Chloride Penetration in Concrete:

Evaluation of Rapid Conductivity Methods and Development of a Service Life Prediction Model for Marine Conditions

A thesis

submitted by

Saarthak Surana

in fulfilment of the requirements for the degree of

DOCTOR OF PHILOSOPHY

Faculty of Engineering and the Built Environment

University of Cape Town

May 2025

Declaration

I declare that this thesis, which is being submitted for the award of PhD at the University of Cape Town, is my own work. Significant contributions of others to this work have been duly acknowledged. This work has not been submitted, in whole or in part, before any other university for any degree.

Saarthak Surana

May, 2025

Abstract

Chloride-induced corrosion is the predominant cause of loss of service life in reinforced concrete structures subjected to marine conditions. To protect reinforcing steel from the corrosive effects of external chloride ions present in these environments, a proper combination of concrete quality and cover depth is needed. Short-term electrical conductivity methods are rapid alternatives to the time-consuming diffusion tests for the characterisation and quality control of concrete mixtures. To estimate the long-term behaviour of a concrete mixture in marine conditions, however, and propose a proper combination of adequate cover depth and concrete quality, a service life prediction model is needed.

In this study, a service life prediction model was developed to predict the rate of chloride ingress in marine environments using conductivity measurements to estimate diffusivity parameters. A comparison between the chloride conductivity test and the Wenner resistivity test was also performed to evaluate the relative impact that pore solution conductivity and unsaturated conditions may have on the proper quantification of chloride penetration resistance of concrete. Diffusivity and conductivity measurements were carried out on various concrete mixtures made with different cementitious binder combinations including fly ash and slag, at different w/b ratios, and cured under wet conditions or plastic wrapping.

The conductivity results of this study showed that the use of the conductivity measurements to assess the ionic transport resistance without regard to the pore solution chemistry can lead to misinterpretations. This effect was especially noticeable in fly ash concretes. These findings address the effect of pore solution on the Wenner resistivity results for practical applications, which has not been explicitly and extensively addressed in the literature. Similarly, the studies on the effect of unsaturation on the Wenner resistivity mostly concern with the effect of surface drying on the Wenner resistivity. In this study, the effect of rewetting on the Wenner resistivity was evaluated on concrete specimens that underwent air drying as part of the curing regime as is common in practical curing regimes before the testing age of 28 days. Despite the use of prolonged specimen rewetting, the moisture gradients in concrete affected the evaluation of the curing efficacy on the cover concrete by the Wenner method. The chloride conductivity test showed more robustness against both these important issues. This study illustrates the constraints of the Wenner resistivity method for compliance testing—an indispensable part of the performance-based quality control process for durability. Notwithstanding this, the Wenner method was found to be very useful in the characterisation of the time-dependence of the instantaneous chloride penetrability of concrete under saturated conditions. A promising application of this finding is in characterising the time-dependence of the chloride diffusivity for service life modelling of reinforced concrete exposed to marine conditions.

On the relationship between the apparent chloride diffusivity and chloride conductivity index (CCI), it was found that the time dependent variation of microstructural penetrability could explain the time

dependent reduction in apparent diffusivity. By accounting the time-dependence of CCI, a general binder-independent correlation was obtained between the apparent diffusivity and CCI. This finding suggests that the differences in the apparent diffusion coefficients in different SCM-blended concretes could be mainly attributed to the continued microstructural development of concrete with time. This is a significant departure from the existing understanding that the chloride resistance of SCMs is to be ascribed to a large extent to their superior binding ability. Instead, the results and analysis of this study strongly suggest that the main differentiating factor is the long-term ageing-dependent reduction in microstructural penetrability. This is a significant improvement of the current understanding of chloride diffusion behaviour in concrete and one of the crucial novel contributions of this study.

Using the laboratory-exposure results of the present study and the field-exposure results of previous studies, a simple user-friendly service life prediction model is developed. A multi-factor model framework based on the error function solution to Fick's 2nd law is used to derive the apparent diffusion coefficient as a function of the test method, curing conditions, and the exposure environment. The general binder-independent correlation between the apparent diffusion coefficient and the time-averaged CCI is used to describe the apparent diffusion coefficient based on early-age CCI and the ageing coefficient of CCI. This approach minimises the need for diffusion testing to characterise the material's resistance to chloride diffusion and its development under moist marine conditions. The quantification of the effect of exposure conditions on the apparent diffusion coefficient was done in terms of a simple empirical factor that could be used to quanitify the severity of exposure conditions pervasive at relevant marine sites. Environmental characterisation parameters were derived for selected South African marine sites using field data from previous studies. The proposed model represents a simplified approach to service life prediction that integtrates design and quality control aspects aimed at providing more effective tools to enable construction of durable reinforced concrete structures.

Acknowledgements

I would like to express my sincere gratitude to my PhD advisors, Prof Hans Beushausen and Prof Mark Alexander, for their guidance, support, and encouragement during this work. It was a deeply enriching experience, for which I thank them.

I appreciate the support of the following people from the Department of Civil Engineering, whose help on the experimental/administrative side was vital to this work:

Mr Nooredien Hassen, Mr Charles May, Mr Christopher Ceaser, Mr Elvino Witbooi, Mr Leonard Adams, the late Mr Tahir Mukadam, Ms Ayesha Dalwai, Ms Rowen Geswindt, and Ms Gill Verster.

I thank Dr Mike Otieno for helpful discussions on chloride analysis and Dr Emmanuel Leo for sharing the XRF results for some of the binder materials used in this study.

I also thank the valuable support of the following organisations:

- Afrisam South Africa (Pty) Ltd – for providing aggregates.
- Ash Resources (Pty) Ltd – for providing fly ash.
- Cement and Concrete SA – for providing access to some valuable literature.
- Pretoria Portland Cement Ltd – for providing Portland cement.
- Sika South Africa (Pty) Ltd – for providing coating materials.

Finally, I would like to extend my deepest gratitude to my father Dr Narendra Mal Surana, my mother Dr Rajkumari Surana, and my brother Nikhil Surana. Without their enduring support, this thesis would not have been completed.

Table of Contents

Declaration i

Abstract ii

Acknowledgements iv

List of Figures xiii

List of Tables xviii

List of Abbreviations and Symbols xx

CHAPTER 1 INTRODUCTION 1

1.1 Background 1

1.2 Research problem and motivation for the study 3

1.3 Research aim 4

1.4 Overall research methodology 4

1.5 Research Significance 5

1.6 Scope and limitations 5

1.7 Thesis organisation 6

CHAPTER 2 LITERATURE REVIEW 8

2.1 Overview 8

Part A: Reinforced concrete in marine environments: an overview 9

2.2 Introduction 9

2.3 Marine exposure 9

2.3.1 Characteristics of the exposure environment 9

2.3.2 Transport processes in marine conditions 10

2.3.3 Degradation mechanisms – An overview 12

2.3.4 Exposure zones – current classifications 14

2.3.5 South African coastline – climatic conditions 15

2.4 Chloride-induced corrosion: the main deterioration mechanism 15

2.4.1 Corrosion initiation 15

2.4.2 Chloride threshold 17

2.5 Conclusions (Part A) 18
Part B: Selected factors affecting chloride penetration resistance of concrete 19
2.6 Introduction 19
2.7 Aggregate 19
2.7.1 Aggregate type 19
2.7.2 Aggregate content 20
2.7.3 Aggregate grading 22
2.8 Binder 23
2.8.1 Portland cement 23
2.8.2 Supplementary cementitious materials (SCM) 24
2.9 w/b ratio 25
2.10 Curing 26
2.11 Exposure conditions 27
2.11.1 Chloride concentration 27
2.11.2 Temperature 28
2.11.3 Exposure zone 29
2.12 Conclusions (Part B) 31
Part C: Chloride modelling and service life prediction 33
2.13 Introduction 33
2.14 Chloride Ingress Modelling 34
2.15 Fick's 2nd Law: Error Function Solutions 34
2.15.1 Principle 34
2.15.2 Apparent parameters: D_a and C_s 36
2.15.3 Time-dependence of D and C_s 38
2.16 Chloride Profile: Practical Considerations 46
2.16.1 Unit of chloride content: by mass of concrete or by mass of binder? 46
2.16.2 Curve-fitting considerations: to extrapolate or to rescale? 47
2.17 Corrosion-Initiation Models 48
2.17.1 Life 365 48

2.17.2 fib Model Code 2010 (modified DuraCrete) 51
2.17.3 ClinConc 52
2.17.4 UCT chloride model 54
2.17.5 Resistivity-based models 55
2.18 Conclusions (Part C) 56
Part D: Formation Factor Approach – theory and testing 57
2.19 Formation factor concept 57
2.19.1 Introduction 57
2.19.2 Principle 57
2.19.3 Description of pore-structure features 58
2.19.4 Pore solution conductivity: composition and influencing factors 59
2.19.5 Determination of formation factor through electrical conductivity: different methodological approaches 60
2.20 Conclusions (Part D) 63
CHAPTER 3 METHODOLOGY 64
3.1 Overview 64
3.2 Experimental variables 64
3.2.1 Supplementary cementitious materials: type and replacement levels 64
3.2.2 Water-binder ratio 65
3.2.3 Curing regime 65
3.2.4 Tests and test parameters 66
Part I - Materials 67
3.3 Concrete materials and mix proportions 67
3.3.1 Binder properties 67
3.3.2 Aggregate properties 70
3.3.3 Mix proportioning, casting, and basic characterisation 71
3.4 Curing methods 74
3.4.1 Wet curing regime 74
3.4.2 Plastic-wrap curing regime 74
3.4.3 Wet-dry curing regime 74

Part II - Testing 76
3.5 Chloride bulk diffusion test 76
3.5.1 Exposure specimens and exposure regime 76
3.5.2 Sample preparation for chloride content testing 77
3.5.3 Chloride content determination through potentiometric titration 77
3.5.4 Chloride profile analysis: curve fitting 79
3.6 Electrical tests 80
3.6.1 Chloride conductivity 80
3.6.2 Surface resistivity 81
3.7 Summary 83
CHAPTER 4 RESULTS 85
4.1 Introduction 85
4.2 Chloride conductivity and surface resistivity results: effect of mix composition and curing 85
4.2.1 Effect of binder 85
4.2.2 Effect of w/b ratio 92
4.2.3 Effect of curing 98
4.2.4 Effect of extended environmental curing 104
4.2.5 Ageing coefficient of penetrability and its estimation 106
4.3 Bulk diffusion results 112
4.3.1 Chloride profile results: general considerations and observations 112
4.3.2 Effect of binder and w/b ratio 115
4.3.3 Effect of curing 119
4.3.4 Prolonged Chloride exposure 121
4.4 Correlation between penetrability (CCI) and diffusivity (D_a) 122
4.5 Correlations of SC with CCI and D_a 125
4.6 Conclusions 127
CHAPTER 5 SERVICE LIFE PREDICTION MODEL 128
5.1 Introduction 128

5.2 Model framework for service life prediction (time-to-corrosion-initiation) 128
5.3 Environment parameter (k_e): Influence of marine environment on D_a 130
5.3.1 Modification for salinity differences between the NaCl solution (lab) and seawater (field) 131
5.3.2 Modification for differences in the environmental conditions between the lab and the field 131
5.4 Ageing coefficient (m): time dependence of D_a 135
5.4.1 Influence of marine exposure zones and macro environments on the ageing coefficient 135
5.4.2 Estimation of ageing coefficient 136
5.5 Test method and curing parameters (k_t and k_c) 139
5.5.1 Relationship between D_a and CCI 139
5.5.2 Effect of lab and field curing 145
5.6 Surface chloride concentration 146
5.7 Service life prediction 148
5.7.1 Proposed model 148
5.7.2 Salient features of the proposed model and a comparison with the previous model 149
5.7.3 Service life estimates 151
5.8 Concluding remarks 153
CHAPTER 6 CONCLUSIONS 154
6.1 Introduction 154
6.2 General discussion and outcome 154
6.3 Experimental findings and conclusions 155
6.3.1 Evaluation of rapid conductivity methods: chloride conductivity and Wenner resistivity 155
6.3.2 Relationship between apparent diffusion coefficient and CCI 157
6.4 Service life prediction model 158
6.4.1 Model development: a summary 158
6.4.2 Practical application of the proposed model 161
6.4.3 Key features of the proposed model: a general discussion 161
6.5 Recommendations for further research 163
LIST OF REFERENCES 165

APPENDICES

APPENDIX A. CHLORIDE BINDING – A CRITICAL REVIEW 185

A.1 Introduction 185

A.2 Mechanisms 185

A.2.1 Chemical binding 186

A.2.2 Physical binding 187

A.3 Chloride binding in diffusion models 188

A.4 Binding isotherms 192

A.4.1 Sorption isotherms 192

A.4.2 'Binding capacity' 192

A.4.3 Comparison of different sorption isotherms 193

A.4.4 Desorption isotherms 196

A.5 Determination of bound and free chlorides 196

A.5.1 Pore solution expression method 197

A.5.2 Sorption equilibrium method 198

A.5.3 Leaching method for 'water-soluble' chlorides 198

A.5.4 Steady-state diffusion cell method 199

A.5.5 Other methods 199

A.6 Factors affecting chloride binding 202

A.6.1 pH (OH^- concentration) 202

A.6.2 Source of chlorides 202

A.6.3 Portland cement phases 205

A.6.4 SCMs and level of substitution 205

A.6.5 w/b ratio 207

A.6.6 Aggregate 207

A.6.7 Temperature 207

A.6.8 Carbonation 207

A.6.9 Electric field 208

A.7 Conclusions 209

APPENDIX B. DIFFUSION AND MIGRATION: AN OVERVIEW OF THEORY AND TESTING 210

B.1 Introduction 210

B.2 Chloride diffusion and migration 210

B.2.1 Ionic Diffusion in solutions 210

B.2.2 Ionic conduction / migration in solutions 211

B.2.3 Nernst-Einstein relation 213

B.2.4 Concentration dependence of ionic diffusion and conduction 214

B.2.5 Diffusion in porous media 216

B.3 Tests for Resistance to Chloride Penetration 219

B.3.1 Steady-state diffusion methods 219

B.3.2 Non-steady-state diffusion methods 219

B.3.3 Steady-state migration methods 221

B.3.4 Non-steady-state migration methods 222

B.3.5 Resistivity/conductivity methods 224

B.4 Chloride Conductivity Test 227

B.4.1 Salient features 227

B.4.2 Preconditioning 230

B.4.3 Vacuum saturation 231

B.4.4 Variability and Revisions 232

B.5 Conclusions 236

APPENDIX C. XRD RESULTS 237

APPENDIX D. CELL CONSTANT CORRECTION FACTOR FOR RESISTIVITY MEASUREMENTS 240

APPENDIX E. COMPRESSIVE STRENGTH RESULTS 243

APPENDIX F. CHLORIDE CONDUCTIVITY RESULTS 244

F.1 Wet cured 244

F.2 Plastic cured 247

APPENDIX G. SURFACE RESISTIVITY RESULTS (150 MM CUBE) 250

APPENDIX H. TYPICAL CALIBRATION RESULTS FOR CHLORIDE CONTENT TESTING 251

H.1 Mortar samples for calibration: Plain Portland cement 251

H.2 Mortar samples for calibration: Fly ash (30%) 252

H.3 Mortar samples for calibration: Blastfurnace slag (50%) 253

APPENDIX I. CHLORIDE PROFILE RESULTS 254

I.1 Exposure duration: 180 days 254

I.2 Exposure duration: 365 days 307

I.3 Exposure duration: 760 days 315

List of Figures

Figure 1.1 An overview of the methodological approach adopted 5

Figure 2.1 A typical seawall depicting transport of aggressive species into concrete under marine exposure (reproduced from (BS 6349-1, 2013)) 10

Figure 2.2 Transport processes in different zones of a typical cover concrete (reproduced from (Alexander, Beushausen & Otieno, 2013)) 11

Figure 2.3 Illustration of (a) microcell corrosion – the anodic and cathodic half-cells are closely spaced and (b) macrocell corrosion – a localized anodic half-cell with an extensive cathodic half-cell (reproduced from (Poursaee & Hansson, 2009)) 16

Figure 2.4 Corrosion-induced damage model that is generally used for service life prediction (reproduced from (Violetta, 2002)) 17

Figure 2.5. Corrosion rates of steel in the presence of chloride ions (reproduced from (Lambert, Page & Vassie, 1991)) 17

Figure 2.6 Chloride profiles for concrete with different paste contents (reproduced from (Buenfeld & Okundi, 1998)) 21

Figure 2.7. The variation of different concrete properties at different w/b ratios on decreasing the aggregate content as the water content increases (reproduced from (Wassermann, Katz & Bentur, 2009)) 22

Figure 2.8 Diffusion coefficient as a function of w/c for Portland cement concretes (reproduced from (Bamforth, Price & Emerson, 1997)) 26

Figure 2.9 Variation of apparent diffusion coefficient of cement paste with chloride concentration (reproduced from (Marchand & Samson, 2009)) 27

Figure 2.10 Presence of atmospheric chlorides with distance from the sea using wet candle method (reproduced from (Meira et al., 2010)) 31

Figure 2.11 Modified Tutti's model for corrosion damage during the life of a structure (reproduced from (Heckroodt, 2002)) 33

Figure 2.12 A typical measured chloride profile in which an error function solution is fitted – the first few data points are ignored in data fitting and the fitted curve is extrapolated to get a hypothetical surface content – C_s [figure reproduced from (Ann, Ahn & Ryou, 2009)] 37

Figure 2.13. Time dependency of instantaneous (D) and apparent (D_a) diffusion coefficients [the crosses signify the exposure period] (reproduced from (Nilsson, 2006)) 39

Figure 2.14. The variation of surface chloride content in 11 concrete bridges located in South Korean coastline in tidal conditions over the years (reproduced from (Pack et al., 2010)) 43

Figure 2.15 Increase in C_s with time in (a) tidal, and (b) splash conditions (reproduced from (Ann, Ahn & Ryou, 2009)) 43

Figure 2.16 The existing nomogram for diffusion coefficient prediction from CCI measurements (reproduced from (Mackechnie, 2001)) 55

Figure 3.1 The binder materials used in this study 69

Figure 3.2 Particle size distribution of fly ash and slag used in this study, measured by laser diffraction 69

Figure 3.3 Particle size distribution of aggregates used in this study 70

Figure 3.4 Schematic illustration of the curing regimes adopted in this study. *Wet-dry regime was only adopted for bulk diffusion testing. 75

Figure 3.5: The pulveriser used for grinding the concrete samples to powder. The salient features are (a) the pneumatic clamping arrangement mounted on a spring-loaded vibrating bench (in the left image), and (b) the sample holder with the pulverizing pellet/disc (enlarged image on the right) 78

Figure 3.6: Automatic potentiometric titrator used in this study 79

Figure 3.7 A schematic of the chloride conductivity test apparatus (adopted from DI-Manual, 2018) 81

Figure 3.8: Surface resistivity test with a 4-point probe on a 150-mm cube 83

Figure 4.1 Variation with fly ash level (% mass): (a) 28-days CCI and (b) 28-day SC (1/SR). Note: The CCI result for PC-0.6 was a statistical outlier (ASTM E178, 2008) and therefore comparisons are made here with an estimated value based on the CCI-w/b relationship for PC concretes. For the original data point, refer to Section 4.2.2. 86

Figure 4.2 Variation with slag level (% mass): (a) 28-days CCI and (b) 28-day SC (1/SR) 86

Figure 4.3 Effect of binder on CCI and SC through 'relative conductivity'. It is calculated by dividing the result with the corresponding result for PC concrete of the same w/b ratio. 87

Figure 4.4 (a) Compressive strength results and (b) Relative compressive strength to illustrate the effect of binder type on the 28-day concrete compressive strength: the ratio (%) of the 28-day compressive strength of concrete to that of the PC concrete of the same w/b ratio 88

Figure 4.5 Relationship between 28-day porosity (based on vacuum saturation with 4.4 M NaCl solution after 7 days of oven drying at 50°C) and SCM level (%, mass) in the binder: FA (a) and BS (b) 88

Figure 4.6 Comparison of the measured CCI of FA concretes with the hypothetical CCI considering FA as an inert filler. The equivalent PC CCI is the calculated CCI of PC concretes at w/b=w/c (column (3),

Table 4.1), whereas the actual PC CCI are those measured at the given w/b ratios (shown on the 'x' axis).....90

Figure 4.7 NIST predictions of pore solution (PS) conductivity for fly ash concretes (NIST, 2019), which are not consistent with the experimental evidence reported in the literature. 92

Figure 4.8 Variation of (a) 28-day CCI and (b) 28-day SC (1/SR), with w/b ratio 93

Figure 4.9 Relationship between CCI and porosity (CCI). The porosity referred to here is based on vacuum saturation with a 4.4 M NaCl solution of oven-dried concrete, as per (SANS 3001-CO3-3, 2015) 94

Figure 4.10 Variation of porosity (CCI) with w/b ratio 95

Figure 4.11 δ_b (binder-dependent intercept parameter for the porosity-w/b ratio relationship) as a function of SCM%. Note the difference between the predictions of a linear and a hypothetical curve for FA beyond the range of experimental data used. 95

Figure 4.12 Comparison of the predicted values of 28-day wet cured CCI with the literature. The legend includes the Portland cement type, water content, and aggregate details. Data sources: SS: present study; AB: (Bakera, 2018); EL: (Leo, 2022); HS: (Sohawon, 2018); MO: (Otieno, 2018), (Otieno, 2014). The predicted values were estimated using Table 4.2. Note: Repeatability SD = 10% (SANS 3001-CO3-3, 2015), n = 4. 97

Figure 4.13 Effect of curing method on 28-day CCI. Wet: continuously wet; Plastic: 7 days under plastic, 21 days in air 99

Figure 4.14 Influence of curing method on (a) 28-day porosity (measured using CCI protocol on near-surface 30-mm discs) and (b) 28-day compressive strength (100-mm cubes). 100

Figure 4.15 Influence of curing method on (a) CCI and (b) SC. The confidence intervals are calculated using the 1s repeatability value of the test method, i.e., for CCI: SD = 10%, n = 4 (SANS 3001-CO3-3, 2015) and for SC: SD = 6%, n = 3 (AASHTO T 358, 2015). 101

Figure 4.16 Schematic illustration of the expected variation of different parameters influencing surface conductivity measurements with depth in the near-surface region under wet and plastic curing regimes 102

Figure 4.17 Schematic variation of measured surface resistivity with the movement of the water-front upon immersion of unsaturated concrete in water (Gowers & Millard, 1999). 103

Figure 4.18 Effect of immersion duration on (a) calculated depth of water penetration, and (b) surface resistivity of 7-day plastic cured 150-mm concrete cubes. Water depth was calculated based on mass gain with immersion duration and concrete porosity. 104

Figure 4.19 Comparison of surface conductivities of plastic cured concretes after 7 days of water immersion with continuously wet cured concrete of the same age 104

Figure 4.20 Variation of CCI with age under two different curing and storage regimes. Results of only one w/b ratio (0.6) are presented for the sake of brevity as these are sufficiently representative of the general trend 105

Figure 4.21 Evolution of CCI with time (log scale) (Note: different ordinate scales; PC-0.6 values were normalised with the 28-day estimated value) 107

Figure 4.22 Evolution of surface conductivity (SC - 1/SR) with time (log scale) (Note: different ordinate scales) 108

Figure 4.23 Comparison between the ageing coefficients for CCI (α_{CCI}) and SC (α_{SC}) 110

Figure 4.24 Relationship of α_{SC} with w/b ratio (left) and SCM level (right) 111

Figure 4.25 Relationship between the SC ageing coefficient and the replacement ratio (i.e., FA%/30 or BS/50%) 111

Figure 4.26 Illustrative chloride profiles for PC (left) and FA (30%) (right) concretes. Each graph includes the chloride profiles of 3 individual specimens (labelled: 1, 2, 3), the points excluded from the regression analysis (represented by unfilled markers), and the average curve for all 3 specimens (labelled: Avg. fit). 112

Figure 4.27 An illustration of the close correspondence between the mean C_s (left) and D_a (right) values of the individual chloride profiles of the specimens and the overall values obtained by regression analysis on the entire sample. Although the values shown here are from 28-day wet cured specimens, similar results were achieved from plastic cured specimens as well. 114

Figure 4.28 Estimation of the total chloride depth: (left) Illustration of the Cl depth calculation method using the internal Cl content as the reference Cl concentration and (right) Comparison of the estimated Cl depth (normalised with the corresponding PC Cl depth) using different references: internal Cl content versus a uniform Cl threshold content = 0.05%, on selected concrete mixtures 114

Figure 4.29 Variation of Cl bulk diffusion parameters according to FA (left) and BS levels (right) after a chloride exposure of 180 days: (i) depth of chloride penetration, (ii) apparent diffusion coefficient (D_a) [caution: log scale], (iii) surface chloride concentration (C_s) [Cautionary note: the scales on the SCM% axis for fly ash and slag are different] 116

Figure 4.30 Variation of bulk diffusion parameters with w/b ratio: (i) depth of chloride penetration, (ii) D_a, and (iii) C_s 117

Figure 4.31 Relative D_a and relative Cl depth with respect to plain cement concretes at corresponding w/b ratios 118

Figure 4.32 Illustration of the possible cause of high variability in the diffusion results 119

Figure 4.33 Effect of curing on chloride diffusion parameters [Note: 95% CI based on average variance, n=3] 120

Figure 4.34 Chloride profile development of selected wet cured concretes with extended duration of exposure 121

Figure 4.35 Variation of C_s and D_a with time for wet cured concretes 122

Figure 4.36 Relationship between the 180-day D_a and 28-day CCI. Part (i) presents all the data together, whereas parts (ii)-(vi) present data specific to a binder group. The error bars represent 95% confidence intervals [D_a (n = 3), CCI (n = 4)]. 123

Figure 4.37 (a) Correlation between the 180-day D_a and the time-integrated equivalent CCI and (b) validation with 365-day and 760-day exposure data 125

Figure 4.38 Correlations between SC and CCI 126

Figure 4.39 Correlations between D_a and SC 126

Figure 5.1 k_e for individual mixes for the Cape Town site (Granger Bay). 25-year D_a values were obtained by extrapolation of time functions determined in a 3.5-year long exposure study (Heiyantuduwa-Beushausen, 2022). 133

Figure 5.2 k_e for individual mixes for the Durban site (Durban Port). 25-year D_a values were obtained by extrapolation of time functions determined in a 3.5-year long exposure study (Heiyantuduwa-Beushausen, 2022). The average values shown represent averaging over all the studied concrete mixtures. 133

Figure 5.3 Comparison of the calculated $k_{e,\,calc}$ (k_{RH} x k_T) (Lindvall, 2003; Life-365 v2.2.3, 2020) and the measured $k_{e,\,meas}$ ($D_{a,field}/D_{a,lab}$) after exposure durations of 2.5 years and 25 years (extrapolated using the derived time functions) for Cape Town and Durban sites based on data from (Heiyantuduwa-Beushausen, 2022). Note: Error bars represent SD values and the bars represent the mean values, averaged over different concrete mixtures (PC, FA, BS; w/b – 0.4, 0.6). 134

Figure 5.4 Illustration of the influence of exposure conditions on the ageing coefficient, m_a, based on (Heiyantuduwa-Beushausen, 2022). The Cape Town site (a) is located on the extreme south-west coast exposed to the Atlantic Ocean and the Durban site (b) is located on the east coast exposed to the Indian Ocean. Binder groups included are PC, FA (30%), and BS (50%) with w/b ratios: 0.4 and 0.6. 136

Figure 5.5 Comparison of calculated m_a (0.7α) and measured m_a 138

Figure 5.6 A hypothetical illustration of possible differences between ageing in lab and field diffusion experiments (excluding the effects of T, RH, and salinity on D_i) 140

Figure 5.7 Correlations between 180-day D_a ($D_{a,180}$) and 28-day CCI (CCI_{28}). Note: (i) w/b was in the range (0.3-0.7) for PC and (0.4-0.6) for the rest. (ii) R^2 were adjusted to account for setting the intercept to zero. 142

Figure 5.8 Evaluation of test correlation constant for $D_{a,180}$-CCI_{28} pair as a function of SCM proportions 143

Figure 5.9 (a) Correlation between the 180-day D_a and the time-integrated equivalent CCI and (b) validation with 365-day and 760-day exposure data..... 144

Figure 5.10 Ratio of lab potential CCI and field potential CCI to assess the effect of curing on CCI on different concrete compositions 146

Figure 5.11 Determination of the w/b ratio factor for $C_{s,ult}$ from experimental data of the present study 147

Figure 5.12 Scheme for modelling D_a in Mackechnie's model [f(): represents correlation] 150

Figure 5.13 Scheme for modelling D_a in the proposed model [f(): represents correlation] 150

Figure 5.14 Sensitivity of estimated cover depth to selected parameter changes (Note: analysis performed with the following selected default conditions (unless otherwise mentioned in the figure): Exposure site: Granger Bay, exposure zone: splash zone, SL= 50 y, w/b: 0.4)..... 151

Figure 5.15 A design chart for selected conditions: the estimated minimum design cover depth based on the 28-day CCI, for different binder types 152

List of Tables

Table 2.1 Exposure classifications in different standards (adapted from (Alexander & Nganga, 2016)) 15

Table 2.2 Phase composition (%) of Portland cement over time 24

Table 2.3 Chloride ingress in exposure zones: trends in literature [*Sub.: submerged, Tid.: tidal, Spl.: Splash, Spr: Spray, Atm: atmospheric] 30

Table 2.4. Development of surface chloride content for different exposure zones (Life-365 v2.2.3, 2020) 50

Table 3.1 Oxide composition of binder materials through XRF and crystalline phases through quantitative XRD 68

Table 3.2 Physical properties of the binder materials 69

Table 3.3 Physical properties of the aggregates used in this study 71

Table 3.4 Concrete mixture details – mixture proportions, slump, and standard compressive strength 73

Table 3.5. Concrete mixes used for wet-dry regime 75

Table 4.1 Comparison of the hypothetical porosity assuming no contribution from FA hydration with the measured porosity 89

Table 4.2 Prediction model for estimating 28-day wet cured CCI (mS/cm) 96

Table 4.3 Results of the Student's t-test for significance of the differences between mean CCI of wet cured and plastic cured concretes 99

Table 4.4 Equivalent PC-Wet w/b ratios based on 28-day CCI. A comparison under the same curing method reveals the effect of binder, and a comparison between curing methods illustrates the effect of curing on a given mix. 100

Table 4.5 Time functions for CCI and SR 109

Table 4.6 SC/CCI ageing coefficient estimation based on polynomial interpolation 112

Table 5.1 Environmental parameter (k_e) for modifying lab D_a for selected South African sites (based on data from (Heiyantuduwa-Beushausen, 2022)) 135

Table 5.2 Ageing coefficients from different sources 137

Table 5.3 CCI ageing coefficient (α): estimation for fly ash and slag 138

Table 5.4 Ageing coefficient selected for apparent diffusion coefficient (D_a) to be used up to 25 years (D_a will be assumed to remain constant after 25 years) 138

Table 5.5 Test correlation factor between $D_{a,180}$ and CCI_{28} 143

Table 5.6 $C_{s,w/b\text{-}0.4}$ values adopted for the model (Mackechnie, 2001). 147

Table 6.1 Summary of the proposed model 161

List of Abbreviations and Symbols

Abbreviations

BS	Ground Granulated Blastfurnace Slag
CCI	Chloride Conductivity Index
FA	Fly Ash
FF	Formation Factor
PC	Portland Cement
RC	Reinforced Concrete
SC	Surface Conductivity
SCM	Supplementary Cementitious Material
SR	Surface Resistivity
w/b	Water-to-Binder ratio
CI	Confidence Interval (n – number of observations)

Symbols

C_s	Surface chloride concentration
D_a	Apparent diffusion coefficient
m	Ageing coefficient of apparent diffusion coefficient
α	Ageing coefficient of instantaneous conductivity/penetrability
t	Age / time
t_{exp}	Exposure duration
T	Temperature
x	Depth (position variable)
k_t	Test method parameter
k_c	Curing parameter
k_e	Environmental parameter

Chapter 1 INTRODUCTION

1.1 Background

Corrosion of reinforcing steel in reinforced concrete (RC) structures is a critical concern for the service life of civil and urban infrastructure (Mackechnie & Alexander, 1997; Koch et al., 2002). It stands out from other deterioration processes affecting RC structures for at least two reasons. One is the geographical scale on which this problem affects RC structures globally. The second is the deceptive nature of rebar corrosion to go undetected, often until it is too late for an inexpensive intervention. In marine regions, chloride ions from seawater are the predominant cause of reinforcing steel corrosion. Structures exposed to seawater directly or through air-borne chlorides are susceptible to chloride-induced corrosion of reinforcing steel. By forming localised pits in reinforcing steel, this type of corrosion can lead to rapid deterioration.

Often, the first and the only defence against this type of deterioration is the concrete in the cover region of steel. Good quality cover concrete can provide resistance against the rapid penetration of aggressive species essential for the initiation and propagation of corrosion. Hence, a large portion of research and design effort to ensure durability in these conditions is focused on controlling the appropriate characteristics of the cover concrete.

The main differences in common design approaches lie in what are deemed to be the 'appropriate characteristics' to focus on regarding durability and how these are 'controlled' through specification. Most current codes and specifications focus on prescribing limits on mix composition parameters, curing, strength grade[1], and cover depth. Amongst the prescribed characteristics, only the compressive strength grade is subject to testing as part of the strength requirement of the structural design. Several criticisms of this prescriptive approach are worth discussing (Anoop et al., 2001; Lobo, Lemay & Obla, 2006; Alexander & Thomas, 2015), however, the principal concerns are:

(i) A lack of verification of the as-built quality of cover concrete through test methods that can evaluate the concrete against the relevant deterioration mechanism(s).

(ii) An inability of these prescriptions to allow for a design process that sufficiently differentiates between the design requirements of a structure, particularly, the service life, and the severity of exposure.

Lacking a proper rational basis, this type of design approach may fail to adequately ensure durability, while at the same time being overly restrictive. An alternative is provided by the so-called 'performance' approach. The performance approach focuses on the end performance rather than the

[1]Strength grade of concrete is evaluated by testing standard specimens, which are wet/moist cured for 28 days in laboratory-controlled environment.

methods or means of achieving it. The emphasis is placed on characterising the as-built cover concrete through test parameters representing resistance to the relevant deterioration mechanism (Alexander, Ballim & Stanish, 2008; Andrade et al., 2013; Baroghel-Bouny, Thiéry & Wang, 2014). The test values to achieve for the given cover depth and prevalent exposure conditions are determined by modelling the material behaviour under the relevant deterioration mechanism(s), through 'service life models'. These test parameters should, on the one hand, reliably characterise the resistance of concrete against the relevant physico-chemical mechanisms of deterioration and on the other hand, be able to identify the effect of common construction practices such as compaction, curing, etc. to assist in quality control (Ballim & Alexander, 2018). Often the timeframes to fulfil the two requirements are at odds with each other. For instance, chloride penetration in marine conditions primarily occurs through the mechanism of non-steady state diffusion, which may take several months to provide useful information, while the quality control procedures are required to be finished within a few weeks.

The onset of chloride-induced corrosion, like many other deterioration mechanisms, mainly depends on the transport characteristics of concrete. As a result, several durability indicator tests have been developed worldwide to provide a rapid assessment of the transport resistance of concrete to address the dual concerns with the prescriptive approach described above. Generally, electrical methods are used. Notable test methods include but are not limited to, the rapid chloride permeability test (RCPT) (ASTM C1202, 2012), the rapid chloride migration test (RCMT) (NT BUILD 492, 1999), the Wenner resistivity test (AASHTO T 358, 2015). The electrical test methods mainly differ in the electrochemical principles used, test design, and specimen preparation requirements. Each method has its advantages and disadvantages. It is important that the chosen test method provides a good balance of accuracy, precision, and practical ease.

Service life models using some of these test methods as the key material parameter have also been developed (Tang & Nilsson, 1996; Polder & De Rooij, 2005; Andrade et al., 2013). Different approaches are adopted for service life modelling, which are broadly classified into: physical (or mechanistic) and empirical (Nilsson, 2006). The physical approaches attempt to model by describing the idealised phenomenon from its individual component parts through physical constitutive laws/equations. On the other hand, the empirical approaches attempt to model the complex phenomenon as a whole through direct empirical observations. In other words, the former is a bottom-up approach and the latter is a top-down approach (Gerlee & Lundh, 2016). The physical approaches are essential to understanding the phenomenon accurately, which would enable accurate predictions. However, chloride penetration is a complex phenomenon, which makes its physical models correspondingly complex. At present, the level of accuracy provided by these models may not justify the attendant complexity (scientific and computational) and cost for practical application. In most cases, empirical or semi-empirical models offer a more practical alternative, which can be built relatively quickly and can be handled by design engineers. Regardless of which approach is preferred, service life models require

site-specific field data as input to make realistic predictions due to the complex and multi-variate nature of the process of chloride transport in concrete.

In the South African context, the chloride conductivity test was developed as a reliable measure of the transport resistance of concrete to chloride ion diffusion (Streicher & Alexander, 1995). The test was designed carefully to address the shortcomings of contemporary methods (Streicher & Alexander, 1994), which resulted in a more accurate, simpler and quicker test method suitable for concrete mixture qualification, quality control, and compliance testing. A service life prediction model was developed for selected South African marine conditions linking long-term chloride penetration performance to the short-term 'chloride conductivity index' (Mackechnie, 1996, 2001). This enabled the use of the chloride conductivity index as a performance assessment parameter by allowing the specification of acceptance criteria using the service life model (for the target service life in the given exposure conditions) (Alexander, Santhanam & Ballim, 2011). Since these initial developments, the test method has been improved (Otieno & Alexander, 2015). In addition, more field data on chloride penetration rates from different South African marine environments have been systematically collected in another study (Heiyantuduwa-Beushausen, 2022).

1.2 Research problem and motivation for the study

The existing service life model (Mackechnie, 1996, 2001) requires three different material parameters, namely, the 28-day CCI, the 98-day modified CCI, and the 'm' value, to predict the long-term chloride ingress. Moreover, the approach is based on direct correlations between the CCI parameters (CCI and modified CCI) and the field-based D_a. This model lacks a straightforward modelling approach and requires diffusion-related data to expand the scope of the model to other materials. These characteristics limit its comprehensibility to practitioners and its flexibility to extend to other materials and exposure conditions. There is therefore a need to move towards a more simplified, straightforward and practical modelling approach that is better suited to development in the scope of materials and exposure conditions. This is especially relevant given the strong impetus to develop more locally relevant sustainable materials (Scrivener, John & Gartner, 2018). These newer materials will have to be quickly assimilated into the scope of the existing service life model so that design decisions can be rationally based on a view to long-term durability.

In addition, finding ways to simplify testing could be similarly beneficial for quality control and for generating input data for service life prediction. It is well recognised that the assessment of chloride resistance of concrete through diffusion testing is quite tedious and time-consuming. Even the more rapid tests such as chloride conductivity often require careful specimen extraction, preparation, and conditioning procedures. As an alternative, the surface resistivity (or conductivity) method has been adopted by many as a non-destructive alternative (Andrade et al., 2013; Presuel-Moreno, Wu & Liu, 2013; Sengul, 2014; Mendes et al., 2018; Balestra et al., 2020; Chidiac & Shafikhani, 2020). A clear

understanding of the advantages and shortcomings of this method is still lacking despite the expanding literature on the subject (Morris, Moreno & Sagüés, 1996; Sengul & Gjørv, 2009; Spragg et al., 2013). This is often due to an underappreciation of the complex interaction of material, environmental, and test design-related factors influencing conductivity measurements and the conductivity-diffusivity relationship. Hence, the effectiveness of the surface resistivity method in quality control and service life prediction of marine structures requires further investigation.

1.3 Research aim

The overarching aim of this thesis is to study the use of electrical conductivity methods in the prediction of chloride ion penetration resistance of concrete exposed to marine environments. This aim is divided into the following specific objectives:

1. To develop an updated service life model incorporating the chloride conductivity index as the quality assessment parameter to predict the corrosion-free service life for RC structures exposed to South African marine environments.
2. To assess the opportunities and pitfalls of the surface resistivity/conductivity method as a non-destructive supplement to the chloride conductivity method.

The main objectives are divided further into the following sub-objectives:

i. To generate a database of the conductivity and diffusivity measures for common concrete constituents, mix proportioning, and curing methods.
ii. To investigate the relationship between the apparent diffusivity and the conductivity parameters.
iii. To illustrate the influence of pore solution conductivity on the conductivity of concrete and how it may affect the interpretation of transport characteristics by conductivity measurements.

1.4 Overall research methodology

An experimental study was undertaken to collect chloride transport and conductivity data for common concrete mixtures and curing methods. The binders included various binary blends of fly ash and slag with Portland cement. The experimental work was conducted in laboratory-controlled conditions. In conjunction with the collected data from this work, field data and findings for marine exposure in South African environments were collected from previous studies (Mackechnie, 1996; Heiyantuduwa-Beushausen, 2022) to develop a service life prediction model. The model framework adopted is based on the multi-factor concept followed by the DuraCrete model (fib bulletin 34, 2006). The overall methodological approach adopted in this study is summarized in Figure 1.1.

.

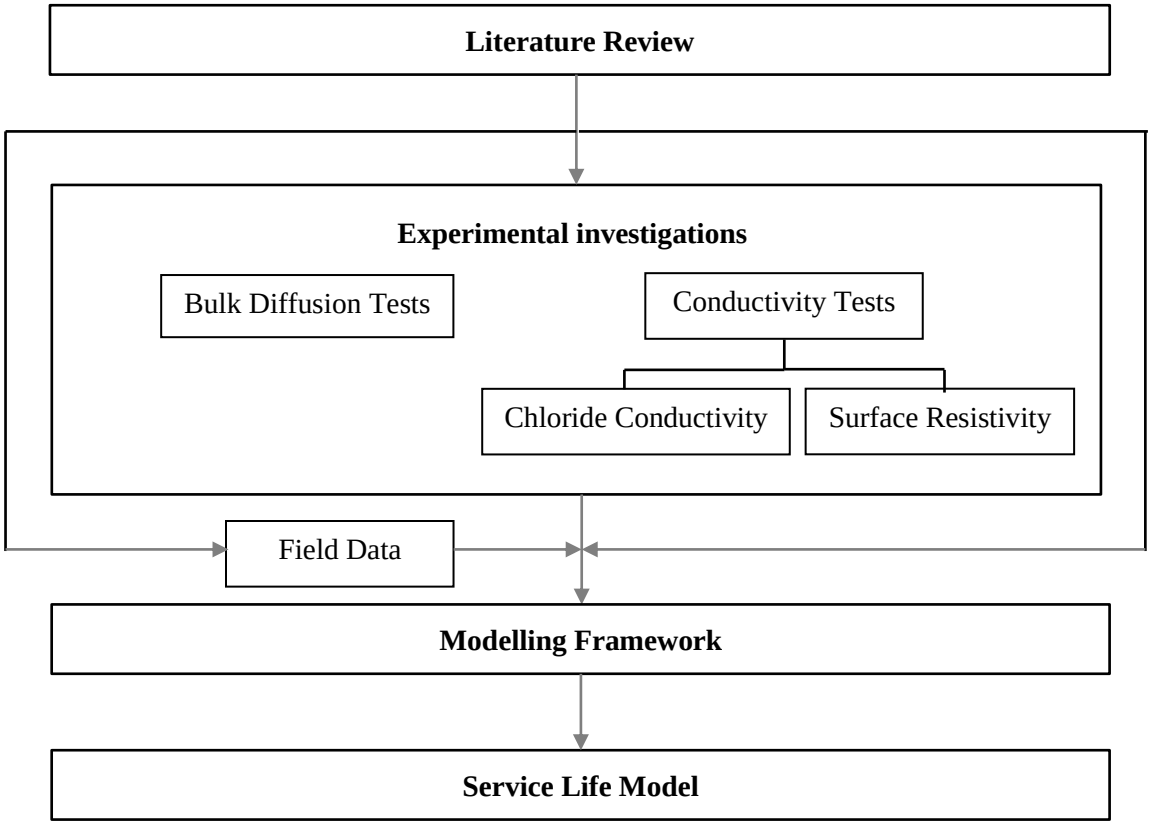

Figure 1.1 An overview of the methodological approach adopted

1.5 Research Significance

The findings of this study provide important new insights into the factors controlling the chloride ion resistance of concrete. This has important implications on the understanding of the chloride transport in concrete and on the optimisation of concrete materials for enhanced chloride resistance. Based on these findings, a generalised empirical approach to address the long-term time-dependent evolution of concrete penetrability in marine environments is presented. This modelling approach can accommodate different binder systems using conductivity measurements and can be extended to different exposure environments without the need for extensive field data. It provides a simpler and more efficient way to generate service life estimates and integrates them with short-term concrete quality requirements, which will improve the process of durability design and quality control. Important insights are also presented on the use of the Wenner resistivity method, which can lead to a more careful interpretation of its results and provide possibilities for its proper integration into the material characterisation process.

1.6 Scope and limitations

The scope of this study is limited to the following:

1. The limit state of unacceptable failure due to deterioration from chlorides is assumed to be the achievement of the critical chloride threshold value at the level of steel or in other words, corrosion initiation. The portion of service life under corrosion propagation is ignored in this study.
2. Concrete is considered crack-free as data are collected on lab specimens. The effect of cracking found normally in RC structures is ignored in the analysis and modelling.
3. The scope of materials and exposure conditions is restricted to those prevalent in South Africa. The specific materials and exposure environment included are covered in Chapter 3.
4. A deterministic approach to modelling is adopted as the information needed to enable a proper probabilistic treatment in this case requires data collection that is not possible in the time frame of a single PhD study.
5. The data collection for time-dependent parameters was restricted to 2 years due to the time restrictions of the study. Studying long-term durability in natural conditions requires a much longer time scale and therefore the findings and conclusions of this study should be interpreted in view of the restricted timeline.

1.7 Thesis organisation

This thesis is organized into the following chapters:

Chapter 2: Literature review

Chloride-induced corrosion is a complex subject and an understanding of the various aspects governing it is highly desirable to properly address the issues identified in this study. Chapter 2 presents a critical review of various aspects pertaining to chloride-induced corrosion initiation and highlights the knowledge gaps in this field. The chapter is divided into four parts, each addressing a different aspect of the subject from general considerations (Part A) and terminology to influencing factors (Part B), modelling practices (Part C), and the formation factor approach (Part D). Facets such as chloride binding, diffusion theory and testing are included in Appendices A and B.

Chapter 3: Methodology

The rationale behind the selection of chosen research parameters for the experimental program is presented in Chapter 3. It also describes the materials and methods used in detail.

Chapter 4: Results

A comparison of the chloride conductivity and surface resistivity results is presented within the context of the formation factor approach in this chapter. How various aspects such as binder type, w/b ratio, and curing affect the chloride resistance of concrete is highlighted. The correlations between different

transport parameters such as diffusion coefficient and different conductivity parameters are also investigated in this chapter.

Chapter 5: Service life prediction

This chapter presents the development of a service life prediction model based on the lab-based experimental results acquired in this study and the field-based results from the literature.

Chapter 6: Conclusions and recommendations

Conclusions drawn from this study are presented in this final chapter. Recommendations for future research are also included.

Chapter 2 LITERATURE REVIEW

2.1 Overview

A critical review of various aspects of the subject of chloride-induced corrosion is presented in this chapter. The emphasis is placed on addressing the transport of chloride ions through concrete. Relevant concepts of steel corrosion are briefly covered, but a more detailed discussion is considered out of the scope of this study. The chapter is divided into the following four parts:

- Part A presents an overview of the various aspects of marine exposure environment and its effects on reinforced concrete. The focus is subsequently placed on the main deterioration mechanism relevant to this study, i.e., the chloride-induced corrosion.

- Part B provides a critical examination of selected relevant factors influencing chloride ion transport in concrete.

- Part C covers selected concepts of modelling chloride transport and a critique of some of the influential service life models.

- Part D presents the principles of the formation factor approach and examines the methodological aspects of its evaluation.

Part A: Reinforced concrete in marine environments: an overview

2.2 Introduction

Corrosion of steel in reinforced concrete structures can severely impair the service life of the structure and increase the life cycle costs through additional repair costs. Corrosion of reinforcing steel is one of the most challenging durability problems in RC structures worldwide, especially in marine environments. Steel corrosion is a part of the many processes that may lead to degradation in marine environments. Marine environments present uniquely harsh exposure conditions combining a multitude of physical and chemical degradation mechanisms. This section presents an overview of the various aspects of marine environments pertaining to RC structures, including, environmental actions, transport processes, degradation mechanisms, and exposure classification used in current durability specifications. Furthermore, issues related to corrosion initiation are briefly discussed. Through this overview, the aim is to lay out the necessary basic concepts and terminology for the rest of the thesis.

2.3 Marine exposure

2.3.1 Characteristics of the exposure environment

The aggressiveness of marine environments to reinforced concrete is primarily the result of the aggressive composition of seawater. Seawater contains aggressive ionic species in the form of dissolved salts, mainly, Na^+, Mg^+, Cl^-, SO_4^{2-} ions, with Na^+ and Cl^- ions in the highest concentrations. Their respective and total quantities vary widely according to the specific geographical and climatic region; however, 35 g/kg (3.5%) is generally considered as an average salinity value for most seawater. Out of 3.5%, approximately 2.8% (0.5 M) is due to NaCl. Total salinity at any location is influenced by the following factors: (i) freshwater discharge from the rivers/streams and precipitation, which reduces the salt concentration, (ii) evaporative loss of water, which increases the salt concentration, (iii) circulation of water, (iv) nature of effluents and solid wastes discharged into the sea, among other things. The pH of seawater generally lies slightly on the basic side, between 7.5 and 8.4 (Otieno & Thomas, 2016).

Another essential characteristic of marine environments that has a major influence on the transport of aggressive species into concrete is seawater movement due to tides and winds. Tides cause surges and decline of sea level as a result of the differential gravitational pull of mainly, the moon, because of its proximity to the earth, but also the sun. Sea level rises and falls twice a day giving rise to “high tides” and “low tides” with an average period of 12 h 25.2 min between two high and two low tides, following the movement of the moon with respect to the earth (Mackie, 2016).

Winds, on the other hand, induce waves on the surface of water by friction. Waves carry enormous amounts of energy and when they come in contact with a structure in the sea or the coast, transfer that energy as impact. When these waves break against a barrier or at the seashore, they generate marine aerosol which can be carried inland by the wind. The portion which is not in direct contact with seawater

but is exposed to these airborne chlorides in the form of marine aerosol is known as the *atmospheric* or *air-borne* zone. The portion completely submerged in seawater is known as the *submerged* zone. The portion of the structure in the tidal range is subjected to semi-diurnal wet and dry cycles with the rise and the fall of tides and is also subjected to the abrasive action of wave splashes. This portion of the structure is known as the *tidal/splash/spray* zone (see Figure 2.1).

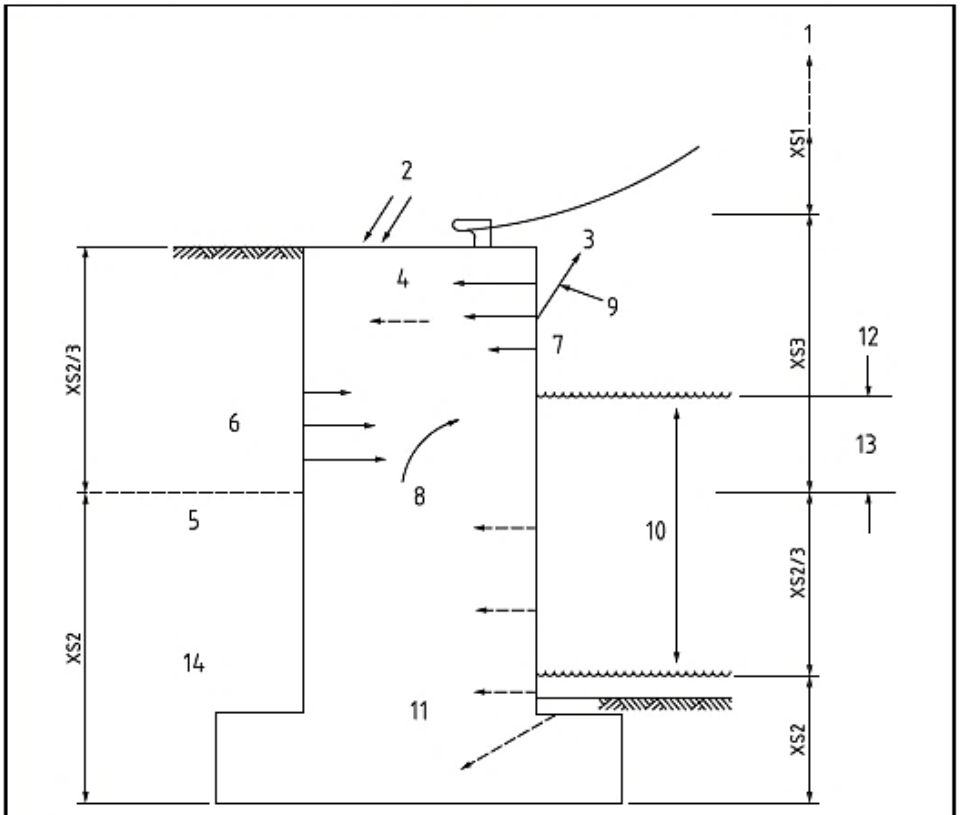

Key

1 Airborne chlorides only (aerosol/mist – less than direct spray)
2 Rain reducing surface salt concentration
3 Evaporation giving a salt concentration
4 Diffusion in response to salt concentration
5 Water table
6 Permeation by pressure head
7 Capillary absorption into partially saturated concrete
8 Wick action, drawing water from wet concrete to the exposed face
9 Splash/spray
10 Tidal range
11 Diffusion of salt from seawater
12 Mean high water springs (MHWS)
13 Approximately one quarter of tidal range below MHWS
14 Permanently submerged

NOTE XS1 exposure class applies to elements not directly in a wetted zone, including superstructures and buildings adjacent to the coast.

Figure 2.1 A typical seawall depicting transport of aggressive species into concrete under marine exposure (reproduced from (BS 6349-1, 2013))

2.3.2 Transport processes in marine conditions

Generally, the aggressive species gets transported into the concrete through a combination of transport processes. However, often the transport is modelled based only on the most dominant transport process involved for ease of study. For example, the first few millimetres of the cover concrete are often

subjected to wetting and drying, which results in a convective transport of fluid and ionic species in that zone. However, the inner zone of concrete is treated as saturated, and the transport is considered to happen only by diffusion (see Figure 2.2).

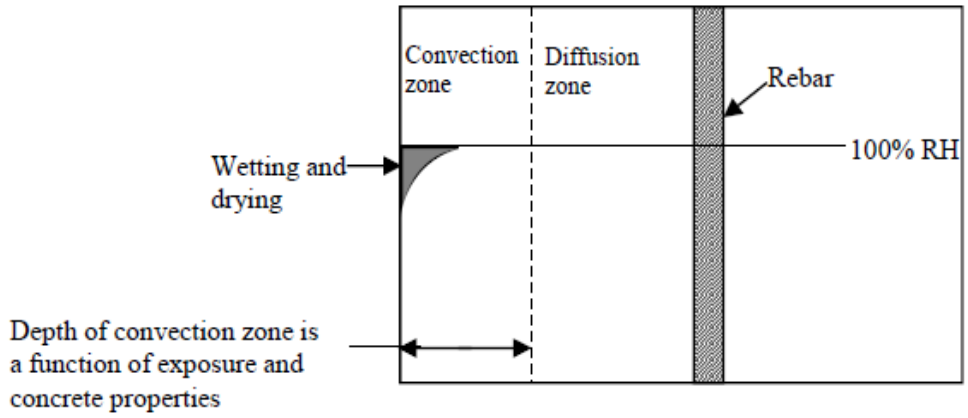

Figure 2.2 Transport processes in different zones of a typical cover concrete (reproduced from (Alexander, Beushausen & Otieno, 2013))

The different hygral conditions of the marine zones result in different transport processes by which aggressive species enter and move into concrete in different zones. Figure 2.1 depicts the relevant transport processes in different marine exposure zones for a typical seawall. In the submerged zone, the concrete is fully immersed in water and is not allowed to dry. Hence, the relevant transport processes for this region are permeation and diffusion. Seawater permeates into the surface of concrete and the ionic species, such as chlorides, sulphates etc, diffuse into the concrete which is considered to be in a saturated condition (Santhanam & Otieno, 2016; Alexander, Bentur & Mindess, 2017).

In case of the tidal zone, as there are wetting and drying cycles, the transport is a combination of diffusion, capillary suction (sorption) and permeation. However, the duration of drying increases with the height from the low tide level for each cycle of tides and so the portion towards the high tide is expected to have an increased contribution from sorption. The region just above this “upper tidal” region is exposed to wave splashes and the resulting spray, and hence will also have increased sorption due to relatively dry (and hence partially saturated) conditions (BS 6349-1, 2013). Tidal and splash zones are also subjected to wave impacts and other abrasive actions of seawater, as explained in the next section.

The atmospheric zone, on the other hand, remains in unsaturated conditions for most of the time, the exception being the occasional or seasonal rains. The unsaturated state of the concrete in this region allows high rates of gaseous and water vapour diffusion. The salt is deposited on the surface by the wind in the form of aerosol, which is absorbed into the dry surface. The chloride buildup rate is inversely proportional to the distance from the sea and depends on climatic and geographical factors. The sorption of rainwater can increase the moisture content temporarily accelerating the diffusion of chlorides deeper

into the concrete. On the other hand, heavy rains can also have an effect of washing away some of the surface salts, slowing down the diffusion process at the surface (Santhanam & Otieno, 2016).

2.3.3 Degradation mechanisms – An overview

Aggressive species penetrate the concrete by various transport processes depending on the marine exposure zone. These species disrupt the concrete's chemical and physical integrity often through a combination of chemical and physical mechanisms as discussed below.

2.3.3.1 Chemical degradation

The chemical degradation mechanisms relevant to marine conditions are sulphate attack, alkali-aggregate reaction (AAR), chloride-induced corrosion, and carbonation-induced corrosion. However, sulphate attack from seawater is mitigated by the presence of chlorides as they compete for aluminates and tend to reduce the expansion of ettringite (Santhanam, Cohen & Olek, 2006). Long-term evidence from Scandinavian field exposed specimens suggests that sulphates in seawater merely cause sulphur enrichment and minor scaling of the surface (Jakobsen, De Weerdt & Geiker, 2016). AAR is a separate consideration when reactive aggregates are used. Hence, the following discussion is restricted to the dominant mechanisms of degradation.

1. Chloride-induced corrosion

Chlorides are the most abundant ionic species found in seawater. Chlorides penetrate concrete through a combination of transport processes depending on the micro and macro environment of concrete. Chlorides are known to react with cement paste to form complex compounds such as Friedel's salt and Kuzel's salt; however, these products are neither expansive nor chemically aggressive to concrete (Glasser, Marchand & Samson, 2008). These reactions are part of the phenomenon of chloride binding.

Chloride binding is defined as the phenomenon in which a part of the chloride ions in the concrete pore solution is captured by solid concrete constituents and rendered immobile. The immobilised chloride ions are known as *bound chloride ions*. The binding phenomenon reduces the concentration of chloride ions available in the pore solution capable of diffusing further into concrete (known as the *free chloride ions*) and effectively reduces the rate of chloride transport. More detailed discussion is presented in Appendix A.

Chlorides affect concrete structures indirectly by attacking the passivity of their steel reinforcement. Chlorides, in sufficient quantity—known as *"critical chloride threshold content"*—can disrupt the passive oxide layer of γ-Fe_2O_3 that protects the steel from corrosion, initiating the active corrosion process. Chlorides take part in the corrosion process as a catalyst, leading to rapid, localised pitting corrosion, also known as macro-cell corrosion (Neville, 1995). This type of deterioration in marine RC structures is so widespread and severe that it has been the subject of extensive research for at least five decades now.

2. Carbonation-induced corrosion

Carbonation involves the consumption of calcium hydroxide and other calcium-bearing phases of concrete by atmospheric or dissolved carbon dioxide in the presence of moisture to form calcium carbonate. This process leads to a reduction in the alkalinity of concrete, which is essential for the protection of steel from corrosion. Hence, the carbonation of concrete leads to steel corrosion.

Carbonation depends on two processes – diffusion of carbon dioxide into concrete and its reaction with lime in the presence of water. Diffusion of carbon dioxide is heavily impeded in the presence of moisture, as much as 10,000 times slower compared to dry conditions. On the other hand, the formation of carbonic acid to react with lime requires the presence of water (Neville, 1995).

In marine environments, carbonation mostly occurs in the atmospheric zone where optimum moisture levels (~60-80%) may exist. For instance, carbonation depths of less than 10 mm were recorded on the exterior faces of 25-75 years old concrete structures at the coast in the South African cape peninsula, where the conditions are moist or too humid for carbonation to progress (Mackechnie, 1996). Carbonation adversely affects the ability of concrete to bind chlorides, which reduces the chloride resistance of concrete and accentuates the threat of chloride-induced corrosion.

Other zones can also get affected by carbonation due to carbon dioxide dissolved in seawater, resulting in the formation of aragonite (calcium carbonate mineral) on the surface. Aragonite layer can have the beneficial effect of reducing the penetrability of concrete surface (Mehta, 1991).

2.3.3.2 Physical degradation

Several physical mechanisms also exist that disrupt concrete in marine environments, such as salt weathering, freeze-thaw, and abrasion. Seawater, from the submerged and tidal zones or the other side exposed to ground water, gets transported to the higher, drier zones through capillary suction, also known as wicking (see Figure 2.1). This seawater takes its dissolved salts along with it. Due to evaporation, the dissolved salt gets gradually deposited on the surface or beneath the surface depending on the rate of evaporation and capillary suction. The crystallization pressure of depositing salts in the evaporative zone, mainly sulphates, is believed to induce cracking in the concrete in addition to the chemical effects of these salts, exacerbating concrete degradation (Haynes & Bassuoni, 2011). However, contrary views also exist. (Liu, Deng & De Schutter, 2014) argue that concrete primarily deteriorates due to chemical attack from sulphates and wicking should be considered only as a transport process.

In cold climates, repeated freezing and thawing of pore water in concrete can also fatigue the concrete, inducing cracking. Floating ice, wave impact, and suspended organic and inorganic substances damage the concrete surface by physical abrasion, in general. This abrasion tends to remove the beneficial aragonite and brucite layers on the surface that protect against seawater penetration (Mehta, 1991;

Santhanam & Otieno, 2016). In addition, sea waves generated by wind carry immense energy, which is released onto the structure in the form of impact, surface friction and cavitation. The situation is aggravated by the presence of various sediments that the seawater carries with it, contributing further to its abrasiveness. The randomness of wave action makes it even more difficult to model and make predictions about.

2.3.4 Exposure zones – current classifications

Marine exposure is characterised by a combination of physical, chemical and biological action, and the severity as well as the nature of which depend on the local environment (Otieno & Thomas, 2016). The primary reason is the differences in the temperature and relative humidity (RH) conditions in different climatic regions.

High temperature tends to accelerate the transport and the chemical reactions. Humidity on the one hand is a necessary participant of degradation mechanisms and on the other hand, its lack may accelerate the transport of aggressive species by creating dry fronts for sorption to happen, worsen the physical deterioration of concrete through salt crystallization and make the concrete accessible to oxygen necessary for steel corrosion. Concretes in the cold marine environments, on the contrary, face damage by freeze-thaw, which is absent in the temperate and tropical environments. It is also important to mention that along with the consideration of the local climatic conditions, it is also essential to take into account the micro-environmental factors such as daily and seasonal exposure to sunlight, wind, etc. in design (Alexander, Bentur & Mindess, 2017). Notwithstanding that, most standards in the world characterise marine exposure conditions only based on the location from sea, see Table 2.1 (Alexander & Nganga, 2016). Most standards categorise the marine exposure zones into atmospheric, submerged, and tidal/splash/spray zones in the order of increasing severity (IS 456, 2000; AS 3600, 2009; BS EN 206, 2013).

The Indian standard (IS 456, 2000) even separates the spray zone and the tidal zone as “very severe” and “extreme”, respectively. The Australian standard differentiates between the coastal structures in the atmospheric zone lying up to 1 km from the coastline and those at 1-50 km from it. On the other hand, the ACI (North American) standard (ACI 318, 2014) provides no demarcation between these categories and puts all the marine exposure zones in a “severe” category. South African standards, however, lack marine exposure classification and thus guidance is drawn from EN 206 and some modifications have been suggested by (Alexander & Beushausen, 2009) to include the highly abrasive conditions of the South African coasts.

It is only reasonable to expect that national standards cater to the specific marine climatic zone the country comes under, directly or indirectly. It is imperative that data specific to South African conditions be considered for developing the local specifications.

Table 2.1 Exposure classifications in different standards (adapted from (Alexander & Nganga, 2016))

Standard	Marine exposure classification	Description
ACI 318, 2014 (American Standard)	C0: Negligible	Concrete dry and protected from moisture
	C1: Moderate	Concrete exposed to moisture, no external source of chlorides
	C2: Severe	Concrete exposed to moisture, and an external source of chlorides
AS 3600, 2009 (Australian Standard)	B-1: Near coastal	1-50 km from coastline
	B-2: Coastal	Up to 1 km from coastline excluding tidal and splash zones
	B-2: Seawater	Permanently submerged
	C: Seawater	Tidal and splash zones
EN 206, 2013 (European Standard)	XS-1: Exposed to airborne salt but not in direct contact with seawater	Surfaces near or on the coast
	XS-2: Permanently submerged	Parts of marine structures
	XS-3: Tidal, splash and spray zone	Parts of marine structures
IS 456, 2000 (Indian Standard)	III: Severe	Concrete completely immersed in seawater / Concrete exposed to the coastal environment
	IV: Very severe	Concrete exposed to seawater spray
	V: Extreme	Surface of members in tidal zone

2.3.5 South African coastline – climatic conditions

South Africa has a coastline of roughly 3000 km (South African Government, 2018). Climatic conditions vary widely between the west and east coasts. While the west coast experiences cold arid to temperate conditions moving towards the southern tip with water temperatures of 9 to 15°C; the east coast has a warmer, subtropical climate with a temperature of 18 to 27°C (Mackie, 2016). The average tidal range is 1.2 m (Mackechnie, 1996). Some South African coasts also have to bear strong winds, especially the south-eastern summer winds.

2.4 Chloride-induced corrosion: the main deterioration mechanism

2.4.1 Corrosion initiation

Corrosion of reinforcing steel in concrete is categorised as microcell and macrocell corrosion based on the extent of separation of anodes and cathodes over the surface of steel, as shown in Figure 2.3. The rate of corrosion in both cases depends on the rate of anodic and cathodic reactions and concrete conductivity (or resistivity).

Microcell corrosion occurs when the passive layer of steel is destroyed over a large area and the surrounding concrete has high resistivity so that the formation of minute corrosion cells is favoured, resulting in a generalised corrosion of the steel surface. This is common in the case of carbonation-

induced corrosion, where a reduction in the pore solution pH due to carbonation leads to a generalised depassivation of steel. In addition, the formation of calcium carbonate increases the resistivity of concrete favouring the passage of low corrosion currents over small extents, forming several microcells in close proximity. On the other hand, macrocell corrosion occurs where steel gets depassivated locally acting as an anode and the rest of the portion acts as the cathode, resulting in localized pitting. This is common in the case of chloride-induced corrosion.

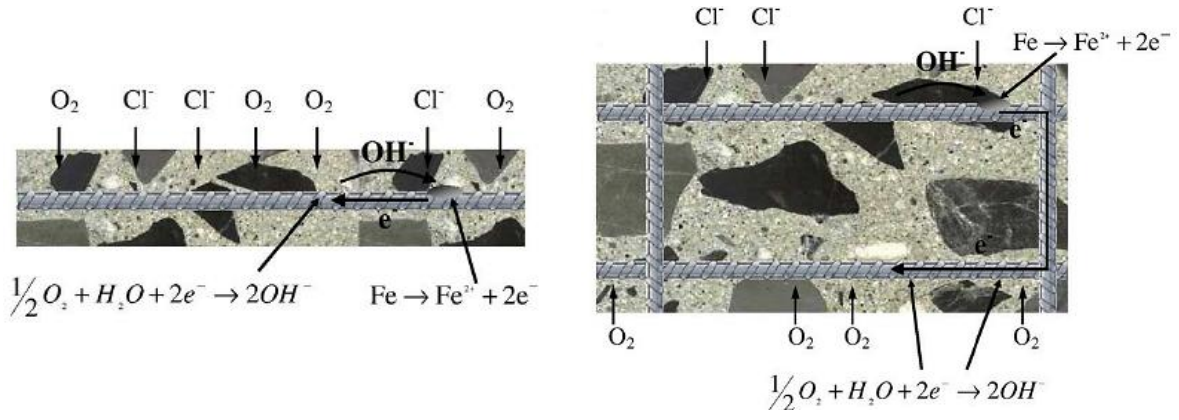

(a) (b)

Figure 2.3 Illustration of (a) microcell corrosion – the anodic and cathodic half-cells are closely spaced and (b) macrocell corrosion – a localized anodic half-cell with an extensive cathodic half-cell (reproduced from (Poursaee & Hansson, 2009))

Chlorides in sufficient concentration (known as *chloride threshold*) are required to disrupt the passive layer and initiate the corrosion process. Once the chloride threshold is reached and the corrosion is initiated, its propagation largely depends on the factors that affect the cathodic reaction, such as the availability of oxygen and moisture, and concrete resistivity. This is because chlorides act only as catalysts and do not get consumed in the process. The products of corrosion—various oxides of iron—generate expansive forces due to a net increase in the volume of products compared to the reacting iron. This leads to cracking in cover concrete thereby further accelerating the deterioration process.

Figure 2.4 shows the general corrosion-induced deterioration model used for characterising the life cycle of a structure. As corrosion propagation is a complex process, corrosion initiation is generally taken as the limit state marking the end of design service life for convenience. Moreover, corrosion propagates rapidly and hence propagation period is relatively short. Thus, the time to corrosion initiation, which is generally taken as the time to attainment of chloride threshold value at the surface of the steel, becomes of prime importance for service life prediction in such models.

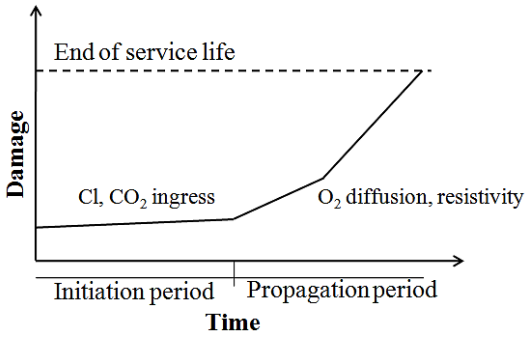

Figure 2.4 Corrosion-induced damage model that is generally used for service life prediction (reproduced from (Violetta, 2002))

2.4.2 Chloride threshold

The chloride threshold value is defined as the concentration of chlorides required at the level of steel to cause its depassivation and initiate active corrosion (Figure 2.5). The chloride threshold is used to define the corrosion-initiation-based limit state for the service life of a structure and thus could easily be deemed as the most crucial parameter for service life estimation.

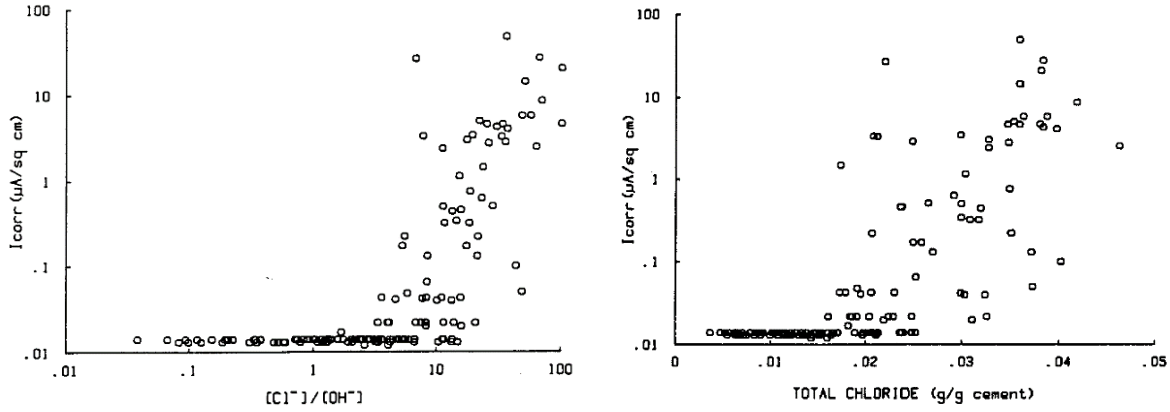

Figure 2.5. Corrosion rates of steel in the presence of chloride ions (reproduced from (Lambert, Page & Vassie, 1991))

Chloride threshold (C_{th}) values depend on various factors connected to the materials and the exposure conditions involved, broadly categorised as (Angst et al., 2009):

1. Steel: type (composition), surface
2. Concrete mix: binder, w/b ratio, degree of hydration, pH
3. Steel-concrete interface
4. Exposure conditions: internal moisture content, access to oxygen, chloride source, temperature

Chloride ions lower the corrosion potential, and the hydroxyl ions provide the inhibitive or buffer capacity against it (Glass & Buenfeld, 1997). Angst et al. (2009) conducted a quantitative analysis of the broad literature on the topic and some of the findings relevant to this study are noted here.

Binder type influences C_{th} by influencing the pH, capacity for binding, and resistivity. High Portland cement contents provide high pH buffer capacity. The effect of fly ash and slag is not clear due to contradictory findings in the literature. An increase in the w/b ratio lowers the C_{th}.

The relative humidity of 90-95% is ideal for corrosion initiation. Too high or too low humidity levels require higher chloride concentration for initiation. In practical terms, this means that submerged and air-borne zones require higher chloride concentrations for initiating corrosion than splash/spray zones. The spread in the C_{th} was however found to be so wide across literature [0.04 to 8.34 % (total chlorides by weight of cement)] that selecting a reliable value for the purpose of service life prediction is not possible. In the same vein, attempts to differentiate between different mix compositions may also be futile at this stage.

Commonly, a conservative value of 0.4% of total chloride content by mass of binder is used for calculating the time to corrosion initiation. Given the statistical uncertainty, the practice of using a common, but conservative value could be acceptable until better ways are available. However, it must always be remembered that the calculated time to corrosion initiation can only be considered notional and comparison between different exposure zones in relation to corrosion initiation solely on the basis of threshold value attainment must be viewed with caution.

2.5 Conclusions (Part A)

1. Marine environments are characteristically harsh and lead to the deterioration of reinforced concrete. Deterioration mechanisms differ based on micro- and macro-climatic conditions and material properties; however, chloride-induced corrosion remains the common and dominant mode of deterioration governing the service life of concrete.
2. Regional climatic conditions influence the nature and aggressiveness of the marine environment and should be integrated with the qualitative aggressiveness classification of marine exposure zones. There is a need to move towards quantitative characterisation of the environment for service life prediction.
3. The transport of chloride ions occurs through various transport processes; however, diffusion is the dominant mechanism by which transport occurs in the interior of concrete across exposure zones. The chloride ion ingress in concrete is, as a result, commonly evaluated and modelled after ionic diffusion.
4. Given the wide dispersion of chloride threshold values across literature, numerous influencing factors, and the mismatch between the actual and test methods, it appears pragmatic to adopt a conservative value of 0.4% (by wt. of binder) regardless of mix proportion or exposure conditions, until more reliable data become available.

Part B: Selected factors affecting chloride penetration resistance of concrete

2.6 Introduction

Many factors affect concrete's resistance to chloride penetration. Some of the important factors are discussed in this part. These factors are mainly categorised as related to concrete mix proportioning, curing, and exposure conditions.

2.7 Aggregate

2.7.1 Aggregate type

Different aggregate types are used in concrete depending on geographical location and availability. In the context of concrete, aggregates are commonly classified in terms of the petrological type in standards, i.e., the mineralogical composition (Alexander & Mindess, 2005). It is important to understand the properties of different aggregate types for their effect on the transport resistance of concrete. This concern can be differentiated into two parts: the penetrability of the aggregates themselves and the effect of aggregate type on the penetrability of the surrounding paste.

The permeability of aggregates, inferred from the permeability of the parent rock, may not be zero as is generally assumed and may have the potential to significantly affect the permeability of concrete, aggregates being concrete's major constituent (Hobbs, 1999). If such is the case, it would be a mistake to consider aggregates as perfect diluents. Price et al. (2003), using water absorption values of aggregates as an indication of their penetrability, found chloride diffusivities of various concretes increasing with aggregate absorption. A limit on the aggregate absorption of 1% for severe marine conditions is therefore recommended by the authors. The aggregates commonly used in South Africa have water absorption values under 0.5% (Alexander & Mindess, 2005). Greywacke, quartzite, and tillite, some of the common aggregate types in South Africa, were found to have no effect on the penetrability indexes of concrete as well as chloride ingress (Githachuri, 2010; Githachuri, Alexander & Moyo, 2012).

The influence of aggregate type on the surrounding paste, particularly the ITZ, has been studied and discussed to a limited extent mostly in relation to calcareous aggregates. Calcareous aggregates such as limestone can undergo a non-deleterious reaction with the cement paste to form calcium carbo-aluminate or other compounds, which may change the composition and potentially the properties of ITZ (Ollivier, Maso & Bourdette, 1995). However, Scrivener (1999) found minimal influence of aggregate type on the microstructure of ITZ between siliceous and limestone aggregates. Surface roughness, on the other hand, was found to have a more significant influence on the ITZ porosity with rougher aggregates densifying the ITZ (Scrivener, 1999). Consequent improvements in the mechanical properties of concrete were also noted. Similarly, improvements in bulk resistivity were reported by replacing smooth-textured gravel with rough-textured crushed limestone aggregates (Sengul, 2014).

2.7.2 Aggregate content

The aggregate content is usually determined by considerations regarding workability and mechanical properties. However, minimum cement content and maximum w/b ratio are also commonly specified in marine conditions with an aim to control the resistance of concrete to chloride penetration. The intention of these specifications may have been to control the quality of the cement paste in concrete when workability could only be achieved by adding water and ensuring minimum cement content was essential to control the w/b ratio, to ensure an adequate bond between concrete and steel, and to provide resistance against corrosion initiation by chlorides or carbonation (Wassermann, Katz & Bentur, 2009). The inevitable consequence of this is a limit on the minimum paste content, which in turn puts a limit on the maximum aggregate content. The experimental evidence is examined in the following paragraphs to evaluate the value of this type of specification.

Increasing the aggregate content is expected to reduce the overall proportion of cement paste—the phase mainly responsible for the transport of aggressive species. However, it might be argued that it would also lead to a higher proportion of ITZ due to the increased surface area of the aggregate phase in contact with the reduced amount of paste. The inter-aggregate spacing reduces with increasing aggregate content. At the same time, ITZ thickness remains about the same with increasing aggregate content (Gao et al., 2014). This could bring the ITZs, conceptualized as shells around aggregates, together to overlap beyond a certain aggregate content. The interconnection of the porous ITZ could result in the "percolation" of the pore space, in other words, creating preferential paths for transport through concrete, which would sharply increase the penetrability. In line with this, the mercury intrusion into mortar was observed to increase steeply when the sand content was increased beyond 45-49%, which is believed to represent the aggregate content beyond which percolation occurs (Winslow et al., 1994). In the case of concrete, where the aggregate content is always in the range 60-80%, which is above the given range, the ITZ phase is always expected to overlap. Such ITZ interconnections were observed through Wood's Metal penetration into concrete subjected to a restraining load of 10 MPa (Scrivener & Nemati, 1996). However, such a spike in the overall penetrability due to the "percolation" effect has not always been observed in the transport behaviour of mortars having the sand fraction between 0 and 70% (Halamickova et al., 1995; Delagrave et al., 1997; Wong et al., 2009; Sengul, 2014).

In terms of the overall relationship between aggregate content and transport coefficients, some contradicting experimental evidence exists. Halamickova et al. (1995) observed an increase in chloride migration and water permeation of mortars with increasing sand contents in the range 0-55%. On the other hand, others have found decreasing trends for diffusivity, conductivity, migration and permeability coefficients with increasing sand fraction (Delagrave et al., 1997; Yang & Su, 2002; Wong et al., 2009; Sengul, 2014). The increased resistance to penetration despite ITZ effects was attributed to the counteracting effect of tortuosity. In another study on mortars, the chloride migration coefficients increased with sand content for finer sand but decreased for coarser sand (Caré, 2003).

Fortunately for concrete practitioners, a more consistent picture emerges for the case of concrete itself. Buenfeld & Okundi (1998) found improvements in a wide variety of transport properties including resistance to chloride diffusion (shown in Figure 2.6) and conduction with an increase in the aggregate content regardless of the binder used.

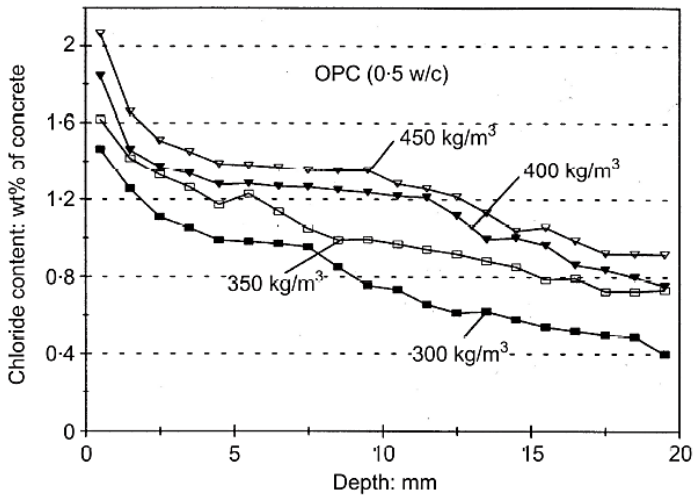

Figure 2.6 Chloride profiles for concrete with different paste contents (reproduced from (Buenfeld & Okundi, 1998))

Similarly, Wassermann et al. (2009) also found the rapid chloride permeability of various concrete mix designs decreasing with increasing aggregate content in the range of 65-78% along with many other penetrability indicators as shown in Figure 2.7. Price et al. (2003) found similar trends with chloride diffusivity although less pronounced. In all these studies, the dilution of cement paste and increase in tortuosity upon the addition of aggregates surpassed the effect of ITZ on the net transport properties of concrete. On the other hand, in another study on major cement types (EN), no major influence of cement content was observed on chloride resistance (Dhir et al., 2004).

The overall effect of increasing the aggregate content, in the practical range relevant to concrete practice, seems therefore to benefit the chloride resistance of concrete provided adequate fresh properties can be achieved. Conversely, lower cement contents for a given w/b ratio will not adversely affect the overall penetrability as assumed implicitly in some codes and may even improve it. However, the effect of cement content on the chloride threshold must also be included to understand the overall effect of cement content on the chloride-induced corrosion initiation.

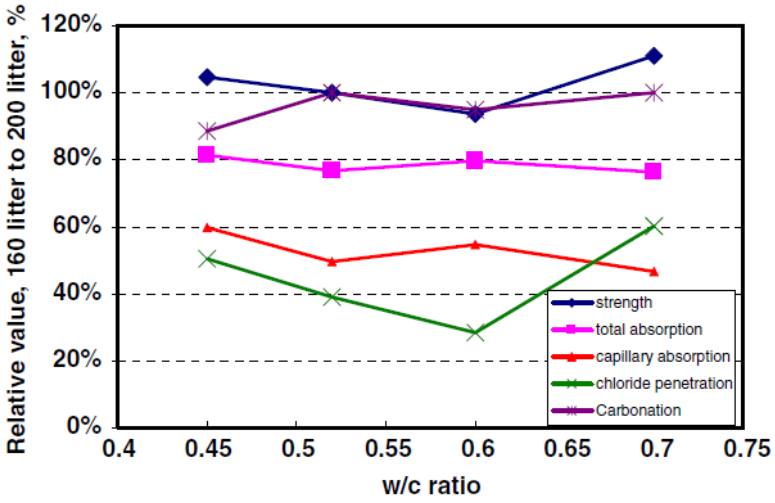

Figure 2.7. The variation of different concrete properties at different w/b ratios on decreasing the aggregate content as the water content increases (reproduced from (Wassermann, Katz & Bentur, 2009))

2.7.3 Aggregate grading

The size grading affects the water demand of aggregates and thus is of particular importance to the workability of concrete. Over the course of construction, there can be slight changes in the grading of natural aggregates. The selection of aggregate considering its grading and the inherent variability are factors that may also influence the chloride resistance of concrete and are discussed as follows in that context.

Smaller aggregates have larger surface area for the same aggregate volume and therefore the proportion of ITZ in concrete at a given paste content would increase with finer size grading. This argument holds true theoretically if the ITZ thickness does not change with aggregate size. It has been argued that the packing of the cement particles at the interface and therefore the ITZ thickness should remain unaffected as long as the aggregate size is an order of magnitude greater than the cement particles, which is largely the case in practice, leaving aside the aggregate fines (Scrivener, 1999). As there is no additional dilution in this case, the other two factors would add to increase the penetrability of the concrete as aggregate fineness increases.

In a study on mortars, this seemed to be the case as the resistance to chloride migration decreased when finer sand was adopted (Caré, 2003). Contrary to this, air permeability decreased while the resistance to carbonation and air diffusion were unaffected by increasing the aggregate fineness (Basheer, Basheer & Long, 2005; Wong et al., 2009). Sengul found coarse aggregates to result in higher bulk resistivity than fine aggregate at a given aggregate content (Sengul, 2014). In another study, no effect of changing the sand fineness in the practical range (FM: 1.6-3.3) was observed on chloride permeability or mechanical properties (Rangaraju, Olek & Diamond, 2010). Chloride conductivity, oxygen

permeability, and sorptivity testing on greywacke aggregate concretes also showed minimal effect of changes within the practical range of aggregate (Loseby, Alexander & Beushausen, 2016).

It is clear that disparate trends and arguments exist in the literature on this matter and direct investigations on chloride diffusivities are not easy to find. However, the weight of the evidence on diffusion-related and chloride conduction-related results tilts towards the relative insensitivity of chloride resistance of concrete to aggregate grading.

2.8 Binder

2.8.1 Portland cement

Portland cement has changed over time in response to various economic, sustainability, and durability concerns by, for example, switching to a more efficient dry kiln process from a wet kiln process and selecting low alkali raw materials, among other things. The C_3S/C_2S ratio increased significantly from 1930s to 1980s (Table 2.2) without changes to the alumina-bearing phases (Nixon, 1975). There was a consequent increase in the strength grade of cement. Since then, there seems to be little change in the cement composition in the UK region based on the data shown in Table 2.2. However, the corresponding changes seem to have occurred in South Africa after the 1990s (see Table 2.2). However, this cannot be confirmed due to the lack of more rigorous evidence.

Higher grade PC has shown long-term (4-5 years) improvements in the permeability properties and the chloride diffusion coefficient over lower grade PC at the same w/c ratio (Ben-Bassat, Nixon & Hardcastlet, 1990; Frey, Balogh & Balfizs, 1994). At the same concrete strength, however, some increase in the concrete permeability under wet marine conditions is to be expected due to the higher w/b ratio involved. The differences were found to be relatively small in one study (Ben-Bassat, Nixon & Hardcastlet, 1990). C_3A content is another compositional factor that influences the chloride diffusion coefficient. Higher C_3A contents are preferable for chloride resistance (Frey, Balogh & Balfizs, 1994).

The properties of PC, such as rate of hydration, and alkali content, can influence the properties of SCM-blended binders. The effect is likely to manifest mainly in the early ages, which can change the short-term values for diffusion coefficient and durability indicators. In contrast, the long-term chloride-related properties are likely to be dictated by the SCM. The influence of the binder content is discussed in detail in Section 2.7.2.

Table 2.2 Phase composition (%) of Portland cement over time

Region	Decade	C_3S	C_2S	C_3A	C_4AF	Reference
UK	1930s	39	32	10	7	(Nixon, 1975)
	1980s	53	18	10	7	(Nixon, 1975)
	2000s (CEM I-42.5N)	53	21	8.5	8.5	(Dhir et al., 2004)
	2000s (CEM I-52.5N)	54	19	7.3	8	(Dhir et al., 2004)
South Africa	1990s	35-55	20-40	5-12	5-10	(Fulton's, 1994)
	2000s	45-65	10-35	4-10	5-10	(Fulton's, 2001)
	2020s	55-65	10-18	6-9	9-12	(Fulton's, 2021)
	1970s	48.5	26.4	8.8	8.5	(Wolhuter & Morris, 1973)
	1990s	66.9	11.2	4.5	10	(Mackechnie, 1996)

The increase in cement strength grade makes it possible to make concretes of a given strength grade (28 days) and workability at a higher w/c ratio (and reduce the cement content). Higher PC grades are also obtained through finer grinding of the same clinker (Nilsson, Sandberg & Sørensen, 1996).

2.8.2 Supplementary cementitious materials (SCM)

Partial replacement of Portland cement (clinker) with supplementary cementitious materials is one of the most effective means of improving the chloride resistance of concrete. Various natural and artificial SCMs are available with varying pozzolanic and hydraulic reactivity. Fly ash (FA), ground granulated blastfurnace slag (BS), and silica fume (SF) are the most utilized SCMs in marine environments. These SCMs differ widely in their composition, physical characteristics, and their effect on the fresh and hardened properties of concrete (Thomas, 2013; Ramezanianpour, 2014). FA and BS react slowly and require longer to develop a given concrete strength than PC. Silica fume on the other hand is highly reactive due to very fine particle sizes and surpasses the strength of PC concrete within a few days. The implication for practice is that FA and BS concretes are required to be designed with a lower w/b ratio than PC for a given strength grade.

In a marine exposure study, FA and BS concretes of the same grade as PC were found to exhibit similar diffusivity as PC concretes under 1 month. However, diffusivities of FA and BS reduced by orders of magnitude with time compared to PC concretes (Thomas & Bamforth, 1999). Similar improvements have also been observed in FA and BS concrete at the same w/b ratio as PC concretes (Bamforth, 1999). Field exposure studies in the tidal zone for 10-25 years have shown that the resistance of concrete to chloride diffusion improves as the levels of BS (25-65%) and FA (>50%) increase (Thomas &

Matthews, 2004; Thomas et al., 2008). However, the diffusivities of FA and BS concretes develop slowly and thus chlorides can penetrate more easily in the first 10 mm of the cover concrete. Therefore, a minimum cover depth is recommended even in the case of SCMs (Thomas & Bamforth, 1999). Scaling due to freeze-thaw or abrasion due to wave action will also influence the decision on minimum cover depth and the concrete composition. Slag concretes and high w/b ratio concretes are more susceptible to scaling or abrasive action (Mackechnie, 1996; Thomas et al., 2008).

The resistance to chloride ingress of SCM concretes is achieved through the refinement of pore structure and superior chloride binding ability. SCMs lead to a refinement of pore sizes, although to varying extent, which reduces the permeability of the pore space (Lothenbach, Scrivener & Hooton, 2011). Silica fume in particular reduces the penetrability of the physical pore structure, which reflects in a highly reduced diffusivity from the early ages. However, due to small further improvements and poor chloride binding ability, the long-term chloride diffusivity of silica fume concretes does not reach the level of FA and BS concretes. Both FA and BS are known to reduce pore sizes, given adequate curing conditions are provided, while the total porosity may remain unaffected or even increase (Thomas, 1989; Matthes et al., 2018). In addition, FA and BS contribute significantly towards chloride binding. Chloride binding in SCM blends is further discussed in Appendix A.

2.9 w/b ratio

The w/b ratio, normally calculated by mass, determines the average interparticle spacing between the binder particles (Bentz & Aitcin, 2008; Aïtcin, 2016). Beyond the maximum volume that the hydration products can fill, the rest of the space remains as capillary porosity. Both the strength and durability of concrete depend on its porosity and thus depend on w/b ratio. The w/b ratio is not a straightforward parameter as the nature of porosity depends on the volume of binder added at a given mass.

Nevertheless, the w/b ratio is such an important parameter for concrete durability with regard to chloride-induced corrosion that a limit on the maximum value is commonly prescribed by national and international codes. Minimum compressive strength for concrete is also prescribed in such cases as it is considered an indicator of the w/b ratio, which itself is difficult to verify on-site (Nixon, 1975). Given the diversity of SCMs used in modern concrete, each of which has a specific w/b – strength relationship, compressive strength is no longer a sufficient indicator of the w/b ratio.

The relationship of the diffusion coefficient in chloride environments with the w/b ratio was investigated through a review of a large number of studies on PC concretes (Figure 2.8) by Bamforth, Price & Emerson (1997). It is clear that the diffusion coefficient increases with w/b ratio. However, particular relationships differ widely, presumably, due to differences in other mix parameters, testing protocols, exposure conditions and duration, etc. Notwithstanding this, service life prediction models such as Life-365 make use of w/b-D relationships for normal Portland cement concrete. The w/b ratio

is also important in other modes of deterioration in the marine environments such as wave action and freeze-thaw scaling.

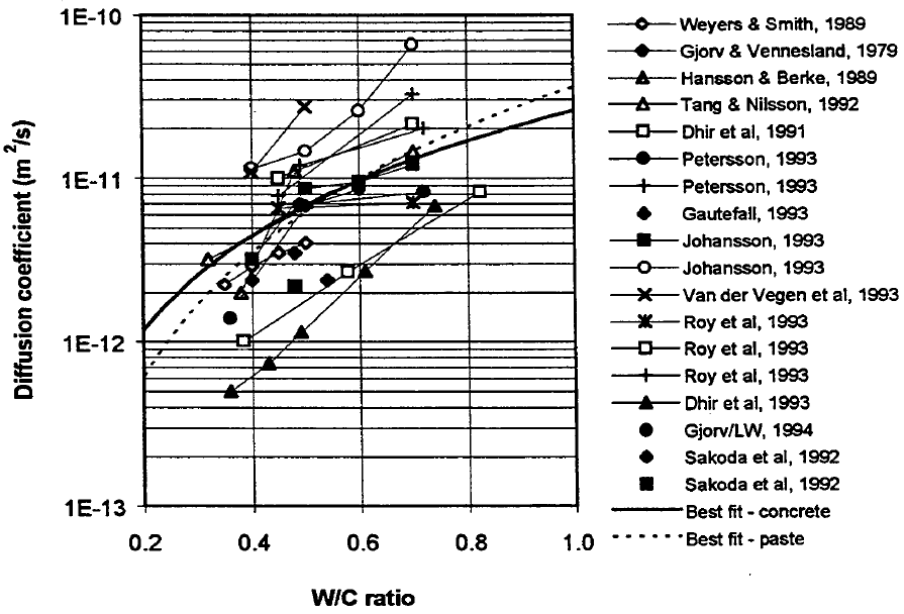

Figure 2.8 Diffusion coefficient as a function of w/c for Portland cement concretes (reproduced from (Bamforth, Price & Emerson, 1997))

2.10 Curing

Several studies have emphasized the importance of the method and duration of initial curing on the penetrability of concrete (Senbetta & Scholer, 1984; Patel et al., 1985; Ballim, 1993; Wasserman & Bentur, 2013; Beushausen, Höhlig & Martin, 2016). The use of SCMs, higher replacement levels, and higher w/b ratios generally make the concrete more sensitive to curing (Thomas, 1989; Zhang et al., 1999). However, the subject of testing curing effectiveness is complex due to the inherent differences between lab and field conditions, which must be considered while consolidating the literature.

For instance, the relationship of temperature with time and depth can be very different between small lab specimens and large field structures during hydration (Thomas, 2013). Also, the temperature and humidity conditions in the lab may be very different from the prevailing field conditions. Furthermore, the age of testing selected for studies in lab and even field conditions is frequently 28 days, which is in line with quality control requirements, but which may not depict the long-term effect of initial curing.

Some studies have considered the issue of long-term environmental conditions, which are discussed as follows. In hot and arid conditions, it was found that the initial curing can make a lasting impact on strength, porosity, and absorptivity even after a year (Alsayed & Amjad, 1994). In contrast, exposure to intermittent rain or sea mist reduced the effects of curing on concrete penetrability considerably in a few months to a year's time (Ewertson & Petersson, 1993; du Preez & Alexander, 2004). Similarly, the

effect of a wet curing duration of up to 28 days on chloride profiles of concretes exposed to the Persian Gulf tidal zone was not consistently visible and the differences diminished with exposure age (Khanzadeh-Moradllo et al., 2015). Marine environments are characterised by high humidity, which, as observed in the aforementioned studies, will likely equalise the effect of different initial curing methods on concrete in the long term. However, chloride penetration in the early period may still be affected by poor curing, leading to increased chloride penetration.

2.11 Exposure conditions

2.11.1 Chloride concentration

The chloride concentration or salinity is an important parameter that determines the severity of chloride penetration and is therefore an important boundary condition. The intrinsic diffusivity of Cl in the pore solution of concrete decreases with an increase in chloride ion concentration of the exposure solution (Bockris & Reddy, 2002; Zhang & Gjorv, 2005). The effect on chloride depth into concrete will however depend on the following competing factors: the reduction of intrinsic diffusivity of Cl ions in pore solution, the increase in the rate of diffusion due to the increase in chloride concentration, and the effect of non-linear chloride binding.

Jee & Pradhan (2019) found higher free chloride depths with higher chloride concentrations of exposure solution in a lab study. Similarly in another study, higher concentration showed higher chloride ingress in lab exposure however only a minor effect of concentration was observed in the field conditions (Lindvall, 2007). This contradiction could not be explained. Results contradicting the theoretical expectation of reduced diffusion coefficient at higher concentrations have also been presented as shown in Figure 2.9.

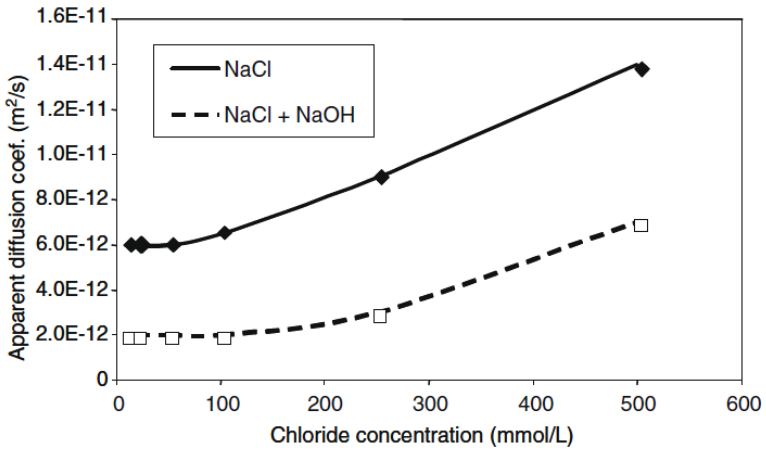

Figure 2.9 Variation of apparent diffusion coefficient of cement paste with chloride concentration (reproduced from (Marchand & Samson, 2009))

An important implication of concentration lies in the use of lab-based bulk diffusion tests (NT BUILD 443, 1995; ASTM C1556, 2016)—which involves concentrated chloride solution (2.8 M; the average seawater concentration is around 0.5 M)—in the quantification of the diffusion parameters for service life predictions such as Life 365 (Life-365 v2.2.3, 2020). The effect of this large difference in the exposure conditions on diffusion parameters is not always recognised. Even migration parameters are also subject to similar effects. In addition, the concentration of seawater changes periodically due to, among other things, temperature variations. Clearly, the effect of concentration must be understood quantitatively to enable realistic service life predictions, especially when using accelerated tests, which as of now has not been adequately addressed.

2.11.2 Temperature

Diffusion, being the result of the random thermal motion of particles, is greatly influenced by temperature. The rate of diffusion increases exponentially with temperature, which is usually modelled using the Arrhenius equation (Eq. (2.1)).

$$D\ (T) = D_0 e^{\frac{E_a}{R}\left(\frac{1}{T_0}-\frac{1}{T}\right)} \tag{2.1}$$

Where,

D(T) and D_0 [m^2/s] are the diffusivities at temperatures T [K] and T_0, respectively.

E_a is the activation energy of chloride diffusion in concrete [KJ/mol] and R is the ideal gas constant.

The activation energy term in the Arrhenius equation is experimentally determined. Most of the studies on the topic are concerned with measuring this parameter. The influence of temperature on chloride diffusion in concrete also extends to chloride binding.

In controlled exposure studies, the chloride penetration, measured through total or free chlorides, was observed to increase with an increase in temperature and so did the diffusivity. However, the change was less than 3 times for an increase of 30˚C in temperature (Dousti et al., 2013; Shao, Li & Liu, 2016). On the other hand, the same direction of variation was observed in diffusivity in the field, but total C_s decreased with temperature (Lindvall, 2007). Temperature also has an indirect influence on exposure severity by affecting the rate of surface drying, which in turn affects chloride accumulation near the concrete surface.

2.11.3 Exposure zone

The exposure zones in marine conditions differ principally with regard to wetness in the context of chloride-induced corrosion. The moisture content in and around the concrete largely determines the rate of chloride build-up at the surface and chloride penetration, biological growth, and the availability of oxygen for corrosion initiation and propagation. Amongst the different exposure zones, the tidal zone is often considered most aggressive when factors such as abrasion damage due to wave action, freeze-thaw damage, chloride build-up rate, etc. are all considered together. In relation to the risk of steel corrosion, the splash/spray zone is considered the most severe zone by some researchers due to sufficient availability of oxygen (Roy, Kok Chye & Northwood, 1993; Thomas & Matthews, 2004; Moore et al., 2022). Systematic field investigations are however needed to investigate this issue. The submerged zone is often neglected from the analysis stating the lack of oxygen availability. Studies have however shown that even low oxygen availability can sustain localised corrosion that can occur in the submerged zone due to the availability of large cathodic area located outside the submerged zone (Walsh & Sagüés, 2016). In addition to the moisture conditions, the exposure zone may also differ with regard to the presence of surface layers such as aragonite, brucite, and organic growth.

A limited review of field studies from around the world (Table 2.3) shows that the predominant trend for the rate of chloride penetration in different exposure zones regardless of the climatic conditions is: submerged > tidal > splash > atmospheric. However, variations in this order in individual cases are very common, especially amongst the submerged, tidal and splash zones (wet or partially wet zones). Variations were even seen between studies conducted in the same local region, example the case of South Africa. A possible reason, in part, for such variations could be that the exposure severity of splash/spray and air-borne zones is influenced by the distance from the sea level (Figure 2.10), wind speed, wind direction, sunlight exposure, etc. Similarly, the frequency of wetting decreases in the tidal zone from the low to high tide mark, which implies a variation in the exposure severity. These details are not always mentioned and additionally, definitive knowledge of their effects is still lacking. The loose use of the term spray zone also contributes to the vagueness. The influence of exposure zones on the apparent diffusion coefficient (D_a) has been observed to be minimal after a length of exposure and the exposure zones seem to act mostly as the boundary condition by affecting the surface concentration (C_s) (Nanukuttan et al., 2008; Heiyantuduwa-Beushausen, 2022). [More on exposure zone in Part A, Sections 2.3and 2.3.4]

Table 2.3 Chloride ingress in exposure zones: trends in literature [*Sub.: submerged, Tid.: tidal, Spl.: Splash, Spr: Spray, Atm: atmospheric]

Region	Climate	Exposure	Depth of chloride	Reference
China	Temperate-sub-tropical (Wheat Island Exposure Station, Yellow Sea)	Duration: 13 m	Sub.>Tid.≃Spl.>Atm.	(Zuquan et al., 2018)
India	Hot semi-arid (Thoothukudi, Indian Ocean)	Duration: 10 y	Spl. ≃Sub.>Atm. Corr. rate: Spl.>Sub.>Atm.	(Kwon et al., 2017)
Portugal	Temperate (Sado Estuary, Atlantic Ocean)	Duration: 5 y	Tid.>Spr.>Atm.	(Costa & Appleton, 1999)
Scotland	Temperate (North Sea)	Duration: 7 y	Low Tid.> High tid.> Spl.>Atm.	(Nanukuttan et al., 2008)
Singapore	Hot tropical (Singapore Strait)	Duration: 1.5 y Sub.:16 m below MSL Tidal: Mid (MTL) Atm.: 3 m above MTL	Sub.>Tid.>Atm.	(Roy, Kok Chye & Northwood, 1993)
South Africa	Temperate: Granger bay (high wind) (Cape Peninsula, Atlantic Ocean)	Duration: 2 y Tid.: Below high tide Spr.: 3 m above MSL	Tid.>Spr. (Granger bay Spr. ≃ Simonstown Tid.)	(Mackechnie, 1996)
	Temperate: Simonstown (Cape Peninsula, Atlantic Ocean)			
	Temperate: Granger bay (Cape Peninsula, Atlantic Ocean)	Duration: 3.5 y Tid.: Below high tide Spl.: 4 m from MSL Atm.: <5 km from coast	Spl.>Tid.>Sub. ≃Atm.	(Heiyantuduwa-Beushausen, 2022)
	Sub-tropical: Durban Port (Indian Ocean)			

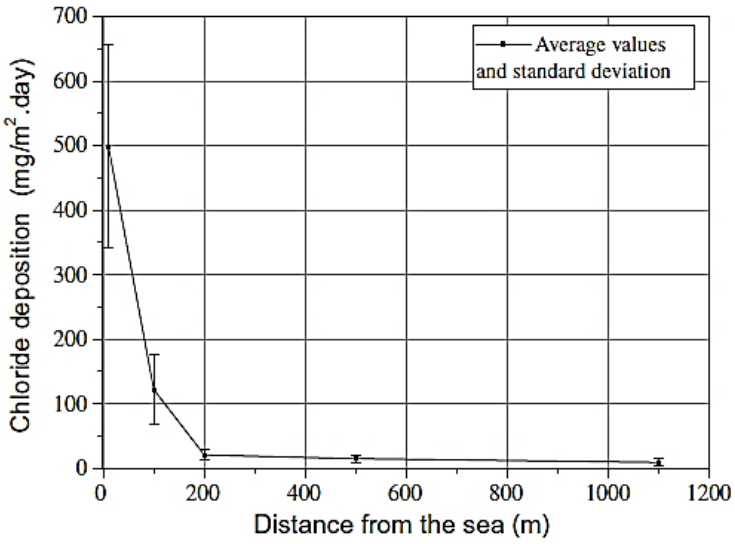

Figure 2.10 Presence of atmospheric chlorides with distance from the sea using wet candle method (reproduced from (Meira et al., 2010))

2.12 Conclusions (Part B)

1. Aggregates influence the microstructure and transport properties by way of dilution, tortuosity, and ITZ phenomena. The aggregate type and size grading may not significantly influence the chloride resistance of concrete. Maximizing the aggregate content without affecting the workability may improve the chloride resistance of concrete. However, most literature on this matter involves indirect tests like electrical migration and permeability. More research using direct chloride ingress tests is required to verify the above findings.
2. Binder type has the most significant effect on the chloride resistance of concrete. SCMs such as FA and BS refine the porosity and improve the chloride binding ability. The short-term evaluation of FA and BS blended concretes however may not always show their long-term benefits. Both short-term and long-term studies are thus needed to quantitatively understand the performance of current South African binder materials in marine conditions.
3. An increase in the w/b ratio increases the diffusion coefficient. However, individual relationships with different binder types need to be evaluated to develop concrete mix proportioning charts.
4. The long-term effect of curing depends on the environmental conditions surrounding the concrete. Under wet/moist conditions prevalent in the sea or near the coast, the effect of curing on chloride ingress appears to diminish over time. Despite this, curing can be an important consideration to prevent degradation by other mechanisms such as abrasion, freeze-thaw, etc.
5. More research is needed on parameters characterising the exposure environment to gain a clear understanding of their individual and combined effects on chloride ingress. Similarly, the severity of different exposure zones in the context of chloride ingress shows considerable

variation in the literature. There is also a dearth of long-term studies, especially longer than 10 years, to enable clarity on the variation of C_s and D_a with time in different environmental conditions.

Part C: Chloride modelling and service life prediction

2.13 Introduction

Reliable estimates of service life are essential to designing structures for durability in a sufficiently differentiated and logical way. In practical terms, the purpose of service life prediction is to enable valid comparison of different material combinations based on their long-term performance in the service environment so that appropriate choices can be made to achieve the desired service life. Service life prediction models are tools that allow the calculation of potential service life for given materials and environmental conditions (Alexander & Beushausen, 2019). Service life itself can be defined in different ways with varying levels of complexity in definition, experimental determination, and mathematical description. Usually, they fall into two categories: i) corrosion initiation and ii) stage of damage during corrosion propagation.

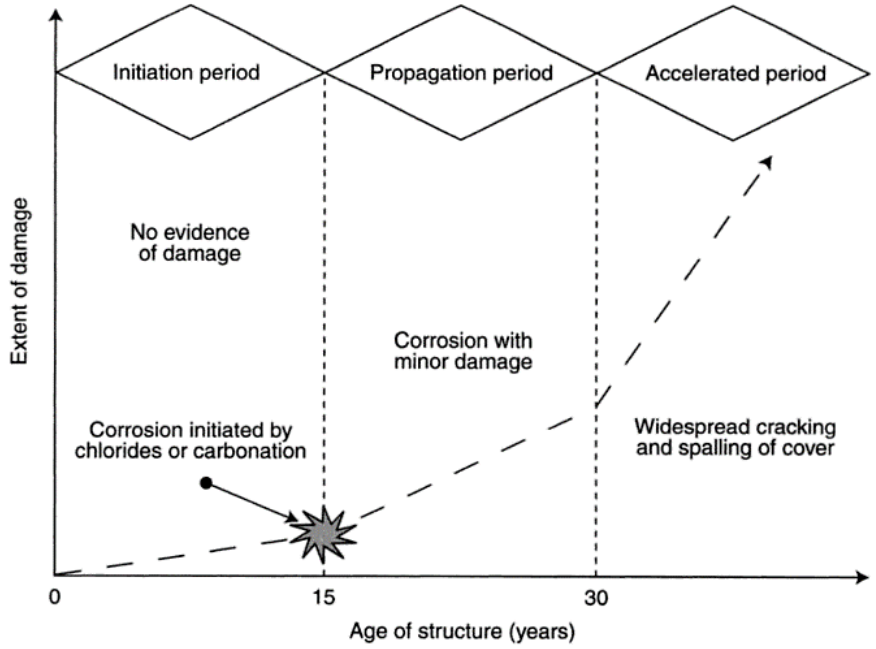

Figure 2.11 Modified Tutti's model for corrosion damage during the life of a structure (reproduced from (Heckroodt, 2002))

The discussion in this section is restricted to service life related to corrosion initiation only. As corrosion is assumed to initiate when the chloride threshold value is achieved at the level of the steel, the predictions based on corrosion initiation can be divided into two steps: chloride ingress modelling and selection of chloride threshold value. The principles of chloride ingress modelling based on Fick's 2nd law are explained in this section. The chloride threshold is discussed in Section 2.4.2. An overview of some of the influential service life prediction models is also presented outlining their principles, merits, and limitations.

2.14 Chloride Ingress Modelling

Chloride ingress occurs through a combination of different transport processes depending upon the marine exposure zone. However, diffusion is considered the dominant transport process. It is commonly assumed that the convective processes influence the development of chloride concentration in the unsaturated near-surface concrete, which then drives the diffusion of chlorides in the nearly saturated interior (Alexander, Bentur & Mindess, 2017). Thus, most of the effort in chloride transport modelling is generally focused on developing diffusion-based models. Chloride diffusion in concrete has been conventionally modelled simply by using Fick's laws. In particular, Fick's 2nd law is used to describe the natural diffusion, which occurs in non-steady state conditions.

There are two approaches to chloride modelling broadly categorised as empirical and physical modelling approaches (Nilsson, 2006). The empirical approaches use empirical observations of material performance in relevant, preferably actual field, environments to prepare a model, which can be used to make predictions for the scope of materials and environments used to develop the model. Such models may or may not require or use the knowledge of the underlying processes involved. Such models are relatively simple but require continuous updating with data to accommodate changes in material properties and extend the model to other materials and exposure conditions. On the other hand, the physical models are based on knowledge of the underlying processes and their scientific descriptions. These models define the environment and material properties in terms of their fundamental measurable constituent parts. This makes the physical models extendable, in theory, to any material and environment as long as their characteristic data are available without having to measure the performance itself. However, this requires a sufficient understanding of the intricate processes that govern the performance and a vast amount of input data.

In this section, the issues common to both physical and empirical approaches are discussed, but the emphasis is given to the empirical approach for its simplicity and relevance to this study.

2.15 Fick's 2nd Law: Error Function Solutions

2.15.1 Principle

The partial differential equation of Fick's 2nd law for unidimensional diffusion as in Eq. (2.2) is commonly solved using the error function solution (Crank, 1975), which is shown in Eq. (2.3).

$$\frac{\partial C_f}{\partial t} = \frac{\partial}{\partial x}\left(D_{NSS} \cdot \frac{\partial C_f}{\partial x}\right) \tag{2.2}$$

Where,

C_f is the free chloride content

D_{NSS} is the non-steady state diffusion coefficient

$$C_x = C_0 \left(1 - erf\left[\frac{x}{2\sqrt{(\mathrm{D}.t)}}\right]\right) \quad (2.3)$$

Where,

C_x is the concentration of the chloride ions at a depth 'x' from the surface (the exposure boundary).

C_o is the concentration of the chloride ions at the surface (x = 0).

D is the diffusion coefficient.

t is the exposure duration.

$erf(z) = \frac{2}{\sqrt{\pi}} \int_0^z e^{-y^2} dy$, 'y' is the variable of integration[2].

$erfc(z) = 1 - \mathrm{erf}\,(z)$

Where, erfc is the error function complement or complementary error function.

This type of solution to Fick's 2nd law is also referred to as error function complement or ERFC solution.

This solution enables the calculation of D from chloride profile data (C_x vs x) for a given exposure duration (t) through curve-fitting or even with one point on the profile if boundary conditions (C_0) are known. In its basic form, the solution is relatively easy to understand because of its mathematical simplicity. The calculations can also be performed quickly using basic Spreadsheet computer programs. However, the ERFC solution is valid only under the following assumptions (Crank, 1975; Tang & Gulikers, 2007; Marchand & Samson, 2009), in addition to the assumptions of pure diffusion of uncharged particles underlying Fick's laws.

1. Unidirectional diffusion into a semi-infinite medium
2. Constant boundary conditions, i.e., constant surface concentration
3. Constant diffusivity with respect to
    a. Position, i.e., the material is homogeneous, and no temperature gradient exists.
    b. Time, i.e., material properties remain constant with time.
    c. Concentration of chloride ions in the pore solution, i.e., only instantaneous linear binding occurs. In the classic case, no interaction between the diffusant and the medium is typically assumed. However, linear binding is also technically valid as the diffusion

[2]This is to distinguish the variable used to define the function being integrated from the limits of integration (z, which in this case is also a variable).

coefficient remains constant in relation to the chloride concentration at any location[3] (refer to Appendix A).

Leaving the edges and corners of concrete members aside, the assumptions of unidirectionality and semi-infinite medium can be accepted given the typically large sizes of concrete structures. The assumptions regarding constant boundary and material conditions are not fulfilled in reality as discussed in subsequent sections. Modifications have been proposed to account for these conditions. However, the available analytical solutions only allow for the violation of one assumption at a time (Crank, 1975). Therefore, while deriving model equations using the ERFC solution, the focus is generally placed on the variation of a single parameter, either diffusivity (case 1) or surface concentration (case 2), while keeping the other parameter constant. The simultaneous variation of both the parameters of diffusivity and surface concentration (case 3) is a common observation in measurements and in some cases also recognised as such in modelling. Each of these approaches has its own limitations, which will be discussed in the following sections.

2.15.2 Apparent parameters: D_a and C_s

The chloride concentration results from concrete specimens typically are arranged with respect to the depth from the surface, in the form of chloride profiles as shown in Figure 2.12. The error function solution is then fitted through regression analysis to obtain the surface chloride concentration and the diffusion coefficient. It is common practice to use acid-soluble (total) chloride concentrations for chloride profile analysis.

The diffusion coefficient and surface concentration measured in the case of chloride penetration in concrete are quite different from the classic ERFC solution and are considered 'apparent' parameters, different from their definition in the classic case. The expression for ERFC solution typically used for chloride diffusion in concrete is shown in Eq. (2.4).

$$C_x = C_s \left(1 - erf\left[\frac{x}{2\sqrt{(D_a . t_{ex})}}\right]\right) \tag{2.4}$$

Where,

C_x is the chloride content at a depth 'x' from the surface.

C_s is the chloride content extrapolated from the fitted curve to the surface (Figure 2.12).

D_a is the apparent diffusion coefficient.

t_{ex} is the exposure duration

[3] $D_{NSS} = \frac{D_{SS}}{\left(1+\frac{\partial C_b}{\partial C_f}\right)}$; linear binding implies that $\frac{\partial C_b}{\partial C_f} = constant$ and D_{NSS} will remain constant with Cl content.

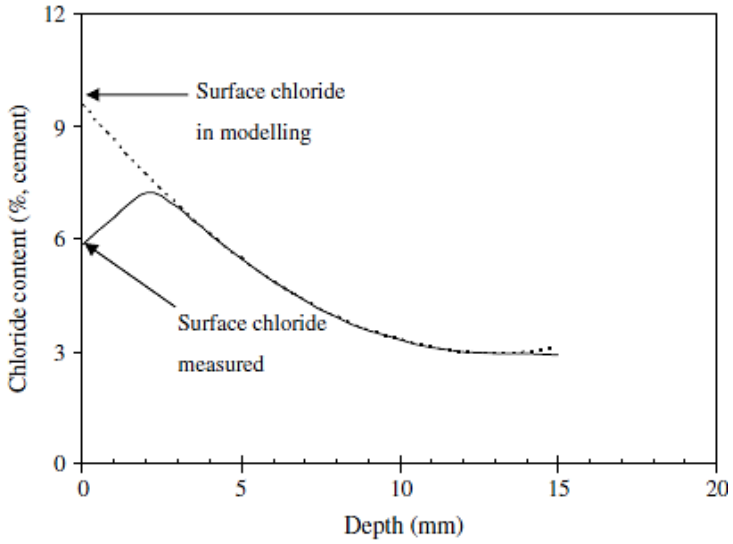

Figure 2.12 A typical measured chloride profile in which an error function solution is fitted – the first few data points are ignored in data fitting and the fitted curve is extrapolated to get a hypothetical surface content – C_s [figure reproduced from (Ann, Ahn & Ryou, 2009)]

The meaning of these apparent parameters must be understood and distinguished from the classic case to avoid misinterpretation and misuse. A variety of differences may exist between the apparent and the true parameters individually or simultaneously depending on the case. The discussions in several of the following sections will attempt to describe the following points:

1. In the classic case, D is the same as D_{SS} or D_{NSS} as there is no binding. In the case of concrete, the ERFC solution is derived from D_{NSS}, which is dependent on chloride binding and thus differs from D_{SS}. *[D_{SS} and D_{NSS} are steady state and non-steady state diffusion coefficients (Appendix A)]*.
2. Since ERFC solution requires a constant D, linear binding[4] must be assumed. Hence, the D obtained by the ERFC solution is not the actual D_{NSS}, but rather an equivalent D_{NSS} assuming linear binding.
3. The chloride concentrations are usually measured in total chloride contents rather than free chloride contents. Because chloride binding occurs non-linearly, these profiles are not equivalent to free chloride profiles. The resulting D from fitting such profiles will be different from the actual D_{NSS}.
4. The concrete's diffusivity evolves with time, which means that the chloride profile develops over the entire exposure duration while the diffusivity undergoes continuous change. Fitting the ERFC solution to a chloride profile will result in a diffusion coefficient averaged over time

[4]Linear binding is the linear approximation for the binding isotherm ($C_b = \alpha.C_f$).

until the end of the exposure. This is perhaps the most important distinction between D_a and D_{NSS}.

5. The surface concentration also increases with time. The ERFC solution in this case will assume that the surface concentration remained constant at its final level throughout the entire exposure period. In relation to this assumption, the achieved diffusion coefficient will be lower than its actual value.

The above reasons show that D_a and C_s are regression parameters, rather than pure material or exposure properties, in a typical chloride profile analysis. However, definitions and treatments differ based on physical or empirical modelling approaches, which must be carefully understood to avoid errors and are described next.

2.15.3 Time-dependence of D and C_s

The variation of diffusivity and surface chloride content with time can have large implications on the service life predictions and are therefore addressed in various ways in the literature. The time-dependencies of D and C_s are described separately in the following sections.

2.15.3.1 Modified ERFC solutions for time-dependent D (D_i and D_a) with constant C_s

The microstructure of concrete in service densifies as the hydration progresses with time under conducive environmental conditions. Consequently, the diffusion coefficient decreases with time in marine environments. Several studies have reported this phenomenon in natural diffusion tests as well as electrical tests on lab- and field-exposed specimens (Mangat & Molloy, 1994; Maage et al., 1996; Mackechnie, 1996; Stanish & Thomas, 2003; Audenaert, Yuan & De Schutter, 2010; Andrade, Castellote & D'Andrea, 2011).

The time-dependence of diffusion coefficient has been observed to follow the exponential form as shown in Eq. (2.5).

Or,
$$D(t) = D_{ref}\left(\frac{t_{ag}}{t_{ag,ref}}\right)^{-m_i} \quad (2.5)$$

Where,

D (t) is the diffusion coefficient at age 't_{ag}'.

D_{ref} is the diffusion coefficient at reference age '$t_{ag,ref}$'.

m_i is the diffusion coefficient decay coefficient

It is crucial to note that the time in this case is the age of concrete as opposed to the exposure duration used in the ERFC solution.

The diffusion coefficient D (t) referred to above is the instantaneous diffusion coefficient (denoted as D_i) from Fick's law at any particular instance. The apparent diffusion coefficient (D_a), on the other hand, represents the average diffusion coefficient in the concerned time period and is different from the instantaneous diffusion coefficient (Maage et al., 1996; Nilsson, 2006). The chloride profile measured after any length of exposure is a result of the evolving instantaneous diffusion coefficient throughout the exposure period. For a constant surface concentration, the ERFC solution fitted to the chloride profile will yield an average or apparent diffusion coefficient.

Both D_i and D_a reduce with age. As D_a is an average value of D_i in the exposure period, D_a will always be higher than D_i at the end of the exposure when the chloride profiles are obtained. With the increase in the exposure period, the difference between the two will increase as D_a will include in its average the entire range of D_i from highest to lowest. This implies that the time-dependence (simplistically, the m value) of D_i and D_a should be different as shown in Figure 2.13 (Nilsson, 2006). Different subscripts for 'm' ('i' for instantaneous and 'a' for apparent) are thus used here to indicate this distinction. These differences have not always been recognised in the literature leading to a great deal of confusion and incorrect mathematical expressions (Nilsson, 2006).

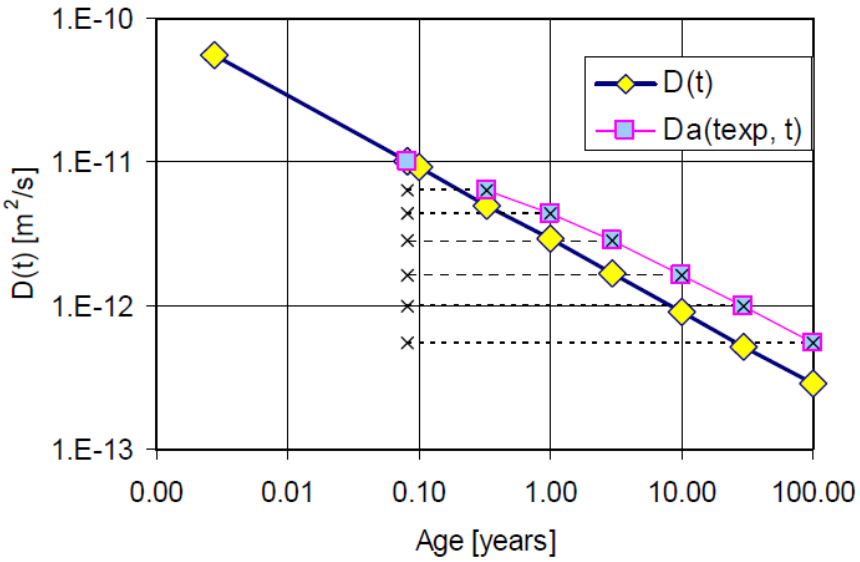

Figure 2.13. Time dependency of instantaneous (D) and apparent (D_a) diffusion coefficients [the crosses signify the exposure period] (reproduced from (Nilsson, 2006))

The mathematical treatment of the time-dependence of the two diffusion coefficients in ERFC solution is discussed henceforth. As previously discussed, the ERFC solution of Fick's 2nd law requires an assumption of a constant diffusion coefficient to yield the true diffusion coefficient. While the change of diffusion coefficient with time invalidates this assumption, it is possible to incorporate this time-dependence into the ERFC solution to have a mathematically valid solution. Such a solution is known as the modified ERFC solution.

1. From instantaneous diffusion coefficient ($D_i(t)$) to apparent diffusion coefficient (D_a)

When the time-dependence of the instantaneous diffusion coefficient is available, the following mathematical expressions can be used to derive the apparent diffusion coefficient.

Fick's 2nd law can be rewritten by substituting the non-steady state diffusion coefficient (D_i) with its time function from Eq. (2.5) as shown in Eq. (2.6) (Crank, 1975).

$$\frac{\partial \mathrm{C}}{\partial t} = D_{ref}\left(\frac{t_{ag}}{t_{ag,ref}}\right)^{-m_i}\frac{\partial^2 C}{\partial x^2} \tag{2.6}$$

Rearranging Eq. (2.6),

$$\frac{1}{D_{ref}\left(\frac{t_{ag}}{t_{ag,ref}}\right)^{-m_i}}\cdot\frac{\partial \mathrm{C}}{\partial t} = \frac{\partial^2 C}{\partial x^2} \tag{2.7}$$

Defining T such that,

$$dT = D_{ref}\left(\frac{t_{ag}}{t_{ag,ref}}\right)^{-m_i} dt \tag{2.8}$$

Fick's second law can then be rewritten as,

$$\frac{\partial \mathrm{C}}{\partial \mathrm{T}} = \frac{\partial^2 C}{\partial x^2} \tag{2.9}$$

Integrating T with respect to time from the age at the start of exposure (t_i) to the age at the end of exposure (t_f) (Stanish & Thomas, 2003; Tang & Gulikers, 2007),

$$\int_0^T dT = \int_{t_{ag,i}}^{t_{ag,f}} D_{ref}\left(\frac{t_{ag}}{t_{ag,ref}}\right)^{-m_i} dt \tag{2.10}$$

Thus,

$$\mathrm{T} = D_{ref}(t_{ag,ref})^{m_i}\left(\frac{{t_{ag,f}}^{1-m_i} - {t_{ag,i}}^{1-m_i}}{1-m_i}\right) \tag{2.11}$$

For a constant C_s, the modified error function solution for Eq. (2.9) will be,

$$C_x = C_s \left(1 - erf\left[\frac{x}{2\sqrt{(T)}}\right]\right) \tag{2.12}$$

After substituting the expression for T, the modified ERFC solution will be,

$$C_x = C_s \left(1 - erf\left[\frac{x}{2\sqrt{\left(D_{ref}(t_{ag,ref})^{m_i}\left(\frac{{t_{ag,f}}^{1-m_i} - {t_{ag,i}}^{1-m_i}}{1-m_i}\right)\right)}}\right]\right) \tag{2.13}$$

Comparing the basic ERFC solution (Eq. (2.3)) to the modified ERFC solution (Eq. (2.13)), the apparent diffusion coefficient can be obtained as,

$$D_a \cdot t_{ex} = T \tag{2.14}$$

Where, t_{ex} is the exposure duration (= $t_{ag,f} - t_{ag,i}$)

Or,
$$D_a = \frac{D_{ref}(t_{ag,ref})^{m_i}\left(\frac{{t_{ag,f}}^{1-m_i} - {t_{ag,i}}^{1-m_i}}{1-m_i}\right)}{t_{ag,f} - t_{ag,i}} \tag{2.15}$$

This D_a is the true average of the D_i over time under constant C_s.

It should be noted that this expression is truly valid only when free chloride contents are used, and the surface (free) chloride content is constant. This is because D_a is derived by incorporating the instantaneous D and its time function into Fick's 2nd law, which is ideally valid when the diffusion driving force is free chlorides. The assumption of constant boundary condition (free chloride concentration at the surface) was necessary simplification to enable the mathematical derivation. In submerged conditions, it is considered a reasonable assumption as the chloride concentration of the surrounding environment remains constant.

It must be noted here that the time development of D_i is assessed through short-term tests, mostly based on migration/conduction or short duration bulk diffusion tests. It does not account for the contribution of the increase in chloride binding capacity with time by assuming instantaneous chloride binding (Tang & Nilsson, 2000).

This solution is used by simplified physical modelling approaches, which use independently measured material properties: D, m_i, and binding coefficients, to predict the chloride profile without using any chloride profile measurements. This treatment is distinct from the empirical approaches where the time function is defined not in terms of the instantaneous diffusion coefficient but rather in terms of the

apparent diffusion coefficient obtained directly from the measured chloride profiles. This is further discussed in the next section.

2. Direct use of apparent diffusion coefficient (D_a)

The time-dependence of the diffusion coefficient is more commonly evaluated through the evolution of the apparent diffusion coefficient. The apparent diffusion coefficient measured from chloride profiles obtained at different exposure durations is used to calculate the ageing factor according to Eq. (2.16).

$$D_a(\mathrm{t}) = D_{a,ref}\left(\frac{t}{t_{ref}}\right)^{-m_a} \tag{2.16}$$

Where,

$D_a(t)$ is the apparent diffusion coefficient.

$D_{a,ref}$ is the apparent diffusion coefficient at reference time 't_{ref}'.

m_a is the ageing factor for the apparent diffusion coefficient.

t is the time: age or exposure duration

It is crucial to note that the definition of time, whether age or exposure duration, among others, is most often left ambiguous. The drawback of using exposure duration is that extrapolating backwards to the start of the exposure period yields an infinitely large D_a, which is physically meaningless. The same thing can be said about age as the time parameter when extrapolated to zero. However, it at least has the advantage that the D_a can be extrapolated to the start of the exposure, which is of much practical importance.

In contrast to the previous case in which the apparent diffusion coefficient was required to be derived from the time function of the instantaneous diffusion coefficient, no such derivation is needed in this case. The reason is that the apparent diffusion coefficient with its time variation ($D_a(t)$) is already available in Eq. (2.16), which can be directly substituted for D_a in the ERFC solution as shown in Eq. (2.17). Using the time integration of Eq. (2.13) will be incorrect as the time-function used in this case is not that of the instantaneous diffusion coefficient (Maage et al., 1996; Mackechnie, 1996).

$$C_x = C_s\left(1 - erf\left[\frac{x}{2\sqrt{\left(D_{a,ref}\left(\frac{t_{ex}}{t_{ex,ref}}\right)^{-m_a}.t_{ex}\right)}}\right]\right) \tag{2.17}$$

2.15.3.2 Surface chloride content (C_s) and its time dependence

In the preceding discussion on the time-dependence of diffusion coefficient, it was assumed that the surface chloride content, C_s, remains constant with time. Several studies however have shown that C_s evolves with time as well, increasing with exposure duration as shown in Figure 2.14 and Figure 2.15 (Ann, Ahn & Ryou, 2009; Pack et al., 2010; Kim et al., 2016; Shakouri & Trejo, 2017, 2018).

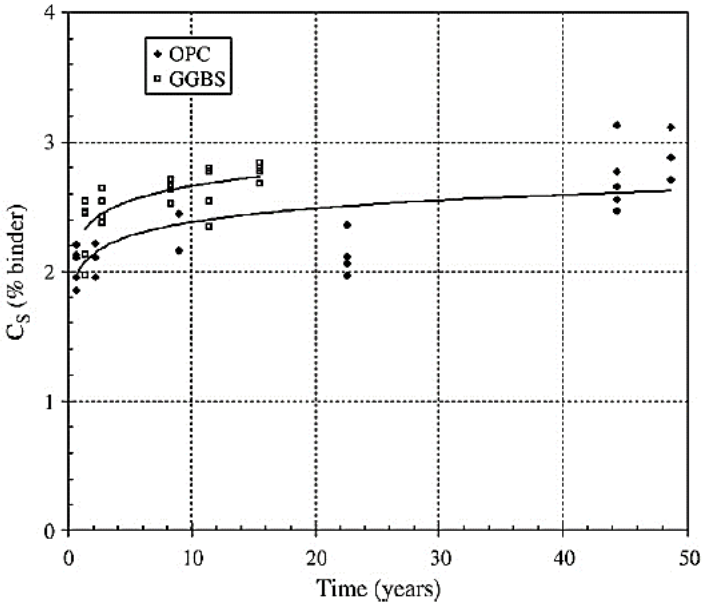

Figure 2.14. The variation of surface chloride content in 11 concrete bridges located in South Korean coastline in tidal conditions over the years (reproduced from (Pack et al., 2010))

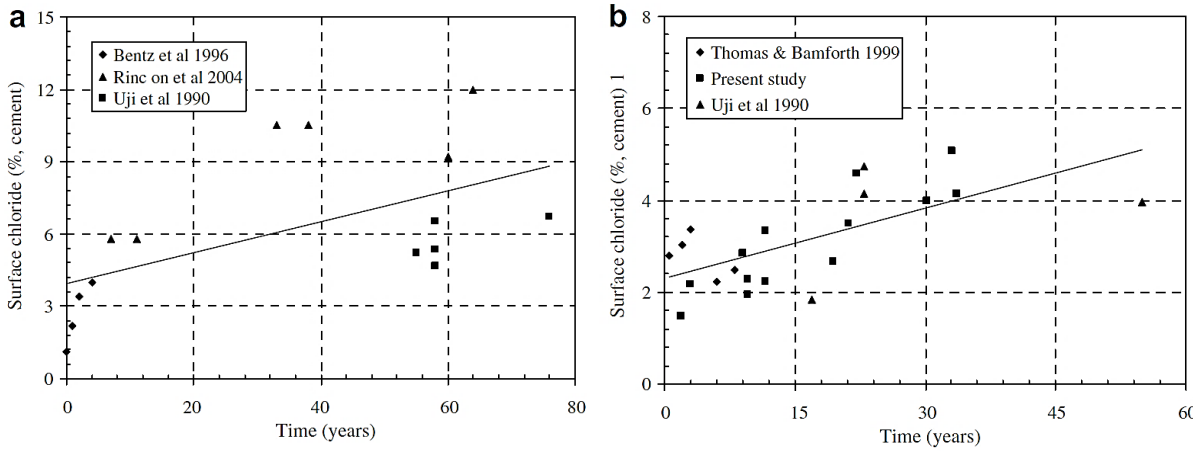

Figure 2.15 Increase in C_s with time in (a) tidal, and (b) splash conditions (reproduced from (Ann, Ahn & Ryou, 2009))

It is normally viewed as a consequence of repeated wetting and drying of the near-surface concrete in exposure zones involving convective processes (Ann, Ahn & Ryou, 2009; Cai et al., 2020). When the

surface of concrete dries, water in the near-surface region evaporates leaving the transported chlorides behind. These additional chlorides are carried rapidly deeper into the near-surface concrete mainly when the dry surface absorbs seawater in the wetting period. Repeated wetting and drying increases the chloride concentration with time near the interior boundary of the wetting-drying zone, also referred to as the convection zone.

These factors have also been used to describe the divergence of chloride profiles from the theoretical curve in the near-surface zone as shown in Figure 2.12. The chloride contents measured in this region are much lower than expected from the diffusion theory. Additional causes such as washout of near-surface chlorides from rain and loss of binding ability due to carbonation have also been frequently used to explain this phenomenon. Normally, the portion of the chloride profile showing the convection zone behaviour is ignored and the rest of the profile is used to enable analysis using the diffusion theory. The surface chloride content is derived by extrapolating the diffusion curve to the surface.

The possibility of convective transport provides a reasonable explanation for the divergent shape of the chloride profiles and the time dependence of surface chloride content in the tidal, splash, spray, and air-borne zones. It can even explain the differences in the severity of chloride penetration between different exposure zones. However, the chloride profiles of continuously submerged concrete have also been observed to have similar divergence behaviour near the surface and a time-dependent increase in surface chloride content (Tang & Nilsson, 2000; Shakouri & Trejo, 2018; Cai et al., 2020).

In submerged conditions, the free chloride ion concentration of the pore solution of concrete at the exposure boundary is, at least in theory, equal to the chloride ion concentration of the surrounding chloride solution (seawater). The chloride binding is assumed to occur instantaneously—in relation to diffusion—which implies the total chloride content at the surface is supposed to remain stable with time in submerged conditions. The empirical observations are however in contradiction with these expectations.

The time-dependence of chloride binding has been argued as a possible explanation (Tang & Nilsson, 2000). Mainly, the leaching of alkali ions and calcium hydroxide from the surface can change the microstructure and composition of the near-surface concrete. Heavy leaching in the first few microns can lower the capacity for chloride binding and light leaching in the inner zones can increase the binding ability. This can result in the typical peak shape observed in the chloride profiles and increase the chloride concentration at the peak with time (De Weerdt et al., 2016; Jakobsen, De Weerdt & Geiker, 2016; Machner, Hemstad & De Weerdt, 2018; Machner et al., 2022). Portlandite leaching can also increase the porosity in this region. However, more research is needed in this regard to find definitive answers, preferably distinguishing the behaviour of free and bound chlorides by direct measurement.

The time-dependence of C_s has been modelled in widely different ways in attempts to best fit the empirical data. There is no consensus yet over a general form for the time-dependence of C_s, such as in

the case of diffusion coefficient. Nevertheless, it is generally accepted that C_s increases non-linearly with time with gradually diminishing rates of increase. Some of the simple models used in the literature are listed below (Kim et al., 2016; Shakouri, 2021).

- $C_s(t) = k.t$
- $C_s(t) = k.\sqrt{t}$
- $C_s(t) = k.t^n$
- $C_s(t) = C_0 + kt^n$
- $C_s(t) = C_0 + k_1 \ln(k_2 t + k_3)$

Where, k_i is a constant, n ϵ (0,1) is the age exponent, and C_0 is the initial instantaneous surface chloride content at the start of the exposure.

2.15.3.3 ERFC solution for simultaneous time-evolution of D_a (t) and C_s (t): the case of reality

The C_s obtained from a chloride profile represents the C_s at the time of measuring the chloride profile, in other words, the end of the exposure period. The D_a, on the other hand, represents the effective diffusion coefficient that will result in the chloride profile with the boundary condition set at the measured C_s. However, in reality, the C_s is not constant but increases continuously over time. This implies that a lower D_a is required to compensate for the higher boundary condition implicit in the chloride profile. For this reason, the measured apparent diffusion coefficient is not a true average of the instantaneous diffusion coefficient in time; it has an additional component that changes with the variation of C_s. As both the C_s and D_a are calculated from the chloride profile data, the direct substitution of their time functions into the ERFC solution gives the correct solution (see Eq. (2.18)). This is because the values of the time functions for C_s and D_a at any time 't' will give the respective value measured at that exposure time. A true mathematical solution for the simultaneous variation of intrinsic diffusion coefficient and C_s with time from material and boundary condition parameters is not possible using the ERFC solution.

As discussed before, the simultaneous time variation of both C_s and D_a changes the definition of D_a from a time-averaged D to a more complex regression parameter, rather than a material property. Only at the start of the exposure, is D_a equal to the instantaneous diffusion coefficient. This can be obtained by extrapolating D_a backwards in time to the start of the exposure. At this point, the calculated D_a is equal to the D_i and has not been affected by the time-evolution of D and C_s. This is why this point is closest to the intrinsic diffusion coefficient, or any indicator of it measured in the lab at the reference age, affected only by any difference in temperature.

$$C_x = C_s(t)\left(1 - erf\left[\frac{x}{2\sqrt{\left(D_{a,ref}\left(\frac{t_{ex}}{t_{ex,ref}}\right)^{-m_a} . t_{ex}\right)}}\right]\right) \quad (2.18)$$

2.16 Chloride Profile: Practical Considerations

2.16.1 Unit of chloride content: by mass of concrete or by mass of binder?

Chloride contents are generally measured in terms of acid-soluble (or total) chloride content. Conventionally, the total chloride contents are expressed in the following units: (i) $\%Cl^-$ – by mass of concrete or material (example, $\%\text{-}kg_{Cl}/kg_{concrete}$), or (ii) $\%Cl^-$ – by mass of cement or binder ($\%\text{-}kg_{Cl}/kg_{binder}$). Expression of $\%Cl^-$ by mass of the material facilitates the comparison of the penetrability of different materials to chloride ions regardless of their composition. It is generally stated that the free chloride profiles would be ideal for this purpose. However, even total chloride contents expressed in this way will provide information on the penetrability through the overall penetration depth (De Weerdt et al., 2023). Additionally, chloride contents by mass of concrete (or material or sample) can be readily converted in terms of %mass-of-binder when the relevant information for unit conversion, i.e., concrete density and binder content, are available. In the case of old field structures, the information on the mix composition may not be available and this type of conversion may not be possible without further assumptions or testing (Angst et al., 2009).

On the other hand, the expression of %Cl by mass of binder is used as a convenient way of describing the chloride threshold value. The threshold values are expressed as the ratio of the deterioration action (or potential) and the potential resistance. Expressing the chloride content in this way facilitates the comparison in terms of the attainment of chloride threshold value in time or distance, i.e., the resistance against corrosion initiation. However, whether total chlorides by mass of binder is the right way of expressing the chloride threshold value is an ongoing debate. Other alternatives have been used such as free chloride content (instead of total chloride content) and $[Cl^-]/[OH^-]$ ratio. Neither of these expressions is considered to be any improvement over the total chloride content by some researchers (Glass & Buenfeld, 1997). The arguments against these expressions are as follows (Glass & Buenfeld, 1997; Angst et al., 2009; Tang, Nilsson & Basheer, 2012):

a) There is a lack of clarity over the involvement of bound chlorides in the initiation of corrosion and hence, it is not clear whether removing bound chlorides is appropriate or not.
b) Processes such as leaching and carbonation can result in the release of bound chlorides.

c) There are difficulties in the reliable measurement of free chloride content—experimental difficulties in the test methods and accurate estimation of the porosity associated with free chlorides.
d) The OH^- content (or pH) may only be a part, not all, of the resistance offered by the binder or concrete to steel depassivation. Moreover, accurate measurement of this term can also pose difficulties.

As already discussed, the unit %Cl by mass of binder is conveniently used to assess the depth of chloride threshold at a given exposure duration and thus enables a comparative analysis of the corrosion-free service life. However, the conversion of %Cl by mass of concrete to %Cl by mass of binder rescales the chloride contents of the profiles based on the binder content. This rescaling operation renders attempts to infer and compare the chloride penetrability of concretes through chloride profiles or penetration depths inappropriate, especially between concretes of different binder contents.

From the preceding discussion, it can be concluded that the appropriateness of a particular unit depends on the purpose of the analysis. However, %concrete can be used for both purposes as is the practice in North America. Since a major goal of this study is to compare the penetrability of different concretes and investigate the relationships between different measures of penetrability, the unit total chlorides by mass of concrete is preferred.

2.16.2 Curve-fitting considerations: to extrapolate or to rescale?

The first few points on the chloride profile near the surface in the so-called convection zone commonly deviate from the theoretical Fick's law curve. Normally, the data points leading to the peak are excluded from curve fitting of the ERFC solution in the rest of the profile. The fitted curve is extrapolated to the surface to determine the effective (or apparent) surface chloride content, C_s.

A different method has been suggested (fib bulletin 34, 2006; Andrade, Climent & de Vera, 2015) by the fib Model Code 2010 for service life design. Because of the influence of fib Model Code on international practices, this approach is analysed in some detail here. The proposed method rescales the profile from the position of the peak as per Eq. (2.19).

$$C_x - C_i = (C_{\max} - C_i)\left(1 - erf\left[\frac{x - \Delta x}{2\sqrt{(D_a.t)}}\right]\right) \quad (2.19)$$

Where,

C_i is the initial chloride content (internal/background chloride content).

C_{max} is the chloride content at the peak.

Δx is the depth of the peak from the surface (convection zone depth).

This operation basically ignores the existence of any material before the peak and shifts the exposure boundary to the peak from the surface. It is argued that this procedure uses a 'real' C_s (C_{max}) in the sense that it is measurable, instead of the extrapolated, not measurable, and thus a 'virtual' C_s. The concentration gradient represented in this manner is argued to be in better alignment with the actual diffusion process underway in the interior of the concrete. While this may limit the variability in the calculation of C_s in the regression analysis, some things must be borne in mind as described below.

1. Neither the extrapolated C_s nor the C_{max} are inherently or completely 'real' as the boundary condition in the diffusion process, as they both generally represent total chloride contents. In the same vein, they are equally 'real' as they fall on the same curve provided an interior concentration is treated as from the interior, not as a boundary condition. It is nonetheless recognised that extrapolating backwards in the convection zone does violate the assumption of diffusion as a transport process and may lead to misinterpretation of C_s values to carry physical meanings that may only be an artefact of extrapolation.
2. Enough data points in the peak region are often unavailable to locate the peak (C_{max} and Δx) with any certainty. In addition, the long-term variation of C_{max} and Δx will constitute additional data required for service life predictions, which is often not easily available.

Given the practical limitations of the fib approach, the conventional approach is preferred in this work.

2.17 Corrosion-Initiation Models

2.17.1 Life 365

Life 365 (Life-365 v2.2.3, 2020) is a freely available computer program, which offers prediction of corrosion initiation time, time to first repair, and life cycle costs for different material selection choices. Although based on a multi-mechanistic model (Boddy et al., 1999), Life 365 only considers diffusion as the transport process responsible for chloride ingress to minimize the number of input variables required from the user and to make it accessible to the practising engineers.

The rate of chloride ingress is predicted by solving the mass-balance equation of Fick's 2nd law using the finite difference method rather than its error function solution. It thus uses an instantaneous diffusion coefficient instead of the apparent diffusion coefficient (Ehlen & Kojundic, 2014). It also allows for 1-D as well as 2-D modelling of chloride ingress in structural elements. Solving Fick's 2nd law partial differential equation using numerical methods has the advantage that the diffusion coefficient can be treated as a material property (in the given conditions: T, C) (Stanish & Thomas, 2003). However, the diffusion coefficients and surface chloride contents are measured through acid-soluble chloride contents following ASTM C1556. Total chlorides are assumed to be responsible for diffusion. Chloride binding is therefore not considered explicitly.

The diffusion coefficient is assumed to be a function of time and temperature as per Eq. (2.20) following the Arrhenius law.

$$D(\mathrm{t},\mathrm{T}) = D_{ref}\left(\frac{t_{ref}}{t}\right)^{m}.\exp\left[\frac{U}{R}\left(\frac{1}{T_{ref}}-\frac{1}{T}\right)\right] \quad (2.20)$$

Where,

D_{ref} is defined at the reference age t_{ref} (= 28 days as D_{28}).

m is the diffusion decay constant.

U is the activation energy of the diffusion process (=35 KJ/mol).

R is the gas constant (8.314 J/(K.mol)).

T_{ref}, T are the reference temperature (293 K) and (absolute) temperature of concrete.

The model can calculate the diffusion coefficient and its evolution with time on the basis of the mix proportioning parameters, which can be selected by the users. These 'default' values have been derived from lab-based data from various sources. The instantaneous diffusion coefficients are calculated from the bulk diffusion tests using acid-soluble chlorides (ASTM C1556, 2016) following the method by Stanish & Thomas (2003). The relationships used in the model are based on the w/c ratio and SCM level as shown below:

1. For Portland cement concretes, D depends only on w/c ratio as per Eq. (2.21). The m value is 0.2.

$$D_{PC,28} = 10^{[-12.06+2.40\left(\frac{w}{c}\right)]} \quad (2.21)$$

2. Silica fume [0-15%] is assumed to modify the diffusivity of concrete according to Eq. (2.22) but not its time development.

$$D_{SF} = D_{PC}e^{-0.1646SF} \quad (2.22)$$

3. Fly ash [up to 50%] and blastfurnace slag [up to 70%] are assumed to have no effect on the early diffusivity of concrete but enhance its reduction with time by increasing the m value (over 0.2 for PC) according to Eq. (2.23).

$$\mathrm{m} = 0.2 + 0.4(\%\frac{\mathrm{FA}}{50} + \%\frac{BS}{70}) \quad (2.23)$$

The reduction of diffusion coefficient in Life 365 is allowed to occur up to 25 years after which D remains constant following the assumption of complete hydration beyond that point.

The surface chloride concentration is considered as the driving force for diffusion. Default values of maximum surface chloride content and its development in time (chloride build-up) are provided according to the exposure conditions in North America. Life 365 caters to both marine conditions and deicing salt exposure. This seems to be based on field data or past experience. The surface chloride content is assumed to increase linearly from 0 to a maximum value and remain constant afterwards according to Table 2.4. Annual temperature trends are obtained from meteorological data.

Table 2.4. Development of surface chloride content for different exposure zones (Life-365 v2.2.3, 2020)

Marine exposure zone	Rate of Cl^- buildup (%/year)	Max. C_s (%, concrete)	Time of chloride buildup (years)
Splash zone (tidal and within 1 m of high tide)	instantaneous	0.8	0
Spray zone (>1 m above high tide)	0.1	1.0	10
Air-borne (<800 m from ocean)	0.04	0.6	15
Air-borne (<1.5 km from ocean)	0.02	0.6	30

Life 365 assumes a chloride threshold value of 0.05% (%, concrete) for most cases, but specific values are provided for special materials. A constant propagation period of 6 years is assumed. Life 365 also allows the use of directly measured values in lab or field instead of the default values.

In essence, Life 365 uses a combination of lab and field data to predict the service life. It allows users to select a mix proportion from a wide range of material combinations, mix parameters, and protection strategies based on the desired service life and life cycle cost thereby allowing an economic analysis of different service scenarios/options. The model operates on a user-friendly interface and requires a small number of input parameters making it accessible to the broad engineering community. It also provides the opportunity to use the local data to improve the accuracy and relevance of predictions.

Although Life 365 acknowledges its simplified approach and advises caution on the interpretation of the results, it is worth looking at some of its specific issues that need clarification other than the limitations of the scope of materials and exposure conditions dealt with within the model:

1. It is not clear how the input parameters are used to produce chloride profiles. There is a lack of transparency in that respect.

2. The model uses instantaneous diffusion coefficient and yet the decay coefficient 'm' is derived from apparent diffusion coefficient data. The time dependence of the two are different and hence will yield different 'm' values.
3. It is assumed that the decay of diffusion coefficient (m) is a function of material properties only. The effect of exposure conditions, RH and temperature in different zones and localities, for example, on the hydration of concrete is ignored.
4. Similarly, the effect of materials on the surface chloride content is ignored even though total chloride contents are considered rather than free chlorides.
5. Diffusion coefficients are measured using the ASTM C1556 method which uses a significantly higher chloride concentration than present in the natural marine environment. The effect of chloride concentration on diffusivity is not accounted for.
6. The method of calculating the instantaneous diffusion coefficient from apparent diffusion results assumes a constant surface chloride concentration in time, which may not be a valid assumption. To what degree this affects the instantaneous diffusion coefficient needs to be analysed.

2.17.2 fib Model Code 2010 (modified DuraCrete)

fib Model Code (fib bulletin 34, 2006) recommends a model based on the ERFC solution as per Eq. (2.24) in a full probabilistic design framework. The apparent diffusion coefficient is considered with its time decay.

$$C_x - C_0 = (C_{s,\Delta x} - C_0)\left(1 - erf\left[\frac{x - \Delta x}{2\sqrt{(D_a . t)}}\right]\right) \quad (2.24)$$

Where, $C_{s,\Delta x}$ is C at Δx depth from the surface and Δx is the depth of convection zone or the peak chloride concentration, C_0 is the initial chloride content.

The reference D_a (Eq. (2.25)) is based on D_{RCM} (NT BUILD 492, 1999) measured in the lab and is modified by an environmental factor, which corrects for the temperature difference between the lab and the field using Arrhenius equation, and a transfer factor whose purpose is not clearly defined.

$$D_a = D_{RCM} . k_e . k_t . \left(\frac{t_0}{t}\right)^m \quad (2.25)$$

Where,

t_0 is time to start of exposure.

k_e, k_t are environmental factor and transfer factor, respectively.

m is 0.30 (PC), 0.60 (FA), 0.45 (BS) based on field data.

It is argued that chloride buildup on the surface takes a short time in relation to the typical service life. Hence, the surface chloride content is assumed constant, which depends on the material and exposure conditions. The ERFC equation suggested, however, requires additional input parameters: the peak chloride concentration and the depth of the convection zone.

The model is quite straightforward in its description. A limited number of parameters are required, which makes the model readily manageable. The probabilistic treatment ensures that the large variability associated with every step of the chloride-induced corrosion process is handled appropriately.

However, the transformation of D_{RCM} to initial D is performed without recognising the difference between the migration coefficient and the diffusion coefficient, i.e., no test method factor. Tang, Nilsson & Basheer (2012) also note that the model lacks a term for the age at the start of exposure in the time function and generally does not define time in specific terms as either age or exposure duration.

2.17.3 ClinConc

ClinConc (Tang & Nilsson, 1996) is a physical model for chloride penetration in submerged conditions. It describes the material and environmental exposure parameters in a detailed and unambiguous manner. The transport of free chlorides in the pore solution is described through Fick's laws while accounting for non-linear binding using Freundlich isotherm. Using the water content in the concrete, free chloride profiles and bound chloride concentrations, the profiles for total chloride contents are generated.

The intrinsic diffusion coefficient of the material is measured in the lab under controlled exposure conditions, which is modified for variation with respect to depth, time and temperature through independent functions as per Eq. (2.26).

$$\mathrm{D}\ (\mathrm{x}, \mathrm{t}, \mathrm{T}) = \frac{D_0}{\varepsilon_p} . f(x) . g(t) . e^{\frac{E}{R}\left(\frac{1}{T_0} - \frac{1}{T}\right)} \tag{2.26}$$

Where,

D (x, t) is the diffusion coefficient as a function of depth, time and temperature.

D_0 is the diffusion coefficient of the matured concrete (determined in the lab under controlled conditions).

ε_p is the porosity.

f(x) is the function describing the variation of diffusion coefficient with depth.

g(t) is the function describing the variation of diffusion coefficient with time.

$e^{\frac{E}{R}\left(\frac{1}{T_0} - \frac{1}{T}\right)}$ describes the variation of diffusion coefficient with temperature according to Arrhenius law.

The intrinsic diffusion coefficient is derived from the RMC test method (NT BUILD 492, 1999), see Eq. (2.27). The time and depth functions are based on appropriate mathematical functions describing the empirical data. The boundary conditions include the free chloride concentration at the surface, and temperature, both of which are defined as periodic functions that describe variation annually. The time-dependence of the surface chloride concentration is dealt with by adding a function for the time-dependence of chloride binding (Tang & Nilsson, 2000).

The model requires a relatively large number of input parameters, some of which are not readily obtained. The complexity of the model will increase and so will the computational effort as the convective processes associated with unsaturated conditions of other exposure zones are introduced.

$$D_0 = \frac{1 + 0.59K_{b6m}}{1 + \frac{\partial c_b}{\partial c_f}} D_{6m} k_{TD} \tag{2.27}$$

Where,

D_{6m} is the migration coefficient at the age of 6 month measured through the RCM method.

k_{TD} is the temperature factor.

K_{b6m} is the unit changing factor as shown below:

$$K_{b6m} = \frac{W_{gel6m}}{1000\varepsilon_{6m}} \tag{2.28}$$

Where W_{gel6m} is the gel content in kg/m^3(concrete) and ε_{6m} is the water-penetrable porosity at 6 months of age. The numerator ($1+0.59\cdot K_{b6m}$) accounts for binding in the presence of electric field in the non-steady state migration coefficient (D_{6m}).

Tang presented a simplified model (Tang, 2008) more suited for engineering application based on the ClinConc model. The simplified version uses a modified ERFC solution considering free chlorides as the diffusing species. A number of simplifying assumptions are made to deal with non-linear binding and what the authors describe as the time-dependence of binding. Total chloride profiles are generated by summing the bound chlorides and the free chlorides. Despite its elaborate nature, the model still requires calibration to avoid under-prediction of the long-term chloride ingress especially for SCM concretes. A large number of input parameters are needed requiring adequate understanding of their derivation and availability of data.

2.17.4 UCT chloride model

The UCT chloride model (Mackechnie, 1996, 2001) is an empirical model for South African conditions. Following the Durability Index approach (Alexander, Ballim & Stanish, 2008), it uses the chloride conductivity index values measured at a relatively early age (28 days) to predict the long-term chloride resistance of concrete in marine conditions. Distinctions are made based on concrete grade, curing, binder type, and the severity of exposure conditions to improve specificity of predictions and practical relevance.

The model is based on a modified ERFC solution that considers the time-dependence of D_a, and keeps the C_s constant for simplicity. The model can be divided into two distinct parts: a. correlation of CCI with the reference D_a, and b. the time decay of D_a in the long-term. The former is achieved by first finding the correlation between 28-day CCI and the modified CCI. The modified CCI is the CCI measured after the 28-day CCI specimens were left immersed in 5 M NaCl solution until the age of 98 days. This was done to approximately simulate the maximum effect of binding using conductivity measurements to enable a reasonable correlation with the reference D_a. The reference D_a was taken as the 2-year D_a measured in the field on lab-made specimens. The decay coefficient for D_a and C_s were however selected on the basis of the data collected on much older field structures and literature, in order to be realistic in the long term.

The model is easy to understand and use (see Figure 2.16). The primary issue is that being an empirical model it needs regular updating so as to align it with newer concrete materials and advances in concrete technology. The exposure conditions of the model are also limited to that of Western Cape Province in South Africa.

The exposure conditions on the Eastern seaboard are very different from the Western seaboard, example sea temperatures, which are as of now out of the scope of the model. In addition, the correlation between the 28-day CCI, modified CCI, and 2-year D_a lacks sufficient theoretical basis and flexibility to tentatively extend it to other materials and exposure conditions using data from the literature. Following the development of the model, more data have been gathered, which can be used to further quantify the environmental effects (Heiyantuduwa-Beushausen, 2022).

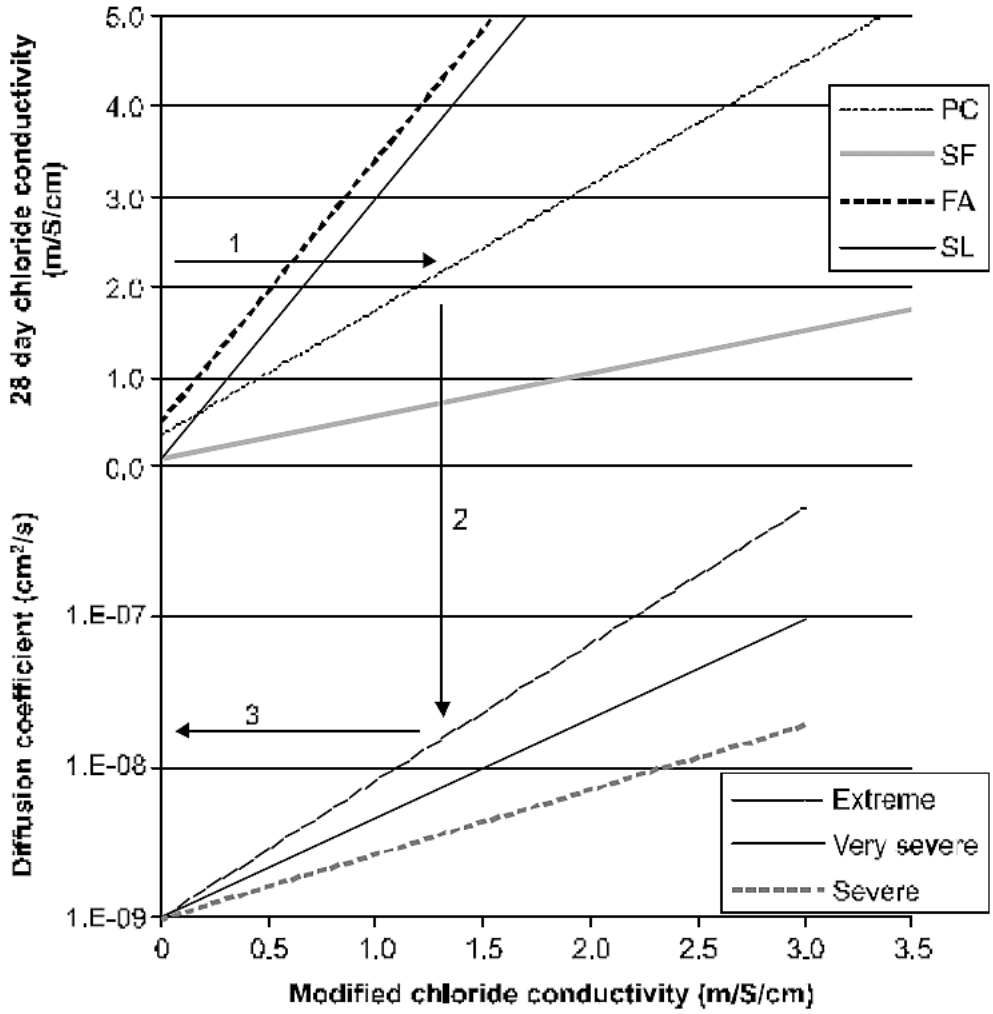

Figure 2.16 The existing nomogram for diffusion coefficient prediction from CCI measurements (reproduced from (Mackechnie, 2001))

2.17.5 Resistivity-based models

Resistivity measurements through the use of methods such as surface resistivity, direct resistivity, etc. on saturated concrete have also been used extensively to predict the service life (Andrade, 2004; Liu, Presuel-Moreno & Paredes, 2015; Balestra et al., 2020; Chidiac & Shafikhani, 2020; Kang et al., 2021). Resistivity is related to the steady-state diffusion coefficient through the Einstein relation. A reaction factor (or retardation factor) has been suggested to empirically relate resistivity to non-steady state diffusivity, which essentially represents the linear rate of binding (Andrade, D'Andrea & Rebolledo, 2014). A more elaborate approach of extracting the formation factor from the resistivity measurements in combination with binding isotherms has also been developed (Qiao et al., 2018). Attempts have been made to derive the decay coefficient for diffusivity through the evolution of resistivity values. The decay coefficient for resistivity is suggested in one study to be about 80% of the decay coefficient of the apparent diffusion coefficient (Andrade, Castellote & D'Andrea, 2011). These approaches present

opportunities for deriving diffusion-related data, perhaps approximately, with much simpler methods and should be investigated further for their practical advantages.

2.18 Conclusions (Part C)

1. Physical approaches of modelling aim for scientifically accurate descriptions of the transport processes, which make them useful towards the goal of a generalised model. However, these are not yet amenable to application in general structural design due to their complexity. Empirical approaches provide more practical solutions to design problems and thus will be adopted in this study.

2. UCT chloride model is an empirical model, which requires updating to account for changes in concrete constituents and test methods. A larger chloride-related database is available, which is expected to improve the representativeness of the model.

Part D: Formation Factor Approach – theory and testing

2.19 Formation factor concept

2.19.1 Introduction

Diffusivity is often measured through electrical conductivity measurements following the Nernst-Einstein relation between the two properties for the ease and economy of electrical testing. The electric field however mobilises all the ionic species present in the pore solution along with the ionic species of interest, in this case, chloride ions (Streicher & Alexander, 1995). The consequent additional conductivity due to other ionic species in the pore solution is not in itself a major issue if it remains uniform in all concretes because a uniform deviation in all measurements does not affect comparisons and can also be accounted for when needed. The problem lies in the fact that the ionic composition of the pore solution and therefore its conductivity contribution varies across different concrete mixtures. An effective way of overcoming this issue is through the use of the formation factor (Archie, 1941).

In this part, the concept of the formation factor is discussed through the conceptual and empirical models used in the literature to gain an understanding of its pore structure underpinnings. A review of pore solution conductivity and selected influencing factors is also provided.

2.19.2 Principle

The transport of chloride ions occurs through the pore solution present in the pore space within concrete. The pore space within concrete consists of a network of interconnected pores of various sizes and morphology. The variability in the size and shape of pores in the cement paste results in highly "tortuous" network passages with variable and often "constricted" cross sections (Atkinson & Nickerson, 1984). The tortuosity and constrictivity of the pore network significantly reduce the effective diffusivity of chlorides through concrete (10^{-10}–10^{-13} m^2/s) by orders of magnitude compared to that in the free pore liquid (10^{-9} m^2/s) unconstrained by the pore network (Snyder, 2001).

In electrically induced ionic transport, the contribution of pore structure to resistivity is expressed in terms of the so-called "formation factor" *FF* (Archie, 1941), which is defined as the ratio of concrete resistivity to the pore solution resistivity (Eq. (2.1)).

$$FF = \frac{\rho}{\rho_{ps}} = \frac{\sigma_{ps}}{\sigma} \tag{2.1}$$

Where ρ, σ refer to the resistivity and conductivity of concrete, ρ_{ps}, σ_{ps} are the resistivity and the conductivity of pore solution, respectively, and F is the formation factor. By applying the Nernst-Einstein relation between the ionic diffusivity and conductivity, the formation factor can also be expressed for chloride diffusion in concrete as in Eq. (1.2) (Atkinson & Nickerson, 1984; Garboczi & Bentz, 1992; Streicher & Alexander, 1995; Snyder, 2001).

$$FF = \frac{\sigma_{cl,ps}}{\sigma_{cl,c}} = \frac{D_{cl,ps}}{D_{cl,c}} \tag{1.2}$$

Where $\sigma_{cl,c}$ and $D_{cl,c}$ are the conductivity and diffusivity (Fick's 1st law) of chlorides in concrete, respectively. Similarly, $\sigma_{cl,ps}$ and $D_{cl,ps}$ are the conductivity and diffusivity (Fick's 1st law) of chlorides in the pore solution, respectively.

It has been shown that the formation factor is independent of the ionic species used and its concentration (Snyder, 2001). Even though the object of interest is the transport of chloride ions through concrete, this implies that the formation factor can be determined through electrical conductivity measurements on virgin concrete specimens as well (Eq. (1.3)). The diffusivity can then be determined through Eq. (1.4). In this case, the pore solution conductivity becomes a crucial factor and therefore is discussed in some detail in a subsequent section after a brief overview of simplified pore structure models that illustrate the concept of the formation factor. Note that the inverse of the formation factor is referred to as the 'penetrability' hereinafter, with a specific reference to the penetration of chloride ions.

$$FF = \frac{\sigma_{ps}}{\sigma} \tag{1.3}$$

$$D_{cl,c} = \frac{D_{cl,ps}}{FF} \tag{1.4}$$

2.19.3 Description of pore-structure features

A simplified parallel resistor model has been used to describe the idea of the formation factor in terms of pore network characteristics (Whittington, McCarter & Forde, 1981). In this model, concrete is assumed to consist of conductive pore conduits of uniform cross-sections spanning the length of the specimen dispersed in a highly resistive solid material (paste solids and aggregates). The resistance of concrete using the parallel resistor arrangement becomes nearly equal to that of the conductive pore phase, which can be rearranged to obtain the formation factor in terms of geometric parameters as in Eq. (1.5) (Sallehi, Ghods & Isgor, 2018).

$$\frac{\sigma}{\sigma_{ps}} = \frac{L}{L_p} \times \frac{A_p}{A} \tag{1.5}$$

Where A and L are the cross-section and length of the concrete specimen. A_p and L_p are the effective cross-section and effective traversed length of the pore conduits. L_p/L is the tortuosity of the current paths, and its inverse is termed pore connectivity (β). A_p/A is equal to the fractional pore volume or

porosity (φ). Eq. (1.5) can be rewritten as Eq. (1.6). In this way, the inverse of the formation factor is conceptualised as a product of the saturated porosity and the connectivity of the pore network.

$$\frac{1}{F} = \beta \times \varphi \tag{1.6}$$

However, Archie found the formation factor to be a power law function of the saturated porosity, which is known as Archie's law, as shown in Eq. (1.7) (Archie, 1941).

$$F = A\varphi^{-m} \tag{1.7}$$

Where φ is the volume fraction of saturated porosity, and A and m are coefficients dependent on the porous medium.

Physical meanings such as tortuosity and pore shape factor or constrictivity, respectively, are sometimes ascribed to the coefficients A and m, based on a comparison with the simplified parallel resistor model. Similarly, β (=1/(A.φ^{1-m})) from Eq. (1.6) is used as a physical property to differentiate the tortuosity of different materials despite the fact that β and φ may not be mutually independent parameters (Eq. (1.7)). Other more complex models are outlined elsewhere (Garboczi, 1990; Christensen et al., 1994).

2.19.4 Pore solution conductivity: composition and influencing factors

The initial 24 hours of cement hydration is a period of rapid change and is reflected in the rapid evolution of the composition of the pore solution in this period. The most notable change that occurs in this period, in the context of pore solution conductivity, is the replacement of most sulphate and calcium ions with hydroxyl and alkali (sodium and potassium) ions as a consequence of aluminate-sulphate reactions to form ettringite. The main constituents of the pore solution after this period are hydroxyl, potassium, and sodium ions with other ions in minor concentrations (Taylor, 1987; Vollpracht et al., 2016). The hydroxyl ion also has the highest ionic mobility among the ionic species found in the pore solution and therefore is predominantly responsible for the conductivity of the pore solution with additional contributions from potassium and sodium ions (Snyder et al., 2003). Much of the literature on pore solution characterisation focuses on the hydroxyl ion concentration ([OH^-]) due to its relevance to other matters of interest such as the alkali-silica reaction. The following discussion therefore is also presented in terms of the hydroxyl ion concentration, which as discussed above is also reflective of the conductivity of the pore solution.

The concentration of hydroxyl and alkali ions in the pore solution increases with continued hydration as more alkali ions are dissolved from the clinker and free water is consumed in hydration. This is partly counteracted by the uptake of alkalis in the CSH. The rate of increase of alkalinity diminishes rapidly after around 10 days and the composition tends to change little beyond 28 days (Diamond, 1981; Scott & Alexander, 2016). The composition of the pore solution and its variation over time is influenced by

the composition of the Portland cement, partial replacement with SCMs, w/b ratio, curing, admixtures, and in some cases aggregates.

In contrast to clinker, in which the majority (~70%) of alkalis are in the form of readily soluble alkali sulphates, SCMs such as fly ash and blast-furnace slag generally contain alkalis in the amorphous portion and require hydration to release them (Schaffer & Meng, 2001). Incorporation of SCMs in the binder blend therefore dilutes the clinker component with a material that may release fewer alkalis into the pore solution. In addition, pozzolanic reactions result in C(A)SH with a low Ca/Si ratio, which can bind additional alkalis. Therefore, besides high alkali Class C (high calcium) fly ashes, fly ash, slag, silica fume, and metakaolin generally lower the alkali content and the OH^- concentration of the pore solution (Diamond, 1981; Duchesne & Berube, 1994; Shehata, Thomas & Bleszynski, 1999; Schaffer & Meng, 2001; Thomas, 2011; Scott & Alexander, 2016). The degree of reduction increases with the replacement level (Duchesne & Berube, 1994; Shehata, Thomas & Bleszynski, 1999; Thomas, 2011; Scott & Alexander, 2016).

The changes in OH^- concentration are generally small after 28 days, however in some cases this period may be extended (Thomas, 2011; Vollpracht et al., 2016). Comparisons of different SCMs in their effectiveness to reduce the OH^- concentration, as reported in separate studies, are presented below. The comparisons vary to some degree possibly due to differences in the alkali contents of the materials used and other compositional and methodological details. More importantly, the quantitative differences can be large depending on the composition of the binder materials used.

PC >25% C fly ash >50% C fly ash >25% F fly ash >10% silica fume >50% slag >20% metakaolin, where the 50% slag blend had only a third of the OH^- concentration compared to the (high alkali) PC after 28 days (Thomas, 2011);

PC >25% slag >50% slag~30% fly ash >75% slag >7% silica fume, where the 50% slag blend had two-thirds the OH^- concentration compared to the PC after 28 days (Scott & Alexander, 2016).

The w/b ratio influences the OH^- concentration by its influence on the degree of hydration and the availability of free water in the pore space. Similarly, curing also affects the degree of hydration. Curing can also influence the amount of free water and loss of alkalis depending on the curing method adopted (Spragg et al., 2017). Other influences such as temperature, chemical admixtures, etc. are out of the scope of this study and are not discussed here.

2.19.5 Determination of formation factor through electrical conductivity: different methodological approaches

Different studies have followed different methodologies for arriving at the formation factor. However, these methodologies can broadly be classified into two groups based on whether the pore solution conductivity of the tested concrete is required to be explicitly determined or not. The measurement of

concrete conductivity can be performed using alternating or direct current methods in the preferred geometric arrangement. The choice of conductivity measurement method does not bear upon this classification and is therefore omitted in the following discussion.

2.19.5.1 Methods requiring explicit determination of pore solution conductivities

The conductivity of the pore solution is determined either by measurements on the actual pore solution or through model calculations. In the first method, the pore solution is squeezed typically out of a companion paste specimen through pore expression (Barneyback & Diamond, 1981). The extracted pore solution is either analysed for its ionic composition and conductivity calculated using an appropriate estimation model (example (Snyder et al., 2003)) or if adequate yield is obtained, direct measurements of conductivity are performed. The tedious and expensive nature of this method makes it impractical for quality control purposes. The second method involves the estimation of pore solution composition (and conductivity as described above) based on the oxide composition of the binder and concrete mix proportions. Two prominent models used for this purpose are Taylor's model (Taylor, 1987) and NIST calculator (NIST, 2019) based on Bentz' model (Bentz, 2007). The former model is too complicated for practical use and the latter, although relatively simple and easy to use, has limited accuracy in the case of fly ash concretes (Mukhopadhyay, Liu & Jalal, 2019).

Concrete is generally kept immersed in water (or in lime water) continuously before electrical conductivity testing. This is to ensure concrete saturation, which is known to have a considerable influence on conductivity measurements (Weiss et al., 2013; Zaccardi & Maio, 2014). However, the storage in water/lime water results in the leaching of alkali ions and affects the pore solution conductivity (Spragg et al., 2017). In order to avoid leaching, sealed curing until the time of testing has been adopted; however self-desiccation can lower the degree of saturation requiring a correction (Weiss et al., 2016). An alternative has been presented to address the shortcomings of these methods, which involves sealed curing to avoid leaching, followed by oven drying and vacuum saturation with lime water (Spragg et al., 2016). This method conserves the pore solution chemistry and saturates the concrete. An approach accounting for deviations from the standard states of saturation and temperature, and the effect of leaching on resistivity and formation factor, has been presented by Weiss and team (Weiss et al., 2018).

2.19.5.2 Methods using normalised pore solutions

The second type of method avoids the need to determine the individual pore solution conductivities altogether and measures pore structure resistance to electrical conduction directly. This is achieved by minimising the differences in the individual pore solution conductivities through external means, which vary across test methods. Two such test methods are discussed below.

The chloride conductivity test (Streicher & Alexander, 1995; SANS 3001-CO3-3, 2015) follows the approach of saturating thin concrete disc specimens with a highly conductive (concentrated NaCl)

solution. It is well known that the ionic conductivity increases with an increase in concentration, but the rate of increase in the ionic conductivity decreases with increasing concentration (Bockris & Reddy, 2002). This fact is utilised in the test design as the high concentration of the NaCl solution reduces the influence of original pore solution species on the final conductivity. In addition, the differences contributed by the pore solution ions induce smaller proportional errors due to the high base conductivity of the saturating solution (Streicher & Alexander, 1995). The formation factor in this case can be calculated simply by assuming the conductivity of the normalised pore solution to be approximately equal to the conductivity of the saturating NaCl solution (Eq. (1.8)). Since the conductivity of the normalised pore solution can be assumed to be constant across concrete mixtures, the conductivity of the concrete specimen saturated with the chloride solution can also be used as a measure of the formation factor inverse.

$$F = \frac{\sigma_{NaCl\ sol.}}{\sigma_{CC}} \tag{1.8}$$

Where $\sigma_{NaCl\ sol.}$ is the conductivity of the normalising NaCl solution and σ_{CC} is the conductivity of the NaCl-saturated concrete (also known as the chloride conductivity index (CCI)).

This approach in conjunction with a preconditioning protocol effectively addresses the issues hindering the previous class of methods such as lack of saturation and errors due to alkali leaching. These are also not constrained by any particular curing and storage regime.

The North American test methods are also moving in the same direction, however, with some salient differences (Weiss et al., 2020; Saraswatula & Mukhopadhyay, 2023; Rios et al., 2024). The bulk conductivity test method (ASTM C1876, 2019) follows the approach of curing the standard concrete cylinders in a simulated (average) pore solution with the stated intention of achieving pore saturation and pore solution equalisation. This method relies on cross-diffusion of the ionic species between concrete pores and the surrounding solution to normalise the pore solution as the simulated pore solution fills the empty portion of the pore space. The large specimen size, lack of oven drying, and use of immersion alone may prevent homogenous equalisation of the pore solution across the specimen for a practical timeline. This would be especially difficult to achieve in the case of dense concretes typically used in marine conditions. Also, the use of an average pore solution may affect the robustness of the method as differences in individual pore solution composition may cause large proportional errors, as explained earlier.

Regardless of the present shortcomings of the latter method, which may improve with further research work, the methodologies using normalised pore solution are a more practical alternative for the measurement of formation factor.

2.20 Conclusions (Part D)

The principle of the formation factor approach and the description of the formation factor in terms of pore structure features were discussed in this part. Factors affecting pore solution conductivity, which is a critical part of the formation factor analysis, were critically reviewed. Factors such as binder properties and w/b ratio were found to be influential. Sufficient evidence exists indicating that slag and fly ash generally decreases the pore solution conductivity. Of particular importance is the case of fly ash in this regard, which is often believed to do the opposite based on some model predictions. In light of present findings, such predictions should be verified carefully before using them to calculate the formation factor or make predictions.

The methodologies for the evaluation of the formation factor were also reviewed. Of the two ways, one using explicit measurement of pore solution conductivity and direct determination through pore solution normalisation, the latter appears a more practical approach for routine testing. The chloride conductivity test effectively utilises this latter approach. The recent ASTM C1876 method following this approach may require further developments to address the potential issues regarding adequate and repeatable specimen saturation, and insufficiently high conductivity of the simulated pore solution.

Chapter 3 METHODOLOGY

3.1 Overview

The key objective of this study is to investigate the relationship between concrete conductivity and the resistance of concrete to chloride diffusion. This relationship, between specific measures of concrete conductivity and diffusivity, may depend on various factors that influence the transport properties of the concrete. In this chapter, the methodological decisions are described and justified followed by an account of the materials and methods used in this study.

Important factors of practical significance to the transport properties of the cover concrete are selected as variables to study. An experimental program was developed to quantify their influence on concrete conductivity and diffusion characteristics in standard controlled conditions of the lab. The rationale behind this selection is discussed first. Thereafter, the selection of the test parameters is discussed. The details of the concrete materials used in this study and the testing procedures adopted are then described in Part I and Part II, respectively.

3.2 Experimental variables

The variables in the chloride transport process identified in the previous chapter as the most important in relation to the damage-free material resistance were selected for investigation in this study as discussed below. The study of factors governing environmental action was not part of this experimental investigation. The relevant information needed in this regard to develop the model was derived from previous studies conducted in the natural marine conditions of South Africa (Mackechnie, 1996; Heiyantuduwa-Beushausen, 2022).

3.2.1 Supplementary cementitious materials: type and replacement levels

The binder type is the most decisive parameter for short-term and long-term performance of concrete in marine environments, as discussed in the previous chapter. Different SCMs have different chloride binding properties and result in different pore structure characteristics. The use of SCMs such as fly ash and ground granulated blast-furnace slag in marine environments is encouraged not only because of the consequent improvement these materials bring to the properties of the concrete but also to reduce the clinker content of the binder in a bid to lower the environmental impact (BS 6349-1-4, 2013; Scrivener, John & Gartner, 2018).

Concrete mix selection must balance multiple design requirements. SCMs differ in their short-term and long-term properties with type and replacement levels and therefore offer versatility in mix optimisation to suit the specific requirements of the project. It is therefore important to investigate the influence of the common SCMs and their replacement levels on the chloride penetration resistance of concrete.

In this study, two types of supplementary cementitious materials were used, namely, fly ash and ground granulated blast-furnace slag. The selection of SCMs was based on general availability and long-standing use in South Africa (Mackechnie & Alexander, 1997). Various replacement levels up to 30% for fly ash and up to 75% for slag were adopted. The replacement levels were restricted to the aforementioned values to avoid excessively low early strengths from the resulting concretes. The specific replacement levels used were:15% and 30% for fly ash; and 25%, 50%, 75% for slag. These replacement levels were selected to cover the EN classified cements (BS EN 197-1, 2011)incorporating fly ash or slag with an intention to improve the direct relevance of the results of this study.

It must be pointed out that the term binder is used in this study to refer to the total mass of Portland cement and SCM. Hence, the term is used to distinguish different combinations of cement and SCMs based on composition.

3.2.2 Water-binder ratio

The w/b ratio is another important parameter influencing the chloride penetrability of concrete as discussed in the previous chapter. Through its deciding effect on a wide range of concrete properties, both fresh and hardened, it is easily the most crucial parameter in mix optimisation. In addition, the choice of w/b ratio also largely governs the binder content for a given set of materials and hence affects the cost and environmental impact of concrete. It was therefore considered essential to investigate a wide range of w/b ratios in this study. This would also help to ascertain whether the limits on the w/b ratio prescribed by the current standards are reasonable or overly restrictive. In combination with different binder blends, this would expand the mix design options and enable mix optimisation for diverse requirements.

In this study, the w/b ratios typically adopted were 0.4, 0.5, and 0.6. A wider range was adopted for plain cement concrete incorporating additional w/b ratios of 0.3 and 0.7. These w/b ratios were selected to produce a wide range of strength grades representative of the range of structural concretes used in marine conditions.

3.2.3 Curing regime

In the absence of proper curing measures, the concrete in the near-surface region experiences a loss of mix water to the environment. This can, on the one hand, leave it with large, open porosity due to hindered hydration and, on the other hand, make it susceptible to shrinkage cracking. Both adversely affect the transport properties of the cover concrete, which makes curing an important durability consideration. Hence, it is important to investigate the influence of different curing methods on the penetrability of concrete to chlorides in marine conditions. Of particular importance to service life prediction is the long-term effects of initial curing on concrete penetrability under marine environments.

In this study, two initial curing methods were adopted, namely, wet curing and plastic-wrap curing. These two methods were intended to provide a comparison between a standard lab curing method and a practical curing method. The selection of 28-day wet curing is based on the definition of potential durability indexes in the South African durability index approach, which is in line with quality control and design practices followed for compressive strength testing by the construction industry (SANS 3001-CO3-1, 2015; DI-Manual, 2018). For the field curing method, plastic curing till the age of 7 days was selected as it is a common practice in South Africa due to the scarcity of water. In addition to the early-age curing regimes, investigations involving prolonged wet curing were also carried out to study the time-development of concrete penetrability in simulated submerged conditions.

3.2.4 Tests and test parameters

3.2.4.1 Non-steady state chloride diffusion: C_s and D_a

The transport of chloride ions in concrete is typically modelled after non-steady state diffusion in saturated conditions to simplify the complex problem of chloride transport by focusing only on the dominant transport mechanism acting under natural marine conditions. In controlled studies, this is studied directly through simulation experiments. To investigate the potential resistance of concrete materials to chloride diffusion, standard bulk diffusion tests (NT BUILD 443, 1995; ASTM C1556, 2016) were adopted in this study, which serve as simulation experiments under submerged conditions. The typical exposure duration used in this study was 180 days. This was a practical compromise between achieving sufficient depth of penetration to ensure reliable chloride profile analysis and the total time required for an experiment. In selected cases, specimens were also exposed for longer durations of up to 760 days to study the time-dependence of diffusion parameters.

The saturated conditions of the bulk diffusion test enable the investigation of the relationship between chloride diffusivity and conductivity in ideal conditions. However, field conditions deviate from ideal conditions due to the following environmental influences: wet-dry cycles, temperature cycles, continuous leaching, chloride concentration differences, wave & other mechanical actions, organic growth, inorganic surface layers. It is essential to account for these influences in the service life model to provide reliable predictions for in-service conditions. In this study, the environmental influences are incorporated using parameters developed or adopted from previous South African field exposure data (Mackechnie, 2001; Heiyantuduwa-Beushausen, 2022). In terms of testing economics, the bulk diffusion test requires substantial time, labour, and equipment investment, which limits its relevance in routine testing.

3.2.4.2 Conduction: Chloride Conductivity and Resistivity

Electrical conductivity tests are used as a more practical alternative to chloride diffusion testing, especially for quality control. Various test methods exist globally and are adopted according to local preferences. The chloride conductivity test (SANS 3001-CO3-3, 2015) is commonly used in the South

African region and was adopted in this study. The chloride conductivity test has the advantage of robustness against the factors affecting conductivity measurements such as differences in moisture content and pore solution compositions between different concrete mixtures and requires relatively short testing duration (Streicher & Alexander, 1995). However, the specimens are required to be extracted from the structure or parent specimen by coring and slicing. In addition, the conditioning process takes over a week's time. While these methodological aspects improve the robustness of the test, they may be unfavourable to the project timeline. Thus, surface resistivity test was also included in this study with the following intentions:

1. A comparison of chloride conductivity results with surface resistivity results would give insight into the mechanistic underpinnings of the two test methods and their comparative advantages and limitations.
2. Surface resistivity being a non-destructive method may serve as a non-destructive counterpart to the chloride conductivity test for on-site use for quality control and compliance testing.

The bulk (uniaxial) resistivity test was also used in a selective way to analyse the effect of unsaturation on surface resistivity and to measure the cell constant correction factor for the specimen type used in the surface resistivity test in this study (Appendix D).

The tests were conducted typically at the age of 28 days to align with the quality control conventions. However, tests were also conducted at later ages to study the time-dependence of the respective conductivity measurements.

3.2.4.3 Other tests

28-day compressive strength of 100-mm concrete cubes was evaluated as a means to characterise the compressive strength grade of concrete mixtures used in this study. Other basic characterisation tests common to typical concrete studies were performed, namely, oxide composition, as deemed relevant to this study, the results of which will be discussed in relevant sections to follow.

Part I - Materials

3.3 Concrete materials and mix proportions

3.3.1 Binder properties

CEM I 52.5 N (Portland cement - PC) cement was used as the "control" binder. A siliceous Fly Ash (designation V (SANS 50197-1, 2013)) and Ground Granulated Blast-furnace Slag were used to partially replace Portland cement. The fly ash (FA) was used at replacement levels of 15 and 30%, whereas the slag (BS) was used at replacement levels of 25, 50, and 75%. PC, FA, and BS were sourced from PPC Ltd., Ash Resources (Lafarge Ltd.), and AfriSam Ltd., respectively. These are major suppliers of these materials in the South African region.

The chemical and physical properties of these binder materials are shown in Table 3.1, Table 3.2, and Figure 3.1. The oxide compositions were determined using wavelength dispersive XRF on fused disc specimens. The mass loss on ignition was measured by heating the specimens at 800°C for 4 hours. The XRD measurements were carried out using a powder diffractometer. The crystalline and amorphous phases were identified using the Bruker Topas 4.1 software and quantification was done by the Rietveld method. The detailed diffractograms for fly ash and slag are provided in Appendix C.

Table 3.1 Oxide composition of binder materials through XRF and crystalline phases through quantitative XRD

Oxide (% mass)	PC[1]	FA	BS
SiO_2	20.0	52.7	35.9
CaO	65.0	4.4	37.7
Al_2O_3	4.1	32.5	13.7
Fe_2O_3	3.5	3.1	0.6
MnO	-	0.0	1.3
MgO	0.9	1.0	7.8
TiO_2	-	1.6	0.6
Na_2O	0.1	0.5	0.1
K_2O	0.7	0.7	1.1
P_2O_5	-	0.5	0.0
SO_3	2.5	0.2	1.0
Cr_2O_3	-	0.0	0.0
NiO	-	0.0	0.0
LOI	3.1	1.1	-0.4[2]
Sum	99.8	98.4	99.5
Bogue Compounds: PC (% mass)		Crystalline phases: FA (%mass)	
C_3S	75.3	Mullite	35.0
C_2S	0.4	Quartz	11.4
C_3A	4.9	Calcite	1.8
C_4AF	10.7	Hatrurite	1.4
		Maghemite	1.4
		Brownmillerite	0.3

[1]From supplier (PPC Ltd.)
[2]An increase in mass occurs when sulphides in slag get oxidized during ignition (Thomas, 2013)

The oxide compositions shown here correspond well with the local literature (Fulton's, 2021). FA and BS are lighter materials compared to PC as reflected by their lower relative densities with the implication of producing more paste volume at a given binder mass than PC. This requires consideration in mix proportioning when using these materials.

The proportion of amorphous content is one of the main indicators of the potential reactivity of an SCM alongside composition and fineness. FA used in this study contained a little less than 50% amorphous content, which is on the lower end of the spectrum in the international context (Ramezanianpour, 2014). On the other hand, the BS used in this study was composed almost entirely of amorphous content. Figure 3.2 presents the particle size distributions of FA and BS, which shows that FA used in this study was finer than BS and contained a somewhat higher proportion of particles in the size range of 1-20 µm.

Table 3.2 Physical properties of the binder materials

Property	PC	FA	BS
Relative density*	3.14	2.36	2.9
Amorphous content^ (%mass)	-	49	>98

* Typical values obtained from the respective manufacturers
^Determined through X-ray diffraction analysis

Figure 3.1 The binder materials used in this study

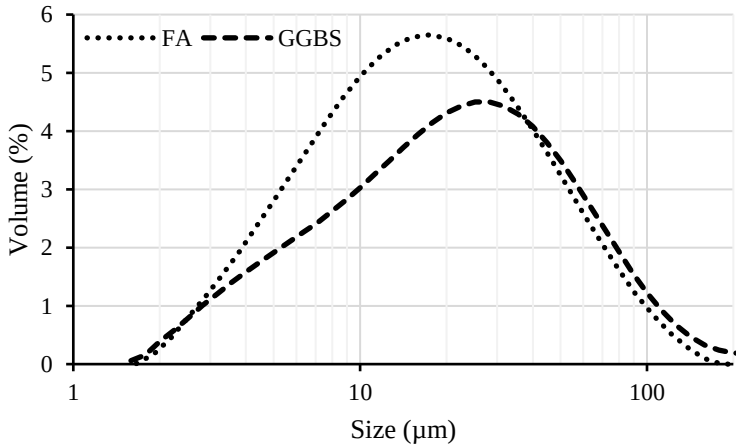

Figure 3.2 Particle size distribution of fly ash and slag used in this study, measured by laser diffraction

3.3.2 Aggregate properties

The Greywacke stone crushed aggregates of maximum size 19 mm are commonly used in concrete construction in the Western Cape region and were also used as the coarse aggregate in this study. For fine aggregate, a blend of natural Phillipi dune sand and crushed Greywacke sand was adopted to optimise mixture properties. The particle size distribution of all the aggregates used in this study were measured using the standard sieve analysis (SANS 201, 2008)and is presented in Figure 3.3.

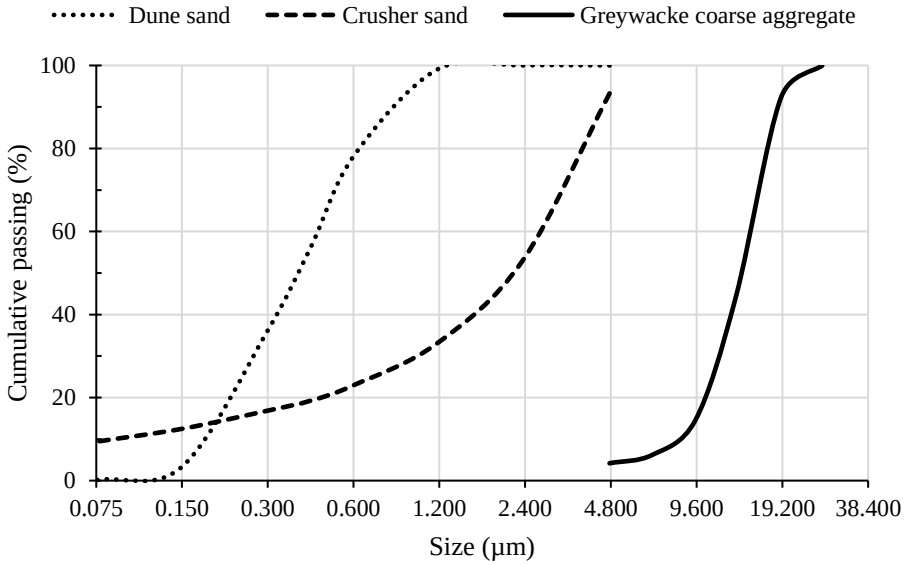

Figure 3.3 Particle size distribution of aggregates used in this study

The coarse aggregate particles were narrowly distributed between 10 and 20 mm. The dune sand was also narrowly distributed mainly in the size range of 0.1 – 1 mm. The crusher sand had a wider gradation with a significant proportion (20%) of fines (passing 425 µm) on the one hand and about half the particles bigger than 2 mm. Blending these two fine aggregates takes advantage of the different size fractions present in the two sands to achieve a well graded fine aggregate for the concrete. In addition, the round particles of the dune sand improve consistency, and the fines present in the crusher sand impart cohesiveness to the mix. On the basis of concrete mix trials, the proportion of dune sand to crushed sand of 60 : 40 was found to result in adequate workability and was therefore adopted for all the mix designs. The relative density and water absoprtion of the aggregates were measured using the pycnometer method (SANS 5844, 2014) are shown in Table 3.3, along with other details.

The fine aggregate was dried in a ventilated oven at 105ºC overnight and then cooled to room temperature before use in the manufacture of concrete. The coarse aggregate was already in a dry state. The aggregates were used in a dry state and a (minor) correction for the water absorption of aggregate was applied through changes in the quantities of mix water and the fine aggregate. It should be noted

that normally this correction is neglected in South African practice for low absorption aggregates such as those used in this study.

Table 3.3 Physical properties of the aggregates used in this study

Property	Dune sand	Crusher sand	Greywacke coarse aggregate
Relative density	2.65	2.72	2.72
Water absorption (%)	0.4	0.3	0
Particle shape	Round	Angular	Angular
Fineness modulus	1.8	3.7	-

3.3.3 Mix proportioning, casting, and basic characterisation

The CCSA method was used to arrive at the first estimate for the concrete mix design (Fulton's, 2021). These estimated proportions were then optimized for binder economy, ease of proportioning, and workability through trial and error. The desired consistency of the mix was obtained with the help of superplasticizers.

The replacement of cement with SCMs was done by keeping the paste volume constant between mixes with the same water-binder ratio, which resulted in differences in the total binder contents and water contents between *control* (PC – CEM I 52.5N) and *treatment* mixes (SCM). This so-called *"paste-equalisation method"* was used instead of keeping the binder and the water contents constant across all the same w/b class of mixes considering that it is the total paste volume through which the transport occurs rather than the binder or the water content. Keeping the binder mass constant across the same class of mixes would result in different total paste volumes—SCMs leading to higher paste contents owing to lower particle relative density compared to Portland cement (see Table 3.2). This would result in a concomitant change in the aggregate content. Since the effects of paste and aggregate are very different in relation to transport properties, variation in their relative proportions between different concrete mixtures would complicate the analysis. To establish control over these influencing parameters, it was preferred to normalise the paste volume and keep the aggregate content the same (at a given w/b ratio) instead of binder content.

The resulting total binder masses in the SCM concretes were lower than the control (PC) concretes. Although the reduction was not significant, it is advantageous in the economic and environmental context. The binder contents (kg/m^3) varied in the ranges: w/b-0.4 (425-407), w/b-0.5 (340-327), w/b-0.6 (283-274) and the water contents varied range: (170-163). Table 3.4 presents the detailed mix proportions. The consistency was perceptibly better in FA and BS mixtures. BS mixtures exhibited better cohesion.

The mixing operations were performed in a concrete pan mixer of 100 L capacity. All the dry materials were added first in the following sequence: coarse aggregate, binder, and fine aggregate. The dry

materials were mixed thoroughly before adding water and superplasticizer to the mix in that order. The slump of concrete, tested as per SANS 5862-1 (2006), was adjusted using a polycarboxylate ether based (PCE) superplasticizer. All the specimens were compacted on a compaction table (~3000 vibrations/min., 0.5-1 mm amplitude) for 15-25 s. The exposed face of the specimens was covered with a plastic sheet to avoid excessive evaporation.

The specimens belonging to a particular concrete mix regardless of the allocated curing regime were all produced on the same day from a continuous batch of concrete and were divided into two groups in a randomised fashion to be placed under either wet curing or plastic curing. This was done to minimize systematic variations other than the applied curing regime.

At the age of 28 days, the compressive strength tests were carried out on the wet cured specimens. The plastic cured concretes were tested after being immersed in water for 48 hours (SANS 5865, 1994). The compressive strength test was conducted using a compression testing machine at a load rate of 0.3 MPa/s, according to SANS 5863 (2006). The results, as shown in Table 3.4, correspond well with contemporary South African studies involving similar materials (Bakera, 2018; Sohawon, 2018; Gopinath, 2020).

Table 3.4 Concrete mixture details – mixture proportions, slump, and standard compressive strength

Binder type	w/b	CEM I 52.5N (kg/m^3)	FA (kg/m^3)	BS (kg/m^3)	Total binder (kg/m^3)	Water (kg/m^3)	Stone (kg/m^3)	Sand[1] (kg/m^3)	SP (l/l-b) %	Paste vol. (%)	Slump (mm)	Calc. density[2] (kg/m^3)	28-day wet cured density (kg/m^3)	28-day C.S.[3] (MPa)
CEM I 52.5 N	0.3	567	-	-	567	170	1000	755	2.8	35.0	>150	2492	2476	83.4 ± 5.8
	0.4	425	-	-	425	170	1000	876	1.1	30.5	90	2471	2472	65.2 ± 0.9
	0.5	340	-	-	340	170	1000	948	1.5	27.8	100	2458	2494	61.0 ± 0.6
	0.6	283	-	-	283	170	1000	997	1.3	26.0	80	2450	2395	44.6 ± 1.6
	0.7	243	-	-	243	170	1000	1031	0.8	24.7	80	2444	2407	33.6 ± 0.5
FA-15%	0.4	353	62	-	415	166	1000	876	1.4	30.5	150	2457	2435	62.8 ± 0.9
	0.5	283	50	-	333	167	1000	948	1.3	27.8	95	2448	2438	56.0 ± 5.5
	0.6	236	42	-	278	167	1000	998	0.9	26.0	115	2443	2424	37.3 ± 0.8
FA-30%	0.4	285	122	-	407	163	1000	877	0.6	30.5	100	2447	2466	61.0 ± 1.1
	0.5	229	98	-	327	163	1000	950	1.0	27.7	120	2440	2392	41.3 ± 0.1
	0.6	192	82	-	274	164	1000	997	1.0	26.0	100	2435	2424	32.5 ± 2.4
BS-25%	0.4	315	-	105	421	168	1000	877	1.6	30.5	140	2466	2406	73.2 ± 1.8
	0.5	252	-	84	337	168	1000	950	1.4	27.8	110	2455	2443	55.9 ± 2.0
	0.6	211	-	70	281	169	1000	998	1.3	26.0	115	2447	2368	45.5 ± 0.2
BS-50%	0.4	208	-	208	416	167	1000	877	0.9	30.5	100	2460	2420	60.4 ± 1.9
	0.5	167	-	167	334	167	1000	948	1.3	27.8	120	2449	2427	48.8 ± 0.4
	0.6	139	-	139	278	167	1000	998	1.2	25.9	90	2443	2397	33.9 ± 2.5
BS-75%	0.4	103	-	310	414	165	1000	876	0.9	30.5	>150	2455	2434	39.4 ± 0.6

[1]Dune sand : crusher sand - 60 : 40 (by mass)

[2]Theoretical density without air content based on constituent densities. Based on a comparison of this density and density measured on 100-mm saturated cubes, average air content was found to be 1%.

[3] C.S. – Mean compressive strength, tested on 100-mm cubes, wet cured for 28-days.
Variability in terms of S.D.

3.4 Curing methods

Two main curing methods were used in this study: wet curing and plastic curing. An additional curing regime was adopted, called here as wet-dry curing, for a specific part of the study. These are described below.

3.4.1 Wet curing regime

This curing regime involved the immersion of specimens in water tanks immediately after demoulding. The temperature of the water was kept at 21 °C ± 2 °C. The typical immersion period was 28 days. However, longer periods were also adopted in some cases for conductivity tests.

3.4.2 Plastic-wrap curing regime

Membrane-based curing methods are routinely used in the field in regions with water scarcity. Curing on the field is normally restricted to 7 days or even less for practical reasons. In addition to that, it has been found that there is little benefit in using membrane-based curing methods on normal strength concretes beyond a period of 7 days, with 3 days being the period of most effectiveness in the context of durability-related properties (Ho & Chirgwin, 1996; Wong et al., 2009). Accordingly, 7-day plastic-wrap curing was considered as the field-applicable curing method in this study. A thin film plastic wrap (cling wrap) was used in 2 layers to cover the specimen surfaces after demoulding. The thin film wrap was adopted for this purpose for the ease of wrapping specimen surfaces while ensuring that no gaps are left from which the moisture might escape. The specimens were stored under plastic wrapping at a temperature of 21 °C ± 2 °C and relative humidity of 55% ± 10% for 6 days (i.e., until the age of 7 days), after which the wrap was removed, and the specimens were stored in the same control environment for 21 days until testing. A schematic representation of the curing regimes is presented in Figure 3.4.

3.4.3 Wet-dry curing regime

The plastic curing regime involved air drying for 21 days, which left the concrete specimens in an unsaturated state. Before immersing these specimens into the NaCl solution for bulk diffusion experiments, these specimens were immersed in the saturated lime solution for 48 hours. This was done to saturate the specimens before the commencement of the diffusion experiments. This prevents capillary absorption and keeps diffusion the dominant transport process. However, immersion for 48 hours can only saturate the first few millimetres of concrete, leaving the remaining concrete partially saturated (Surana, Beushausen & Alexander, 2022). The diffusion coefficient decreases rapidly with the decrease in the degree of saturation (Zhang & Zhang, 2014). On the one hand, the effect of inferior curing is to increase the diffusion coefficient, but on the other hand, the lower degree of saturation may reduce the diffusion coefficient. In addition, capillary absorption also takes place in partially saturated concretes, albeit at a slow, diminishing rate after the first 48 hours. The net effect will be an interplay

of these factors. In order to distinguish between the effects of inferior curing on the pore structure development and the degree of saturation effects, a third curing regime was adopted—wet-dry curing.

Directly measuring the degree of saturation of concrete under non-steady conditions, for example, using an RH probe, is a tedious and time-consuming process (Rajabipour et al., 2005). More importantly, such measurements, useful as they are, cannot provide any direct evidence on their own on the significance of the internal unsaturation, if found, on chloride diffusion. Thus, it was decided to instead adopt a simpler phenomenological approach and simulate the air-drying part of the plastic curing regime on some of the wet cured specimens before diffusion experiments. A comparison of the diffusion results of the continuously wet cured specimens and the wet cured but dried specimens was expected to reveal the effect of drying on chloride diffusion, which was the main issue. In other words, concrete specimens were wet cured for 28 days and then, like the plastic curing regime, left to dry for 21 days in the lab before bulk diffusion experiments (Figure 3.4).

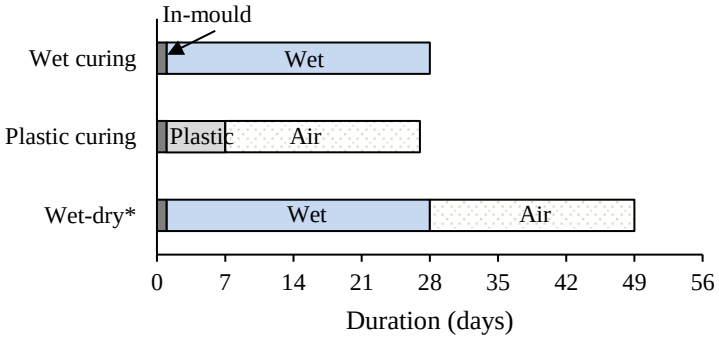

Figure 3.4 Schematic illustration of the curing regimes adopted in this study. *Wet-dry regime was only adopted for bulk diffusion testing.

It must be acknowledged that this approach comes with a possible drawback, that is, of introducing an error associated with further hydration during the drying period. However, it was found in this study that the plastic cured specimens stored in the same environment showed negligible changes in CCI over time, implying that this issue is not likely to significantly affect the analysis. It must be noted that this regime was adopted only for a few selected mixes deemed sufficient to enable a reasonably representative analysis. The selected mixes are listed in Table 3.5.

Table 3.5. Concrete mixes used for wet-dry regime

Binder type	w/b
PC	0.3, 0.4, 0.7
FA (15%)	0.4, 0.5, 0.6
FA (30%)	0.4
BS (50%)	0.4
BS (75%)	0.4

Part II - Testing

3.5 Chloride bulk diffusion test

3.5.1 Exposure specimens and exposure regime

100-mm cube specimens were used as the exposure specimens. The wet-cured specimens were taken out of the curing tanks and washed thoroughly under water using a nylon brush to remove any leaching residue or organic growth. The specimens were then surface dried using paper towels and left to further dry for about 6 hours before applying the epoxy coating. The washing step was unnecessary for the plastic cured specimens and thus was omitted. Five faces of each cube, leaving one face, were sealed with two layers of epoxy coating applied 4-6 hours apart and left in air to cure the coating overnight. Only one, moulded, face was exposed to the chloride solution with an intention for unidirectional chloride ingress into the specimes. Moulded faces are less susceptible to variable surface preparation and segregation effects during casting. This was consistent with the protocol used for the durability index testing (DI-Manual, 2018). Following the same protocol, the top 5 mm thick portion of concrete was cut off to avoid surface effects such as the wall effect, carbonation, demoulding oil absorption, etc. that could influence chloride ingress, (NT BUILD 443, 1995; DI-Manual, 2018).

The specimens were then immersed in a saturated calcium hydroxide solution for 48 hours. This was to ensure that the specimens were in a reasonably saturated condition before they were exposed to the chloride solution thereby ensuring that the chloride transport was only via diffusion. The standards for bulk diffusion testing recommend that the specimens be kept in the saturation solution until the mass change is less than 0.1 % in 24 h (NT BUILD 443, 1995; ASTM C1556, 2016). However, it is also noted that moist cured specimens typically need 48 hours to reach that limit (ASTM C1556, 2016). In this study, a duration of 48 h was selected for saturation on that basis. The duration was kept uniform across all the curing methods in the interest of time.

A sodium chloride solution with a molarity of 2.8 M (165 $g_{NaCl}/l_{solution}$) was used as the exposure solution using tap water (ASTM C1556, 2016). The tap water chloride content must be less than 300 mg/l (SANS 241, 2015), which is within the tolerance of 1 g/l specified by ASTM C 1556 for making the chloride solution. The specimens were removed from the lime solution after 48 h, washed to remove any residual lime, surface dried, and transferred to the exposure solution. Six specimens were stored in one exposure tank containing 15 litres of NaCl solution, i.e. 40 cm^2 exposed surface per litre of chloride solution, which is under the prescribed limits (20-80 cm^2/l) (NT BUILD 443, 1995; ASTM C1556, 2016). The exposure surfaces were laid horizontally facing the closing lid. The tanks were sealed to avoid evaporative loss of water through them and were stored at 21ºC for the entire exposure duration.

3.5.2 Sample preparation for chloride content testing

At the end of the exposure duration, exposure specimens were removed from the chloride solution and the exposed surface was washed immediately to remove any leaching products that may carbonate when exposed to air. 70-mm diameter cores were then extracted from the cube specimens using a minimal amount of water as a coolant. Cores were extracted to avoid the epoxy coating and the edge effects of the outer 5-10 mm section of concrete on the test results. The cores were lightly washed to remove any sludge from the coring process and were surface dried using paper towels. They were then left to dry for 24 hours in the lab air before they were sealed in thin-film plastic wrap to prevent any further moisture exchange with the environment. Because of the relatively large number of specimens tested in this study, it was not always possible to perform chloride profiling immediately after taking the specimens out of the solution. Therefore, in the meantime, cores, sealed with plastic wrapping, were stored at -15 ºC to arrest the diffusion process (NT BUILD 443, 1995; ASTM C1556, 2016).

In the next step, the cores were cut into thin slices using a concrete cutting machine, within a day of taking them out of the freezer. The amount of water during this process was kept to a minimum to avoid dissolving chlorides. ASTM C1218 (2020) notes that the amount of chlorides dissolved in the cooling water is generally very limited. Surface grinding using a milling machine was not used for this purpose as it was too time-consuming, hazardous due to the large amounts of dust generated in the surrounding air, and deemed unnecessary for the purposes of this study. ASTM C1556 (2016) also permits the use of water-cooled saw cutting procedure when the extent of chloride penetration is sufficient to obtain the minimum number of slices required (6-8) for the curve fitting operation. This was more-or-less the case in this study.

The length of the cores was measured, at four points, before and after cutting every slice and the thickness of the blade (2 mm) was subtracted to determine the average thickness of each slice and its position with respect to the exposed face. After cutting, the slices were dried overnight at 105ºC (BS EN 14629, 2007) to remove evaporable water from the concrete. After the drying period, the slices were taken out of the oven and cooled in air for 1-2 hours. Slices were ground to a fine powder (passing a 150-µm sieve) using a mechanical pulveriser (see Figure 3.5). The powdered sample was collected and stored in a resealable plastic bag until testing.

3.5.3 Chloride content determination through potentiometric titration

The measurement of total chloride content was preferred in this study to avoid uncertainties involved in the measurement of the free chloride content. The acid dissolution method was used to extract the total chloride content. The chloride content was measured by potentiometric titrations. An in-house procedure was used for the determination of acid-soluble chloride content as described below (Streicher, 1997). This method was preferred as it uses a smaller sample size for testing than the ASTM method for potentiometric titrations (ASTM C1152, 2004).

3.5.3.1 Sample preparation

1. Between 2.1 and 2.5 g of concrete sample was weighed into a plastic cup. The sample is brought to a suspension by adding enough water to cover the sample and then swirling the cup.
2. 2.0 ml of diluted nitric acid (1:1) was added to the suspension and left to stand for 30 minutes to bring all the chloride into solution.
3. 2.5 ml of sodium acetate solution was added after 30 minutes to adjust the pH to within the range of 4 to 7.
4. Deionized water was added to the cup to fill it to the 60 ml mark.

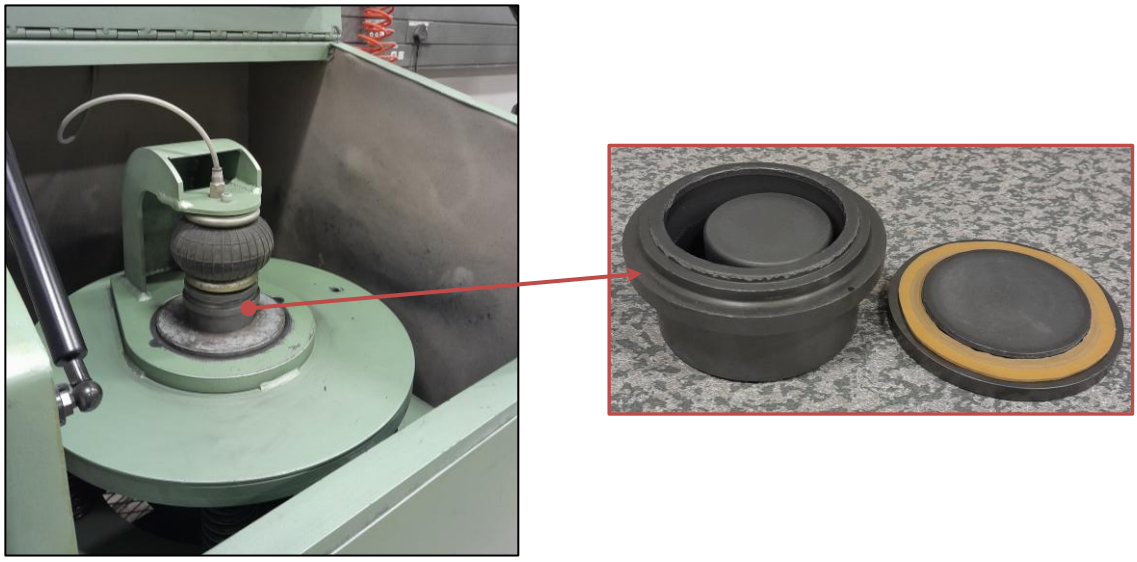

Figure 3.5: The pulveriser used for grinding the concrete samples to powder. The salient features are (a) the pneumatic clamping arrangement mounted on a spring-loaded vibrating bench (in the left image), and (b) the sample holder with the pulverizing pellet/disc (enlarged image on the right)

3.5.3.2 Testing

The chloride content was measured by titrating the prepared sample with 0.1 M silver nitrate solution using an automatic potentiometric titrator (Figure 3.6). The amount of silver nitrate required to reach the equivalence point is obtained, which is then converted into the percentage mass of chlorides with respect to the mass of concrete/binder using Eq. (3.1). Calibration testing was conducted at regular intervals. Typical calibration results on mortar samples with admixed chlorides are presented in Appendix H.

According to these results, the typical accuracy (trueness) and precision (variability, SD) of the measurements were typically within 6% and 1%, respectively. Higher percentage error and variability were encountered for very low chloride contents (<0.1%, bwc.). However, for the purpose of an investigation such as this, very low chloride contents are of minor significance. Considering the high accuracy and low variability of these measurements, a single test value was considered adequate.

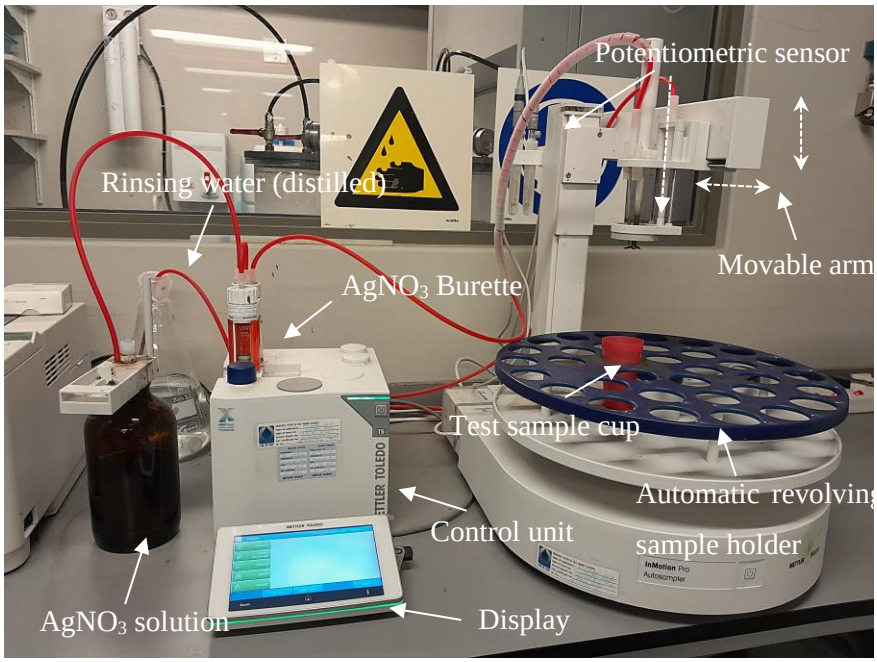

Figure 3.6: Automatic potentiometric titrator used in this study

$$C_{Cl,\%b} = \frac{V_{AgNO_3} \times M_{AgNO_3} \times m_{Cl}}{m_{w,c}} \times \frac{\rho_c}{m_{w,b}} \times 100 \quad (3.1)$$

Where

$C_{Cl,\%b}$	Chloride content by mass of binder, %
V_{AgNO_3}	Volume of titrant ($AgNO_3$), L
M_{AgNO_3}	Molarity of titrant ($AgNO_3$), M – moles/L
m_{Cl}	Molar mass of chlorine (35.5 x 10^{-3} kg/mol.)
$m_{w,c}$	Mass of concrete sample, kg
ρ_c	Density of concrete, kg/m^3
$m_{w,b}$	Binder content in concrete, kg/m^3

3.5.4 Chloride profile analysis: curve fitting

Chloride profiles are constructed by arranging the chloride contents on the 'y' axis and the mean chloride penetration depth on the 'x' axis. The ERFC solution is fitted into the measured chloride

profiles through non-linear regression analysis. This was performed using the CurveFit2003 spreadsheet program developed by Prof Tang Luping (Tang, 2003). The input parameters required for curve fitting for unidirectional diffusion are: chloride profile measurements, exposure duration, and initial chloride content. The analysis provides the following output: surface chloride content/concentration (C_s), apparent diffusion coefficient (D_a), and the fitted curve. Other details are described in the results chapter.

3.6 Electrical tests

3.6.1 Chloride conductivity

The chloride conductivity test was performed according to the method provided in the current South African standard (SANS 3001-CO3-1, 2015; SANS 3001-CO3-3, 2015; DI-Manual, 2018). Nevertheless, a brief description of the specimen preparation, preconditioning, and test process is also provided below.

3.6.1.1 Specimen preparation

70-mm diameter cores were extracted from 100-mm cube specimens at the end of the curing regime in the direction perpendicular to that of casting. Two 30-mm thick slices were obtained from the outer 5 – 35 mm depth range of the opposite ends of the core. The specimens were washed thoroughly with water and a nylon brush (SANS 3001-CO3-1, 2015; DI-Manual, 2018).

3.6.1.2 Preconditioning

The cylindrical disc specimens so obtained were dried in a ventilated oven at 50ºC for 7 days. After 7 days, the specimens were removed from the oven and kept in a desiccator for 2 to 4 hours to allow the specimens to cool down to the laboratory temperature of 21ºC. The dimensions of each specimen—diameter and thickness—were measured. The specimens were then vacuum-saturated with a solution of 292 g of NaCl per L of water using the standard procedure (SANS 3001-CO3-3, 2015).

3.6.1.3 Test method

The test method involves applying a potential difference across the concrete specimen saturated with the NaCl solution and measuring the current drawn. A potential difference of about 10 V is applied using two conduction cells positioned on either side of the specimen (see Figure 3.7).

These conduction cells are filled with the same NaCl solution which is used to saturate the specimens. The chloride ions are expected to migrate through concrete due to the applied potential difference in a steady state condition causing a current in the circuit. The current and the potential difference across the opposite faces of the specimens are measured, and the chloride conductivity index (CCI) is calculated using Eq. (3.2). In addition, the porosity penetrable to the NaCl solution was also calculated

by measuring the NaCl solution absorbed by the dried specimens, at the end of the vacuum saturation procedure. Four replicate specimens were tested for each result.

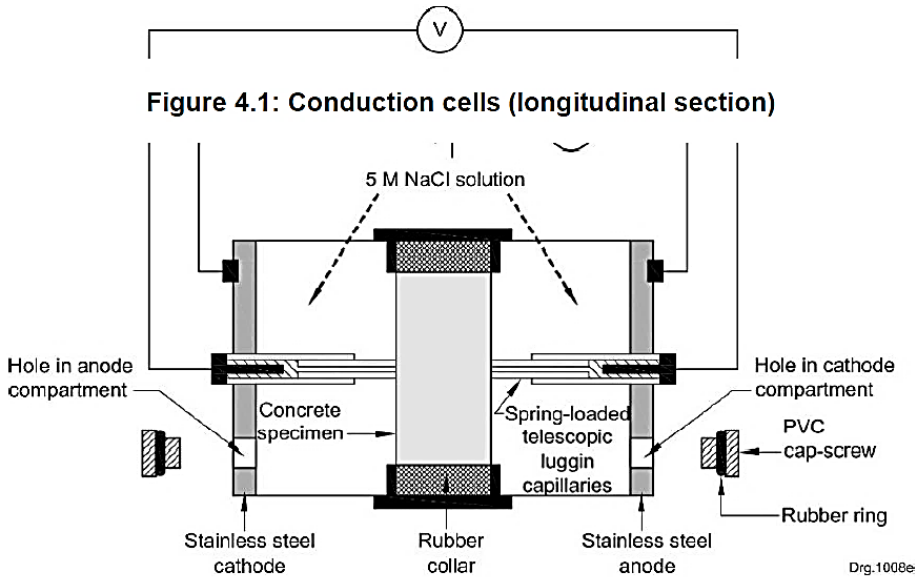

Figure 4.1: Conduction cells (longitudinal section)

Figure 3.7 A schematic of the chloride conductivity test apparatus (adopted from DI-Manual, 2018)

$$CCI = \frac{Id}{VA} \tag{3.2}$$

Where,

I	Current (mA)
V	Voltage (V)
d	Thickness of the specimen (mm)
A	Cross-sectional area (mm^2)

3.6.2 Surface resistivity

The surface resistivity (SR) method was performed largely in accordance with the AASHTO standard (AASHTO T 358, 2015), with the exception of the specimen design. 150-mm cube specimens were used in this study for resistivity testing as opposed to cylindrical specimens suggested in this standard. The cube specimens were selected instead of cylinder specimens following the quality control practices in South Africa, where cubes are preferred for compressive strength testing rather than cylinders, which is a standard practice in the US. Furthermore, both the specimens have the same limitation that they do

not have semi-infinite dimensions and require cell constant correction on the Wenner expression to arrive at the true resistivity. Conversely, both can be used for the purpose of comparison.

3.6.2.1 Specimen preparation

150-mm cube specimens were used for the determination of surface resistivity using the Wenner four probe method. Measurements were made only on the moulded faces for consistency. No additional surface preparation was done.

3.6.2.2 Preconditioning

The specimens were immersed in the curing tanks alongside other concrete specimens for 48 ± 2 h at the test age prior to testing. At the end of 48 hours, the specimens were taken out of the curing tanks, and the excess water was wiped off the surfaces. The measurements were taken as quickly as possible to avoid drying of the specimens. The continuously wet cured specimens and the plastic cured specimens were stored in the same curing tank for the saturation period to prevent any effect of a temperature difference between the two sets of specimens on the resistivity results.

3.6.2.3 Test method

A Proceq probe (Figure 3.8) with a probe spacing of 50 mm was used to take resistivity measurements with alternating current at a frequency of 40 Hz (Proceq SA, 2013). The resistivity is calculated automatically by the Proceq device using the Wenner expression for resistivity (Eq. (3.3)) (Wenner, 1915). Measurements were taken along the two diagonals of each tested face keeping the Wenner probe centred on the centre of the cube face as shown in Figure 3.8. The probes were wetted with tap water before every measurement to ensure proper electrical contact with the concrete surface. In total, 8 readings were taken per cube and 3 cubes were tested per result, i.e., every result is an average of 24 readings.

Previous studies have found that geometrical constraints of the specimen relative to the probe spacing and probe placement can affect the magnitude of resistivity measured (Gowers & Millard, 1999; Sengul & Gjørv, 2009; Angst & Elsener, 2014). These constraints include edge distance of the probe, specimen shape, depth/probe spacing ratio, and edge distance. The positioning of the end probes (current injecting probes), specifically, which are too close to the end in these specimens (25 mm), appear to have no practical influence on the measurements (Gowers & Millard, 1999). Regardless, the Wenner resistivity measurements conducted on small specimens such as used in this study cannot be taken to represent true resistivity of the material. Measurements taken on the same type of specimen can nevertheless be used beneficially for the purpose of comparison. In this study, the observed Wenner measurements are used as is for the purpose of comparison. The cell constant correction factor to convert these measurements to true resistivity is provided in Appendix D, if needed.

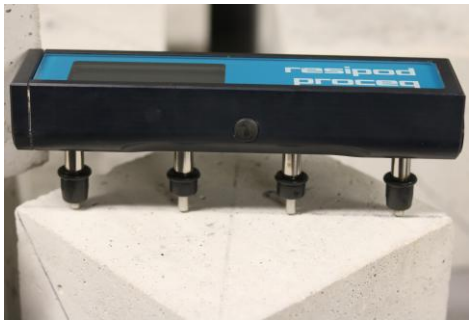

Figure 3.8: Surface resistivity test with a 4-point probe on a 150-mm cube

$$\rho = 2\pi a \frac{V}{I} \tag{3.3}$$

Where,

a Probe spacing (= 50 mm)

3.7 Summary

A lab-based experimental program was devised to investigate the relationship between conductivity index and diffusivity with a larger goal of formulating a service life prediction model addressing chloride-induced corrosion in marine conditions. Of the multitude of variables that characterise chloride transport in marine conditions, the most influential variables were selected based on the review of the literature. This simplification was essential to enable the study of this complex process under the practical constraints of a single study and also to allow the construction of a simple, yet informative model. The variables relevant to the material's resistance were included in the experimental program and the information on the variables relevant to the environmental actions were derived from previous studies.

The variables selected were binder type, w/b ratio, and curing method. The scope of variables used are as follows: 1. Binder type: plain Portland cement (CEM I 52.5N), fly ash blends with PC (15%, 30%), and slag blends with PC (25%, 50%, 75%); 2. w/b ratio: 0.3, 0.4, 0.5, 0.6, 0.7; 3. Curing methods: 28-day wet curing, 7-day plastic curing, 28-day wet/21-day dry curing.

The resistance of concrete to diffusion was studied through non-steady state diffusion experiments according to the bulk diffusion test protocol. These tests were selected as they simulate the natural chloride transport in an accelerated manner. Mainly two types of conductivity test methods were performed, namely: chloride conductivity and surface resistivity. The chloride conductivity test is

preferred in the South African durability approach. A chloride ingress model with chloride conductivity as an input parameter is highly desired. The surface resistivity test is selected in addition as a means of comparison and a possible non-destructive counterpart to the chloride conductivity tests. In essence, the methodology consists of exploring means of linking 28-day conductivity to the apparent diffusion coefficient and using other parameters to enable the prediction of chloride profiles.

Chapter 4 RESULTS

4.1 Introduction

This chapter presents the results of the experimental testing conducted in this study. The chapter is divided into three main sections comprising: (i) the analysis of conductivity results – chloride conductivity and surface resistivity, (ii) the analysis of the bulk diffusion results, and (iii) the investigation of the relationship between conductivity and diffusivity. The experimental methods and materials adopted in this study are described in Chapter 3.

More specifically, this chapter addresses the following objectives of the study:

1. To evaluate the influence of mix composition and curing on electrical and diffusion parameters.
2. To investigate the relationship between the apparent diffusion coefficient from the lab-based bulk diffusion tests and the chloride conductivity, for service life prediction using chloride conductivity measurements.
3. To assess the potential of using the surface resistivity method as an accompaniment to the chloride conductivity test.

In the presentation of data, the following notations are used to convey the meaning of the statistical parameters used:

a) ⊥ : Error bar
b) n: number of independent test observations per result
c) 95% CI: 95% confidence interval, which is calculated assuming Student's t distribution for sample data as per Eq. (4.1).

$$CI = t.\frac{SD}{\sqrt{n}} \tag{4.1}$$

Where, SD is the population standard deviation estimate based on sample dispersion. t is a constant for the t-distribution for n-1 degrees of freedom.

The outlier selection is based on 5% significance level according to ASTM E178 (2008).

4.2 Chloride conductivity and surface resistivity results: effect of mix composition and curing

4.2.1 Effect of binder

The 28-day chloride conductivity index (CCI) results of wet cured concretes in relation to the fly ash (FA) and blast furnace slag (BS) levels in the binder are presented in Figure 4.1 (a) and Figure 4.2 (a), respectively. The CCI results obtained in this study correspond well with the recent literature, which is demonstrated in Section 4.2.2.1. The surface resistivity (SR) values (in kΩ-cm) were inverted (i.e.,

1/SR) to obtain the surface conductivity (SC) values. This was done to facilitate easy comparison with CCI results. The variation of SC results with FA and BS levels are presented in Figure 4.1 (b) and Figure 4.2 (b), respectively. The SC values obtained in this study also generally agree with the literature (Dhanya, 2015).

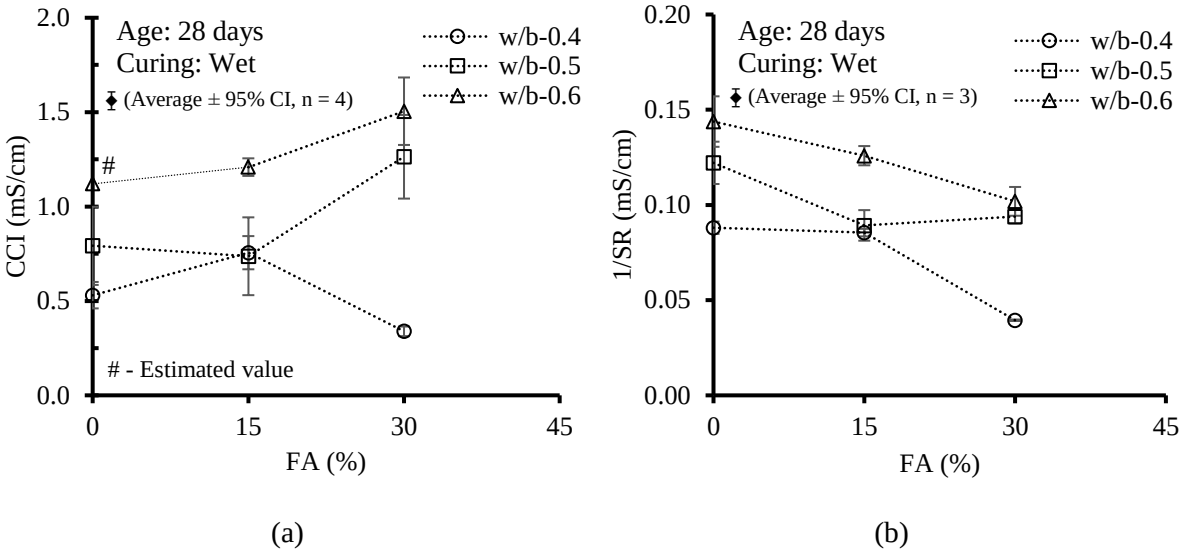

Figure 4.1 Variation with fly ash level (% mass): (a) 28-days CCI and (b) 28-day SC (1/SR). Note: The CCI result for PC-0.6 was a statistical outlier (ASTM E178, 2008) and therefore comparisons are made here with an estimated value based on the CCI-w/b relationship for PC concretes. For the original data point, refer to Section 4.2.2.

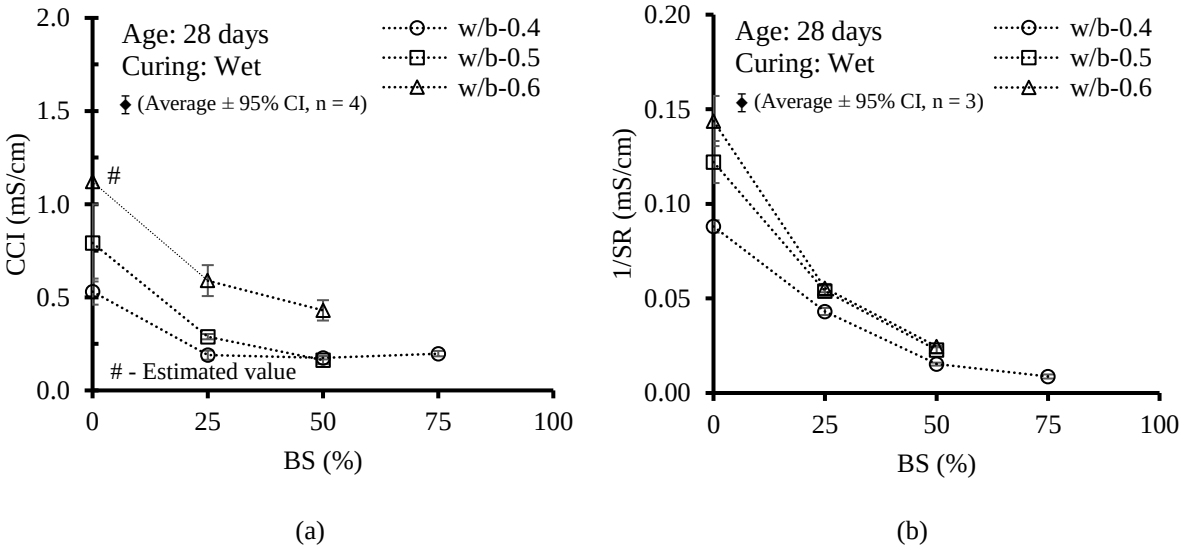

Figure 4.2 Variation with slag level (% mass): (a) 28-days CCI and (b) 28-day SC (1/SR)

In general, the CCI at the age of 28 days showed a moderate increase with the increase in FA levels. FA (30%), at the w/b ratio of 0.4 exhibited an exception to this trend by showing a decrease in the CCI. Besides this exception, the relative increase in the CCI appears to increase with the FA level (Figure

4.3). Since the CCI is inversely related to the formation factor (Eq. (1.8)), an increase in the CCI implies a reduction in the formation factor and vice versa. In contrast, the use of BS brings about sharp reductions in the CCI. The CCI reduces non-linearly with the BS%, i.e., the relative reduction decreases as the BS% increases and appears to produce no further gains beyond the BS level of 50%. Similar effects of FA and BS were observed on the 28-day gas (oxygen) permeability in recent previous studies (Omar, 2018; Gopinath, 2020).

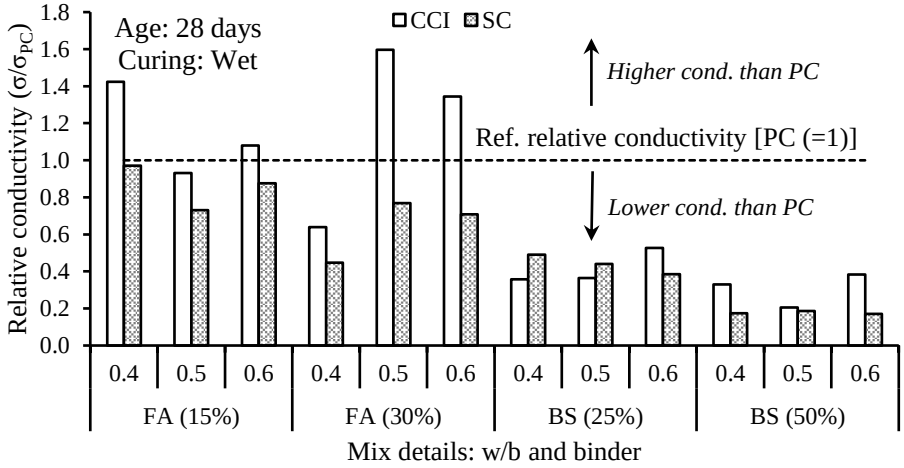

Figure 4.3 Effect of binder on CCI and SC through 'relative conductivity'. It is calculated by dividing the result with the corresponding result for PC concrete of the same w/b ratio.

It is important to consider that the findings under discussion from this study and elsewhere are based on a comparison at the same w/b ratio as opposed to a comparison at the same strength grade. The comparison at the same strength grade often necessitates a reduction of the w/b ratio in the case of slowly hydrating SCMs to reach the 28-day strength grade of the control mix. For instance, FA and BS in this study affected the compressive strength of concrete depending on the replacement level and w/b ratio as shown in Figure 4.4 (refer to Table 3.4 for other details). A comparison at the same grade could lead to different trends than a comparison at the same w/b ratio. Another possible reason for an apparent reversal in trends is an increase in CCI values of the control concretes due to the use of lower-grade cement. In a previous study, the CCI for FA and BS concretes were very similar to those found in this study, but the CCI of PC concretes were much higher due to the use of CEM I-42.5, resulting in the conclusion that FA produces superior microstructure within a month (Githachuri, Alexander & Moyo, 2012).

Under wet curing and w/b ratios ranging between 0.4-0.6, the mean 28-day CCI values were found to vary in the range 0.5-1.1 mS/cm for PC concretes, 0.3-1.5 mS/cm for FA concretes, and 0.2-0.6 mS/cm for BS concretes. The 28-day CCI values for FA concretes largely overlap the range of values for PC concretes, while most BS concretes showed superior (lower) CCI than PC concretes regardless of the w/b ratio and replacement level. Similar trends were reflected in the porosity results shown in Figure

4.5. This porosity was calculated based on the vacuum-saturated absorption of concrete to NaCl solution after oven drying (at 50˚C for 7 days) as part of the CCI testing. FA concretes showed either similar or higher porosities than PC concretes. Replacement with BS, on the other hand, exhibited larger reductions in porosity than were possible by reducing the w/b ratio from 0.6 to 0.4 in PC concretes.

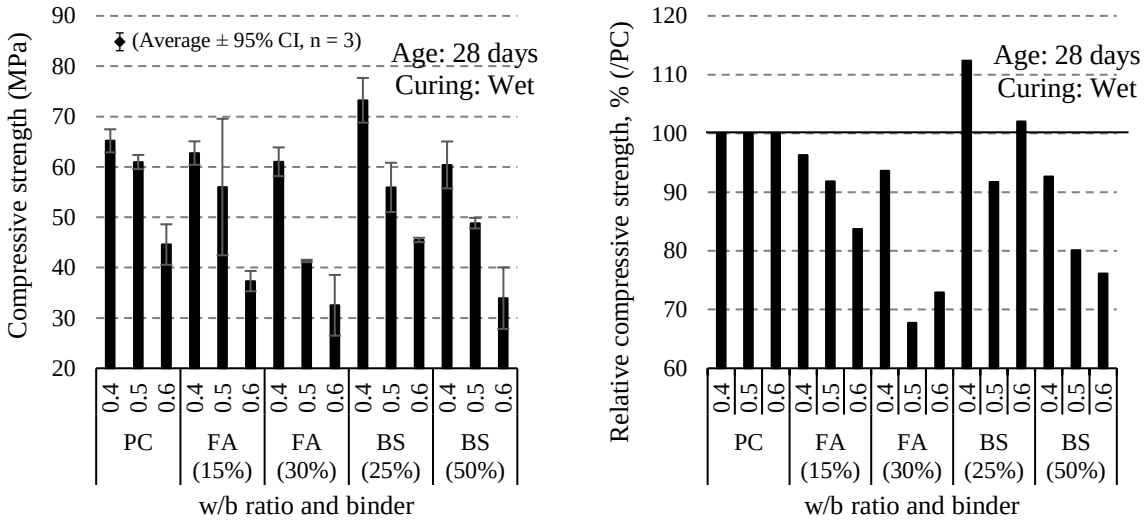

(a) (b)

Figure 4.4 (a) Compressive strength results and (b) Relative compressive strength to illustrate the effect of binder type on the 28-day concrete compressive strength: the ratio (%) of the 28-day compressive strength of concrete to that of the PC concrete of the same w/b ratio

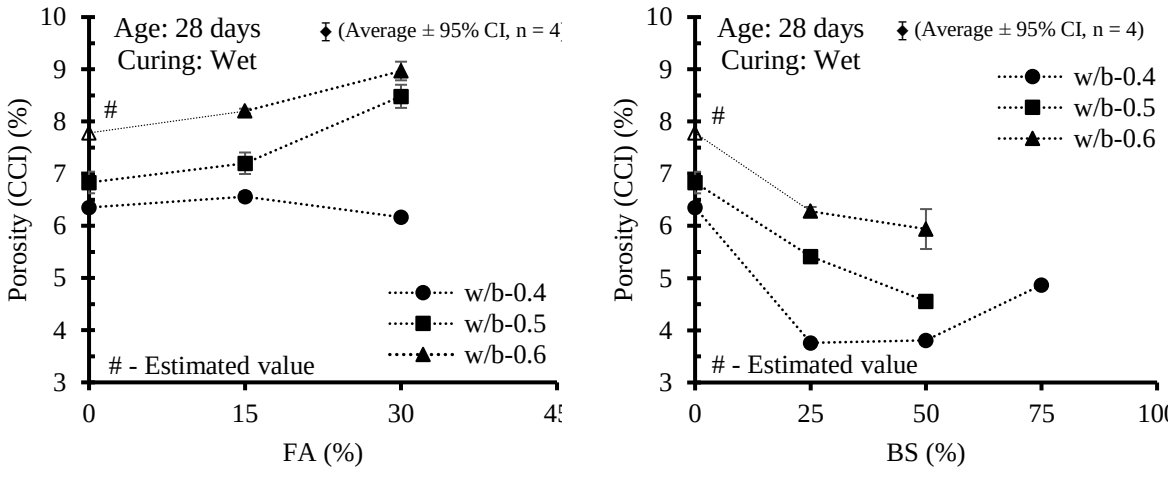

(a) (b)

Figure 4.5 Relationship between 28-day porosity (based on vacuum saturation with 4.4 M NaCl solution after 7 days of oven drying at 50°C) and SCM level (%, mass) in the binder: FA (a) and BS (b)

A preliminary analysis is performed to gain insights into the observed behaviour of FA up to 28 days in the context of penetrability. As a starting point, FA is assumed to be an inert filler for the sake of argument. The porosity and CCI calculated based upon this assumption are compared to the actual values and those of PC concretes at corresponding w/b ratios to evaluate the assumption made (Table 4.1 and Figure 4.6). The measured porosities of FA concretes are lower but lie close to the porosities calculated based on the above assumption. The measured CCI values on the other hand show a larger proportional reduction than porosities.

This improvement could be due to the filler effect and/or partial hydration of fly ash (Gutteridge & Dalziel, 1990). The overall behaviour of fly ash observed in this study is consistent with the reports of low reactivity of siliceous FA that it may stay nearly dormant for a week until very high pH (>13.2) is developed by the hydration of PC and may attain low degrees of hydration under the age of 1 month (Fraay, Bijen & De Haan, 1989; Berodier & Scrivener, 2015). The dissimilarity in the proportional effects on porosity and penetrability indicates that the presence of FA may have resulted in some pore refinement within the first 28 days. However, pore refinement due to FA is not consistently observed in the literature (Pandey & Sharma, 2000; Canut, 2011; Yu & Ye, 2013; Berodier & Scrivener, 2015; Dhandapani & Santhanam, 2017) and hence further studies are imperative to gain a better understanding of the behaviour of FA at the microstructure level. It is crucial to note that the discussion of FA blends so far has excluded the effect of continued curing (beyond 28 days), which may dramatically change its long-term performance and is discussed in Section 4.2.4. It should also be emphasised that SCMs vary in their properties based on their source and consequently, their influence on concrete properties is also subject to some variation.

Table 4.1 Comparison of the hypothetical porosity assuming no contribution from FA hydration with the measured porosity

(1)	(2)	(3)	(4)	(5)	(6)
Binder	w/b	w/c	Measured porosity[1] (%)	Estimated porosity (%)	Difference (%) (4)-(5)
FA (15%)	0.4	0.47	6.6	6.7	-2.0
	0.5	0.59	7.2	7.7	-7.0
	0.6	0.71	8.2	8.7	-6.0
FA (30%)	0.4	0.57	6.2	7.5	-22.4
	0.5	0.71	8.5	8.7	-2.9
	0.6	0.85	9.0	9.9	-10.7

Terminology: w/b: actual w/b ratio; w/c: w/b assuming FA inert; Estimated porosity: porosity of pure PC concrete at same w/c; Difference= (Measured porosity – estimated porosity)/Measured porosity

[1]Porosity measured through absorption of NaCl solution in oven-dried vacuum-saturated concrete

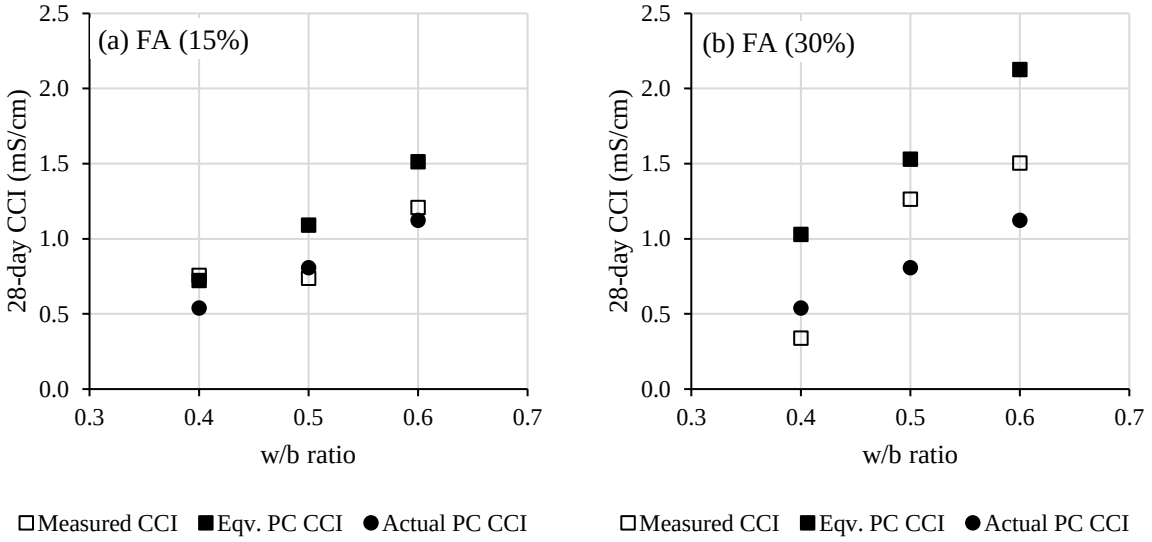

Figure 4.6 Comparison of the measured CCI of FA concretes with the hypothetical CCI considering FA as an inert filler. The equivalent PC CCI is the calculated CCI of PC concretes at w/b=w/c (column (3), Table 4.1), whereas the actual PC CCI are those measured at the given w/b ratios (shown on the 'x' axis).

The substitution with BS on the other hand had a major influence on the pore structure within the first 28 days as observed through the reductions in the overall porosity and CCI. Past studies have also shown that BS inclusion significantly refines the pore structure within the first 28 days due to the high reactivity of slag (Manmohan & Mehta, 1981; Berodier & Scrivener, 2015). However, the reduction in overall porosity with BS substitution observed in this study is contrary to the trends reported for MIP porosities (Pandey & Sharma, 2000; Yu & Ye, 2013; Berodier & Scrivener, 2015). In addition, increasing replacement levels may suppress the hydration of PC and tend to leave more unreacted slag in the mix (Lothenbach, Scrivener & Hooton, 2011). This could explain the reversal of trends beyond the 50% BS levels. In summary, the differences between the CCI trends of FA and BS are a reflection of their respective rates of hydration and arise from different rates of microstructure development.

A comparison of the CCI and SC results (Figure 4.1, Figure 4.2, and Figure 4.3) reveals interesting differences in trends as listed below:

1. A notable difference is in the range of conductivities of the two test methods within which the results lie as seen by the difference of an order of magnitude between the CCI and SC values.
2. The surface conductivity decreased with FA inclusion, which is contrary to the general trend observed in the CCI results.
3. A sharp reduction in surface conductivity was observed with the BS%, which corresponds with the CCI trends. However, the surface conductivity results did not exhibit a minimum

around 50% slag level like the CCI and porosity (CCI) results, instead the surface conductivity decreased further when the slag level reached 75%.

To understand the cause(s) of these differences, one must analyse the differences in the measurement processes of the two test methods given that the material (concrete) itself, which was prepared and cured in common batches per mix, is likely to be similar between the two test methods. The measurement of the CCI and the SC differ in the following aspects: (i) specimen preparation (including (pre-/)conditioning) and (ii) conductivity measurement technique (AC/DC, geometric arrangement of probes).

The geometric arrangement of probes (uniaxial/surface) used for the electrical measurements on small specimens may result in different conductivity values (Morris, Moreno & Sagüés, 1996). For instance, the Wenner 4-probe arrangement results in conductivities that are generally 0.72 times the uniaxial conductivities, both measured on the same specimens (refer to Appendix D). Similarly, a comparison of the surface conductivity of continuously immersed cubes with the uniaxial conductivities of disc specimens (oven dried and vacuum saturated with lime water) to include the effect of specimen preparation and preconditioning indicates a ratio of 0.5 between the two. The lower conductivity ratio of 0.5 could be partly a result of the differences in the pre-/conditioning procedures, namely (i) higher effectiveness of oven-drying and vacuum saturation in saturating the specimen, and (ii) potential microstructural damage due to these procedures.

The most important difference however lies in the use of a highly conductive saturating solution for specimen conditioning in the CCI method. Using a saturating solution of conductivity 2-5 times that of the concrete pore solution is likely the major cause of the differences in the absolute values of the conductivity measured in the two methods. The saturation of concrete specimen with concentrated NaCl solution prior to conductivity measurement in the CCI method ensures that the variable contribution of the original pore solution is diminished. Therefore, the influence of mix composition, such as binder or w/b ratio, on pore solution conductivity is also diminished. A change in the CCI upon a change in the concrete mixture design (or treatment such as curing) consequently is indicative largely of the influence of the given change on the penetrability of the concrete pore structure to the transport of chloride ions. Although the binding of chloride and alkali ions from the saturating solution to the hydration products is likely, the high initial concentration of the solution and relatively short exposure period are expected to mitigate the differential errors.

The SC method on the other hand is influenced by the pore solution conductivity, which in turn is dependent on the pore solution composition and the degree of pore saturation. Under continuous immersion for 27 days, the differences in the degree of saturation in different concrete mixtures may become relatively small. This would suggest that the difference between the trends of CCI and SC is likely to mainly emanate from the differences in the pore solution composition/conductivity.

This could explain the contrasts observed between the CCI and SC trends for FA concretes. It is well documented that increasing the replacement of cement with siliceous fly ash, without high alkali content, generally decreases the pore solution conductivity (Diamond, 1981; Shehata, Thomas & Bleszynski, 1999; Thomas, 2011; Scott & Alexander, 2016). This means that despite no general improvement in the pore structure due to substitution by fly ash up to 28 days as evidenced by the CCI results, the surface conductivity would have reduced owing to the reduction in the pore solution conductivity. In the case of slag, the conductivity reduced significantly due to a reduction in penetrability, and the reductions due to a decrease in pore solution conductivity further would have added to lowering the concrete conductivity. This may explain the reduction of SC upon increasing the BS levels from 50% to 75% contrary to the CCI trends.

Such influences of pore solution conductivity can make interpretation of conductivity measurements difficult and may even lead to misunderstandings. This is particularly the case when pore solution effects are ignored, or sometimes with the use of simplified models for determining pore solution composition. For instance, the pore solution conductivities predicted by the NIST calculator (NIST, 2019) for 28-day old wet cured fly ash concretes (Figure 4.7) increase with FA%, which contradicts the experimental evidence from the literature and inferences from this study. This conclusion is consistent with the findings of a previous study (Mukhopadhyay, Liu & Jalal, 2019).

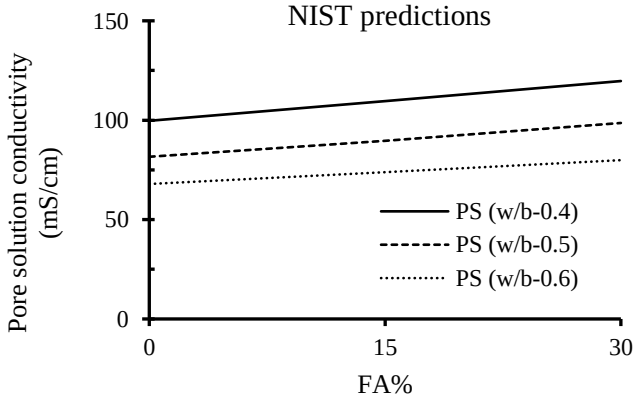

Figure 4.7 NIST predictions of pore solution (PS) conductivity for fly ash concretes (NIST, 2019), which are not consistent with the experimental evidence reported in the literature.

4.2.2 Effect of w/b ratio

The variation of the CCI and the SC results with the w/b ratio for different binders is presented in Figure 4.8. In general, both the CCI and SC increased with increasing w/b ratio, independent of the binder group. The increase in the CCI with the increase in the w/b ratio can be ascribed to the rise in capillary pore volume, which also increases the pore connectivity resulting in an increase in the penetrability of concrete (Goto & Roy, 1981).

The relationship of the SC with the w/b ratio, on the other hand, depends on the effect of the w/b ratio on the pore structure as well as on the conductivity of the pore solution. While an increase in the w/b ratio would increase the penetrability of the pore structure, it may decrease the conductivity of the pore solution. The effect of the w/b ratio on the pore solution conductivity is a function of the degree of hydration (↑), the volume of free water (↓), the concentration dependence of the ionic conductivity (↑, with a diminishing rate), and the degree of leaching (↓) during curing and conditioning of the specimen (Snyder et al., 2003; Bentz, 2007). Among the listed factors, the dilution effects that lower the ionic concentration of the pore solution tend to dominate and the pore solution conductivity tends to decrease with the increase in the w/b ratio, as reported by Christensen et al. (1994). The net effect of these two counteracting effects may explain the observed lower sensitivity (visibly flatter slopes) of the SC with respect to the w/b ratio, compared to the CCI.

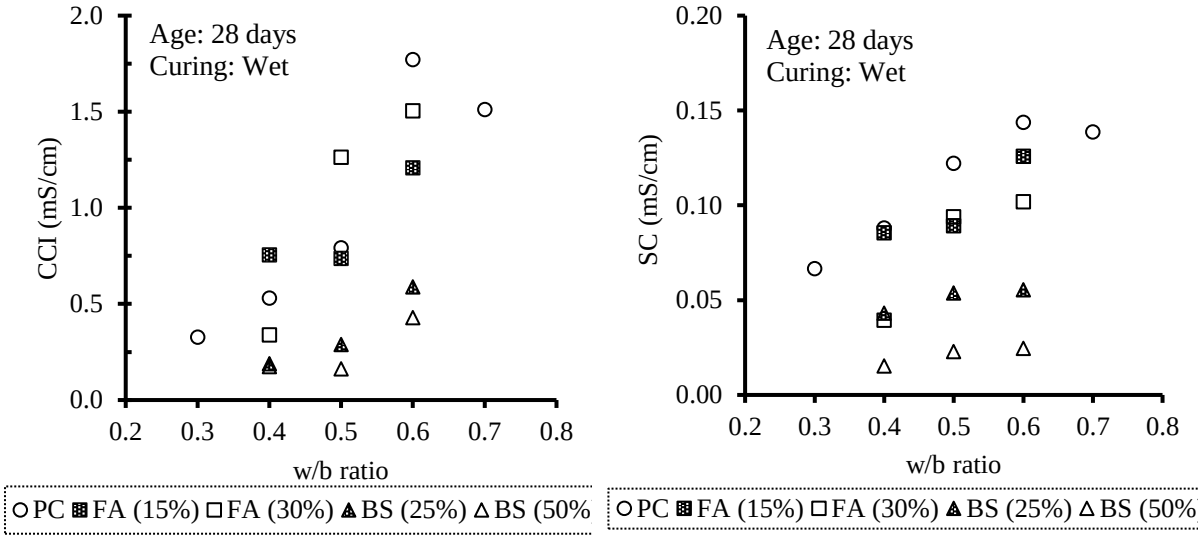

(a) (b)

Figure 4.8 Variation of (a) 28-day CCI and (b) 28-day SC (1/SR), with w/b ratio

In terms of binder-specific trends, the PC concretes showed a very clear and close relationship between CCI and w/b ratio. The FA concretes on the other hand exhibited a larger scatter around the average FA trends with respect to the w/b ratio. For instance, the FA (30%), w/b-0.4 concrete showed a lower-than-expected value of 0.34 mS/cm. The same concrete had yielded a value of 0.6 mS/cm in a previous batch. It is also interesting to note that changing the w/b ratio from 0.6 to 0.4 in PC concretes produces a smaller change in the CCI than replacing 25% of cement with slag at a w/b ratio of 0.6. This shows that substitution with slag is far more efficient in reducing the penetrability while decreasing the total binder content.

4.2.2.1 *CCI prediction*

The relationship between the 28-day CCI and the w/b ratio can be derived using the CCI-porosity relationship, shown in Figure 4.9, which strongly resembles the empirical relation of Archie's law (Eq. (1.7)). For the purpose of exploring this relationship, the porosity used was measured using the CCI protocol, which in brief involves vacuum saturation of oven-dried specimens with a 4.4 M NaCl solution (SANS 3001-CO3-3, 2015). The relationship between CCI and porosity appears independent of the binder blends. It also appears to be largely independent of curing and age, not shown in the figure, although these factors do introduce additional scatter in the data. Based on these observations, the 28-day wet-cured CCI can be expressed as a function of the porosity as shown in Eq. (4.2).

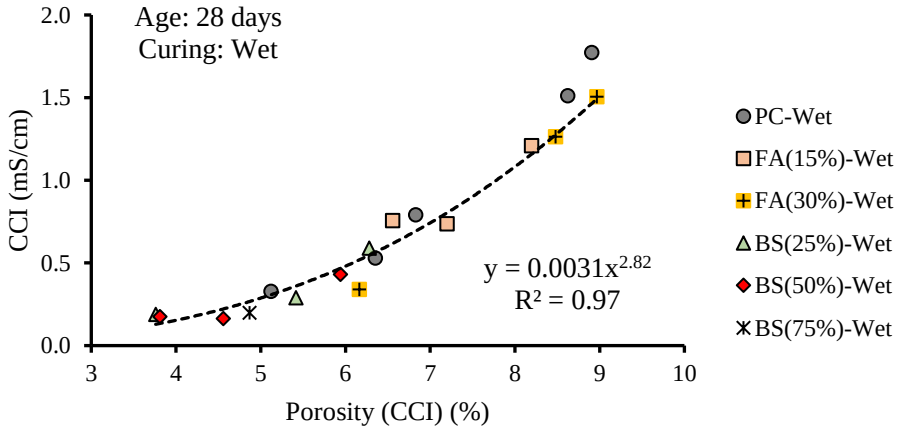

Figure 4.9 Relationship between CCI and porosity (CCI). The porosity referred to here is based on vacuum saturation with a 4.4 M NaCl solution of oven-dried concrete, as per (SANS 3001-CO3-3, 2015)

$$CCI = (3.08 \times 10^{-3}) \cdot {\varphi_{CCI}}^{2.82} \tag{4.2}$$

Where, φ_{CCI} is the porosity measured by the CCI method.

Figure 4.10 shows the relationships between porosity (CCI protocol) and w/b ratio for different binder groups. The porosity varies linearly with the w/b ratio and the linear function seems to remain approximately uniform across different binder types and only requires translation on the porosity axis depending on the binder type as shown in Figure 4.10 and Eq. (4.2).

The intercept (on the porosity axis) was estimated and described as a function of the SCM level as shown in Figure 4.11 and Eq. (4.4). As observed in the porosity results of BS, the porosity follows a non-linear relationship with the BS level, where porosity decreases with the BS level up to a certain point and starts increasing thereafter. Hence, a quadratic function seems justifiable and is used to describe porosity (intercept) as a function of the BS level (Figure 4.11).

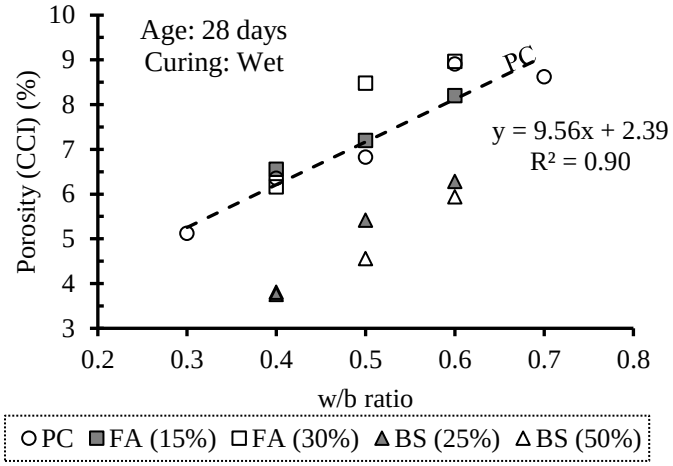

Figure 4.10 Variation of porosity (CCI) with w/b ratio

$$\varphi_{CCI} = 9.56\frac{w}{b} + \delta_b \tag{4.3}$$

Where, δ_b is a constant dependent on the binder type.

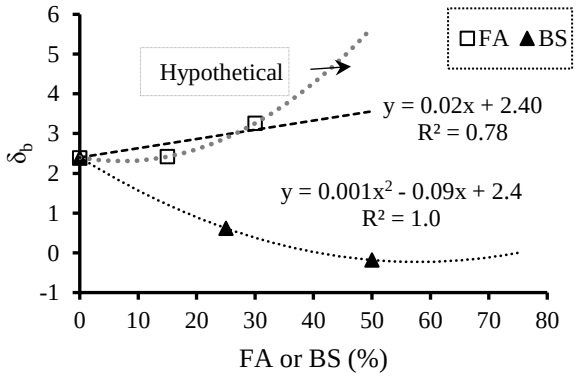

Figure 4.11 δ_b (binder-dependent intercept parameter for the porosity-w/b ratio relationship) as a function of SCM%. Note the difference between the predictions of a linear and a hypothetical curve for FA beyond the range of experimental data used.

$$\delta_b = \begin{cases} 2.4 + 0.02 \cdot FA\%, & SCM: FA \\ 2.4 - 0.09 \cdot BS\% + 0.001(BS\%)^2, & SCM: BS \end{cases} \tag{4.4}$$

The value of δ_b for plain Portland cement (CEM I-52.5N) is 2.4.

Similarly, the FA%-porosity relationship is likely to follow a non-linear function. However, due to a lack of sufficient data points, errors are likely, which tend to compound in a non-linear function. To avoid the risk of excessive errors upon possible extrapolation, a linear function is used for now until more data on higher replacement levels become available. The potential CCI at 28 days can be estimated

using Eq. (4.2)-(4.4) or the combined form presented in Table 4.2. A more fundamental w/b-porosity relationship can also be derived in future studies from theoretical considerations to enable further generalization.

Table 4.2 Prediction model for estimating 28-day wet cured CCI (mS/cm)

$$CCI = (3.08 \times 10^{-3}) \cdot \left(9.56\frac{w}{b} + \delta_b\right)^{2.82}$$

$$\text{Where, } \delta_b = \begin{cases} 2.4 + 0.02 \cdot FA\%, & SCM: FA \\ 2.4 - 0.09 \cdot BS\% + 0.001(BS\%)^2, & SCM: BS \end{cases}$$

**FA: fly ash, BS: blastfurnace slag*

Studying and predicting the effect of the w/b ratio on concrete is not as straightforward as paste due to practical constraints involved in mix proportioning. The w/b ratio can be varied while keeping the paste volume constant across all w/b ratios by adjusting the binder content and water content, thereby keeping the aggregate proportion and its effect uniform. However, rather than keeping the paste volume constant across different w/b ratios, often the water content is kept constant to obtain similar workability and reduce cost, among other things. The reduction in the paste content, for example, by increasing the w/b ratio is compensated by increasing the aggregate content. The same practice was followed in the present study for its practical relevance. A likely practical drawback of using a uniform water content is that the resulting property-w/b relationships may not lend themselves to other water contents. Since the water content changes in accordance with aggregate properties and workability requirements, this could be an impediment to the generalization of the derived relationships. Hence, a comparison with various past studies is used to assess this matter and validate the derived relationships.

The data were collected from relatively recent studies, from year 2015 onwards after the revision of the CCI test setup in 2014 (Otieno & Alexander, 2015). Other criteria for data collection to maintain consistency with the present data were as follows: PC type (CEM I or II (42.5N or 52.5N)), curing (continuous wet curing), and age (28 days). The coarse aggregate content was also generally uniform across the data at around 1000 kg/m^3. The selected studies were performed in well controlled laboratory conditions at the University of Cape Town and the University of the Witwatersrand by different researchers. The range of water contents used (160-200 kg/m^3) represents the typical range in practical use. The results are shown in Figure 4.12. Although more than one variable unavoidably varied at the same time, overall conclusions can be drawn from this analysis as presented below:

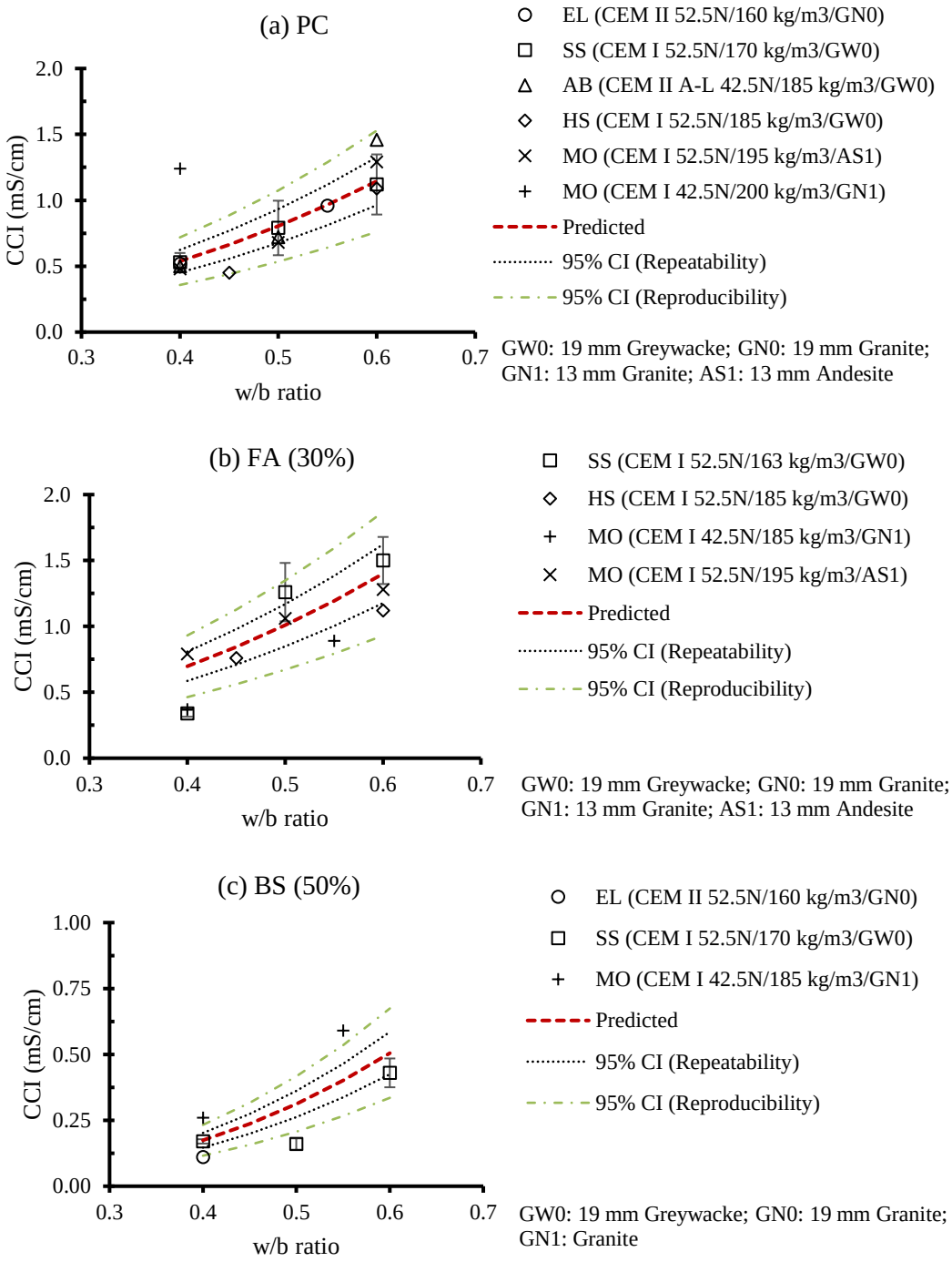

Figure 4.12 Comparison of the predicted values of 28-day wet cured CCI with the literature. The legend includes the Portland cement type, water content, and aggregate details. Data sources: SS: present study; AB: (Bakera, 2018); EL: (Leo, 2022); HS: (Sohawon, 2018); MO: (Otieno, 2018), (Otieno, 2014). The predicted values were estimated using Table 4.2. Note: Repeatability SD = 10% (SANS 3001-CO3-3, 2015), n = 4.

A total of 6 data sets were collected for PC concretes based on the criteria mentioned above. The CCI results for PC concretes from these data sets generally show a strong correspondence at a given w/b ratio. Although to a limited degree, the aggregate type and size varied in the studies used for this analysis

as shown in the figure legend. Past studies have found no identifiable influence of aggregate type and size, commonly in use in South Africa, on CCI results (Githachuri, 2010; Loseby, Alexander & Beushausen, 2016). In the absence of a significant competing/cancelling effect of aggregate characteristics, the general lack of significant differences in various data sets points to a corresponding lack of influence of water content on the CCI results. Practically small and inconsistent effects on CCI with large changes in water content have also been reported previously (Angelucci, 2013). Fewer data sets could be obtained for SCM concretes for this analysis.

Model estimates were evaluated for prediction accuracy against the data collected from different studies, through significance testing under repeatability and reproducibility conditions. Repeatability conditions refer to tests conducted by a single operator in a single laboratory with identical materials and setups (ASTM E177, 2020). Reproducibility conditions refer to tests conducted on identical materials in different laboratories by different operators (ASTM E177, 2020). While repeatability conditions are used to assess the differences between results within a single study, reproducibility conditions are used to compare results between different studies. Although the data are collected from different studies, most of the data points for PC concretes (8/11, excluding data from the present study) lie within the 95% confidence intervals for repeatability condition. This shows an excellent agreement between the collected PC data and the predicted values and the dominant influence of the w/b ratio on the CCI. In contrast, the agreement appears less certain in the case of SCM concretes, although only a few data sets were available. More data, especially on fly ash and slag concretes and other cement grades, are needed to further validate and possibly improve the predictions.

4.2.3 Effect of curing

The CCI results for the two curing methods compared in this study, namely wet and plastic curing, are presented in Figure 4.13. Wet curing refers to continuous immersion in water until testing, whereas plastic curing refers to plastic wrapping until the age of 7 days and thereafter open-to-air storage in the lab until the age of testing.

A statistical analysis was performed to evaluate the significance of the observed mean differences in the CCI of the two studied curing methods and the outcome is reported in Table 4.3. The results show that plastic curing led to higher CCI than wet curing in most of the SCM concretes at a statistical significance level of 5%. On the other hand, the PC concretes mostly showed statistically insignificant increases in CCI due to plastic curing.

PC typically exhibits high rates of hydration in the first few days, which decreases substantially after the first week as higher degrees of hydration are achieved. Therefore, only small improvements in the penetrability can be observed by increasing the curing duration to 28 days (Ballim, 1993; Li, Otsuki & Yuan, 2009; Surana, Pillai & Santhanam, 2017). The present results indicate the same phenomenon.

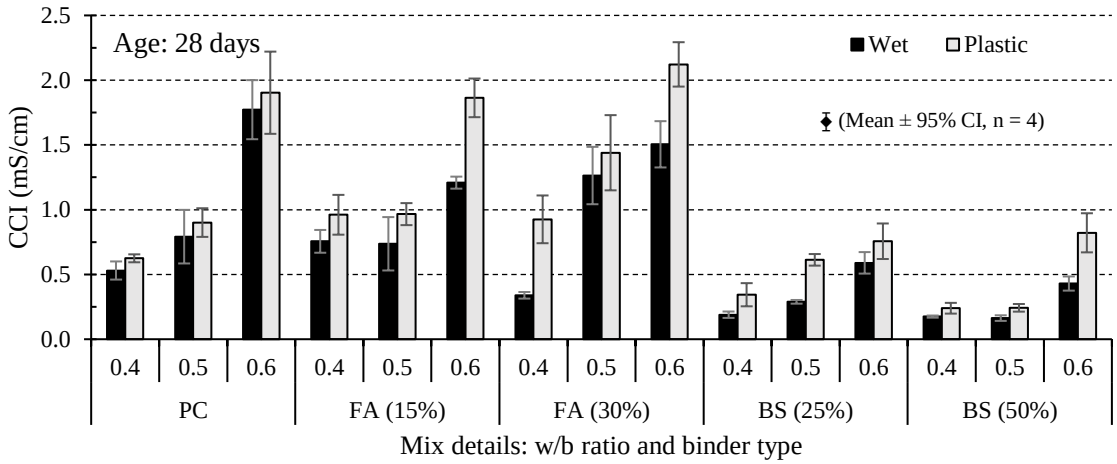

Figure 4.13 Effect of curing method on 28-day CCI. Wet: continuously wet; Plastic: 7 days under plastic, 21 days in air

Table 4.3 Results of the Student's t-test for significance of the differences between mean CCI of wet cured and plastic cured concretes

Mix	S/NS	Mix	S/NS	Mix	S/NS
PC-0.3	NS	FA(15%)-0.4	S	BS(25%)-0.4	S
PC-0.4	S	FA(15%)-0.5	S	BS(25%)-0.5	S
PC-0.5	NS	FA(15%)-0.6	S	BS(25%)-0.6	S
PC-0.6	NS	FA(30%)-0.4	S	BS(50%)-0.4	S
PC-0.7	S	FA(30%)-0.5	NS	BS(50%)-0.5	S
		FA(30%)-0.6	S	BS(50%)-0.6	S
				BS(75%)-0.4	S

*Note: One-tailed t-test, degrees of freedom – 6, significance level – 0.05 | Significant (S): $t > 1.943$, Not significant (NS): $t \leq 1.943$

FA and BS concretes on the other hand were affected to a larger degree than PC concretes. This is consistent with the literature and is generally ascribed to the slower rates of hydration typical of FA and BS compared to PC (Thomas, 1989; Mackechnie, 1996; Streicher, 1997; Zhang et al., 1999; Beushausen, Höhlig & Martin, 2016). The degree to which an individual mix was affected varied such that approximately half the mixes showed a large increase, and the other half showed a relatively modest increase. No consistent trend was observed with respect to the replacement level or the w/b ratio. The effect of curing and binder can be quantitatively appreciated in terms of equivalent w/c ratio in reference to the wet cured PC concretes as shown in Table 4.4.

The effect of curing was also apparent on the porosity (CCI) and the cube compressive strength at 28 days (Figure 4.14). These results constitute additional evidence of the effect of curing on concrete specimens used in this study. A contrast in the degrees to which curing affects near-surface properties such as CCI (and near-surface porosity) and bulk properties such as compressive strength can also be observed through these results.

Table 4.4 Equivalent PC-Wet w/b ratios based on 28-day CCI. A comparison under the same curing method reveals the effect of binder, and a comparison between curing methods illustrates the effect of curing on a given mix.

Actual w/b	PC		FA (15%)		FA (30%)		BS (25%)		BS (50%)	
	Wet	Plastic	Wet	Plastic	Wet	Plastic	Wet	Plastic	Wet	Plastic
0.4	0.40	0.45	0.50	0.55	0.30	0.55	0.20	0.30	0.20	0.25
0.5	0.50	0.55	0.50	0.55	0.65	0.70	0.30	0.45	0.20	0.25
0.6	0.75	0.80	0.60	0.80	0.70	0.85	0.40	0.50	0.35	0.50

Note: Eqv. w/b ratios are estimated using the CCI-w/b relationship for PC (wet cured) concretes (Table 4.2). The w/b ratios have been rounded off to the nearest 0.05. The cases with a difference of or over 0.1 w/b ratio are highlighted.

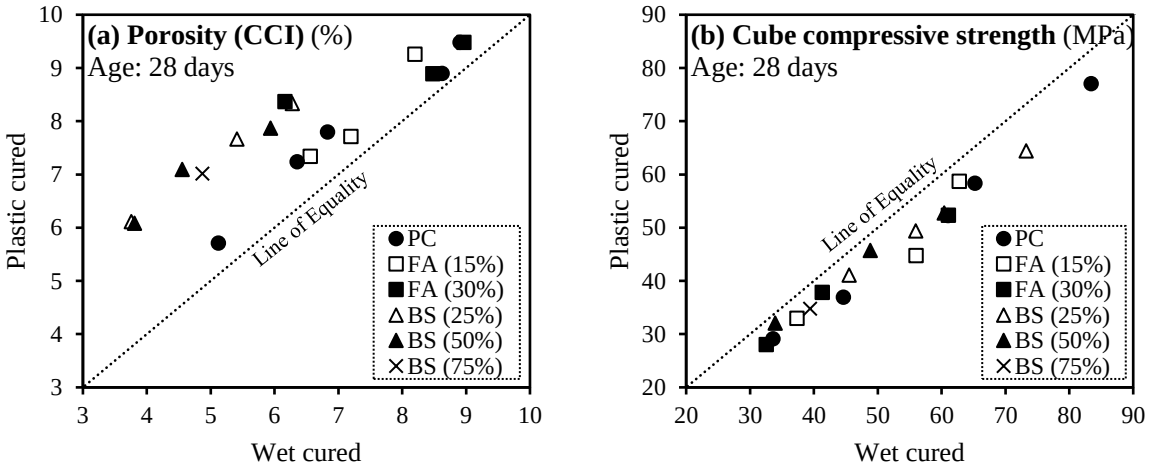

Figure 4.14 Influence of curing method on (a) 28-day porosity (measured using CCI protocol on near-surface 30-mm discs) and (b) 28-day compressive strength (100-mm cubes).

The effect of curing was also evaluated through the surface conductivity method. To avoid the lack of saturation interfering with a valid comparison between the two curing methods, the plastic cured specimens were immersed in water for 48 hours before testing, based on a common practice followed for the strength tests (BS 1881-120, 1983). The CCI and SC results for wet cured and plastic cured specimens are compared in Figure 4.15, which gives a sense that the measured surface conductivities were not affected by the curing method. However, it has already been demonstrated through CCI and other results that wet curing produced a more densified pore structure. Pertaining to SC measurements, at least three differences can be identified between the wet cured and plastic cured specimens as described below and summarised in Figure 4.16:

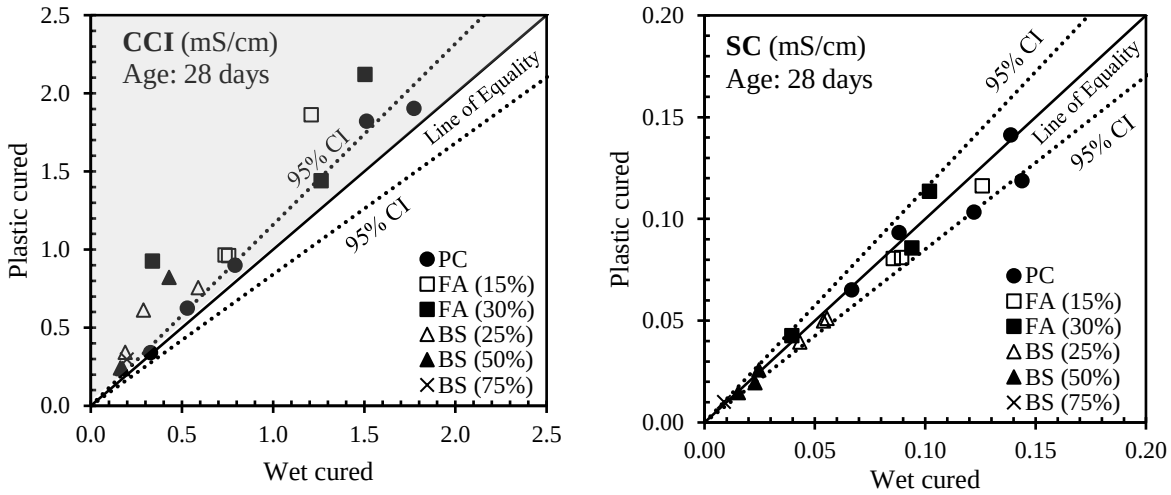

(a) (b)

Figure 4.15 Influence of curing method on (a) CCI and (b) SC. The confidence intervals are calculated using the 1s repeatability[5] value of the test method, i.e., for CCI: SD = 10%, n = 4 (SANS 3001-CO3-3, 2015) and for SC: SD = 6%, n = 3 (AASHTO T 358, 2015).

i. Pore structure gradient: Drying from the surface of concrete, following the removal of plastic wrapping at 7 days, may produce a moisture level gradient in concrete, which could in turn produce a gradient of degree of hydration and a consequent gradient of penetrability. This aspect is of primary interest to the study of chloride resistance of concrete.

ii. Degree of saturation or pore relative humidity: Immersion in water is expected to progressively eliminate the RH gradient produced by surface drying as the water-front moves deeper into concrete.

iii. Gradient of pore solution composition: Immersion of concrete in water will lead to leaching of ions from the pore solution to the surrounding water, producing a gradient of pore solution conductivity. Wet cured concretes will be more susceptible to leaching effects than plastic cured specimens due to longer immersion durations involved.

These differences will have counteracting effects on concrete conductivity and the net conductivity will depend on their relative proportions. The conductivity measured by the SC method will depend on the relative proportion of these effects and the sensitivity of the surface resistivity test method to near-surface changes in concrete conductivity. The sensitivity of the Wenner surface resistivity method to near-surface properties can be explored through the relationship of measured resistivity with the depth of specimens relative to the probe spacing.

[5] Repeatability SD is the average single-laboratory and single-operator SD of the test method.

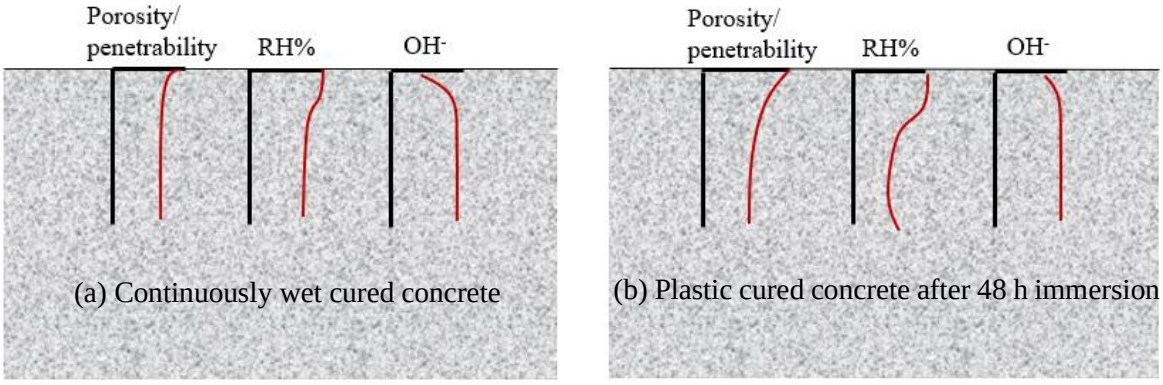

Figure 4.16 Schematic illustration of the expected variation of different parameters influencing surface conductivity measurements with depth in the near-surface region under wet and plastic curing regimes

4.2.3.1 Exploring the factors influencing the sensitivity of the SC method to curing

In the 4-probe arrangement, the current density varies inversely with the square of the distance from the current probes and reduces to negligible levels beyond a distance equal to the probe spacing (Angst & Elsener, 2014). Furthermore, a specimen thickness of two to four times the probe spacing is recommended to prevent excessive errors in using the Wenner expression (Gowers & Millard, 1999; Angst & Elsener, 2014). In view of these findings, it seems reasonable to conclude that the test region in a (reasonably) homogeneous specimen may extend beyond what is typically deemed to be the near-surface region. However, an air-dried specimen subjected to surface wetting cannot be considered a homogeneous specimen due to the creation of a low resistivity layer in the near-surface region by water absorption. In this case, concrete specimens can be viewed as composed of at least two parallel resistors: saturated layer with low resistance and unsaturated or dry layer with high resistance.

In a parallel resistor system, the overall resistance is given by Eq. (4.5), which implies that depending on the relative magnitude of the two resistances, the overall resistance may depend on both or is controlled by the lower resistance. Note that this relationship should be expressed in terms of impedance terms instead of resistance terms; however, impedance largely represents resistance in the frequency range used in the Wenner method. The resistance depends on the cross-sectional area of the resistor, which in this case can be represented by the depth of the water-front and the thickness of the remaining portion of the specimen. The effect of the depth of the water-front on the measured surface resistivity can be understood in relation to the probe spacing using the work of (Millard & Gowers, 1992), as shown in Figure 4.17. It is shown that when water depths are lower than the probe spacing (=50 mm), the surface resistivity measurements would be affected by the unsaturated portion. This argument can be extended to other causes of low surface resistivity such as poorer pore structure formation due to,

for example, poor finishing, bleeding etc. to show limitations with regard to the sensitivity of the test method to the near-surface properties.

$$\frac{1}{R} = \frac{1}{R_1} + \frac{1}{R_2} \tag{4.5}$$

Where, R is the overall resistance of the parallel resistor system; R_1 and R_2 are resistances of the individual resistors.

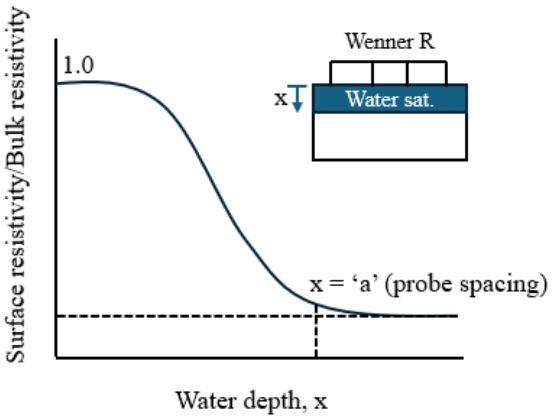

Figure 4.17 Schematic variation of measured surface resistivity with the movement of the water-front upon immersion of unsaturated concrete in water (Gowers & Millard, 1999).

The influence of the immersion period on the surface resistivity measurements of plastic cured specimens was investigated on selected concrete mixtures. Figure 4.18 shows the variation of the water-front into concrete and the measured surface resistivity with immersion duration. It can be observed that surface resistivity reduces sharply in the first 24 hours and continues to decrease albeit with a decreasing rate. Water depths varied extensively with the type of concrete, but in no case surpassed 50 mm in the immersion durations used. Hence, it is expected that the lack of saturation in the remaining section will be variable and produce higher surface resistivity measurements over and above the sensitivity issues. This is also observed when comparing curing methods with much more pronounced differences, such as shown in Figure 4.19. In this figure, the SC values of the plastic cured concrete increased by extending the immersion period from 2 days to 7 days, showing the effect of increased saturation. However, the benefit of the increased immersion duration was so limited that the SC values were still lower than the SC values of the corresponding continuously wet cured and thus more densified concretes, demonstrating the pronounced effect of the lack of saturation on the SC measurements.

From the preceding discussion, it appears reasonable to deduce that the perceived lack of influence of curing on the 28-day SC values is an indication of the involvement of other parameters, mainly the lack of saturation and the lower (than a method such as CCI) sensitivity of the method to near-surface changes.

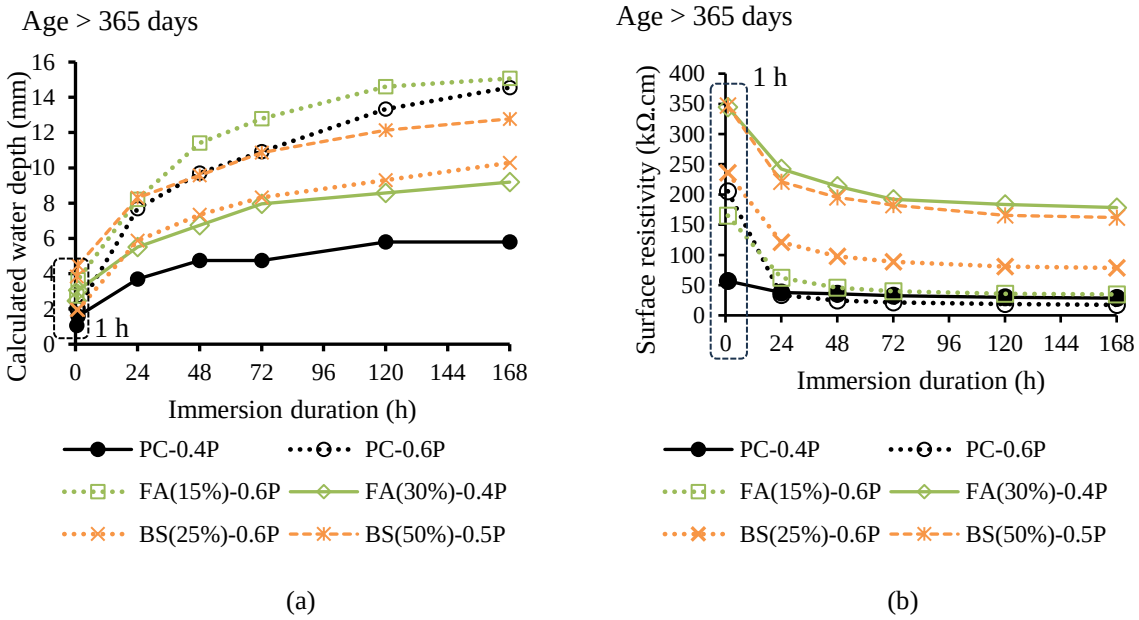

(a) (b)

Figure 4.18 Effect of immersion duration on (a) calculated depth of water penetration, and (b) surface resistivity of 7-day plastic cured 150-mm concrete cubes. Water depth was calculated based on mass gain with immersion duration and concrete porosity.

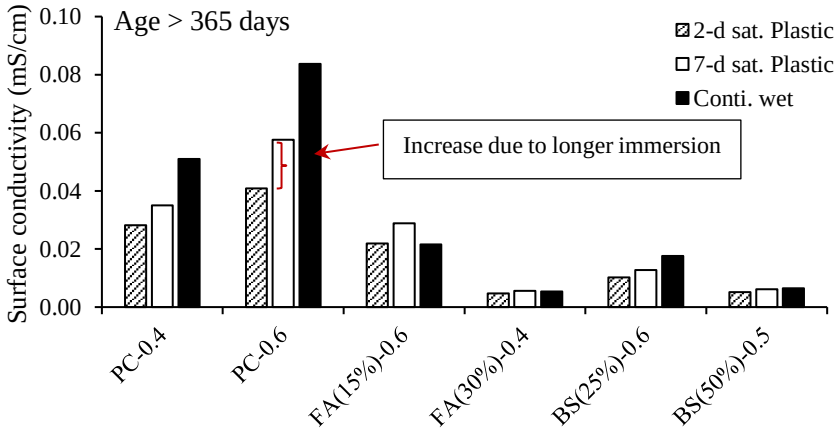

Figure 4.19 Comparison of surface conductivities of plastic cured concretes after 7 days of water immersion with continuously wet cured concrete of the same age

4.2.4 Effect of extended environmental curing

In the previous section, the effect of curing on the 28-day results was described. The compressive strength of 28-day wet cured concrete is generally treated as the indicator of the long-term strength of concrete in practice. This could be justified at least for PC concretes, which tend to reach a large proportion of their final strength in the first 28 days. More importantly, the concrete may continue to hydrate in the interior region beyond the active curing period owing to the protection provided from excessive drying by the near-surface concrete. Since the compressive strength is influenced more by the interior region, the 28-day 'wet cured' compressive strength is a better indicator of the long-term strength of field cured concrete than using the actual curing method itself.

The case of durability is quite different in contrast. The long-term durability performance depends on the quality of the near-surface region, which forms the cover zone. The cover zone may not have the same opportunities as the interior region to hydrate from the internal moisture. Therefore, it depends on the quality of active curing and the surrounding environmental conditions thereafter for its long-term performance.

In this section, the effect of storage conditions beyond 28 days on the penetrability of the pore structure is discussed. To that end, two cases were selected to represent the two ends of the spectrum of possible availability of moisture in the exposure environment. Figure 4.20 shows the evolution of CCI with age stored/cured under these conditions, namely, (a) continuously wet cured after demoulding, and (b) plastic wrapping until the age of 7 days and thereafter stored in air at 21˚C/50% RH. It can be observed in the results that the CCI decreased substantially with time in wet surroundings, while it remained relatively unaffected in dry air.

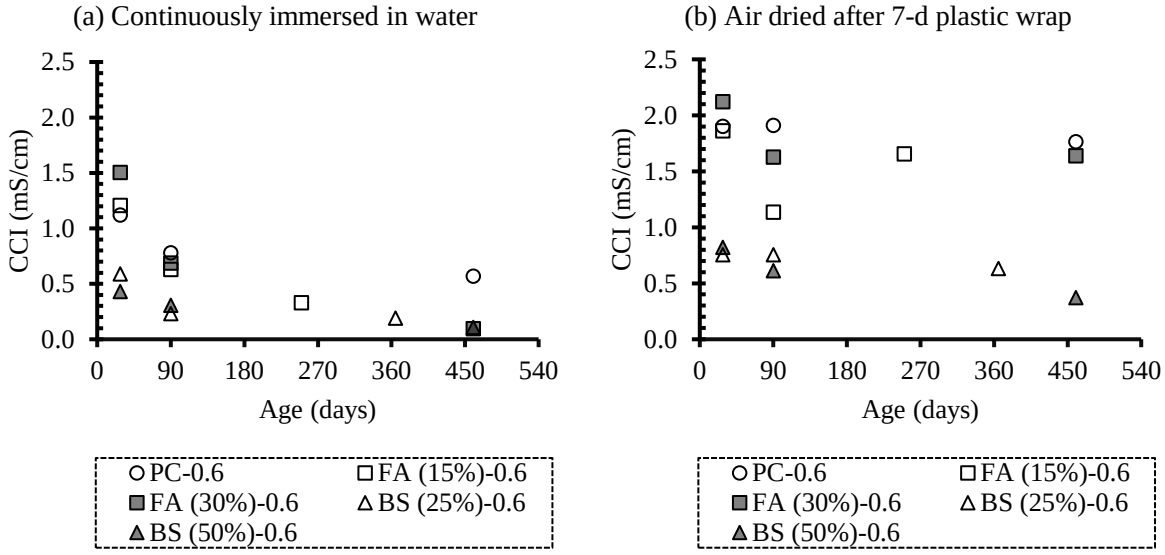

Figure 4.20 Variation of CCI with age under two different curing and storage regimes. Results of only one w/b ratio (0.6) are presented for the sake of brevity as these are sufficiently representative of the general trend.

The moist environmental conditions experienced by surfaces directly in contact with seawater may alleviate some of the concerns regarding less effective curing methods, provided these do not prevent moisture uptake by concrete in the long term. In moderate to mild conditions, even surfaces in contact with seawater aerosol may also continue to hydrate after the active curing period. By contrast, the cover region may not improve, or only slowly improve, without significant contact with seawater much beyond the active curing period in relatively dry environments. Recommendations for longer curing duration (>7 days) for fly ash concretes would produce some benefit as shown in the previous section; however, they would be quite limited given that extended curing periods are needed for appreciable

improvement in the penetrability of fly ash concretes. The selection of fly ash in such circumstances should be performed in view of these limitations. Future studies should be directed to evaluate and understand the performance of fly ash especially under exposure conditions with intermediate humidity such as where susceptibility to steel corrosion is increased by the combination of external/internal chlorides and carbonation.

4.2.5 Ageing coefficient of penetrability and its estimation

The typical practice for the structural design of concrete is to adopt the 28-day compressive strength as the potential (final) strength of concrete as previously discussed. The same practice can be applied to durability design and base the design on 28-day potential transport properties. However, the long-term improvement of transport properties in conducive conditions if utilised may improve the efficiency of material use and cost-effectiveness of the design. Service life prediction models facilitate this process by accounting for long-term changes in transport properties. The evolution of the chloride diffusion coefficient with time represents such a change in the case of chloride penetration in marine conditions, which follows a power function relationship (Mangat & Molloy, 1994; Maage et al., 1996; Tang & Nilsson, 1996). The evolution of the formation factor or penetrability with time may assist or provide an alternative to long-term diffusion measurements. To that end, the time-development functions are derived for continuously wet cured CCI and SC based on Eq. (4.6) using the experimental data from this study.

$$CCI\ (t) = CCI_{ref}\left(\frac{t}{t_{ref}}\right)^{-\alpha} \tag{4.6}$$

Where,

CCI (t): CCI at age ‘t’

CCI_{ref}: CCI at the reference age ‘t_{ref}’

α: ageing coefficient

The time dependence of CCI and SC are presented in Figure 4.21 and Figure 4.22. The time functions obtained through non-linear regression analysis are presented in Table 4.5. High R^2 values were obtained (>0.83) showing a good fit of the power function to the data. The data were collected up to an age of 1.25 years. Longer periods, which were not practical for this study, however, will invariably improve the reliability of the derived relationships for long term prediction.

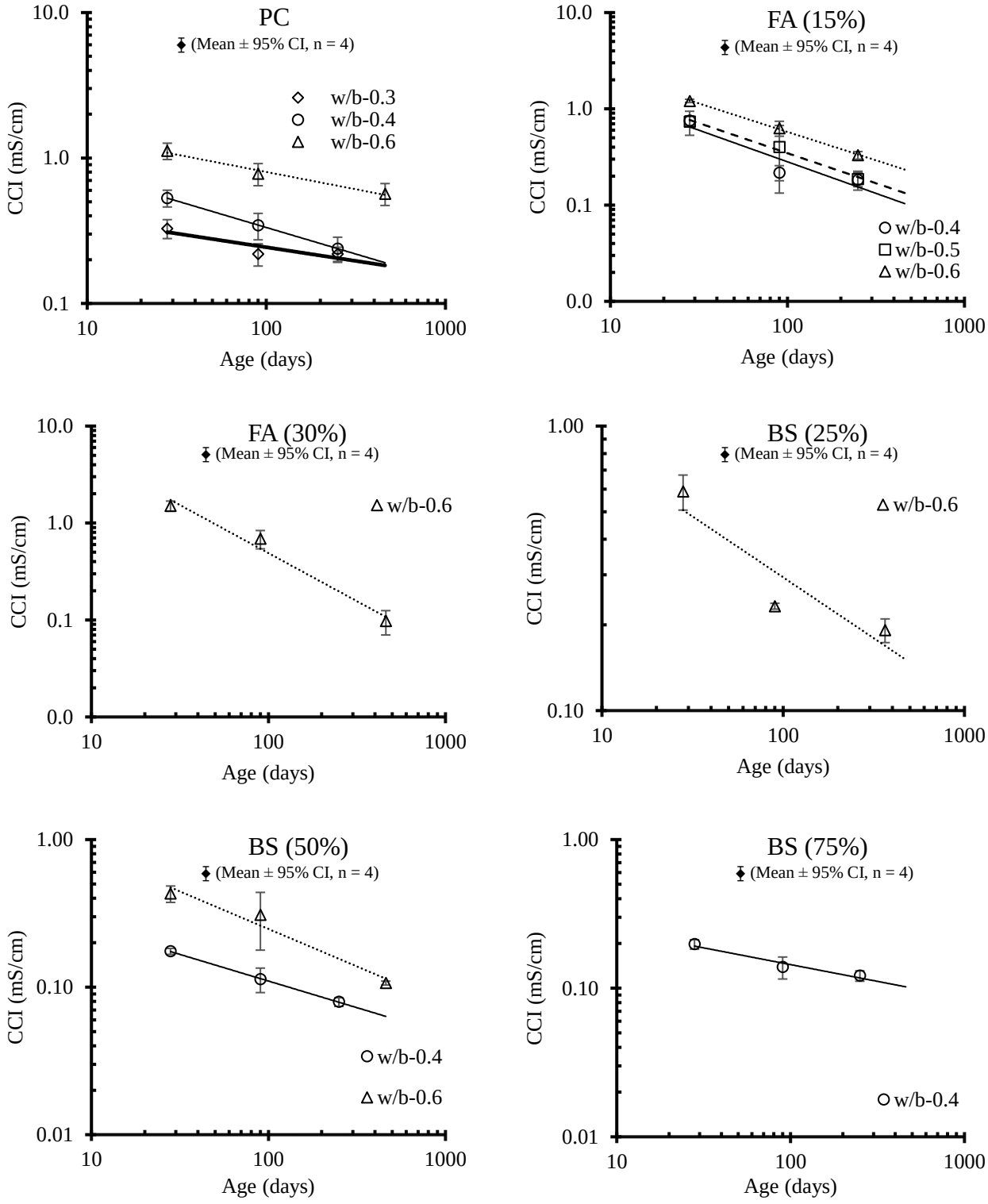

Figure 4.21 Evolution of CCI with time (log scale) (Note: different ordinate scales; PC-0.6 values were normalised with the 28-day estimated value)

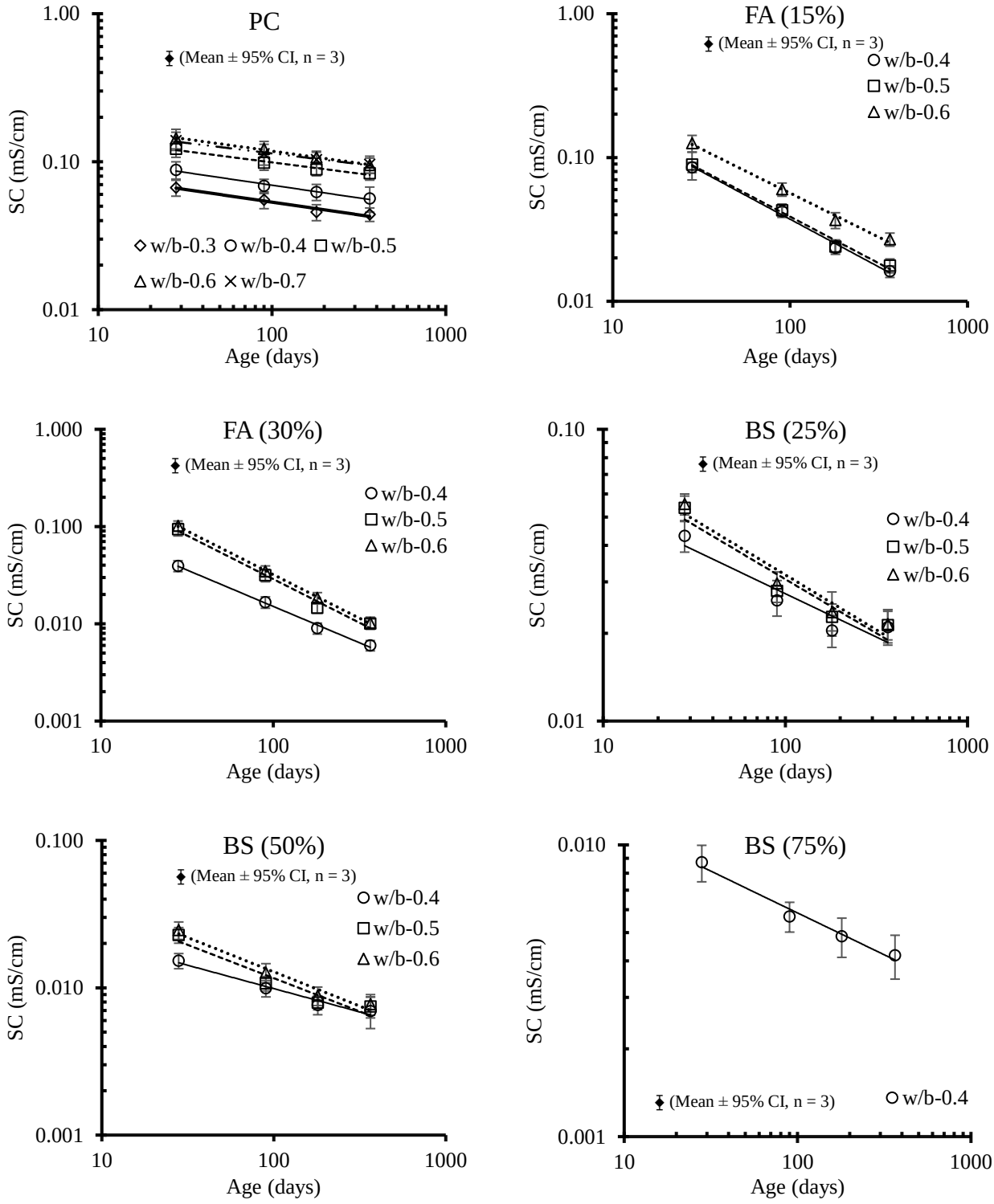

Figure 4.22 Evolution of surface conductivity (SC - 1/SR) with time (log scale) (Note: different ordinate scales)

Table 4.5 Time functions for CCI and SR

Binder	w/b ratio	CCI-t relationship		SR-t relationship	
PC	0.3	$CCI(t) = 0.58t^{-0.19}$	$[R^2=0.83]$	$SC(t) = 0.12t^{-0.17}$	$[R^2=0.97]$
	0.4	$CCI(t) = 1.8t^{-0.37}$	$[R^2=1]$	$SC(t) = 0.15t^{-0.17}$	$[R^2=0.99]$
	0.5			$SC(t) = 0.20t^{-0.15}$	$[R^2=0.98]$
	0.6	$CCI(t) = 2.4t^{-0.24}$	$[R^2=0.98]$	$SC(t) = 0.22t^{-0.16}$	$[R^2=0.99]$
	0.7			$SC(t) = 0.25t^{-0.14}$	$[R^2=0.99]$
FA (15%)	0.4	$CCI(t) = 5.8t^{-0.66}$	$[R^2=0.94]$	$SC(t) = 0.79t^{-0.66}$	$[R^2=1]$
	0.5	$CCI(t) = 6.1t^{-0.62}$	$[R^2=0.99]$	$SC(t) = 0.77t^{-0.65}$	$[R^2=1]$
	0.6	$CCI(t) = 8.8t^{-0.59}$	$[R^2=1]$	$SC(t) = 0.95t^{-0.61}$	$[R^2=1]$
FA (30%)	0.4			$SC(t) = 0.47t^{-0.75}$	$[R^2=1]$
	0.5			$SC(t) = 1.8t^{-0.9}$	$[R^2=1]$
	0.6	$CCI(t) = 47t^{-0.99}$	$[R^2=0.97]$	$SC(t) = 2.0t^{-0.9}$	$[R^2=1]$
BS (25%)	0.4			$SC(t) = 0.11t^{-0.3}$	$[R^2=0.93]$
	0.5			$SC(t) = 0.17t^{-0.37}$	$[R^2=0.94]$
	0.6	$CCI(t) = 2.1t^{-0.43}$	$[R^2=0.9]$	$SC(t) = 0.18t^{-0.38}$	$[R^2=0.96]$
BS (50%)	0.4	$CCI(t) = 0.58t^{-0.36}$	$[R^2=1]$	$SC(t) = 0.04t^{-0.32}$	$[R^2=0.98]$
	0.5			$SC(t) = 0.09t^{-0.45}$	$[R^2=0.96]$
	0.6	$CCI(t) = 2.6t^{-0.51}$	$[R^2=0.94]$	$SC(t) = 0.11t^{-0.47}$	$[R^2=0.98]$
BS (75%)	0.4	$CCI(t) = 0.41t^{-0.23}$	$[R^2=0.96]$	$SC(t) = 0.02t^{0.29}$	$[R^2=0.98]$

The ageing coefficients obtained from CCI and SC results were generally found to be within 15% (the average 95% CI of CCI and SC methods) of each other as shown in Figure 4.23. The close correspondence in the ageing coefficients of CCI and SC indicates that the effect of changes in pore solution conductivity with hydration did not appreciably affect the evolution of SC. This is in agreement with the literature on pore solution conductivity, which suggests that the changes in pore solution conductivity are small after the age of 28 days (Thomas, 2011; Vollpracht et al., 2016). However, PC concretes were an exception to this trend and α_{CCI} differed significantly from α_{SC}.

Keeping this exception in mind, it would be reasonable to conclude that the Wenner method can be used as a convenient practical method for determining the ageing coefficients for penetrability/formation factor. A significant advantage of this method is that there is no need for additional specimens for long term measurements in addition to minimal specimen/test preparation.

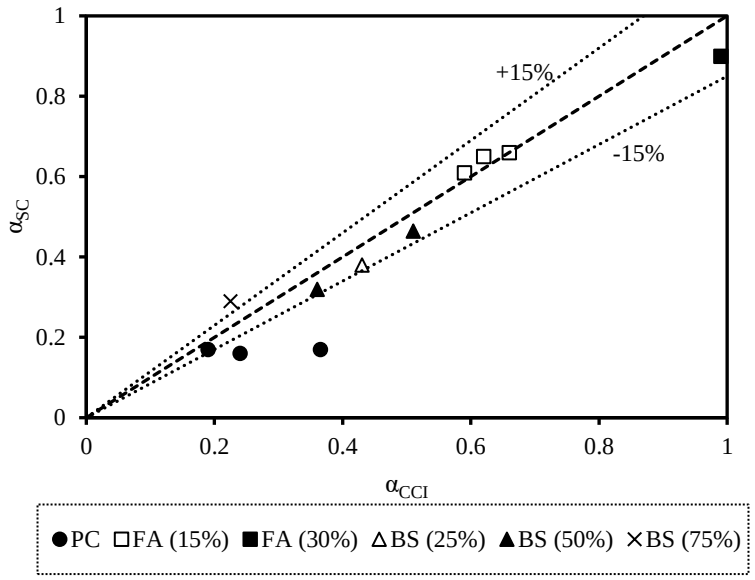

Figure 4.23 Comparison between the ageing coefficients for CCI (α_{CCI}) and SC (α_{SC})

Based on the ageing coefficients from CCI and SR, PC concretes showed a mildly decreasing trend with w/b (Figure 4.24). However, a consistent relationship with w/b ratio across different mix groups was not observed. The differences between different w/b ratios in a mix group range from moderate to small and a mean value is adopted in the absence of more extensive data. The ageing coefficient however changed considerably with the binder type, increasing with substitution levels of fly ash and slag (Figure 4.24). The results clearly show the dependence of SCM% on the ageing coefficient.

Higher ageing coefficients and steeper changes with respect to substitution level were observed for fly ash compared to slag, as expected from earlier discussions. Average ageing coefficients based on SC results were: 0.16 for plain cement, 0.64-0.81 for fly ash, 0.35-0.41 for slag. The ageing coefficients increase in the order: Plain cement < Slag < Fly ash. The binders that hydrate faster within the first month, achieve a higher proportion of their potential faster within this period. Further hydration and the consequent reduction in penetrability slows down afterwards, which is reflected in the lower ageing coefficients such as for plain cement. Fly ash in contrast hydrates slowly and takes longer to manifest its potential, which is reflected in a higher ageing coefficient. The rate of hydration of slag blends is intermediate and so are their ageing coefficients.

As shown earlier, the ageing coefficients vary with the SCM replacement level without a consistent effect of the w/b ratio. A relationship therefore can be derived to estimate the ageing coefficients based

only on the SCM replacement level without a significant loss of accuracy. Based on the data from this study, the relationships are derived for fly ash and slag (Figure 4.25). The ageing coefficients from SC measurements are used due to larger available dataset. Since SC ageing coefficients exhibited a lack of agreement with the CCI ageing coefficients in case of PC concretes as discussed previously, the CCI ageing coefficients were adopted for PC concretes to derive the relationships in Figure 4.25.

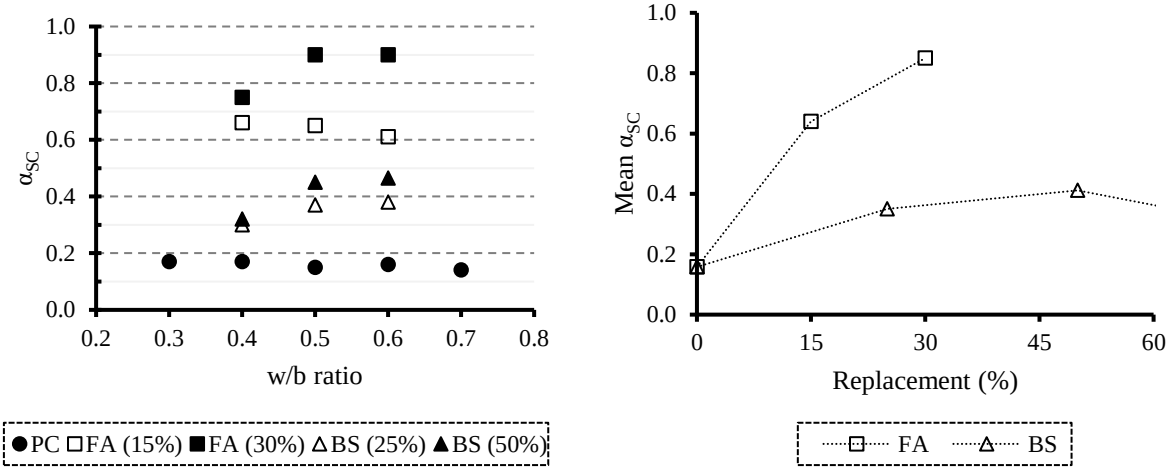

(a) (b)

Figure 4.24 Relationship of α_{SC} with w/b ratio (left) and SCM level (right)

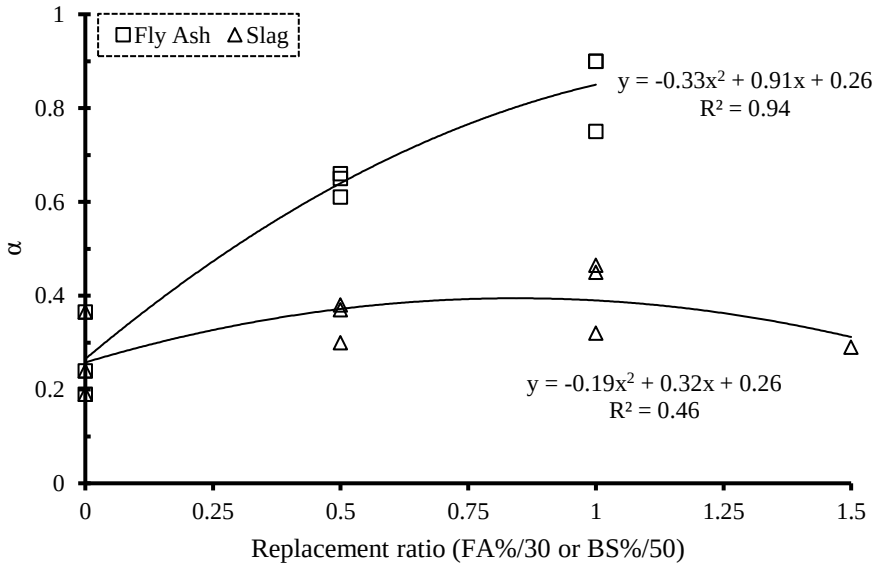

Figure 4.25 Relationship between the SC ageing coefficient and the replacement ratio (i.e., FA%/30 or BS/50%)

The polynomial relationships obtained are presented in Table 4.6. The polynomial form, which starts decreasing beyond a maxima, enables extrapolation of the relationships to higher replacement levels than used in deriving them, i.e., 30% for fly ash and 50% for slag, with reasonable accuracy. The accuracy/reliability of these relationships can be improved when more data become available.

Table 4.6 SC/CCI ageing coefficient estimation based on polynomial interpolation

Fly ash	$\alpha = 0.26 + 0.91\left(\frac{FA\%}{30}\right) - 0.33\left(\frac{FA\%}{30}\right)^2$
Slag	$\alpha = 0.26 + 0.32\left(\frac{BS\%}{50}\right) - 0.19\left(\frac{BS\%}{50}\right)^2$

4.3 Bulk diffusion results

4.3.1 Chloride profile results: general considerations and observations

The chloride profile results were collected from bulk diffusion experiments typically for the exposure duration of 180 days. Three individual specimens were tested for each concrete sample. Illustrative chloride profiles obtained in this study are shown in Figure 4.26. The chloride concentration is presented as percentage by mass of concrete and the depth represents the mean depth of the slice from the exposed surface.

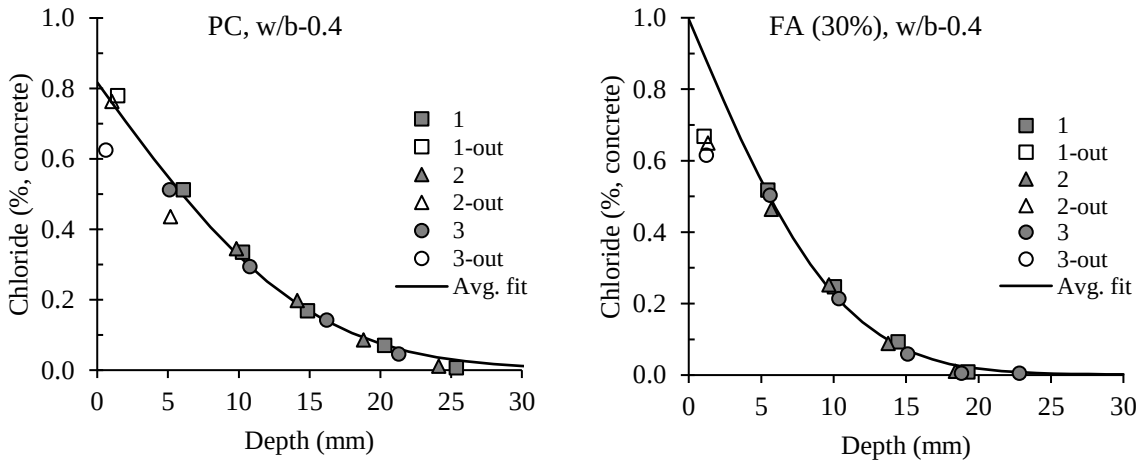

Figure 4.26 Illustrative chloride profiles for PC (left) and FA (30%) (right) concretes. Each graph includes the chloride profiles of 3 individual specimens (labelled: 1, 2, 3), the points excluded from the regression analysis (represented by unfilled markers), and the average curve for all 3 specimens (labelled: Avg. fit).

The shape of the chloride profile in the first few millimetres (generally 2-3 mm, but <5 mm) varied to some extent depending on the concrete mix. The classic peaking phenomenon (De Weerdt et al., 2016)

was consistently and prominently observed in FA (30%) and BS (50%) concretes regardless of w/b ratio and curing regime. On the other hand, PC concretes rarely showed such a peaking phenomenon and the first point on the chloride profile generally did not deviate much from the remainder of the profile (see Figure 4.26). The concretes with other SCM replacement levels showed inconsistent occurrence of this phenomenon. A consistent and clear dependence of the binder type, w/b ratio, or curing regime on this phenomenon could not be established from the results of this study.

For the purpose of curve fitting, the first point was always excluded from the analysis regardless of its deviation from the rest of the profile considering that this portion of the concrete was influenced by the interface effects between concrete and the chloride solution as opposed to the rest of the profile. The only exception to this rule was BS (75%) because of the lack of sufficient data points in the steep portion of the profile. Some subsequent points may also have been affected, but presumably, to a lesser extent from such effects. This is however difficult to ascertain without additional data. It should be noted that the first 5 mm of the specimen was truncated before chloride exposure so a gradient of concrete microstructure due to the wall effect is unlikely. Hence, the interface effect of importance or consequence would be the leaching of ionic species given the specimens were exposed to fully submerged conditions. This was practically observed in plain cement specimens in the form of leachate 'clusters' on their exposed surfaces. This however was only characteristic of plain cement concretes, perhaps due to the high alkalinity of the hydrated cement. Other binders showed white precipitates at the bottom of the exposure container.

Other points in the chloride profile were excluded with discretion only if they clearly appeared to deviate from the rest of the profile. This was performed in less than 10% of cases. The scatter in the data of individual chloride profiles and among the individual profiles of a sample was found to be minimal as evidenced by the high R^2 values of the fitted curves. The R^2 values generally remained above 0.9 with most specimens showing R^2 values of 0.98 or more. The only exception to this was PC, w/b-0.7 in which case R^2 of 0.76 and 0.88 were obtained. The high w/b ratio of 0.7 results in an open pore structure, which increases the rate and depth of leaching. The leaching profiles affect the binding ability of concrete with respect to depth, which may have caused deviations from the typical profile shapes (Machner et al., 2022).

To obtain the average chloride profile for a sample, a regression analysis was conducted on the combined data of the entire sample, i.e., 3 specimens. This is termed as the overall fit. However, the mean and variance of C_s and D_a obtained from individual specimens were also obtained. The mean values and the values obtained by overall fitting are compared in Figure 4.27. These values are practically identical. Where it was not possible to fit curves to individual profiles due to a lack of sufficient data points such as in the case of some slag concretes (BS (75)), only overall fit values are available. For the sake of consistency, all the analysis presented uses the overall values. The average and variance from the individual specimens are used to calculate the confidence intervals/ error bars for

each case. In addition to the apparent surface chloride content (C_s) and apparent diffusion coefficient (D_a), the depth of chloride penetration was also determined from the fitted chloride profiles as the depth at which the external chloride content became zero (i.e., Cl content reaches the internal Cl levels) as shown in Figure 4.28.

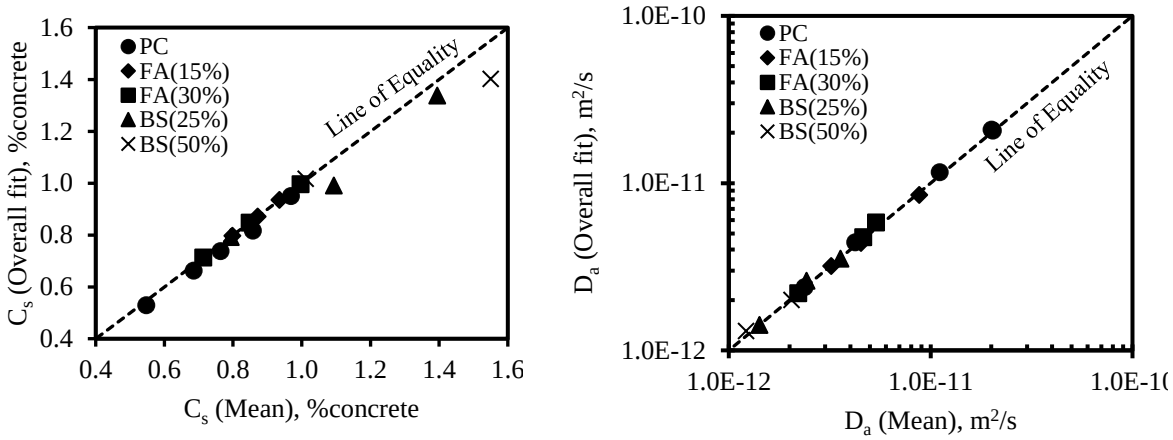

Figure 4.27 An illustration of the close correspondence between the mean C_s (left) and D_a (right) values of the individual chloride profiles of the specimens and the overall values obtained by regression analysis on the entire sample. Although the values shown here are from 28-day wet cured specimens, similar results were achieved from plastic cured specimens as well.

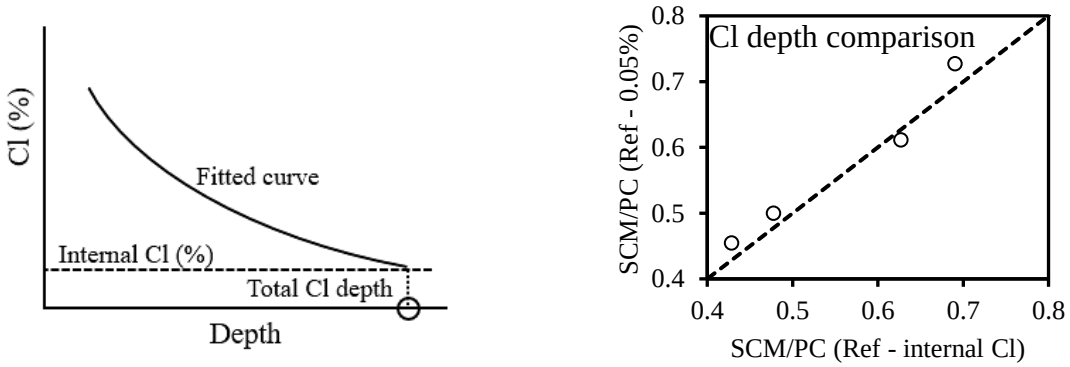

Figure 4.28 Estimation of the total chloride depth: (left) Illustration of the Cl depth calculation method using the internal Cl content as the reference Cl concentration and (right) Comparison of the estimated Cl depth (normalised with the corresponding PC Cl depth) using different references: internal Cl content versus a uniform Cl threshold content = 0.05%, on selected concrete mixtures

C_s and D_a are vital parameters for prediction but require careful interpretation. The chloride penetration depth provides a simple and direct means of comparing the resistance of concretes to chloride penetration regardless of whether free or total chlorides were measured. It encompasses the effects of C_s and D_a. In this study, the unit of chloride content was chosen as the % by mass of concrete rather than % by mass of binder, as mentioned earlier. The objective of this investigation is to study the

penetrability of concrete to chloride diffusion, which cannot be readily done using the latter unit as it skews the unit scale depending on the concrete mix proportions used, rendering a fair comparison of concretes with different mix proportions (for example, different w/b ratios) for penetrability difficult. The unit % by mass of binder requires the use of chloride threshold values, taken in the same unit, to enable meaningful comparisons of different concretes in terms of 'corrosion initiation time'. However, given that the chloride concentration of the exposure solution used in this study was significantly higher than the average concentration of seawater, such an analysis is susceptible to misinterpretation, for instance, if attempts are made to translate the resulting quantitative observations (of time-to-corrosion-initiation) to the actual field conditions. Therefore, to enable fair comparisons of the chloride penetrability of concrete, the % by mass of concrete unit is used and the entire depth of penetration estimated from the fitted curve is used to calculate the Cl depth. Since the purpose of this analysis is not to compare the corrosion initiation time, any Cl concentration can be used from the main body of the Cl profile as the reference. As shown in Figure 4.28, the comparisons based on Cl depth do not appear to depend on the chosen reference. Analyses along the same lines have been adopted elsewhere (Wilson, Georget & Scrivener, 2024).

4.3.2 Effect of binder and w/b ratio

The bulk diffusion results are summarised in relation to the SCM levels in the binder in Figure 4.29 and in relation to the w/b ratio in Figure 4.30. It must be noted that the results from bulk diffusion/ non-steady state diffusion experiments are averaged values of the measured parameters in time as opposed to the strength or penetrability values that are instantaneous parameters (Mangat & Molloy, 1994; Nilsson, 2006).

The results after 180 days of exposure showed that fly ash (FA) and slag (BS) reduced the chloride (Cl) depth and hence improved the resistance of concrete to chloride diffusion, as observed in the literature (Thomas & Bamforth, 1999; Thomas & Matthews, 2004; Thomas et al., 2008; Heiyantuduwa-Beushausen, 2022). The increase in the replacement with these SCMs had the effect of reducing the Cl depths, however with decreasing effectiveness with an increase in replacement levels. The apparent decrease in the effectiveness of increasing SCM additions produced an optimum replacement level with the lowest Cl depth, see for example the case of BS (w/b-0.4). The decrease in effectiveness with increasing replacement level is consistent with the long-term penetrability (CCI) results and is generally explained by the decline in the pH of the pore solution due to dilution of PC, which decreases the rate of hydration by reducing the rate of binder dissolution (Lothenbach, Scrivener & Hooton, 2011).

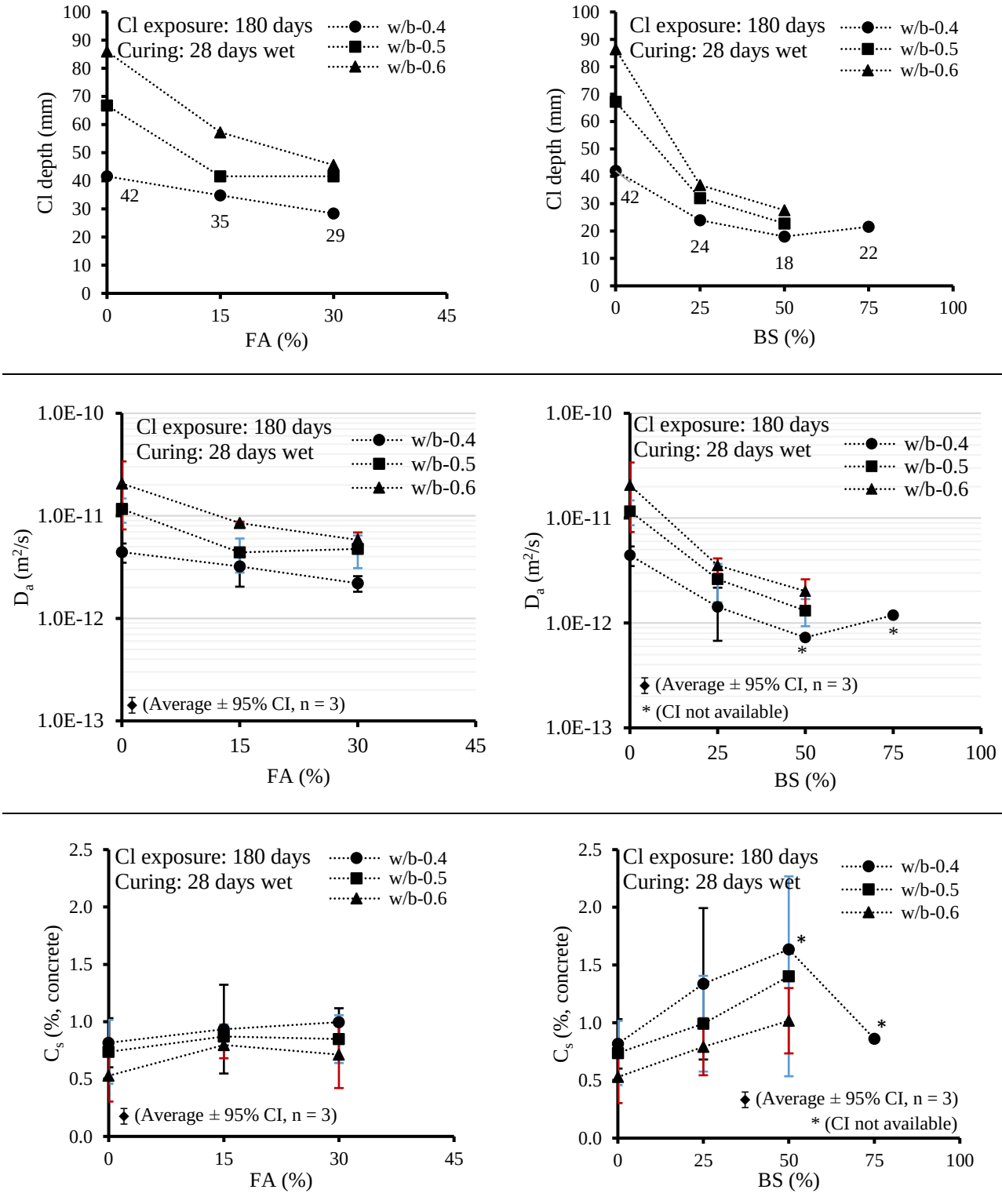

Figure 4.29 Variation of Cl bulk diffusion parameters according to FA (left) and BS levels (right) after a chloride exposure of 180 days: (i) depth of chloride penetration, (ii) apparent diffusion coefficient (D_a) [caution: log scale], (iii) surface chloride concentration (C_s) [Cautionary note: the scales on the SCM% axis for fly ash and slag are different]

i.

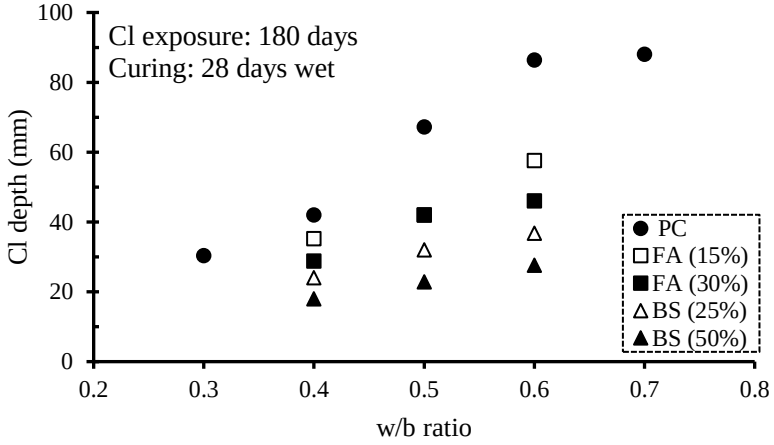

ii.

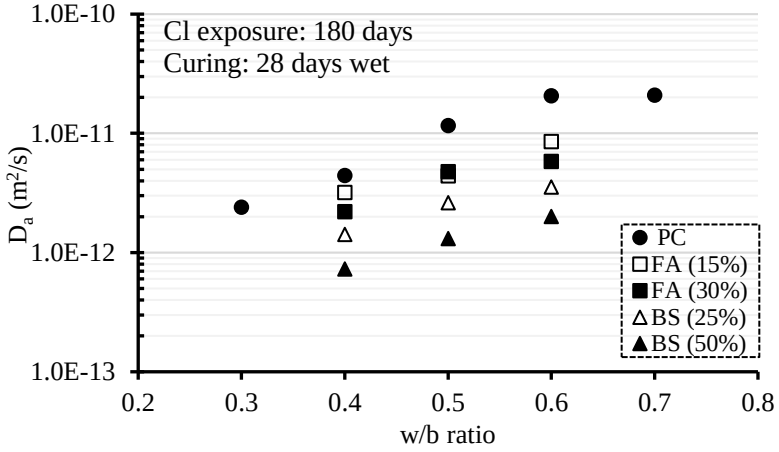

iii.

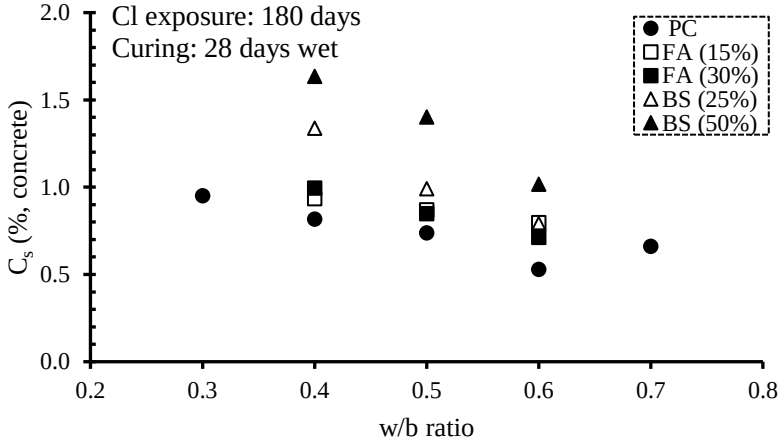

Figure 4.30 Variation of bulk diffusion parameters with w/b ratio: (i) depth of chloride penetration, (ii) D_a, and (iii) C_s

Similarly, the 180-day D_a also reduced with FA and BS levels. Although generally, the 180-day D_a remained in the order of 10^{-12} m/s^2, a change of up to 1 order of magnitude was observed with high levels of BS. The degree of improvement in D_a and chloride depth over PC concretes in FA and BS concretes is presented in Figure 4.31. In this figure, it can be seen that the Cl depth consistently follows

the variation of D_a. Also interesting to note is that the effectiveness of SCMs improves with increasing w/b ratio (Figure 4.31). In contrast, the same was not observed for the 28-day CCI results (Figure 4.3). This suggests that the pronounced effect of SCM addition at a higher w/b ratio on Cl depths is a result of larger subsequent reductions in penetrability, of SCM concretes compared to PC concretes, over the 6-month period in the presence of the NaCl solution. It must be remembered that the ageing behaviour was found to be independent of the w/b ratio in this study (Section 4.2.5). Even though the CCI of SCM concretes at the w/b ratio of, for example, 0.6 was similar to or higher than the CCI of PC concrete at the w/b ratio of 0.4, the higher ageing coefficients of SCM concretes reduced the penetrability to below that of the PC concrete at w/b-0.4. Since the ageing coefficients are dependent on the binder type rather than the w/b ratio, the SCM concrete undergoes the same rate of reduction for both a low and a high w/b ratio. This refutes another plausible explanation of this observation that concretes at low w/b ratios are already so dense that they require less assistance from SCMs, at least in the context of chloride penetration. The practical significance of this observation is that introducing SCMs or increasing the replacement levels will be more effective than reducing the w/b ratio, provided conducive conditions for long-term improvements are present as discussed in Section 4.2.4.

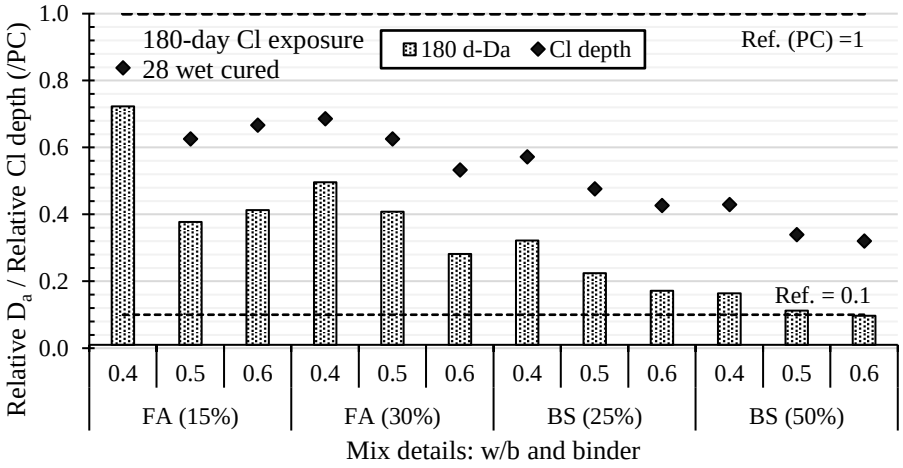

Figure 4.31 Relative D_a and relative Cl depth with respect to plain cement concretes at corresponding w/b ratios

The 180-day C_s results (Figure 4.29) showed practically no influence of FA, which is likely to change with longer exposure durations. In the case of BS blends, on the other hand, the C_s increased but reached a maximum around the BS level of 50%. The diffusion results were generally characterised by high variability. The effect of SCMs appears larger on D_a than C_s given the larger effect size (mean difference/standard deviation) observed for the former. The high variability in the diffusion results can be attributed to the large sensitivity of the non-linear curve to small deviation in chloride content in the near-surface region as shown through a typical case in Figure 4.32. It can be observed that the chloride

profiles were more or less identical except for the small difference in the near-surface points, which led to quite different fitted curves.

A dependence of the diffusion parameters on the w/b ratio can be observed in the results, in agreement with the literature (Nilsson, Sandberg & Sørensen, 1996; Bamforth, Price & Emerson, 1997). The Cl depth and D_a increase with an increase in the w/b ratio, while the C_s decreases. The effect of the w/b ratio on Cl depth and D_a can be explained through the influence of the w/b ratio on the penetrability. The influence of the w/b ratio on C_s is more complex. While the porosity increases due to an increase in the w/b ratio, which increases the amount of free Cl ions, the decrease in binder content decreases the amount of bound Cl ions. In addition, the effect of the w/b ratio on the convection depth could also influence the measurement of C_s values through its influence on the extrapolation of the fitted curve to the surface.

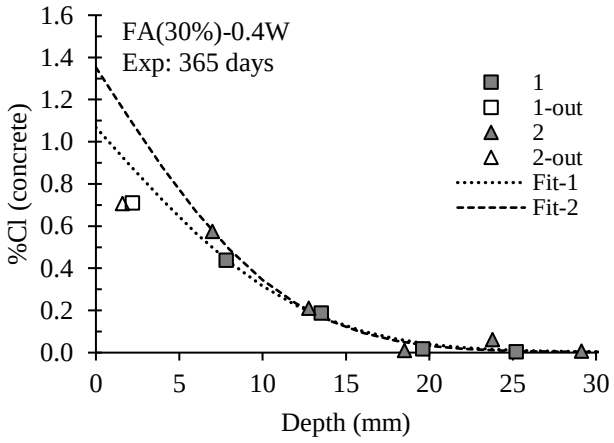

Figure 4.32 Illustration of the possible cause of high variability in the diffusion results

4.3.3 Effect of curing

The effect of curing on chloride diffusion parameters is demonstrated in Figure 4.33. The plastic and wet cured concretes almost invariably resulted in practically the same diffusion parameters. This is despite the differences in the penetrability of concretes due to curing (Section 4.2.3) at the start of exposure. A similar lack of influence of curing on chloride penetration was also observed previously (Mackechnie, 1996; Thomas & Matthews, 2004). It is possible that plastic cured concretes may have lower pore saturation levels than wet cured concrete despite immersion in lime water for 48 hours prior to the start of Cl exposure as seen in the surface conductivity specimens as well. The internal relative humidity has been shown to reduce the diffusion coefficient in previous studies (Saetta, Scotta & Vitaliani, 1993; Zhang, Zhang & Ye, 2018).

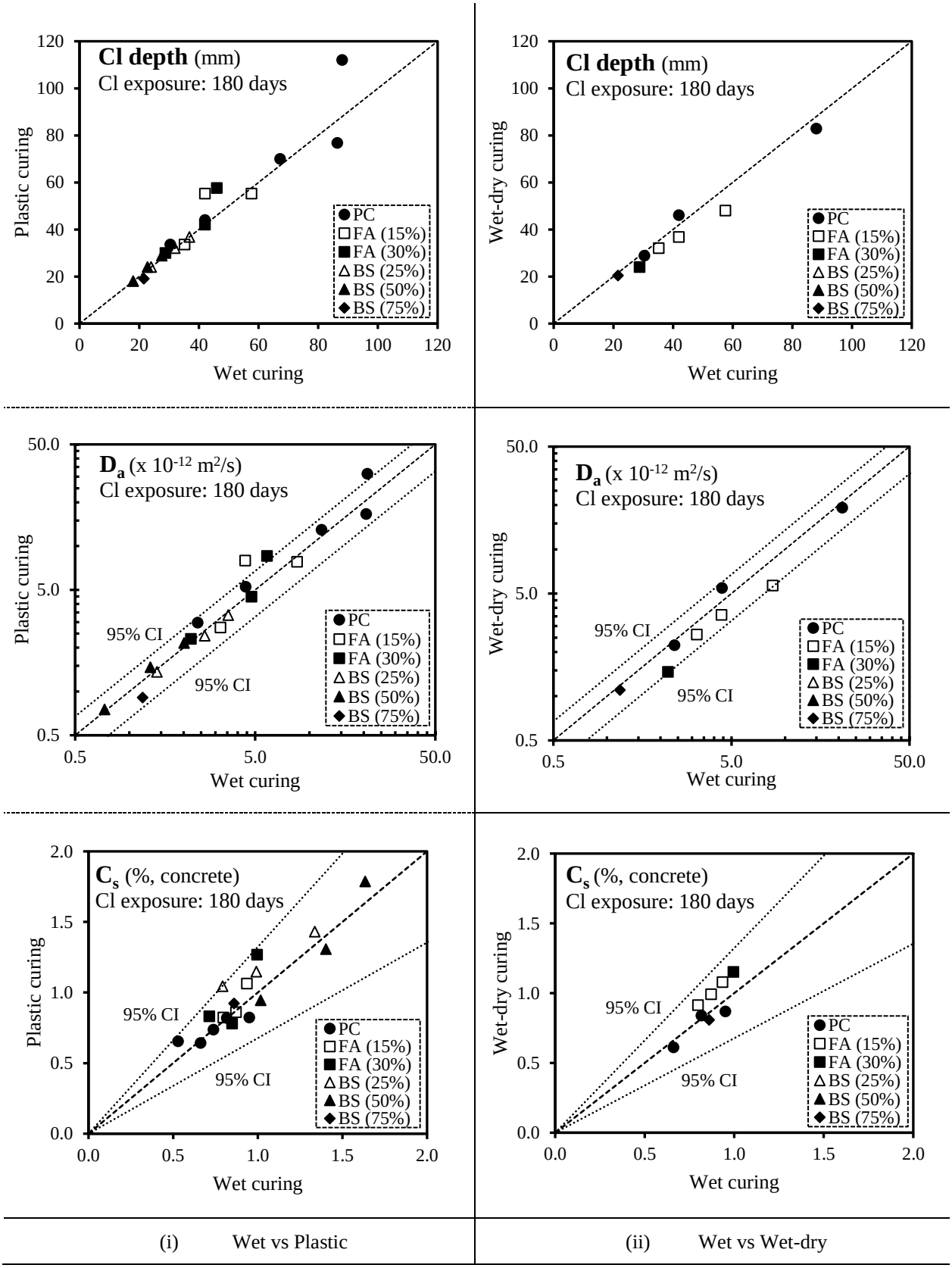

Figure 4.33 Effect of curing on chloride diffusion parameters [Note: 95% CI based on average variance, n=3]

Hence, an investigation was conducted to evaluate the net effect of the drying portion of the plastic curing regime on the diffusion results. The drying regime was simulated for the 28-day wet cured

specimens so that continuously wet cured specimens could be compared with the wet cured and dried (for 21 days as the plastic cured specimens) to isolate the effect of the drying regime. The results are shown in Figure 4.33 (ii) and compared with the results for wet curing shown in Figure 4.33 (i).

The comparison showed no influence of the drying regime on chloride diffusion. Although the simulation was performed on wet cured specimens, which could have led to somewhat different internal RH states than plastic cured specimens, the comparison is acceptable on a practical level. This means that the effect of drying on the rate of diffusion was either not a major factor or was counteracted by other factors. The likely cause seems to be the improvement in the pore structure of plastic cured concretes due to continued hydration under the presence of moisture from the chloride solution.

4.3.4 Prolonged Chloride exposure

A limited number of concrete mixtures were subjected to longer chloride exposure for over 2 years and the chloride profile results are compared in Figure 4.34. The development of C_s and D_a with time is presented in Figure 4.35.

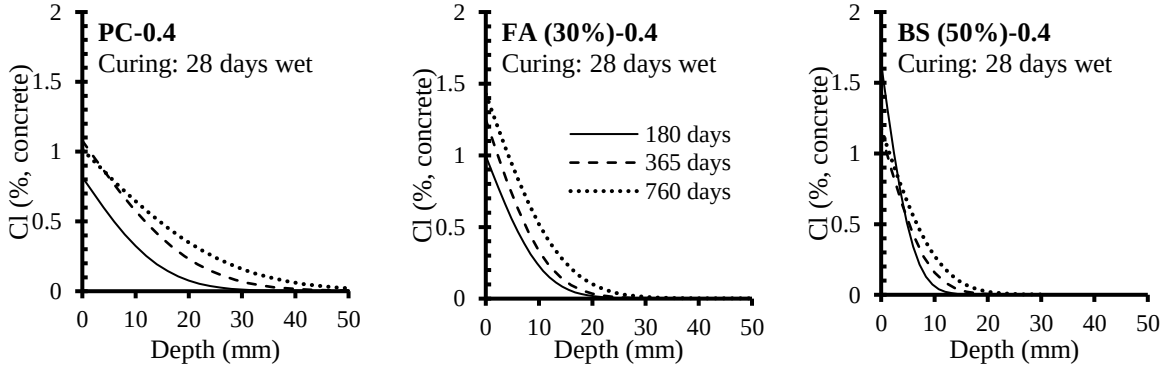

Figure 4.34 Chloride profile development of selected wet cured concretes with extended duration of exposure

The results showed that the D_a decreased with exposure time continuously even under a concentrated Cl solution, in agreement with the literature (Stanish & Thomas, 2003). The rate of reduction, inferred from the ageing coefficients of the D_a-t relationships shown in Figure 4.35, depended on the binder type. The fly ash concrete improved significantly during this period and if continuing at the same rate, may surpass the slag concrete.

The C_s generally increased over time, with a diminishing rate, in the immersed conditions, which has been interpreted as indicating increased chloride binding with time by some researchers (Tang & Nilsson, 2000). However, the interpretation of these data is complicated by the time-development of the convection zone characteristics and the need for very fine depth increments to capture the position of the peak. This is especially the case with the BS concretes, which due to their higher chloride resistance, exhibit very steep chloride profiles and are thus more sensitive to experimental error. This

may have partly caused the anomalous variation observed in the C_s and D_a values of the BS concrete, which could also have influenced the measured ageing coefficient in this case. The possible causes for the observed long-term behaviour of the diffusion parameters are discussed in the next section. It must be acknowledged that the time scale used in this study is restricted for practical purposes and longer exposure durations of the order of decades are needed to more reliably study these phenomena.

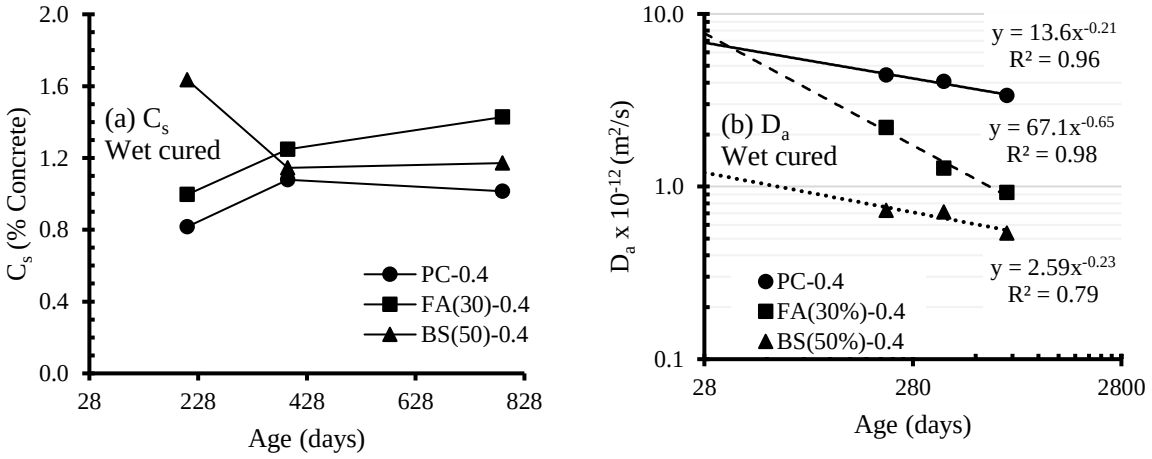

Figure 4.35 Variation of C_s and D_a with time for wet cured concretes

4.4 Correlation between penetrability (CCI) and diffusivity (D_a)

The relationship between the apparent diffusion coefficient and chloride penetrability was investigated by assessing the correlation between 180-day D_a and 28-day CCI as shown in Figure 4.36. Data from all three curing regimes used in bulk diffusion experiments were used. Since CCI testing was not done for the wet-dry regime, the 28-day wet cured CCI was adopted for this dataset. It is not expected that the CCI would have changed in any major way in the drying period of 21 days following 28 days of wet curing. This could be supported by the lack of significant changes in CCI over time in the drying regime of plastic curing. The correlations were found to be binder-group-specific. Within the respective binder groups, the correlations could be expressed through linear regression curves.

The strength of the correlations varied considerably between binder groups from strong (R^2>0.8) to weak (R^2=0.47). This can partially be ascribed to the differences in the effect of curing on CCI and D_a between different binder groups. The correlations differed in some cases with the curing method, but the differences were quite inconsistent. Therefore, a distinction between different curing regimes seemed unnecessary in deriving the correlations at this stage given the mostly small and inconsistent effect observed. The other part of the problem of weak correlations is expected to be resolved to some extent by expanding the database through further studies.

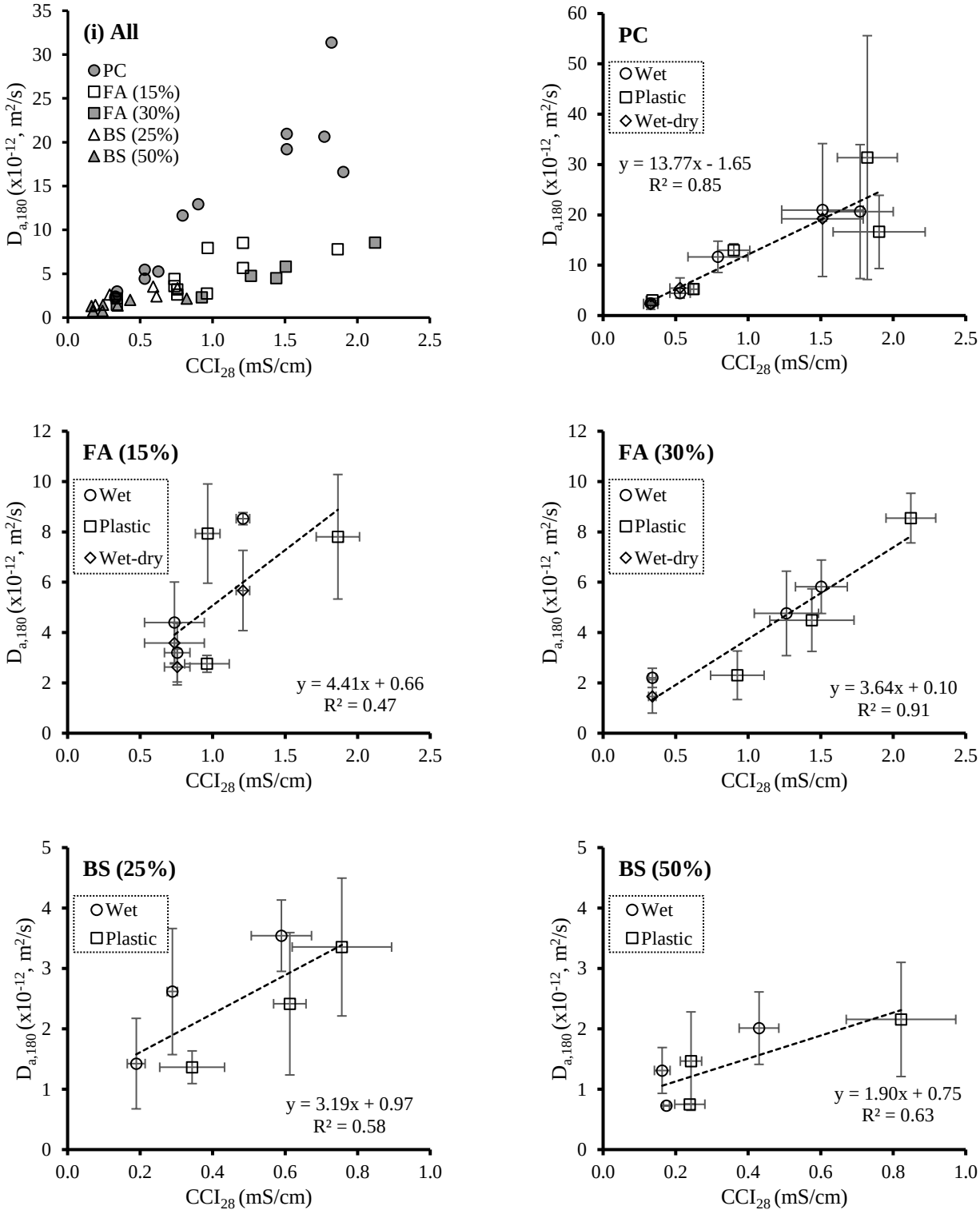

Figure 4.36 Relationship between the 180-day D_a and 28-day CCI. Part (i) presents all the data together, whereas parts (ii)-(vi) present data specific to a binder group. The error bars represent 95% confidence intervals [D_a (n = 3), CCI (n = 4)].

The linear relationships obtained through regression analysis exhibited an intercept on the y-axis. Although the intercept in these relationships seemed mostly of the positive kind, closer inspection of

the relationships for different curing methods reveals that both negative and positive intercepts are observed without any apparent preference for binder type or curing method. Hence, the occurrence of an intercept may likely be due to random errors rather than one with a physical meaning. What is therefore important to observe is the slope of these curves, which depends strongly on the binder group and is the characteristic feature of these correlations. The dependence of these correlations on the binder group could be possibly ascribed to the binder-specific differences in the time-dependence of the inherent diffusivity and the binding ability inherent in D_a. It is important to note that the correlations discussed so far have been investigated on a time-averaged value (D_a) and an instantaneous value (CCI at 28 days). Therefore, these correlations include the effect of time dependence of the diffusion coefficient along with other effects. To evaluate the effect of these influences, a time-averaged value of CCI is also derived and correlations between the two time-averaged parameters are explored as follows.

Similar to the apparent diffusion coefficient, the equivalent CCI can be defined as the CCI averaged over the time period between the start and end of the chloride exposure period and computed by integrating Eq. (4.6) with respect to time (Eq. (4.7) and (4.8)). Similar treatment has been previously reported (Liu, Presuel-Moreno & Paredes, 2015). The ageing coefficient (α) adopted is that which was derived from the continued curing regime and summarised in Table 4.6.

$$CCI_{eqv} = \frac{\int_{28}^{28+t_{exp}} CCI_{28}\left(\frac{t}{28}\right)^{-\alpha} dt}{\int_{28}^{28+t_{exp}} dt} \tag{4.7}$$

Where,

CCI_{28} is the instantaneous CCI at the age of 28 days

CCI_{eqv} is the average CCI over the time period that D_a is measured, i.e., it describes the average penetrability of concrete during this period.

t_{exp} is the exposure duration.

$$CCI_{eqv} = CCI_{28} \cdot \left[\frac{(28 + t_{exp})^{1-\alpha} - 28^{1-\alpha}}{(1-\alpha) \cdot 28^{-\alpha} \cdot t_{exp}}\right] \tag{4.8}$$

The relationship between the two time-averaged penetrability parameters, the apparent diffusion coefficient and the equivalent CCI, for different binder groups is evaluated in Figure 4.37 (a). Results for other exposure periods also follow the same correlation (Figure 4.37 (b)) validating, at least in part, the occurrence of a single predominant correlation. It should be noted that the ageing coefficients used to derive the equivalent CCI do not include the long-term effects of binding as these were derived from concrete stored in plain water and measured via conductivity testing (contact with chlorides was short, only during conditioning and testing). Hence, the occurrence of one major correlation suggests that the differences in the D_a between different binder materials used in this study mainly emanate from the

differences in the rate of development of their physical pore structure or penetrability instead of differences in the binding abilities of these binders.

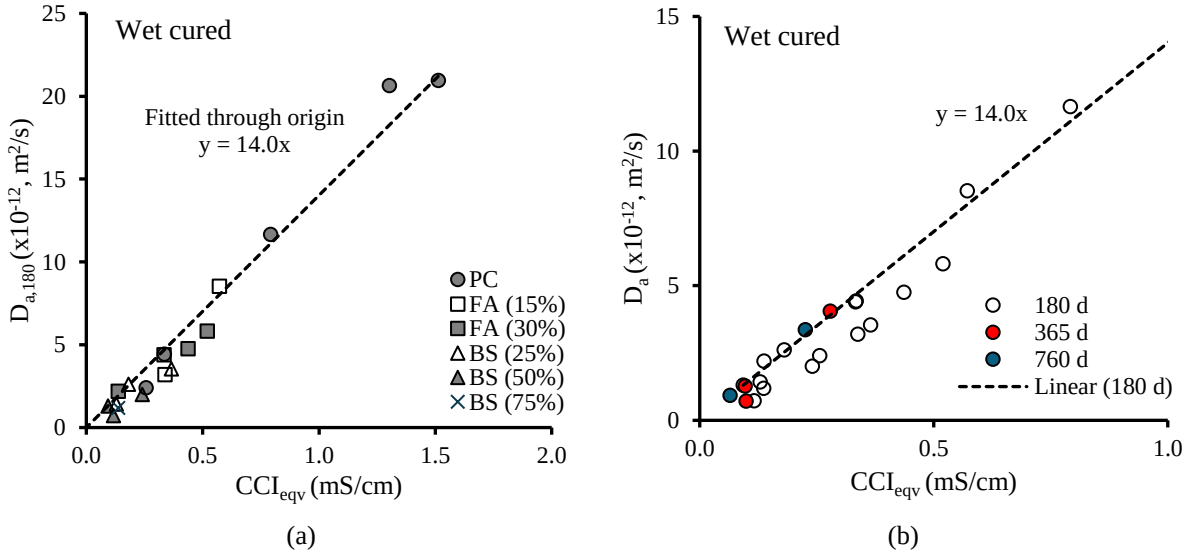

Figure 4.37 (a) Correlation between the 180-day D_a and the time-integrated equivalent CCI and (b) validation with 365-day and 760-day exposure data

Note: Data at t_{ex} = 365 / 760 days belong to PC-0.4, FA (30%)-0.4, BS (50%)-0.4.

This is a significant finding as it refutes the emphasis often placed on chloride binding as the main differentiating characteristic of the chloride resistant binders and instead shows that pore structure penetrability plays a dominant role in determining the chloride penetration resistance. Some previous studies had come to a similar conclusion in the recent past (Loser et al., 2010; Wilson, Georget & Scrivener, 2024) . A mathematically more rigorous analysis presented in this study provides a stronger case in support of this conclusion.

The apparent lack of net differences in the binding abilities or their effect on the D_a implies that the ageing coefficients for D_a may be calculated from the ageing coefficients of formation factor/conductivity testing, reducing the need for tedious bulk diffusion testing. This finding shows that pore structure penetrability plays a dominant role in determining the chloride penetration resistance.

4.5 Correlations of SC with CCI and D_a

The relationship between CCI and SC is investigated in Figure 4.38 at 28 days and 90 days of curing. SC results were found to group into different bands in relation to CCI. These bands appear to be related to the binder group, as can be observed in the 90-day results.

Notably, different SC values can occur for the same CCI depending on the pore solution conductivity, which demonstrates how unaccounted pore solution conductivity may complicate the interpretation of

penetrability in the electrical methods. Similarly, the relationships between D_a and SC for different binder groups are found to lie in binder-specific bands as shown in Figure 4.39.

An overall linear relationship may be derived by disregarding the deviating PC values. However, the sensitivity of the prediction of D_a value would be diminished. For example, a given change in the SC value in PC or BS concretes, say, due to w/b ratio change, will produce a lower estimated change than it would be in reality. Nonetheless, binder-specific correlations as obtained in Figure 4.39 (b) can be used to derive empirical models.

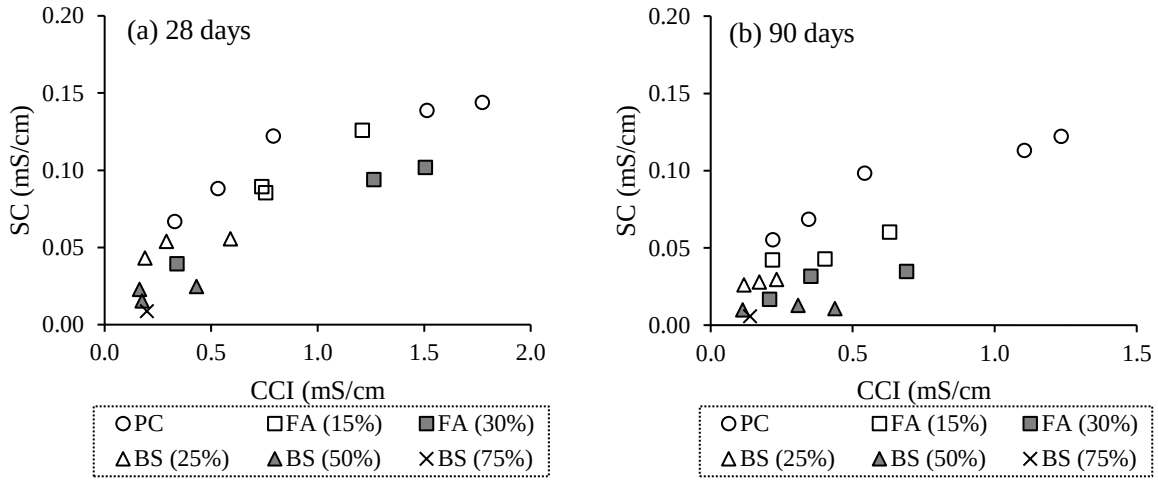

Figure 4.38 Correlations between SC and CCI

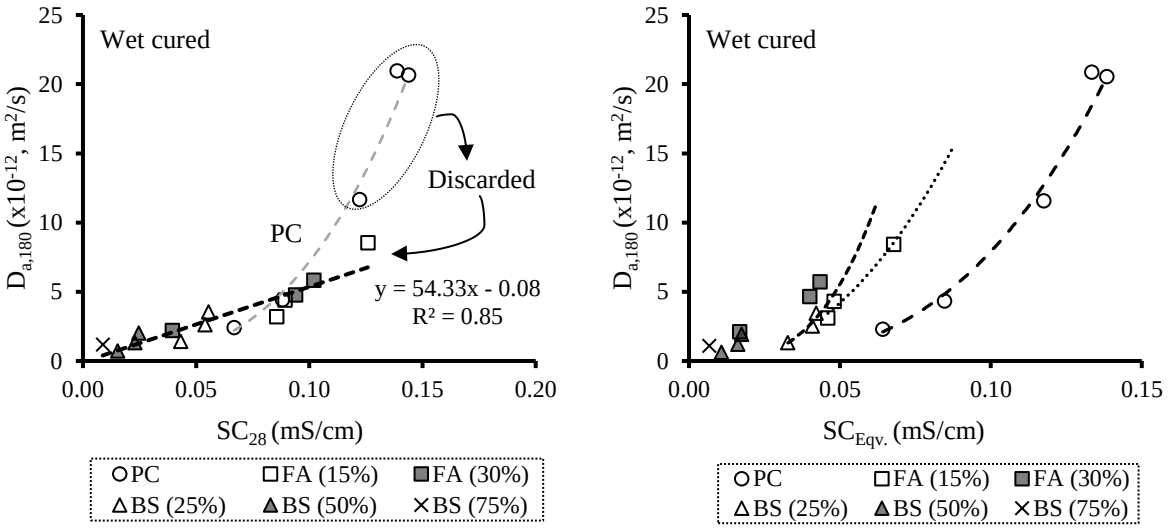

(a) 180-day D_a (log_{10} scale) vs 28-day SC (b) 180-day D_a (log_{10} scale) vs Equivalent SC

Figure 4.39 Correlations between D_a and SC

4.6 Conclusions

The main conclusions drawn from the preceding discussion of the experimental observations are as follows:

1. The surface conductivity values include the effect of pore solution conductivity, among other things. In consequence, a comparison of surface conductivity values to select a durable concrete mix may lead to inaccurate judgements. For instance, fly ash concretes in this study showed opposite trends for chloride conductivity and surface conductivity relative to Portland cement concretes, illustrating the influence of pore solution conductivity. Hence, either pore solution conductivity should be accounted for explicitly or a direct formation factor test such as chloride conductivity be adopted to evaluate the resistance of concrete to chloride penetration.
2. Despite these limitations, the Wenner resistivity method offers a reasonably good and quick alternative to evaluate the time dependence of penetrability. It may also function as an internal quality control alternative through a case-specific relationship with CCI.
3. A simple empirical model is proposed to estimate the chloride conductivity index based on Archie's law. The model has been validated using past data from the literature and is found to predict well for PC concrete. More data on slag and fly ash concretes are needed for proper validation.
4. The relationship between the apparent diffusion coefficient and CCI for different binder types seems to vary mainly due to the differing rates of microstructure development in different binders. Contrary to the present understanding, this indicates minimal differences in the binding ability of different binders. It demonstrates the determining influence of the penetrability of the pore structure on chloride resistance. Further investigations are however needed to investigate this finding further.

Chapter 5 SERVICE LIFE PREDICTION MODEL

5.1 Introduction

A service life prediction model is proposed in this chapter making use of the experimental results from this study and field data from previous studies conducted in South Africa. The service life in the context of this study is defined as the time to reach the chloride threshold value at the level of reinforcing steel. The chapter begins with laying out the modelling framework adopted. The individual model parameters are developed thereafter. The chapter concludes with a summary of the final model, its key features, and its application in design.

5.2 Model framework for service life prediction (time-to-corrosion-initiation)

A model framework is proposed in this study based on the typical multi-factor approach used in scientific modelling and followed by the DuraCrete framework (Lindvall, 2003; fib bulletin 34, 2006). The DuraCrete approach is favoured for its conceptual and computational simplicity in addressing the material and environmental effects on the rate of chloride penetration. The salient features of the proposed model framework are summarised as follows.

1. Error function solution (ERFC equation)

The error function solution (ERFC) to the non-steady state diffusion process is used to model chloride transport in marine conditions according to Eq. (5.1). Diffusion is assumed to be the predominant transport mechanism; however, convective transport can also be accommodated implicitly in the ERFC solution. In the present model, the explicit rescaling of the chloride profile to remove the convection zone as proposed in the fib model (fib bulletin 34, 2006; Andrade, Climent & de Vera, 2015) has not been adopted for simplicity and to reduce the variables needed for modelling.

$$C_x = C_s \left(1 - erf \left[\frac{x}{2\sqrt{(D_a \cdot t_{exp})}} \right] \right) \tag{5.1}$$

Where, 'C_x' is the chloride content at a depth 'x'; 'C_s' is the surface chloride content; 'D_a' is the apparent diffusion coefficient; and 't_{exp}' is the exposure time.

The chloride binding is assumed to occur: (i) instantaneously and (ii) follow a linear binding isotherm (Tutti, 1982). In the absence of these assumptions, a numerical solution will be necessitated (Nilsson, Massat & Tang, 1994), which is avoided to enable practical ease for model use. Moreover, a linear binding isotherm has been observed in some field and field-simulations studies, where the hydroxyl ion leaching can change the pH and consequently influence the binding behaviour (Sandberg, 1999; Mohammed & Hamada, 2003; Wang et al., 2020). The linear approximation also allows the use of total chloride profiles for non-steady-state diffusion measurements.

2. Apparent diffusion coefficient (D_a)

The apparent diffusion coefficient (D_a) is modelled as a function of the short-term formation factor of concrete determined in controlled conditions, which is converted through various (transfer) parameters according to Eq. (5.2) to represent long-term field conditions. The formation factor approach provides a theoretically sound and practically convenient means of deriving the apparent diffusion coefficient from conductivity measurements. It enables the use of the Nernst-Einstein equation by accounting for the inevitable involvement of additional ionic species present in the concrete pore solution during concrete conductivity measurements. The use of conductivity instead of diffusivity also reduces the testing time and cost, making it more practical for quality assessment and control testing. In the present study, the chloride conductivity index (CCI) has been opted as a direct measure of the formation factor ($CCI_0 \propto \frac{1}{FF_0}$) (Mackechnie, 1996; Streicher, 1997), obtained according to the Chloride Conductivity test (SANS 3001-CO3-3, 2015). Although the formation factor can be calculated by explicitly accounting for the pore solution conductivity contribution, the chloride conductivity test provides a practical protocol for directly measuring an index representing the formation factor characteristic of concrete.

Note that the inverse of the formation factor is termed in this study as the 'chloride penetrability' or in short 'penetrability'.

$$D_a = k_e \cdot k_c \cdot k_t \cdot \frac{1}{FF_0} \cdot f(t) \tag{5.2}$$

Where,

'FF_0' is the formation factor measured typically on the 28-day standard wet cured specimens used for quality control. The present study adopts CCI as an index of the formation factor inverse.

'k_t' is the test method parameter: it connects the penetrability measure (CCI) to the lab-based diffusion coefficient of the standard lab-cured concrete.

'k_c' is the curing parameter: it corrects for the differences in the effectiveness of field and lab (standard wet) curing methods on short-term diffusivity.

'k_e' is the environmental parameter: it modifies the lab-based diffusivity in accordance with the field exposure conditions and accounts for the effect of environmental influences, such as temperature, relative humidity, salinity, etc.

f(t) is the time-development parameter/function: it accounts for the development of D_a with time.

't' is the age at testing.

't_0' is the reference age, which is typically adopted as 28 days to align it with quality control practices. Note, $t = t_0 + t_{exp}$, where t_0 is the age at the start of exposure and t_{exp} is the exposure duration.

3. Surface chloride concentration (C_s)

The surface chloride concentration (C_s) is the chloride concentration obtained by extrapolating the fitted chloride profile back to the exposure surface. It sets the boundary condition for the chloride ingress model. It should ideally be expressed as a time function to account for its variation with time. However, as discussed in Section 5.6, this is not possible at this stage in the present study due to a lack of long-term field data. Hence, only expressions presenting the ultimate C_s value will be included in this study. These will enable the calculation of the time-to-corrosion-initiation or corrosion-free life but is likely to over-estimate the chloride profiles for short to medium lengths of exposure.

4. Critical chloride threshold concentration (C_{crit})

The critical chloride threshold concentration depends on various factors related to material properties and exposure conditions. However, large variability has been observed in the reported values across the literature (Angst et al., 2009). A differentiated approach accounting for the variation of materials and exposure conditions is not preferred at this stage given the extent of uncertainty underlying their relevance to field conditions. The classic conservative approach is adopted. The critical chloride concentration (C_{crit}) for predicting corrosion initiation is assumed to be 0.05% (by mass of concrete) as a conservative estimate of the typically used value of 0.4% (by mass of binder) following Life-365 (Life-365 v2.2.3, 2020).

The proposed framework differs from the fib's DuraCrete-based framework (fib bulletin 34, 2006) in the following ways:

1. The proposed framework uses the formation factor approach to characterise the concrete diffusivity instead of the rapid chloride migration coefficient.
2. A combined-effect empirical coefficient is proposed to account for environmental influences on the apparent diffusivity instead of temperature-related corrections according to the Arrhenius law as proposed by the fib model.
3. The extrapolated C_s is used in the proposed model instead of the peak region chloride content. Furthermore, long-term field values are adopted, which includes all the exposure zones, instead of relying on chloride-binding isotherms for saturated conditions.

These modifications are intended to simplify the modelling framework, reduce the input parameters, and improve its field relevance.

5.3 Environment parameter (k_e): Influence of marine environment on D_a

The environmental exposure conditions differ geographically as well as with respect to the position (distance and height) of the site from the ocean. These external influences can be divided into: relative humidity, temperature, salinity, and position-related parameters such as wind speed and direction, tidal height, topography of the landscape, etc. These factors affect the boundary conditions for chloride transport, but these may also affect the D_a. The relative humidity of the environment and the wetting-

drying cycles affect the internal relative humidity of the concrete in the tidal, splash and air-borne zones. It has been shown that the diffusion coefficient decreases considerably with the decrease in the internal RH (Saetta, Scotta & Vitaliani, 1993). This means that the D_a measured/calculated for submerged conditions would require a modification to translate it to the other zones. Similarly, the difference in the reference and exposure temperature would require a modification, which is typically done using the Arrhenius equation (Nilsson, Sandberg & Sørensen, 1996; Bamforth, Price & Emerson, 1997). The effect of salinity on D_a appears less clear from the literature (Lindvall, 2007; Marchand & Samson, 2009).

5.3.1 Modification for salinity differences between the NaCl solution (lab) and seawater (field)

In the present study, the D_a values were measured in the lab following ASTM C1556 (ASTM C1556, 2016), which specifies the use of a 16.5% NaCl solution. These D_a values are used to obtain a lab-based correlation between CCI and D_a. The salinity used in the bulk diffusion tests is significantly different from the average seawater NaCl concentration of 2.8%. Due to contradicting factors that determine the role of chloride concentration on D_a and a lack of sufficient quantitative research available on this aspect, the influence of this difference in salinity on D_a is not clear. A factor of 1.0 is thus assumed until better correlations are found.

5.3.2 Modification for differences in the environmental conditions between the lab and the field

The combined or net influence of the environmental influences on D_a is addressed in the model through a multiplicative correction parameter, k_e. It must be pointed out that k_e may not completely address the influence of field conditions on its own and the ageing coefficient may also be affected by field conditions. Because the modelling approach adopted in this study uses D_a (which combines multiple influences) instead of D_i for practical purposes, it is often difficult to express individual influences as mutually independent multiplicative parameters. Thus, a more comprehensive analysis of the influence of exposure conditions on 'D_a' and 'm' is included in this chapter.

Generally, the environmental parameter, when defined explicitly, is expressed as a function of the individual influencing environmental actions based on mechanistic descriptions or established physical relations (Tang & Nilsson, 1996; Lindvall, 2003; fib bulletin 34, 2006; Life-365 v2.2.3, 2020). However, this type of approach requires handling the complex interplay of the environment-material interactions and may be computationally more challenging, which makes it less attractive for practical use. In this study, a more simplified empirical approach is proposed to derive k_e. The k_e is defined herein as the ratio of the apparent diffusion coefficients measured in the field to those measured in the lab for a given concrete and exposure duration (Eq. (5.3). To account for the variation of this ratio with time, k_e is calculated at a relatively early age (example, 2.5 y) and at a later age (example, 25 y). The two values are then averaged to obtain an average k_e value for the model. Ideally, the environmental effects should be traced from the short to the long term using real field data. However, long-term field data is

not always available and thus the long-term value can be obtained by extrapolation, which requires the time-development data for the given exposure conditions. In the absence of time-development data for D_a, the ratio based on a single exposure duration can also be used as an initial practical approximation. This could also be accomplished through linear regression if sufficient data points are available.

$$k_{e,meas} = \frac{D_{a,field}}{D_{a,lab}} \tag{5.3}$$

Where, $k_{e,meas}$ is the k_e determined through the measured D_a data, $D_{a,field}$ refers to D_a measured on field-exposed concrete, and $D_{a,lab}$ refers to D_a measured on lab-exposed concrete.

For the present model, the data from a previous study (Heiyantuduwa-Beushausen, 2022) were used to derive the k_e values. In this past study, concrete specimens of various compositions were exposed to different exposure zones in two climatically different exposure sites in South Africa. The field exposure programme spanning 3.5 years included four exposure zones: submerged, upper tidal, splash/spray, and air-borne at two exposure sites representing two different classes of marine environments on the western and eastern coastlines of South Africa. The principal difference between the western coastline (Cape Town) and the eastern coastline (Durban) is the higher average temperature prevalent in the latter (details about the South African marine environments are included in Section 2.3.5). Parallel exposure was also conducted in the lab through immersion experiments with 2.8% NaCl solution to simulate the prevalent seawater Cl content. Since the lab- and field-exposed specimens differed mainly in the environmental exposure conditions, a comparison between the same can yield k_e values for the South African sites used in the study.

The k_e values based on the extrapolated 25-year exposure for various concrete mixtures and exposure zones are presented in Figure 5.1 for the Cape Town site and in Figure 5.2 for the Durban site. From these figures, it is clear that the k_e values vary substantially between concrete mixtures within a given exposure zone on a particular site. A similar variation was observed when the exposure duration of 2.5 years was selected (but not presented here for brevity). Hence, the variation observed is regardless of the exposure duration chosen.

A comparative analysis of these observations using the more mechanistic modelling approaches from the literature could provide useful explanatory information on the environmental influences. Lindvall quantified individual modification parameters for moisture and temperature to arrive at the overall environmental transfer parameter as in Eq. (5.4) (Lindvall, 2003). The RH parameter was quantified based on a D-RH model and RH profile data from Swedish field specimens as 1.0 (submerged conditions), 0.9 (tidal), 0.4 (splash), and 0.4 (air-borne). These deterministic values selected in the study were near the higher end of the widely variable distribution of values. These values show that the diffusion coefficient is expected to reduce in unsaturated exposure conditions due to the expected

reduction in the internal RH of concrete in such conditions. The temperature parameter can be defined following Life-365 for the reference temperature of 23°C as in Eq. (5.5) (Life-365 v2.2.3, 2020).

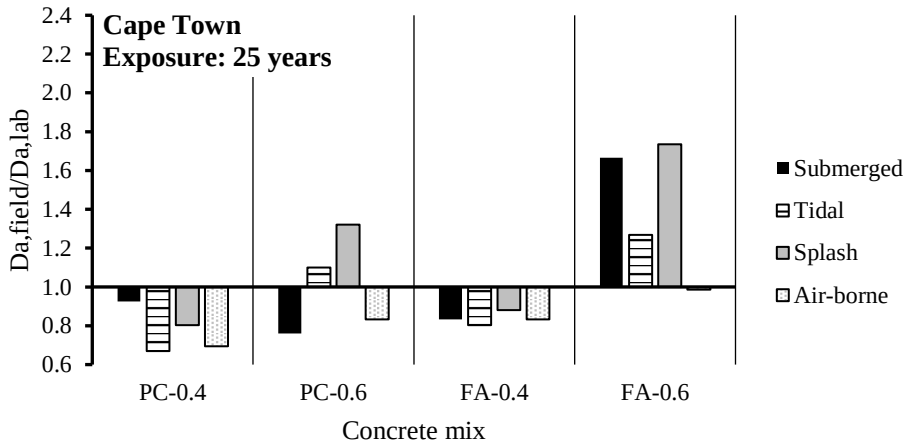

Figure 5.1 k_e for individual mixes for the Cape Town site (Granger Bay). 25-year D_a values were obtained by extrapolation of time functions determined in a 3.5-year long exposure study (Heiyantuduwa-Beushausen, 2022).

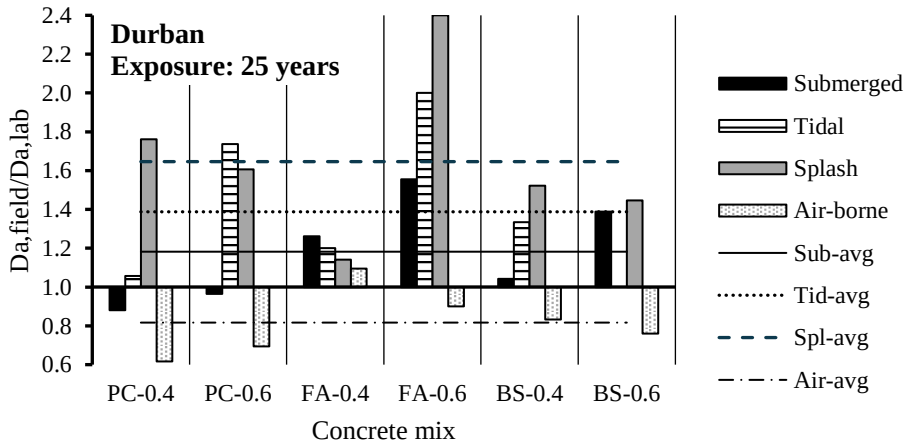

Figure 5.2 k_e for individual mixes for the Durban site (Durban Port). 25-year D_a values were obtained by extrapolation of time functions determined in a 3.5-year long exposure study (Heiyantuduwa-Beushausen, 2022). The average values shown represent averaging over all the studied concrete mixtures.

$$k_e = k_{RH} \times k_T \tag{5.4}$$

Where, k_{RH} is the RH correction parameter and k_T is the temperature correction parameter.

$$k_T = e^{\left[4210\left(\frac{1}{296}-\frac{1}{273+T}\right)\right]} \quad (5.5)$$

Where, k_T is the temperature correction parameter and T is the temperature in °C.

The average annual seawater temperatures at Cape Town and Durban sites are 16°C and 23°C (Climate-data.org, 2024). The average values of k_T for Cape Town and Durban sites would be 0.7 and 1.0, respectively, assuming that the discrepancy arising due to temperature differences between concrete and the environment would be minimal and ignoring temperature cycling. It must be emphasised that seawater/air temperature varies widely both temporally and spatially, but average values are considered sufficient for a simplified analysis. The average salinities on the two sites are close to 2.8% (NaCl) and the variation of salinity over time and space is ignored for simplicity. The k_e calculated using the selected theoretical considerations are compared with the average k_e values derived from the data collected by (Heiyantuduwa-Beushausen, 2022) in Figure 5.3. The point of showing values pertaining to two exposure durations, i.e., 2.5-year and 25-year is to enable a distinction between the effect of small differences between individual m values and the environmental effects on the D_a values, as discussed before.

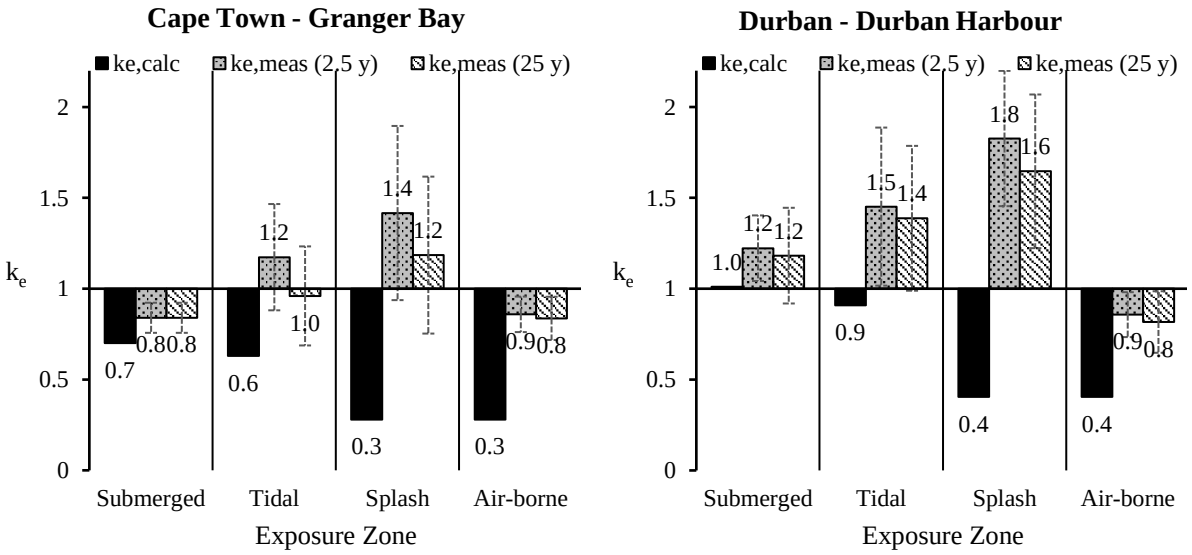

(a) (b)

Figure 5.3 Comparison of the calculated $k_{e,\,calc}$ (k_{RH} x k_T) (Lindvall, 2003; Life-365 v2.2.3, 2020) and the measured $k_{e,\,meas}$ ($D_{a,field}/D_{a,lab}$) after exposure durations of 2.5 years and 25 years (extrapolated using the derived time functions) for Cape Town and Durban sites based on data from (Heiyantuduwa-Beushausen, 2022). Note: Error bars represent SD values and the bars represent the mean values, averaged over different concrete mixtures (PC, FA, BS; w/b – 0.4, 0.6).

For submerged conditions, the measured and theoretical values show agreement. For other exposure zones, these show significant differences. Even when the moisture and temperature factors were applied

in isolation, these did not agree with the measured values for either site. The interesting thing to note in this comparison is that the tidal and splash zones exhibited higher diffusion coefficients than submerged conditions when the opposite was expected due to an expected lower degree of saturation. Even if the concrete is assumed to be saturated in these zones as in the submerged conditions, the field observations cannot be explained from this perspective. The air-borne zone also had much higher diffusion coefficients than expected from this analysis. This analysis shows that the practice of using only k_T (temperature factor) to describe the environmental influences on D_a adopted by some models (fib bulletin 34, 2006; Life-365 v2.2.3, 2020) can only be justified for the submerged zone. It also shows that a more sophisticated theoretical framework is required that also addresses other possible factors at play such as convective transport under wetting-drying conditions. More importantly, it emphasises the importance of an empirical treatment such as presented in this study as a simple and reliable means of addressing the environmental influences in the chloride model, until better quantitative models are developed.

For the service life model, k_e values are derived from the empirical data (Heiyantuduwa-Beushausen, 2022) by averaging the 2.5-year and 25-year values obtained for all the concretes, shown in Figure 5.3. Table 5.1 shows the k_e selected for the two sites for which data are available. The mean values are presented for simple deterministic analysis, but these can be converted to 95th percentile values (or to other probabilistic levels), if desired. It must be recognised that the environmental effects vary widely at all the levels of analyses in time and space, which gets translated to these parameters as well. Therefore, more such investigations are needed, preferably long term, to sufficiently characterise the environmental effects and assess the potential for generalisation. Until this happens, the parameters derived in this study may be used for guidance with a clear recognition of the limits of a single study.

Table 5.1 Environmental parameter (k_e) for modifying lab D_a for selected South African sites (based on data from (Heiyantuduwa-Beushausen, 2022))

Exposure Zone	Cape Town: Granger Bay	Durban: Durban Harbour
	(Mean)	(Mean)
Submerged and Lower tidal	0.8	1.2
Upper tidal	1.1	1.4
Splash/spray	1.3	1.7
Air-borne	0.8	0.8

Note: Average SD = 25%

5.4 Ageing coefficient (m): time dependence of D_a

5.4.1 Influence of marine exposure zones and macro environments on the ageing coefficient

It appears reasonable to hypothesise that concrete in different marine exposure zones may exhibit different rates of hydration with time owing to the different degrees of wetness prevalent in each zone.

Similarly, the environmental conditions on a regional geographical level such as prevalent temperature and salinity ranges, among other things, would also have an influence. In consequence, the intrinsic diffusivity of concrete may evolve as a function of the exposure zone and the regional environmental conditions. In addition, these factors may also affect the surface chloride concentration (C_s), the rate of evolution of which will affect the apparent diffusion coefficient and its evolution. Because of all the above factors, the ageing coefficient of the apparent diffusion coefficient (m_a) may differ with exposure zones and climatic/regional zones.

A comparison of the ageing coefficient, m_a, from lab and field based on the field study described in Section 5.3.2 (Heiyantuduwa-Beushausen, 2022) is presented in Figure 5.4. This comparison shows that the differences due to environmental conditions do not follow a consistent pattern and when non-negligible, they are often comparable to the variation among concretes of the same binder group (with different w/b ratios). This is the case both when compared between exposure zones from the same marine environment and between different marine environments included in the study. Based on these findings, it appears reasonable to assume for the time being, that m_a is independent of the exposure conditions in South African marine environments for all practical purposes and can be estimated through lab-based immersion experiments.

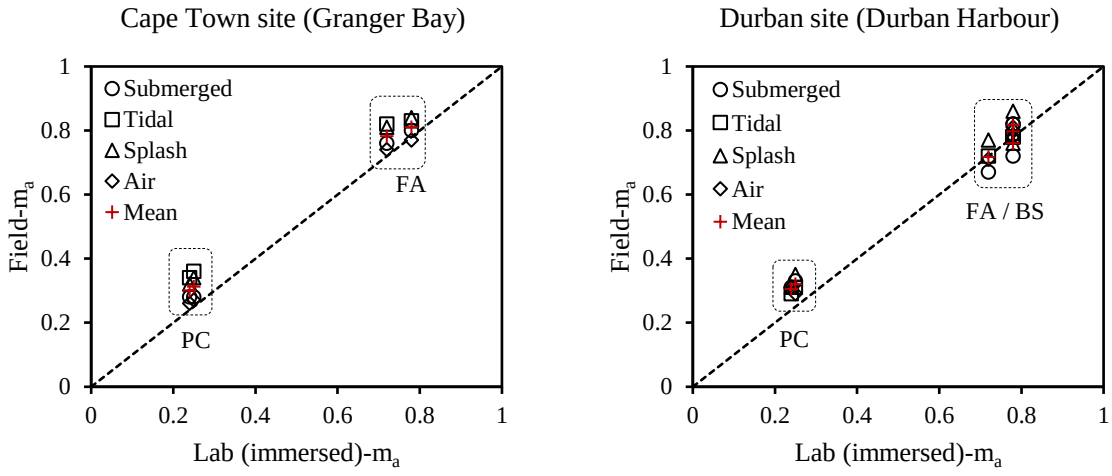

Figure 5.4 Illustration of the influence of exposure conditions on the ageing coefficient, m_a, based on (Heiyantuduwa-Beushausen, 2022). The Cape Town site (a) is located on the extreme south-west coast exposed to the Atlantic Ocean and the Durban site (b) is located on the east coast exposed to the Indian Ocean. Binder groups included are PC, FA (30%), and BS (50%) with w/b ratios: 0.4 and 0.6.

5.4.2 Estimation of ageing coefficient

A comparison of the present (see Section 4.2.5) and published ageing coefficient values is shown in Table 5.2. It is clear that the ageing coefficients determined or adopted vary significantly between

studies. The same conclusion was drawn on the basis of a wider literature review (Dhandapani & Santhanam, 2023). There are numerous possible reasons for this wide variation such as differences in the materials used—especially binder properties, differences in exposure conditions, different time definitions used (age, exposure duration, etc.) in D-t relationships, different test methods used, different exposure durations adopted, different curing ages used before the start of exposure, etc.

In addition, the treatment of the ageing coefficient as a constant itself is under question. It has been shown that the ageing coefficient related to the microstructure development decreases with time (Frederiksen, Mejlbro & Nilsson, 2008; Presuel-Moreno, Wu & Liu, 2013). This implies that the ageing coefficients measured in short-term studies may result in unconservative long-term estimates of diffusivities. Similar thinking is reflected in the use of a time-development cut-off point of 25 years for the ageing coefficients in Life-365 (Life-365 v2.2.3, 2020).

Furthermore, the ageing coefficients derived from bulk diffusion testing (m_a) and electrical testing (α) may be different in that the former represents time-averaged diffusivities and the latter represents instantaneous conductivity values. A factor of 0.7 applied over α appears to provide a reasonable practical approximation for m_a as shown in Figure 5.5. In the absence of better relationships between these two parameters, this approximation will reduce dependence on reported values from the past and enable rapid expansion of the database with different materials.

Table 5.2 Ageing coefficients from different sources

Region	Source	Ageing coeff.[1]	PC	FA (30%)	BS (50%)
South Africa	Present study (Chapter 4): Lab	α	0.26	0.85	0.41
		m_a	0.21	0.65	0.23
	(Heiyantuduwa-Beushausen, 2022): Field	m_a	0.3	0.8	0.8
	(Mackechnie, 1996): Field case studies	m_a	0.29	0.68	0.68
International	(Presuel-Moreno, Wu & Liu, 2013)	α	0.11	0.66-0.47[2]	-
	(Bamforth, 1999)	m_a	0.25	0.7	0.62
	(Life-365 v2.2.3, 2020)[3]	m_a	0.2	0.44	0.49
	(fib bulletin 34, 2006)	m_a	0.3	0.6	0.45

Note:
1. m_a refers to the ageing coefficient for apparent diffusion coefficient; α refers to the ageing coefficient for CCI/surface conductivity (see Section 4.2.5).
2. The range represents the reduction of the age factor with time from 140 days to 1000 days.
3. Conservative values based on (Bamforth, 1999). Life-365 uses these values as m_i values.

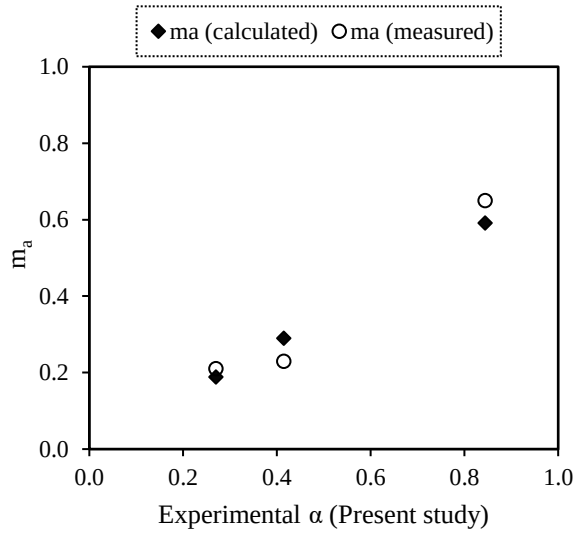

Figure 5.5 Comparison of calculated m_a (0.7α) and measured m_a

The relationship derived between the penetrability ageing coefficients and SCM levels in Chapter 4 (Table 5.3) is modified by multiplying with a factor of 0.7 [i.e., m = 0.7α]. The equations derived for fly ash and slag are combined after rounding off into a single equation by linear superposition (summation). This way of representing has the advantage that a single equation is more manageable, and it could also be used in the case of ternary binders with both fly ash and slag. Evidently, the equation does not account for the combined effect of fly ash and slag hydrating together over and above their individual effects. Nonetheless, it may still be useful as a first approximation. The equation is presented in Table 5.4. The reduction of D_a with time will be restricted to 25 years following Life-365 to account for a possible reduction in the m value over time, as discussed earlier. It is worth noting that materials in general and SCMs in particular vary in composition and properties, which may affect the accuracy of these estimates in particular cases. Hence, it is recommended that this input information is verified in case the binder materials in question differ significantly from those used in this study.

Table 5.3 CCI ageing coefficient (α): estimation for fly ash and slag

$$\alpha = 0.25 + 0.9\left(\frac{FA\%}{30}\right) + 0.35\left(\frac{BS\%}{50}\right) - \left[0.3\left(\frac{FA\%}{30}\right)^2 + 0.2\left(\frac{BS\%}{50}\right)^2\right]$$

Table 5.4 Ageing coefficient selected for apparent diffusion coefficient (D_a) to be used up to 25 years (D_a will be assumed to remain constant after 25 years)

$$m = 0.2 + 0.6\left(\frac{FA\%}{30}\right) + 0.2\left(\frac{BS\%}{50}\right) - \left[0.2\left(\frac{FA\%}{30}\right)^2 + 0.1\left(\frac{BS\%}{50}\right)^2\right]$$

FA%: Percentage mass of fly ash in binder; %BS: Percentage mass of blast-furnace slag in binder

5.5 Test method and curing parameters (k_t and k_c)

5.5.1 Relationship between D_a and CCI

Two different approaches to correlate D_a and CCI are presented as follows.

5.5.1.1 Approach I

A relationship between instantaneous diffusivity and formation factor can be derived by applying the Nernst-Einstein equation. The D_i is directly proportional to penetrability (inverse of formation factor) with the coefficient of proportionality describing the effects of pore solution composition on chloride diffusivity and chloride binding. Between these two effects, the chloride binding is generally considered the main differentiating factor.

At the start of the exposure (t_0), the relationship between D_i and FF can be represented as in Eq. (5.6).

$$D_{i,0} = \frac{k_0}{FF_0} \tag{5.6}$$

Where, $D_{i,0}$ and FF_0 are instantaneous diffusivity and formation factor at age t_0, respectively.

The time-dependent apparent diffusivity can thus be expressed in terms of the short-term formation factor, as shown in Eq. (5.7). The effect of field conditions on D_a is covered in Section 5.3.

$$D_a(t) = \frac{k_0}{FF_0} \cdot \left(\frac{t}{t_0}\right)^{-m_a} \tag{5.7}$$

In the present study, the chloride conductivity index is adopted as a measure of penetrability or formation factor inverse. Thus, Eq. (5.7) can be rewritten as Eq. (5.8).

$$D_a(t) = k_{t,0} \cdot CCI_0 \cdot \left(\frac{t}{t_0}\right)^{-m_a} \tag{5.8}$$

Where, '$k_{t,0}$' is the test method parameter and 'CCI_0' is the chloride conductivity index at t_0. $k_{t,0}$ will depend on the test methods used to measure FF and D_i, the material properties influencing chloride binding and pore solution.

Since instantaneous diffusivity cannot be directly measured through non-steady diffusion state experiments, it must be computed from the apparent diffusivities in the present scheme. Thus, to establish the correlation between the instantaneous diffusivity and formation factor as shown in Eq. (5.6), the ageing coefficient, m_a, for the apparent diffusion coefficient must first be established so that $D_{i,0}$ can be ascertained through back-extrapolation of D_a to the start of exposure. Alternatively, attempts can be made to directly correlate the short-term CCI, normally measured at the age of 28 days, with D_a measured over a finite period. D_a was measured in lab-controlled conditions in this study. If, assuming the ageing coefficient varies in relation to the exposure conditions such as exposure zone, the

$D_{a,ref}$ measured in the lab may not be compatible with the field time function of D_a as shown in Figure 5.6. In this case, $D_{i,0}$ must first be computed using the time function applicable to lab conditions as shown in Eq. (5.9), which can then be substituted in the field applicable time function for D_a as in Eq. (5.10).

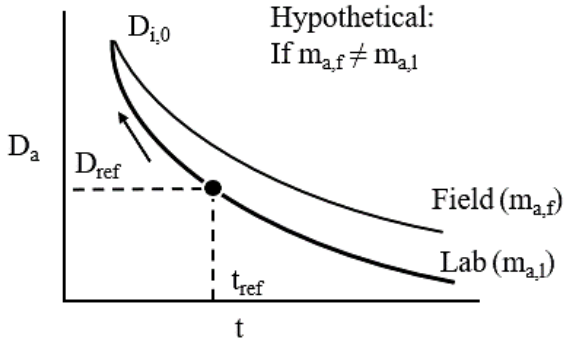

Figure 5.6 A hypothetical illustration of possible differences between ageing in lab and field diffusion experiments (excluding the effects of T, RH, and salinity on D_i)

Using lab bulk diffusion experiments, $D_{i,0}$ can be calculated as:

$$D_{i,0} = D_{a,ref}\left(\frac{t_0}{t_{ref}}\right)^{-m_{a,l}} \tag{5.9}$$

Where, $D_{a,ref}$ is the apparent diffusion coefficient measured in lab. $m_{a,l}$ is the ageing coefficient in lab conditions.

D_a for field conditions can be described, excluding the effect of T, RH, and salinity on D_i (see Section 5.3):

$$D_a = D_{a,ref}\left(\frac{t_0}{t_{ref}}\right)^{-m_{a,l}}\left(\frac{t}{t_0}\right)^{-m_{a,f}} \tag{5.10}$$

However, it was shown in Section 5.4.1 that ageing coefficients can be considered independent of the exposure conditions (Heiyantuduwa-Beushausen, 2022). Hence, the ageing coefficients from lab and field can be considered to be the same. Note that the effect of difference in salinity between seawater and bulk diffusion experiments is ignored in the present study due to lack of more information in this regard. Thus, Eq. (5.10) becomes:

$$D_a = D_{a,ref(lab)}\left(\frac{t}{t_{ref}}\right)^{-m_a} \tag{5.11}$$

From Eq. (5.8), $D_{a,ref}$ can be expressed as a function of CCI:

$$D_{a,ref} = k_{t,0} \cdot CCI_0 \cdot \left(\frac{t_{ref}}{t_0}\right)^{-m_a} \quad (5.12)$$

Defining $k_{t,ref}$ as shown below,

$$k_{t,ref} = k_{t,0} \cdot \left(\frac{t_{ref}}{t_0}\right)^{-m_a} \quad (5.13)$$

$D_{a,ref}$ can then be expressed as, from Eq. (5.12) and (5.13):

$$D_{a,ref} = k_{t,ref} \cdot CCI_0 \quad (5.14)$$

Thus, from Eq. (5.12) and (5.14), D_a becomes:

$$D_a(t) = k_{t,ref} CCI_0 \left(\frac{t}{t_{ref}}\right)^{-m_a} \quad (5.15)$$

In the present study, bulk diffusion experiments were conducted in standard lab conditions and data were collected for an exposure duration of 180 days. The 28-day CCI was also determined as per the standard quality control practices. These results are presented and analysed in Chapter 4. In the following discussion, correlations between the 180-day D_a and 28-day CCI are examined on the basis of the general equation derived above. The correlations are presented in Figure 5.7.

The correlations are found to be binder specific. This is to be expected as the $k_{t,ref}$ combines the effect of binding, pore solution, and time development, all of which are a function of the binder type. The predominant effect, however, is that of the time-dependent improvement of the microstructure as shown in Section 4.4. In most cases, a significant influence of curing was not observed on the correlations. Hence, the curing parameter (k_c) is assumed to be 1. Consequently, data from all curing methods are used to determine correlations to improve the degree of generalisation. The correlations show good fit to linear trendlines following Eq. (5.14). Note that the fitted line is forced through the origin as required by Eq. (5.14). Adjustments are made to the R^2 values accordingly.

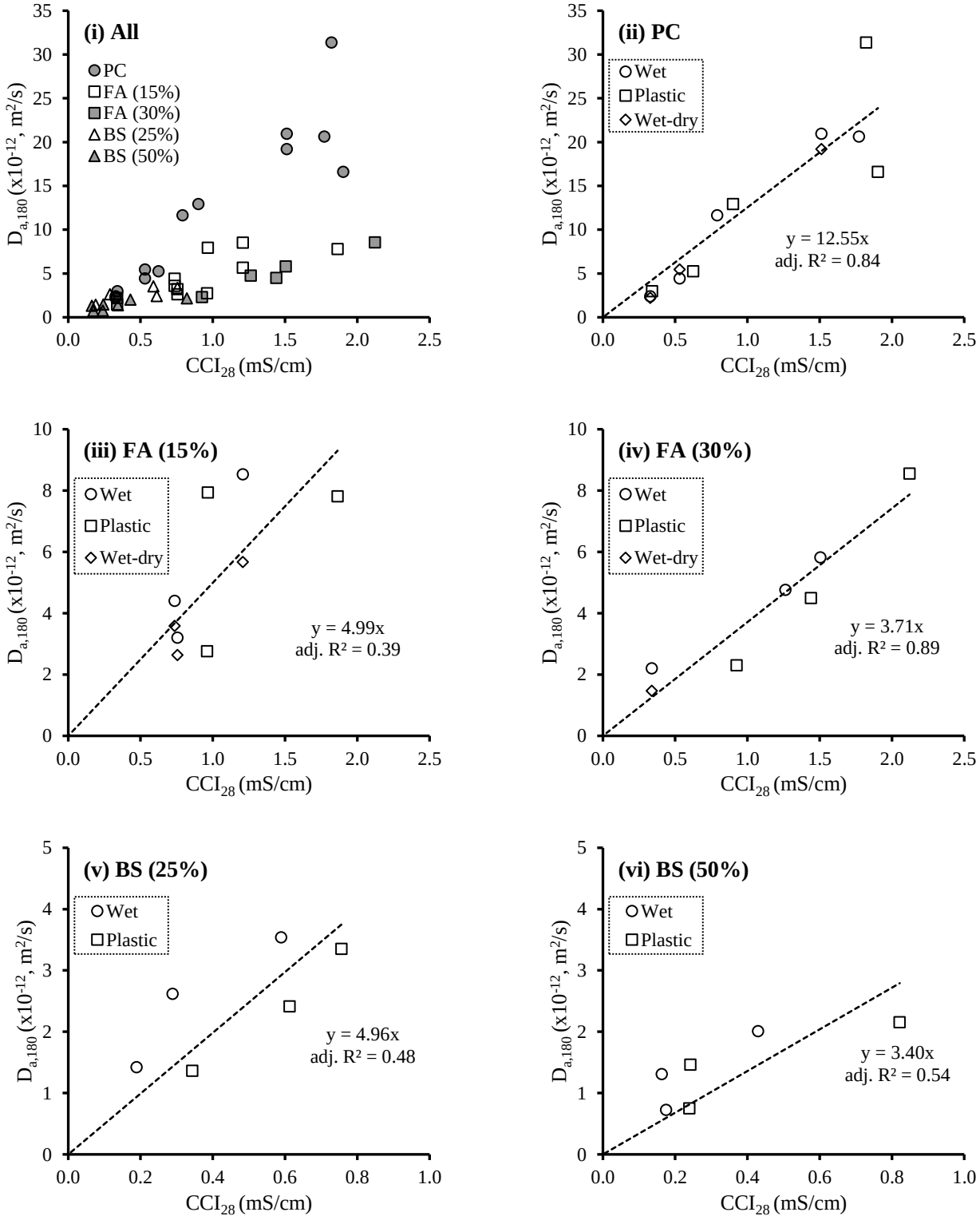

Figure 5.7 Correlations between 180-day D_a ($D_{a,180}$) and 28-day CCI (CCI_{28}). Note: (i) w/b was in the range (0.3-0.7) for PC and (0.4-0.6) for the rest. (ii) R^2 were adjusted to account for setting the intercept to zero.

The test correlation factors obtained following Eq. (5.14) as the slope of the fitted line also exhibit a dependence on the binder type as shown in Figure 5.8. It is considered useful to express these constants

as non-linear functions of the SCM levels. In this case, exponential functions are preferred over polynomial functions to avoid over-fitting and over linear functions to avoid under-fitting. Moreover, further efforts to find a better fit or more scientifically aligned function may not improve the accuracy in the absence of more data. These empirical correlations are used to develop an expression for D_a, which requires CCI_{28} and SCM% as input apart from the ageing coefficient as shown in Eq. (5.16) and Table 5.5.

$$D_a(t) = k_{t,180}.CCI_{28}\left(\frac{t}{28+180}\right)^{-m_a} \quad (5.16)$$

Where,

t_{ref} = 208 days (Reference age = Age at the start of exposure (28 days) + exposure duration (180 days))

CCI_{28}: Chloride conductivity index at the age of 28 days

$k_{t,180}$: Test method correlation parameter for $t_{ref} = t_{180}$; $(\frac{cm}{mS} \cdot \frac{m^2}{s})$

Table 5.5 Test correlation factor between $D_{a,180}$ and CCI_{28}

$k_{t,180} = 11.5 \times 10^{-12}.e^{-1.26\left(\frac{FA\%}{30}+\frac{BS\%}{50}\right)}$

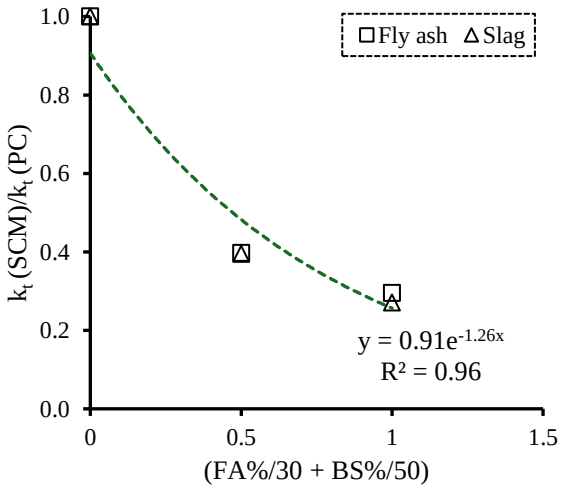

Figure 5.8 Evaluation of test correlation constant for $D_{a,180}$-CCI_{28} pair as a function of SCM proportions

5.5.1.2 Approach II

As discussed in Section 4.4, the correlation between the time-averaged (i.e., integrated) CCI[6] (termed as the equivalent CCI) and the apparent diffusion coefficient is largely independent of the binder type and holds regardless of the length of exposure. The linear regression model, shown in Figure 5.9, fits the data well in practical terms and provides conservative estimates for the low diffusivity SCM concretes that are of most practical relevance in marine conditions. This correlation can be used to derive D_a from the 28-day CCI and α (ageing coefficient of CCI) as shown in Eq. (5.17) and (5.18). The time-dependent reduction in D_a is limited to 25 years in this approach following Life-365, as previously discussed (Section 5.4.2).

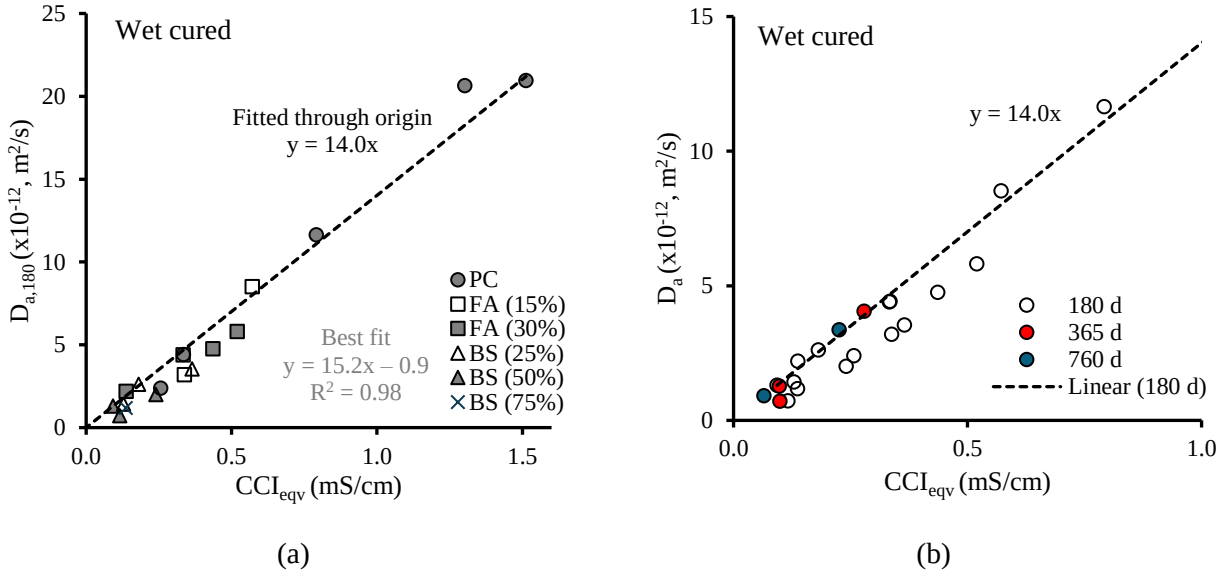

Figure 5.9 (a) Correlation between the 180-day D_a and the time-integrated equivalent CCI and (b) validation with 365-day and 760-day exposure data.
Note: scope of concrete mix designs and curing: binder type (CEM I 52.5N, fly ash (15%, 30%), slag (25%, 50%, 75%)), w/b ratio (0.3-0.7), curing (28-day wet immersion)

$$D_{a,lab}(t) = k_t \frac{1}{FF_{28}} f(t) = \left(14.0 \cdot CCI_{eqv.}\right) \times 10^{-12} \quad (5.17)$$

Where,

$D_{a,lab}$ (t) [m^2/s] is the laboratory-based apparent diffusion coefficient at age 't' [days].

[6] $CCI_{eqv} = \frac{\int_{28}^{28+t_{exp}} CCI_{28}\left(\frac{t}{28}\right)^{-\alpha} dt}{\int_{28}^{28+t_{exp}} dt}$

k_t is the test method parameter.

FF_{28} is the formation factor of concrete at the age of 28 days.

f (t) is the time development parameter.

$$CCI_{eqv} = \begin{cases} CCI_{28} \cdot \left[\dfrac{\left(28 + t_{exp}\right)^{1-\alpha} - 28^{1-\alpha}}{(1-\alpha) \cdot 28^{-\alpha} \cdot t_{exp}}\right], & 0 < t_{exp} \leq 9125\ days\ (25\ years) \\ CCI_{28} \cdot \left[\dfrac{(28 + 9125)^{1-\alpha} - 28^{1-\alpha}}{(1-\alpha) \cdot 28^{-\alpha} \cdot 9125}\right], & t_{exp} > 9125\ days\ (25\ years) \end{cases} \quad (5.18)$$

CCI_{28} [mS/cm] is the CCI at the age of 28 days.

α is the ageing coefficient of CCI.

t_{exp} [days] is the exposure duration.

The main advantages of this approach are that it eliminates the need for individual D_a-CCI correlations for each binder type and only requires electrical parameters (28-day CCI and α) to expand the model to other concrete binder materials. Due to these significant advantages, Approach-II is preferred over Approach-I for service life prediction. As data on other binder materials become available in the future, this correlation can be validated and refined.

5.5.2 Effect of lab and field curing

As discussed in the previous section, the effect of curing on the correlations between CCI and D_a is not clear from the results of this study. This is primarily due to differences in the effect of curing on CCI and D_a as test parameters and different binder systems. Curing influences the 28-day CCI values as shown in Section 4.2.3, but it does not affect D_a beyond the first month of exposure. Hence, differences in CCI values between lab wet cured concrete and field cured concrete should be expected and accounted for in design recommendations even though it is not considered in the D_a-CCI relationship.

The 28-day CCI after 28 days of wet curing in the lab (considered as the lab potential CCI) and the 28-day CCI after 7 days of plastic wrapping in the lab (considered as field potential CCI), from the experimental results of the present study are compared in Figure 5.10. This comparison reveals that the lab potential CCI is lower than the field potential CCI by 10% for PC concretes, and 30-40% on average for FA/BS concretes. Since the D_a-CCI correlations are based on both wet-cured and plastic-cured CCI values, the effect of curing can be halved.

Thus, it is recommended that the following tolerances based on curing differences between the lab and the field be given, for PC: 5%, FA/BS: 15%. Within these tolerances, the expected diffusion coefficient and the service life are not expected to change.

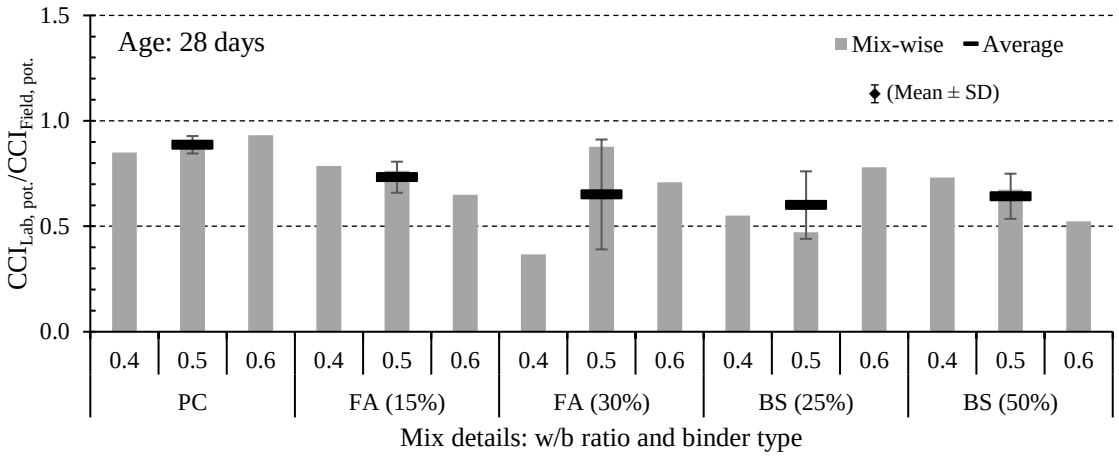

Figure 5.10 Ratio of lab potential CCI and field potential CCI to assess the effect of curing on CCI on different concrete compositions

5.6 Surface chloride concentration

The surface chloride concentration represents the boundary condition in the ERFC model based on the total chloride profile even though it is not purely an environmental action parameter. It rather includes the material response within it. This means that the C_s depends not only on the seawater salinity, temperature, characteristics specific to the exposure zone, and weather conditions, but it also varies with the type of binder, w/b ratio, compaction, and curing. The empirical approach is to model C_s values directly based on the analysis of chloride profiles obtained from field observations. Due to the inherent variability of the environmental conditions from one place to another, and the large variety of concrete materials used, large variability in the long-term C_s values and their time-dependence has been reported (Ann, Ahn & Ryou, 2009). Sufficiently long studies (i.e., until C_s stabilises to some extent, for instance, >10-15 years) tracking the variation of C_s with time are not available at present for the South African conditions, which can be used to model the time variation of C_s in a reliable manner. Therefore, the time development of C_s is ignored in the present model. Nevertheless, the long-term C_s to expect in different exposure zones in the Western Cape region according to the binder type was presented in a previous study based on an extensive chloride profile survey of existing structures of ages 1-75 years (Mackechnie & Alexander, 1997).

These published long-term C_s values are adopted for the present model (after conversion in terms of %mass of concrete). However, a simplified factor is added to account for the effect of the w/b ratio based on the immersion results of the present study as discussed in Chapter 4. The $C_{s,max}$ values represent the C_s values corresponding to the w/b ratio of 0.4. This factor modifies the C_s value for any deviation of the w/b ratio from 0.4. Figure 5.11 shows how the relationship was derived.

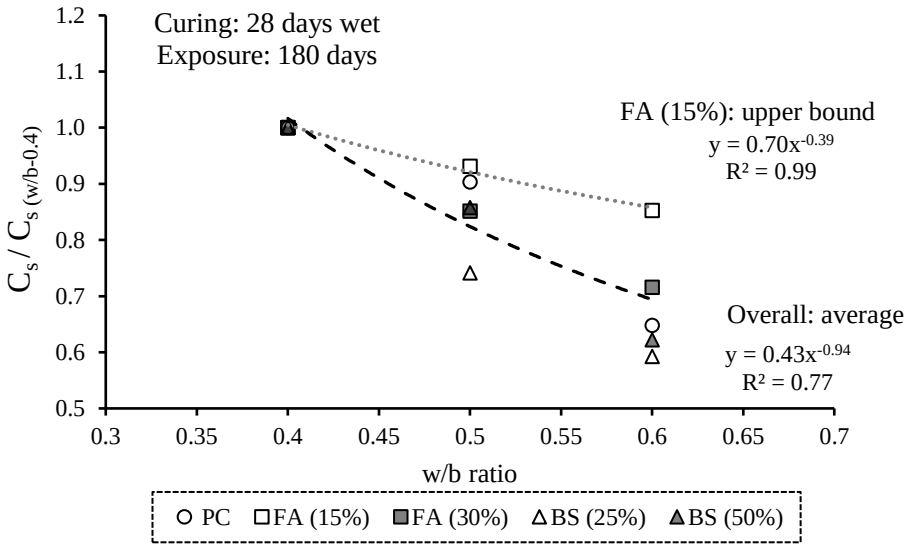

Figure 5.11 Determination of the w/b ratio factor for $C_{s,ult}$ from experimental data of the present study

The average relationship based on all the data is adopted as shown in Eq. (5.19) because it seems to provide a reasonable conservative estimate for most of the concrete mixtures. The values obtained from the adopted relationship agree well with the range recommended by previous research (Mackechnie, 2001). Regarding the effect of curing, the experimental results of this study (see Section 4.3.3) indicate that the variation in C_s values in relation to curing is minimal for curing durations longer than 7 days. In view of the present results, curing is assumed to have no effect on C_s in the proposed model.

$$C_{s,ult} = 0.43\left(\frac{w}{b}\right)^{-0.94} C_{s,\frac{w}{b}-0.4} \tag{5.19}$$

Where,

$C_{s,ult}$ represents the ultimate surface chloride concentration by %mass of concrete.

$C_{s,w/b-0.4}$ is according to Table 5.6.

Table 5.6 $C_{s,w/b-0.4}$ values adopted for the model (Mackechnie, 2001).

Binder	$C_{s,max}$ (%concrete)	
	Tidal/Splash	Air-borne
PC	0.7	0.4
FA (30%)	0.9	0.5
BS (50%)	1.1	0.6

Note: $C_{s,max}$ values for intermediate SCM levels can be estimated through linear interpolation.

5.7 Service life prediction

5.7.1 Proposed model

The proposed model for estimating the corrosion-free service life in selected South African marine environments is summarised as follows.

Governing Equation
$C_x = C_{\text{s,ult}} \left(1 - erf\left[\frac{x}{2\sqrt{(D_a . t_{exp})}}\right]\right)$
$D_a = k_e \cdot \left(14.0 \cdot CCI_{28} \cdot f(t)\right) \times 10^{-12}$ [m²/s]

Input Parameters	
CCI_{28}	28-day CCI [mS/cm]
f (t)	$f(t) = \begin{cases} \left[\frac{(28 + t_{exp})^{1-\alpha} - 28^{1-\alpha}}{(1-\alpha) \cdot 28^{-\alpha} \cdot t_{exp}}\right], & 0 < t_{exp} \leq 9125\ days\ (25\ years) \\ \left[\frac{(28 + 9125)^{1-\alpha} - 28^{1-\alpha}}{(1-\alpha) \cdot 28^{-\alpha} \cdot 9125}\right], & t_{exp} > 9125\ days\ (25\ years) \end{cases}$
α	$\alpha = 0.25 + 0.9\left(\frac{FA\%}{30}\right) + 0.35\left(\frac{BS\%}{50}\right) - \left[0.3\left(\frac{FA\%}{30}\right)^2 + 0.2\left(\frac{BS\%}{50}\right)^2\right]$

	Exposure Zone (→) / Site (↓)	Submerged/ lower tidal	Upper tidal	Splash	Air-borne (<5 km from sea)
k_e	Granger Bay (Cape Town)	0.8	1.1	1.3	0.8
	Durban Harbour (Durban)	1.2	1.4	1.7	0.8

$C_{s,ult}$	$C_{s,ult} = 0.43\left(\frac{w}{b}\right)^{-0.94} \cdot C_{s,\frac{w}{b}-0.4}$ [%-mass of concrete]			
	$C_{s,w/b-0.4}$	Binder	Tidal/Splash	Air-borne
		PC	0.7	0.4
		FA (30%)	0.9	0.5
		BS (50%)	1.1	0.6

C_{crit}	0.05% [%-mass of concrete]

The $C_{s,ult}$ values are based on observations of long-term C_s values in the Western Cape region (Mackechnie, 2001). Long-term C_s data for the Durban region are presently unavailable. Further research should try to bridge this gap. In the meantime, C_s values for the Western Cape region can be used for the purpose of comparing mix designs for the Durban region. However, higher values than in the Western Cape region have been observed in Durban after a few years of exposure (Heiyantuduwa-Beushausen, 2022). Therefore, service life design for the Durban region must be performed with due caution (i.e., conservatively) until better estimates are available.

5.7.2 Salient features of the proposed model and a comparison with the previous model

A salient feature that differentiates the proposed model from most other chloride models in the international context (Mangat & Molloy, 1994; Polder & De Rooij, 2005; fib bulletin 34, 2006; Tang, 2008; Andrade et al., 2013; Life-365 v2.2.3, 2020) is the use of the formation factor measure as an indicator of the short-term diffusivity of concrete. Some attempts have been made in the recent past (Isgor & Weiss, 2019; Yang et al., 2020) to utilise the formation factor for service life prediction. However, these are complex computational models based on physical modelling approaches. More importantly, these models are so far only applicable to the laboratory environment and have yet to be extended to the real field marine environment. These aspects limit the practical relevance of these models at present. Other models that include field influences, such as the fib model code (fib bulletin 34, 2006), consider temperature as the sole environmental influence on diffusivity, which may limit their applicability in wet-dry exposure zones. The present model instead proposes the use of an empirical coefficient that accounts for the net effect of the various field influences on the apparent diffusion coefficient.

The proposed model uses the chloride conductivity index (CCI) as a practical measure of the formation factor following previous research (Streicher & Alexander, 1995). The CCI has been used previously in a similar way by Mackechnie (Mackechnie, 1996) to generate a service life prediction model for selected South African marine conditions (Mackechnie, 2001). However, there are important methodological differences between Mackechnie's model and the modelling approach presented in this study. Mackechnie's model requires the following two input parameters/functions related to the material's resistance (Figure 5.12).

I. Correlations between the 28-CCI and the so-called 'modified CCI'[7] ($CCI_{mod.}$) values
II. Ageing coefficients for the apparent diffusion coefficient ('m' value)

Both the required inputs are a function of the binder type. While the CCI_{28}-$CCI_{mod.}$ correlations require relatively short-term and simple electrical testing; the measurement of m values necessitates the more

[7] Modified CCI: It is defined as the CCI measured on the specimens stored in 5 M NaCl solution between the ages of 28 days and 98 days. The $CCI_{mod.}$is postulated to provide a quick measure of the long-term binding and hydration on the CCI and thus on the diffusion coefficient (Mackechnie, 1996).

tedious diffusion testing. On the other hand, the proposed model does not require measuring the $CCI_{mod.}$ or the m value (Figure 5.13). The only parameter needed to relate CCI to the long-term D_a is the ageing coefficient of CCI (α), which eliminates the requirement of diffusion testing for extending the model to other concrete materials, except for intermittent validation work. Evidently, measuring α is far easier than measuring m, which can even be further simplified by using the Wenner resistivity test instead of the chloride conductivity test as shown in Section 4.2.5.

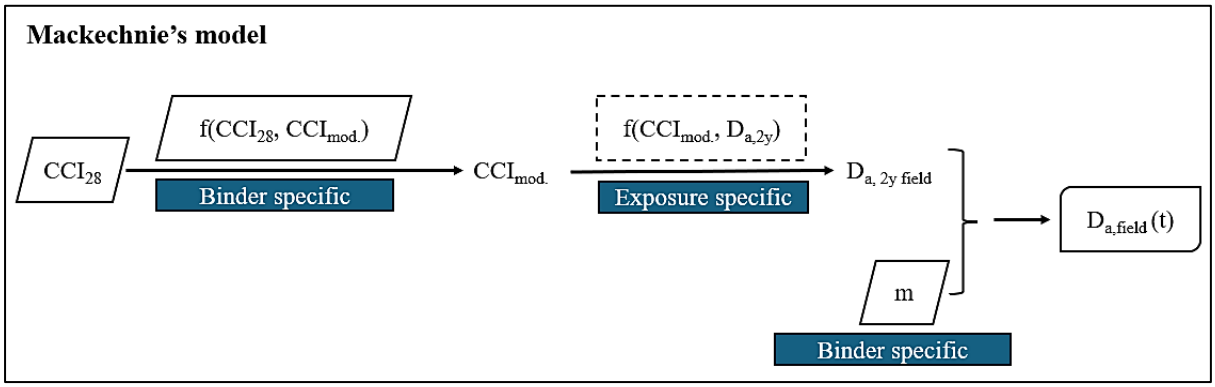

Figure 5.12 Scheme for modelling D_a in Mackechnie's model [f(): represents correlation]

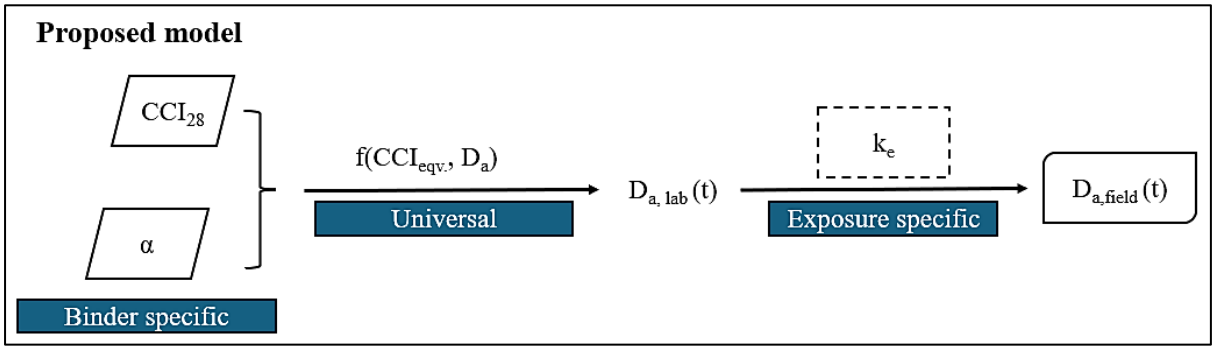

Figure 5.13 Scheme for modelling D_a in the proposed model [f(): represents correlation]

Through further simplification and clear delineation of the laboratory and field influences, the present modelling approach provides better comprehensibility. This is expected to minimise errors and increase adoption by the industry. Furthermore, fewer and simpler input parameters required for modelling will significantly reduce the efforts needed to incorporate new materials into the scope of the model. The incorporation of other exposure sites will however still require time and effort. Further simplification in this regard could go a long way to minimise the effort needed to include other sites of relevance.

A limitation of the proposed model, which it shares with Mackechnie's model, is that C_s values needed for modelling are only available for selected binder (SCM) types: fly ash and blast-furnace slag. Since long-term C_s values will not be available for new binders in the foreseeable future, further work is needed to find ways of approximating this information and enable service life prediction for such

materials. Another limitation that persists in this model is that acquiring reliable data for calculating the ageing coefficient (α) may take a few months in the design phase, which may not be available in some cases. However, this limitation can be readily circumvented by generating a database of α for a wide range of relevant binder materials, in advance.

5.7.3 Service life estimates

5.7.3.1 Sensitivity to influencing parameters

The predicted chloride profiles show sensitivity to crucial material and exposure parameters. A limited sensitivity analysis is presented in Figure 5.14. This analysis shows that crucial parameters such as SCM level, w/b ratio, exposure zone, expected service life produce significant changes in the estimated cover depth requirements. Within the parameters selected, the greatest change on the required cover depth occurs by the incorporation of SCMs in the binder.

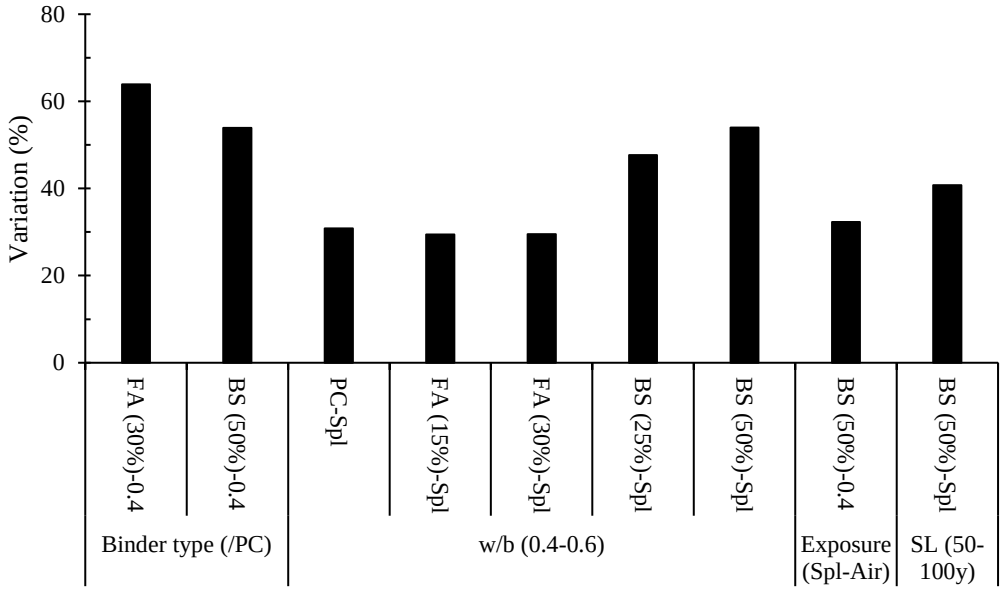

Figure 5.14 Sensitivity of estimated cover depth to selected parameter changes (Note: analysis performed with the following selected default conditions (unless otherwise mentioned in the figure): Exposure site: Granger Bay, exposure zone: splash zone, SL= 50 y, w/b: 0.4)

5.7.3.2 Design application

Based on the model predictions, a simple design chart has been developed for a desired service life of 50 years under the splash zone at Granger Bay as shown in Figure 5.15. This illustrative chart provides a means of selecting mix properties (binder type and CCI) based on the desired cover depth or any other combination of these parameters. Similar charts can be developed for other conditions for easy use, if desired. It can be observed that different binders require different CCI for a given cover depth. In other words, it can be stated that a given CCI may lead to different durability performance depending on the binder type. This is a consequence of differences in the long-term improvements in the chloride

resistance of different binders. It is also clear from the model predictions that plain Portland cement concretes even at very low water w/b ratios (or low CCI) cannot provide adequate protection to rebar in marine environments, necessitating the proper use of SCMs in these environments.

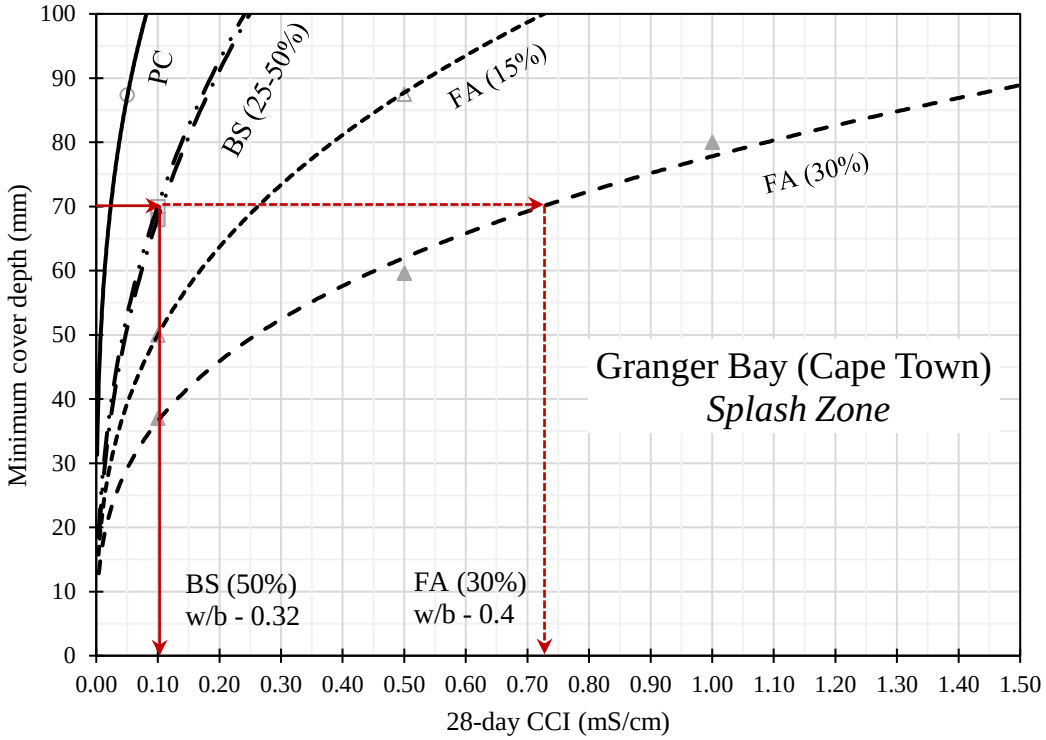

Figure 5.15 A design chart for selected conditions: the estimated minimum design cover depth based on the 28-day CCI, for different binder types

Since binder materials may differ in their reactivity depending on the grade and source, it is important to collect data for the local materials to be used. These differences are important for the purpose of long-term modelling and short-term quality control. The model framework presented in this study can be conveniently used to extend the model to materials out of the present scope of the model.

Using the model predictions, a designer will be able to specify the required CCI values corresponding to the specified binder options and the cover depth. Alternatively, a mix design can be directly specified by the designer and quality can be monitored through CCI. In both cases, the as-achieved CCI should be used to update the service life predictions, which could be used to plan subsequent steps in the construction process and future maintenance. Given the binder-specific nature of the long-term chloride resistance of concrete, the 28-day CCI must be specified with a corresponding binder type.

The input parameters are established in this chapter following a deterministic approach for the sake of simplicity. The model parameters vary around a central value and the variability of individual parameters results in a probability distribution for the output. It is recommended that these aspects be

addressed through a full- or semi-probabilistic design approach in the next stage of model development. Guidance can be availed from the literature (Alexander, Ballim & Stanish, 2008; Muigai, Moyo & Alexander, 2012).

5.8 Concluding remarks

A model is proposed in this chapter to estimate the corrosion-free service life for concrete structures exposed to chlorides in selected marine conditions of South Africa to aid the process of durability design. Some concluding remarks are provided below:

1. The proposed model uses the error function solution to Fick's 2nd law as the governing equation. It uses a generalised relationship between CCI and D_a to enable the use of 28-day chloride conductivity index as the main short-term input parameter and the ageing coefficient of CCI as the long-term parameter. The effect of exposure conditions on chloride diffusivity is addressed through simple empirical coefficients developed using laboratory and field data.
2. The proposed model is relatively simple and integrates quality control parameters with the long-term effects of materials and exposure conditions. It is sensitive to important influencing factors, namely, binder type, w/b ratio, exposure zone, and exposure climate.
3. Although the model incorporates macro and one level of micro (exposure zones) exposure conditions, it must be emphasized that the local variation in a single region and in different parts of the same structure are naturally wide.
4. The current treatment is deterministic in nature for simplicity but may be extended to probabilistic terms.
5. Based on service life modelling, a performance specification for marine conditions should properly require the following components in regard to chloride ingress for the desired service life:
    a. Classification of exposure conditions based on regional climatic conditions and local exposure conditions in terms of marine exposure zones and position from the sea
    b. Binder options and minimum binder-specific CCI values to achieve a minimum cover depth

Finally, it must be emphasised that validation of the proposed model with independent long-term data is essential to evaluate its accuracy and identify possible limitations and shortcomings.

Chapter 6 CONCLUSIONS

6.1 Introduction

This research was undertaken with the main aim of developing a service life prediction model for chloride penetration in marine environments, using the chloride conductivity index as one of the main material parameters, particularly for South African conditions. The potential of the surface conductivity method as an indicator of the resistance of concrete to chloride diffusion was also studied. The experimental program consisted of the penetrability characterisation of lab concretes using the chloride conductivity index (CCI), surface resistivity, and bulk diffusion tests. Concrete mixes were prepared using w/b ratios ranging between 0.3 and 0.7, binders incorporating fly ash (0 – 30%) or slag (0 – 75%), and cured under either wet conditions or 7 days of plastic wrapping. This chapter presents a summary of the main findings and highlights the main conclusions derived from the experimental and modelling work undertaken in this study and weighed against other evidence from the literature. Recommendations for further studies are also included.

6.2 General discussion and outcome

Electrical tests are being increasingly adopted to characterise the durability potential of concrete materials and extend use of these tests to quality control and durability design of reinforced concrete structures. Electrical tests enable rapid assessment of relevant concrete properties and thus provide a substantial practical benefit over durability tests such as bulk diffusion. The advantage of convenience and economy in testing is not to be underestimated in practical applications. However, in the selection of a suitable electrical test, one must weigh convenience with the accuracy and reliability that a method provides in measuring the relevant transport properties of the cover concrete. The ability to unambiguously test the near-surface region of the as-built concrete is fundamental to the performance approach to durability.

Furthermore, the focus in using these methods is often to characterise concrete at early ages, which is in line with quality control requirements. However, it is the long-term properties that are of concern to durability, which depends on the long-term evolution of the material properties and their interaction with the exposure environment. An effective durability design strategy must properly take account of these long-term changes to assess the suitability of materials for the intended exposure environment.

These aspects were investigated in this research. The findings of this research, as described in the following sections, suggest that it is possible to use the rapid electrical methods to not only characterise the short-term quality of concrete but also determine the long-term changes concrete undergoes in marine environments. It is however imperative to select the test method carefully and to be aware of the limitations to avoid misinterpreting their results. The Wenner resistivity method in this regard was found to be less robust than the chloride conductivity method against common material- and

environment-related influences that can interfere with the evaluation of concrete quality. Nevertheless, the Wenner resistivity was useful in characterising the long-term evolution of concrete penetrability. This study presents a new generalised empirical approach to predicting the long-term chloride diffusivity solely through electrical penetrability measurements. Based on this and other contributions, a simple service life model was formulated, which is the main practical outcome of this work.

6.3 Experimental findings and conclusions

6.3.1 Evaluation of rapid conductivity methods: chloride conductivity and Wenner resistivity

As a non-destructive method, the Wenner resistivity method, also known as the surface resistivity method, has found favour with several researchers as a quality control method for concrete durability. In this study, the opportunities and limitations of the Wenner method were investigated through a comparative analysis of the surface resistivity and chloride conductivity results. The quality of the tested concrete was varied by changing composition and curing method. In total, 6 different binder blends with either fly ash (15% / 30%) or slag (25% / 50% / 75%), 5 different w/b ratios (0.3-0.7), and 2 different curing methods (continuous wet and 7-day plastic) were included. The surface resistivity was measured using a Wenner probe diagonally placed on a standard 150-mm cube specimen after a minimum immersion period of 48 hours when the specimen was not kept continuously wet as part of the selected curing regime. The chloride conductivity was measured using a direct current setup on small disc specimens extracted from the near-surface concrete and saturated with concentrated NaCl solution after oven drying.

The results of this study showed that the surface resistivity produced a different assessment of the concrete quality compared to the CCI. The assessment of concrete's transport resistance as evaluated through CCI was well supported by other experimental results of this study and the literature. The surface resistivity results on the other hand showed different, even contradicting, trends in some cases. This inconsistency was particularly noticeable in fly ash concretes in which increased levels of fly ash led to an increase in the early-age (28-day) surface resistivity despite the contrary evidence provided by the CCI results of increased early-age chloride penetrability in such concretes. Through a literature review of the effects of fly ash on the pore solution composition, it was shown that this contradiction can be attributed to the lowering of the pore solution conductivity due to fly ash addition. Similarly, the effects of curing on concrete penetrability were also obscured in surface resistivity results by incomplete saturation of the internal concrete that persisted despite the immersion of the plastic cured concrete in water for 2 days before testing. Efforts to saturate the concrete by extending the immersion in water beyond 2 days, to more than a week, proved to be inadequate given that the depth of influence in the Wenner method was found to far exceed the depth that could be saturated through normal absorption in a practical timeframe.

The time dependence of the CCI and surface resistivity under wet conditions was investigated for a time frame of 1.25 years. The ageing coefficients were computed by fitting the power law function to the conductivity-time data. As expected, both CCI and surface resistivity decreased with time under wet conditions in response to continued hydration. The SCM type and replacement level strongly affected the ageing coefficients. However, a clear influence of w/b ratio on these ageing coefficients could not be ascertained in this study. In a more substantial finding, the ageing coefficients measured for CCI corresponded well with those measured for the surface resistivity. The only major exceptions to this general trend were PC concretes. The reasons for their deviation are not yet well understood. A limited comparison of these ageing coefficient (α) with those of the apparent diffusion coefficient (m) revealed that the latter is approximately 0.7 times the former (i.e., $m = 0.7\alpha$). The difference mainly lies in the instantaneous or time-averaged nature of the electrical and diffusion parameters that results in the lower ageing coefficient for the diffusion coefficient.

Based on the findings of this study, the following main conclusions can be drawn on the effectiveness of the Wenner resistivity method in assessing the chloride resistance of cover concrete:

1. Although the Wenner resistivity method has the benefit of non-destructive evaluation, the measurements are subject to confounding influences from concrete composition and practical curing regimes through their effects on the pore solution conductivity. Similar difficulties due to the influences of pore solution have been reported for the RCPT method in the past. This prevents the Wenner method from reliably giving an unambiguous and accurate measure of the quality of the cover concrete regardless of the materials and production processes involved. A more robust test method, such as the chloride conductivity method, with a properly designed method to minimise the influence of extraneous factors on the cover concrete properties is recommended for the purpose of material characterisation and quality control. The formation factor analysis can also be used to properly understand the Wenner resistivity results. However, proper quantification of various influences on pore solution conductivity is difficult, which may limit the practical application of this type of analysis.
2. Despite these limitations, the Wenner resistivity method was found to produce reasonably accurate estimates of the ageing coefficients of the CCI (or in other words, penetrability). Hence, the Wenner method can be used as a convenient alternative to measuring the ageing coefficients of instantaneous penetrability of concrete.
3. The ageing coefficient of the apparent diffusion coefficient can be approximated as 0.7 times that of the ageing coefficient of CCI (i.e., $m = 0.7\alpha$). The convenience of the electrical methods can be advantageously used by using this simple relationship for estimating the time-dependence data (m values) necessary for chloride ingress modelling.

6.3.2 Relationship between apparent diffusion coefficient and CCI

A key objective of this study and a necessary step towards developing the service life model was to investigate the relationship between the apparent chloride diffusion coefficient (D_a) and the CCI. The D_a was measured using laboratory-based bulk diffusion experiments following the ASTM C1556 protocol for exposure. In this investigation, consistent correlations were observed between the 180-day exposed D_a and the 28-day CCI. These correlations were found to be dependent on the binder type. Based on these correlations, a given 28-day CCI predicted the 180-day D_a in the following decreasing order [Binder or SCM type (SCM level in %)]: PC > FA (15%) ≈ BS (25%) > FA (30%) ≈ BS (50%), where PC: Portland cement, FA: fly ash, and BS: blast-furnace slag.

Both D_a and CCI are time-variant parameters. The D_a was measured over the exposure duration of 6 months (age: 208 days) for all the concrete mixtures and also over exposure durations up to 2 years for selected concrete mixtures. The CCI was measured at different ages up to an age of 1.25 years. Since the 28-day CCI is an instantaneous value, the relationship of D_a with a time-averaged or equivalent CCI was explored in an attempt to separate the effects of time development due to ongoing hydration and the binding ability, on chloride penetration.

The relationship between D_a and the equivalent CCI was found to be largely independent of the binder type as opposed to the relationship between D_a and 28-day CCI. This relationship was also validated with longer exposure data (up to 2 years). The relationship is presented as follows.

$$D_{a,lab}\left(\frac{m^2}{s}\right) = \left(14.0 \cdot CCI_{eqv.}\right) \times 10^{-12} \tag{6.1}$$

Where,

$$CCI_{eqv} = CCI_{28} \cdot \left[\frac{\left(28 + t_{exp}\right)^{1-\alpha} - 28^{1-\alpha}}{(1-\alpha) \cdot 28^{-\alpha} \cdot t_{exp}}\right] \tag{6.2}$$

CCI_{28}: 28-day CCI (mS/cm); t_{exp}: exposure duration (days); α: ageing coefficient of CCI

The following inferences and conclusions can be drawn from this general relationship:

1. On the basis of Fick's 2nd law, the conductivity-diffusivity relationship, when time-dependences have been accounted for, is generally expected to vary with the binder type mainly due to the different binding abilities of different binders. However, a single common relationship irrespective of the binder type implies that chloride diffusion behaves as if there is an invariance in the binding abilities of different binders, contrary to the current understanding of the binding behaviour of common binder systems and its relationship to diffusive transport.
2. The pore penetrability can describe the apparent diffusion coefficient by its time variation without the need for a separate binding component for every binder. It implies that the time-

dependence of the apparent diffusion coefficient is mainly a result of the densification of the pore structure due to the ongoing hydration under conducive conditions offered by the marine environment. This means that the microstructural penetrability and the ability for pore refinement play a dominant role in determining the long-term resistance of concrete to chloride penetration.

3. A general D_a-CCI relationship, which can be extended to other concrete binder materials such as different SCMs, can serve as a generalised model for the apparent diffusion coefficient requiring only CCI-based parameters as input values, while eliminating the need for the diffusion-based 'm' value to describe the time-dependence of D_a. This is a significant development towards a simplified and unified modelling approach.

These findings significantly deviate from the existing understanding that the chloride resistance of SCMs is to be ascribed to a large extent to their superior binding ability. Instead, the results and analysis of this study strongly suggest that the main differentiating factor is the long-term ageing-dependent reduction in microstructural penetrability. This is a significant improvement of the current understanding of chloride diffusion behaviour in concrete and one of the crucial novel contributions of this study.

6.4 Service life prediction model

6.4.1 Model development: a summary

The primary aim of this study was to develop a model for the time-to-corrosion-initiation or the corrosion-free service life of reinforced concrete structures exposed to South African marine conditions. This was accomplished with the help of the experimental results collected in this study and the field data obtained from previous studies. Since the goal was to produce a practice-oriented model, the error-function solution approach was favoured for its simplicity and general acceptance. The error function solution to Fick's 2nd law of non-steady state diffusion requires two defining parameters: the apparent diffusion coefficient (D_a) as the material's resistance parameter and the surface chloride concentration (C_s) as the boundary condition. The methodology selected for describing these two parameters constitutes the development of the model proposed in this study, as summarised below.

6.4.1.1 Description of the apparent diffusion coefficient (D_a)

It is well known that the diffusion coefficient can be affected by, inter alia, the environmental influences such as temperature and relative humidity, and reduces with increasing exposure duration. Hence, these influencing parameters must be accounted for in any model of the D_a. In this model, the D_a was expressed as a function of the early-age CCI following the Nernst-Einstein relation and the formation factor concept, modified appropriately for the above-mentioned influences using separate modifying parameters. The task of modelling was accomplished in two steps. The first part comprised linking the

early-age CCI (28-day CCI) to the laboratory-based D_a. The second part consisted of modifying the laboratory-based D_a according to the environmental conditions of the field in order to arrive at the field-based D_a.

In the first step, two approaches to linking the short-term CCI with D_a in the laboratory conditions were explored. In the first approach, direct correlations between the 28-day CCI and 180-day exposed D_a were established. These correlations were found to be dependent on the binder type and required binder-specific correlations to derive D_a using the 28-day CCI. This approach required the use of the binder-dependent ageing coefficient of the D_a (m) to describe the time-dependence of D_a. In the second approach, the correlation between the time-integrated or equivalent CCI and D_a was used to relate the 28-day CCI to the long-term D_a. Because this correlation is extendable to any concrete binder type and requires 'α' (CCI ageing coefficient) instead of 'm', this approach was favoured in this model.

In the second step, a simplified empirical approach to derive the environmental parameter, k_e, was presented. In this approach, the environmental influences on the D_a are quantified by comparing and normalising the field-based D_a with the corresponding laboratory-based D_a. Using the sets of field and lab D_a available from a previous study (Heiyantuduwa-Beushausen, 2022), k_e values were derived for different macro and micro-exposure conditions in South Africa. This approach relies on actual empirical data contrary to the more common practice of using the Arrhenius equation with or without the RH factors. The latter approaches were observed in this study to only produce satisfactory results in the case of the submerged zone.

6.4.1.2 Description of the surface chloride concentration (C_s)

Long-term total C_s values were adopted from Mackechnie's model (Mackechnie, 2001) as the boundary condition for service life prediction. The adopted C_s values are sensitive to the exposure zone, regional climate, and the binder type. A calibrating factor was developed based on the bulk diffusion results of the present study to account for the influence of the w/b ratio on the C_s values (expressed in terms of %mass of concrete). The time-dependence of C_s could not be addressed in this model due to insufficient information available in this regard in the South African context.

The final form of the proposed model along with the input parameters derived for selected material and environmental conditions are presented in Table 6.1

.

Table 6.1 Summary of the proposed model

Governing Equation
$C_x = C_{s,ult}\left(1 - erf\left[\frac{x}{2\sqrt{(D_a \cdot t_{exp})}}\right]\right)$
$D_a = k_e \cdot \left(14.0 \cdot CCI_{28} \cdot f(t)\right) \times 10^{-12}$ [m²/s]

Input Parameters	
CCI_{28}	28-day CCI [mS/cm]
f (t)	$f(t) = \begin{cases} \left[\frac{(28+t_{exp})^{1-\alpha} - 28^{1-\alpha}}{(1-\alpha)\cdot 28^{-\alpha}\cdot t_{exp}}\right], & 0 < t_{exp} \le 9125\ days\ (25\ years) \\ \left[\frac{(28+9125)^{1-\alpha} - 28^{1-\alpha}}{(1-\alpha)\cdot 28^{-\alpha}\cdot 9125}\right], & t_{exp} > 9125\ days\ (25\ years) \end{cases}$
α	$\alpha = 0.25 + 0.9\left(\frac{FA\%}{30}\right) + 0.35\left(\frac{BS\%}{50}\right) - \left[0.3\left(\frac{FA\%}{30}\right)^2 + 0.2\left(\frac{BS\%}{50}\right)^2\right]$

	Exposure Zone (→) / Site (↓)	Submerged/ lower tidal	Upper tidal	Splash	Air-borne (<5 km from sea)
k_e	Granger Bay (Cape Town)	0.8	1.1	1.3	0.8
	Durban Harbour (Durban)	1.2	1.4	1.7	0.8

$C_{s,ult}$	$C_{s,ult} = 0.43\left(\frac{w}{b}\right)^{-0.94} \cdot C_{s,\frac{w}{b}-0.4}$ [%-mass of concrete]			
	$C_{s,w/b-0.4}$	Binder	Tidal/Splash	Air-borne
		PC	0.7	0.4
		FA (30%)	0.9	0.5
		BS (50%)	1.1	0.6

C_{crit}	0.05% [%-mass of concrete]

Glossary: 'x' is the depth into concrete (m); 'C_x' is the chloride content at depth 'x'; 't_{exp}' is the exposure duration (days); 'D_a' is the apparent diffusion coefficient (m²/s); 'α' is the ageing coefficient of CCI; 'k_e' is the environmental modification parameter for 'D_a'; '$C_{s,ult}$' is the ultimate (long-term) surface chloride content (%-mass of concrete); 'C_{crit}' is the critical chloride threshold content for corrosion initiation ((%-mass of concrete)

6.4.2 Practical application of the proposed model

The proposed model facilitates the durability design of new reinforced concrete structures by providing a means of quantitatively specifying the cover depth and concrete mix design (binder and CCI) required under given exposure conditions to achieve the target service life. Different combinations of mix design choices and required cover depth, all leading to the given target service life, can be explored using this model, thereby providing flexibility in designing and addressing other structural and durability design concerns.

A designer will be able to specify the following parameters using this model:

1. Minimum cover depth to rebar
2. Binder type and 28-day CCI

The binder type must be specified with the 28-day CCI as it dictates both the short-term and long-term chloride resistance of concrete. While the 28-day CCI indicates the short-term chloride resistance, the ageing coefficient determines the long-term evolution of the chloride resistance, which is a function of the binder type. To provide some flexibility to the concrete supplier and the contractor, different binder options with attached CCI values can be specified.

The 28-day CCI value is intended as the quality control target value. The acceptance values for the as-achieved CCI of the as-built cover concrete can be decided by the designer based on the degree of quality control available on-site. The findings of this study on the disparity between the effects of curing on CCI and chloride diffusivity can be utilised in this regard. In this study, it was found that the 7-day plastic cured CCI was, on average, 30% higher than the 28-day wet cured CCI for SCM concretes. In contrast, the 180-day D_a remained unaffected by changing the curing method from 28-day wet curing to 7-day plastic curing. Therefore, it can be recommended that a tolerance of up to 30% in the 28-day CCI of SCM concretes can be allowed for differences in curing quality between laboratory and field in the as-built values without a significant loss of service life.

In any case, the as-built values should be used to update the service life model for the constructed structure and the predicted chloride profiles can be used to plan and manage maintenance and preventive strategies. The use of this model must be accompanied by a proper appreciation of the uncertainty and limitations inherent in the models of chloride transport. Hence, efforts to excessively fine tune parameters are likely to be in vain. A conservative approach is expected to yield better long-term outcomes and is therefore recommended

6.4.3 Key features of the proposed model: a general discussion

The salient features of the proposed model are discussed as follows.

1. Various factors influence the ability of concrete to resist the ingress of chloride ions. These factors range from mix design choices such as the binder type and w/b ratio to construction

quality control such as compaction and curing, among other things. Through their influence on the transport properties of the cover concrete, these factors influence the service life of the built structure. The proposed model adopts the chloride conductivity index as an unambiguous, accurate, and rapid measure of the transport resistance of the concrete in the cover region. The CCI, being sensitive to changes in these practical influencing factors, can reflect relevant changes in the cover concrete properties, which could in turn influence the service life predictions. It can also serve as a practical means to monitor the quality of construction and manage the quality control processes. Furthermore, CCI being a direct measure of the formation factor, there is a strong theoretical basis for a relationship between CCI and the diffusion coefficient.

2. The model follows a simplified approach to linking the early-age CCI to the long-term diffusivity. The general relationship found between the time-integrated CCI and the apparent diffusion coefficient independent of the binder type was used to derive the laboratory-based D_a from the 28-day CCI. In a major contribution to the empirical approach to chloride modelling, this relationship, being independent of the binder type, enables the inclusion of new binder materials only based on the ageing coefficient of CCI—the 'α' value. It is a significant outcome of this study that this approach eliminates the necessity of diffusion data pertaining to D_a or m to expand the scope of the model. In a further simplification, based on the evidence of this study, it is proposed that the 'α' value be conveniently measured through the Wenner resistivity method, thereby minimising even the effort of acquiring the CCI-t data.
3. A simplified empirical approach to the quantification of the environmental influences on the apparent diffusion coefficient was presented. The proposed approach is based on direct measurement of the apparent diffusion coefficient under the given field conditions and its normalisation with the corresponding laboratory-based apparent diffusion coefficient. Using this approach the field influences can be quantified through a single set of measurements (i.e., a single concrete mix) as opposed to needing a series of measurements required for a regression analysis. This enables better quantification of the macro- and micro-environmental conditions with regard to their influences on the material's resistance. This type of quantification goes beyond the qualitative classification system of the exposure environment currently prevalent in terms of exposure zones and integrates the macro-climatic conditions into the environmental characterisation. This simplified approach, together with the long-term C_s data, where possible, could be used to generate 'environmental severity maps' for sites of importance or on a national level. In this study, the environmental parameters were quantified for the Granger Bay (Western Cape) and the Durban Harbour sites.

In conclusion, a simplified approach to modelling and the compact nature of the proposed model will promote comprehensibility and ease of use. The minimisation of the input requirements will help

service life modelling keep pace with the ongoing rapid development of new materials intended to improve sustainability. The underlying philosophy underpinning and guiding this work is encapsulated in the following statement.

"All models are wrong, but some are useful!"[8]

This simplified approach intended to be practically useful is expected to help in increasing the adoption of the performance-based approach to durability and to ultimately contribute towards constructing more durable structures.

6.5 Recommendations for further research

The following suggestions are made to overcome some of the limitations of the present study and advance this field of research:

1. Although the D_a-CCI relationship was validated in this study, the proposed model as a whole must be validated with independent data to verify its accuracy and identify possible deficiencies.
2. Presently, the proposed model includes various replacement levels of fly ash and slag as binder options. This can be significantly increased to include other binder options by collecting the ageing data for CCI or Wenner resistivity.
3. Characterisation of the environmental influences on D_a (k_e) and the long-term C_s values to include other marine sites can assist in building quantitative exposure classification for the marine environment and expand the applicability of the model. Although long-term data are more reliable, relatively short-term D_a measurements on corresponding specimens exposed to laboratory and field conditions can be used for generating k_e values. The long-term C_s values on the other hand will require chloride profiling of selected existing structures in service under long-term marine exposure.
4. The effect of chloride concentration on D_a could not be determined in this study. Future research should investigate this aspect and assist in further refinement of the relationship between the laboratory and field D_a.
5. The proposed model considers concrete in a crack-free, unloaded state, which is a simplification/idealisation of the actual state of concrete in structures. These aspects must also be investigated in future research.
6. The proposed model follows a deterministic approach for the sake of simplicity. However, given the uncertainty inherent in the material and exposure parameters, it is recommended that

[8] Credited to George E. P. Box, 1976

a probabilistic framework is generated and used to enable the analysis of the output in probabilistic terms.

LIST OF REFERENCES

AASHTO T 358. 2015. Surface resistivity indication of concrete's ability to resist chloride ion penetration. *American Association of State Highway and Transportation Officials*.

ACI 318. 2014. *Building Code Requirements for Structural Concrete*. Farmington Hills, MI: American Concrete Institute.

Aïtcin, P.C. 2016. The importance of the water-cement and water-binder ratios. In *Science and Technology of Concrete Admixtures*. Elsevier Inc. 3–13. DOI: 10.1016/B978-0-08-100693-1.00001-1.

Alexander, M. & Beushausen, H. 2019. Durability, service life prediction, and modelling for reinforced concrete structures – review and critique. *Cement and Concrete Research*. 122(February):17–29. DOI: 10.1016/j.cemconres.2019.04.018.

Alexander, M. & Mindess, S. 2005. *Aggregates in Concrete*. 1st ed. Taylor & Francis.

Alexander, M. & Thomas, M. 2015. Service life prediction and performance testing - Current developments and practical applications. *Cement and Concrete Research*. 78:155–164. DOI: 10.1016/j.cemconres.2015.05.013.

Alexander, M.G. & Beushausen, H. 2009. Performance-based durability testing, design and specification in South Africa : latest developments. In *Excellence in Concrete Construction through Innovation*. Limbachiya & Kew, Eds. Taylor & Francis Group, London. 429–434.

Alexander, M.G. & Nganga, G. 2016. Introduction: importance of marine concrete structures and durability design. In *Marine Concrete Structures : Design, Durability and Performance*. M.G. Alexander, Ed. Woodhead Publishing, Elsevier Ltd. 1–13.

Alexander, M.G., Ballim, Y. & Stanish, K. 2008. A framework for use of durability indexes in performance-based design and specifications for reinforced concrete structures. *Materials and Structures*. 41(5):921–936. DOI: 10.1617/s11527-007-9295-0.

Alexander, M.G., Santhanam, M. & Ballim, Y. 2011. Durability design and specification for concrete structures—the way forward. *International Journal of Advances in Engineering Sciences and Applied Mathematics*. 2(3):95–105. DOI: 10.1007/s12572-011-0027-x.

Alexander, M.G., Beushausen, H. & Otieno, M.B. 2013. Research Monograph No. 9 - Corrosion of steel in reinforced concrete : Influence of cover cracking and concrete quality. *University of Cape Town*.

Alexander, M.G., Bentur, A. & Mindess, S. 2017. *Durability of Concrete: Design and Construction*. CRC Press.

Alsayed, S.H. & Amjad, M.A. 1994. Effect of curing conditions on strength, porosity, absorptivity, and shrinkage of concrete in hot and dry climate. *Cement and Concrete Research*. 24(7):1390–1398.

Andrade, C. 2004. Calculation of initiation and propagation periods of service life of reinforcements by using the electrical resistivity. In *International RILEM Symposium on Concrete Science and Engineering: A Tribute to Arnon Bentur*.

Andrade, C., Castellote, M. & D'Andrea, R. 2011. Measurement of ageing effect on chloride diffusion coefficients in cementitious matrices. *Journal of Nuclear Materials*. 412(1):209–216. DOI: 10.1016/j.jnucmat.2010.12.236.

Andrade, C., Prieto, M., Tanner, P., Tavares, F. & D'Andrea, R. 2013. Testing and modeling chloride penetration into concrete. *Construction and Building Materials*. 39:9–18.

Andrade, C., D'Andrea, R. & Rebolledo, N. 2014. Chloride ion penetration in concrete: The reaction factor in the electrical resistivity model. *Cement and Concrete Composites*. 47:41–46. DOI: 10.1016/j.cemconcomp.2013.09.022.

Andrade, C., Climent, M.A. & de Vera, G. 2015. Procedure for calculating the chloride diffusion coefficient and surface concentration from a profile having a maximum beyond the concrete surface. *Materials and Structures/Materiaux et Constructions*. 48(4):863–869. DOI: 10.1617/s11527-015-0543-4.

Angelucci, M. 2013. The influence of mix design parameters and compressive strength on durability indices. MSc. University of Cape Town.

Angst, U.M. & Elsener, B. 2014. On the applicability of the Wenner method for resistivity measurements of concrete. *ACI Materials Journal*. 111(6):661–672. DOI: 10.14359/51686831.

Angst, U., Elsener, B., Larsen, C.K. & Vennesland, Ø. 2009. Critical chloride content in reinforced concrete - A review. *Cement and Concrete Research*. 39(12):1122–1138. DOI: 10.1016/j.cemconres.2009.08.006.

Ann, K.Y., Ahn, J.H. & Ryou, J.S. 2009. The importance of chloride content at the concrete surface in assessing the time to corrosion of steel in concrete structures. *Construction and Building Materials*. 23(1):239–245. DOI: 10.1016/j.conbuildmat.2007.12.014.

Anoop, M., Balaji Rao, K., Appa Rao, T. & Gopalakrishnan, S. 2001. International standards for durability of RC structures Part 1 - A critical review. *The Indian Concrete Journal*. (September):559–569.

Archie, G.E. 1941. The Electrical Resistivity Log as an Aid in Determining Some Reservoir Characteristics. *Transactions of the AIME*. 146(01):54–62. Available: http://onepetro.org/TRANS/article-pdf/146/01/54/2179020/spe-942054-g.pdf.

AS 3600. 2009. Australian Standard, Concrete Structures. *Standards Austrailia Limited, Sydney*.

ASTM C1152. 2004. Standard Test Method for Acid-Soluble Chloride in Mortar and Concrete. *ASTM International*. DOI: 10.1520/C1152.

ASTM C1202. 2012. Standard Test Method for Electrical Indication of Concrete's Ability to Resist Chloride Ion Penetration. *American Society for Testing and Materials*. (C):1–8. DOI: 10.1520/C1202-12.2.

ASTM C1218. 2020. Standard Test Method for Water-Soluble Chloride in Mortar and Concrete. *ASTM International*. DOI: 10.1520/C1218_C1218M-20.

ASTM C1556. 2016. Standard Test Method for Determining the Apparent Chloride Diffusion Coefficient of Cementitious Mixtures by Bulk Diffusion. *ASTM International*. 1–7. DOI: 10.1520/C1556-11A.2.

ASTM C1876. 2019. Standard Test Method for Bulk Electrical Resistivity or Bulk Conductivity of Concrete. *ASTM International*. DOI: 10.1520/C1876-19.

ASTM E177. 2020. Standard Practice for Use of the Terms Precision and Bias in ASTM Test Methods. *ASTM International*. i:1–9. DOI: 10.1520/E0177-20.2.

ASTM E178. 2008. Standard Practice for Dealing With Outlying Observations. *ASTM International*. (October, 1). DOI: 10.1520/E0178-08.

Atkinson, A. & Nickerson, A.K. 1984. The diffusion of ions through water-saturated cement. *Journal of Materials Science*. 19:68–3078.

Audenaert, K., Yuan, Q. & De Schutter, G. 2010. On the time dependency of the chloride migration coefficient in concrete. *Construction and Building Materials*. 24(3):396–402. DOI: 10.1016/j.conbuildmat.2009.07.003.

Bakera, A.T. 2018. Properties of Western Cape concrete with metakaolin. MSc. University of Cape Town.

Balestra, C.E.T., Reichert, T.A., Pansera, W.A. & Savaris, G. 2020. Evaluation of chloride ion penetration through concrete surface electrical resistivity of field naturally degraded structures present in marine environment. *Construction and Building Materials*. 230. DOI: 10.1016/j.conbuildmat.2019.116979.

Ballim, Y. 1993. Curing and the durability of OPC, fly ash and blast-furnace slag concretes. *Materials and Structures*. 26:238–244.

Ballim, Y. & Alexander, M.G. 2018. Guiding principles in developing the South African approach to durability index testing of concrete. *6th International Conference on Durability of Concrete Structures, ICDCS 2018*. (July):36–45.

Bamforth, P.B. 1999. The derivation of input data for modelling chloride ingress from eight-year UK coastal exposure trials. *Magazine of Concrete Research*. 51(2):87–96.

Bamforth, P.B., Price, W.F. & Emerson, M. 1997. An international review of chloride ingress into structural concrete. *Transport Research Laboratory, Edinburgh*. Report 359.

Barneyback, R.S. & Diamond, S. 1981. Expression and analysis of pore fluids from hardened cement pastes and mortars. *Cement and Concrete Research*. II:279–285.

Baroghel-Bouny, V., Thiéry, M. & Wang, X. 2014. Performance-based assessment of durability and prediction of RC structure service life: Transport properties as input data for physical models. *Materials and Structures/Materiaux et Constructions*. 47(10):1669–1691. DOI: 10.1617/s11527-013-0144-z.

Basheer, L., Basheer, P.A.M. & Long, A.E. 2005. Influence of coarse aggregate on the permeation, durability and the microstructure characteristics of ordinary Portland cement concrete. *Construction and Building Materials*. 19(9):682–690. DOI: 10.1016/j.conbuildmat.2005.02.022.

Ben-Bassat, M., Nixon, P.J. & Hardcastlet, J. 1990. The effect of differences in the composition of Portland cement on the properties of hardened concrete. *Magazine of Concrete Research*. 42(151):59–66.

Bentz, D.P. 2007. A virtual rapid chloride permeability test. *Cement and Concrete Composites*. 29(10):723–731. DOI: 10.1016/j.cemconcomp.2007.06.006.

Bentz, D.P. & Aitcin, P.-C. 2008. The Hidden Meaning of Water-Cement Ratio. *Concrete International*. 30(5):51–54. Available: https://www.researchgate.net/publication/234838616.

Berodier, E. & Scrivener, K. 2015. Evolution of pore structure in blended systems. *Cement and Concrete Research*. 73:25–35. DOI: 10.1016/j.cemconres.2015.02.025.

Beushausen, H., Höhlig, B. & Martin, M. 2016. The influence of curing methods on durability indicators & micro- and macro porosity of concrete. In *fib Symposium*. Cape Town.

Bockris, J. & Reddy, A. 2002. *Modern Electrochemistry 1 - Ionics*. 2nd ed. Kluwer Academic Publishers.

Boddy, A., Bentz, E., Thomas, A. & Hooton, R.D. 1999. An overview and sensitivity study of a multimechanistic chloride transport model. *Cement and Concrete Research*. 29:827–837.

BS 1881-120. 1983. Method for determination of the compressive strength of concrete cores. *British Standards Institute*. (1).

BS 6349-1. 2013. Maritime Structures. Code of practice for general practice. *British Standards*.

BS 6349-1-4. 2013. Maritime works – Part 1-4 : General – Code of practice for materials. *British Standards*.

BS EN 197-1. 2011. Cement Part 1: Composition, specifications and conformity criteria for common cements. *BSI Standards Publication*. (November):50.

BS EN 206. 2013. BSI Standards Publication Concrete — Specification , performance , production and conformity. *British Standard*. (May):30.

BS EN 14629. 2007. Products and systems for the protection and repair of concrete structures - Test methods - Determination of chloride content of hardened concrete. *British Standards*.

Buenfeld, N.R. & Okundi, E. 1998. Effect of cement content on transport in concrete. *Magazine of Concrete Research*. 50(4):339–351.

Cai, R., Hu, Y., Yu, M., Liao, W., Yang, L., Kumar, A. & Ma, H. 2020. Skin effect of chloride ingress in marine concrete: A review on the convection zone. *Construction and Building Materials*. 262:120566. DOI: 10.1016/j.conbuildmat.2020.120566.

Canut, M.M.C. 2011. Pore structure in blended cement pastes. PhD. Technical University of Denmark. Available: www.byg.dtu.dk.

Caré, S. 2003. Influence of aggregates on chloride diffusion coefficient into mortar. *Cement and Concrete Research*. 33(7):1021–1028. DOI: 10.1016/S0008-8846(03)00009-7.

Chidiac, S.E. & Shafikhani, M. 2020. Electrical resistivity model for quantifying concrete chloride diffusion coefficient. *Cement and Concrete Composites*. 113. DOI: 10.1016/j.cemconcomp.2020.103707.

Christensen, B.J., Coverdale, T., Olson, R.A., Ford, S.J., Garboczi, E.J., Jennings, H.M. & Mason, T.O. 1994. Impedance Spectroscopy of Hydrating Cement-Based Materials: Measurement, Interpretation, and Application. *Journal of the American Ceramic Society*. 77(11):2789–2804. DOI: 10.1111/j.1151-2916.1994.tb04507.x.

Climate-data.org. 2024. *https://en.climate-data.org/africa/south-africa/western-cape/cape-town-788/*.

Costa, A. & Appleton, J. 1999. Chloride penetration into concrete in marine environment - Part I: Main parameters affecting chloride penetration. *Materials and Structures/Materiaux et Constructions*. 32(4):252–259. DOI: 10.1007/bf02479594.

Crank, J. 1975. *The Mathematics of Diffusion*. Second ed. Oxford University Press. DOI: 10.1021/ja01562a072.

Delagrave, A., Bigas, J.P., Ollivier, J.P., Marchand, J. & Pigeon, M. 1997. Influence of the Interfacial Zone on the Chloride Diffusivity of Mortars. *Adv. Cem. Based Mat.* 5:86–92.

Dhandapani, Y. & Santhanam, M. 2017. Assessment of pore structure evolution in the limestone calcined clay cementitious system and its implications for performance. *Cement and Concrete Composites*. 84:36–47. DOI: 10.1016/j.cemconcomp.2017.08.012.

Dhandapani, Y. & Santhanam, M. 2023. On the correlations between different chloride transport parameters and their role in service life estimation. *Sustainable and Resilient Infrastructure*. 8(2):240–255. DOI: 10.1080/23789689.2022.2097771.

Dhanya, B.S. 2015. Study of the influence of supplementary cementitious materials on selected durability parameters of concrete. PhD. Indian Institute of Technology Madras.

Dhir, R.K., McCarthy, M.J., Zhou, S. & Tittle, P.A.J. 2004. Role of cement content in specifications for concrete durability: cement type influences. In *Proceedings of the institution of Civil Engineers - Structures & Buildings*. 113–127.

Diamond, S. 1981. Effects of two Danish fly ashes on alkali contents of pore solutions of cement-fly ash pastes. *Cement and Concrete Research*. II:383–394.

DI-Manual. 2018. Durability index testing procedure manual, Version 4.5.1. *University of Cape Town*. 43. Available: http://www.theconcreteinstitute.org.za/durability.

Dousti, A., Rashetnia, R., Ahmadi, B. & Shekarchi, M. 2013. Influence of exposure temperature on chloride diffusion in concretes incorporating silica fume or natural zeolite. *Construction and Building Materials*. 49:393–399. DOI: 10.1016/j.conbuildmat.2013.08.086.

Duchesne, J. & Berube, M.A. 1994. The effectiveness of supplementary cementing materials in suppressing expansion due to ASR: another look at the reaction mechanisms part 2: pore solution chemistry. *Cement and Concrete Research*. 24(2):221–230.

Ehlen, M.A. & Kojundic, A.N. 2014. Life 365 v2.2: Adding user estimates of chloride exposure. *Concrete international*. (May):41–44.

Ewertson, C. & Petersson, P.E. 1993. The influence of curing conditions on the permeability and durability of concrete: results from a field exposure test. *Cement and Concrete Research*. 23:683–692.

fib bulletin 34. 2006. Model code for service life design. *International Federation for Structural Concrete, Lausanne, Switzerland*.

Fraay, A.L.A., Bijen, J.M. & De Haan, Y.M. 1989. The Reaction of Fly Ash in Concrete. A Critical Examination. *Cement and Concrete Research*. 19(2):235–246.

Frederiksen, J.M., Mejlbro, L. & Nilsson, L.-O. 2008. Fick's 2nd law - Complete solutions for chloride ingress into concrete -with focus on time dependent diffusivity and boundary condition. *Lund Institute of Technology*. Reprt TVBM-3146. Available: www.byggnadsmaterial.lth.se.

Frey, R., Balogh, T. & Balfizs, G.L. 1994. Kinetic method to analyse chloride diffusion in various concretes. *Cement and Concrete Research*. 24(5):863–873.

Fulton's. 1994. *Fulton's Concrete Technology*. 7th ed. B. Addis, Ed. Portland Cement Institute, South Africa.

Fulton's. 2001. *Fulton's Concrete Technology*. 8th ed. B. Addis & G. Owens, Eds. Cement & Concrete Institute.

Fulton's. 2021. *Fulton's Concrete Technology*. 10th ed. M.G. Alexander, Ed. Midrand: The Concrete Institute.

Gao, Y., De Schutter, G., Ye, G., Tan, Z. & Wu, K. 2014. The ITZ microstructure, thickness and porosity in blended cementitious composite: Effects of curing age, water to binder ratio and aggregate content. *Composites Part B: Engineering*. 60:1–13. DOI: 10.1016/j.compositesb.2013.12.021.

Garboczi, E.J. 1990. Permeability, diffusivity, and microstructural parameters: A critical review. *Cement and Concrete Research*. 20(4):591–601. DOI: 10.1016/0008-8846(90)90101-3.

Garboczi, E.J. & Bentz, D.P. 1992. Computer simulation of the diffusivity of cement-based materials. *Journal of Material Science*. 27:2083–2092.

Gerlee, P. & Lundh, T. 2016. *Scientific Models*. Cham: Springer International Publishing. DOI: 10.1007/978-3-319-27081-4.

Githachuri, K. 2010. Influences on the transport properties of a range of South African marine concretes. MSc. University of Cape Town.

Githachuri, K., Alexander, M. & Moyo, P. 2012. Durability performance of a range of marine concretes and the applicability of the South African Service Life Prediction Model. *Materials and Structures*. 45(1–2):185–198. DOI: 10.1617/s11527-011-9759-0.

Glass, G.K. & Buenfeld, N.R. 1997. The presentation of the chloride threshold level for corrosion of steel in concrete. *Corrosion Science*. 39(5):1001–1013.

Glasser, F.P., Marchand, J. & Samson, E. 2008. Durability of concrete - Degradation phenomena involving detrimental chemical reactions. *Cement and Concrete Research*. 38(2):226–246. DOI: 10.1016/j.cemconres.2007.09.015.

Gopinath, R. 2020. Concrete Carbonation Prediction For Varying Environmental Exposure Conditions. PhD. University of Cape Town.

Goto, S. & Roy, D.M. 1981. The effect of w/c ratio and curing temperature on the permeability of hardened cement paste. *Cement and Concrete Research*. 11(4):575–579. DOI: 10.1016/0008-8846(81)90087-9.

Gowers, K.R. & Millard, S.G. 1999. Measurement of concrete resistivity for assessment of corrosion severity of steel using wenner technique. *ACI Materials Journal*. 96(5):536–541. DOI: 10.14359/655.

Gutteridge, W.A. & Dalziel, J.A. 1990. Filler cement: the effect of the secondary component on the hydration of Portland cement Part 2: Fine hydraulic binders. *Cement and Concrete Research*. 20:853–861.

Halamickova, P., Detwiler, R.J., Bentz, D.P. & Garboczi, E.J. 1995. Permeability and Chloride Diiffusion. *Cement and Concrete Research*. 25(4):790–802.

Haynes, H. & Bassuoni, M.T. 2011. Physical Salt Attack on Concrete. *Concrete International*. (November):38–42.

Heckroodt, R.O. 2002. *Guide to deterioration and failure of building materials*. Thomas Telford Publishing.

Heiyantuduwa-Beushausen, R. 2022. The influence of concrete mix composition and environmental exposure on long-term chloride ingress in concrete. PhD Thesis. University of Cape Town.

Hobbs, D.W. 1999. Aggregate influence on chloride ion diffusion into concrete. *Cement and Concrete Research*. 29(12):1995–1998. DOI: 10.1016/S0008-8846(99)00188-X.

IS 456. 2000. Plain and Reinforced Concrete - Code of Practice. *Bureau of Indian Standards*. (July).

Isgor, O.B. & Weiss, W.J. 2019. A nearly self-sufficient framework for modelling reactive-transport processes in concrete. *Materials and Structures/Materiaux et Constructions*. 52(1). DOI: 10.1617/s11527-018-1305-x.

Jakobsen, U.H., De Weerdt, K. & Geiker, M.R. 2016. Elemental zonation in marine concrete. *Cement and Concrete Research*. 85:12–27. DOI: 10.1016/j.cemconres.2016.02.006.

Jee, A.A. & Pradhan, B. 2019. Study on development of empirical relationships between durability parameters of concrete made with different types of binder and exposed to chloride environment. *Construction and Building Materials*. 212:799–817. DOI: 10.1016/j.conbuildmat.2019.04.048.

Kang, S., Lloyd, Z., Behravan, A. & Tyler Ley, M. 2021. The relationship between the apparent diffusion coefficient and surface electrical resistivity of fly ash concrete. *Construction and Building Materials*. 299. DOI: 10.1016/j.conbuildmat.2021.123964.

Khanzadeh-Moradllo, M., Meshkini, M.H., Eslamdoost, E., Sadati, S. & Shekarchi, M. 2015. Effect of Wet Curing Duration on Long-Term Performance of Concrete in Tidal Zone of Marine Environment. *International Journal of Concrete Structures and Materials*. 9(4):487–498. DOI: 10.1007/s40069-015-0118-3.

Kim, J., McCarter, W.J., Suryanto, B., Nanukuttan, S., Basheer, P.A.M. & Chrisp, T.M. 2016. Chloride ingress into marine exposed concrete: A comparison of empirical- and physically- based models. *Cement and Concrete Composites*. 72:133–145. DOI: 10.1016/j.cemconcomp.2016.06.002.

Koch, G., Brongers, M., Thompson, N., Virmani, Y. & Payer, J. 2002. *Corrosion Cost and Preventive Strategies in the United States*.

Kwon, S.J., Lee, H.S., Karthick, S., Saraswathy, V. & Yang, H.M. 2017. Long-term corrosion performance of blended cement concrete in the marine environment – A real-time study. *Construction and Building Materials*. 154:349–360. DOI: 10.1016/j.conbuildmat.2017.07.237.

Lambert, P., Page, C.L. & Vassie, P.R.W. 1991. Investigations of reinforcement corrosion. 2. Electrochemical monitoring of steel in chloride-contaminated concrete. *Materials and Structures*. 24:351–358.

Leo, E.S. 2022. Development of low-clinker concrete: Partial replacement of cement with calcined clay and limestone, based on selected African raw materials. PhD thesis. University of Cape Town.

Li, G., Otsuki, N. & Yuan, Y. shu. 2009. Effects of the initial water curing time on the corrosion behavior of steel bar corrosion in fly ash concrete. *Procedia Earth and Planetary Science*. 1(1):742–749. DOI: 10.1016/j.proeps.2009.09.117.

Life-365 v2.2.3. 2020. Life-365 Service life prediction model and computer program for predicting the service life and life-cycle cost of reinforced concrete exposed to chlorides. *Life-365 Consortium III*.

Lindvall, A. 2003. Environmental actions on concrete exposed in marine and road environments and its response : consequences for the initiation of chloride induced reinforcement corrosion. PhD Thesis. Chalmers University of Technology.

Lindvall, A. 2007. Chloride ingress data from field and laboratory exposure - Influence of salinity and temperature. *Cement and Concrete Composites*. 29(2):88–93. DOI: 10.1016/j.cemconcomp.2006.08.004.

Liu, Y., Presuel-Moreno, F.J. & Paredes, M. 2015. Determination of chloride diffusion coefficients in concrete by electrical resistivity method. *ACI Materials Journal*. 112(5):631–640.

Liu, Z., Deng, D. & De Schutter, G. 2014. Does concrete suffer sulfate salt weathering? *Construction and Building Materials*. 66:692–701. DOI: 10.1016/j.conbuildmat.2014.06.011.

Lobo, C., Lemay, L. & Obla, K. 2006. Performance-based specifications for concrete. *AEI 2006: Building Integration Solutions - Proceedings of the 2006 Architectural Engineering National Conference*. 2006(July 2020):45. DOI: 10.1061/40798(190)45.

Loseby, M., Alexander, M.G. & Beushausen, H. 2016. The influence of aggregate grading on concrete potential durability and penetrability. *Concrete Beton*. 147:19–27.

Loser, R., Lothenbach, B., Leemann, A. & Tuchschmid, M. 2010. Chloride resistance of concrete and its binding capacity - Comparison between experimental results and thermodynamic modeling. *Cement and Concrete Composites*. 32(1):34–42. DOI: 10.1016/j.cemconcomp.2009.08.001.

Lothenbach, B., Scrivener, K. & Hooton, R.D. 2011. Supplementary cementitious materials. *Cement and Concrete Research*. 41(12):1244–1256. DOI: 10.1016/j.cemconres.2010.12.001.

Maage, M., Helland, S., Poulsen, E., Vennesland, O. & Carlsen, J.E. 1996. Service Life Prediction of Existing Concrete Structures Exposed to Marine Environment. *ACI Materials Journal*. 93(6).

Machner, A., Hemstad, P. & De Weerdt, K. 2018. Towards the Understanding of the pH Dependency of the Chloride Binding of Portland Cement Pastes. *Nordic Concrete Research*. 58(1):143–162. DOI: 10.2478/ncr-2018-0009.

Machner, A., Bjørndal, M., Šajna, A., Mikanovic, N. & De Weerdt, K. 2022. Impact of leaching on chloride ingress profiles in concrete. *Materials and Structures/Materiaux et Constructions*. 55(1). DOI: 10.1617/s11527-021-01730-w.

Mackechnie, J.R. 1996. Predictions of Reinforced Concrete Durability in the Marine Environment. PhD Thesis. University of Cape Town.

Mackechnie, J.R. 2001. Predictions of reinforced concrete durability in the marine environment. *Research Monograph 1*. 1–28.

Mackechnie, J.R. & Alexander, M.G. 1997. Durability Findings from Case Studies of Marine Concrete Structures. *Cement, Concrete, and Aggregates*. 22–25.

Mackie, K.P. 2016. Concrete durability in small harbours: the Southern African experience. In *Marine Concrete Structures : Design, Durability and Performance*. M.G. Alexander, Ed. Woodhead Publishing, Elsevier Ltd. 371–426.

Mangat, P.S. & Molloy, B.T. 1994. Prediction of long term chloride concentration in concrete. *Materials and Structures*. 27(6):338–346. DOI: 10.1007/BF02473426.

Manmohan, D. & Mehta, P. 1981. Influence of Pozzolanic, Slag, and Chemical Admixtures on Pore Size Distribution and Permeability of Hardened Cement Pastes. *Cement, Concrete, and Aggregates*. 3(1):63–67. DOI: 10.1520/CCA10203J.

Marchand, J. & Samson, E. 2009. Predicting the service-life of concrete structures - Limitations of simplified models. *Cement and Concrete Composites*. 31(8):515–521. DOI: 10.1016/j.cemconcomp.2009.01.007.

Matthes, W., Vollpracht, A., Villagrán, Y., Kamali-Bernard, S., Hooton, D., Gruyaert, E., Soutsos, M. & De Belie, N. 2018. Ground granulated blast-furnace slag. In *RILEM State-of-the-Art Reports*. V. 25. Springer Netherlands. 1–53. DOI: 10.1007/978-3-319-70606-1_1.

Mehta, P.K. 1991. *Concrete in the Marine Environment*. New York: Elsevier Science Publishers Ltd.

Meira, G.R., Andrade, C., Alonso, C., Borba, J.C. & Padilha, M. 2010. Durability of concrete structures in marine atmosphere zones - The use of chloride deposition rate on the wet candle as an environmental indicator. *Cement and Concrete Composites*. 32(6):427–435. DOI: 10.1016/j.cemconcomp.2010.03.002.

Mendes, S.E.S., Oliveira, R.L.N., Cremonez, C., Pereira, E., Pereira, E. & Medeiros-Junior, R.A. 2018. Electrical resistivity as a durability parameter for concrete design: Experimental data versus estimation by mathematical model. *Construction and Building Materials*. 192:610–620. DOI: 10.1016/j.conbuildmat.2018.10.145.

Millard, S.G. & Gowers, K.R. 1992. Resistivity assessment of in-situ concrete: the influence of conductive and resistive surface layers. In *Proc. Instn Civ. Engrs Structs & Bldgs*. 389–396.

Mohammed, T.U. & Hamada, H. 2003. Relationship between free chloride and total chloride contents in concrete. *Cement and Concrete Research*. 33(9):1487–1490. DOI: 10.1016/S0008-8846(03)00065-6.

Moore, A., Beushausen, H., Otieno, M., Ndawula, J. & Alexander, M. 2022. Oxygen Availability and Corrosion Propagation in RC Structures in the Marine Environment—Inferences from Field and Laboratory Studies. *Corrosion and Materials Degradation*. 3(3):363–375. DOI: 10.3390/cmd3030022.

Morris, W., Moreno, E.I. & Sagüés, A.A. 1996. Practical evaluation of resistivity of concrete in test cylinders using a Wenner array probe. *Cement and Concrete Research*. 26(12):1779–1787. DOI: 10.1016/S0008-8846(96)00175-5.

Muigai, R., Moyo, P. & Alexander, M. 2012. Durability design of reinforced concrete structures: a comparison of the use of durability indexes in the deemed-to-satisfy approach and the full-probabilistic approach. *Materials and Structures*. 45(8):1233–1244. DOI: 10.1617/s11527-012-9829-y.

Mukhopadhyay, A.K., Liu, K.W. & Jalal, M. 2019. An innovative approach to fly ash characterization and evaluation to prevent alkali-silica reaction. *ACI Materials Journal*. 116(4):173–181. DOI: 10.14359/51716751.

Nanukuttan, S. V., Basheer, L., John McCarter, W., Robinson, D.J. & Muhammed Basheer, P.A. 2008. Full-scale marine exposure tests on treated and untreated concretes-initial 7-year results. *ACI Materials Journal*. 105(1):81–87. DOI: 10.14359/19210.

Neville, A.M. 1995. *Properties of Concrete*. Fourth ed. Pearson Education Inc.

Nilsson, L.O. 2006. Present limitations of models for predicting chloride ingress into reinforced concrete structures. In *Journal de Physique IV (Proceedings)*. V. 122. 1–7.

Nilsson, L.O., Massat, M. & Tang, L. 1994. The effect of non-linear chloride binding on the prediction of chloride penetration into concrete structures. In *ACI SP-145*. V.M. Malhotra, Ed. 469–486.

Nilsson, L.-O., Sandberg, P. & Sørensen, H.E. 1996. *HETEK: Chloride penetration into concrete - State-of-the-Art*. DOI: 10.13140/RG.2.1.2771.7526.

NIST. 2019. *Estimation of pore solution conductivity*.

Nixon, P.J. 1975. Changes in Portland cement properties and their effects on concrete. *Building Research Establishment*.

NT BUILD 443. 1995. Accelerated chloride penetration. *Nord test method*. 1–5.

NT BUILD 492. 1999. Chloride migration coefficient from non-steady-state migration experiments. *Nord test method*. 1–8.

Ollivier, J.P., Maso, J.C. & Bourdette, B. 1995. Interfacial Transition Zone in Concrete. *Adv. Cem. Bas. Mat.* 2:30–38.

Omar, N. 2018. Carbonation and Permeability Characteristics of Modern South African Concretes. MSc. University of Cape Town.

Otieno, M. 2018. Sensitivity of the rapid chloride conductivity index test to concrete quality and changes in various test parameters. *Cement and Concrete Composites*. 86:110–116. DOI: 10.1016/j.cemconcomp.2017.11.011.

Otieno, M.B. 2014. The Development of Empirical Chloride-induced Corrosion Rate Prediction Models for Cracked and Uncracked Steel Reinforced Concrete Structures in the Marine Tidal Zone. PhD. University of Cape Town.

Otieno, M. & Alexander, M. 2015. Chloride conductivity testing of concrete – past and recent developments. *Journal of South African Institution of Civil Engineering*. 57(Cci):55–64. DOI: 10.17159/2309-8775/2015/v57n4a7.

Otieno, M. & Thomas, M. 2016. Marine exposure environments and marine exposure sites. In *Marine Concrete Structures : Design, Durability and Performance*. M.G. Alexander, Ed. Woodhead Publishing, Elsevier Ltd. 171–193.

Pack, S.W., Jung, M.S., Song, H.W., Kim, S.H. & Ann, K.Y. 2010. Prediction of time dependent chloride transport in concrete structures exposed to a marine environment. *Cement and Concrete Research*. 40(2):302–312. DOI: 10.1016/j.cemconres.2009.09.023.

Pandey, S.P. & Sharma, R.L. 2000. The influence of mineral additives on the strength and porosity of OPC mortar. *Cement and Concrete Research*. 30:19–23.

Patel, R.G., Parrott, L.J., Martin, J.A. & Killoh, D.C. 1985. Gradients of microstructure and diffusion properties in cement paste caused by drying. *Cement and Concrete Research*. 15(2):343–356. DOI: 10.1016/0008-8846(85)90046-8.

Polder, R.B. & De Rooij, M.R. 2005. Durability of marine concrete structures-field investigations and modelling. *HERON*. 50.

Poursaee, A. & Hansson, C.M. 2009. Potential pitfalls in assessing chloride-induced corrosion of steel in concrete. *Cement and Concrete Research*. 39(5):391–400. DOI: 10.1016/j.cemconres.2009.01.015.

du Preez, A.A. & Alexander, M.G. 2004. A site study of durability indexes for concrete in marine conditions. *Materials and Structures*. 37(267):146–154. DOI: 10.1617/13998.

Presuel-Moreno, F., Wu, Y.Y. & Liu, Y. 2013. Effect of curing regime on concrete resistivity and aging factor over time. *Construction and Building Materials*. 48:874–882. DOI: 10.1016/j.conbuildmat.2013.07.094.

Price, W.F., Jones, M.R., Ting, S.C. & Dhir, R.K. 2003. Effect of aggregate porosity on chloride ingress into concrete. In *Role of Concrete In Sustainable Development: Proceedings of the International Symposium dedicated to Professor Surendra Shah, Northwestern University, USA held on 3–4 September 2003 at the University of Dundee, Scotland, UK*. 287–297.

Proceq SA. 2013. Resipod family: instruction manual.

Qiao, C., Coyle, A.T., Isgor, O.B. & Weiss, W.J. 2018. Prediction of chloride ingress in saturated concrete using formation factor and chloride binding isotherm. *Advances in Civil Engineering Materials*. 7(1):206–220. DOI: 10.1520/ACEM20170141.

Rajabipour, F., Weiss, J., Shane, J.D., Mason, T.O. & Shah, S.P. 2005. Procedure to interpret electrical conductivity measurements in cover concrete during rewetting. *Journal of Materials in Civil Engineering*. 17(5):586–594. DOI: 10.1061/(ASCE)0899-1561(2005)17:5(586).

Ramezanianpour, A.A. 2014. *Cement Replacement Materials: Properties, Durability, and Sustainability*. Springer. Available: http://www.springer.com/series/10171.

Rangaraju, P.R., Olek, J. & Diamond, S. 2010. An investigation into the influence of inter-aggregate spacing and the extent of the ITZ on properties of Portland cement concretes. *Cement and Concrete Research*. 40(11):1601–1608. DOI: 10.1016/j.cemconres.2010.07.002.

Rios, R.T., Rigaud, T., Kopp, T., Lolli, F. & Kurtis, K.E. 2024. Impact of curing solution on concrete surface resistivity and formation factor. *Construction and Building Materials*. 426. DOI: 10.1016/j.conbuildmat.2024.136070.

Roy, S.K., Kok Chye, L. & Northwood, D.O. 1993. Chloride ingress in concrete as measured by field exposure tests in the atmospheric, tidal and submerged zones of a tropical marine environment. *Cement and Concrete Research*. 23:1289–1306.

Saetta, A., Scotta, R. & Vitaliani, R. 1993. Analysis of Chloride Diffusion into Partially Saturated Concrete. *ACI Materials Journal*. 90(5). DOI: 10.14359/3874.

Sallehi, H., Ghods, P. & Isgor, O.B. 2018. Formation factor of fresh cementitious pastes. *Cement and Concrete Composites*. 91:174–188. DOI: 10.1016/j.cemconcomp.2018.05.011.

Sandberg, P. 1999. Studies of chloride binding in concrete exposed in a marine environment. *Cement and Concrete Research*. 29:473–477.

SANS 201. 2008. Sieve analysis, fines content and dust content of aggregates. *South African National Standards*.

SANS 241. 2015. *Drinking water. Part 1: Microbiological, physical, aesthetic and chemical determinands*. South African National Standards.

SANS 3001-CO3-1. 2015. Civil engineering test methods Part CO3-1: Concrete durability index testing — Preparation of test specimens. *South African National Standards*. (1):4.

SANS 3001-CO3-3. 2015. South African National Standard Civil engineering test methods Part CO3-3 : Concrete durability index testing — Chloride conductivity test. *South African National Standards*.

SANS 5844. 2014. Particle and relative densities of aggregates. *South African National Standard*.

SANS 5862-1. 2006. Concrete tests - Consistence of freshly mixed concrete - Slump test. *South African National Standard*.

SANS 5863. 2006. Concrete tests - Compressive strength of hardened concrete. *South African National Standards*.

SANS 5865. 1994. Concrete tests - The drilling, preparation, and testing for compressive strength of cores taken from hardened concrete. *South African National Standards*.

SANS 50197-1. 2013. Cement Part 1: Composition, specifications and conformity criteria for common cements. *South African National Standard*.

Santhanam, M. & Otieno, M. 2016. Deterioration of concrete in the marine environment. In *Marine Concrete Structures : Design, Durability and Performance*. Woodhead Publishing, Elsevier Ltd. 137–170.

Santhanam, M., Cohen, M. & Olek, J. 2006. Differentiating seawater and groundwater sulfate attack in Portland cement mortars. *Cement and Concrete Research*. 36(12):2132–2137. DOI: 10.1016/j.cemconres.2006.09.011.

Saraswatula, P. & Mukhopadhyay, A. 2023. Increasing the Reliability of Formation Factor-Based Transport Property Prediction for High Performance Concrete Mixtures Through Innovative Matching Pore Solution Curing. *Transportation Research Record*. 2677(11):36–50. DOI: 10.1177/03611981231164078.

Schaffer, E. & Meng, B. 2001. Influence of cement and additions on the quantity of alkalis available for an alkali-silica reaction. *Beton*. 145–155.

Scott, A. & Alexander, M.G. 2016. Effect of supplementary cementitious materials (binder type) on the pore solution chemistry and the corrosion of steel in alkaline environments. *Cement and Concrete Research*. 89:45–55. DOI: 10.1016/j.cemconres.2016.08.007.

Scrivener, K. 1999. Characterisation of the ITZ and its quantification by test methods. In *Engineering of the Interfacial Transition Zone in Cementitious Composites—State-of-the-Art Report*. Report No. 20 ed. M.G. Alexander, G. Arliguie, G. Ballivy, A. Bentur, & J. Marchand, Eds. RILEM Publications.

Scrivener, K. & Nemati, K.M. 1996. The percolation of pore space in the cement paste/aggregate interfacial zone of concrete. *Cement and Concrete Research*. 26(1):35–40.

Scrivener, K.L., John, V.M. & Gartner, E.M. 2018. Eco-efficient cements: Potential economically viable solutions for a low-CO2 cement-based materials industry. *Cement and Concrete Research*. 114(February):2–26. DOI: 10.1016/j.cemconres.2018.03.015.

Senbetta, E. & Scholer, C.F. 1984. A New Approach for Testing Concrete Curing Efficiency. *ACI Journal*. 81(1):82–86.

Sengul, O. 2014. Use of electrical resistivity as an indicator for durability. *Construction and Building Materials*. 73:434–441. DOI: 10.1016/j.conbuildmat.2014.09.077.

Sengul, O. & Gjørv, O.E. 2009. Electrical Resistivity Measurements for Quality Control During Concrete Construction. *ACI Materials Journal*. (105):541–547. DOI: 10.14359/20195.

Shakouri, M. 2021. Time-dependent concentration of chlorides at the concrete surface revisited. *Sustainable and Resilient Infrastructure*. 8(2):222–239. DOI: 10.1080/23789689.2021.1892965.

Shakouri, M. & Trejo, D. 2017. A time-variant model of surface chloride build-up for improved service life predictions. *Cement and Concrete Composites*. 84:99–110. DOI: 10.1016/j.cemconcomp.2017.08.008.

Shakouri, M. & Trejo, D. 2018. A study of the factors affecting the surface chloride maximum phenomenon in submerged concrete samples. *Cement and Concrete Composites*. 94(December 2017):181–190. DOI: 10.1016/j.cemconcomp.2018.09.006.

Shao, W., Li, J. & Liu, Y. 2016. Influence of Exposure Temperature on Chloride Diffusion into RC Pipe Piles Exposed to Atmospheric Corrosion. *Journal of Materials in Civil Engineering*. 28(5). DOI: 10.1061/(asce)mt.1943-5533.0001489.

Shehata, M.H., Thomas, M.D.A. & Bleszynski, R.F. 1999. The effects of fly ash composition on the chemistry of pore solution in hydrated cement pastes. *Cement and Concrete Research*. 29(12):1915–1920. DOI: 10.1016/S0008-8846(99)00190-8.

Snyder, K.A. 2001. The relationship between the formation factor and the diffusion coefficient of porous materials saturated with concentrated electrolytes: theoretical and experimental considerations. *Concrete Science and Engineering*. 3(12):216–224.

Snyder, K.A., Feng, X., Keen, B.D. & Mason, T. 0. 2003. Estimating the electrical conductivity of cement paste pore solutions from OH-, K+ and Na+ concentrations. *Cement and Concrete Research*. 33(6):793–798. Available: www.sciencedirect.c-om.

Sohawon, H. 2018. Service life extension of reinforced concrete structures using hydrophobic impregnation. MSc Thesis. University of Cape Town.

South African Government. 2018. *Geography and climate*. Available: https://www.gov.za/about-sa/geography-and-climate [2018, March 27].

Spragg, R., Villani, C., Snyder, K., Bentz, D., Bullard, J. & Weiss, J. 2013. Factors that influence electrical resistivity measurements in cementitious systems. *Transportation Research Record*. 11(2342):90–98. DOI: 10.3141/2342-11.

Spragg, R., Qiao, C., Barrett, T. & Weiss, J. 2016. Assessing a concrete's resistance to chloride ion ingress using the formation factor. In *Corrosion of steel in concrete structures*. A. Poursaee, Ed. Woodhead Publishing.

Spragg, R., Jones, S., Bu, Y., Lu, Y., Bentz, D., Snyder, K. & Weiss, J. 2017. Leaching of conductive species: Implications to measurements of electrical resistivity. *Cement and Concrete Composites*. 79:94–105. DOI: 10.1016/j.cemconcomp.2017.02.003.

Stanish, K. & Thomas, M. 2003. The use of bulk diffusion test to establish time dependent concrete chloride diffusion coefficients. *Cement and Concrete Research*. 33(1):55–62. DOI: http://dx.doi.org/10.1016/S0008-8846(02)00925-0.

Streicher, P.E. 1997. The development of a rapid chloride test for concrete and its use in engineering practice. PhD Thesis. University of Cape Town.

Streicher, P.E. & Alexander, M.G. 1994. A critical evaluation of chloride diffusion test methods for concrete. In *Third CANMET/ACI International Conference on Concrete Durability*. Nice, France: Supplementary papers, ACI, Detroit. 517–530.

Streicher, P.E. & Alexander, M.G. 1995. A chloride conduction test for concrete. *Cement and Concrete Research*. 25(6):1284–1294.

Surana, S., Pillai, R.G. & Santhanam, M. 2017. Performance evaluation of curing compounds using durability parameters. *Construction and Building Materials*. 148. DOI: 10.1016/j.conbuildmat.2017.05.055.

Surana, S., Beushausen, H. & Alexander, M. 2022. The effect of curing, specimen thickness, and saturation on surface resistivity of concrete. *MATEC Web of Conferences*. 364:03010. DOI: 10.1051/matecconf/202236403010.

Tang, L. 2003. *Curve fitting program for apparent Cs and Da*.

Tang, L. 2008. Engineering expression of the ClinConc model for prediction of free and total chloride ingress in submerged marine concrete. *Cement and Concrete Research*. 38(8–9):1092–1097. DOI: 10.1016/j.cemconres.2008.03.008.

Tang, L. & Gulikers, J. 2007. On the mathematics of time-dependent apparent chloride diffusion coefficient in concrete. *Cement and Concrete Research*. 37(4):589–595. DOI: 10.1016/j.cemconres.2007.01.006.

Tang, L. & Nilsson, L. 1996. A numerical method for prediction of chloride penetration into concrete structures. In *H. Jennings et al. (eds.), The modelling of Microstructure and Its potential for Studying Transport Properties and Durability*. Kluwer Academic Publishers. 539–552.

Tang, L. & Nilsson, L.-O. 2000. Modeling of chloride penetration into concrete - Tracing five years' field exposure. In *Concrete Science and Engineering*. 170–175.

Tang, L., Nilsson, L. & Basheer, P.A.M. 2012. *Resistance of Concrete to Chloride Ingress - Testing and Modelling*. CRC Press.

Taylor, H.F.W. 1987. A method for predicting alkali ion concentrations in cement pore solutions. *Advances in Cement Research*. 1(1):5–17.

Thomas, M. 2011. The effect of supplementary cementing materials on alkali-silica reaction : A review. *Cement and Concrete Research*. 41:1224–1231. DOI: 10.1016/j.cemconres.2010.11.003.

Thomas, M. 2013. *Supplementary Cementing Materials in Concrete*. 1st ed. CRC Press. DOI: 10.1201/b14493.

Thomas, M.D.A. 1989. The effect of curing on the hydration and pore structure of hardened cement paste containing pulverized fuel ash. *Advances in Cement Research*. 2(8):181–188.

Thomas, M.D.A. & Bamforth, P.B. 1999. Modeling chloride diffusion in concrete effect of fly ash and slag. *Cem Concr Res*. 29:487–495.

Thomas, M.D.A. & Matthews, J.D. 2004. Performance of pfa concrete in a marine environment - 10-year results. *Cement and Concrete Composites*. 26(1):5–20. DOI: 10.1016/S0958-9465(02)00117-8.

Thomas, M., Scott, A., Bremner, T., Bilodeau, A. & Day, D. 2008. Performance of slag concrete in marine environment. *ACI Materials Journal*. 105(6):628–634.

Tutti, K. 1982. Corrosion of steel in concrete. PhD Thesis. Lund University.

Violetta, B. 2002. Life-365 Service Life Prediction Model ™. *Concrete International*. (December):53–57.

Vollpracht, A., Lothenbach, B., Snellings, R. & Haufe, J. 2016. The pore solution of blended cements: a review. *Materials and Structures/Materiaux et Constructions*. 49(8):3341–3367. DOI: 10.1617/s11527-015-0724-1.

Walsh, M.T. & Sagüés, A.A. 2016. Steel corrosion in submerged concrete structures-part 1: Field observations and corrosion distribution modeling. *Corrosion*. 72(4):518–533. DOI: 10.5006/1945.

Wang, Y., Liu, C., Tan, Y., Wang, Y. & Li, Q. 2020. Chloride binding capacity of green concrete mixed with fly ash or coal gangue in the marine environment. *Construction and Building Materials*. 242. DOI: 10.1016/j.conbuildmat.2020.118006.

Wasserman, R. & Bentur, A. 2013. Efficiency of curing technologies: strength and durability. *Materials and Structures*. 46(11):1833–1842. DOI: 10.1617/s11527-013-0021-9.

Wassermann, R., Katz, A. & Bentur, A. 2009. Minimum cement content requirements: A must or a myth? *Materials and Structures/Materiaux et Constructions*. 42(7):973–982. DOI: 10.1617/s11527-008-9436-0.

De Weerdt, K., Orsáková, D., Müller, A.C.A., Larsen, C.K., Pedersen, B. & Geiker, M.R. 2016. Towards the understanding of chloride profiles in marine exposed concrete, impact of leaching and moisture content. *Construction and Building Materials*. 120:418–431. DOI: 10.1016/j.conbuildmat.2016.05.069.

De Weerdt, K., Wilson, W., Machner, A. & Georget, F. 2023. Chloride profiles – What do they tell us and how should they be used? *Cement and Concrete Research*. 173. DOI: 10.1016/j.cemconres.2023.107287.

Weiss, J., Snyder, K., Bullard, J. & Bentz, D. 2013. Using a saturation function to interpret the electrical properties of partially saturated concrete. *Journal of Materials in Civil Engineering*. 25(8):1097–1106. DOI: 10.1061/(ASCE)MT.1943-5533.0000549.

Weiss, J., Qiao, C., Isgor, B. & Olek, J. 2020. Implementing Rapid Durability Measure for Concrete Using Resistivity and Formation Factor. *Joint Transport Research Program*. FHWA/IN/JTRP-2020/08. DOI: 10.5703/1288284317120.

Weiss, W.J., Barrett, T.J., Qiao, C. & Todak, H. 2016. Toward a Specification for Transport Properties of Concrete Based on the Formation Factor of a Sealed Specimen. *Advances in Civil Engineering Materials*. 5(1):179–194. DOI: 10.1520/ACEM20160004.

Weiss, W.J., Spragg, R.P., Isgor, O.B., Ley, M.T. & Van Dam, T. 2018. Toward performance specifications for concrete: Linking resistivity, RCPT and diffusion predictions using the formation factor for use in specifications. In *fib Symposium*. fib. The International Federation for Structural Concrete. 2057–2065. DOI: 10.1007/978-3-319-59471-2_235.

Wenner, F. 1915. A method of measuring earth resistivity. *Bulletin of the Bureau of Standards*. 12(3):469–478.

Whittington, H.W., McCarter, J. & Forde, M.C. 1981. The conduction of electricity through concrete. *Magazine of Concrete Research*. 33(114):48–60. DOI: 10.1680/macr.1981.33.114.48.

Wilson, W., Georget, F. & Scrivener, K.L. 2024. Towards a two-step assessment of the chloride ingress behaviour of new cementitious binders. *Cement and Concrete Research*. 184. DOI: 10.1016/j.cemconres.2024.107594.

Winslow, D.N., Cohen, M.D., Bentz, D.P., Snyder, K.A. & Garboczi, E.J. 1994. Percolation and pore structure in mortars and concrete. *Cement and Concrete Research*. 24(1):25–37. DOI: 10.1016/0008-8846(94)90079-5.

Wolhuter, C.W. & Morris, R.M. 1973. Aspects of steel corrosion in concrete. *Civil Engineering= Siviele Ingenieurswese*. (9):245–250.

Wong, H.S., Zobel, M., Buenfeld, N.R. & Zimmerman, R.W. 2009. Influence of the interfacial transition zone and microcracking on the diffusivity, permeability and sorptivity of cement-based materials after drying. *Magazine of Concrete Research*. 61(8):571–589. DOI: 10.1680/macr.2008.61.8.571.

Yang, C.C. & Su, J.K. 2002. Approximate migration coefficient of interfacial transition zone and the effect of aggregate content on the migration coefficient of mortar. *Cement and Concrete Research*. 32:1559–1565.

Yang, P., Dhandapani, Y., Santhanam, M. & Neithalath, N. 2020. Simulation of chloride diffusion in fly ash and limestone-calcined clay cement (LC3) concretes and the influence of damage on service-life. *Cement and Concrete Research*. 130. DOI: 10.1016/j.cemconres.2020.106010.

Yu, Z. & Ye, G. 2013. The pore structure of cement paste blended with fly ash. *Construction and Building Materials*. 45:30–35. DOI: 10.1016/j.conbuildmat.2013.04.012.

Zaccardi, Y.A. V. & Maio, A.A. 2014. Electrical resistivity measurement of unsaturated concrete samples. *Magazine of Concrete Research*. 66(10):484–491.

Zhang, T. & Gjorv, O. 2005. Effect of chloride source concentration on chloride diffusivity in concrete. *ACI Materials Journal*. 102(5):295–298.

Zhang, Y. & Zhang, M. 2014. Transport properties in unsaturated cement-based materials - A review. *Construction and Building Materials*. 72:367–379. DOI: 10.1016/j.conbuildmat.2014.09.037.

Zhang, M.H., Bilodeau, A., Malhotra, V.M., Kim, K.S. & Kim, J.C. 1999. Concrete incorporating supplementary cementing materials: Effect on compressive strength and resistance to chloride-ion penetration. *ACI Materials Journal*. 96(2):181–189. DOI: 10.14359/443.

Zhang, Y., Zhang, M. & Ye, G. 2018. Influence of moisture condition on chloride diffusion in partially saturated ordinary Portland cement mortar. *Materials and Structures/Materiaux et Constructions*. 51(2). DOI: 10.1617/s11527-018-1162-7.

Zuquan, J., Xia, Z., Tiejun, Z. & Jianqing, L. 2018. Chloride ions transportation behavior and binding capacity of concrete exposed to different marine corrosion zones. *Construction and Building Materials*. 177:170–183. DOI: 10.1016/j.conbuildmat.2018.05.120.

Appendix A. Chloride binding – a critical review

A.1 Introduction

Chloride binding is defined as the phenomenon in which a part of the chloride ions in the concrete pore solution is captured by solid concrete constituents and rendered immobile. The binding phenomenon reduces the concentration of chloride ions available in the pore solution capable of diffusing further into concrete (i.e., free chloride ions) and effectively reduces the rate of chloride transport. Chloride binding also reduces the concentration of free chloride ions available at the steel surface to disrupt the passivation layer of steel. This makes understanding chloride binding crucial to: (i) understanding the chloride transport behaviour of concrete exposed to external chlorides in marine conditions, (ii) developing appropriate methods to test chloride resistance realistically, and (iii) making better predictions of time to corrosion initiation. The subject of chloride binding is complex and our understanding of it is still under development.

An adequate understanding of chloride binding is crucial to the understanding of the overall chloride transport in concrete. It also enables a comprehensive and critical outlook needed for analysing chloride test methods and prediction models. In this part, an attempt is made to critically review the literature on the subject to summarise the current state of knowledge in relation to the mechanisms involved, mathematical descriptions used, test methods used, and the important factors that influence chloride binding.

A few extensive reviews are available on the subject, most notably (Zibara, 2001; Yuan et al., 2009), that effectively covers the breadth of topics this subject entails. Therefore, the emphasis was on reviewing the most relevant and well-performed studies published in the last two decades unless where the lack of recent literature or the importance of past studies dictated otherwise.

Reviewing recent literature in this case becomes even more important because a lot of what we know about chloride binding comes from the studies on admixed/internal chlorides (Byfors, Hansson & Tritthart, 1986; Tritthart, 1989a,b; Arya & Xu, 1995; Suryavanshi, Scantlebury & Lyon, 1996; Xu, 1997). There seems to be a clear realization since the late 1990s that even though some overlap might exist, the findings from the studies on internal chlorides may not adequately represent the case of external chlorides, perhaps partly due to the awareness of a more convenient method of testing (equilibrium method, see later) for chloride binding than the previous cumbersome method (pore expression, see later). This review is therefore restricted to studies on external chlorides only.

A.2 Mechanisms

Two main mechanisms are used to explain chloride binding in concrete: chemical binding and physical binding. Chemical binding involves chemical interactions of chloride ions with the hydration products,

while physical binding involves the physical adsorption of chloride ions on the surface of hydration products. The aluminate phases are believed to be mainly responsible for chemical binding and CSH gel for physical binding.

A.2.1 Chemical binding

The main mechanism responsible for chemical binding is thought to be the reaction involving C_3A and Cl^- ions producing Friedel's salt ($C_3A.CaCl_2.10H_20$). Through an extensive review of the literature published between 1962 and 1999, Zibara, (2001) reported that it was believed that C_3A reacts directly with chlorides in the presence of gypsum to form Friedel's salt in the case of internal chlorides although with some debate on the competition between sulphates and chlorides. However, confusion in the case of external chlorides existed in the early literature regarding whether chlorides react with the hydration products of C_3A or the remaining unhydrated C_3A. In later years, the chemical binding of external chlorides was increasingly explained through the process of ion-exchange in which chlorides replace hydroxyl ions present in the interlayers of the AFm phases.

AFm refers to aluminate-ferrite-monosubstituent phases and represents the collection of calcium aluminate hydrate phases with the general formula $[Ca_2(Al, Fe)\ (OH)_6]^+\ X^-\ n{\cdot}H_2O$ (Birnin-Yauri & Glasser, 1998). Its crystalline structure is analogous to that of $Ca(OH)_2$ [or $Ca_3(OH)_6$] in which each divalent Ca ion is replaced by a trivalent Al/Fe ion leaving a residual positive charge (Zibara, 2001). This residual positive charge may be balanced by any anion(s) 'X' such as OH^-, SO_4^{-2}, CO_3^{-2}, Cl^- (Birnin-Yauri & Glasser, 1998; Zibara, 2001). Various AFm phases exist depending on the exposure conditions as shown in Figure A.1.

In Portland cements without significant carbonate content, sulphate AFm reacts with chlorides at low concentration to form Kuzel's salt, which contains both sulphates and chlorides as anions (Cl^-/SO_4^{-2}=2:1) (see Figure A.2). At high chloride concentrations (below 1 M), AFm converts to Friedel's salt (Cl-AFm) (Zibara, 2001) (Eq. (A.1)). Both reactions leave sulphate ions as by-products (Eq. (A.1)), which react with AFm to form ettringite (AFt) (Hirao et al., 2005). An increase in total volume has been reported (Balonis et al., 2010) but the formation of ettringite has not been considered as a deleteriously expansive reaction. Although AFm contributes the most, several other calcium aluminate hydrate phases have been reported to contribute to chloride binding (Zibara, 2001). Ettringite has also been reported to convert to Friedel's salt at chloride concentrations above 3 M (Zibara, 2001). The current understanding of chemical binding is however much more complex than described here.

$$C_3A.CaSO_4.12H_2O + 2NaCl \rightarrow C_3A.CaCl_2.10H_2O + 2Na^+ + SO_4^{-2} + 2H_2O \qquad (A.1)$$

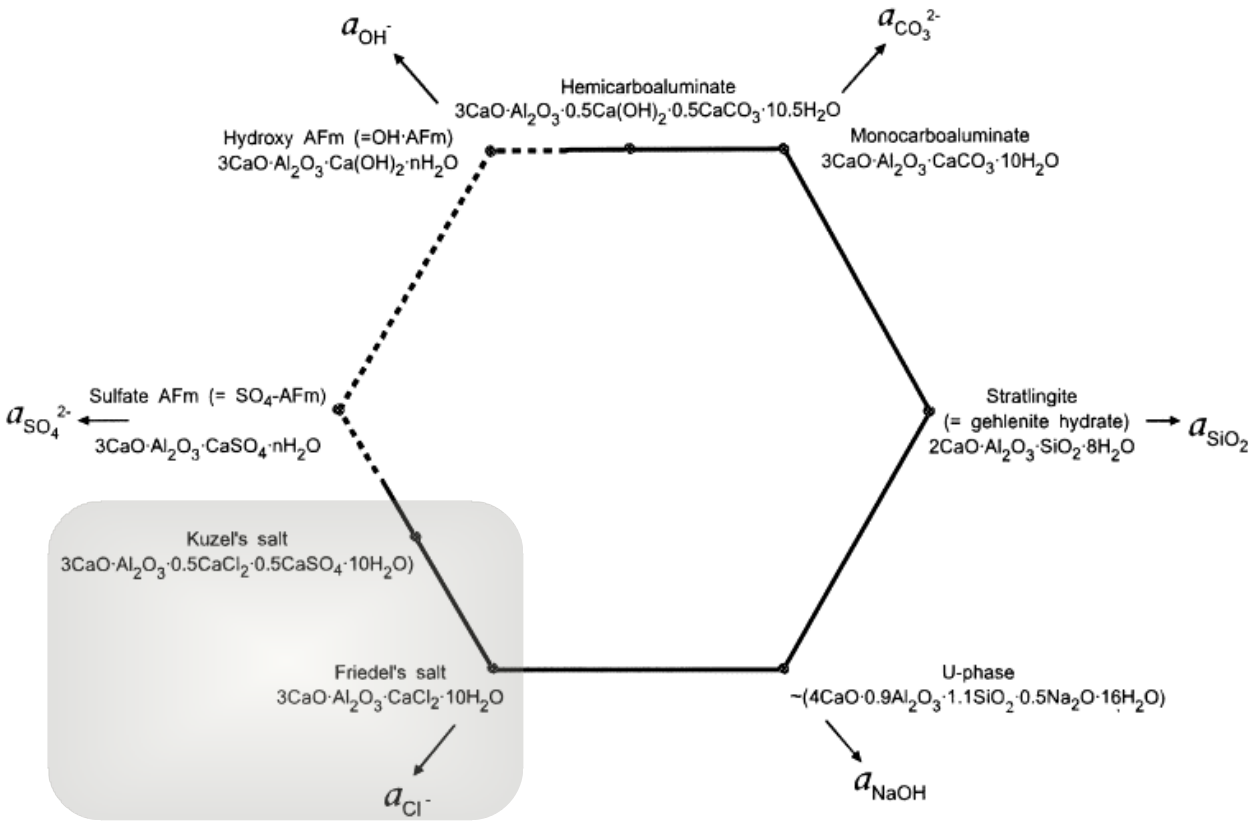

Figure A.1 Various AFm phases in hydrated cement (Glasser, Kindness & Stronach, 1999). The dotted lines represent the unstable AFm phases and AFm phases with chlorides are highlighted in the shaded rectangle in the figure.

A.2.2 Physical binding

Electrical double layer theory has been used to explain the mechanism of physical binding. Cement hydrates such as CSH acquire a negative surface charge due to missing cations from their crystal structures. These negative charges are compensated by the positively charged Ca, Na ions from the pore solution forming a positive Stern-layer, which is followed by a negatively charged diffuse layer of chloride ions. The mechanisms of physical binding, however, are not well understood. As physical adsorption involves weaker forces, the physically bound chlorides are loosely held, and the chemically bound chlorides strongly held. However, desorption of both types of bound chlorides may occur depending on the exposure conditions.

The binding capacity of CSH is much lower than AFm on a per g basis, around 1/5th; however, because CSH has a much higher volume than AFm, its overall contribution to binding can be significant (Hirao et al., 2005).

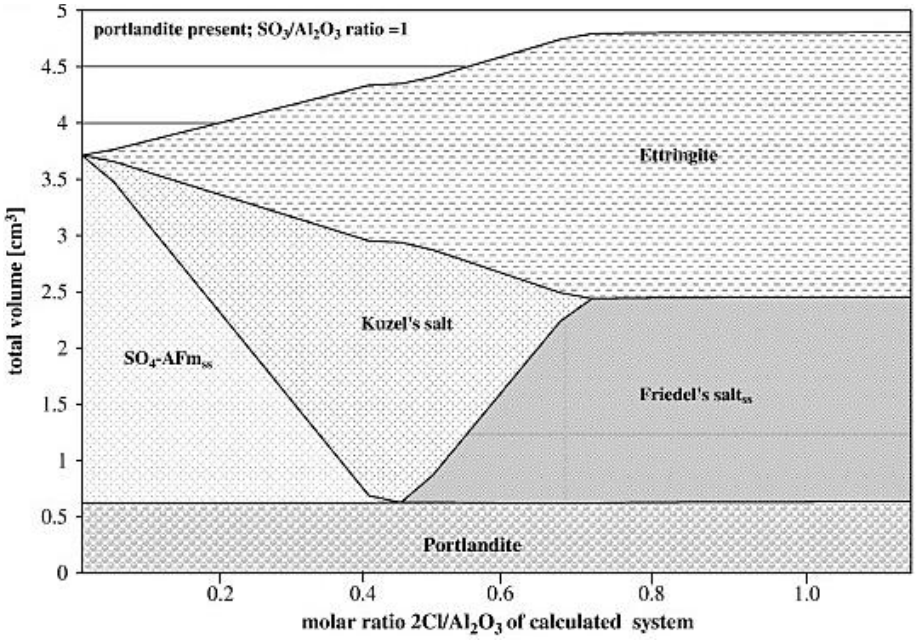

Figure A.2 The dependence of the total phase volume (calculated) on chloride concentration in a hydrated model mixture containing representative quantities of C_3A, portlandite, water, and sulphates (Balonis et al., 2010)

A.3 Chloride binding in diffusion models

Diffusion is the major transport process through which chloride ions penetrate concrete. The governing equations for diffusion are described by Fick's 1st and 2nd laws for steady and non-steady (unsteady) state diffusion. In the following section, the mathematical expression for Fick's 1st law is presented and 2nd law derived. A common approach to account for chloride binding in the diffusion process is then described (based on (Tang, Nilsson & Basheer, 2012)).

The rate at which a material (measured in mass) flows across a unit section is termed 'flux' (meaning flow) as described in Eq. (A.2). In a steady state transport process such as steady state diffusion, the flux at a given location remains constant with time. Therefore, the flux going into an infinitesimal element will be equal to the flux coming out of it. In other words, no material is retained in the element.

$$J = \frac{1}{A}\frac{\partial m}{\partial t} \tag{A.2}$$

Where,

J: Flux (moles/s/m^2) (moles in place of kg depending on the unit of 'C')

m: Mass (kg)

t: Time (s)

A: Area of cross-section (m^2)

Under steady state conditions, the diffusion flux is directly proportional to the concentration gradient across the element according to Fick's first law in one dimension (x) (Eq. (A.3)).

$$J = -D_{SS}\frac{\partial C}{\partial x} \tag{A.3}$$

Where,

C: Concentration (moles/m^3)

'D_{SS}' is the constant of proportionality and is termed the steady state diffusion coefficient. The negative sign signifies that the direction of flow occurs in the direction of decreasing concentration gradient.

As opposed to steady state conditions, the incoming and the outgoing flux are not equal at a given time in non-steady state conditions, Eq. (A.4).

$$J_{in} \neq J_{out} \tag{A.4}$$

The difference in incoming and outgoing flux leads to an accumulation of ions with time in the infinitesimal element according to the law of conservation of mass. Therefore, the concentration at a given location will change with time (see Eq. (A.5), (A.6)). Applying Eq. (A.2) and Eq. ((A.3)) to Eq. (A.6), leads to the equation for Fick's 2nd law of non-steady state diffusion (Eq. (A.8) and (A.9)).

$$\frac{\partial C}{\partial t} = -\frac{m_{out} - m_{in}}{\Delta V \cdot \Delta t} \tag{A.5}$$

or,

$$\frac{\partial C}{\partial t} = -\frac{m_{out} - m_{in}}{A \cdot \Delta x \cdot \Delta t} \tag{A.6}$$

or,

$$\frac{\partial C}{\partial t} = -\frac{J_{out} - J_{in}}{\Delta x} \tag{A.7}$$

or,
$$\frac{\partial C}{\partial t} = -\frac{\partial J}{\partial x} \tag{A.8}$$

Fick's 2nd law
$$\frac{\partial C}{\partial t} = \frac{\partial}{\partial x}\left(D_{SS}\frac{\partial C}{\partial x}\right) \tag{A.9}$$

'D_{SS}' is the steady state diffusion coefficient.

When the diffusant (the diffusing species) does not interact with the porous material, the non-steady state usually is a transient state before the steady state is reached. In the case of chlorides diffusing in concrete, the binding phenomenon creates a sink for chloride ions, whereby the chloride concentration at any location is composed of bound chlorides and free chlorides, of which only free chlorides participate in diffusion. Therefore, the change in chloride concentration with time is due to two processes: the chloride binding and an increase in incoming free chloride ions (left-hand side term of Eq. (A.8)). But the driving force for diffusion comes only from the free chlorides (right hand side term of Eq. (A.8)). It should be noted that the amount of bound chlorides depends on the amount of free chlorides at that location, thus as the free chlorides move ahead, a part of them turns into bound chlorides and the rest remain free to move. Fick's 2nd law can be rewritten for this case:

$$\frac{\partial C_t}{\partial t} = \frac{\partial}{\partial x}\left(D_{SS}\frac{\partial C_f}{\partial x}\right) \tag{A.10}$$

'C_t' is the total chloride content and is composed of bound chlorides ('C_b') and free chlorides ('C_f'). The unit of concentration is with respect to the volume of concrete.

$$C_t = C_b + C_f \tag{A.11}$$

Using Eq. (A.10) and (A.11):

$$\frac{\partial}{\partial t}\left(C_b + C_f\right) = \frac{\partial}{\partial x}\left(D_{SS}\frac{\partial C_f}{\partial x}\right) \tag{A.12}$$

or,
$$\frac{\partial C_f}{\partial t}\left(\frac{\partial C_b}{\partial C_f} + 1\right) = \frac{\partial}{\partial x}\left(D_{SS}\frac{\partial C_f}{\partial x}\right) \tag{A.13}$$

or,

$$\frac{\partial C_f}{\partial t} = \frac{\partial}{\partial x}\left(\frac{D_{SS}}{\left(\frac{\partial C_b}{\partial C_f} + 1\right)} \cdot \frac{\partial C_f}{\partial x}\right) \quad \text{(A.14)}$$

or,

$$\frac{\partial C_f}{\partial t} = \frac{\partial}{\partial x}\left(D_{NSS} \cdot \frac{\partial C_f}{\partial x}\right) \quad \text{(A.15)}$$

where,

$$D_{NSS} = \frac{D_{SS}}{\left(1 + \frac{\partial C_b}{\partial C_f}\right)} \text{ [m}^2\text{/s]} \quad \text{(A.16)}$$

'D_{NSS}' is the non-steady state diffusion coefficient. It represents the rate of chloride transport in non-steady state conditions.

The free, bound, and total chloride concentrations in the aforementioned expressions are in per m^3 of concrete. However, most often, different types of chloride concentrations are defined with respect to different quantities, due to the different methods of determination involved in each case. For example, total and bound chloride concentrations are expressed in moles per m^3 of concrete, whereas free chloride concentrations are expressed in moles per m^3 (or L) of pore solution. In such cases, the proportion of pore solution involved in diffusion in concrete is used to account for these differences. Usually, the following assumptions are made in this regard: 1. all the pore solution participates in diffusion, 2. concrete is completely saturated, and porosity is uniformly distributed in concrete, and 3. the pore solution content is equal to the capillary porosity or the evaporable water content.

When C_f is expressed in mol per m^3 (solution) and C_b, C_t in mol per m^3 (concrete), Eq. (A.11) will be modified by using the pore solution content (assumed to be the porosity 'ε'= vol. of porosity/vol. of concrete):

$$C_t = C_b + \varepsilon . C_f \text{ [moles/m}^3\text{(concrete)]} \quad \text{(A.17)}$$

Consequently, the expression for the Fick's 2nd law and D_{NSS} will change as follows:

$$\frac{\partial}{\partial t}\left(C_b + \varepsilon \cdot C_f\right) = \frac{\partial}{\partial x}\left(D_{SS} \cdot \varepsilon \cdot \frac{\partial C_f}{\partial x}\right) \quad \text{(A.18)}$$

Or,

$$D_{NSS} = \frac{D_{SS}}{\left(1 + \frac{1}{\varepsilon} \cdot \frac{\partial C_b}{\partial C_f}\right)} \quad \text{(A.19)}$$

$\frac{\partial C_b}{\partial C_f}$ represents the rate of binding relative to the free chloride concentration. Chloride binding would imply a positive value to this parameter, and it is obvious considering Eq. (A.16) that binding would lead to a reduction in the diffusion coefficient. The values for this parameter are obtained from binding isotherms, explained in the next section.

A.4 Binding isotherms

A.4.1 Sorption isotherms

Binding isotherms describe the relationship between bound chlorides and free chlorides at a particular temperature. Also called adsorption isotherms or sorption (adsorption and ion exchange) isotherms, the binding isotherms are common in various fields to describe sorption processes. In other words, binding isotherms describe the amount of sorbate (bound chlorides) sorbed on the sorbent (substrate–concrete) as a function of the concentration (free chlorides) at constant temperature. Figure A.3 illustrates a typical chloride binding isotherm measured on paste samples. The binding isotherm does not capture the progress of binding with time. It only presents the bound chloride content in equilibrium with the given chloride concentration, i.e., it assumes instantaneous binding. It is well known that the relationship between bound and free chloride concentration is non-linear and the increase in binding decreases with an increase in concentration (Tang & Nilsson, 1993; Castellote, Andrade & Alonso, 1999). Hence, the amount of binding depends on the concentration. A wide range of chloride concentrations is of practical interest. Seawater on average has a chloride concentration of 0.5 M, typical lab diffusion tests use a chloride concentration of ~3 M, migration tests use a range of chloride concentrations up to 5 M.

A.4.2 'Binding capacity'

$\frac{\partial c_b}{\partial c_f}$ is the slope of the binding isotherm and is termed 'binding capacity' by (Nilsson, Massat & Tang, 1994). Nilsson, Massat & Tang (1994) define the binding capacity as "the ability of a material to bind further chlorides when the chloride concentration increases". As shown in Figure A.3, the chloride binding

isotherm follows a non-linear trend, which means that the binding capacity decreases continuously as the chloride concentration increases. However, this definition is not always recognised in the literature (Tang & Nilsson, 1993; Thomas et al., 2012) and the term binding capacity is often used to refer to the maximum ability of the material to bind chlorides.

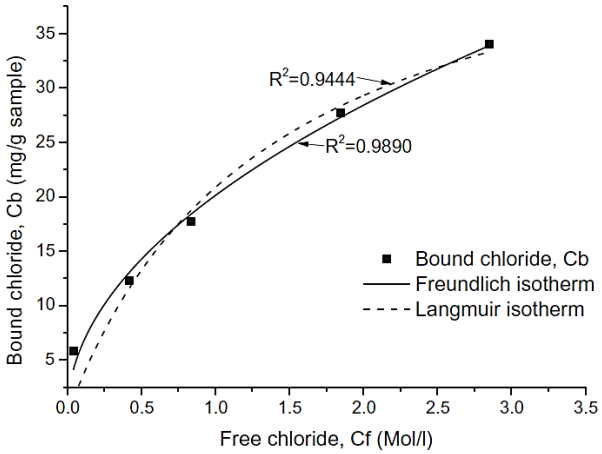

Figure A.3 A typical chloride binding isotherm (Ogirigbo & Black, 2017)

A.4.3 Comparison of different sorption isotherms

Various isotherms have been used in the literature to describe chloride binding, most notably, linear, Langmuir, and Freundlich.

The linear isotherm passing through the origin has been criticised, despite its simplicity, for underestimating binding at low to moderate chloride concentrations and overestimating binding at moderate to high chloride levels, with a recommendation to consider non-linearity of binding for more accurate predictions as shown in Figure A.4 (Nilsson, Massat & Tang, 1994; Martín-Pérez et al., 2000).

The most widely accepted (cited) finding on non-linear binding is that chloride binding follows Freundlich isotherm best at chloride concentration >0.01 M and Langmuir isotherm best at chloride levels <0.05 M (Tang & Nilsson, 1993). On this basis, it was argued that monolayer adsorption should be the mechanism at low chloride levels, but more complex mechanisms might be involved at higher chloride levels. However, subsequent studies have shown that using either of these isotherms through the entire range of chloride concentrations results in extremely good fits (R^2>0.9) and the difference between the two is marginal (Zibara, 2001; Thomas et al., 2012; Ogirigbo & Black, 2017).

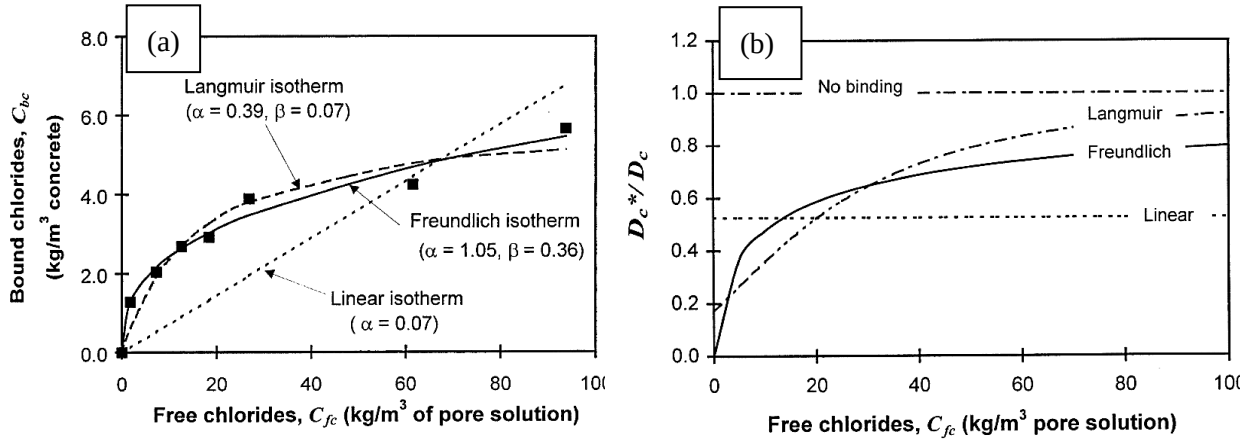

Figure A.4 (a) and (b) show the comparison of different binding isotherms and their effect on the diffusion coefficient (relative to no binding), respectively for ggbs (40%) concrete with w/b-0.3 (adapted from (Martín-Pérez et al., 2000))

The issue of importance is therefore the ease with which these isotherms can be used to derive the diffusion coefficient. It has been recognised that Fick's 2nd law cannot be solved mathematically while using non-linear binding due to the consequent concentration dependence of the non-steady state diffusion coefficient (see Table A.1) and therefore numerical methods are needed (Nilsson, Massat & Tang, 1994).

Table A.1 Types of binding isotherms used to describe chloride binding in concrete

Type of isotherm	*Mathematical expression*	*Binding capacity and diff. coeff.* (Martín-Pérez et al., 2000)	*Properties*
Linear	$C_b = \alpha \cdot C_f + \beta$	$\frac{\partial C_b}{\partial C_f} = \alpha$ $D_{NSS} = \frac{D_{SS}}{1 + \frac{\alpha}{\varepsilon}}$	1. α, β = 0 implies no binding 2. β = 0 implies straight line through origin 3. α, β > 0 implies straight line with an intercept on the bound chloride axis. No theoretical explanation for C_b= β>0 at C_f=0 (Tang, Nilsson & Basheer, 2012)
Langmuir	$C_b = \frac{\alpha \cdot C_f}{1 + \beta \cdot C_f}$	$\frac{\partial C_b}{\partial C_f} = \frac{\alpha}{(1 + \beta \cdot C_f)^2}$ $D_{NSS} = \frac{D_{SS}}{1 + \frac{1}{\varepsilon} \cdot \frac{\alpha}{(1+\beta \cdot C_f)^2}}$	1. Non-linear binding 2. Plateaus at chloride concentration indicating exhaustion of adsorption sites (Martín-Pérez et al., 2000) 3. Derived with the assumption of, among others, monolayer adsorption on a homogenous substrate in a reversible process (Atkins & Paula, 2006)
Freundlich	$C_b = \alpha \cdot C_f^{\beta}$	$\frac{\partial C_b}{\partial C_f} = \alpha \cdot \beta \cdot C_f^{\beta-1}$ $D_{NSS} = \frac{D_{SS}}{1 + \frac{1}{\varepsilon} \cdot \alpha \cdot \beta \cdot C_f^{\beta-1}}$	1. Non-linear binding 2. Empirical expression 3. Keeps increasing with chloride concentration; however, with a decreasing rate

Note:
1. α, β – binding constants obtained by fitting the isotherm equations into the experimental data
2. the unit for C_f is moles/m^3(pore solution), other chloride contents in terms of m^3(concrete)
3. BET (Brunauer-Emmette-Teller) isotherm is not included here because of the complexity of the mathematical expression involved and the lack of its use in description of chloride binding. The expression can be found in ref. (Castellote, Andrade & Alonso, 1999; Yuan et al., 2009).

A.4.4 Desorption isotherms

Desorption of bound chlorides has been shown to occur upon exposure to a solution of lower chloride content. However, desorption exhibits hysteresis (Zibara, 2001) and therefore a significant portion of bound chlorides remains bound unless the chloride concentration becomes very low as shown in Figure A.5. It is clear from this figure that a portion of bound chlorides is reversibly bound. However, conflicting interpretations exist in the literature on whether a portion of bound chlorides is irreversibly bound when the concentration is lowered to zero (Tang & Nilsson, 1993; Thomas et al., 2012). Desorption becomes of importance, especially at the surface of chloride-exposed structures where rainfall or flooding can lower the chloride levels. It can also influence the measurement of bound (or free) chlorides when leaching-based test methods are adopted, see later.

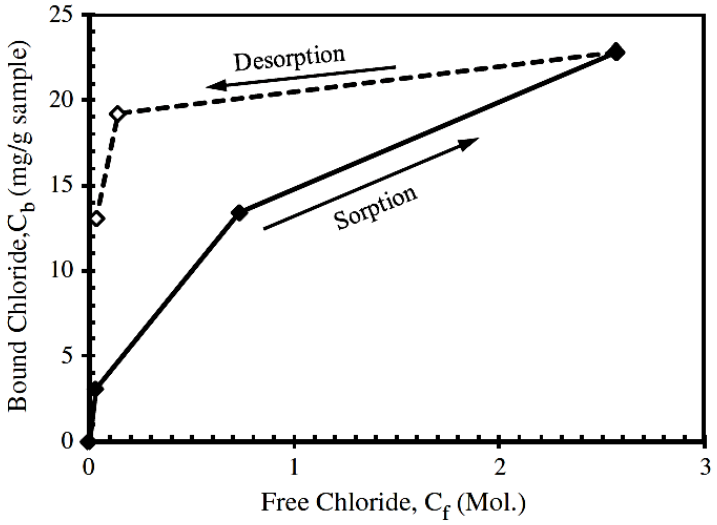

Figure A.5 Sorption and desorption isotherms [metakaolin paste (w/b-0.5); pH-13 (sorption), pH-12.5 (desorption)] (Thomas et al., 2012)

A.5 Determination of bound and free chlorides

The determination of bound chlorides (and binding isotherms) generally consists of extracting the free chloride portion, measuring the free chloride content using chloride measurement techniques, and subtracting that from the total chloride concentration. This indirect scheme is used because isolating the bound chlorides is prone to many experimental errors and often is more tedious than isolating the free chloride portion. The common methods used in this regard are briefly described below.

A.5.1 Pore solution expression method

In this type of method, the pore solution is pressed out of the cementitious system and analysed for chlorides to determine the free chloride content. A common arrangement (Barneyback & Diamond, 1981) uses roughly 250 g of specimen placed in a 53 mm (2 in.) diameter cavity inside a pre-compressed die, and a high pressure of up to 550 MPa is applied on it through a piston on top (see Figure A.6). An O-ring channel carved on the top of the platen collects the pore solution and delivers it through a drain. The pore solution can be collected directly into a syringe using a rubber pipe connected to the drain. The limited exposure to air ensures that carbonation is avoided.

Pore solution can be extracted from paste or mortar specimens using this arrangement. The yield of pore solution from this method is quite low and depends on various factors. For example, the yield of mortars with cement:sand:water of 1:2:0.5 decreases, as the hydration progresses, from 10 ml right after setting to 1-2 ml after several days. Likewise, paste will yield more pore solution than mortar, and a high w/b ratio will yield more than low w/b ratio pastes. The obtained pore solution is diluted to obtain sufficient volume for reliable chloride content determination.

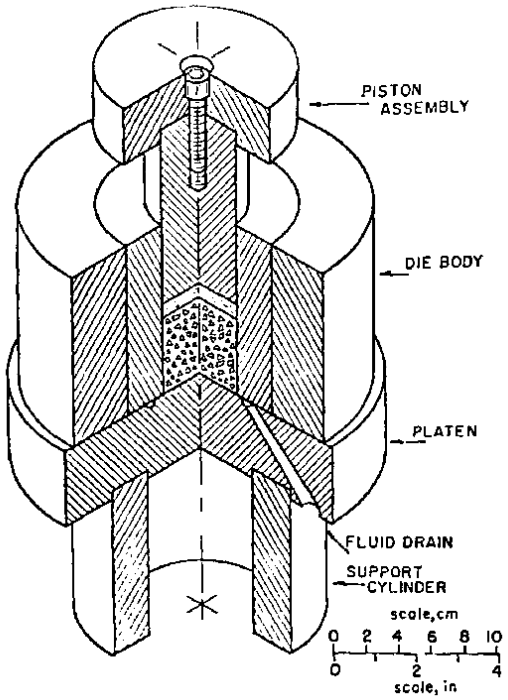

Figure A.6 Device for the extraction of pore solution (Barneyback & Diamond, 1981)

A.5.2 Sorption equilibrium method

In this type of method, crushed samples are stored in chloride solutions of concentrations of interest separately until no more sorption of chloride occurs, i.e., equilibrium is reached. The most extensive method used for bound chloride determination, proposed by (Tang & Nilsson, 1993), uses a well-hydrated sample with a particle size in the range of 0.25-2 mm obtained through wet crushing and water sieving to avoid carbonation. The wet sample is vacuum-dried for 3 days and then stored at 11% RH in a carbon dioxide-free environment for 7 days to ensure only a monolayer of adsorbed water remains on the gel. 25 g of sample is mixed with NaCl solution of a certain concentration saturated with $Ca(OH)_2$. The volume of the solution is not stipulated, but researchers have used a variety of solution-to-sample ratios: 15 ml/30 g (De Weerdt et al., 2015); 20 ml /15 g (Machner, Hemstad & De Weerdt, 2018); 4 ml/g (Avet & Scrivener, 2020). Moreover, in place of $Ca(OH)_2$, NaOH, KOH, or a combination of alkali hydroxides have been used. According to (Tang & Nilsson, 1993), equilibrium could be reached in under 2 weeks for OPC pastes although others (De Weerdt et al., 2015; Avet & Scrivener, 2020) have reported longer durations of 2 months for OPC pastes, and Thomas et al. (2012) found the duration to depend on factors such as SCM and w/b ratio for 3-mm thick discs (see Figure A.7). After reaching sorption equilibrium, the solution is analysed for chlorides to measure free chloride content. This process is repeated for a range of chloride strengths and an adsorption isotherm can be drawn.

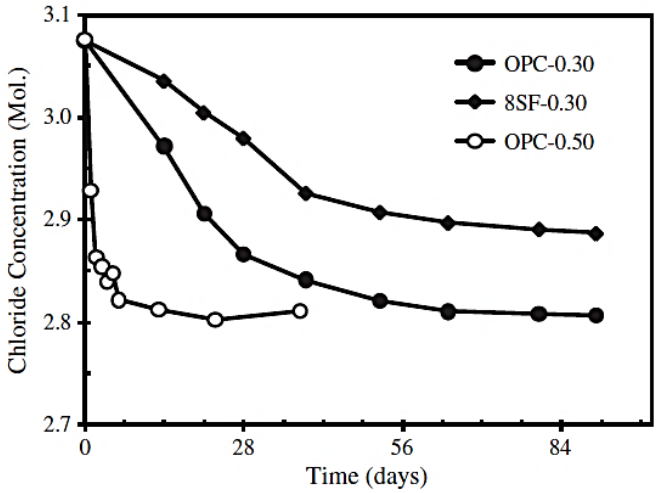

Figure A.7 Time to reach equilibrium concentration in 3-mm thick discs (Thomas et al., 2012)

A.5.3 Leaching method for 'water-soluble' chlorides

In this type of method, crushed chloride contaminated samples, the same as used for total chloride content, are immersed in a chloride-free solution to dissolve the free chlorides in the solution. The filtrate is analysed

for chlorides to determine the free chloride content. Several methods have been used (refer for details (Castellote & Andrade, 2001a)). The ASTM method (ASTM C1218, 2020) states that a pulverized sample (850 μm sieve passing) be boiled in reagent water (10 g in 50 ml) for 5 minutes and the filtrate is obtained after 24 hours. The RILEM recommended method for soluble chlorides (RILEM TC 178-TMC, 2002a), based on a round-robin study (Castellote & Andrade, 2001a), states that a pulverized sample (315 μm sieve passing) be stirred in reagent water (5 g in 50 ml) for 3 minutes and filtrate is obtained immediately thereafter for analysis. Another method has been proposed (Castellote et al., 2001), which uses a 0.3 M NaOH solution instead of distilled water to avoid the effect of pH differences on the soluble chloride content (see Section A.6.1 for more information).

A.5.4 Steady-state diffusion cell method

In this type of method, free chloride contents are estimated for steady-state conditions, i.e., linear variation, in a diffusion cell using the upstream and downstream cell concentrations, which are then subtracted from the total chloride contents at each depth to obtain bound chloride contents. A method proposed by (Glass, Stevenson & Buenfeld, 1998) makes use of a 10-mm mortar/concrete disc specimen exposed to NaCl solution on one side and NaOH solution on the other. Free chlorides in the specimen are estimated after steady state conditions are achieved, and total chloride contents are measured through chloride profiling.

A.5.5 Other methods

Using analytical methods such as XRD and SEM-EDS, attempts have been made to distinguish between physically and chemically bound chlorides (Sui et al., 2019). Physically bound chlorides are assumed to be associated with C-A-S-H and chemically bound chloride are assumed to mainly exist as Friedel's salt. These assumptions may be limited by our understanding of the mechanisms of chloride binding, especially in the case of SCM concretes. These methods are only appropriate for research, not routine testing.

The merits and demerits of the common test methods for assessing bound/free chloride content are discussed in Table A.2.

Table A.2 A comparison of different binding methods

Method	*Advantages*	*Disadvantages*
Pore solution expression method	1. High accuracy and low within-lab variability for chloride and hydroxide content (Tritthart, 1989b) 2. Binding isotherm can be obtained on a single specimen subjected to non-steady state chloride diffusion. 3. The specimen is not subjected to any chemical changes in the test environment that can affect binding. 4. Other properties of the pore solution can be measured on part of the same sample.	1. Expensive as specialized equipment is needed. 2. Safety is a concern as high pressures are involved. 3. Large sample size is required to obtain a sufficient volume of pore solution; testing concrete is impractical. 4. Concrete requires the sample to be broken into small pieces, which are susceptible to carbonation-related errors (Tritthart, 1989b). 5. The pore solution content (or solution-filled porosity) is required to calculate chloride content per m^3 of material, which is difficult to measure accurately. 6. The expression of pore solution might lead to the release of some of the bound chlorides due to the high pressures involved (Glass, Wang & Buenfeld, 1996).
Equilibrium method	1. Test procedure is easy to follow. 2. No need of special/expensive equipment. 3. Small sample size is required.	1. Equilibrium could take a long time to establish, from weeks to months. 2. Crushing the specimen may result in exposing higher surface area/portions than happens in the actual diffusion process (Alexander & Streicher, 1998). 3. Crushing (wet storage) also makes the specimen susceptible to a higher degree of hydration thereby changing the composition. 4. Risk of leaching during water sieving. 5. The composition of the exposure solution will affect the binding isotherm, e.g., pH.

Method	*Advantages*	*Disadvantages*
Leaching methods	1. The quickest and most straightforward among the available methods. 2. Concrete samples can be tested easily. 3. Field chloride-exposed samples can be tested.	1. Uncertainty around the accuracy, esp. at low chloride contents. 2. Highly dependent on the ionic composition of the solution. Desorption of bound chlorides is likely due to lower solution pH. 3. Some of the bound chlorides get into the solution with water, which affects the accuracy of the method. The ratio of free chlorides determined by pore expression to the water soluble chlorides (C_f/C_w) varies widely (0.5-0.8) in the literature (Otsuki, Nagataki & Nakashita, 1993; Yuan et al., 2013).
Steady-state diffusion cell method	1. Realistic conditions; pore structure remains intact during the test 2. Diffusion coefficient and binding isotherms can be measured through the same test.	1. Long durations are required to establish steady-state conditions. 2. Thin specimens required to reduce the test duration will lead to difficulty in chloride profiling.

A.6 Factors affecting chloride binding

A.6.1 pH (OH^- concentration)

The pH or the hydroxyl ion (OH^-) concentration of the concrete pore solution has a direct influence on the chloride binding capacity of concrete. Various studies have shown that generally with a reduction in pH, the binding capacity increases (Tritthart, 1989a; Machner, Hemstad & De Weerdt, 2018; Avet & Scrivener, 2020). As the OH^- ion concentration decreases, it is thought that the competition for adsorption sites also reduces leaving more sites to occupy for Cl^- ions (Tritthart, 1989a). However, recent research shows that chloride binding follows this trend only until a minimum pH (around 12 for OPC) is reached (see Figure A.8), below which it can decrease severely (Machner, Hemstad & De Weerdt, 2018). Some possible reasons for this phenomenon have been suggested by the authors: the decomposition of 'chloride binding phases', their inability to bind chlorides beyond a certain pH, the decalcification of CSH resulting in a lower positive charge, which could reduce chloride ions in diffuse layer, and reduction in the amount of CSH. The exact mechanism(s) by which pH influences the chloride binding capacity still requires clarification and experimental verification.

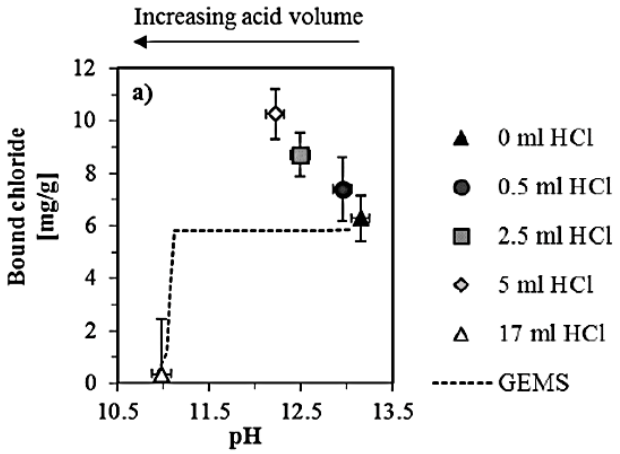

Figure A.8 The influence of pH on binding in Portland cement. The pH was adjusted by adding HCl to the binding solution of 1.5 M NaCl used to quantify the amount of bound chloride ions by the equilibrium method (Machner, Hemstad & De Weerdt, 2018).

There are various implications of the pH-binding relationship for the chloride ingress behaviour of concrete. The pH of the pore solution is affected by the concrete constituents, in particular, the type of the binder. Excessive leaching and carbonation at the exposed surface of marine structures can also reduce the pH to the level where the concrete starts losing its binding capacity. Furthermore, the binding capacity determination itself can be erroneous if the pH of the solution, in equilibrium or leaching method, is not kept at a realistic level (Avet & Scrivener, 2020).

A.6.2 Source of chlorides

Seawater contains many ionic species, mainly, Na^+ (Sodium), K^+ (Potassium), Ca^{2+} (Calcium), Mg^{2+} (Magnesium), SO_4^{-2} (Sulphate), and Cl^- (Chloride) ions. These ions can influence the chloride binding

behaviour of concrete. Furthermore, different chloride salts such as NaCl, $CaCl_2$, and $MgCl_2$ are used as deicing salts in cold weather conditions. The different cations associated with chlorides in these salts can have different effects on the chloride binding behaviour of concrete. Similarly, where ground water chloride attack is a concern, the accompanying ions in the ground water can be an influencing factor.

The chloride salts of Mg^{2+} and Ca^{2+} lead to more bound chlorides than the chloride salts of Na^{+} and K^{+} in Portland cement systems (Delagrave et al., 1997; Zhu et al., 2012; De Weerdt et al., 2015) (see Figure A.9a). An associated reduction in pH is also observed with increasing concentration of Ca/Mg ions, which is thought to be behind the increased binding capacity in the presence of Ca^{2+} or Mg^{2+} ions (see Figure A.10a) (De Weerdt et al., 2015). It has been argued that Mg^{2+} and Ca^{2+} ions combine with OH^{-} ions and remove them from the solution due to the limited solubilities of $Ca(OH)_2$ and $Mg(OH)_2$ (Tritthart, 1989a). However, the mechanisms involved are highly debated. Metakaolin and metakaolin-limestone blends have also shown higher binding in the case of $CaCl_2$ compared to NaCl (Shi et al., 2017). However, the mechanisms at play in the case of metakaolin could be different from Portland cement pastes as shown in Figure A.11.

The SO_4^{-2} ions react with AFm preferentially to chlorides to form ettringite leaving less for chlorides to bind with. In addition, sulphates also compete with chlorides for sorption on CSH, thus reducing the chloride binding capacity (De Weerdt, Orsáková & Geiker, 2014). Furthermore, the increased chloride binding of Mg^{2+} disappears when similar amounts of SO_4^{-2} ions are present in the solution without affecting the pH (compare Figure A.9b and Figure A.10b) (De Weerdt, Orsáková & Geiker, 2014). It can also be seen that binding in the case of seawater is quite similar to NaCl. This is possible because the amount of Mg^{2+} and Ca^{2+} in seawater is very small compared to Na^{+} and the presence of sulphates should contradict their effect even further.

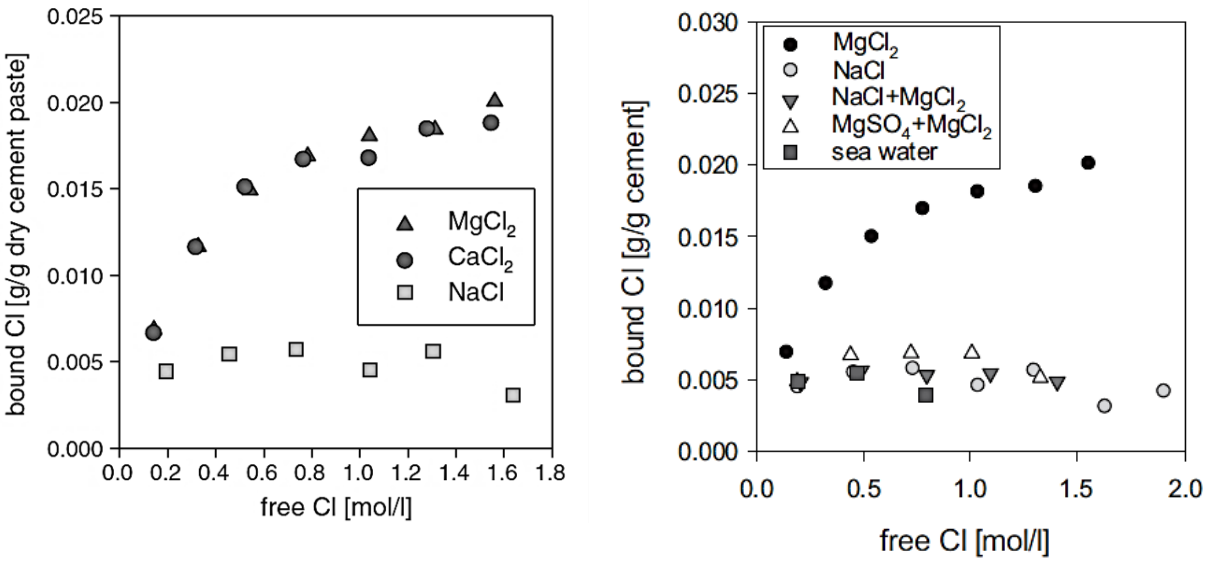

(a) (De Weerdt et al., 2015) (b) (De Weerdt, Orsáková & Geiker, 2014)

Figure A.9 Chloride binding isotherms for different cation-anion combinations

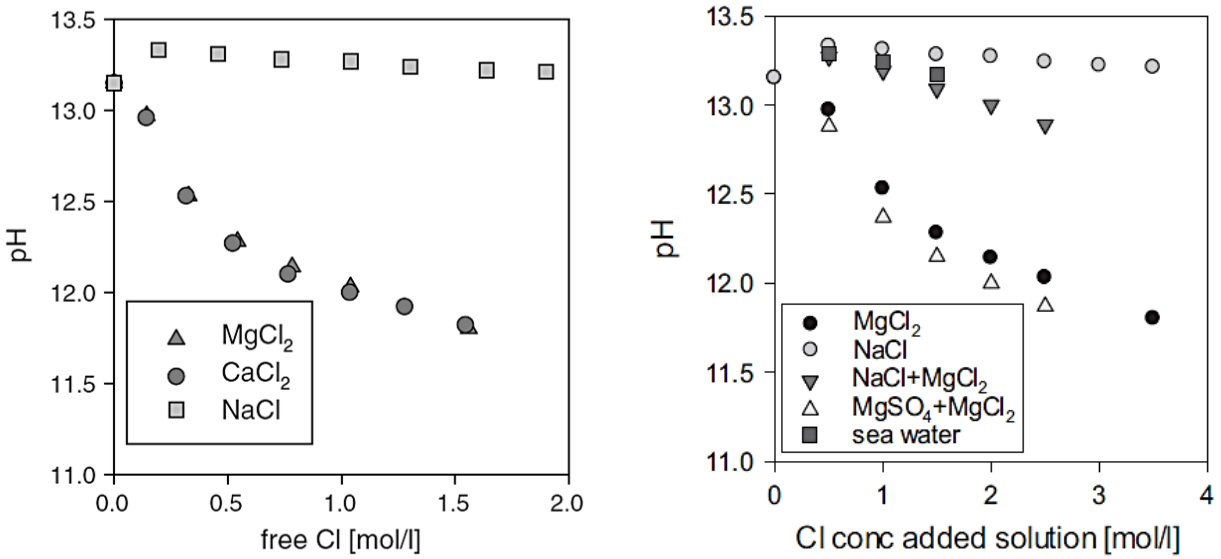

(a) (De Weerdt et al., 2015) (b) (De Weerdt, Orsáková & Geiker, 2014)

Figure A.10 The pH of the respective exposure solutions in relation to their chloride concentration in an equilibrium test for chloride binding where 0.5 ml of chloride solution was used per gram of the ground paste sample

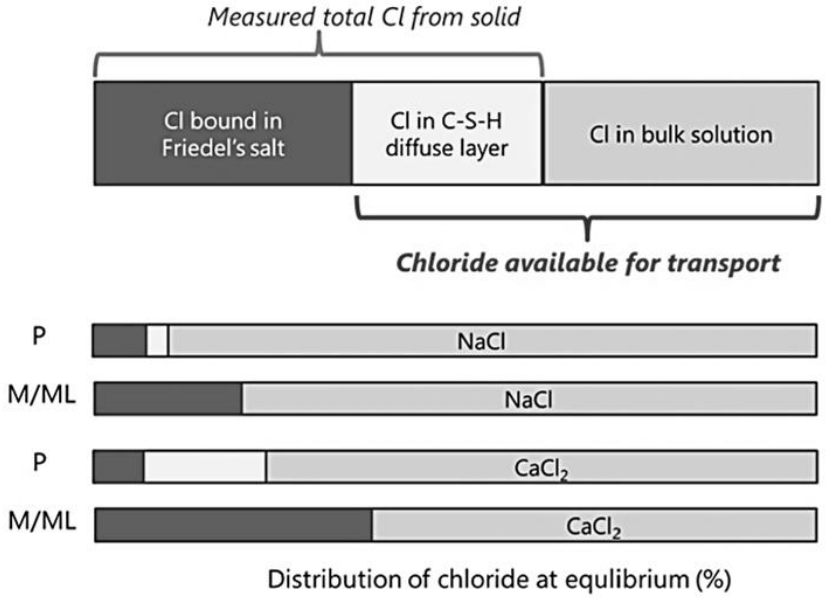

Figure A.11 The proportion of physically and chemically bound chlorides in Portland cement paste (P), metakaolin and metakaolin-limestone blends (M, ML) when exposed to NaCl or $CaCl_2$ solution (Shi et al., 2017)

A.6.3 Portland cement phases

Zibara (2001) found that C_3A plays a major role in chloride binding and the C_3A content is a good predictor of the binding capacity of Portland cement in the moderate to high chloride concentration range (1-3 M), but not in the low concentration range (0.1 M). C_4AF was also estimated in this study to have 1/3rd of the binding capacity of C_3A. On the other hand, SO_3^- content was found to reduce the binding capacity by forming mono-sulphate and ettringite, especially at low chloride concentrations. C_3S and C_2S were reported to contribute about 25-50% to the total binding capacity as physically bound chlorides.

A.6.4 SCMs and level of substitution

1. Ground granulated blast-furnace slag

GGBS is known to have a high active alumina content. The hydration of GGBS in the presence of cement produces some changes in the hydration products. The hydration of slag blends results in CSH with a lower Ca/Si ratio but with a higher Al/Si ratio (therefore – C(A)SH) and is likely to contain hydrotalcite[a]-like phase due to high Mg content (Lothenbach, Scrivener & Hooton, 2011). Previous studies have found higher Friedel's salt content with GGBS suggesting the presence of more AFm (Luo et al., 2003) and yet many recent studies suggest that more alumina content does not necessarily lead to more AFm and AFt phases, rather more Al is found to be incorporated into CSH (Lothenbach, Scrivener & Hooton, 2011).

[a] Hydrotalcite – $Mg_6Al_2(OH)_{16}(CO_3).4H_2O$ [Mg-Al-OH-X phase] (Lumley et al., 1996)

GGBS has been shown to improve chloride binding ability (Dhir, El-Mohr & Dyer, 1996; Luo et al., 2003). The chloride binding ability increases with increasing replacement levels between 0 and 66.7% in a study by (Dhir, El-Mohr & Dyer, 1996), as shown in Figure A.12. A similar increase in binding was also observed with an increase in the replacement level up to 50% in another study; however, 100% replacement resulted in significantly reduced binding, suggesting an optimum replacement level (Zibara, 2001).

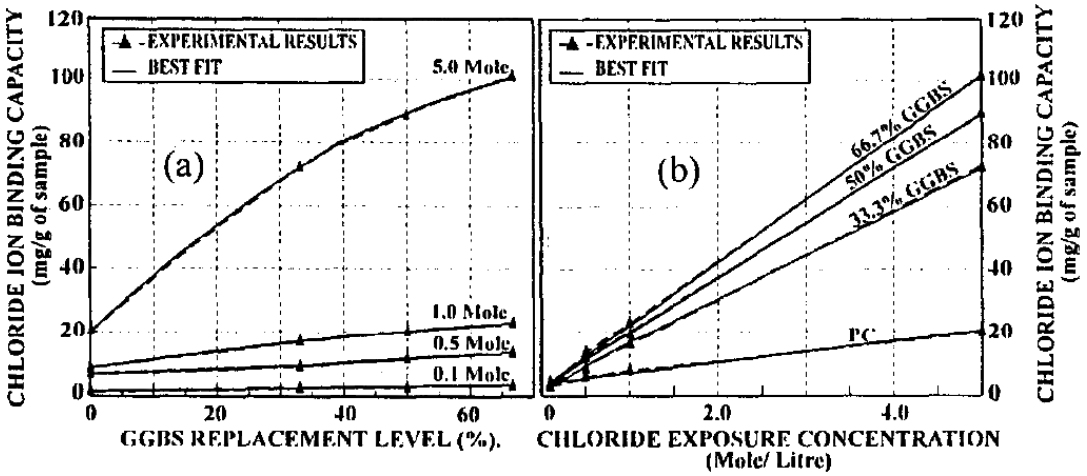

Figure A.12 Effect of GGBS level on chloride binding (Dhir, El-Mohr & Dyer, 1996)

It is generally believed that Friedel's salt formation due to higher alumina content in slag is behind the superior binding capacity of slag-blended binders (Dhir, El-Mohr & Dyer, 1996; Luo et al., 2003). However, it has been shown that hydrotalcite in hydrated slag blends has a high chloride binding potential and therefore could be behind slag's high binding capacity in addition to Friedel's salt formation (Kayali, Khan & Sharfuddin Ahmed, 2012). It has also been suggested that the lower sulphate content of GGBS might be one of the leading causes of its high binding capacity (Xu, 1997; Luo et al., 2003).

The binding ability of common SCMs has been reported in a study in the following order: MK>GGBS>FA>PC>SF[b] (Thomas et al., 2012). Except for FA, the binding capacity for the rest appeared to be correlated with their alumina content in this study. GGBS with higher alumina contents bind more chlorides; however, the relative magnitude also depends on the type of cement with which it is blended (Mapa et al., 2023).

2. Fly ash

Fly ash also contains a large amount of alumina. However, a large part of alumina in FA is present in the form of crystalline Mullite and thus not available for binding, which means that total alumina content is not a reliable indication of FA's binding ability (Thomas et al., 2012). Cheewaket, Jaturapitakkul & Chalee (2010) tested concretes with a range of FA substitution levels (0-50%) and w/b ratios in a tropical marine tidal zone. Their

[b] MK (Metakaolin), FA (Fly Ash), SF (Silica Fume)

results show that binding capacity increased, by about 10% for 50% FA, with the substitution level in an approximately linear fashion and the binding capacity of FA concretes reached a maximum value in 3-4 years.

A.6.5 w/b ratio

Studies on paste have shown that an increase in w/b ratio leads to an increase in bound chlorides per unit sample mass without SCMs (Tang & Nilsson, 1993). In contrast, another study found this trend only with SCMs (Thomas et al., 2012). Studies on concrete and mortar differ in their findings. (Mangat & Molloy, 1995) found increased binding with higher w/b at constant cement content, while (Tang & Nilsson, 1993; Cheewaket, Jaturapitakkul & Chalee, 2010) found no effect of w/b on binding.

Given the same curing, a higher w/b ratio results in a higher degree of hydration at a given cement content. The amount of bound chlorides would depend on the amount of hydration products (or the interface of chlorides with it). The amount of hydration products, in turn, would depend on the w/b ratio and the cement content. A higher degree of hydration with a higher w/b ratio would increase the binding, but a concomitant reduction in cement content to keep the water content constant would more than negate that effect.

A.6.6 Aggregate

Tang & Nilsson (1993) found in a study on OPC pastes and mortars that bound chloride contents of mortars were lower than the pastes when compared on a per-sample mass basis; however, no discernible differences remained when the amount of bound chlorides was normalized with the gel content. Apart from diluting the cement paste, aggregates were not found to bind any chlorides.

A.6.7 Temperature

Zibara (2001) reported that the effect of temperature on chloride binding is concentration-dependent. The binding capacity reduces with increasing temperature between 0-38˚C below the chloride concentration of 1 M although the reduction is marginal. Whereas at a chloride concentration of 3 M, significant increases in binding capacity were observed with increasing temperature. This type of concentration dependence has not been reported by some recent studies. Furthermore, there is a lack of agreement on whether temperature increases (Nguyen, Lorente & Carcasses, 2009; Panesar, Eng & Chidiac, 2011) or decreases binding (Dousti et al., 2013). Nevertheless, the effect of temperature as observed in these studies is marginal and not always consistent. It is therefore uncertain that temperature will play a crucial and definite role in chloride binding in the temperature range of practical significance.

A.6.8 Carbonation

Carbonation reduces the pH of the pore solution and consequently affects the ability of hydrates to bind chlorides. Carbonated concrete loses the ability to bind chloride, and similarly, subsequent carbonation in chloride contaminated concrete releases bound chlorides (Saillio, Baroghel-Bouny & Barberon, 2014; Chang,

2017; Bahman-Zadeh, Ramezanianpour & Zolfagharnasab, 2022). The binding ability decreases sharply with the degree of carbonation and is completely lost upon complete carbonation.

A.6.9 Electric field

An understanding of the influence of electric field on chloride binding is likely to: 1. lead to better interpretations of the migration test results and clarify their relationship to the chloride diffusivity of concrete, 2. reveal if the possibility of developing a better—quicker and simpler—test for binding ability exists using electrical migration, and 3. lead to improvements in the process of electrically-induced chloride extraction. The task of understanding the influence of an electric field on chloride binding can be divided into investigating two main issues: 1. what is the nature of chloride binding when transport occurs under an electric field? and 2. how does the application of an electric field affect the bound chlorides that already exist in concrete? Only a few studies have investigated these questions, as described below.

A study on non-steady state migration conditions (DC) found substantially different relationships between bound and free chlorides compared to those in a natural diffusion test (Castellote, Andrade & Alonso, 1999). The amount of bound chlorides was found to be much lower in case of migration unless at very high chloride concentrations (see Figure A.13). Practically no binding was seen when the catholyte concentration was less than 0.1 M. It is suggested that transport is much quicker in migration than the reaction step and the opposite in the natural diffusion, which was reflected as the difference between the chloride profiles.

In contrast, Yuan et al. (2013) found minimal effect of the applied electric field (DC) on binding in non-steady state conditions. In another study, steady-state conditions for chloride penetration were reached using an applied DC voltage and the amount of bound chlorides expressed thereafter from the specimens was found to be no different from those measured through the typical equilibrium method (Voinitchi, Julien & Lorente, 2008). Even though the time to reach equilibrium in the two types of measurements was different, the same results were obtained. This suggests no adverse influence of the electric field on binding.

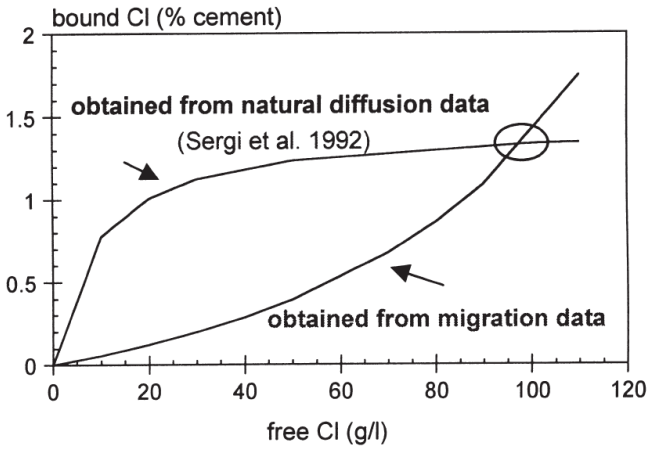

Figure A.13 Binding isotherms obtained from non-steady state migration and diffusion tests (Castellote, Andrade & Alonso, 1999)

It is clear that major contradictions are present, and thus more research is necessary on this topic, especially considering its practical importance. In any case, the only takeaway seems to be that binding does occur in the presence of an electric field; its magnitude and nature need clarification.

A.7 Conclusions

1. The formation of Kuzel's salt and Friedel's salt at low-to-moderate and moderate-to-high chloride concentrations mainly through the reaction between AFm phase and chloride ions is the main mechanism of chemical binding in plain Portland cement systems with or without SCMs. However, other hydrates can also play a significant role, especially in the case of SCMs. The CSH gel and its large surface area are mainly believed to be behind the physical binding.
2. Non-linear binding isotherms satisfactorily express the relationship between free and bound chlorides regardless of the mechanisms involved in chloride binding. Freundlich and Langmuir isotherms are the most widely used; however, the use of non-linear binding in diffusion models requires numerical methods for the solution.
3. The most commonly used method to test for bound chlorides on lab samples is the equilibrium method. The leaching method is the practical option for field/lab samples. However, it needs to be appreciated that the results from any of these tests depend on how closely the test conditions resemble the reality. As it stands, quantification of free Cl contents involves uncertainty in accuracy, which makes total Cl contents preferable in a practical context. These aspects are however of high practical significance and should be researched further.
4. Chloride binding is influenced by a multitude of factors, among which the most important appear to be the pH, the cation associated with the chloride salt, sulphate content, the composition of the binder, and carbonation.
5. Much research effort is still required to investigate the effects of these factors in order to model the chloride transport process better and develop better test methods. In this author's view, a better understanding of the influence of SCMs and the electric field on chloride binding will have the most impact on practice.

Appendix B. Diffusion and Migration: An Overview of Theory and Testing

B.1 Introduction

Chloride transport of concrete in marine conditions is generally modelled on diffusion. The related testing is consequently based on diffusion but also includes (electro-)migration. This part presents an overview of the theoretical background for diffusion and migration. The fundamentals are explained using the case of transport in ionic solutions at both particle and phenomenological level. Fair bit of emphasis is given to the relationship between the mechanisms of diffusion and migration in ionic transport, in particular, for its use in developing efficient test methods for diffusion. The differences between transport in ionic solution and saturated media are then discussed to provide relevance for transport in concrete. Common test methods to assess resistance of concrete to chloride diffusion based on diffusion and migration are critically reviewed in detail. Particular attention is given to the chloride conductivity test for its relevance to this study.

B.2 Chloride diffusion and migration

The fundamental electrochemical principles of ionic diffusion and migration have existed for more than 100 years. These principles have been used extensively across fundamental and applied fields since then. Several textbooks are now available, which describe the subject in detail. Much of the following discussion draws on the indispensable textbooks on Physical Chemistry and Electrochemistry by: (Bockris & Reddy, 2002; Atkins & Paula, 2006).

B.2.1 Ionic Diffusion in solutions

At a particle level, diffusion can be described in this way. Particles move randomly in all directions owing to their kinetic energy at a given temperature. The particles move randomly between the region of high concentration and the region of low concentration in both directions. However, simply because there are larger number of particles in the region of high concentration, more particles travel from the region of high concentration to the region of low concentration. At the phenomenological level, this appears as a net movement of matter (or property, such as temperature) in a specific direction, the direction of decreasing concentration, to establish equilibrium. This flow of particles such as ions due to a concentration gradient is defined as diffusion.

The instantaneous rate of movement under diffusion is directly proportional to the concentration gradient. This is known as Fick's 1st law. Fick's 1st law (Eq. (B.1)) describes diffusion in the steady state, which means that it is applicable when the concentration gradient remains constant with time. Under non-steady state conditions, Fick's 2nd law (Eq. (B.2)) is used.

Fick's 1st law

$$J = -\mathrm{D}\frac{\partial C}{\partial x} \quad \text{(B.1)}$$

Where,

J: Flux (moles/(s.m^2)). It is the amount of mass diffused through a unit cross-section in a unit time.

C: Concentration (moles/m^3)

D: Diffusion coefficient or diffusivity (m^2/s)

Fick's 2nd law

$$\frac{\partial C}{\partial t} = -\frac{dJ}{dx} = \frac{\partial}{\partial x}\left(\mathrm{D}\frac{\partial C}{\partial x}\right) \quad \text{(B.2)}$$

The diffusion coefficient or diffusivity is a constant of proportionality and represents a property that describes the ability of an ion to diffuse through a given electrolyte/medium. It is not an intrinsic property of the ion or the medium. It is specific to the ion-medium pair. This means that the diffusivity of say hydroxyl ions in a concrete pore solution is different from the diffusivity of chloride ions. The diffusion coefficient is not an intrinsic property for another reason that it depends on the concentration of the ionic species.

It is worth noting that the same diffusion coefficient appears in both the laws as does the same concentration term. However, in the case of reactive transport such as chloride ion diffusion through concrete, the concentration terms are more complicated due to the ion-medium interaction, which leads to different diffusion coefficients. Refer to chloride binding (Appendix A) for more details.

In the presented forms, these laws ideally apply to the diffusion of uncharged particles. These can also be applied to ions at infinitely low concentrations where the ions can be assumed to behave like uncharged particles. The case of charged ions like Cl is handled either through the Nernst-Planck equation or the errors associated are ignored in practical situations relevant to concrete.

B.2.2 Ionic conduction / migration in solutions

As mentioned previously, ions in an aqueous solution move randomly and constantly collide with other ions/molecules without producing any net movement in the absence of any external interference. When an electric field is applied, the force due to the applied electric field causes the ions to gain a component of velocity parallel to the electric field. The ionic movement remains zigzag but now has a net movement in the direction of the electric field. This net movement is known as 'drift'. The ions accelerating due to the applied electric field encounter a drag force by the colliding ions and the solvent molecules in the electrolyte that is proportional to the speed of the ions. When the speed of the accelerating ion reaches a point where the drag force is equal to the force due to the electric field, the

forces balance each other and the ions drift with a net average speed in the direction parallel to the electric field, called the drift speed. The force balance results in the expression for the drift speed as shown in Eq. (B.3). However, the assumption underlying this relationship must be pointed out, which is that the drag force is proportional to the speed.

Drift speed (s) ($F_{drag}=F_{elec}$)
$$s = \frac{zeE}{f} \tag{B.3}$$

Where,

z: Valence

e: Charge per valence unit (ze: total charge on the ion)

E: Magnitude of the applied electric Field ($\frac{dV}{dx}$)

f: Drag coefficient ($F_{drag} \propto s$)

This shows that the drift speed is proportional to the force due to the applied electric field. The constant of proportionality represents the ease with which the ion moves in the medium and is termed ionic mobility. Generally, ionic mobility is defined as the drift speed per unit electric field (Eq. (B.4)).

Ionic mobility (u)
$$u = \frac{s}{E} = \frac{ze}{f} \tag{B.4}$$

It is worth noting here that ions dissolved in polar solvents like water are in a state of solvation (known as hydration, in the case of water), i.e., they are surrounded closely by solvent molecules that remain attached to the ions with weak intermolecular bonds. So, the solvated ion as a whole encounters the drag force. Hence, the mobility of a small ion (example, Na) may be lower compared to a large ion (example, Cl) because of the different radii of solvation in the two cases.

The ease of ionic movement through a medium is usually evaluated by measuring the conductivity at the phenomenological level. The conductivity is a part of the constant of proportionality in Ohm's law, which relates the flux ($J=I.A$) due the electric field (V/l) in the form of voltage-current relationship (Eq. (B.5)). The mobility similarly is the constant of proportionality for the relationship between a flux term—the drift speed, and electric field (Eq. (B.4)). It follows therefore that the conductivity is intimately related to the mobility (Eq. (B.6))[3].

[3] The charge passing with a drift speed s through area A in time t is equal to the charge contained in a volume with length = s.t and area A. Thus, J = [(s.t).A.($zeCN_A$)]/A.t]. J=szCF; Thus, I=szCF.A=V/R. Since, s=u.V/l, σ=zCuF

Conductivity (σ)

$$\sigma = \left(\frac{I}{V}\right)\frac{l}{A} \quad \text{(B.5)}$$

Where, I is the current, V is the voltage, l is the length, and A is the cross-section area.

$$\sigma = \mathrm{z}\mathrm{C}uF \quad \text{(B.6)}$$

Where, F is Faraday's constant ($e \times N_A$ = 9648.5 C/mol).

However, in electrolytic conductors, the conductivity also depends on the concentration of the ions and the charge they carry. This implies that as the total charge carried increases by increasing the ionic concentration or/and the valency of the ions, the ionic conductivity also increases. Another quantity is therefore used to normalize the effect of concentration (c) and valence (z) called the equivalent conductivity:

Equivalent conductivity (Λ)

$$\Lambda = \frac{\sigma}{Cz} = uF \quad \text{(B.7)}$$

B.2.3 Nernst-Einstein relation

When the electric field is such that the migration flux balances the diffusion flux, there is no net movement (Eq. (B.8)). Under these balanced conditions, the laws of statistical mechanics can be applied to determine the distribution of ions (Eq. (B.9)), i.e., the concentration gradient. It follows from these two considerations, that the diffusion coefficient is related to the mobility by the Einstein relation as shown in Eq. ((B.10)-(B.12)).

$J_{dif} = J_{mig} \quad \Rightarrow$

$$D\frac{dC}{dx} = C.s \quad \text{(B.8)}$$

Maxwell-Boltzmann distribution

$$C = C^0 e^{-\frac{U}{kT}} \quad \text{(B.9)}$$

Where U is the potential energy, k is the Boltzmann constant, T is the temperature, and C^0 is the concentration at zero potential energy.

Einstein relation

$$D = \frac{uRT}{zF} = \left(\frac{u}{zF}\right)RT \quad \text{(B.10)}$$

Or,

$$D = \left(\frac{u}{zF}\right)RT = BRT \quad \text{(B.11)}$$

Or,

$$B = \left(\frac{u}{zF}\right) \tag{B.12}$$

An important conclusion of this relation, most relevant to this study, is that this relation leads to a relationship between conductivity and diffusivity as both conductivity and diffusivity are a function of mobility. This is described by the Nernst-Einstein equation (Eq. (B.13)), which can be used as the basis for the prediction of diffusivity through the measurement of conductivity.

Nernst-Einstein equation

$$\Lambda = \frac{zDF^2}{RT} \tag{B.13}$$

More precisely, for 1:1 valent cation (+)-anion (-) pair, it can be presented as:

Nernst-Einstein equation

$$\Lambda = \frac{F^2}{RT}(D_+ + D_-) \tag{B.14}$$

An important issue concerning the use of this equation in the case of concrete is in regard to the presence of other ions in the pore solution of concrete. While the diffusion coefficient of NaCl can be measured without considerable error, other ions will significantly affect the conductivity.

B.2.4 Concentration dependence of ionic diffusion and conduction

Ionic diffusion and migration were discussed in the previous section assuming ideal conditions, i.e., the ions were far apart from other ions so that there was no ion-ion interaction. However, these conditions are possible only near infinite dilution. As the concentration increases, the transporting ions are no longer independent of the influence of surrounding ions. The attractive forces of the surrounding oppositely charged ions impede the motion of the moving ions. Consequently, the rate of transport is less than should be expected at that concentration using the ideal laws. This is remedied by using 'activity' in place of concentration as an effective concentration. The concept of activity enables the use of ideal laws in non-ideal conditions of high concentration.

In the context of migration, the ion-ion interactions are discussed in terms of asymmetry and electrophoretic effects. In solutions of finite concentrations, the ions of opposite charge form a symmetric sheath around an ion, termed as the ionic atmosphere. When an electric field is applied, the ion starts moving under its influence. The ions in the ionic atmosphere also move along in response to the movement of the ion. However, the ion moves first and then the ionic atmosphere, therefore what was initially a symmetric sheath around the ion is now lagging behind the ion and becomes asymmetrical. This separation of charge produces an electric field that opposes the movement of the ion. This is known as the asymmetry effect.

The ionic atmosphere is formed of ions of opposite charge, which are attracted to the opposite electrode. This exerts a drag force on the moving ion further impeding its movement. This is known as the electrophoretic effect. These two effects work to reduce the effective concentration of the solution. However, as the ionic concentration increases, more solvent ions are involved in the solvation of these ions and less are available as free solvent ions. This effectively increases the concentration. Therefore, the activity decreases with concentration until the ion-ion interactions are dominant and then it starts rising again when the ion-solvent interactions become dominant (see this for NaCl in Table B.1). In all this, however, what is of importance to this study is how the concentration affects the diffusivity, the conductivity, and their relationship.

Table B.1. Mean activity coefficients ($\gamma = (\gamma_+\gamma_-)^{\frac{1}{2}}$) for NaCl in aqueous solution of various concentrations at 25˚C (adapted from (Haynes, Lide & Bruno, 2014))

Mol/kg (m[1])	0.001	0.010	0.050	0.100	0.200	0.500	1.000	2.000	5.000
Activity coefficient	0.965	0.903	0.822	0.779	0.734	0.681	0.657	0.668	0.874

[1]m is the molality of the solution defined as the moles of NaCl per L of water added to make a solution.

The diffusion coefficient is dependent on concentration because in non-ideal conditions concentration must be replaced by activity and activity is dependent on the concentration. Ideally, the concentration term should be replaced by activity in the diffusion equations. Using activity in Fick's first law results in Eqs. (B.15) and (B.16). Eq. (B.17) shows that using activity results in an extra term since the activity itself is concentration-dependent (see Table B.1). This shows that the diffusion coefficient calculated using the classical forms of Fick's laws is concentration-dependent and therefore is not an intrinsic material property.

$$J = -\overbrace{\mathrm{BRT}}^{D^0}\frac{\mathrm{d(C.}\gamma)}{\mathrm{dx}} \tag{B.15}$$

Where, B is a constant, R is gas constant, T is temperature, and γ is the activity coefficient.

Or,
$$J = -\mathrm{BRT}\frac{\mathrm{dC}}{\mathrm{dx}}\left(1+\frac{C}{\gamma}\frac{d\gamma}{dc}\right) \tag{B.16}$$

Or,
$$J = -\overbrace{\left[BRT\left(1+\frac{C}{\gamma}\frac{d\gamma}{dc}\right)\right]}^{D}\frac{\mathrm{dC}}{\mathrm{dx}} \tag{B.17}$$

Where,

D is the diffusion coefficient from Fick's law when concentration is used instead of activity.

If the range of concentration change is such that the activity coefficient remains almost constant, then the term $\left(\frac{c}{\gamma}\frac{d\gamma}{dc}\right)$ becomes negligible and can be ignored. In the case of chlorides, this range seems to be from 0.5 M to 2.0 M. In this range, the diffusion coefficient can be assumed to be independent of concentration. The concentration dependence of the diffusion coefficient can be derived from the Debye-Huckle limiting law for the activity coefficient (Eq. (B.18)).

$$\log\gamma = -A\sqrt{c} \tag{B.18}$$

D

$$D = D^{\circ}(1 - \frac{1}{2}A\sqrt{c}) \tag{B.19}$$

Similarly, the concentration dependence of equivalent conductivity is described by Eq. (B.20) according to Kohlrausch's law.

Equivalent conductivity (Λ)

$$\Lambda = \Lambda^{\circ} - A\sqrt{c} \tag{B.20}$$

The diffusion coefficient and the equivalent conductivity have different relationships with concentration. This is also shown in Figure B.1. This shows the differences in the mechanisms of influence of ionic interactions on diffusion and migration. The implication is that in the absence of modification to the equation accounting for these differences, a concentration-specific conductivity-diffusivity relationship will have to be experimentally developed. A relationship at a particular concentration, however, cannot be used at other concentrations.

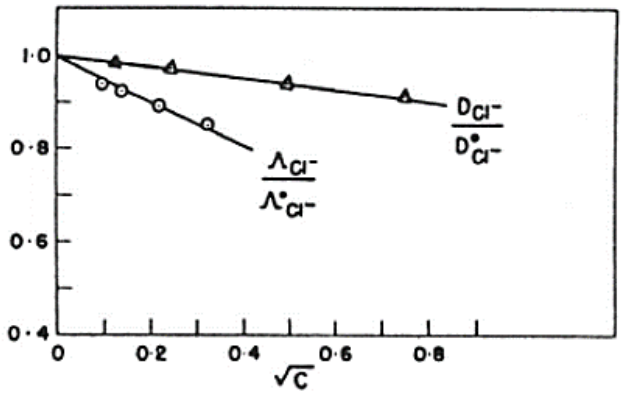

Figure B.1. The ionic diffusivity and conductivity vary in different ways with the concentration (reproduced from (Bockris & Reddy, 2002))

B.2.5 Diffusion in porous media

This discussion is mainly based on Atkinson & Nickerson (1984).

The diffusion in porous media is more complicated than in an electrolyte free of solid boundaries. In porous media, the electrolyte is contained in the pore volume of the medium. The pore volume is generally not composed of straight cylindrical conduits of uniform cross-section parallel to the concentration gradient. Instead, the pores form a longer, more 'tortuous', route with 'constricted' cross-sections at several locations (see Figure B.2). The tortuous and constricted nature of the pore volume prolongs the travel time which translates into a much lower diffusivity (D_p) compared to the free electrolyte (D_f).

The diffusion occurs in the pore solution contained in the pore volume. Hence, the flux and concentration terms of Fick's first law are defined in relation to the volume of the pore solution just as in the case of free solution (Eq. (B.1)).

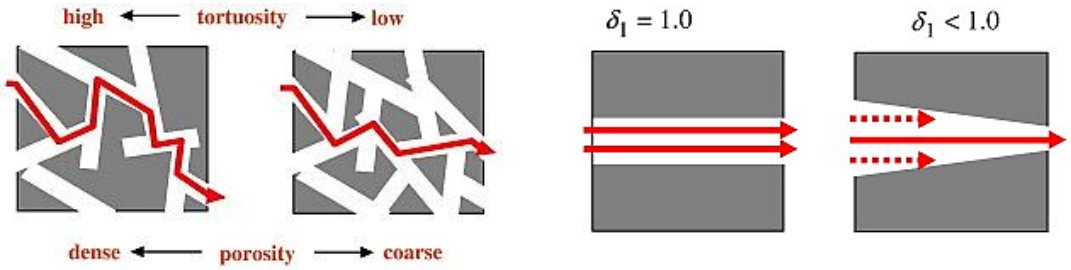

(a) Tortuosity (b) Constrictivity

Figure B.2. Schematic representation of diffusion paths in a tortuous and constricted pore volume (illustrations from (Ishida, Iqbal & Anh, 2009))

In contrast to the diffusion in free solution, the diffusion coefficient (D_p) in case of porous media will be different ($D_p < D$) due to the reasons explained above (see Eq. (B.21)).

D_p
(p – porous medium)

$$J_l = -D_p \frac{\partial C_l}{\partial x} \qquad \text{(B.21)}$$

Where, J_l and C_l are flux and concentration defined with respect to the volume of the pore solution.

It is however more convenient to calculate the flux over the entire cross-section of the medium (J_p). Applying simplifying assumptions that the pores remain continuous in the direction of net movement and fully saturated, porosity can be used to relate the cross-sections as well as the volumes of the pores with the total volume of the porous media (Eq.(B.22)). The flux terms can be modified using Eq. (B.22).

This will modify the diffusion coefficient as well from D_p to D_{eff} (Eq. (B.23)). The D_{eff} [4] is also referred to as the steady-state diffusion coefficient (D_{ss}).

$$A_l = \varepsilon . A_p \tag{B.22}$$

D_{eff} (or D_{ss})

$$J_p = -D_{eff} \frac{\partial C_l}{\partial x} \tag{B.23}$$

Where J_p is the flux term calculated over the cross-section of the porous medium (A_p). The diffusion coefficients for porous media are related in this way: $D_{eff} = \varepsilon . D_p$ (thus, $D_{eff} < D_p$).

In order to separate the effect of pore structure formation on the diffusivity, the 'diffusibility' of the medium is defined as the ratio of the effective diffusivity to the diffusivity in free liquid. The inverse of diffusibility, known as the Formation Factor, is also used in this context. This provides a useful means of characterising the transport property of the medium.

Diffusibility, Q

$$Q = \frac{D_{eff}}{D_f} = \frac{\varepsilon \delta}{\tau^2} \tag{B.24}$$

Where, ε is the pore volume fraction, δ is the constrictivity factor, and τ is the tortuosity factor.

Following the Nernst-Einstein relation, the diffusibility can be measured through conductivity measurements as well.

Diffusibility, Q

$$\frac{D_{eff}}{D_f} = \frac{\sigma_s}{\sigma_f} \tag{B.25}$$

Where σ_s is the conductivity of the medium saturated with the electrolyte and σ_f is the conductivity of the electrolyte in the free state.

Because the numerator and denominator have the same concentration dependence, which applies to both sides of the equation, diffusibility nullifies the effect of different concentration dependence of diffusion coefficient and conductivity (Streicher, 1997). This enables, at least in theory, the use of conduction experiments in lieu of the longer and tedious diffusion experiments to characterise concrete's resistance to chloride diffusion. However, the underlying assumption that the pore structure

[4] [One needs to be careful about which diffusion coefficient the notation represents as same notations could refer to different diffusion coefficients in different sources. For example, (NT BUILD 443, 1995) uses D_{eff} for time-averaged non-steady state diffusion coefficient rather than steady state diffusion coefficient. The "eff" notation refers to different aspects: in the steady state, it refers to the combined effect of electro-diffusion and in the non-steady state, it refers to the combined effect of electro-diffusion, binding, and age.]

responds in the same way to conduction as it does to diffusion must be remembered. Another matter of practical importance in designing test methods and interpreting the results is whether the diffusibility is independent of the ion type used or not. This especially concerns the bulk and surface resistivity tests, which do not use chloride ions to evaluate the resistivity/conductivity of concrete.

So far, the reaction of transporting ions with the porous medium has not been considered. Concrete however is a reactive material which binds chloride ions in its matrix. This also lowers the rate of transport of chloride ions. This aspect has been covered in Appendix A.

B.3 Tests for Resistance to Chloride Penetration

The chloride resistance tests are here classified according to the type of measurement used. A comparison of the common test methods is provided in Table B.2.

B.3.1 Steady-state diffusion methods

A classic diffusion cell arrangement is used which consists of two cells on opposite sides of the specimen, one with a chloride solution and the other containing a chloride-free alkaline solution. The chloride concentration in the downstream cell is monitored and the test is run until a constant flux is established. A constant flux is established when the chloride ions have penetrated the entire thickness of the specimen and the chloride capture through binding is complete. The steady-state diffusion test enables direct measurement of the steady-state diffusion coefficient (using Fick's 1st law). Since the steady-state diffusion coefficient is taken to be the physical transport property governing the resistance of concrete to chloride diffusion, this test is considered fundamental to transport studies and the validation of the migration methods. A great benefit of this method is the straightforward mathematics involved.

As far as the test arrangement is concerned, the chloride solution needs to be replaced at regular intervals to keep the chloride concentration in the upstream cell nearly constant during the time to reach a steady state. Another alternative is to use a larger upstream reservoir (Dhir et al., 1990). The large volume of solution relative to the chloride ion uptake in the specimen keeps the concentration nearly constant without the need to replace the solution frequently. The main drawback of the steady-state diffusion method is that it takes the order of 1 year to reach the steady state for thin concrete specimens. This is too long for practical purposes and can only be feasible in research settings. Even in research work, mostly only paste specimens are used to reduce the time of testing from months to weeks. The thickness of the paste specimens can be acceptably reduced to a considerable extent without compromising the representativeness, which makes only such specimens suitable for this method.

B.3.2 Non-steady-state diffusion methods

The chloride penetration occurs in a non-steady state until it reaches the steady-state conditions, which can take a long time in the case of concrete. This is also the state in which diffusion naturally occurs in

real structures. The non-steady-state diffusion tests utilise this non-steady portion of the chloride ingress to evaluate the chloride resistance of concrete. Tests under complete immersion are known as bulk diffusion tests after the ASTM test (ASTM C1556, 2016) or the accelerated chloride penetration tests after the NORD test (NT BUILD 443, 1995). The use of a relatively high concentration of chloride ions (2.8 M) shortens the test duration further. This method is most widely used for measuring the diffusion parameters in some instances with changes in the test conditions—mostly the solution concentration.

The standard method, same in both the standards, in summary, is as follows. Concrete specimens are sealed with coatings on all but one face through which the chloride ions will be allowed to penetrate. The specimens are saturated with $Ca(OH)_2$ solution to ensure the predominant transport process is diffusion. The saturated specimens are immersed in a 2.8 M NaCl solution (165 g/L_{sol}) for at least 35 days to ensure that chloride ions penetrate in sufficient concentration. At the end of the exposure period, the specimens are taken out of the exposure solution and concrete powder samples are obtained in successive layers into the depth of concrete using profile grinding or slicing techniques. The exposure period of 35 days was found to be very short in this study. Such short durations necessitate the use of very small depth increments only possible through profile grinding. Profile grinding using a lathe or mill was found to be an extremely laborious, time-consuming, and hazardous process, which makes it impractical to use on more than a few specimens. Thus, this method typically requires a few months for completion. Chloride analysis of the powder samples is performed to obtain the chloride content at successive depths into concrete, which constitutes the chloride profile (Figure B.3).

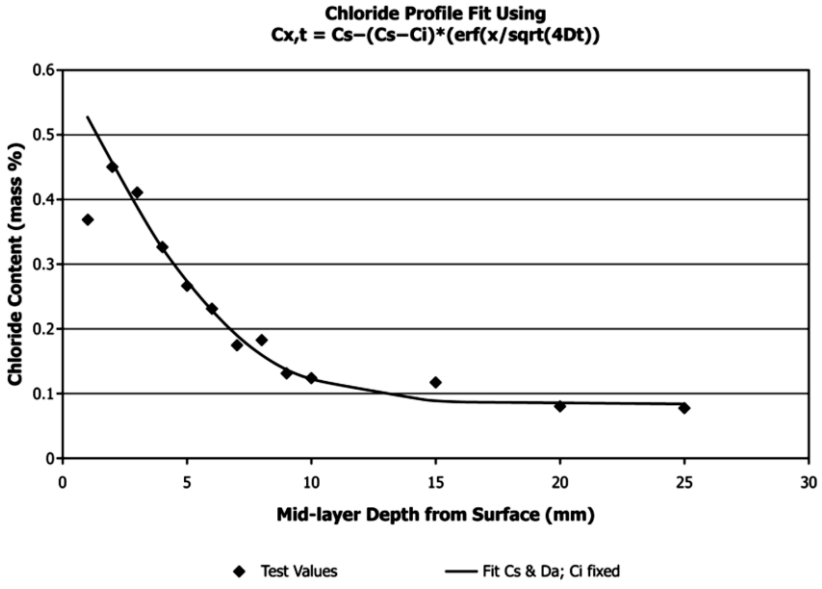

Figure B.3. A typical chloride profile (reproduced from (ASTM C1556, 2016))

In order to obtain the diffusion parameters from these results, the error function solution to Fick's second law is fitted in the chloride profile data through non-linear regression. ASTM C1556 (2016) considers the diffusion coefficient obtained to be an apparent diffusion coefficient (D_a) while the NT

BUILD 443 (1995) defines it as an effective chloride transport coefficient, D_e. This difference in terminology creates confusion in the literature.

B.3.3 Steady-state migration methods

A diffusion-cell type arrangement is used for this test as well, but a DC voltage is applied to accelerate the penetration of chlorides. The test is run until steady-state conditions are achieved, i.e., when the chloride binding is complete in the specimen and therefore constant flux of chlorides is received in the downstream chamber (see Figure B.4).

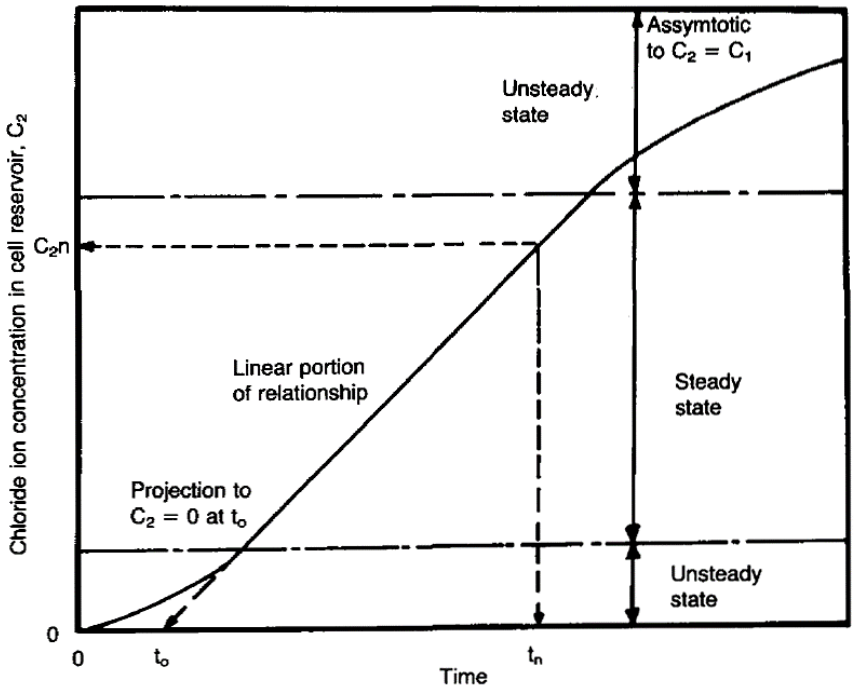

Figure B.4. A schematic of the ideal evolution of the downstream chloride concentration in steady-state diffusion and migration tests (reproduced from (Dhir et al., 1990)).
Note: In both diffusion and migration ($c_{us} >> c_{ds}$), the flux becomes constant in a steady state and hence an equal number of ions entering the downstream cell in a given time leads to a linear increase in concentration with time. It must be noted however that the concentration profiles in the specimen will be different in the two cases due to different mechanisms at play.

This may take one or two weeks depending on the quality of concrete tested and the test conditions (Dhir et al., 1990). This test duration may be too long for most cases. A standard test method is NT BUILD 355 (NT BUILD 355, 1997). The steady-state methods are used to determine the steady-state diffusion coefficient of the material by measuring the steady-state conductivity—a direct application of the Nernst-Einstein equation. In that respect, these tests are firmly grounded in theory. However, chloride ions can get oxidized to chlorine gas at the anode, which could introduce errors in the measurement of chloride concentration in the downstream cell. Additionally, the test needs constant monitoring of the downstream chloride concentration. It also needs adjustment to account for chloride

depletion in the upstream cell and the decrease in pH in the downstream cell due to the release of H^+ ions in anodic reactions, which can be detrimental to the electrode and concrete (Streicher, 1997).

B.3.4 Non-steady-state migration methods

The Tang and Nilsson method, also known as the rapid chloride migration test (RCMT), is widely used internationally as such or with some modifications (Tang & Nilsson, 1992). NT BUILD 492 (1999) provides the standardised procedure. A brief description of the method is provided here. A migration cell arrangement is used consisting of cathodic and anodic half-cells with NaCl solution and NaOH solution respectively on either side of the specimen (Figure B.5). An initial current measurement under a DC voltage of 30 V is measured. Essentially, a measure of resistance, this measurement is used to select the test conditions, namely, voltage and test period. The specimen is split at the end of the test period and the chloride depth is determined by spraying $AgNO_3$ solution.

The distinguishing feature of this method is that the migration coefficient is derived from the chloride penetration depth obtained with the applied test conditions rather than the current. This way the errors associated with the contribution of other ions present in the pore solution to the measured current are avoided. The test is based on a sound mathematical model and the test design addresses the main concerns encountered in migration testing. However, some things must be kept in mind.

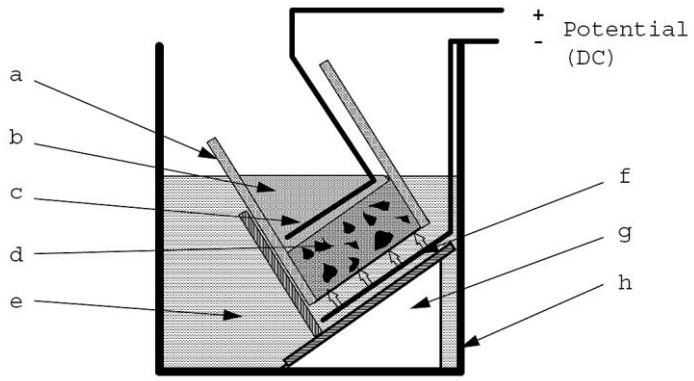

Figure B.5. The typical test arrangement for RCMT (reproduced from (NT BUILD 492, 1999))

The migration coefficient as measured in this test does get influenced by chloride binding in the presence of an electric field, which may or may not be the same as in a diffusion process. The current decreases—and the applied voltage across the specimen—in some cases over the test period due to polarisation effects, which can affect the penetration depth. In addition, the test period exceeds 24 hours for high-quality concrete needed for marine conditions. While this is not a very long duration for such

a test, maintaining the test conditions for this long may become a problem, for instance, in places where power supply is unreliable. Multiple critical steps are involved to complete the test, which makes it prone to error and somewhat tedious. The use of colourimetric measurement of chloride penetration depth as the main measurement also limits the use to only initially chloride-free specimens and thus it is not suitable as a condition assessment tool (Andrade, Castellote & D'Andrea, 2011).

The theory behind this method is described below (Tang, Nilsson & Basheer, 2012):

The migration flux due to an electric field:

Migration flux (J_m)
$$J_m = \frac{zFEDC}{RT} \tag{B.26}$$

In non-steady state conditions, applying mass balance equation:

$$\frac{\partial C_t}{\partial t} = -\frac{\partial J_m}{\partial x} = -\frac{zFED}{RT}\frac{\partial C_f}{\partial x} \tag{B.27}$$

Accounting for chloride binding during migration:

$$\frac{\partial C_t}{\partial t} = \frac{\partial C_f}{\partial t}\left(1 + \frac{\partial C_b}{\partial C_f}\right) = -\frac{zFED}{RT}\frac{\partial C_f}{\partial x} \tag{B.28}$$

Or,
$$\frac{\partial C_f}{\partial t} = -\frac{D}{\left(1 + \frac{\partial C_b}{\partial C_f}\right)}\frac{zFE}{RT}\frac{\partial C_f}{\partial x} \tag{B.29}$$

Or,
$$\frac{\partial x}{\partial t} = -\frac{D}{\left(1 + \frac{\partial C_b}{\partial C_f}\right)}\frac{zFE}{RT} \tag{B.30}$$

The non-steady migration coefficient will be:

$$D_{NSSM} = \frac{D}{\left(1 + \frac{\partial C_b}{\partial C_f}\right)} \tag{B.31}$$

However, the presence of an electric field will alter the binding behaviour. Integrating for the test period, in which the chloride penetration will be x_f, the migration coefficient can be obtained by measuring the penetration depth, assuming constant electric field:

Or,
$$D_{nssm} = \frac{RT}{zFE}.\frac{x_f}{t} \tag{B.32}$$

B.3.5 Resistivity/conductivity methods

The most common test methods using conduction measurements are described in this section. The rapid chloride permeability test is also classified under this category as current measurements are central to this method. The chloride conductivity method also falls under this category. It is covered in much more detail than other tests as it forms the focus of this study and is therefore placed under a separate section of its own.

1. Rapid chloride permeability test (RCPT)

RCPT (ASTM C1202, 2012) is one of the earliest electrical methods to evaluate the chloride resistance of concrete. It uses a diffusion/migration cell in which one cell contains a chloride solution and the other an alkaline solution. A voltage of 60 V is applied for 6 hours, and the current is monitored at half-hour intervals. The total charge passed in 6 hours is used as the measure of the chloride penetration resistance of concrete. This method has been criticized severely for issues such as a lack of theoretical basis, the contribution of ions other than chlorides, excessive temperature increases and so on. The shortcomings of RCPT created opportunities for the development of new tests, such as the rapid migration test, the chloride conductivity test, and the like. Despite all the criticism, the test persists. ASTM provided a conduction method that utilizes the RCPT setup (ASTM C1760, 2012), the only difference is that only the initial reading is taken to measure the resistivity. However, this method has now been withdrawn.

2. Resistivity methods

In contrast to the methods using the migration of chloride ions through concrete, resistivity methods measure the instantaneous electrical resistivity of the concrete ideally in its uncontaminated, but saturated condition. Various test arrangements are possible. The two most common arrangements are axial or direct resistivity and surface resistivity. In the direct resistivity arrangement, the voltage is applied across the longitudinal axis of the specimen and the current runs perpendicular to the cross-section of the specimen. This is referred to as the two-electrode method or the bulk resistivity method. Whereas in the surface resistivity arrangement, both the electrodes across which the voltage is applied are kept on the same side of the surface and two separate electrodes, also on the same side of the surface, measure the current. This is known as the four-electrode method or four-point method or the Wenner method (Wenner, 1915). Both methods use alternating current. The schematic representation of the two methods is shown in Figure B.6.

ASTM C1876 (2019) provides the standard method for bulk resistivity measurement. There is no ASTM method for surface resistivity however a standard method is available in AASHTO T 358 (2015). Both these methods prescribe the use of standard cylinders in line with the practice of using cylinders for the compressive strength test in the US. The resistivity calculations are performed without the assumption of a particular shape of the specimen and hence cube specimens are just as valid.

The conduction in concrete occurs in the pore solution as the solid matrix is nearly non-conductive. The degree of saturation, by its effect on the conducting fluid (pore solution), has a significant influence on resistivity. The pore solution composition also plays an important role. In recognition of this, ASTM C1876 requires saturating the specimen in a simulated pore solution by simple immersion for a minimum of 6 days. In contrast, the AASHTO method states that the lab specimens should always remain in a saturating environment with 100% RH after demoulding. It includes field cores as possible test specimens without providing a method of saturation. In summary, only standard moist-cured lab specimens can be tested with this method.

Both methods are simple and rapid. Minimal specimen preparation is necessary. The surface resistivity method is also non-destructive and can be applied to field structures. The separation of the probes to measure the current and potential difference in the 4-point arrangement prevents the error due to contact resistance (Morris, Moreno & Sagüés, 1996). However, there are many influencing factors that need careful consideration for proper interpretation of the results, such as the degree of saturation and temperature. The proper use of these methods for mix comparison in relation to chloride penetration requires the formation factor analysis.

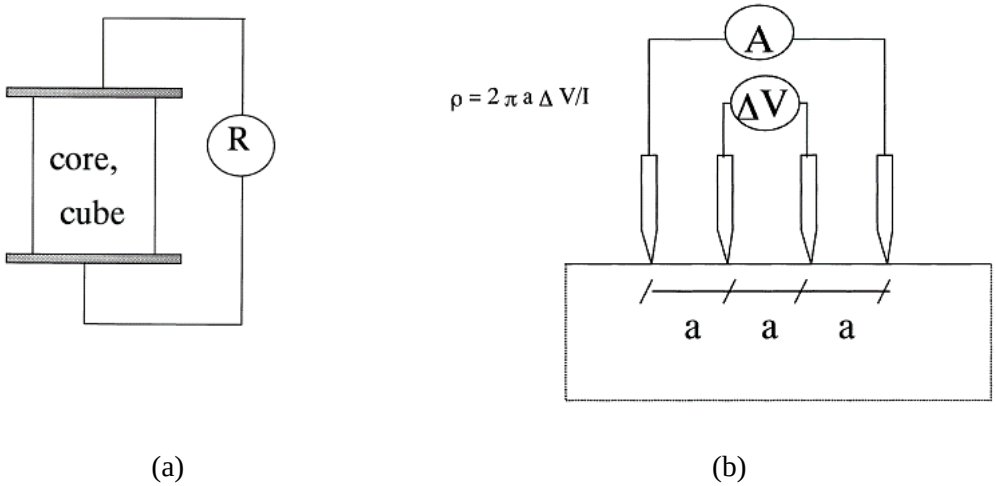

(a) (b)

Figure B.6. The schematic of bulk resistivity (a) and surface resistivity (b) arrangements (reproduced from (Polder, 2001))

Table B.2. A summary of the salient features of common chloride tests

Test method	*Test Specimen*	*Parent specimen*	*Preconditioning*	*Measurements*	*Test duration*	*Variability (1s %)*
RCMT (NT Build 492)	Cyl.: 100 mm (dia.) 50 mm (tk.)	Lab:100 mm (dia.) cyl. Field:100 mm (dia.) core	Vacuum saturation with sat. $Ca(OH)_2$ sol. (ASTM C1202 method)	1.Initial current @ 30 V 2.Applied voltage (10-60 V) 3.Temperature (catholyte chamber) 4.Chloride penetration depth 5.Thickness	6 h – 4 days; For high quality concretes: 24 h or more	Repeatability: 9% Reproducibility: 13-24%
RCPT (ASTM C1202)	Cyl.: 100 mm (dia.) 50 mm (tk.)	Lab: 100 mm (dia.) cyl. Field: 100 mm (dia.) core	Vacuum saturation with sat. $Ca(OH)_2$ sol.	Current at half-hour intervals for 6 hours	6 h	Repeatability: 12% Reproducibility: 18%
CCI (SANS 3001-CO3-3)	Cyl.: 70 mm (dia.) 30 mm (tk.)	Lab:100 mm cube Field: 70 mm (dia.) core	1.Oven-drying at 50˚C for 7 days 2.Vacuum sat. with NaCl solution	1.Voltage 2.Current 3.Thickness & diameter	~2-5 min.	Repeatability: 9% Reproducibility: 21%
Bulk resistivity (ASTM C1876)	Lab: Cyl. 100 mm (dia.) x 200 mm (tk.) -min. 1:1 core field (>3 x agg.)		Immersion in simulated pore sol. for at least 6 days	1.Voltage 2.Current 3.Thickness & diameter	~2-5 min.	Repeatability: 4% Reproducibility: 13%
Surface resistivity (AASHTO T358)	Cyl. 100 mm (dia.) x 200 mm (tk.)		Moist cured	1.Voltage 2.Current 3.Thickness & diameter	~2-5 min.	Repeatability: 6% Reproducibility: 12%
Bulk diffusion (NT Build 443, ASTM C1556)	>75 mm (>3 x agg.)	-	Immersion in sat. $Ca(OH)_2$ sol. Until mass change < 0.1 % in a day	1.Depth of layer 2.Chloride content	At least 35 days; profile grinding and cl analysis extra	C_s:(ASTM C1556, 2016) Repeatability: ~13% Reproducibility: ~18%
						D_a:(ASTM C1556, 2016) Repeatability: ~14% Reproducibility: ~20%

1.1 Chloride Conductivity Test

The chloride conductivity test was developed by (Streicher & Alexander, 1995; Streicher, 1997, 1999) with the aim to address the shortcomings of the existing electrical test methods for chloride resistance of concrete (Streicher & Alexander, 1994). In principle, the test involves applying a direct voltage across a disc specimen saturated with a standard NaCl solution to measure the conductivity. The major steps in the test procedure are as follows (SANS 3001-CO3-3, 2015; DI-Manual, 2018):

1. Test specimen preparation: A cylindrical disc with dimensions of 70 mm (dia.) x 30 mm (thick) is used as the test specimen. The test specimens are extracted from the near-surface region of the cores drilled from larger parent specimens or real structures by removing the top 5 mm.
2. Preconditioning: The preconditioning involves two steps: drying and saturation. The specimens are dried in a ventilated oven at 50˚C for 7 days. The dried specimens are submerged in a 5 M NaCl solution to achieve saturation following a standard vacuum saturation procedure.
3. Testing: A standard test setup (Figure B.7) consists of two half cells closely fitted on opposite sides of the specimen. Each half-cell contains a steel electrode and 5 M NaCl solution as the electrolyte. In addition, fittings are provided in each cell for applying the voltage to the test setup and measuring the potential difference across the specimen. A DC voltage is applied across the circuit such that the potential difference across the specimen is about 10 V. The exact potential difference and current are recorded. The conductivity is calculated from Ohm's law and referred to as the chloride conductivity or chloride conductivity index (CCI).

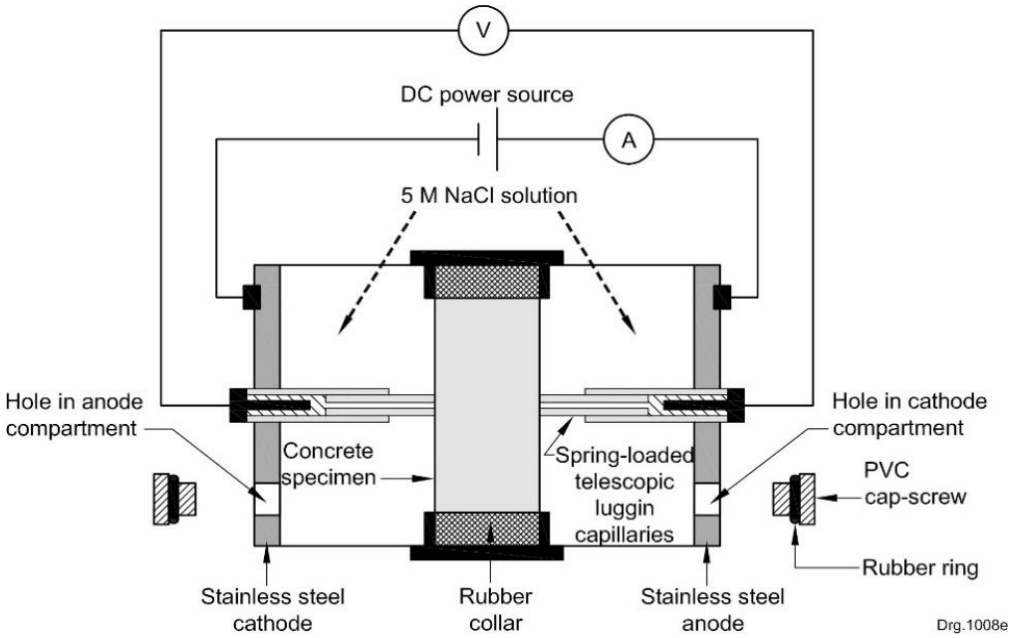

Figure B.7. Schematic of the current CCI rig (fig. reproduced from (Otieno & Alexander, 2015))

1.1.1Salient features

The distinguishing features of this test method and the considerations that led to the development of these features are discussed below (Streicher, 1997).

1.1.1.1 Principle: steady state conditions through saturation

The transport of chloride ions in concrete is impeded by the resistance offered by the physical pore structure of concrete and by the removal of diffusing chloride ions through the process of chloride binding. The ease with which chloride ions diffuse in the pore solution contained in the pore structure of concrete without the effect of binding is described by the steady-state diffusivity, while the non-steady-state diffusivity contains the effect of binding too. Chloride binding, although a complex process with multiple influences, is affected mainly by the choice of binder and to a much smaller extent by the concrete production process and the degree of quality control exercised. On the other hand, the characteristics of the physical pore structure depend heavily on the mix design, production process, and quality control. Therefore, it follows that while proper selection of binder can largely account for chloride binding, a quality control test must clearly measure the 'physical' (non-reactive) resistance of concrete to chloride diffusion that is sensitive to construction practices.

The steady-state diffusivity represents such a property. However, steady-state conditions require very long durations to establish, making it unsuitable as a quality control test. The demand for short testing duration is inherent to the adoption of any quality control test in practice as prolonging the project timeline for any reason incurs additional cost. Given that ionic diffusivity is related to ionic conductivity through the Nernst-Einstein relation, conductivity measurements can provide a rapid means of measuring the diffusivity. The issue with measuring the conductivity of concrete is that not only chlorides but all the other ions present in the pore solution also contribute to the overall conductivity of concrete. The interest however is only in the conductivity (and thus diffusivity) of the chloride ions through concrete. The difficulty arises mainly because the pore solution composition varies across different concretes.

To eliminate the pore solution conductivity misrepresenting the chloride ion conductivity, the concept of diffusibility is used to extract the effect of pore structure by normalising the overall conductivity with the pore solution conductivity. The same is possible for diffusivity. It is assumed that as diffusivity and conductivity are related, the pore structure resistance to both processes remains the same in both cases. The steady-state migration tests achieve that by driving the chloride ions through the concrete until a steady flux is obtained on the other side of the specimen, which may take one to several weeks.

The chloride conductivity test attempts to reach the steady state simply by saturating the concrete specimens with a concentrated 5 M NaCl solution before measuring conductivity, which also takes much shorter than the classic migration tests. Hence, the underlying assumption is that absorption can simulate or establish steady-state conditions.

1.1.1.2 Pore solution standardisation: saturation with 5 M NaCl solution

The use of a concentrated 5 M chloride solution is based on the consideration that the pore solution conductivity is largely governed by the conductivity of the saturating solution at high chloride concentration (see Figure B.8). The errors in the measurement of chloride conductivity due to possible errors in the chloride

concentration are also minimized at high chloride concentrations. Streicher demonstrated that at high chloride concentrations, the errors in diffusibility calculation due to differences in pore solution composition are small (see Figure B.9).

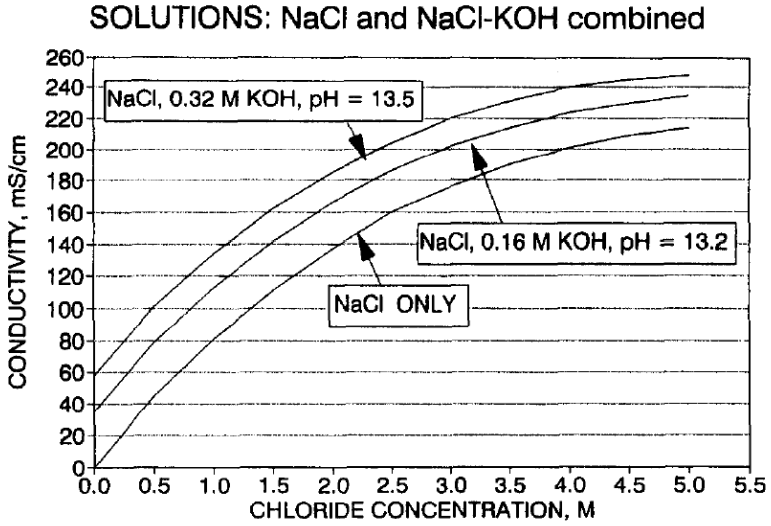

Figure B.8. The conductivity of NaCl solution at different concentrations with and without KOH (reproduced from (Streicher & Alexander, 1995)). The relative deviation of overall conductivity from the NaCl only conductivity becomes small at high NaCl concentrations.

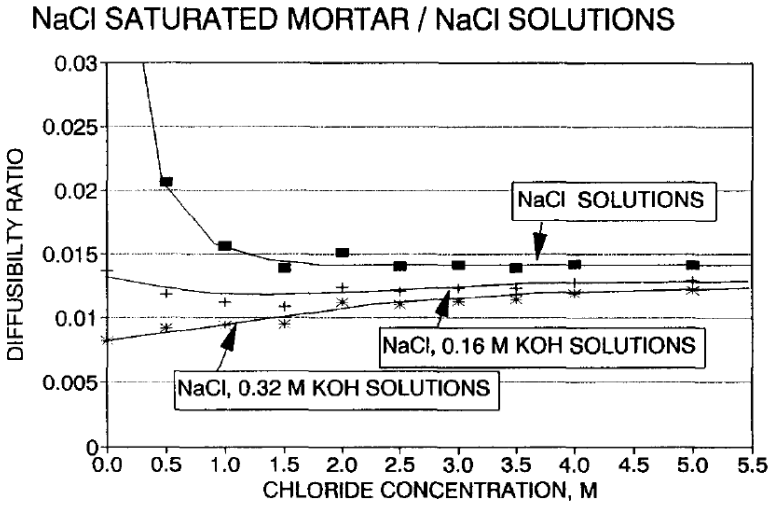

Figure B.9. Diffusibility ratios for mortar calculated considering different saturating solution compositions (reproduced from (Streicher & Alexander, 1995)). The top curve considers only the conductivity of the chloride solution at the chloride concentration, but not other ions from the original pore solution. The lower two curves consider two different original pore solution contributions to the chloride solutions.

In contrast, errors in determining the pore solution conductivity lead to a large error in diffusibility at low chloride concentrations. The foregoing demonstrations imply the robustness of the procedure to experimental errors and material variability.

These findings also imply that the chloride conductivity should provide a reasonable measure of diffusibility as the saturating solution effectively normalises/standardises the pore solution conductivity across all the concretes.

1.1.1.3 Accurate voltage measurement: Luggin capillaries

The voltage applied at the source drives the current in the circuit. However, the current is not entirely dependent on the resistance of the concrete specimen. There are other contributions from the circuit to the overall resistance. These are the resistance of the connecting wires, the resistance of the electrolyte between the electrode and the specimen, and the apparent resistance at the electrode-electrolyte interface, known as the polarisation resistance (Figure B.10). The net potential drop across the specimen is therefore smaller than the voltage applied at the source. Among the listed, the potential loss mainly occurs due to polarisation. If ignored, this can lead to an appreciable error in the conductivity measurement. The chloride conductivity setup includes Luggin capillaries on both sides of the specimen (Figure B.7) to allow the measurement of the potential difference across the specimen. Since the potential loss in the highly conductive 5 M NaCl solution is minimal, the Luggin capillaries provide a reasonably accurate means of measuring the potential difference. This feature improves the accuracy of the test method.

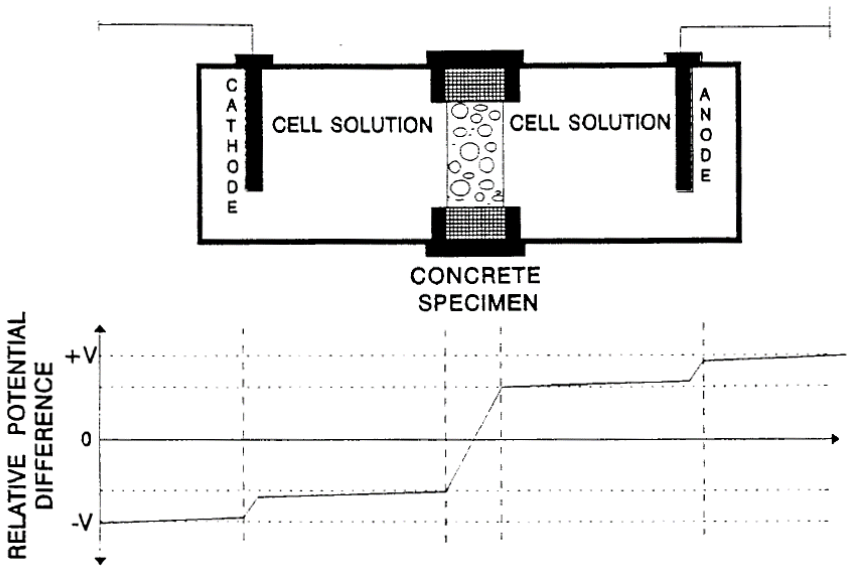

Figure B.10. Schematic representation of the potential drop at various points in the test circuit (reproduced from (Streicher, 1997))

1.1.2Preconditioning

1.1.2.1 Oven drying

The CCI specimens are dried in a ventilated oven at a temperature of 50 ˚C for 7 days. Drying before saturation was included in the preconditioning process to prevent dilution of the standardising solution by the water present in the concrete (Streicher, 1997). Streicher (1997) showed that 7 days of oven drying at 50˚C removes

most of the moisture and results in similar moisture content in concretes of different qualities without excessive microstructural damage in a relatively short time (Figure B.11). Later on, Mukadam, Alexander & Beushausen (2016) also investigated the effect of the duration of oven drying on the CCI of concretes with different binders and w/b ratios. It was found that extending the duration of drying can have a significant effect on CCI results. It was concluded that the duration of oven drying for the test needs to be controlled within a tolerance of 1 day to avoid significant variability in results.

The preconditioning in other tests discussed so far does not include oven drying to avoid the risk of excessive micro-cracking. Skipping this step however leaves the issue of different initial moisture states of the concrete, which can be very different depending on the curing, environment, and type of concrete. The oven drying in that respect creates reproducible conditions.

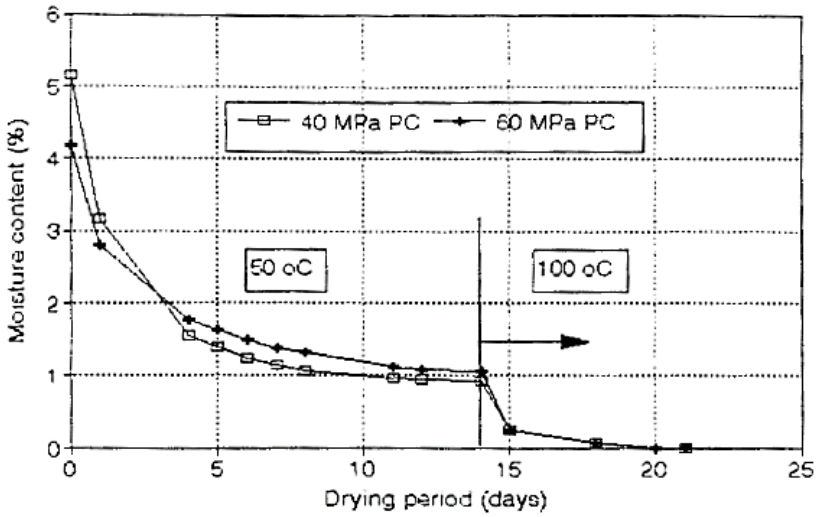

Figure B.11. The effectiveness of oven-drying at 50˚C and 100 ˚C with duration (reproduced from (Streicher, 1997))

1.1.2.2 Vacuum saturation

The ruggedness study on the chloride conductivity test showed that major changes in the vacuum saturation procedure (tested durations - vacuum saturation (2 h / 5 h); immersion time (0 h / 18 h)) can have a significant effect on CCI results (Streicher, 1999). Therefore, the procedure needs to be followed closely within tight tolerances. The difficulty of saturating dense concretes such as those made of SCMs was recognised and it was suggested that the use of a pre-evacuation step before vacuum saturation may resolve the issue. The vacuum saturation method produces improved saturation over methods such as cold-water saturation and boiling-water saturation (Safiuddin & Hearn, 2005). However, it may not be necessary that the specimens will be completely saturated. Mukadam, Alexander & Beushausen (2016), through investigations of chloride penetration depth on the split surfaces of saturated CCI specimens, showed that SCM and low w/b concretes were susceptible to lack of saturation with the NaCl solution.

Prolonging the immersion time in a bid to improve the saturation with NaCl solution will have an associated effect of reducing the conductivity of the specimen due to increased binding (Figure B.12). In any case, the rate of absorption drops precipitously after the 18-hour immersion period (Moore, Bakera & Alexander, 2022) and hence it is unlikely to help.

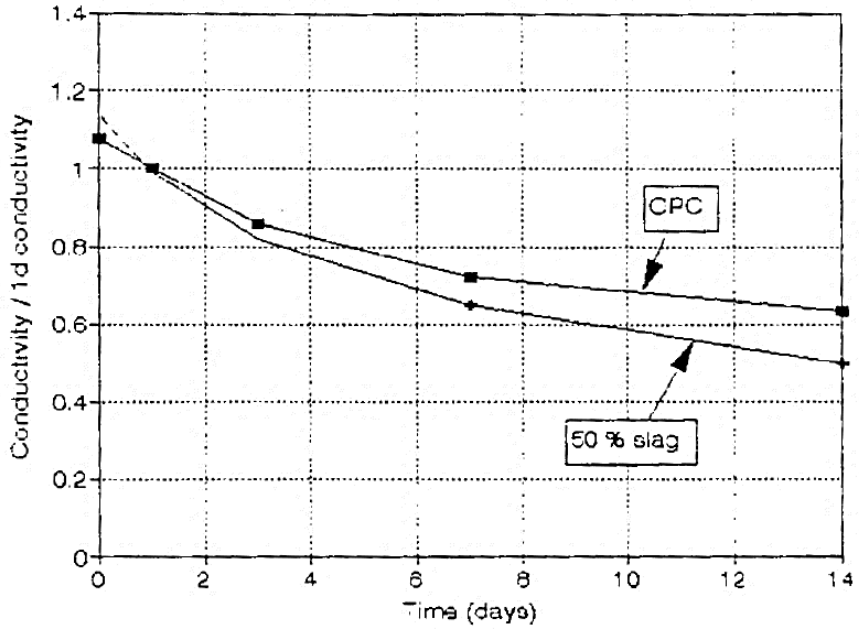

Figure B.12. Reduction in CCI with immersion time (reproduced from (Streicher, 1997))

1.1.3Variability and Revisions

Some preliminary round-robin studies showed large variability in the CCI test and led to the rewriting of the test method to improve clarity, tighten tolerances, and simplify the procedure to make it easier to follow. A round-robin test was conducted subsequently to assess the variability of the test method (Stanish, Alexander & Ballim, 2006). Nine different labs tested ten different concretes covering four different binders, two w/b ratios, and two local aggregate combinations. A good repeatability (9%) was observed in this program; however, a high reproducibility (21%) was recorded. The inexperience of the operators with the method and possible deficiencies in the test method itself were cited as possible causes. It was also found that the rubber rings holding the specimens in the rig need to be made available in a few different diameters to accommodate differences in the core barrel diameters used in different labs. The rubber ring must fit properly and provide a seal between the two cells to prevent leakage.

Some revisions have also been made to the CCI rig over the years as documented in Otieno & Alexander (2015). The $Cu/CuSO_4$ cells used to measure the potential difference across the specimen through the Luggin capillaries were discontinued early on. A steel electrode immersed in the test solution was found to be just as effective, compare Figure B.13 and Figure B.14.

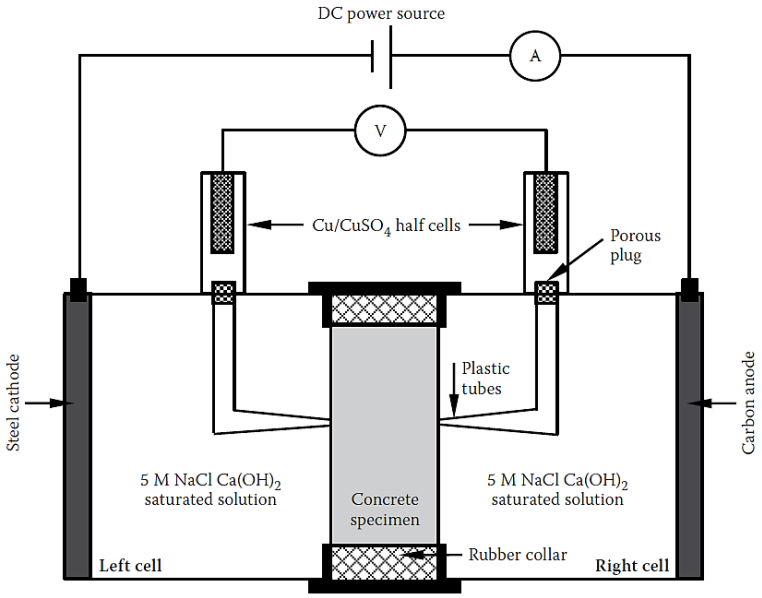

Figure B.13. Schematic of the original CCI rig (reproduced from (Otieno & Alexander, 2015))

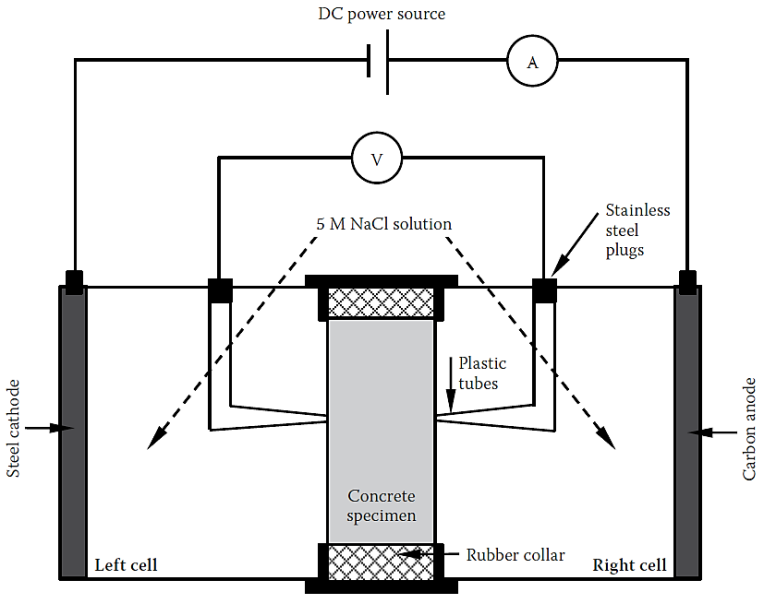

Figure B.14. Schematic of the CCI rig after the first modification (reproduced from (Otieno & Alexander, 2015))

The main revision in design happened in 2014 when the new CCI rig was adopted. There were three main changes:

1. Telescopic spring-loaded Luggin capillaries that project out of the chambers are used in the new rig. In this arrangement, Luggin capillaries are always in contact with the specimen regardless of small differences in thickness. This was not possible in the previous arrangement as the Luggin capillaries were fixed in a position.

2. The anode was made of stainless steel along with the cathode in place of carbon. The test is conducted for a very short time, and it is unlikely that appreciable oxide formation will happen at the steel anode to be disruptive to the test.
3. Filling holes are provided in both the cells to enable complete filling of both the cells with the NaCl solution. This was found to be the most important modification. Mukadam (2014) found significant differences between the results of the two test rigs, the new rig giving a higher conductivity. Otieno & Alexander (2015) demonstrated that the differences mainly occurred due to the incomplete filling of the anodic chamber in the old rig and recommended that filling holes be drilled in the old rig to avoid such differences (compare Figure B.15 and Figure B.16). The new CCI test rig results in systematically different results from the original test rig.

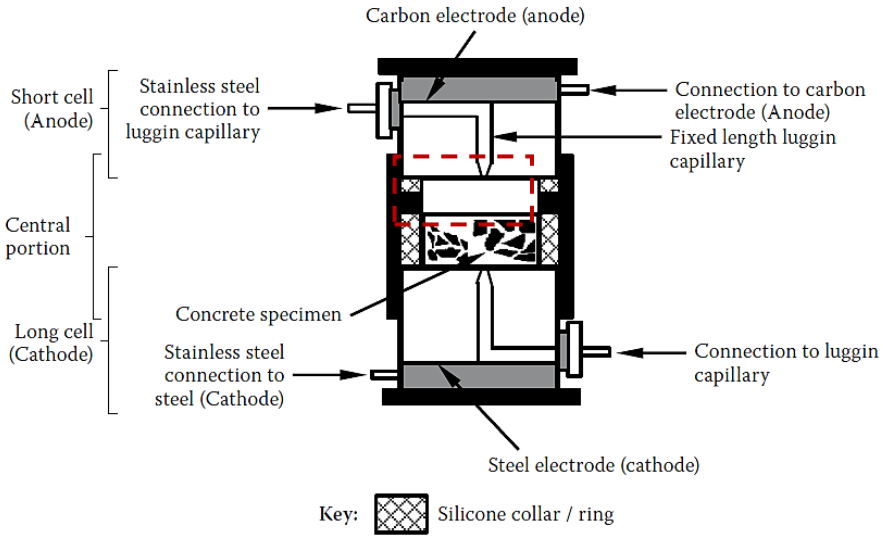

Figure B.15. Cross-section of the old CCI rig (reproduced from (Otieno & Alexander, 2015))

In another study, Otieno (2018) investigated the influence of varying the test parameters, namely, solution concentration (3-5 M), test duration (10-120 s), and capillary voltage (7-15 V) on concretes containing different binders and w/b ratios to evaluate if the test is robust for different concrete types. Looking at the reported results closely, it was found that the effect of test duration and capillary voltage on the measured CCI was minimal for most of the concretes. The concretes that deviated from this trend also had large variability in their results. Generally, fly ash concretes showed larger variability than PC and Corex slag concretes. The effect of changing the concentration seems to manifest itself in the expected way, i.e., reducing the NaCl concentration generally reduces the CCI. The concentration was reduced from 4.4 M to 2.8 M (the concentrations were calculated as moles/L(water) in the paper, but reported as 5 M and 3 M, which are here converted to M (moles/L(solution))) and the consequent reduction in CCI was generally 10-15%. Such a change in concentration can have a significant effect on CCI values. However, it needs to

be pointed out that the change in concentration is quite large and is not expected in a proper lab environment.

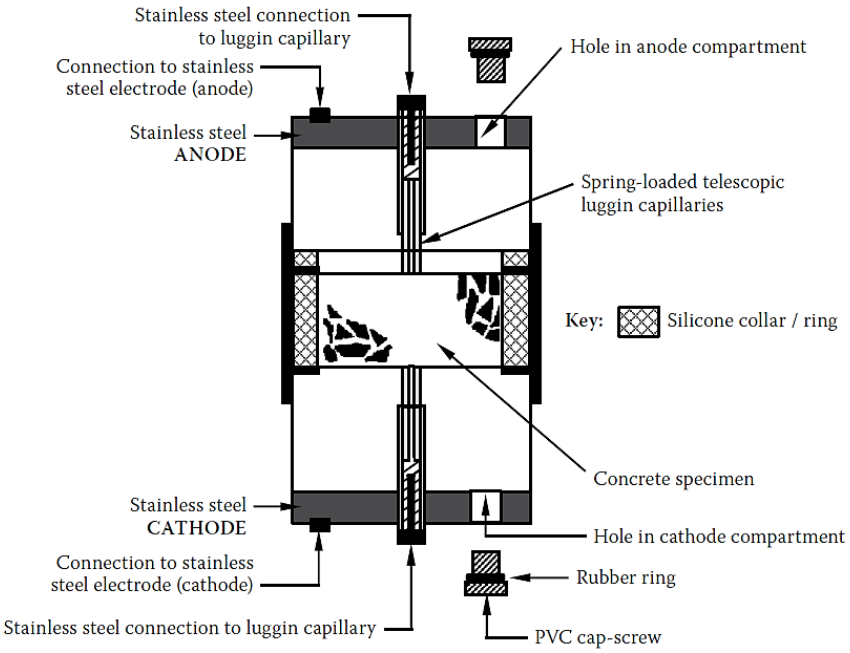

Figure B.16. Cross-section of the current CCI rig (reproduced from (Otieno & Alexander, 2015))

The concentration of NaCl solution also saw a revision from 5 M to 5 m (molality) around the time of the adoption of the SANS standard. The new concentration corresponds to 4.4 M. This revision happened possibly in an attempt to clarify the test method. It is understandably easier to follow instructions on how much salt to add to 1 L of water to make the solution than how much salt to add to make 1 L of the solution. Instead of mixing 5 moles per L of the solution, it is now 5 moles per L of water. In Streicher's ruggedness test, the influence of changing the concentration from 5 M to 4.5 M was found to be statistically insignificant for PC concrete. However, this is also a systematic change, which means that CCI results now may be different from Streicher's time in one more way. The timeline of the important developments in chloride testing at UCT is summarised in Table B.3.

Table B.3. The timeline of the developments in the UCT chloride testing

Year	*Development*
1995	Test method developed (Streicher & Alexander, 1995)
1995	UCT chloride model (Mackechnie, 1996)
1997	CC method - standardisation (Streicher, 1999)
1999	The first modification to the CCI rig
2001	Site repeatability testing (Gouws, Alexander & Maritz, 2001)
2006	Round-robin test (Stanish, Alexander & Ballim, 2006)
2008	Design approach (Muigai, 2008)
2014	New rig adopted
2015	Adoption of the SANS test method (SANS 3001-CO3-3, 2015)

1.2 Conclusions

1. The ideal laws relating ionic diffusivity and conductivity produce deviations in real conditions. Methods based on such theoretical considerations may be considered theoretically sound but should not be expected to yield completely accurate results in real conditions.
2. Most chloride tests must consider a basis in theory to be extendable to different situations. Practical considerations however are also crucial and often dictate the design of the method.
3. Migration tests are preferred over diffusion tests when efficiency is critical as in quality control. CCI and resistivity methods stand out in this regard. Additionally, the surface resistivity method offers the possibility of non-destructive testing.
4. Most migration tests, including the most carefully designed, have similar variability in results (15%/25%), except for bulk and surface resistivity methods. However, the accuracy of resistivity methods can be severely affected by factors such as the saturation level.
5. The chloride conductivity test has undergone revisions in design since the UCT chloride model was first developed. These must be updated in line with the current CCI procedures/setup.

Appendix C. XRD results

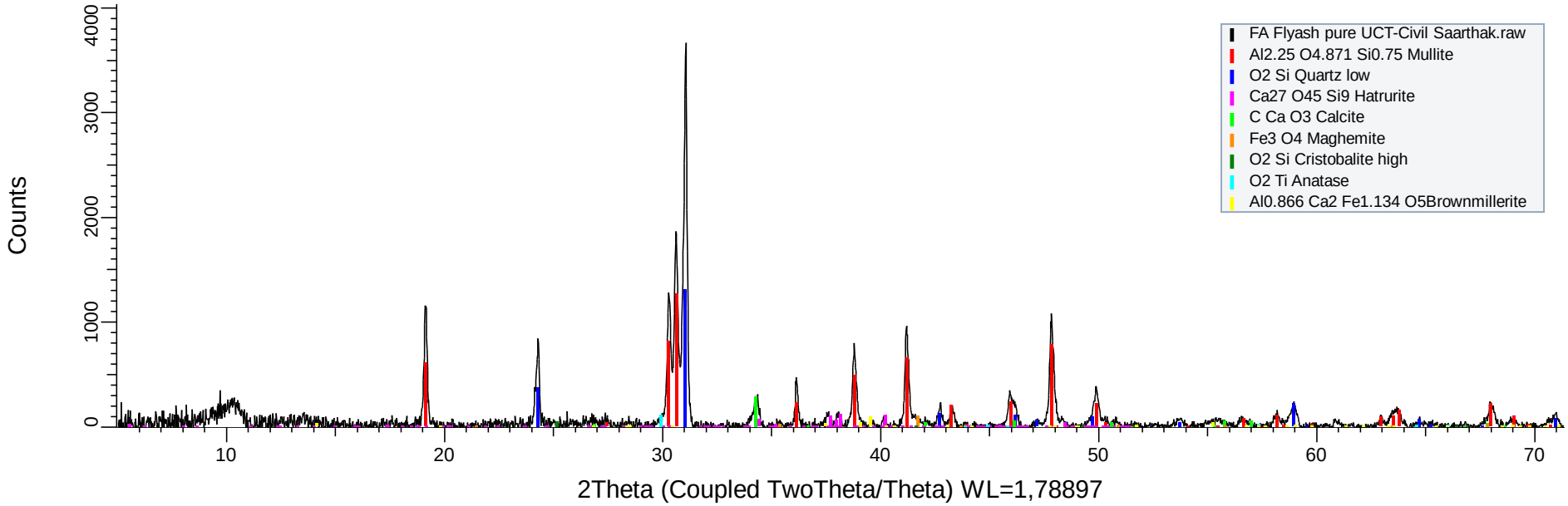

Figure C.1 XRD results for fly ash without background

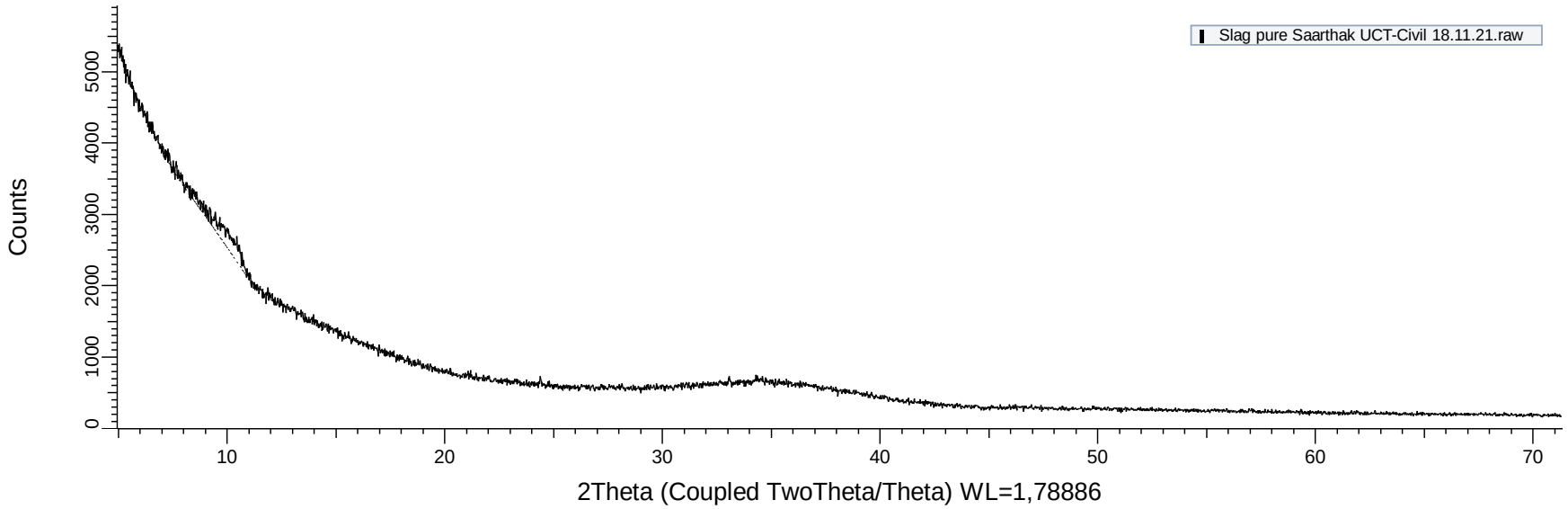

Figure C.2 XRD results for blast-furnace slag with background

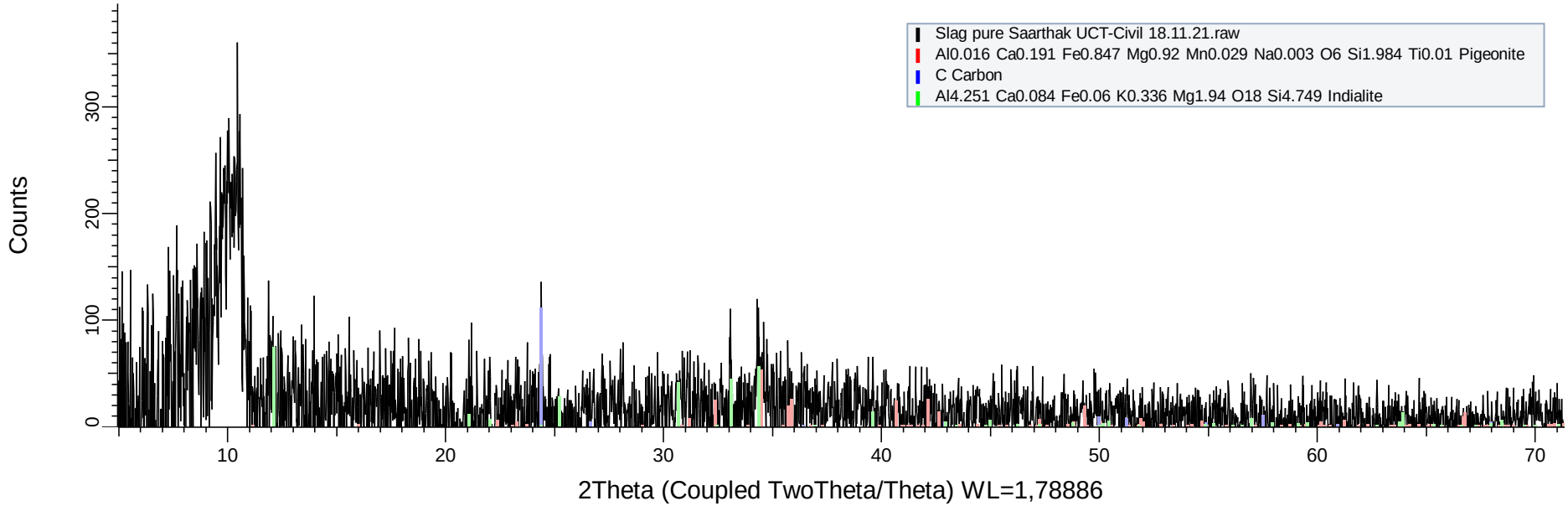

Figure C.3 XRD results for blast-furnace slag without background

Appendix D. Cell constant correction factor for resistivity measurements

It has been shown that the surface resistivity measured on small specimens differs from the true resistivity (Morris, Moreno & Sagüés, 1996). This is because the small volume of the specimens does not fulfil the assumption of semi-infinite volume involved in the derivation of the cell constant, $2\pi a$, used to convert the surface resistivity to true resistivity. Hence, a correction factor is needed.

As described earlier, the surface resistivity measurements were performed on 150-mm cube specimens in this study. The uniaxial resistivity measurements were performed on the same 150-mm cube specimens, and also on smaller cylindrical disc specimens of diameter 70 mm and thickness 30 mm extracted from the cubes. The RILEM TC 154-EMC recommendations (Polder et al., 2001) were followed to measure uniaxial resistivity.

Uniaxial resistivity (UR) was performed using the 2-electrode setup, which consists of two steel metal plates encased in an acrylic housing and clamped tightly on either side of the specimen (see Figure 3.8). A thin (about 2 mm thick) layer of paper towels soaked with lime water (which is a conductive solution) was inserted between the electrodes and the concrete surface to ensure proper electrical contact. The setup was then connected to the Wenner probe, and the results obtained were corrected for the difference in the cell constants between the SR and UR arrangements.

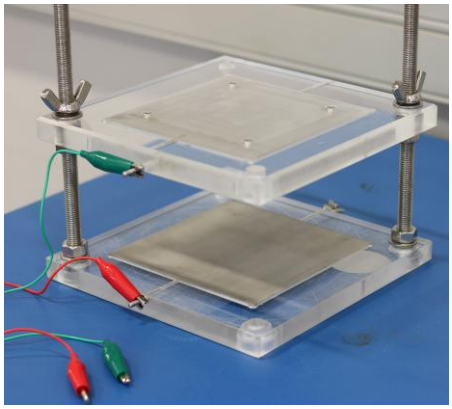

Figure 3.8: Two electrode setup for measuring uniaxial resistivity

The disc specimens were extracted and preconditioned following the protocol used for the durability indicator specimens, i.e., they were extracted from the cover zone (5-35 mm) and oven-dried at 50°C for 7 days. In addition, these specimens were vacuum-saturated with lime water before testing. The results depicting the relationship of surface resistivity with the uniaxial resistivities of 150-mm cubes and 30-mm discs are presented in the figure below (Figure D.2).

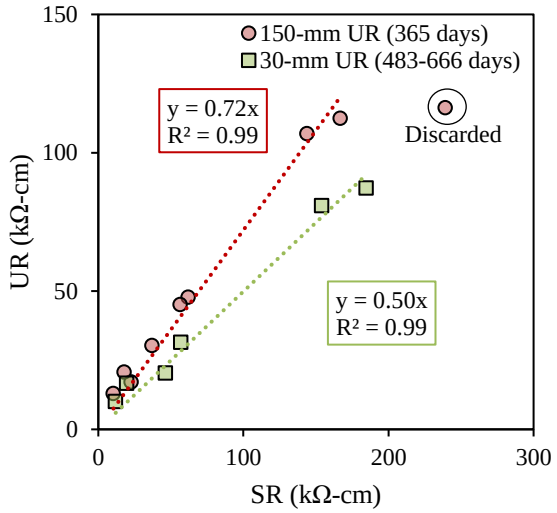

Figure D.2 Relationships between surface resistivity (probe spacing, a = 50 mm) with uniaxial resistivity measured on 150-mm cube and 70-mm ϕ, 30-mm thick cylindrical disc specimen (oven-dried and vacuum-saturated with lime water) for various concrete mixes, with the intercept set at zero. The UR of cubes is an average of a total 6-12 readings on 2-3 specimens, while the UR of discs is an average of a total of 2 readings on 2 specimens.

A general linear relationship relating the surface resistivity with the uniaxial resistivity was found independent of mix proportions and age as expected but with a few exceptions. The uniaxial resistivities measured on cube and disc specimens were found to be different. The bulk resistivity of the disc specimens was on average 33% lower than the cube specimens. Possible reasons include the following, but may not be limited to these:

1. Even though the cube specimens were immersed for 365 days in water, the pore saturation levels may have been less than 100%, increasing the apparent resistivity of the specimen.
2. The disc specimens were extracted from the outer regions of the cubes and would have undergone more leaching-induced pore structural changes than the bulk of the specimens, which may have increased their penetrability.
3. Drying at 50 °C for 7 days would have induced some micro-structural damage in the form of micro-cracking, which may have increased the penetrability and decreased the resistivity of concrete.
4. The use of lime water for saturating disc specimens may have contributed to the increased conductivity of the specimens.

The cell constant correction factor or the geometry factor for surface resistivity measurements was generally found to be 0.72 for the 150-mm cubes and 0.5 for the discs. A few exceptions (PC, BS (75%)) were found to these typical values (Figure D.3), the reasons for which are unclear. In a previous study, the geometry factor was found to be independent of the mix properties, although the observed values varied up to approximately 25% from the mean (Ghosh & Tran, 2015). In comparison, besides the obvious exceptions, values in the present study varied up to 12% from the mean.

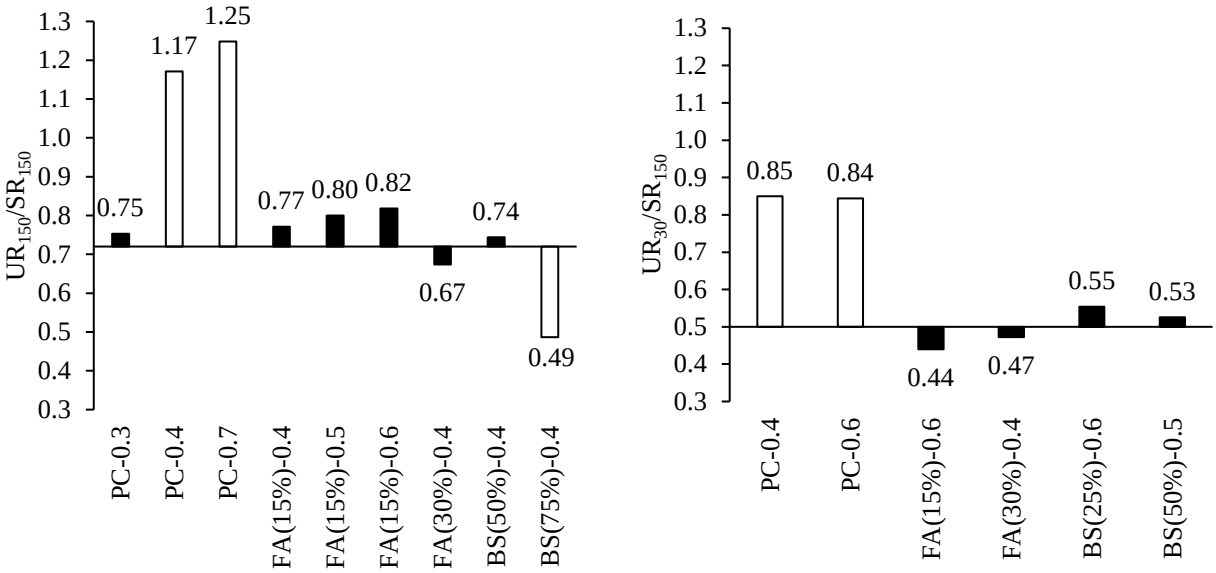

(a) UR on 150-mm cube

(b) UR on 30-mm disc

Figure D.3 Cell constant correction factor (UR/SR): (a) 150-mm cube: average value was found to be 0.72 and (b) case 2: 30-mm disc: average value was found to be 0.5. The average values were calculated disregarding mixes showing large deviations (statistical outliers at a 5% significance level) from the more typical range observed.

The theoretical geometry factors have been presented in a previous study as a function of the specimen height, breadth, and edge distance relative to the probe spacing, i.e., h/a, b/a, and x/a, respectively (Gowers & Millard, 1999). For a 150-mm cube, the geometry factor can be calculated with h/a=3, b/a=3, x/a=1.5 in the range 0.9-0.76. The SR measurements were conducted diagonally; however, the edge distance factor was calculated considering the probe to be aligned parallel to the edges due to the unavailability of theoretical values for diagonal arrangement. However, another study found that both diagonal and parallel arrangements gave essentially the same SR values (Sengul & Gjørv, 2009). Assuming the findings apply to the present case, the measured average value of 0.72 appears to be close to the theoretical range. Further studies, on concrete specimens or on conductive solutions, should be undertaken to validate or calibrate the presented geometry factors and investigate the possible causes for the exceptions/anomalies observed in this study.

Appendix E. Compressive strength results

28-day compressive strength	Wet cured			Plastic cured		
	Av.	SD	COV	Av.	SD	COV
PC 0.3	83.4	5.8	7.0	77.0	3.0	3.9
PC 0.4	65.2	0.9	1.4	58.4	1.0	1.8
PC 0.5	61.0	0.6	0.9	52.3	0.2	0.3
PC 0.6	44.6	1.6	3.6	37.0	2.8	7.5
PC 0.7	33.6	0.5	1.6	29.1	1.3	4.5
FA (15) 0.4	62.8	0.9	1.5	58.7	1.7	2.9
FA (15) 0.5	56.0	5.5	9.7	44.8	0.7	1.6
FA (15) 0.6	37.3	0.8	2.2	33.0	0.4	1.2
FA (30) 0.4	61.0	1.1	1.9	52.3	1.4	2.7
FA (30) 0.5	41.3	0.1	0.2	37.8	1.5	4.0
FA (30) 0.6	32.5	2.4	7.5	28.0	0.4	1.3
BS (25) 0.4	73.2	1.8	2.8	64.5	3.6	5.6
BS (25) 0.5	55.9	2.0	3.5	49.4	1.1	2.2
BS (25) 0.6	45.5	0.2	0.4	41.1	2.0	4.7
BS (50) 0.4	60.4	1.9	3.1	52.8	2.9	5.5
BS (50) 0.5	48.8	0.4	0.9	45.7	2.1	4.6
BS (50) 0.6	33.9	2.5	7.2	32.0	0.1	0.3
BS (75) 0.4	39.4	0.6	1.5	34.8	1.4	4.0

Appendix F. Chloride conductivity results

F.1 Wet cured

28-day CCI	1	2	3	4	Mean	SD	COV
PC-0.3	0.30	0.33	0.31	0.37	0.33	0.03	9.4
PC-0.4	0.59	0.53	0.52	0.49	0.53	0.04	8.3
PC-0.5	0.81	0.96	0.65	0.75	0.79	0.13	16.4
PC-0.6	1.6	1.9	1.8	1.9	1.77	0.14	8.1
PC-0.7	1.4	1.7	1.4	1.5	1.51	0.18	11.7
FA (15)-0.4	0.79	0.81	0.69	0.73	0.76	0.06	7.3
FA (15)-0.5	0.81	0.60	0.88	0.66	0.74	0.13	17.6
FA (15)-0.6	1.17	1.24	1.22	1.20	1.21	0.03	2.4
FA (30)-0.4	0.32	0.34	0.35	0.34	0.34	0.02	4.7
FA (30)-0.5	1.2	1.3	1.1	1.4	1.26	0.14	11.0
FA (30)-0.6	1.4	1.6	1.6	1.4	1.50	0.11	7.5
BS (25)-0.4	0.18	0.20	0.17	0.20	0.19	0.02	8.2
BS (25)-0.5	0.28	0.28	0.30	0.29	0.29	0.01	3.1
BS (25)-0.6	0.65	0.53	0.61	0.57	0.59	0.05	8.9
BS (50)-0.4	0.11	0.17	0.17	0.18	0.17	0.01	2.9
BS (50)-0.5	0.16	0.15	0.16	0.18	0.16	0.01	8.3
BS (50)-0.6	0.46	0.40	0.40	0.46	0.43	0.03	8.0
BS (75)-0.4	0.19	0.20	0.21	0.20	0.20	0.01	4.6

28-day Porosity (CCI)	1	2	3	4	Mean	SD	COV
PC-0.3	5.1	5.4	4.8	5.2	5.1	0.03	4.6
PC-0.4	7.3	5.8	6.4	5.9	6.4	0.04	10.9
PC-0.5	6.9	6.9	6.4	7.1	6.8	0.13	4.5
PC-0.6	8.9	8.9	9.1	8.6	8.9	0.14	2.3
PC-0.7	8.3	9.4	8.1	8.7	8.6	0.18	6.7
FA (15)-0.4	6.7	6.4	6.2	6.9	6.6	0.06	4.9
FA (15)-0.5	7.0	6.4	8.0	7.5	7.2	0.13	9.5
FA (15)-0.6	8.1	8.3	8.4	8.0	8.2	0.03	2.4
FA (30)-0.4	6.3	6.1	6.3	5.9	6.2	0.02	3.1
FA (30)-0.5	8.3	8.3	8.7	8.7	8.5	0.14	2.8
FA (30)-0.6	8.9	9.4	8.7	8.8	9.0	0.11	3.5
BS (25)-0.4	3.6	4.1	3.6	3.8	3.8	0.02	6.1
BS (25)-0.5	5.2	5.2	5.4	5.8	5.4	0.01	5.2
BS (25)-0.6	6.1	6.4	7.0	5.7	6.3	0.05	8.8
BS (50)-0.4	3.5	3.8	3.6	4.3	3.8	0.03	9.3
BS (50)-0.5	4.7	4.4	4.5	4.6	4.6	0.01	2.6
BS (50)-0.6	6.1	5.8			5.9	0.24	4.0
BS (75)-0.4	4.4	4.7	5.2	5.2	4.9	0.01	8.1

90-day CCI	1	2	3	4	Mean	SD	COV
PC-0.3	0.20	0.25	0.20	0.21	0.22	0.02	11.0
PC-0.4	0.39	0.29	0.38	0.33	0.35	0.04	13.0
PC-0.5	0.6	0.78	0.52	0.54	0.54	0.0	4.6
PC-0.6	1.4	1.0	1.3	1.3	1.2	0.1	10.9
PC-0.7	1.2	1.1	1.1	1.0	1.1	0.1	5.4
FA (15)-0.4	0.22	0.24	0.23	0.18	0.22	0.02	11.2
FA (15)-0.5	0.28	0.24	0.57	0.52	0.40	0.17	42.0
FA (15)-0.6	0.62	0.55	0.72	0.63	0.63	0.07	11.1
FA (30)-0.4	0.20	0.22	0.22	0.18	0.21	0.02	8.9
FA (30)-0.5	0.4	0.3	0.4	0.3	0.4	0.0	6.5
FA (30)-0.6	0.8	0.6	0.6	0.7	0.7	0.1	13.5
BS (25)-0.4	0.10	0.12	0.13	0.12	0.12	0.01	9.4
BS (25)-0.5	0.16	0.19	0.15	0.18	0.17	0.02	10.0
BS (25)-0.6	0.24	0.24	0.23	0.23	0.23	0.00	1.5
BS (50)-0.4	0.11	0.10	0.11	0.13	0.11	0.01	11.9
BS (50)-0.5	0.40	0.48	0.43		0.44	0.04	9.5
BS (50)-0.6	0.35	0.25	0.40	0.23	0.31	0.08	26.5
BS (75)-0.4	0.12	0.13	0.15	0.15	0.14	0.01	10.6

90-day Porosity (CCI)	1	2	3	4	Mean	SD	COV
PC-0.3	4.3	4.4	4.0	4.3	4.2	0.02	4.2
PC-0.4	5.6	5.1	5.6	5.4	5.4	0.04	4.1
PC-0.5	5.9	6.2	6.1	6.4	6.2	0.12	3.6
PC-0.6	8.4	7.4	7.8	7.5	7.8	0.13	5.8
PC-0.7	8.9	8.9	9.2	8.9	9.0	0.06	1.5
FA (15)-0.4	5.0	5.1	4.7	5.3	5.0	0.02	4.9
FA (15)-0.5	5.3	5.4	6.7	6.7	6.0	0.17	13.2
FA (15)-0.6	8.6	7.4	8.4	8.3	8.2	0.07	6.1
FA (30)-0.4	4.3	3.9	4.9	4.1	4.3	0.02	9.6
FA (30)-0.5	5.9	5.1	6.2	6.0	5.8	0.02	8.4
FA (30)-0.6	8.0	7.4	7.1	7.6	7.5	0.09	5.0
BS (25)-0.4	3.0	3.0	3.4	3.0	3.1	0.01	6.2
BS (25)-0.5	4.2	4.5	4.1	4.3	4.3	0.02	3.4
BS (25)-0.6	5.2	5.1	5.7	5.5	5.4	0.00	4.8
BS (50)-0.4	3.0	3.0	3.4	3.0	3.1	0.01	6.2
BS (50)-0.5	3.5	3.3	3.1	3.4	3.4	0.19	5.7
BS (50)-0.6	4.9	4.2	4.2	4.5	4.5	0.08	7.0
BS (75)-0.4	4.4	4.6	4.5	4.6	4.5	0.01	1.8

250-day CCI	1	2	3	4	Mean	SD	COV
PC-0.3	0.21	0.22	0.21	0.24	0.22	0.02	7.02
PC-0.4	0.20	0.26	0.23	0.26	0.24	0.03	12.36
PC-0.7	1.40	1.31			1.4	0.1	4.71
FA (15)-0.4	0.17	0.20			0.2	0.03	13.95
FA (15)-0.5	0.20	0.17			0.19	0.02	10.64
FA (15)-0.6	0.35	0.31	0.33	0.34	0.33	0.02	5.70
FA (30)-0.4	0.30	0.33	0.36	0.34	0.33	0.02	7.01
BS (50)-0.4	0.08	0.08	0.08	0.15	0.08	0.00	0.04
BS (75)-0.4	0.12	0.13	0.12	0.12	0.12	0.01	5.04

250-day Porosity (CCI)	1	2	3	4	Mean	SD	COV
PC-0.3	3.2	3.7	3.7	3.5	3.5	0.0	6.7
PC-0.4	3.9	4.5	4.2	4.5	4.3	0.0	7.0
PC-0.7	9.5	9.4			9.5	0.1	1.3
FA (15)-0.4	3.7	4.3			4.0	0.4	9.8
FA (15)-0.5	3.9	3.8			3.8	0.1	2.3
FA (15)-0.6	6.4	5.5	6.2	6.1	6.1	0.0	6.3
FA (30)-0.4	3.2	3.0	3.2	3.3	3.2	0.0	3.5
BS (50)-0.4	2.5	2.6	2.8	2.8	2.7	0.0	4.3
BS (75)-0.4	4.4	4.9	3.9	4.3	4.4	0.0	9.6

365-day CCI	1	2	3	4	Mean	SD	COV
BS (25)-0.6	0.19	0.20	0.18	0.20	0.19	0.01	6.01

365-day Porosity (CCI)	1	2	3	4	Mean	SD	COV
BS (25)-0.6	4.0	4.0	3.5	4.0	3.9	0.0	6.6

460-day CCI	1	2	3	4	Mean	SD	COV
PC-0.6	0.9	0.8	1.0	1.0	0.9	0.1	10.8
FA (30)-0.6	0.08	0.08	0.11	0.11	0.1	0.0	17.7
BS (50)-0.6	0.11	0.10	0.11	0.16	0.11	0.00	1.95

460-day Porosity (CCI)	1	2	3	4	Mean	SD	COV
PC-0.6	8.9	8.3	8.2	8.1	8.4	0.1	4.4
FA (30)-0.6	2.9	3.1	3.1	3.1	3.0	0.0	3.9
BS (50)-0.6	3.8	3.7	3.6	3.4	3.6	0.0	4.1

F.2 Plastic cured

28-day CCI	1	2	3	4	Mean	SD	COV
PC-0.3	0.31	0.34	0.34	0.37	0.34	0.03	7.9
PC-0.4	0.65	0.60	0.63	0.62	0.62	0.02	3.1
PC-0.5	0.90	0.82	0.99	0.90	0.90	0.07	7.7
PC-0.6	1.7	1.8	2.2	1.9	1.9	0.2	10.5
PC-0.7	2.0	1.8	1.7	1.8	1.8	0.1	7.1
FA (15)-0.4	0.86	1.07	0.90	1.01	0.96	0.10	10.1
FA (15)-0.5	0.98	0.89	0.98	1.02	0.97	0.05	5.5
FA (15)-0.6	2.00	1.85	1.77	1.84	1.86	0.09	5.0
FA (30)-0.4	1.02	0.80	0.85	1.03	0.93	0.12	12.5
FA (30)-0.5	1.5	1.3	1.7	1.3	1.4	0.2	12.7
FA (30)-0.6	2.2	2.1	2.0	2.2	2.1	0.1	5.1
BS (25)-0.4	0.32	0.30	0.33	0.43	0.34	0.06	16.4
BS (25)-0.5	0.58	0.60	0.65	0.62	0.61	0.03	4.6
BS (25)-0.6	0.67	0.82	0.69	0.85	0.76	0.09	11.4
BS (50)-0.4	0.24	0.21	0.27	0.24	0.24	0.03	10.9
BS (50)-0.5	0.23	0.23	0.27	0.24	0.24	0.02	7.6
BS (50)-0.6	0.96	0.76	0.75	0.82	0.82	0.09	11.6
BS (75)-0.4	0.27	0.32	0.31	0.29	0.30	0.02	7.3

28-day Porosity (CCI)	1	2	3	4	Mean	SD	COV
PC-0.3	5.4	6.0	5.7	5.7	5.7	0.0	4.4
PC-0.4	7.1	7.1	7.3	7.3	7.2	0.0	1.8
PC-0.5	8.2	7.5	7.9	7.5	7.8	0.1	4.7
PC-0.6	9.1	9.9	9.6	9.3	9.5	0.2	3.8
PC-0.7	9.4	8.9	8.6	8.7	8.9	0.1	3.9
FA (15)-0.4	7.6	8.3	6.3	7.2	7.3	0.1	11.0
FA (15)-0.5	7.9	7.9	7.7	7.3	7.7	0.1	3.5
FA (15)-0.6	9.6	9.5	9.1	8.8	9.3	0.1	3.9
FA (30)-0.4	9.1	8.2	8.2	8.0	8.4	0.1	5.5
FA (30)-0.5	8.6	8.8	9.5	8.7	8.9	0.2	5.0
FA (30)-0.6	9.7	9.9	9.1	9.2	9.5	0.1	4.1
BS (25)-0.4	5.9	6.0	6.4	6.1	6.1	0.1	3.4
BS (25)-0.5	7.5	7.9	7.4	7.9	7.7	0.0	3.6
BS (25)-0.6	8.1	8.4	8.0	8.8	8.3	0.1	4.3
BS (50)-0.4	6.0	5.9	6.5	5.9	6.1	0.0	4.7
BS (50)-0.5	6.7	6.3	8.0	7.3	7.1	0.0	10.4
BS (50)-0.6	8.7	7.0			7.9	1.2	15.1
BS (75)-0.4	6.6	7.4	7.3	6.8	7.0	0.0	5.4

90-day CCI	1	2	3	4	Mean	SD	COV
PC-0.3	0.29	0.33	0.30	0.33	0.31	0.02	7.0
PC-0.4	0.55	0.56	0.67	0.73	0.63	0.09	13.8
PC-0.5	0.85	1.00	0.99	1.11	0.99	0.11	10.7
PC-0.6	2.0	1.8	2.2	1.7	1.9	0.2	12.5
PC-0.7	1.5	1.5	1.8	1.5	1.6	0.1	8.4
FA (15)-0.4	0.58	0.68	0.67	0.61	0.64	0.05	7.9
FA (15)-0.5	1.12	0.93	0.85	1.06	0.99	0.12	12.6
FA (15)-0.6	1.30	1.06	1.01	1.18	1.14	0.13	11.4
FA (30)-0.4	0.84	0.79	0.65	0.68	0.74	0.09	12.1
FA (30)-0.5	1.2	1.3	1.5	1.3	1.3	0.1	9.7
FA (30)-0.6	1.6	1.5	1.6	1.8	1.6	0.1	8.5
BS (25)-0.4	0.22	0.21	0.23	0.21	0.22	0.01	3.9
BS (25)-0.5	0.50	0.47	0.55	0.50	0.51	0.03	6.2
BS (25)-0.6	0.56	0.63	0.56	0.57	0.58	0.03	5.6
BS (50)-0.4	0.29	0.30	0.36	0.27	0.30	0.04	12.6
BS (50)-0.5	0.36	0.42	0.49	0.49	0.44	0.06	14.3
BS (50)-0.6	0.56	0.74	0.49	0.66	0.61	0.11	17.3
BS (75)-0.4	0.20	0.22	0.21	0.22	0.21	0.01	4.8

90-day Porosity (CCI)	1	2	3	4	Mean	SD	COV
PC-0.3	5.6	6.3	5.9	6.6	6.1	0.02	7.2
PC-0.4	6.9	6.3	7.6	8.2	7.3	0.09	11.7
PC-0.5	7.3	7.5	7.4	7.9	7.5	0.11	3.3
PC-0.6	10.5	10.2	11.3	9.6	10.4	0.24	6.8
PC-0.7	9.5	9.4	10.3	9.3	9.6	0.13	4.9
FA (15)-0.4	7.4	8.3	8.0	7.5	7.8	0.05	5.6
FA (15)-0.5	7.6	7.9	7.8	7.7	7.7	0.12	1.7
FA (15)-0.6	10.2	9.1	8.7	9.6	9.4	0.13	7.0
FA (30)-0.4	7.8	8.3	7.6	7.0	7.7	0.09	7.4
FA (30)-0.5	8.0	8.9	8.9	8.9	8.7	0.13	5.1
FA (30)-0.6	9.1	8.5	9.3	9.9	9.2	0.14	6.3
BS (25)-0.4	5.1	5.2	5.2	5.5	5.2	0.01	3.2
BS (25)-0.5	8.0	8.0	8.3	7.8	8.0	0.03	2.6
BS (25)-0.6	8.0	8.4	7.9	8.2	8.1	0.03	3.0
BS (50)-0.4	6.1	6.4	6.9	6.0	6.4	0.04	6.3
BS (50)-0.5	6.1	6.0	6.8	6.0	6.2	0.06	6.4
BS (50)-0.6	8.7	8.9	8.7	8.3	8.7	0.11	2.7
BS (75)-0.4	7.0	6.4	6.8	6.9	6.8	0.01	3.6

250-day CCI	1	2	3	4	Mean	SD	COV
PC-0.3	0.33	0.34	0.32	0.29	0.32	0.02	6.4
PC-0.4	0.67	0.60	0.58	0.64	0.62	0.04	6.8
FA (15)-0.4	0.93	0.74	0.77	0.98	0.85	0.12	13.5
FA (15)-0.5	1.26	1.01	1.02	1.39	1.17	0.19	16.3
FA (15)-0.6	1.55	1.64	1.57	1.87	1.66	0.15	8.8
FA (30)-0.4	1.06	1.01	0.88	1.67	1.16	0.35	30.5
BS (50)-0.4	0.21	0.26	0.41	0.25	0.24	0.03	10.9
BS (75)-0.4	0.23	0.19	0.29	0.21	0.23	0.04	18.5

250-day Porosity (CCI)	1	2	3	4	Mean	SD	COV
PC-0.3	5.8	6.4	5.8	5.6	5.9	0.02	5.9
PC-0.4	7.2	6.7	6.5	7.3	6.9	0.04	5.7
FA (15)-0.4	7.8	7.0	6.6	7.4	7.2	0.12	7.5
FA (15)-0.5	8.2	8.3	7.9	8.4	8.2	0.19	2.4
FA (15)-0.6	8.6	9.1	9.0	10.0	9.2	0.15	6.4
FA (30)-0.4	8.1	8.4	7.9		8.1	0.24	3.0
BS (50)-0.4	6.3	6.7	6.2	6.4	6.4	0.09	3.6
BS (75)-0.4	7.8	7.0	7.6	7.3	7.4	0.04	4.8

365-day CCI	1	2	3	4	Mean	SD	COV
BS (25)-0.4	0.40	0.33	0.38	0.35	0.37	0.03	8.6
BS (25)-0.6	0.62	0.62	0.60	0.69	0.63	0.04	6.0

365-day Porosity (CCI)	1	2	3	4	Mean	SD	COV
BS (25)-0.4	6.2	6.7	6.6	6.4	6.5	0.03	3.7
BS (25)-0.6	8.4	8.2	8.1	8.4	8.3	0.04	2.0

460-day CCI	1	2	3	4	Mean	SD	COV
PC-0.6	1.8	1.9	1.7	1.7	1.8	0.1	5.0
FA (30)-0.6	1.5	1.8	1.8	1.5	1.6	0.2	9.5
BS (50)-0.6	0.41	0.42	0.34	0.33	0.37	0.05	12.2

460-day Porosity (CCI)	1	2	3	4	Mean	SD	COV
PC-0.6	9.2	9.4	9.2	9.8	9.4	0.1	2.9
FA (30)-0.6	8.9	8.9	9.1	8.8	8.9	0.2	1.5
BS (50)-0.6	8.7	8.6	7.9	7.6	8.2	0.05	6.6

Appendix G. Surface resistivity results (150 mm cube)

Probe spacing: 50 mm

Wet cured	28 days	90 days	180 days	365 days
PC-0.3	15.0	18.1	22.0	22.7
PC-0.4	11.4	14.6	16.0	17.7
PC-0.5	8.2	10.2	11.3	12.0
PC-0.6	7.0	8.2	9.3	10.6
PC-0.7	7.2	8.9	9.7	10.4
FA (15)-0.4	11.7	23.7	42.5	62.0
FA (15)-0.5	11.2	23.3	41.7	56.4
FA (15)-0.6	7.9	16.6	27.3	37.1
FA (30)-0.4	25.4	59.9	111.1	166.8
FA (30)-0.5	10.6	31.6	68.6	99.4
FA (30)-0.6	9.8	28.7	54.2	97.7
BS (25)-0.4	23.2	38.6	48.9	47.7
BS (25)-0.5	18.6	35.8	43.9	46.9
BS (25)-0.6	18.0	33.7	42.3	46.5
BS (50)-0.4	65.5	100.7	130.6	143.7
BS (50)-0.5	43.8	93.2	126.0	134.1
BS (50)-0.6	40.6	78.8	113.1	129.1
BS (75)-0.4	114.7	175.8	205.7	239.1

Plastic cured	28 days	90 days	180 days	365 days
PC-0.3	15.4	20.7	29.1	30.4
PC-0.4	10.7	13.9	17.9	19.8
PC-0.5	9.7	12.8	15.0	18.7
PC-0.6	8.4	9.5	12.0	15.0
PC-0.7	7.1	9.1	10.8	11.2
FA (15)-0.4	12.4	23.8	41.4	53.3
FA (15)-0.5	12.4	24.2	40.9	54.7
FA (15)-0.6	8.6	16.4	26.3	29.0
FA (30)-0.4	23.5	59.0	114.4	141.6
FA (30)-0.5	11.7	29.3	56.9	103.3
FA (30)-0.6	8.8	22.6	38.5	68.6
BS (25)-0.4	25.3	44.1	65.0	90.7
BS (25)-0.5	20.1	38.0	55.5	65.6
BS (25)-0.6	19.5	36.2	49.7	59.7
BS (50)-0.4	67.8	119.0	162.1	184.2
BS (50)-0.5	51.1	97.6	128.3	166.6
BS (50)-0.6	38.7	78.6	111.1	121.4
BS (75)-0.4	98.9	149.7	182.3	177.0

Appendix H. Typical calibration results for chloride content testing

H.1 Mortar samples for calibration: Plain Portland cement

Mortar Density (kg/m^3)	2320
Cement Content (kg/m^3)	640
Molarity of titrant (M)	0.1
Molar mass of Cl (g)	35.45

Binder	Admixed chlorides	Mass of sample	Volume of titrant consumed	Chloride Content	Chloride Content	Chloride Content (%, by mass of cement)					
	% (by mass of cement)	(g)	(ml)	% (by mass of concrete)	% (by mass of cement)	Average	SD	COV, %	Net	Error	Error (%)
PC	0.0	3.635	0.062	0.0060	0.022	0.02	0.004	20	0.02	-	-
		3.838	0.052	0.0048	0.017						
		3.461	0.07	0.0072	0.026						
	0.5	2.332	0.891	0.1354	0.491	0.49	0.0005	0.09	0.47	-0.03	-6
		2.203	0.843	0.1357	0.492						
		2.225	0.850	0.1354	0.491						
	1.0	2.265	1.746	0.2733	0.991	0.99	0.003	0.29	0.97	-0.03	-3
		2.471	1.894	0.2717	0.985						
		2.352	1.810	0.2728	0.989						
	2.0	2.220	3.446	0.5503	1.995	2.00	0.008	0.40	1.98	-0.02	-1
		2.340	3.635	0.5507	1.996						
		2.152	3.365	0.5543	2.010						
	6.0	2.479	11.371	1.6261	5.895	5.89	0.004	0.06	5.87	-0.13	-2
		2.381	10.914	1.6250	5.891						
		2.284	10.463	1.6240	5.887						

Note: The mass of sample used for testing 0% Cl samples was increased from 2.1-2.5 g to >3 g to bring the chloride content of the test solution above the detection limit and improve the resolution of the test method. “Net” cl content = Av. – zero error.

H.2 Mortar samples for calibration: Fly ash (30%)

Mortar Density (kg/m^3)	2275
Cement Content (kg/m^3)	640
Molarity of titrant (M)	0.1
Molar mass of Cl (g)	35.45

Binder	Admixed chlorides	Mass of sample	Volume of titrant consumed	Chloride Content	Chloride Content	Chloride Content (%, by mass of cement)					
	% (by mass of cement)	(g)	(ml)	% (by mass of concrete)	% (by mass of cement)	Average	SD	COV, %	Net	Error	Error (%)
FA (30%)	0.0	3.240	0.033	0.0036	0.013	0.02	0.003	19	0.02	-	-
		4.990	0.067	0.0048	0.017						
	0.07	2.441	0.123	0.0179	0.065	0.07	0.0004	0.56	0.04	-0.03	-38
		2.357	0.120	0.0180	0.065						
		2.438	0.123	0.0179	0.065						
	0.35	2.405	0.654	0.0964	0.349	0.35	0.003	0.90	0.33	-0.02	-6
		2.293	0.628	0.0971	0.352						
		2.115	0.569	0.0954	0.346						
	1.05	2.199	1.748	0.2818	1.022	1.02	0.001	0.07	1.00	-0.05	-5
		2.447	1.946	0.2819	1.022						
		2.383	1.897	0.2822	1.023						

H.3 Mortar samples for calibration: Blastfurnace slag (50%)

Mortar Density (kg/m^3)	2301
Cement Content (kg/m^3)	640
Molarity of titrant (M)	0.1
Molar mass of Cl (g)	35.45

Binder	Admixed chlorides	Mass of sample	Volume of titrant consumed	Chloride Content	Chloride Content	Chloride Content (%, by mass of cement)					
	% (by mass of cement)	(g)	(ml)	% (by mass of concrete)	% (by mass of cement)	Average	SD	COV, %	Net	Error	Error (%)
BS (50%)	0.0	3.183	0.139	0.0155	0.056	0.05	0.003	5.5	0.05		-
		3.039	0.127	0.0148	0.054						
		3.422	0.134	0.0139	0.050						
	0.075	2.238	0.194	0.0307	0.111	0.11	0.002	1	0.09	0.01	18
		2.257	0.191	0.0300	0.109						
		2.317	0.201	0.0308	0.111						
	0.375	2.155	0.686	0.1128	0.409	0.41	0.001	0.16	0.39	0.01	3
		2.412	0.766	0.1126	0.408						
		2.480	0.790	0.1129	0.409						
	1.5	2.150	2.588	0.4267	1.547	1.54	0.003	0.18	1.52	0.02	1
		2.260	2.711	0.4252	1.542						
		2.395	2.875	0.4255	1.543						

Appendix I. Chloride profile results

I.1 Exposure duration: 180 days

PC-0.3

Bulk diffusion results - Wet cured

1		2		3	
Depth	% Cl	Depth	% Cl	Depth	% Cl
[mm]	[conc.]	[mm]	[conc.]	[mm]	[conc.]
2.6	0.86	1.4	0.89	1.8	0.50
8.2	0.37	6.1	0.50	6.9	0.31
12.5	0.17	10.7	0.25	11.8	0.15
16.8	0.04	15.5	0.05	17.3	0.02
21.1	0.01	20.7	0.01	22.7	0.004
25.7	0.01	25.3	0.004	--	--
30.5	0.01	--	--	--	--

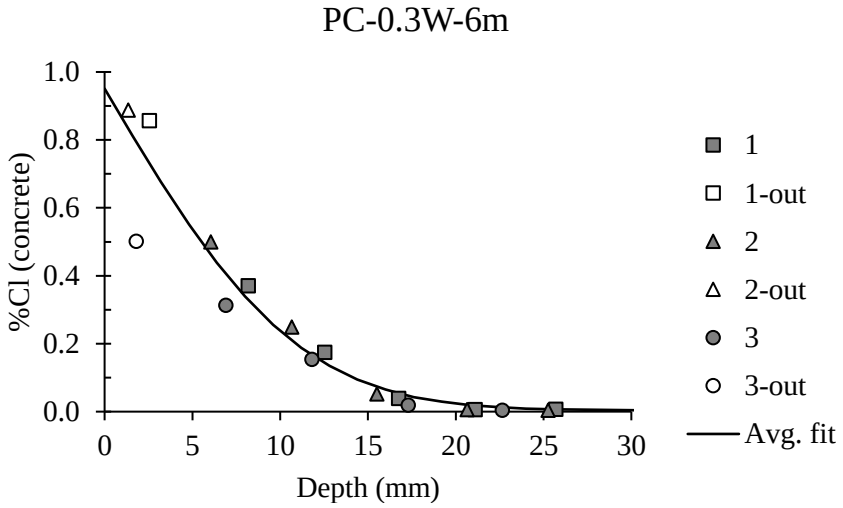

Bulk diffusion results - Plastic cured

1		2		3	
Depth	% Cl	Depth	% Cl	Depth	% Cl
[mm]	[conc.]	[mm]	[conc.]	[mm]	[conc.]
1.6	0.75	2.3	0.92	2.3	0.64
6.4	0.37	7.5	0.37	8.2	0.36
11.1	0.21	12.0	0.21	13.2	0.17
16.3	0.05	17.1	0.05	18.0	0.02
21.3	0.01	22.1	0.01	22.9	0.003
25.7	0.005	26.5	0.004	27.5	0.006

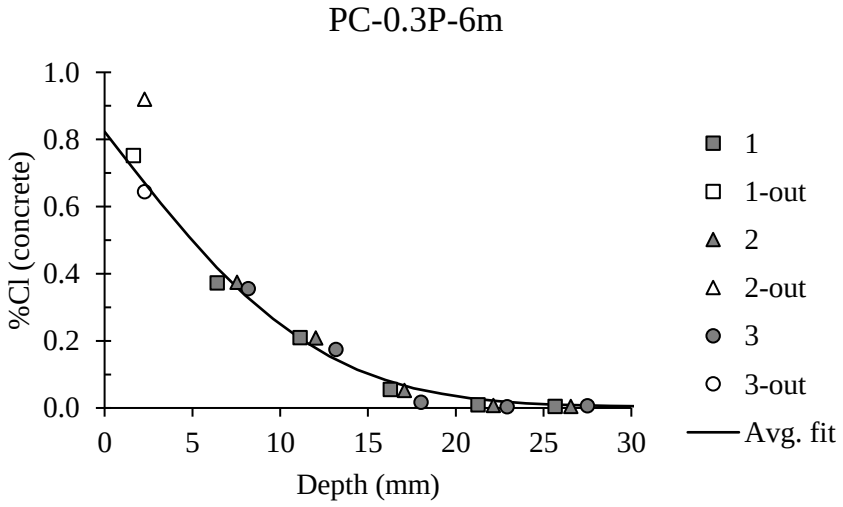

Bulk diffusion results - Wet-dry

1		2		3	
Depth	% Cl	Depth	% Cl	Depth	% Cl
[mm]	[conc.]	[mm]	[conc.]	[mm]	[conc.]
1.5	0.71	1.2	0.71	--	--
6.4	0.38	6.1	0.41	--	--
11.7	0.17	9.8	0.21	--	--
17.1	0.03	14.4	0.06	--	--
22.2	0.01	20.7	0.005	--	--
27.2	0.01	26.3	0.005	--	--

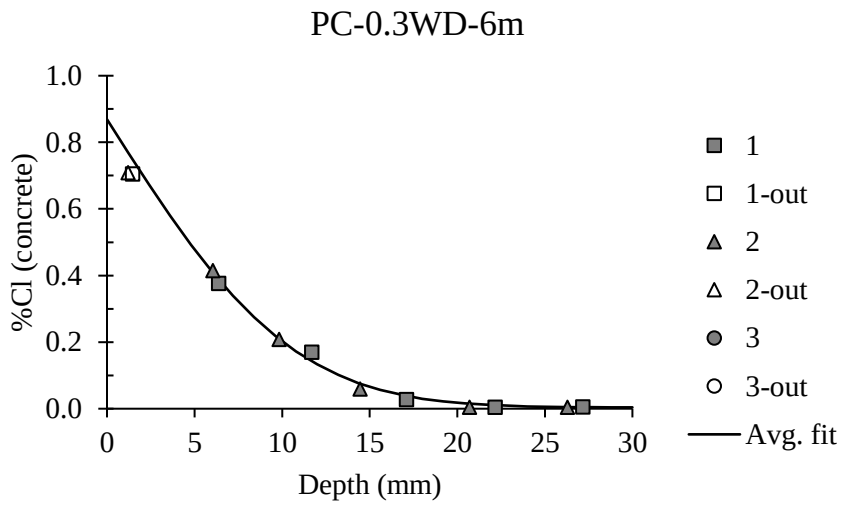

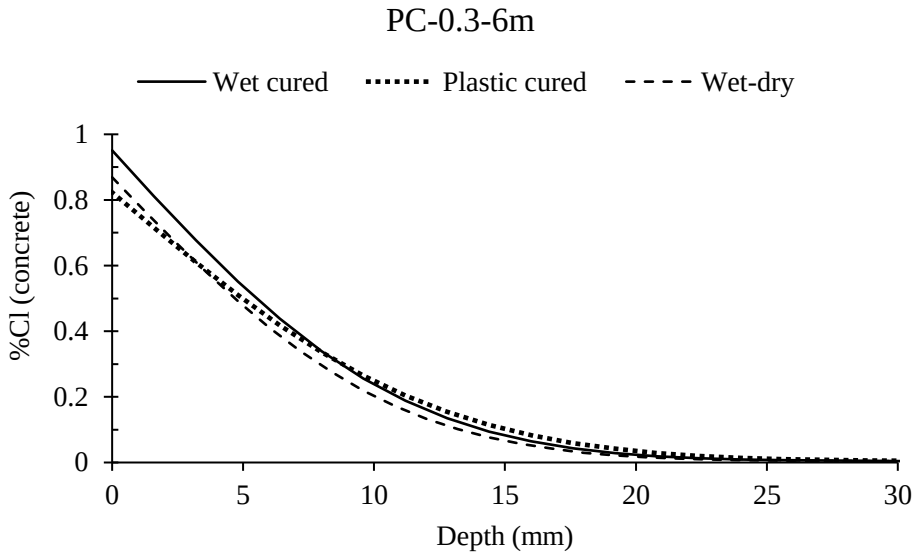

Fitted profiles – overall (PC-0.3)					
Wet cured		**Plastic cured**		**Wet-dry**	
0.0	0.951	0.0	0.823	0.0	0.9
1.6	0.811	1.6	0.715	1.2	0.770
3.2	0.677	3.2	0.610	2.4	0.673
4.8	0.551	4.8	0.510	3.6	0.580
6.4	0.438	6.4	0.418	4.8	0.492
8.0	0.339	8.0	0.336	6.0	0.411
9.6	0.256	9.6	0.265	7.2	0.339
11.2	0.188	11.2	0.204	8.4	0.275
12.8	0.135	12.8	0.154	9.6	0.219
14.4	0.094	14.4	0.114	10.8	0.172
16.0	0.065	16.0	0.083	12.0	0.133
17.6	0.043	17.6	0.059	13.2	0.102
19.2	0.029	19.2	0.042	14.4	0.076
20.8	0.019	20.8	0.029	15.6	0.057
22.4	0.013	22.4	0.020	16.8	0.042
24.0	0.009	24.0	0.014	18.0	0.030
25.6	0.007	25.6	0.010	19.2	0.022
27.2	0.006	27.2	0.008	20.4	0.016
28.8	0.005	28.8	0.006	21.6	0.012
30.4	0.004	30.4	0.005	22.8	0.009
32.0	0.004	32.0	0.005	24.0	0.007
33.6	0.004	33.6	0.004	25.2	0.006
35.2	0.004	35.2	0.004	26.4	0.005
36.8	0.004	36.8	0.004	27.6	0.005
38.4	0.004	38.4	0.004	28.8	0.004
40.0	0.004	40.0	0.004	30.0	0.004
Cl depth (mm)	30		34		29

Initial Cl content= 0.004

Overall fit

Curing	D_a	C_s	r^2
W	2.4E-12	1.0	0.96
P	3.0E-12	0.8	0.98
WD	2.2E-12	0.9	0.99

Individual fit

W	D_a	C_s	r^2
Core 1	2.3E-12	1.1	0.99
Core 2	2.3E-12	1.1	0.99
Core 3	2.5E-12	0.7	0.99
Mean	**2.4E-12**	**1.0**	
SD	1.4E-13	0.21	
CV, %	6	22	

P	D_a	C_s	r^2
Core 1	2.9E-12	0.8	0.99
Core 2	2.9E-12	0.9	0.99
Core 3	2.6E-12	1.0	0.98
Mean	**2.8E-12**	**0.9**	
SD	1.7E-13	0.11	
CV, %	6	13	

WD	D_a	C_s	r^2
Core 1	2.5E-12	0.8	0.99
Core 2	2.0E-12	0.9	1.00
Mean	**2.3E-12**	**0.9**	
SD	4.0E-13	0.10	
CV, %	18	12	

PC-0.4

Bulk diffusion results - Wet cured

1		2		3	
Depth	% Cl	Depth	% Cl	Depth	% Cl
[mm]	[conc.]	[mm]	[conc.]	[mm]	[conc.]
1.4	0.78	1.0	0.76	0.6	0.62
6.1	0.51	5.2	0.44	5.1	0.51
10.3	0.33	9.8	0.34	10.8	0.29
14.8	0.17	14.1	0.20	16.2	0.14
20.3	0.07	18.8	0.09	21.3	0.04
25.4	0.01	24.1	0.01	--	--

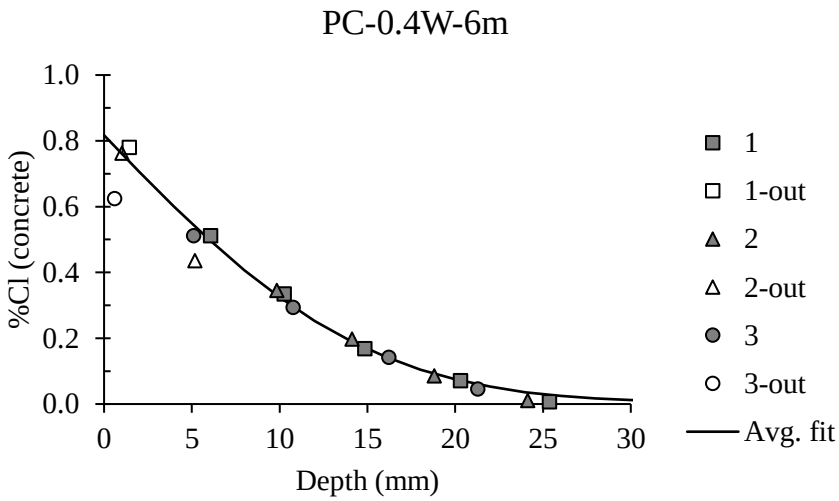

Bulk diffusion results - Plastic cured

1		2		3	
Depth	% Cl	Depth	% Cl	Depth	% Cl
[mm]	[conc.]	[mm]	[conc.]	[mm]	[conc.]
1.4	0.81	1.6	0.60	1.6	0.69
6.6	0.51	6.2	0.38	6.8	0.48
12.1	0.28	11.4	0.31	11.7	0.29
17.2	0.16	16.9	0.17	16.3	0.18
22.0	0.04	21.8	0.08	21.2	0.09
--	--	26.7	0.01	26.0	0.02

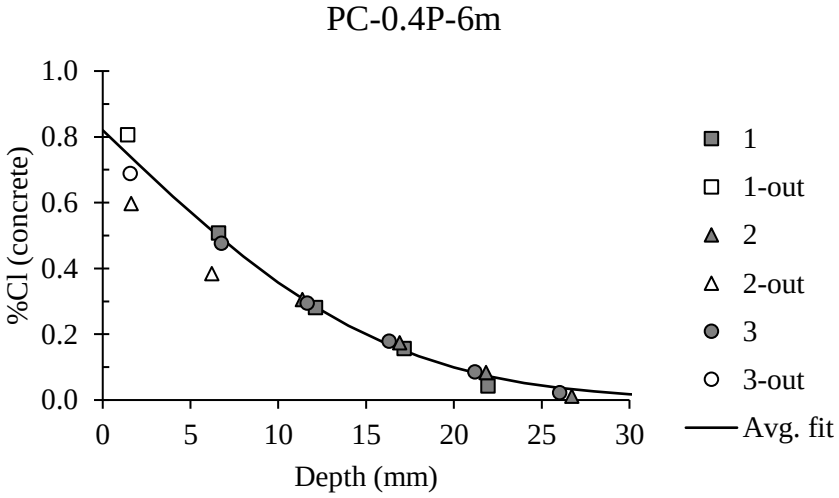

Bulk diffusion results - Wet-dry

1		2		3	
Av. depth [mm]	% Cl [conc.]	Av. depth [mm]	% Cl [conc.]	Av. depth [mm]	% Cl [conc.]
2.15	0.75	1.94	0.74	--	--
8.08	0.49	7.875	0.41	--	--
13.63	0.24	13.63	0.27	--	--
19.30	0.14	18.84	0.14	--	--
25.08	0.03	24.04	0.03	--	--
0.00	0.00	29.35	0.00	--	--

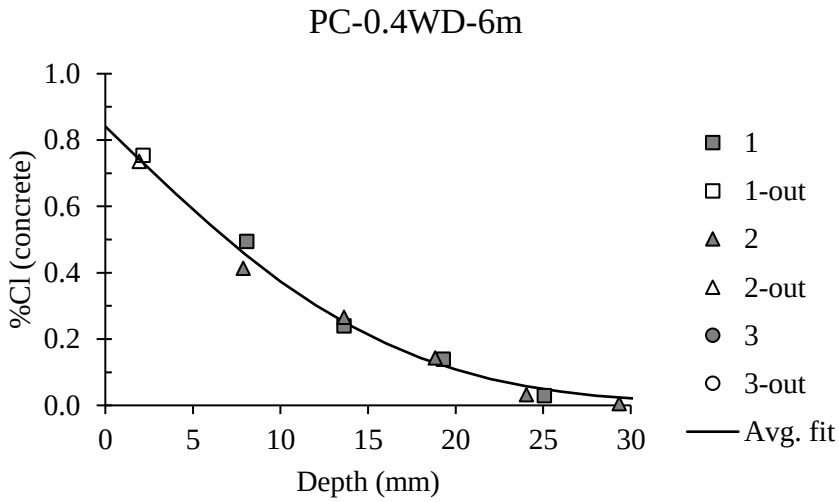

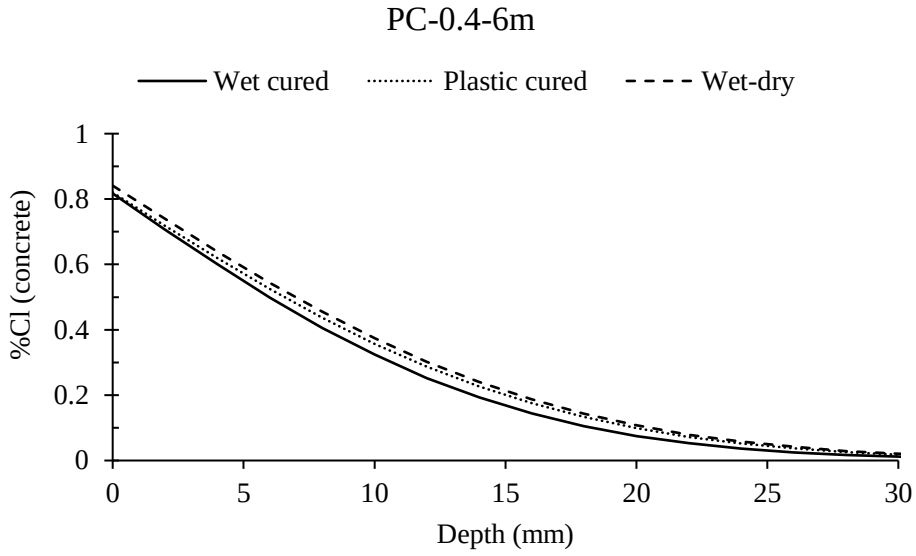

Fitted profiles - overall (PC-0.4)					
Wet cured		**Plastic cured**		**Wet-dry**	
0.0	0.817	0.0	0.820	0.0	0.8
2.0	0.706	2.0	0.718	2.0	0.739
4.0	0.6	4.0	0.619	4.0	0.639
6.0	0.499	6.0	0.525	6.0	0.544
8.0	0.406	8.0	0.437	8.0	0.455
10.0	0.324	10.0	0.357	10.0	0.374
12.0	0.252	12.0	0.287	12.0	0.302
14.0	0.193	14.0	0.226	14.0	0.240
16.0	0.144	16.0	0.175	16.0	0.187
18.0	0.105	18.0	0.133	18.0	0.143
20.0	0.075	20.0	0.099	20.0	0.108
22.0	0.053	22.0	0.072	22.0	0.079
24.0	0.036	24.0	0.052	24.0	0.058
26.0	0.025	26.0	0.037	26.0	0.042
28.0	0.017	28.0	0.026	28.0	0.029
30.0	0.012	30.0	0.018	30.0	0.021
32.0	0.008	32.0	0.013	32.0	0.015
34.0	0.006	34.0	0.009	34.0	0.011
36.0	0.005	36.0	0.007	36.0	0.008
38.0	0.004	38.0	0.005	38.0	0.006
40.0	0.004	40.0	0.004	40.0	0.005
42.0	0.003	42.0	0.004	42.0	0.004
44.0	0.003	44.0	0.003	44.0	0.004
46.0	0.003	46.0	0.003	46.0	0.003
48.0	0.003	48.0	0.003	48.0	0.003
50.0	0.003	50.0	0.003	50.0	0.003
Cl depth (mm)	42		44		46

Initial Cl content= 0.003

Overall fit

Curing	D_a	C_s	r^2
W	4.4E-12	0.8	0.99
P	5.2E-12	0.8	0.99
WD	5.5E-12	0.8	0.97

Individual fit

W	D_a	C_s	r^2
Core 1	4.2E-12	0.9	1.00
Core 2	3.9E-12	0.9	0.99
Core 3	4.6E-12	0.8	1.00
Mean	**4.2E-12**	**0.9**	
SD	3.8E-13	0.09	
CV, %	9	10	

P	D_a	C_s	r^2
Core 1	4.8E-12	0.9	0.99
Core 2	5.5E-12	0.8	0.98
Core 3	5.5E-12	0.8	1.00
Mean	**5.3E-12**	**0.8**	
SD	4.1E-13	0.04	
CV, %	8	5	

WD	D_a	C_s	r^2
Core 1	4.9E-12	1.0	0.99
Core 2	6.0E-12	0.8	0.98
Mean	**5.4E-12**	**0.9**	
SD	8.1E-13	0.14	
CV, %	15	17	

PC-0.5

Bulk diffusion results - Wet cured

1		2		3	
Av. depth	% Cl	Av. depth	% Cl	Av. depth	% Cl
[mm]	[conc.]	[mm]	[conc.]	[mm]	[conc.]
0.2	0.66	0.8	0.63	2.0	0.72
3.9	0.54	5.1	0.58	6.8	0.61
8.3	0.47	9.0	0.45	10.5	0.54
12.3	0.36	13.4	0.40	14.1	0.30
16.4	0.27	19.0	0.24	17.8	0.26
20.8	0.19	23.7	0.15	21.5	0.22
24.7	0.11	28.0	0.10	28.5	0.11

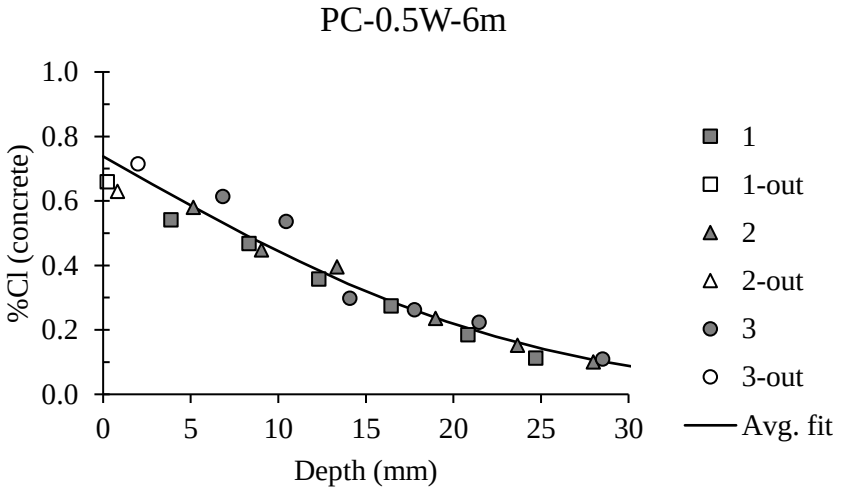

Bulk diffusion results - Plastic cured

1		2		3	
Av. depth	% Cl	Av. depth	% Cl	Av. depth	% Cl
[mm]	[conc.]	[mm]	[conc.]	[mm]	[conc.]
0.7	0.76	0.5	0.49	1.2	0.86
5.1	0.56	3.9	0.59	5.8	0.66
9.4	0.47	7.9	0.43	10.2	0.47
13.5	0.43	11.9	0.39	13.5	0.43
18.2	0.26	16.3	0.33	17.2	0.29
23.0	0.16	20.4	0.21	21.7	0.23

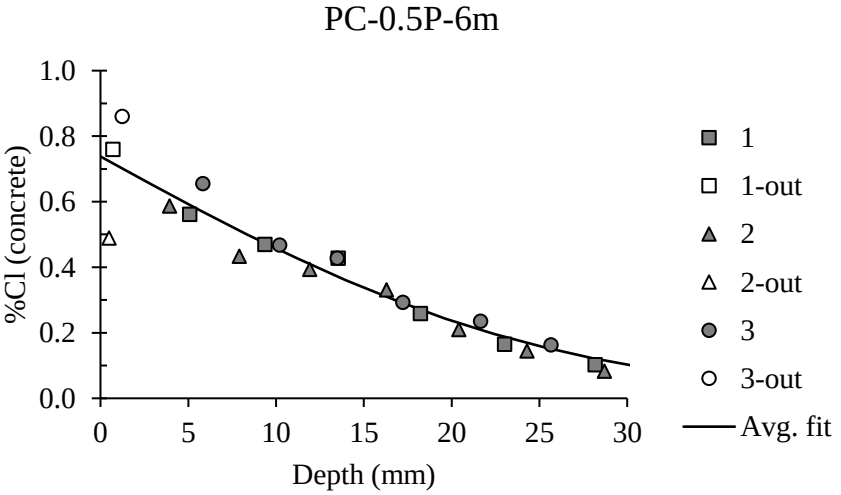

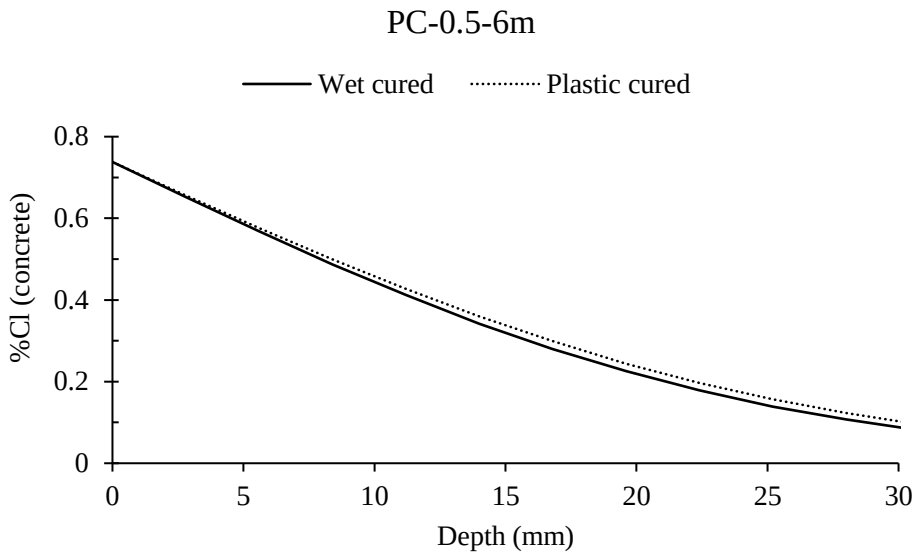
PC-0.5-6m
Wet cured
Plastic cured
%Cl (concrete)
0.8
0.6
0.4
0.2
0
0
5
10
15
20
25
30
Depth (mm)

Fitted profiles - overall (PC-0.5)			
Wet cured		**Plastic cured**	
0.0	0.738	0.0	0.738
2.8	0.652	2.8	0.656
5.6	0.568	5.6	0.576
8.4	0.487	8.4	0.499
11.2	0.412	11.2	0.427
14.0	0.342	14.0	0.360
16.8	0.28	16.8	0.299
19.6	0.226	19.6	0.244
22.4	0.179	22.4	0.197
25.2	0.139	25.2	0.157
28.0	0.107	28.0	0.123
30.8	0.081	30.8	0.095
33.6	0.06	33.6	0.072
36.4	0.044	36.4	0.054
39.2	0.032	39.2	0.040
42.0	0.023	42.0	0.030
44.8	0.017	44.8	0.022
47.6	0.012	47.6	0.016
50.4	0.009	50.4	0.012
53.2	0.007	53.2	0.009
56.0	0.005	56.0	0.007
58.8	0.004	58.8	0.005
61.6	0.004	61.6	0.005
64.4	0.004	64.4	0.004
67.2	0.003	67.2	0.004
70.0	0.003	70.0	0.003
Cl depth (mm)	67		70
Initial Cl content=			0.003

Overall fit

Curing	D_a	C_s	r^2
W	1.2E-11	0.7	0.94
P	1.3E-11	0.7	0.95
WD	0.0E+00	0.0	0.00

Individual fit

W	D_a	C_s	r^2
Core 1	1.2E-11	0.7	0.99
Core 2	1.2E-11	0.7	0.99
Core 3	9.7E-12	0.9	0.95
Mean	**1.1E-11**	**0.8**	
SD	1.2E-12	0.11	
CV, %	11	15	

P	D_a	C_s	r^2
Core 1	1.3E-11	0.7	0.97
Core 2	1.3E-11	0.7	0.98
Core 3	1.2E-11	0.8	0.98
Mean	**1.3E-11**	**0.7**	
SD	5.3E-13	0.08	
CV, %	4	10	

PC-0.6

Bulk diffusion results - Wet cured

1		2		3	
Depth	% Cl	Depth	% Cl	Depth	% Cl
[mm]	[conc.]	[mm]	[conc.]	[mm]	[conc.]
1.7	0.70	2.8	0.61	1.2	0.55
7.0	0.41	8.5	0.47	5.8	0.41
12.0	0.33	12.5	0.36	10.3	0.30
17.2	0.28	16.2	0.28	14.3	0.27
22.0	0.17	19.6	0.24	18.5	0.28
26.0	0.14	23.1	0.19	22.9	0.20
29.7	0.13	27.1	0.17	27.1	0.14

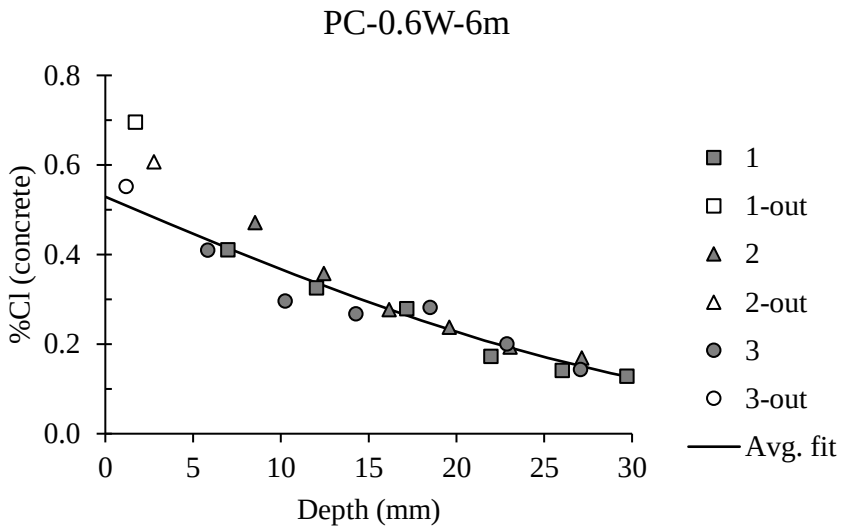

Bulk diffusion results - Plastic cured

1		2		3	
Depth	% Cl	Depth	% Cl	Depth	% Cl
[mm]	[conc.]	[mm]	[conc.]	[mm]	[conc.]
2.2	0.50	1.2	0.64	2.0	0.56
7.4	0.44	5.1	0.53	7.4	0.55
11.6	0.42	8.6	0.49	12.1	0.35
16.3	0.30	12.4	0.41	16.8	0.25
21.1	0.23	16.7	0.33	21.5	0.20
25.5	0.18	20.7	0.20	25.9	0.18

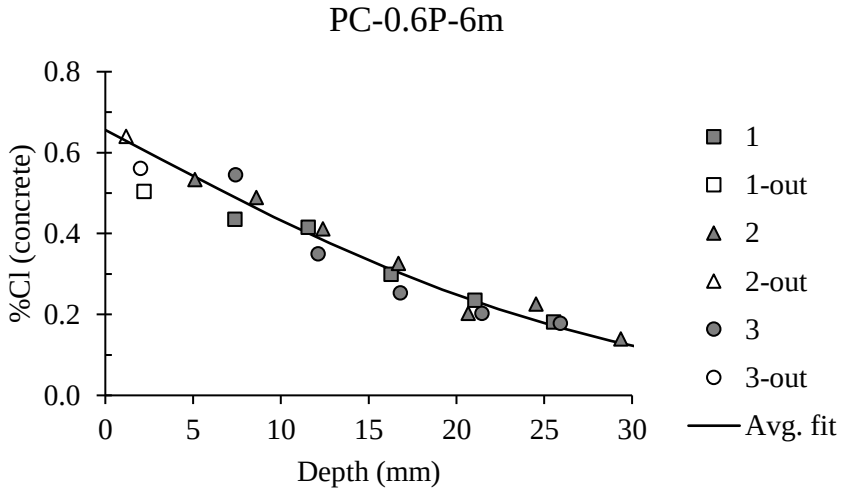

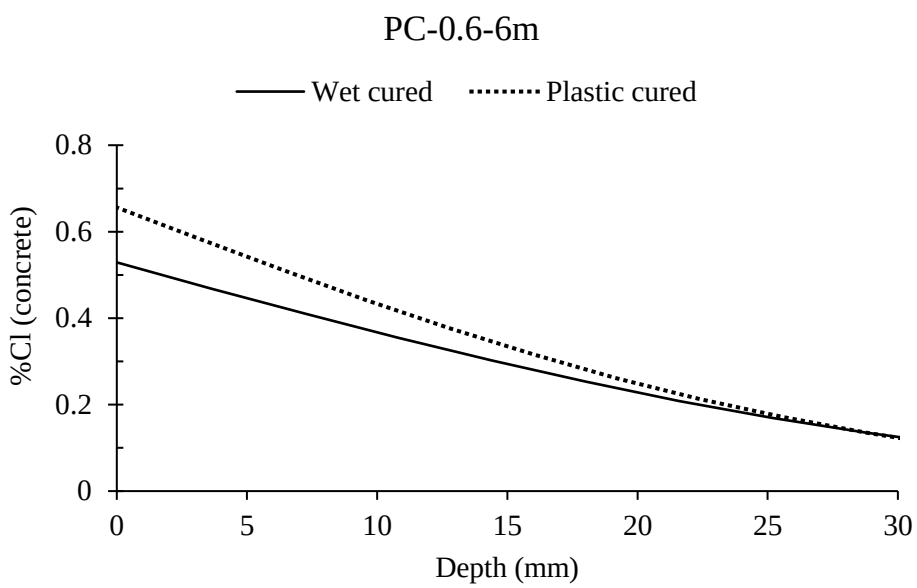
PC-0.6-6m
Wet cured
Plastic cured
0.8
0.6
0.4
0.2
0
%Cl (concrete)
0
5
10
15
20
25
30
Depth (mm)

Fitted profiles - overall			
Wet cured		**Plastic cured**	
0.0	0.529	0.0	0.656
3.6	0.469	3.2	0.583
7.2	0.411	6.4	0.511
10.8	0.355	9.6	0.441
14.4	0.302	12.8	0.376
18.0	0.253	16.0	0.316
21.6	0.208	19.2	0.261
25.2	0.169	22.4	0.213
28.8	0.135	25.6	0.171
32.4	0.106	28.8	0.135
36.0	0.082	32.0	0.104
39.6	0.063	35.2	0.080
43.2	0.047	38.4	0.060
46.8	0.034	41.6	0.044
50.4	0.025	44.8	0.032
54.0	0.018	48.0	0.023
57.6	0.012	51.2	0.016
61.2	0.008	54.4	0.011
64.8	0.006	57.6	0.007
68.4	0.004	60.8	0.005
72.0	0.002	64.0	0.003
75.6	0.002	67.2	0.002
79.2	0.001	70.4	0.001
82.8	0.001	73.6	0.001
86.4	0.000	76.8	0.000
90.0	0.000	80.0	0.000
Cl depth (mm)	86		77

Initial Cl content= 0

Overall fit

Curing	**D_a**	**C_s**	**r^2**
W	2.1E-11	0.5	0.90
P	1.7E-11	0.7	0.95

Individual fit

W	**D_a**	**C_s**	**r^2**
Core 1	1.9E-11	0.5	0.98
Core 2	1.6E-11	0.6	0.97
Core 3	2.6E-11	0.5	0.90
Mean	**2.0E-11**	**0.5**	
SD	5.3E-12	0.09	
CV, %	26	17	

P	**D_a**	**C_s**	**r^2**
Core 1	1.9E-11	0.6	0.98
Core 2	1.8E-11	0.7	0.97
Core 3	1.4E-11	0.7	0.95
Mean	**1.7E-11**	**0.7**	
SD	2.9E-12	0.05	
CV, %	17	8	

PC-0.7

Bulk diffusion results - Wet cured

1		2		3	
Depth	% Cl	Depth	% Cl	Depth	% Cl
[mm]	[conc.]	[mm]	[conc.]	[mm]	[conc.]
1.8	0.69	2.5	0.72	2.0	0.77
6.7	0.46	8.2	0.59	7.2	0.55
11.2	0.38	12.4	0.44	11.3	0.45
15.2	0.33	16.9	0.35	15.1	0.34
18.8	0.28	21.1	0.26	19.1	0.26
22.9	0.23	25.1	0.27	23.5	0.22
27.7	0.19	29.5	0.21	28.0	0.23

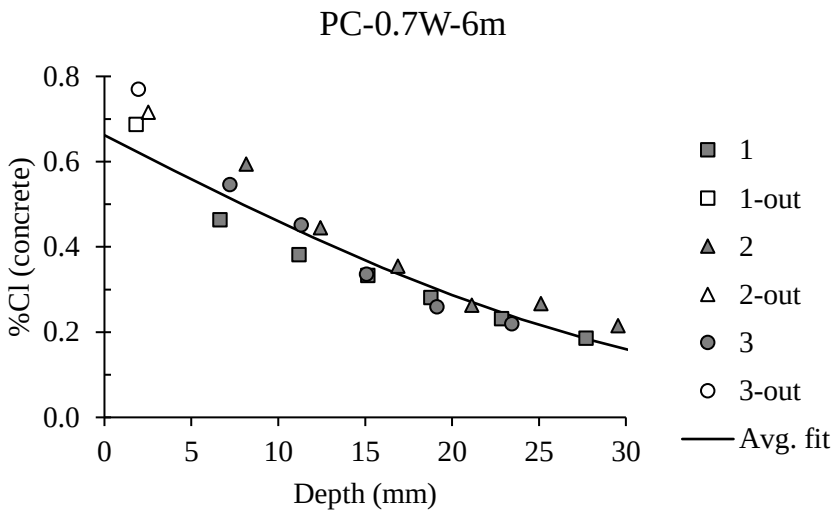

Bulk diffusion results - Plastic cured

1		2		3	
Depth	% Cl	Depth	% Cl	Depth	% Cl
[mm]	[conc.]	[mm]	[conc.]	[mm]	[conc.]
2.0	0.58	0.7	0.34	1.6	0.50
6.9	0.39	4.5	0.50	6.1	0.41
10.9	0.36	8.3	0.32	9.6	0.33
15.2	0.37	11.9	0.34	14.2	0.42
19.4	0.30	16.1	0.45	19.4	0.34
23.7	0.24	20.9	0.36	23.6	0.27

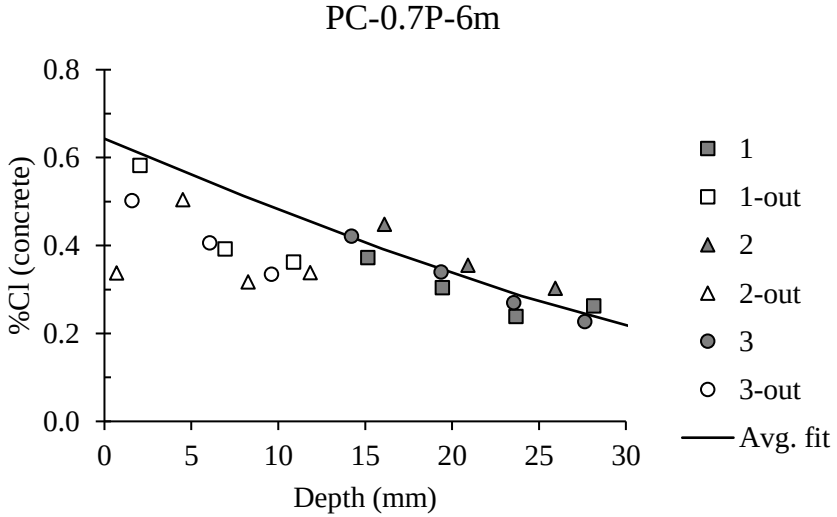

Bulk diffusion results - Wet-dry

1		2		3	
Depth [mm]	% Cl [conc.]	Depth [mm]	% Cl [conc.]	Depth [mm]	% Cl [conc.]
4.3	0.49	4.4	0.57	--	--
14.9	0.36	13.9	0.32	--	--
25.6	0.21	23.1	0.19	--	--
35.2	0.10	32.4	0.12	--	--
44.4	0.04	41.1	0.03	--	--
52.5	0.02	50.9	0.03	--	--

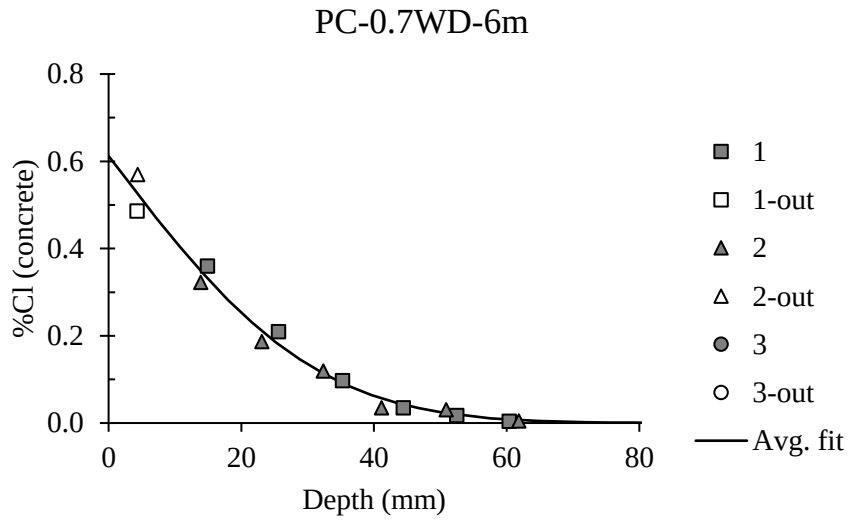

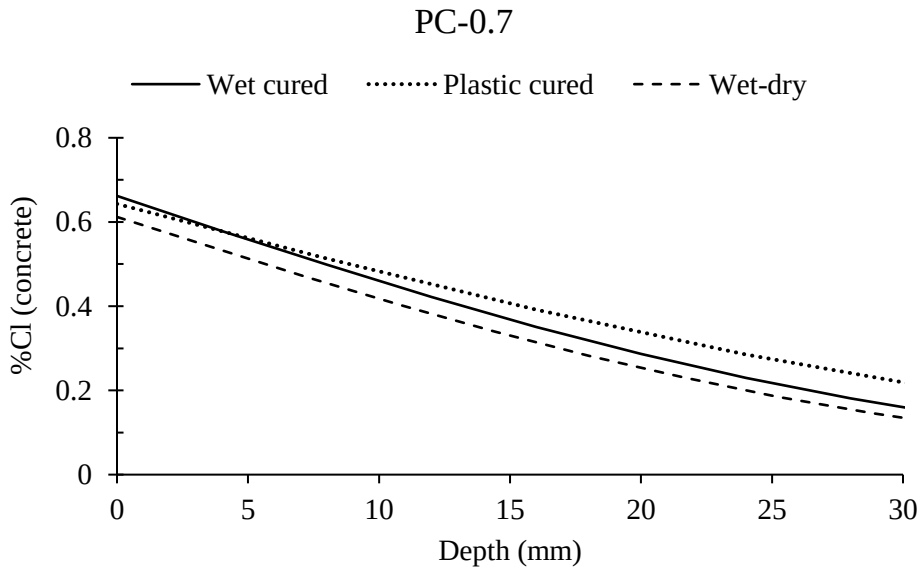

Fitted profiles – overall (PC-0.7)					
Wet cured		**Plastic cured**		**Wet-dry**	
0.0	0.662	0.0	0.643	0.0	0.6
4.0	0.579	8.0	0.513	3.6	0.541
8.0	0.499	16.0	0.392	7.2	0.470
12.0	0.422	24.0	0.285	10.8	0.403
16.0	0.351	32.0	0.197	14.4	0.340
20.0	0.287	40.0	0.129	18.0	0.282
24.0	0.23	48.0	0.080	21.6	0.231
28.0	0.181	56.0	0.047	25.2	0.185
32.0	0.139	64.0	0.026	28.8	0.146
36.0	0.105	72.0	0.014	32.4	0.113
40.0	0.078	80.0	0.007	36.0	0.086
44.0	0.056	88.0	0.003	39.6	0.064
48.0	0.04	96.0	0.001	43.2	0.047
52.0	0.028	104.0	0.001	46.8	0.034
56.0	0.019	112.0	0.000	50.4	0.024
60.0	0.012	120.0	0.000	54.0	0.017
64.0	0.008	128.0	0.000	57.6	0.011
68.0	0.005	136.0	0.000	61.2	0.008
72.0	0.003	144.0	0.000	64.8	0.005
76.0	0.002	152.0	0.000	68.4	0.003
80.0	0.001	160.0	0.000	72.0	0.002
84.0	0.001	168.0	0.000	75.6	0.001
88.0	0	176.0	0.000	79.2	0.001
92.0	0	184.0	0.000	82.8	0.000
96.0	0	192.0	0.000	86.4	0.000
100.0	0	200.0	0.000	90.0	0.000
Cl depth (mm)	88		112		83

Initial Cl content= 0

Overall fit

Curing	D_a	C_s	r^2
W	2.1E-11	0.7	0.88
P	3.1E-11	0.6	0.76
WD	1.9E-11	0.6	0.98

Individual fit

W	D_a	C_s	r^2
Core 1	2.5E-11	0.6	1.00
Core 2	2.1E-11	0.7	0.95
Core 3	1.4E-11	0.7	0.99
Mean	**2.0E-11**	**0.7**	
SD	5.3E-12	0.10	
CV, %	26	15	

P	D_a	C_s	r^2
Core 1	4.4E-11	0.5	0.77
Core 2	3.1E-11	0.7	0.98
Core 3	2.5E-11	0.7	1.00
Mean	**3.4E-11**	**0.6**	
SD	9.7E-12	0.11	
CV, %	29	17	

WD	D_a	C_s	r^2
Core 1	1.9E-11	0.7	1.00
Core 2	1.9E-11	0.6	0.99
Mean	**1.9E-11**	**0.6**	
SD	1.8E-13	0.08	
CV, %	1	13	

FA(15)-0.4

Bulk diffusion results - Wet cured

1		2		3	
Depth	% Cl	Depth	% Cl	Depth	% Cl
[mm]	[conc.]	[mm]	[conc.]	[mm]	[conc.]
1.0	1.05	1.3	0.83	1.4	0.84
5.3	0.63	5.5	0.46	6.7	0.47
9.1	0.36	9.5	0.32	12.1	0.22
12.5	0.24	13.8	0.18	17.1	0.05
16.9	0.07	17.9	0.05	25.8	0.00
22.0	0.00	21.8	0.01	85.1	0.03
0.0	0.00	26.4	0.00	0.0	0.00

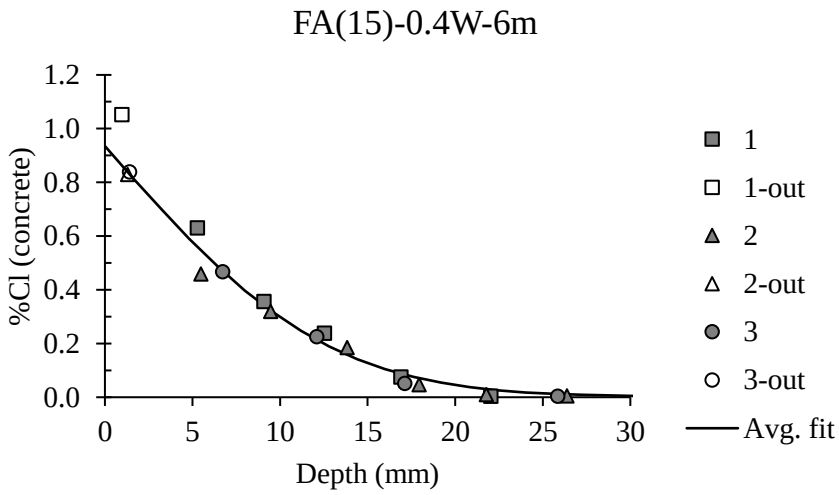

Bulk diffusion results - Plastic cured

1		2		3	
Depth	% Cl	Depth	% Cl	Depth	% Cl
[mm]	[conc.]	[mm]	[conc.]	[mm]	[conc.]
1.6	0.96	1.7	0.93	1.7	0.83
6.8	0.52	6.5	0.49	6.2	0.55
11.2	0.23	10.4	0.21	9.9	0.34
15.6	0.13	14.6	0.15	14.1	0.16
20.3	0.02	19.4	0.03	18.5	0.04
83.6	0.03	87.3	0.01	26.6	0.00

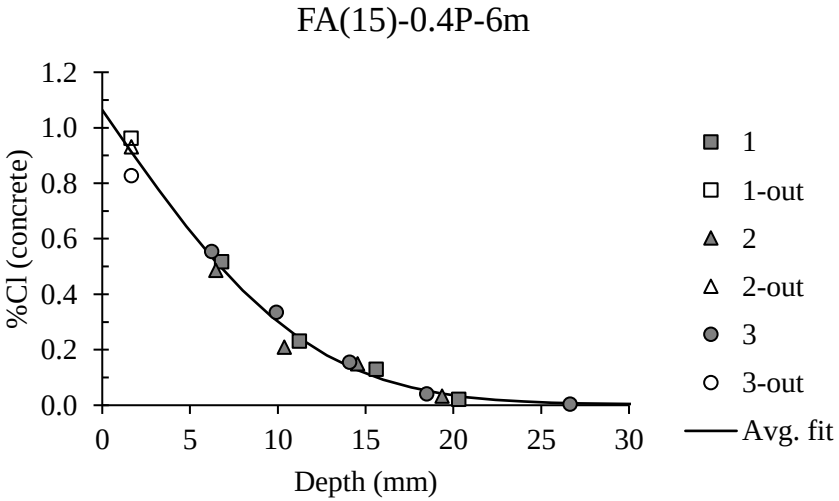

Bulk diffusion results - Wet-dry

1		2		3	
Depth [mm]	% Cl [conc.]	Depth [mm]	% Cl [conc.]	Depth [mm]	% Cl [conc.]
1.61	0.62	1.3	0.77	--	--
6.96	0.48	6.5	0.50	--	--
11.36	0.27	12.0	0.20	--	--
15.69	0.08	17.0	0.04	--	--
21.26	0.01	--	--	--	--
27.20	0.004	--	--	--	--

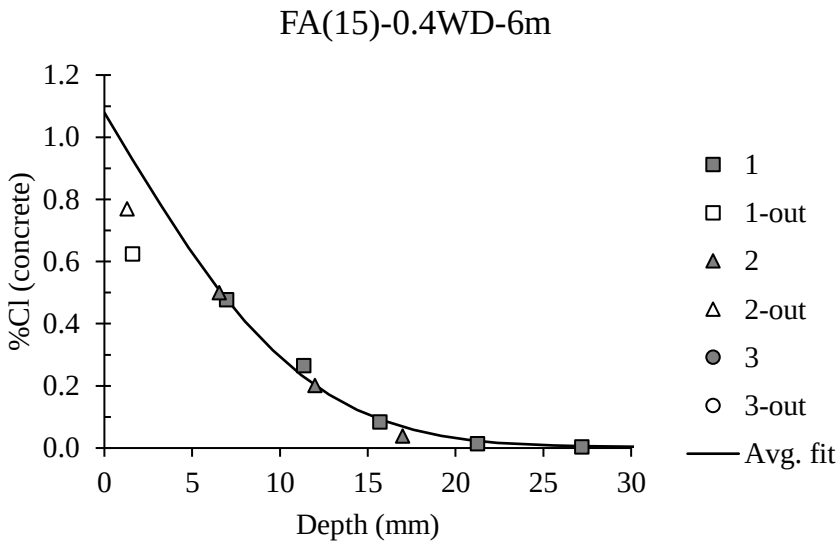

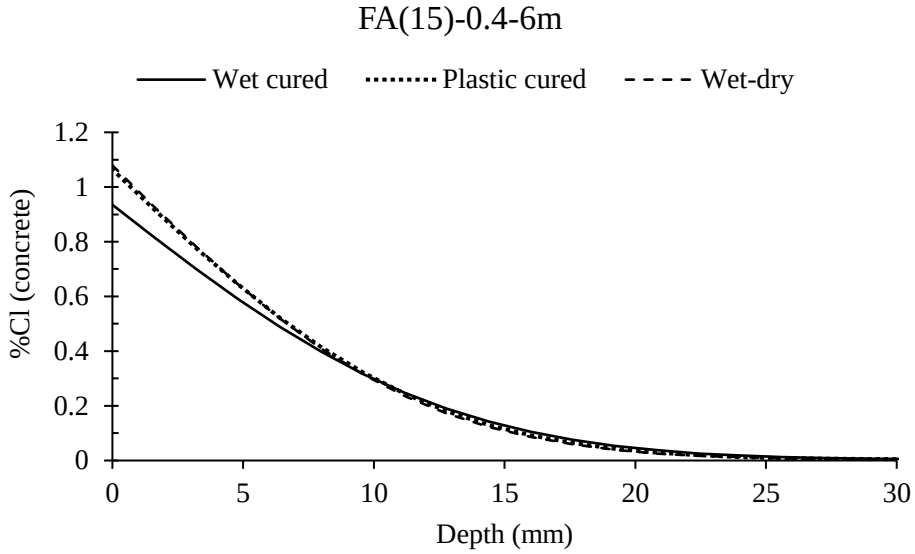

Fitted profiles - overall (FA(15)-0.4)

Wet cured		Plastic cured		Wet-dry	
0.0	0.935	0.0	1.064	0.0	1.1
1.6	0.816	1.6	0.918	1.6	0.928
3.2	0.701	3.2	0.777	3.2	0.782
4.8	0.591	4.8	0.644	4.8	0.644
6.4	0.489	6.4	0.522	6.4	0.519
8.0	0.397	8.0	0.414	8.0	0.408
9.6	0.316	9.6	0.321	9.6	0.314
11.2	0.247	11.2	0.243	11.2	0.235
12.8	0.189	12.8	0.180	12.8	0.172
14.4	0.142	14.4	0.130	14.4	0.123
16.0	0.105	16.0	0.092	16.0	0.086
17.6	0.076	17.6	0.064	17.6	0.059
19.2	0.054	19.2	0.043	19.2	0.039
20.8	0.038	20.8	0.029	20.8	0.026
22.4	0.026	22.4	0.019	22.4	0.017
24.0	0.018	24.0	0.013	24.0	0.012
25.6	0.013	25.6	0.009	25.6	0.008
27.2	0.009	27.2	0.007	27.2	0.006
28.8	0.007	28.8	0.005	28.8	0.005
30.4	0.005	30.4	0.004	30.4	0.004
32.0	0.004	32.0	0.004	32.0	0.003
33.6	0.004	33.6	0.003	33.6	0.003
35.2	0.003	35.2	0.003	35.2	0.003
36.8	0.003	36.8	0.003	36.8	0.003
38.4	0.003	38.4	0.003	38.4	0.003
40.0	0.003	40.0	0.003	40.0	0.003
Cl depth (mm)	35		34		32

Initial Cl content= 0.003

Overall fit

Curing	D_a	C_s	r^2
W	3.2E-12	0.9	0.97
P	2.8E-12	1.1	0.98
WD	2.6E-12	1.1	0.99

Individual fit

W	D_a	C_s	r^2
Core 1	2.9E-12	1.1	0.99
Core 2	3.8E-12	0.8	0.98
Core 3	2.9E-12	1.0	0.99
Mean	**3.2E-12**	**0.9**	
SD	4.7E-13	0.16	
CV, %	15	17	

P	D_a	C_s	r^2
Core 1	2.7E-12	1.1	0.99
Core 2	2.6E-12	1.0	0.97
Core 3	2.9E-12	1.1	1.00
Mean	**2.7E-12**	**1.1**	
SD	1.3E-13	0.06	
CV, %	5	6	

WD	D_a	C_s	r^2
Core 1	2.8E-12	1.1	0.99
Core 2	2.4E-12	1.1	1.00
Mean	**2.6E-12**	**1.1**	
SD	2.9E-13	0.04	
CV, %	11	4	

FA(15)-0.5

Bulk diffusion results - Wet cured

1		2		3	
Depth	% Cl	Depth	% Cl	Depth	% Cl
[mm]	[conc.]	[mm]	[conc.]	[mm]	[conc.]
0.6	0.55	1.8	0.68	1.6	0.76
4.7	0.60	7.6	0.44	5.9	0.43
9.0	0.38	12.7	0.26	9.6	0.33
12.6	0.25	17.5	0.11	13.6	0.22
16.0	0.13	22.4	0.02	17.5	0.12
20.0	0.05	0.0	0.00	22.4	0.04
24.4	0.01	0.0	0.00	27.4	0.00

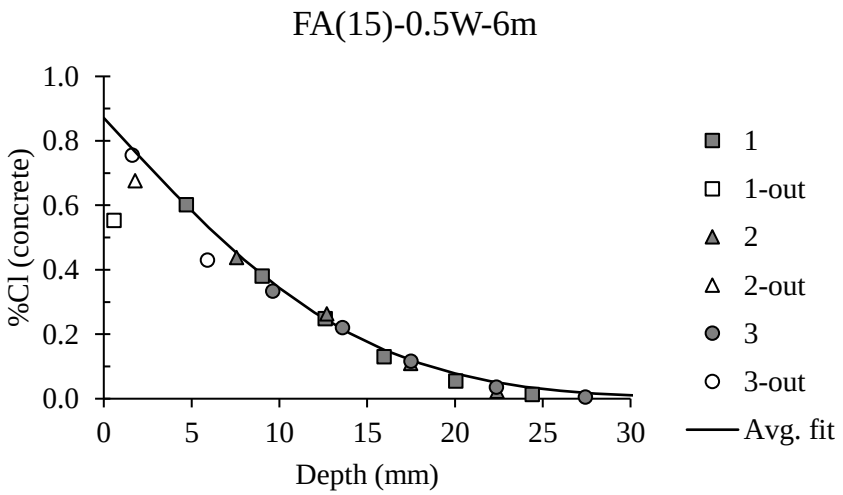

Bulk diffusion results - Plastic cured

1		2		3	
Depth	% Cl	Depth	% Cl	Depth	% Cl
[mm]	[conc.]	[mm]	[conc.]	[mm]	[conc.]
1.6	0.82	1.8	0.78	1.6	0.96
6.2	0.49	7.1	0.58	6.5	0.59
10.5	0.42	12.0	0.38	11.1	0.39
14.9	0.30	17.0	0.27	15.8	0.27
19.2	0.20	21.7	0.14	20.6	0.16
23.1	0.13	26.3	0.08	25.4	0.09

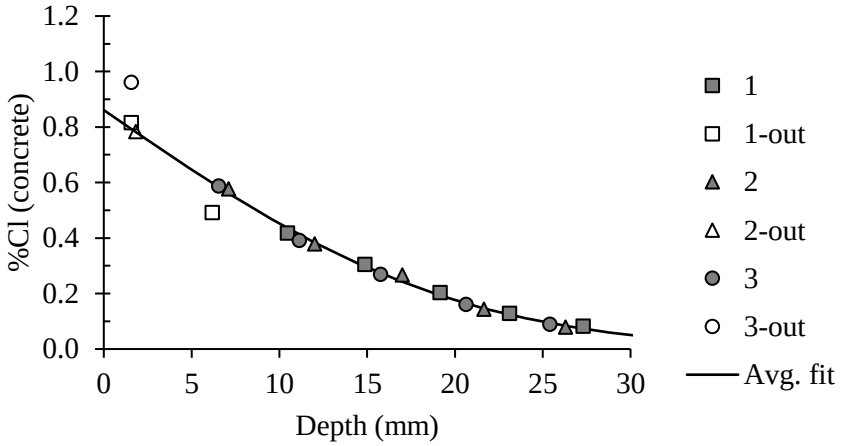

Bulk diffusion results - Wet-dry

1		2		3	
Depth	% Cl	Depth	% Cl	Depth	% Cl
[mm]	[conc.]	[mm]	[conc.]	[mm]	[conc.]
1.8	0.778	1.8	0.840	--	--
7.3	0.476	7.4	0.486	--	--
12.1	0.238	11.9	0.280	--	--
16.5	0.109	16.2	0.142	--	--
21.5	0.032	21.6	0.037	--	--
27.2	0.003	26.6	0.004	--	--

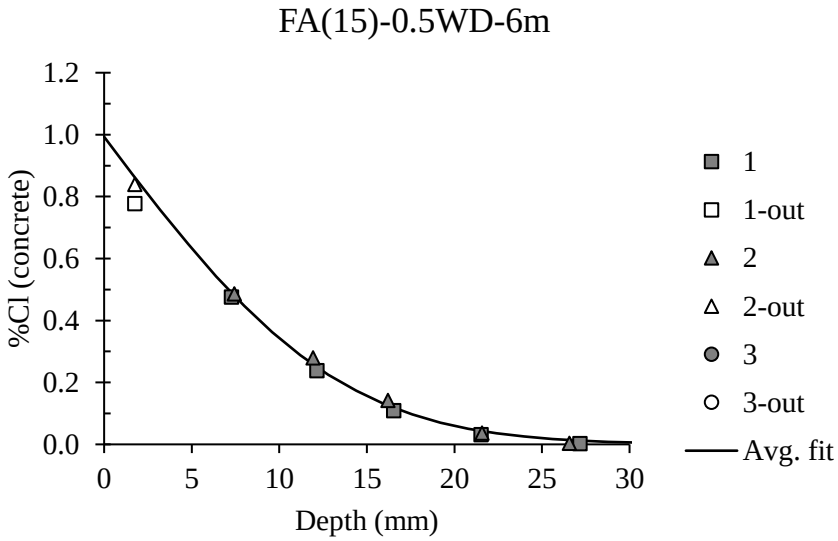

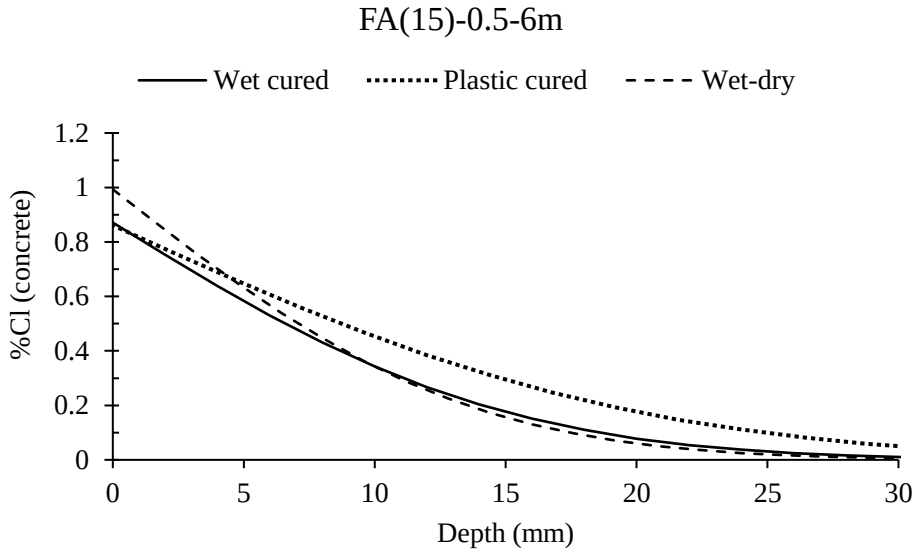

Fitted profiles – overall (FA(15)-0.5)

Wet cured		Plastic cured		Wet-dry	
0.0	0.871	0.0	0.861	0.0	1.0
2.0	0.753	2.4	0.757	1.6	0.874
4.0	0.638	4.8	0.655	3.2	0.757
6.0	0.53	7.2	0.558	4.8	0.646
8.0	0.431	9.6	0.467	6.4	0.542
10.0	0.343	12.0	0.384	8.0	0.447
12.0	0.267	14.4	0.311	9.6	0.362
14.0	0.203	16.8	0.247	11.2	0.288
16.0	0.151	19.2	0.192	12.8	0.225
18.0	0.11	21.6	0.147	14.4	0.173
20.0	0.078	24.0	0.111	16.0	0.130
22.0	0.054	26.4	0.082	17.6	0.097
24.0	0.037	28.8	0.059	19.2	0.070
26.0	0.025	31.2	0.042	20.8	0.050
28.0	0.016	33.6	0.030	22.4	0.036
30.0	0.011	36.0	0.021	24.0	0.025
32.0	0.007	38.4	0.014	25.6	0.017
34.0	0.005	40.8	0.010	27.2	0.012
36.0	0.004	43.2	0.007	28.8	0.008
38.0	0.003	45.6	0.005	30.4	0.006
40.0	0.003	48.0	0.004	32.0	0.004
42.0	0.002	50.4	0.003	33.6	0.003
44.0	0.002	52.8	0.003	35.2	0.003
46.0	0.002	55.2	0.002	36.8	0.002
48.0	0.002	57.6	0.002	38.4	0.002
50.0	0.002	60.0	0.002	40.0	0.002
Cl depth (mm)	42		55		37

Initial Cl content= 0.002

Overall fit

Curing	D_a	C_s	r^2
W	4.4E-12	0.9	0.99
P	7.9E-12	0.9	1.00
WD	3.6E-12	1.0	0.99

Individual fit

W	D_a	C_s	r^2
Core 1	3.9E-12	0.9	1.00
Core 2	5.2E-12	0.8	0.98
Core 3	4.4E-12	0.8	0.99
Mean	**4.5E-12**	**0.9**	
SD	6.5E-13	0.04	
CV, %	14	5	

P	D_a	C_s	r^2
Core 1	9.0E-12	0.8	1.00
Core 2	7.8E-12	0.9	1.00
Core 3	7.5E-12	0.9	1.00
Mean	**8.1E-12**	**0.8**	
SD	7.9E-13	0.05	
CV, %	10	6	

WD	D_a	C_s	r^2
Core 1	3.3E-12	1.0	1.00
Core 2	3.8E-12	1.0	1.00
Mean	**3.6E-12**	**1.0**	
SD	3.3E-13	0.01	
CV, %	9	1	

FA(15)-0.6

Bulk diffusion results - Wet cured

1		2		3	
Depth	% Cl	Depth	% Cl	Depth	% Cl
[mm]	[conc.]	[mm]	[conc.]	[mm]	[conc.]
0.8	0.53	1.8	0.64	1.7	0.67
5.1	0.58	6.5	0.43	7.3	0.53
10.3	0.45	10.9	0.37	12.3	0.39
15.7	0.28	15.7	0.26	16.8	0.23
21.1	0.15	20.4	0.17	22.1	0.15
26.1	0.08	24.8	0.09	27.0	0.09
31.0	0.03	30.0	0.04	31.1	0.04

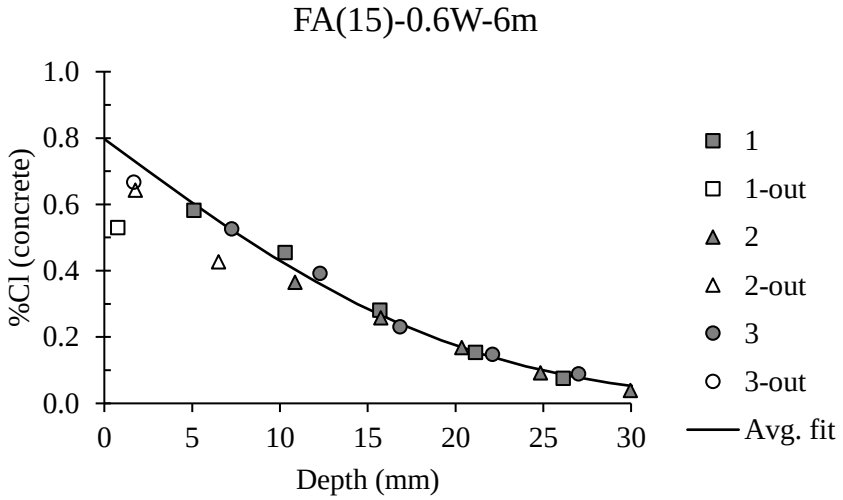

Bulk diffusion results - Plastic cured

1		2		3	
Depth	% Cl	Depth	% Cl	Depth	% Cl
[mm]	[conc.]	[mm]	[conc.]	[mm]	[conc.]
2.1	0.67	2.0	0.61	1.7	0.70
8.0	0.46	7.2	0.58	6.8	0.49
13.4	0.35	11.2	0.30	11.8	0.36
18.1	0.22	15.5	0.27	16.1	0.23
22.6	0.13	20.6	0.14	20.3	0.17
27.5	0.05	25.1	0.07	24.7	0.09

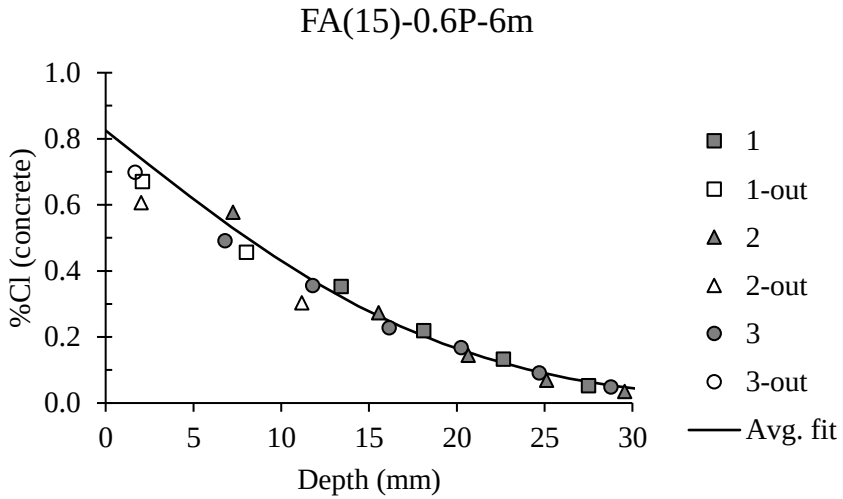

Bulk diffusion results - Wet-dry

1		2		3	
Depth	% Cl	Depth	% Cl	Depth	% Cl
[mm]	[conc.]	[mm]	[conc.]	[mm]	[conc.]
2.0	0.588	0.6	0.658	--	--
8.4	0.374	5.1	0.693	--	--
15.1	0.205	10.2	0.453	--	--
21.5	0.102	15.9	0.242	--	--
27.6	0.032	22.0	0.106	--	--
33.5	0.008	27.4	0.047	--	--

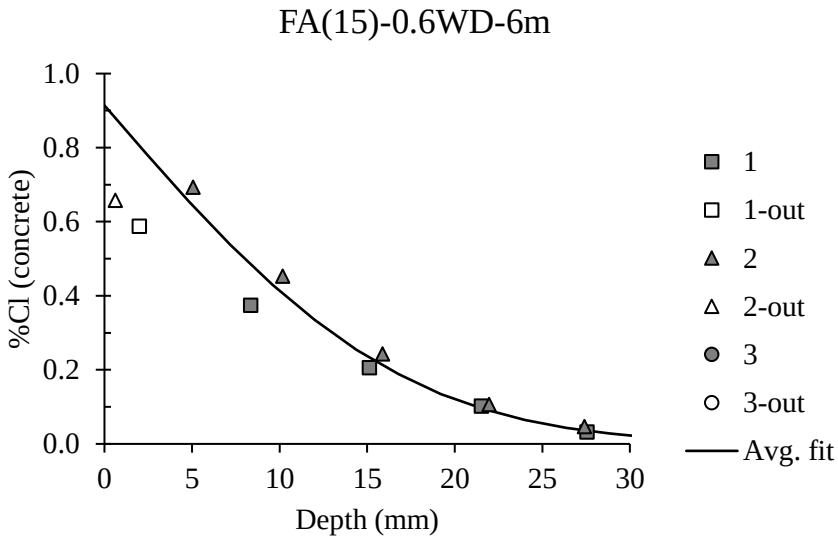

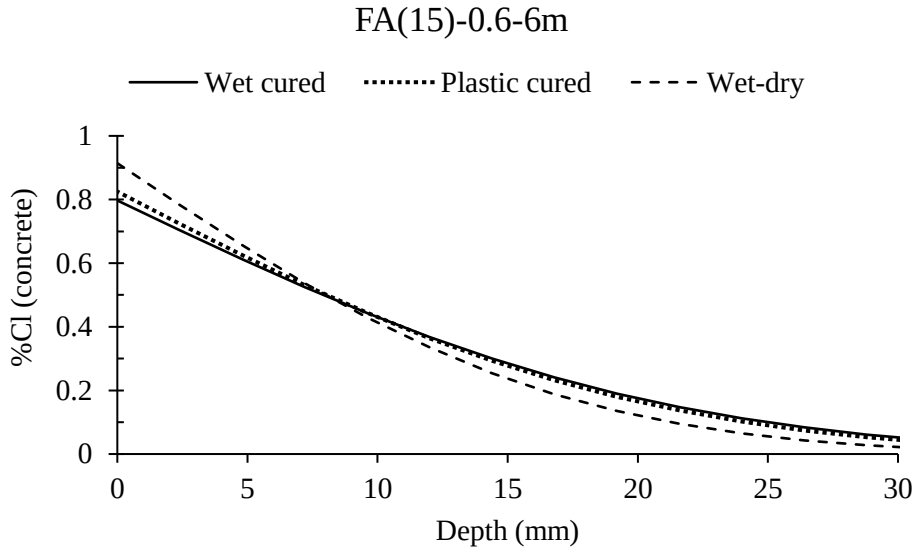

Fitted profiles – overall (FA(15)-0.6)

Wet cured		Plastic cured		Wet-dry	
0.0	0.797	0.0	0.825	0.0	0.9
2.4	0.704	2.4	0.724	2.4	0.783
4.8	0.612	4.8	0.625	4.8	0.656
7.2	0.525	7.2	0.531	7.2	0.537
9.6	0.443	9.6	0.444	9.6	0.429
12.0	0.368	12.0	0.364	12.0	0.335
14.4	0.3	14.4	0.293	14.4	0.254
16.8	0.241	16.8	0.232	16.8	0.188
19.2	0.19	19.2	0.180	19.2	0.135
21.6	0.147	21.6	0.137	21.6	0.095
24.0	0.112	24.0	0.102	24.0	0.065
26.4	0.084	26.4	0.074	26.4	0.043
28.8	0.061	28.8	0.053	28.8	0.028
31.2	0.044	31.2	0.037	31.2	0.017
33.6	0.031	33.6	0.026	33.6	0.010
36.0	0.022	36.0	0.017	36.0	0.006
38.4	0.015	38.4	0.011	38.4	0.004
40.8	0.01	40.8	0.007	40.8	0.002
43.2	0.006	43.2	0.005	43.2	0.001
45.6	0.004	45.6	0.003	45.6	0.001
48.0	0.003	48.0	0.002	48.0	0.000
50.4	0.002	50.4	0.001	50.4	0.000
52.8	0.001	52.8	0.001	52.8	0.000
55.2	0.001	55.2	0.000	55.2	0.000
57.6	0	57.6	0.000	57.6	0.000
60.0	0	60.0	0.000	60.0	0.000
Cl depth (mm)	58		55		48

Initial Cl content= 0

Overall fit

Curing	D_a	C_s	r^2
W	8.5E-12	0.8	0.99
P	7.8E-12	0.8	0.98
WD	5.7E-12	0.9	0.96

Individual fit

W	D_a	C_s	r^2
Core 1	8.8E-12	0.8	0.99
Core 2	8.9E-12	0.7	0.99
Core 3	8.7E-12	0.8	0.99
Mean	**8.8E-12**	**0.8**	
SD	9.7E-14	0.05	
CV, %	1	6	

P	D_a	C_s	r^2
Core 1	7.1E-12	1.0	1.00
Core 2	6.7E-12	0.9	1.00
Core 3	8.6E-12	0.7	1.00
Mean	**7.5E-12**	**0.9**	
SD	9.9E-13	0.13	
CV, %	13	15	

WD	D_a	C_s	r^2
Core 1	7.0E-12	0.7	1.00
Core 2	6.1E-12	1.0	1.00
Mean	**6.6E-12**	**0.8**	
SD	6.4E-13	0.22	
CV, %	10	27	

FA(30)-0.4

Bulk diffusion results - Wet cured

1		2		3	
Depth	% Cl	Depth	% Cl	Depth	% Cl
[mm]	[conc.]	[mm]	[conc.]	[mm]	[conc.]
1.1	0.67	1.3	0.65	1.2	0.62
5.5	0.52	5.7	0.46	5.6	0.50
10.1	0.25	9.7	0.25	10.4	0.21
14.5	0.09	13.8	0.09	15.1	0.06
19.3	0.01	18.4	0.01	18.8	0.00
--	--	--	--	22.8	0.00

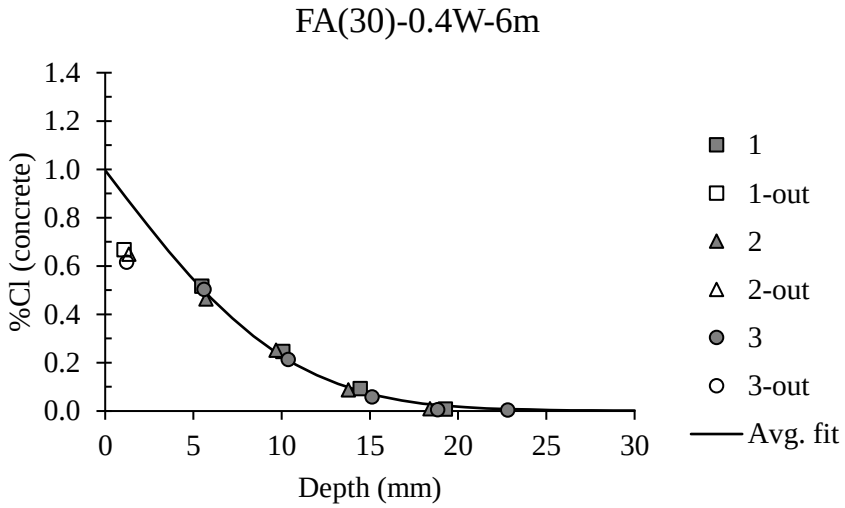

Bulk diffusion results - Plastic cured

1		2		3	
Depth	% Cl	Depth	% Cl	Depth	% Cl
[mm]	[conc.]	[mm]	[conc.]	[mm]	[conc.]
1.0	0.83	0.9	0.77	1.5	0.91
4.9	0.69	5.1	0.72	6.2	0.60
9.0	0.32	9.8	0.31	10.3	0.32
13.4	0.15	14.2	0.09	14.1	0.17
17.9	0.04	18.6	0.01	18.1	0.03
22.4	0.01	23.6	0.002	23.8	0.004

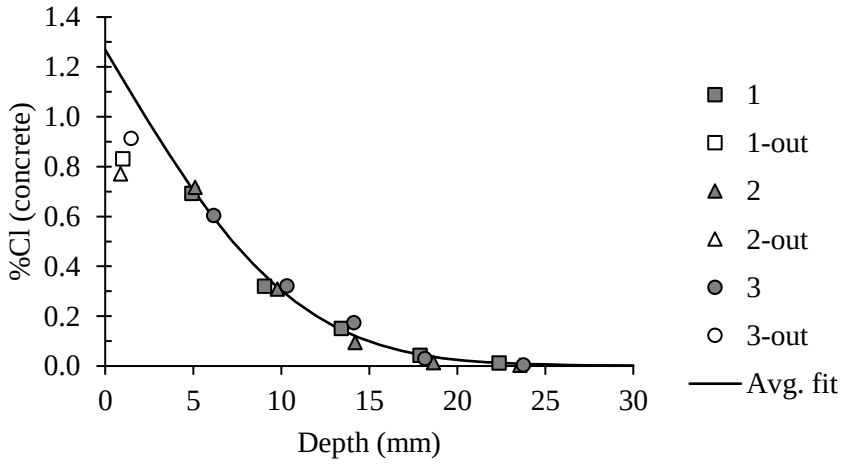

Bulk diffusion results - Wet-dry

1		2		3	
Depth	% Cl	Depth	% Cl	Depth	% Cl
[mm]	[conc.]	[mm]	[conc.]	[mm]	[conc.]
1.6	0.699	1.9	0.665	--	--
6.3	0.414	7.3	0.302	--	--
10.9	0.152	12.3	0.067	--	--
15.5	0.025	17.2	0.004	--	--
20.1	0.005	21.8	0.002	--	--

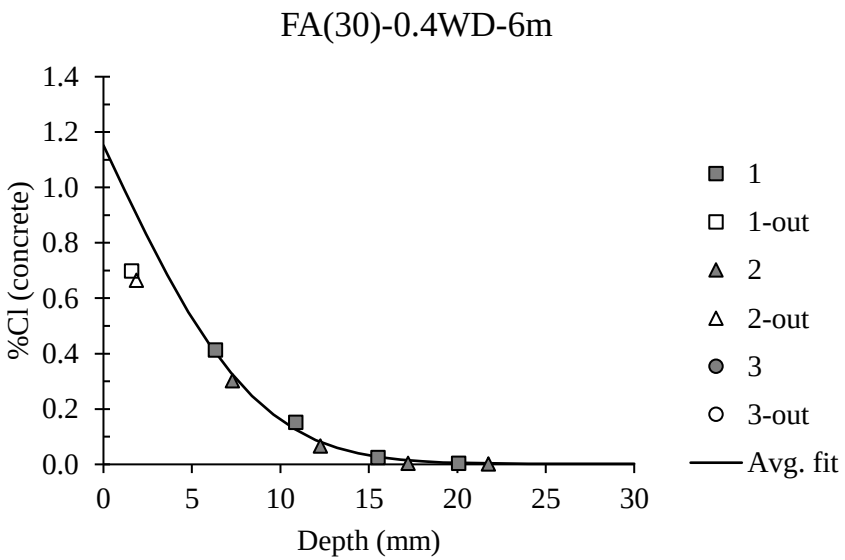

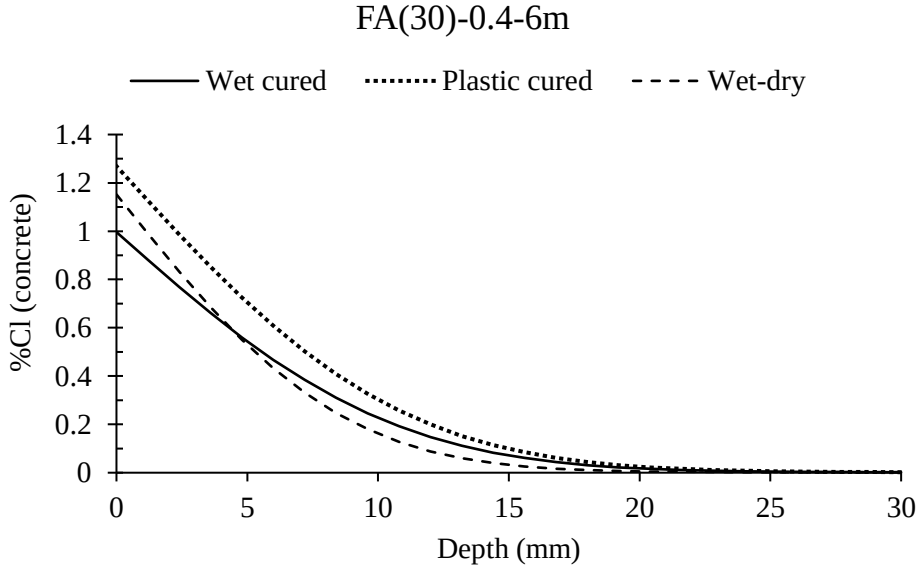

Fitted profiles – overall (FA(30)-0.4)

Wet cured		Plastic cured		Wet-dry	
0.0	0.996	0.0	1.269	0.0	1.2
1.2	0.881	1.2	1.126	1.2	0.990
2.4	0.769	2.4	0.986	2.4	0.832
3.6	0.661	3.6	0.852	3.6	0.685
4.8	0.56	4.8	0.725	4.8	0.550
6.0	0.467	6.0	0.608	6.0	0.432
7.2	0.384	7.2	0.502	7.2	0.331
8.4	0.31	8.4	0.409	8.4	0.247
9.6	0.246	9.6	0.327	9.6	0.180
10.8	0.192	10.8	0.258	10.8	0.128
12.0	0.148	12.0	0.200	12.0	0.088
13.2	0.112	13.2	0.152	13.2	0.060
14.4	0.083	14.4	0.114	14.4	0.040
15.6	0.061	15.6	0.085	15.6	0.026
16.8	0.044	16.8	0.062	16.8	0.017
18.0	0.031	18.0	0.044	18.0	0.011
19.2	0.022	19.2	0.031	19.2	0.007
20.4	0.016	20.4	0.022	20.4	0.005
21.6	0.011	21.6	0.016	21.6	0.004
22.8	0.008	22.8	0.011	22.8	0.003
24.0	0.006	24.0	0.008	24.0	0.002
25.2	0.004	25.2	0.006	25.2	0.002
26.4	0.003	26.4	0.004	26.4	0.002
27.6	0.003	27.6	0.003	27.6	0.002
28.8	0.002	28.8	0.003	28.8	0.002
30.0	0.002	30.0	0.002	30.0	0.002
Cl depth (mm)	29		30		24

Initial Cl content= 0.002

Overall fit

Curing	D_a	C_s	r^2
W	2.2E-12	1.0	1.00
P	2.3E-12	1.3	0.99
WD	1.5E-12	1.2	0.99

Individual fit

W	**D_a**	**C_s**	**r^2**
Core 1	2.3E-12	1.0	1.00
Core 2	2.2E-12	0.9	1.00
Core 3	2.0E-12	1.0	1.00
Mean	**2.2E-12**	**1.0**	
SD	1.5E-13	0.05	
CV, %	7	5	

P	**D_a**	**C_s**	**r^2**
Core 1	2.2E-12	1.2	1.00
Core 2	2.0E-12	1.4	1.00
Core 3	2.7E-12	1.2	0.99
Mean	**2.3E-12**	**1.3**	
SD	3.9E-13	0.10	
CV, %	17	8	

WD	**D_a**	**C_s**	**r^2**
Core 1	1.7E-12	1.1	1.00
Core 2	1.3E-12	1.2	1.00
Mean	**1.5E-12**	**1.2**	
SD	2.7E-13	0.08	
CV, %	18	7	

FA(30)-0.5

Bulk diffusion results - Wet cured

1		2		3	
Depth	% Cl	Depth	% Cl	Depth	% Cl
[mm]	[conc.]	[mm]	[conc.]	[mm]	[conc.]
1.0	0.67	1.1	0.60	0.2	0.51
5.5	0.57	5.4	0.59	3.8	0.57
9.4	0.25	9.9	0.36	8.6	0.42
12.4	0.28	14.4	0.21	12.9	0.28
16.1	0.16	18.3	0.09	16.7	0.16
20.3	0.06	21.8	0.05	20.0	0.05
24.3	0.01	25.4	0.01	23.1	0.03

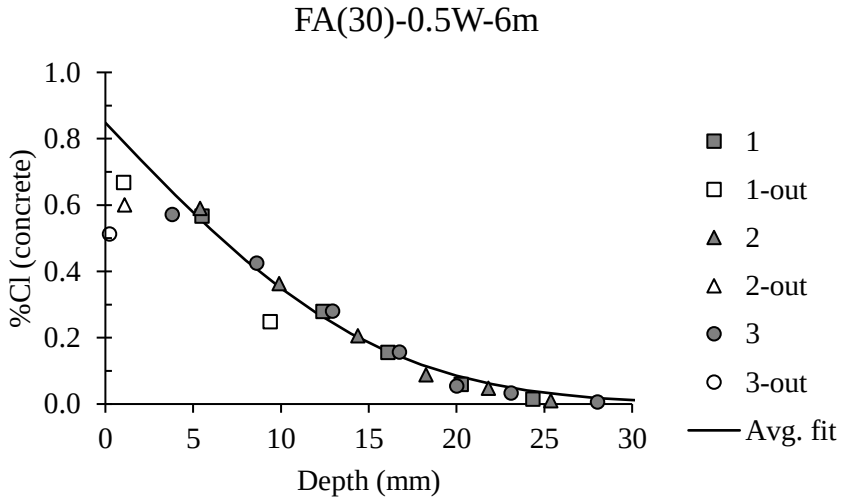

Bulk diffusion results - Plastic cured

1		2		3	
Depth	% Cl	Depth	% Cl	Depth	% Cl
[mm]	[conc.]	[mm]	[conc.]	[mm]	[conc.]
0.2	0.51	1.7	0.64	0.6	0.79
4.0	0.52	6.5	0.39	4.5	0.60
8.7	0.38	10.6	0.31	9.6	0.41
12.8	0.24	14.0	0.16	14.1	0.18
16.9	0.12	17.5	0.12	16.9	0.12
21.4	0.03	21.7	0.04	20.1	0.04

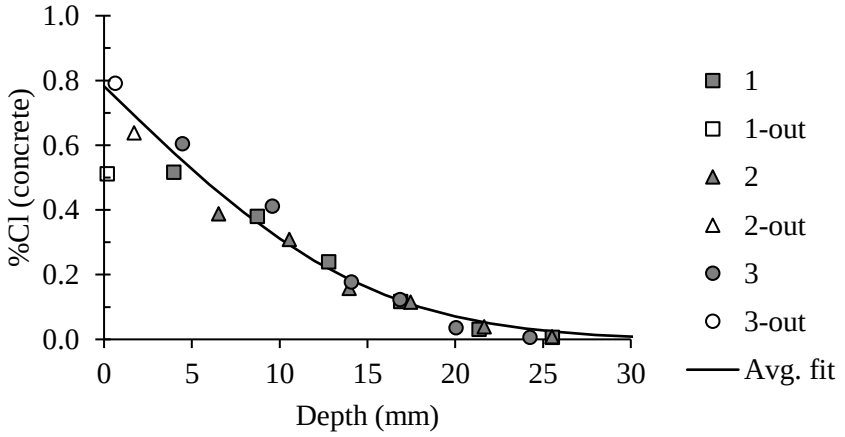

Fitted profiles - overall (FA(30)-0.5)

Wet cured		Plastic cured	
0.0	0.848	0.0	0.782
2.0	0.737	2.0	0.677
4.0	0.63	4.0	0.575
6.0	0.527	6.0	0.478
8.0	0.433	8.0	0.390
10.0	0.349	10.0	0.311
12.0	0.275	12.0	0.242
14.0	0.212	14.0	0.185
16.0	0.16	16.0	0.137
18.0	0.118	18.0	0.100
20.0	0.085	20.0	0.071
22.0	0.06	22.0	0.049
24.0	0.041	24.0	0.033
26.0	0.028	26.0	0.022
28.0	0.018	28.0	0.014
30.0	0.012	30.0	0.009
32.0	0.007	32.0	0.005
34.0	0.004	34.0	0.003
36.0	0.003	36.0	0.002
38.0	0.002	38.0	0.001
40.0	0.001	40.0	0.001
42.0	0	42.0	0.000
44.0	0	44.0	0.000
46.0	0	46.0	0.000
48.0	0	48.0	0.000
50.0	0	50.0	0.000
Cl depth (mm)	42		42

Initial Cl content= 0

Overall fit

Curing	D_a	C_s	r^2
W	4.8E-12	0.8	0.99
P	4.5E-12	0.8	0.96

Individual fit

W	D_a	C_s	r^2
Core 1	4.4E-12	0.9	1.00
Core 2	4.1E-12	0.9	1.00
Core 3	5.4E-12	0.8	0.98
Mean	**4.6E-12**	**0.9**	
SD	6.7E-13	0.08	
CV, %	15	10	

P	D_a	C_s	r^2
Core 1	5.0E-12	0.7	0.98
Core 2	4.9E-12	0.7	0.97
Core 3	4.1E-12	0.9	0.98
Mean	**4.7E-12**	**0.8**	
SD	5.0E-13	0.12	
CV, %	11	16	

FA(30)-0.6

Bulk diffusion results - Wet cured

1		2		3	
Depth	% Cl	Depth	% Cl	Depth	% Cl
[mm]	[conc.]	[mm]	[conc.]	[mm]	[conc.]
0.7	0.48	0.7	0.53	1.7	0.47
4.9	0.53	4.0	0.50	6.0	0.37
9.8	0.38	7.6	0.37	9.8	0.39
14.4	0.22	11.4	0.28	13.8	0.25
18.5	0.09	15.2	0.17	17.6	0.14
22.1	0.04	18.9	0.08	21.5	0.08
25.7	0.01	22.8	0.06	25.3	0.04

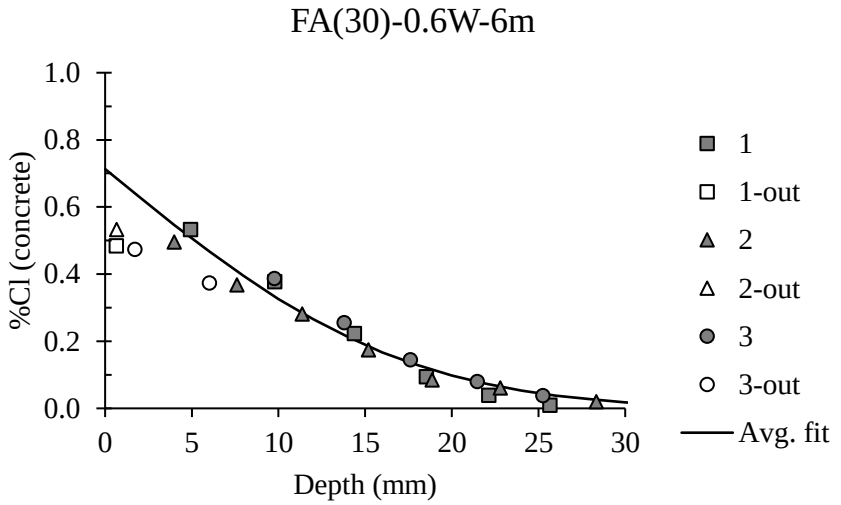

Bulk diffusion results - Plastic cured

1		2		3	
Depth	% Cl	Depth	% Cl	Depth	% Cl
[mm]	[conc.]	[mm]	[conc.]	[mm]	[conc.]
0.7	0.60	1.3	0.45	0.7	0.53
5.1	0.52	5.9	0.49	4.1	0.44
9.5	0.44	10.0	0.49	8.4	0.50
13.4	0.30	14.4	0.35	12.5	0.35
17.1	0.16	22.4	0.15	16.9	0.27
20.5	0.16	27.2	0.08	22.0	0.14

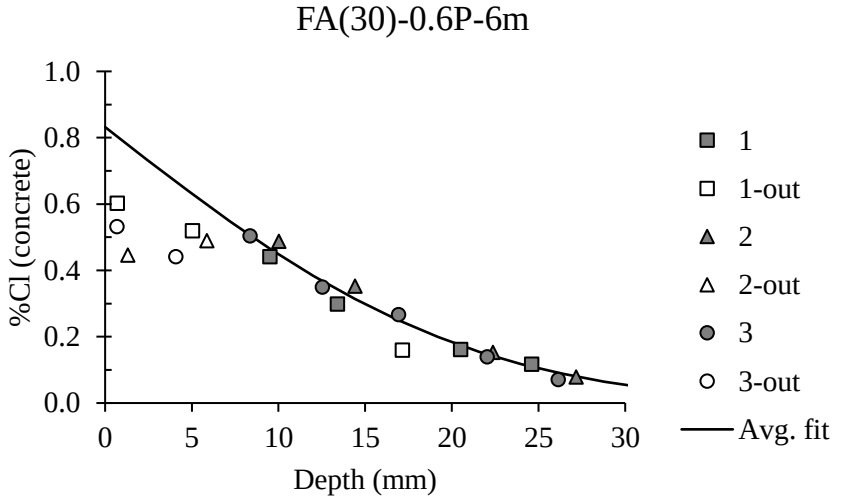

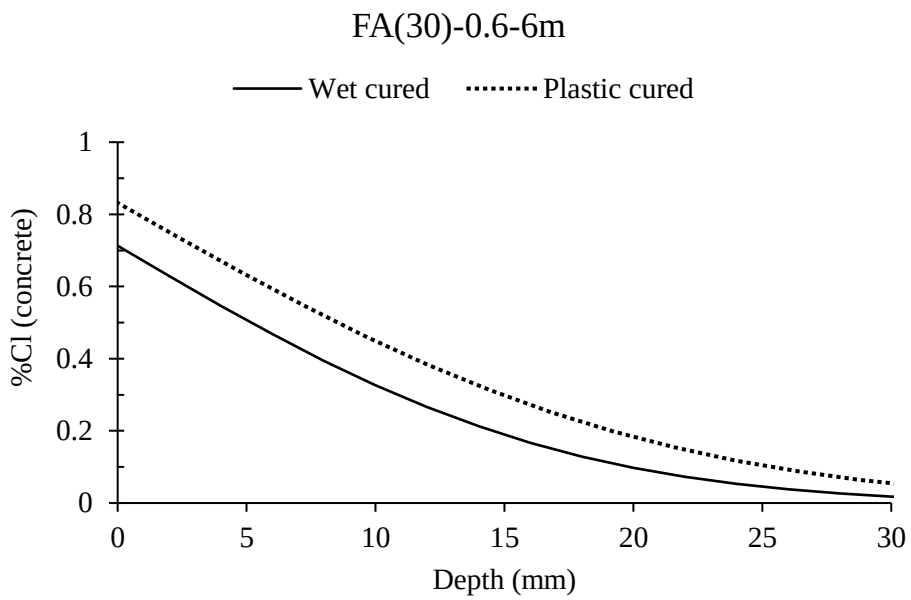
FA(30)-0.6-6m
Wet cured
Plastic cured
%Cl (concrete)
1
0.8
0.6
0.4
0.2
0
0
5
10
15
20
25
30
Depth (mm)

Fitted profiles - overall (FA(30)-0.6)

Wet cured		Plastic cured	
0.0	0.713	0.0	0.832
2.0	0.629	2.4	0.734
4.0	0.546	4.8	0.639
6.0	0.468	7.2	0.548
8.0	0.394	9.6	0.462
10.0	0.326	12.0	0.384
12.0	0.266	14.4	0.314
14.0	0.213	16.8	0.252
16.0	0.167	19.2	0.199
18.0	0.129	21.6	0.154
20.0	0.098	24.0	0.117
22.0	0.073	26.4	0.088
24.0	0.053	28.8	0.064
26.0	0.038	31.2	0.046
28.0	0.027	33.6	0.033
30.0	0.018	36.0	0.023
32.0	0.012	38.4	0.015
34.0	0.008	40.8	0.010
36.0	0.005	43.2	0.007
38.0	0.003	45.6	0.004
40.0	0.002	48.0	0.003
42.0	0.001	50.4	0.002
44.0	0.001	52.8	0.001
46.0	0	55.2	0.001
48.0	0	57.6	0.000
50.0	0	60.0	0.000
Cl depth (mm)	46		58

Initial Cl content= 0

Overall fit

Curing	D_a	C_s	r^2
W	5.8E-12	0.7	0.97
P	8.5E-12	0.8	0.98

Individual fit

W	D_a	C_s	r^2
Core 1	5.1E-12	0.8	0.99
Core 2	5.9E-12	0.7	0.99
Core 3	5.2E-12	0.9	1.00
Mean	**5.4E-12**	**0.8**	
SD	4.3E-13	0.12	
CV, %	8	15	

P	D_a	C_s	r^2
Core 1	9.0E-12	0.8	0.99
Core 2	8.4E-12	0.9	1.00
Core 3	8.2E-12	0.8	0.99
Mean	**8.5E-12**	**0.8**	
SD	4.0E-13	0.08	
CV, %	5	10	

BS(25)-0.4

Bulk diffusion results - Wet cured

1		2		3	
Depth	% Cl	Depth	% Cl	Depth	% Cl
[mm]	[conc.]	[mm]	[conc.]	[mm]	[conc.]
1.4	0.90	0.5	0.94	1.0	1.00
6.0	0.51	4.0	0.80	4.2	0.61
9.4	0.17	8.1	0.33	7.7	0.36
12.6	0.08	11.9	0.10	11.9	0.10
17.0	0.01	15.9	0.01	15.5	0.01
21.6	0.01	19.6	0.01	19.6	0.00
26.3	0.01	23.2	0.00	24.7	0.00

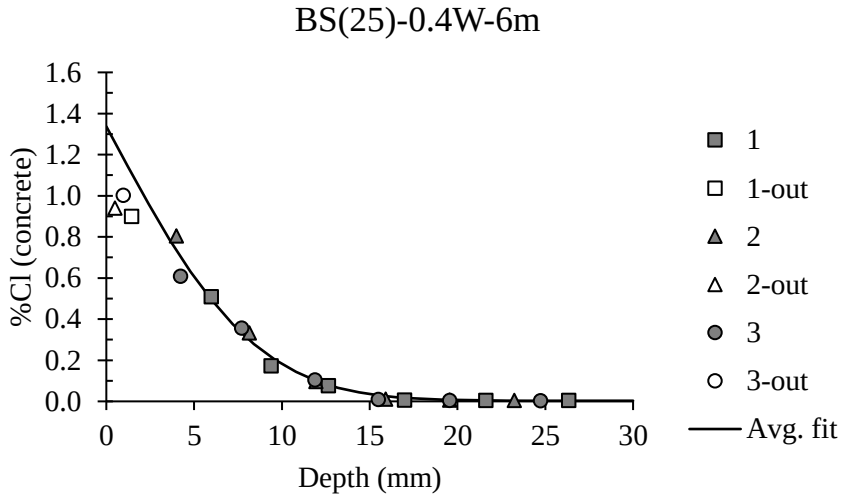

Bulk diffusion results - Plastic cured

1		2		3	
Depth	% Cl	Depth	% Cl	Depth	% Cl
[mm]	[conc.]	[mm]	[conc.]	[mm]	[conc.]
0.5	0.63	0.6	0.84	1.5	0.71
4.4	0.67	4.1	0.82	5.8	0.48
9.1	0.25	8.0	0.37	9.5	0.20
12.9	0.09	12.3	0.08	13.5	0.04
16.7	0.01	16.9	0.01	17.9	0.01
21.6	0.01	21.2	0.00	22.3	0.01

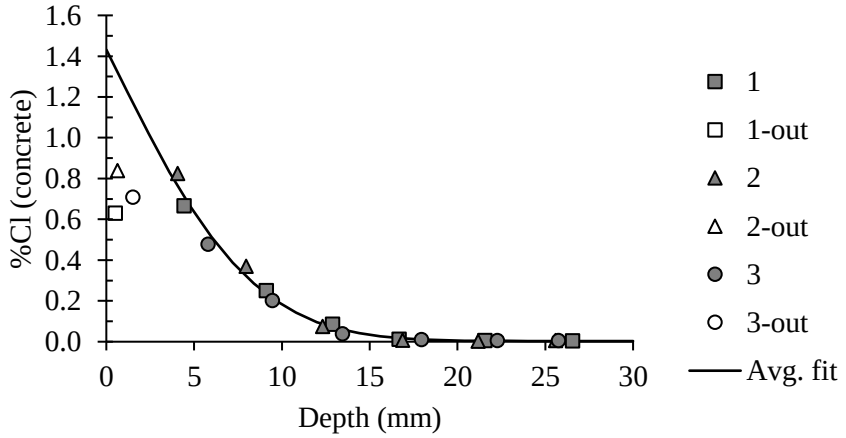

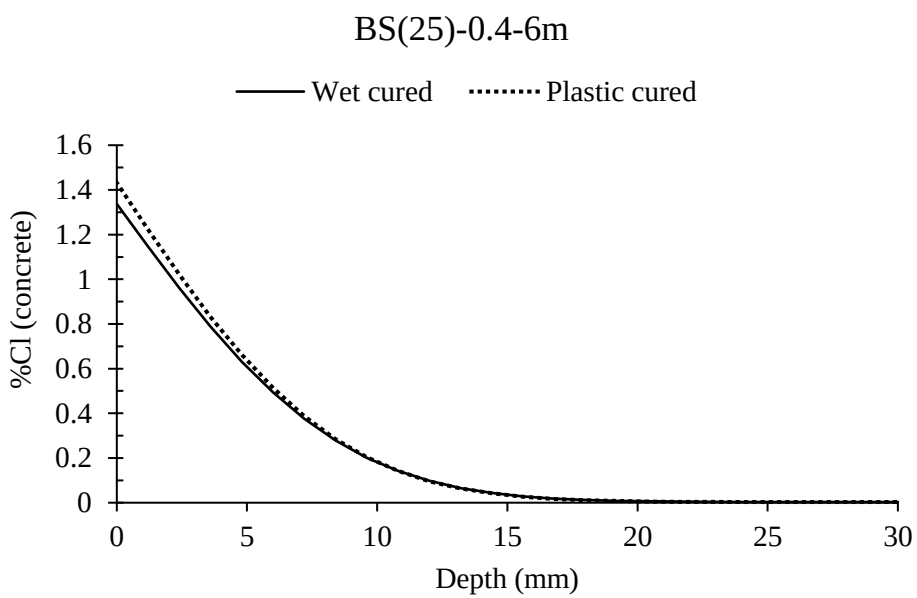
BS(25)-0.4-6m
Wet cured
Plastic cured
%Cl (concrete)
1.6
1.4
1.2
1
0.8
0.6
0.4
0.2
0
0
5
10
15
20
25
30
Depth (mm)

Fitted profiles - overall (BS(25)-0.4)

Wet cured		Plastic cured	
0.0	1.337	0.0	1.432
1.2	1.146	1.2	1.223
2.4	0.961	2.4	1.021
3.6	0.788	3.6	0.832
4.8	0.631	4.8	0.662
6.0	0.493	6.0	0.513
7.2	0.376	7.2	0.387
8.4	0.279	8.4	0.285
9.6	0.202	9.6	0.204
10.8	0.143	10.8	0.142
12.0	0.098	12.0	0.096
13.2	0.066	13.2	0.064
14.4	0.044	14.4	0.042
15.6	0.028	15.6	0.027
16.8	0.018	16.8	0.017
18.0	0.012	18.0	0.011
19.2	0.008	19.2	0.008
20.4	0.006	20.4	0.005
21.6	0.005	21.6	0.004
22.8	0.004	22.8	0.004
24.0	0.003	24.0	0.003
25.2	0.003	25.2	0.003
26.4	0.003	26.4	0.003
27.6	0.003	27.6	0.003
28.8	0.003	28.8	0.003
30.0	0.003	30.0	0.003
Cl depth (mm)	24		24

Initial Cl content= 0.003

Overall fit

Curing	D_a	C_s	r^2
W	1.4E-12	1.3	0.98
P	1.4E-12	1.4	0.99

Individual fit

W	D_a	C_s	r^2
Core 1	1.1E-12	1.6	1.00
Core 2	1.4E-12	1.5	1.00
Core 3	1.7E-12	1.1	0.99
Mean	**1.4E-12**	**1.4**	
SD	3.0E-13	0.26	
CV, %	21	19	

P	D_a	C_s	r^2
Core 1	1.6E-12	1.3	1.00
Core 2	1.4E-12	1.5	1.00
Core 3	1.4E-12	1.3	1.00
Mean	**1.5E-12**	**1.4**	
SD	1.1E-13	0.16	
CV, %	7	12	

BS(25)-0.5

Bulk diffusion results - Wet cured

1		2		3	
Depth	% Cl	Depth	% Cl	Depth	% Cl
[mm]	[conc.]	[mm]	[conc.]	[mm]	[conc.]
1.3	0.83	0.9	0.57	1.1	0.82
5.2	0.47	5.3	0.53	5.6	0.53
9.2	0.34	10.4	0.21	10.3	0.30
13.9	0.13	15.5	0.07	15.3	0.09
18.0	0.03	20.0	0.01	20.2	0.02
21.7	0.01	23.5	0.00	24.7	0.00
0.0	0.00	0.0	0.00	29.8	0.00

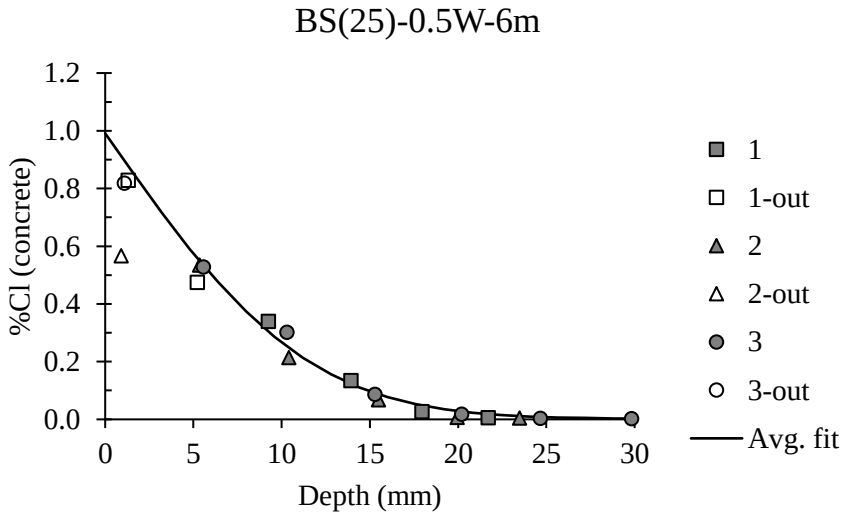

Bulk diffusion results - Plastic cured

1		2		3	
Depth	% Cl	Depth	% Cl	Depth	% Cl
[mm]	[conc.]	[mm]	[conc.]	[mm]	[conc.]
1.7	0.72	1.5	0.79	0.7	0.84
6.9	0.47	6.2	0.65	4.7	0.63
11.7	0.23	10.2	0.24	8.5	0.33
16.4	0.07	13.8	0.14	11.9	0.22
24.1	0.00	17.6	0.05	16.5	0.06
29.8	0.00	22.2	0.01	21.7	0.01

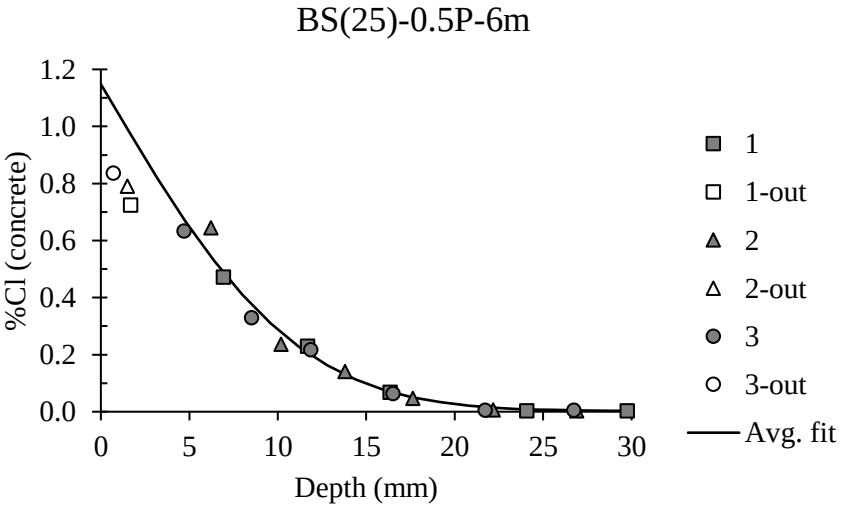

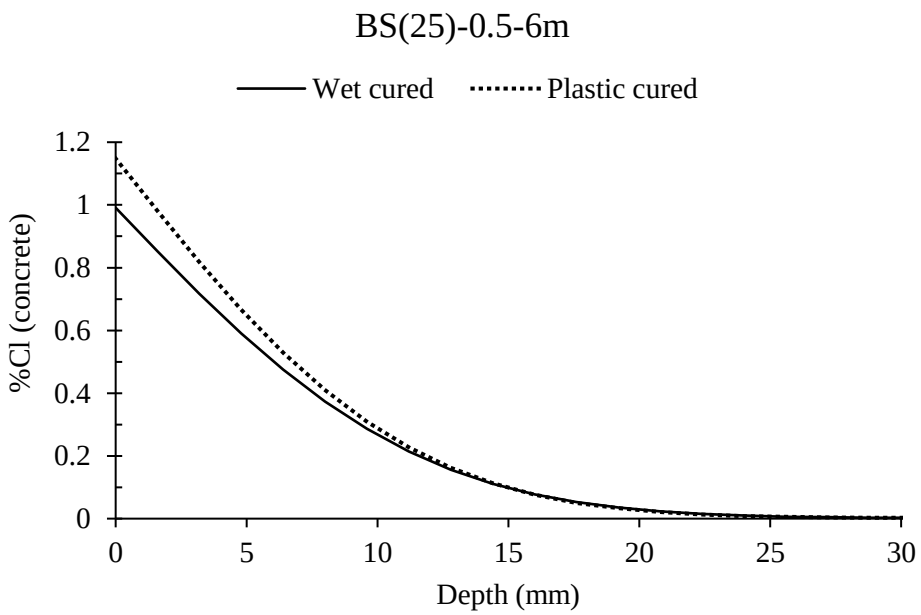
BS(25)-0.5-6m
Wet cured
Plastic cured
%Cl (concrete)
1.2
1
0.8
0.6
0.4
0.2
0
0
5
10
15
20
25
30
Depth (mm)

Fitted profiles - overall (BS(25)-0.5)

Wet cured		Plastic cured	
0.0	0.991	0.0	1.148
1.6	0.852	1.6	0.980
3.2	0.717	3.2	0.818
4.8	0.59	4.8	0.666
6.4	0.475	6.4	0.529
8.0	0.373	8.0	0.410
9.6	0.286	9.6	0.309
11.2	0.214	11.2	0.227
12.8	0.156	12.8	0.162
14.4	0.111	14.4	0.113
16.0	0.077	16.0	0.076
17.6	0.053	17.6	0.050
19.2	0.035	19.2	0.033
20.8	0.023	20.8	0.021
22.4	0.015	22.4	0.013
24.0	0.01	24.0	0.008
25.6	0.006	25.6	0.006
27.2	0.005	27.2	0.004
28.8	0.003	28.8	0.003
30.4	0.003	30.4	0.003
32.0	0.002	32.0	0.002
33.6	0.002	33.6	0.002
35.2	0.002	35.2	0.002
36.8	0.002	36.8	0.002
38.4	0.002	38.4	0.002
40.0	0.002	40.0	0.002
Cl depth (mm)	32		32

Initial Cl content= 0.002

Overall fit

Curing	D_a	C_s	r^2
W	2.6E-12	1.0	0.99
P	2.4E-12	1.1	0.98

Individual fit

W	D_a	C_s	r^2
Core 1	2.2E-12	1.3	0.99
Core 2	2.2E-12	1.0	1.00
Core 3	2.9E-12	1.0	0.99
Mean	**2.4E-12**	**1.1**	
SD	4.2E-13	0.17	
CV, %	17	15	

P	D_a	C_s	r^2
Core 1	2.7E-12	1.1	1.00
Core 2	1.8E-12	1.6	0.99
Core 3	2.5E-12	1.1	1.00
Mean	**2.4E-12**	**1.2**	
SD	4.7E-13	0.29	
CV, %	20	24	

BS(25)-0.6

Bulk diffusion results - Wet cured

1		2		3	
Depth	% Cl	Depth	% Cl	Depth	% Cl
[mm]	[conc.]	[mm]	[conc.]	[mm]	[conc.]
1.2	0.66	1.5	0.81	1.6	0.63
6.1	0.49	5.8	0.44	6.1	0.38
11.1	0.26	9.6	0.33	10.1	0.28
16.0	0.11	13.2	0.16	14.3	0.13
21.0	0.02	17.4	0.06	19.0	0.04
25.5	0.005	22.5	0.01	23.6	0.004

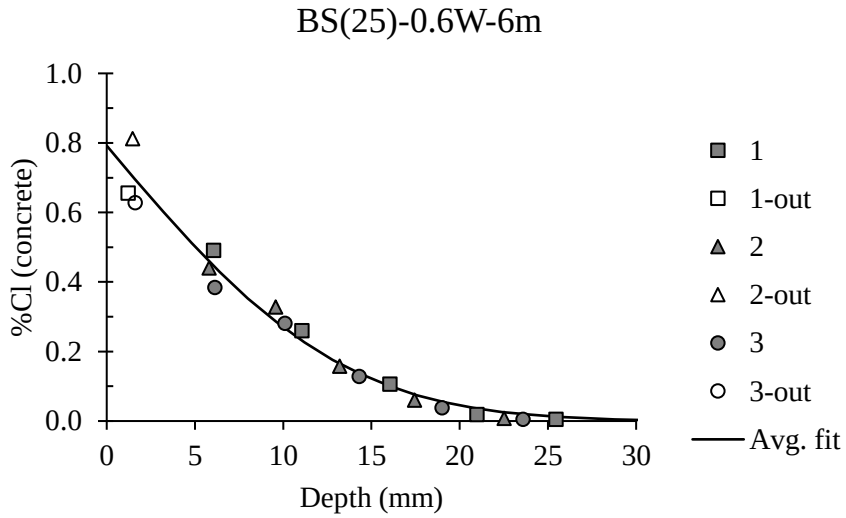

Bulk diffusion results - Plastic cured

1		2		3	
Depth	% Cl	Depth	% Cl	Depth	% Cl
[mm]	[conc.]	[mm]	[conc.]	[mm]	[conc.]
1.1	0.87	1.7	0.85	1.6	0.84
5.4	0.69	6.7	0.52	6.5	0.47
9.8	0.39	11.1	0.25	11.3	0.29
14.2	0.20	15.4	0.15	15.8	0.13
18.6	0.07	20.2	0.05	20.1	0.06
23.2	0.01	25.1	0.01	24.6	0.01

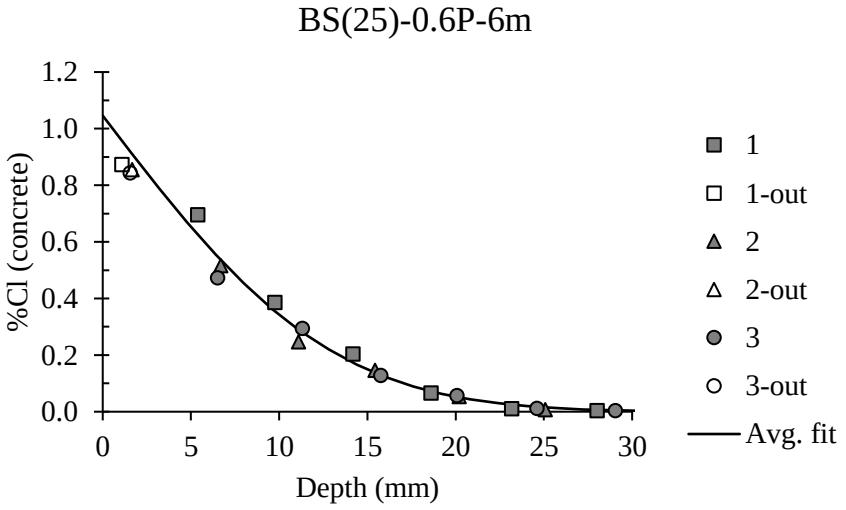

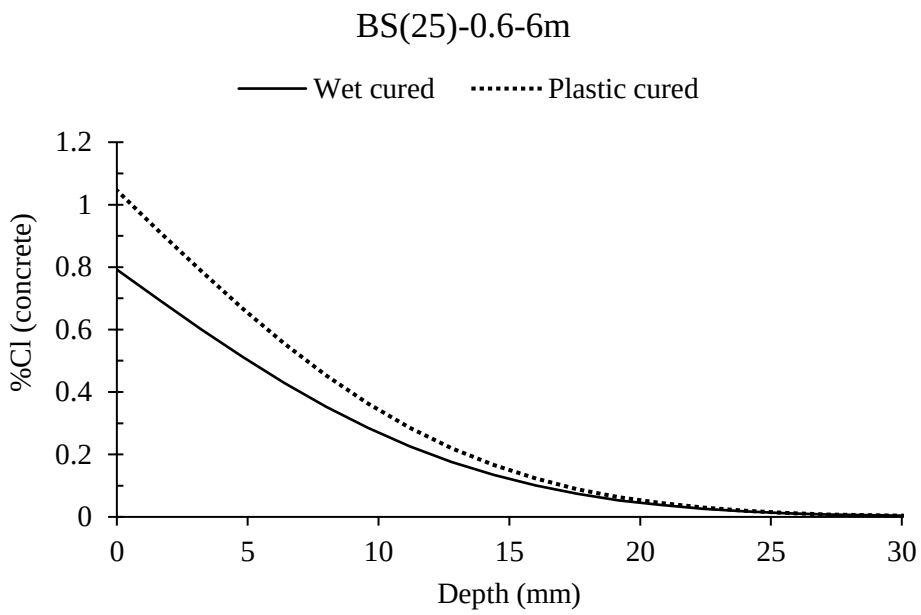
BS(25)-0.6-6m
Wet cured
Plastic cured
%Cl (concrete)
1.2
1
0.8
0.6
0.4
0.2
0
0
5
10
15
20
25
30
Depth (mm)

Fitted profiles - overall

Wet cured		Plastic cured	
0.0	0.792	0.0	1.046
1.6	0.696	1.6	0.916
3.2	0.602	3.2	0.789
4.8	0.513	4.8	0.668
6.4	0.429	6.4	0.555
8.0	0.353	8.0	0.453
9.6	0.285	9.6	0.363
11.2	0.226	11.2	0.285
12.8	0.176	12.8	0.220
14.4	0.135	14.4	0.166
16.0	0.101	16.0	0.123
17.6	0.074	17.6	0.089
19.2	0.053	19.2	0.063
20.8	0.038	20.8	0.044
22.4	0.026	22.4	0.030
24.0	0.018	24.0	0.020
25.6	0.012	25.6	0.013
27.2	0.008	27.2	0.008
28.8	0.005	28.8	0.005
30.4	0.003	30.4	0.003
32.0	0.002	32.0	0.002
33.6	0.001	33.6	0.001
35.2	0.001	35.2	0.001
36.8	0	36.8	0.000
38.4	0	38.4	0.000
40.0	0	40.0	0.000
Cl depth (mm)	37		37

Initial Cl content= 0

Overall fit

Curing	D_a	C_s	r^2
W	3.5E-12	0.8	0.98
P	3.4E-12	1.0	0.98

Individual fit

W	D_a	C_s	r^2
Core 1	3.3E-12	0.9	1.00
Core 2	3.6E-12	0.8	0.98
Core 3	3.8E-12	0.7	0.98
Mean	**3.6E-12**	**0.8**	
SD	2.4E-13	0.10	
CV, %	7	13	

P	D_a	C_s	r^2
Core 1	3.3E-12	1.2	1.00
Core 2	3.3E-12	1.0	0.99
Core 3	4.1E-12	0.9	0.99
Mean	**3.5E-12**	**1.0**	
SD	4.6E-13	0.16	
CV, %	13	16	

BS(50)-0.4

Bulk diffusion results - Wet cured

1		2		3	
Depth	% Cl	Depth	% Cl	Depth	% Cl
[mm]	[conc.]	[mm]	[conc.]	[mm]	[conc.]
1.8	0.81	2.1	0.78	1.2	0.75
6.6	0.24	7.5	0.22	5.6	0.40
10.7	0.03	12.0	0.03	10.1	0.05
15.0	0.01	16.5	0.01	14.5	0.01
19.5	0.01	21.1	0.01	19.1	0.01
24.3	0.01	25.4	0.01	24.0	0.01

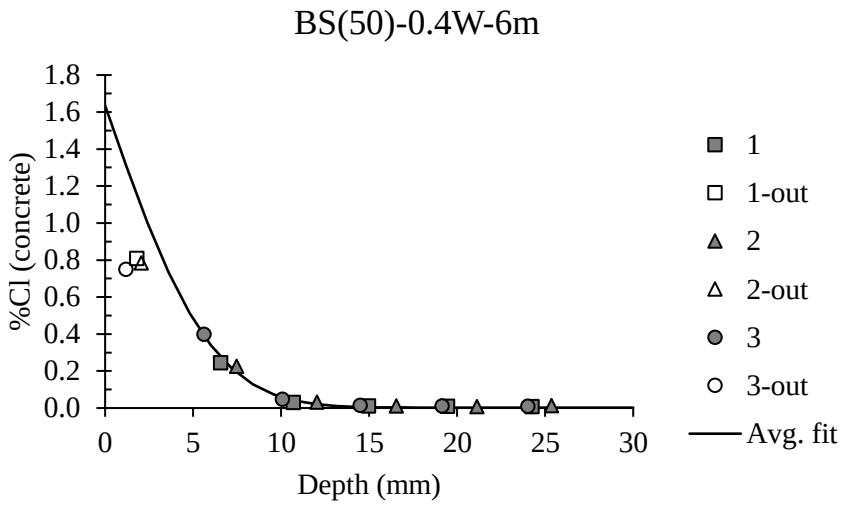

Bulk diffusion results - Plastic cured

1		2		3	
Depth	% Cl	Depth	% Cl	Depth	% Cl
[mm]	[conc.]	[mm]	[conc.]	[mm]	[conc.]
1.3	0.68	0.9	0.72	1.2	0.76
6.0	0.39	5.2	0.51	5.8	0.40
10.6	0.05	10.1	0.07	10.2	0.07
14.9	0.01	15.2	0.00	19.3	0.01
19.7	0.01	20.4	0.01	--	--

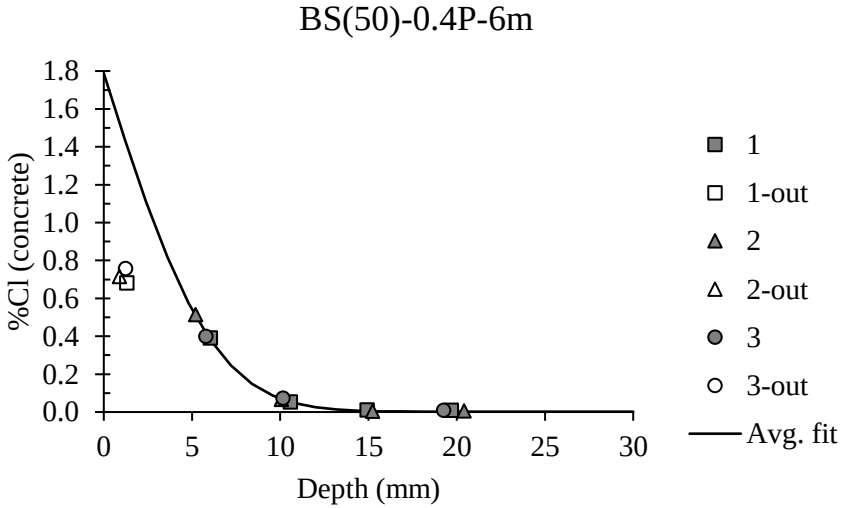

Bulk diffusion results - Wet-dry

1		2		3	
Depth	% Cl	Depth	% Cl	Depth	% Cl
[mm]	[conc.]	[mm]	[conc.]	[mm]	[conc.]
2.4	0.744	1.8	0.773	--	--
7.2	0.130	7.2	0.431	--	--
15.1	0.014	12.0	0.097	--	--
19.1	0.014	16.4	0.025	--	--
23.9	0.009	21.0	0.012	--	--
--	--	25.8	0.008	--	--

*Few data points and high scatter resulted in a poor fit. As a result, the data was discarded.

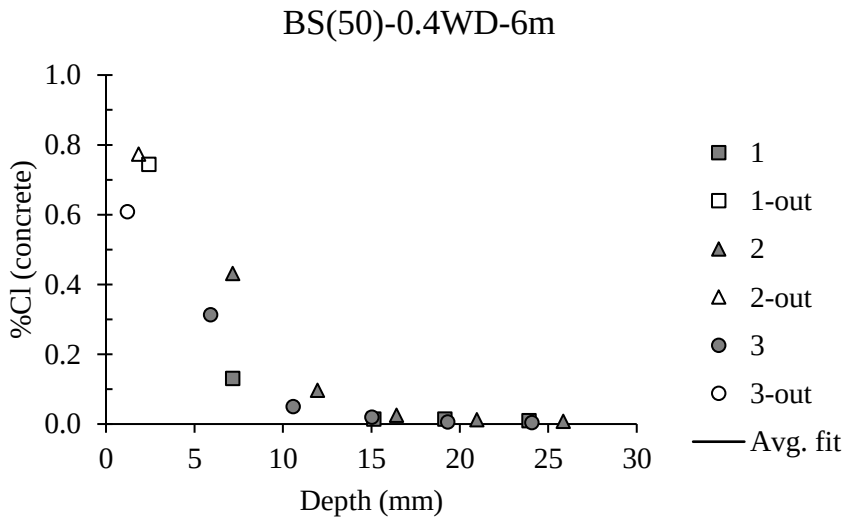

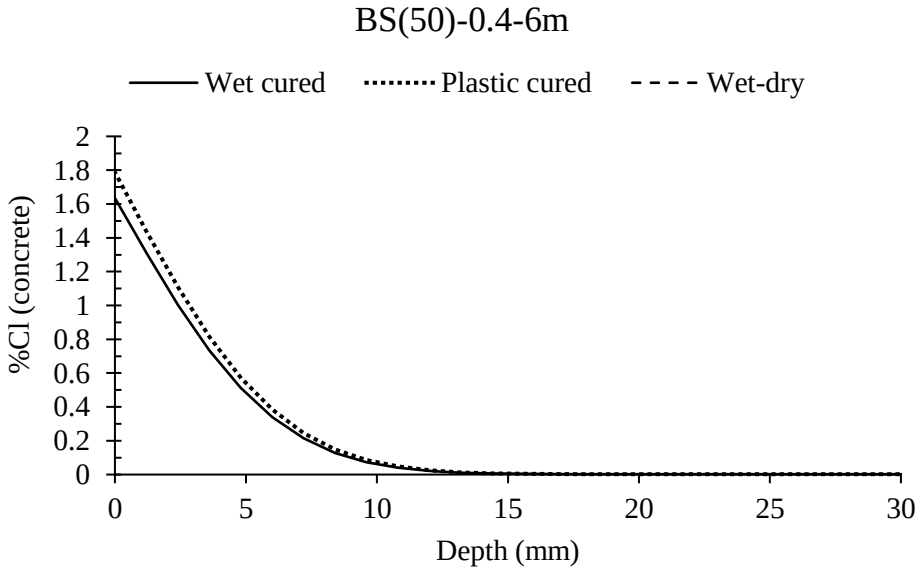

Fitted profiles - overall (BS(50)-0.4)

Wet cured		Plastic cured	
0.0	1.635	0.0	1.788
1.2	1.31	1.2	1.438
2.4	1.004	2.4	1.109
3.6	0.735	3.6	0.817
4.8	0.513	4.8	0.575
6.0	0.34	6.0	0.385
7.2	0.214	7.2	0.246
8.4	0.128	8.4	0.149
9.6	0.073	9.6	0.086
10.8	0.04	10.8	0.048
12.0	0.021	12.0	0.025
13.2	0.011	13.2	0.013
14.4	0.006	14.4	0.007
15.6	0.004	15.6	0.004
16.8	0.003	16.8	0.003
18.0	0.002	18.0	0.002
19.2	0.002	19.2	0.002
20.4	0.002	20.4	0.002
21.6	0.002	21.6	0.002
22.8	0.002	22.8	0.002
24.0	0.002	24.0	0.002
25.2	0.002	25.2	0.002
26.4	0.002	26.4	0.002
27.6	0.002	27.6	0.002
28.8	0.002	28.8	0.002
30.0	0.002	30.0	0.002
Cl depth (mm)	18		18
Initial Cl content=			0.002

Overall fit

Curing	D_a	C_s	r^2
W	7.3E-13	1.6	0.99
P	7.5E-13	1.8	1.00

Individual fit

*Curve-fitting was not possible for individual data set due to few data points

BS(50)-0.5

Bulk diffusion results - Wet cured

1		2		3	
Depth	% Cl	Depth	% Cl	Depth	% Cl
[mm]	[conc.]	[mm]	[conc.]	[mm]	[conc.]
0.8	0.61	2.0	0.91	1.0	0.49
5.2	0.57	6.5	0.50	5.6	0.50
10.4	0.14	10.4	0.14	10.5	0.14
14.5	0.03	15.1	0.01	15.3	0.02
18.4	0.01	20.3	0.00	20.1	0.01
23.0	0.01	25.1	0.00	25.0	0.00
27.5	0.00	29.6	0.00	29.9	0.00

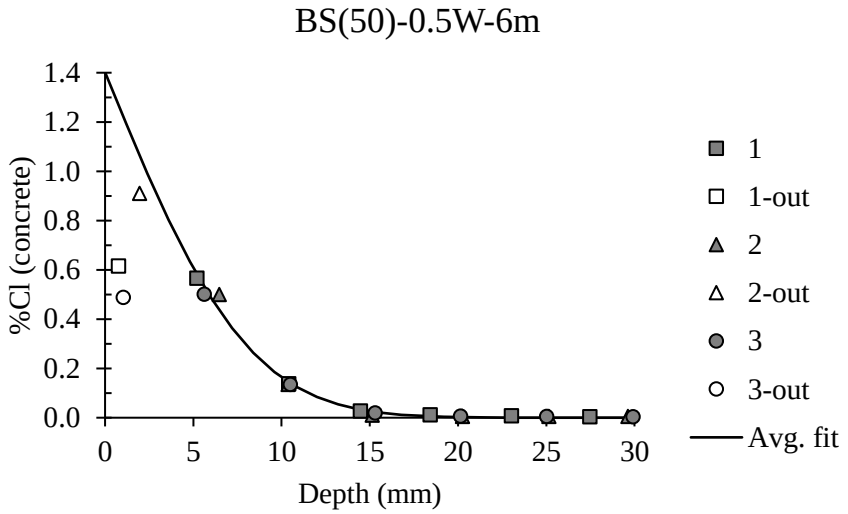

Bulk diffusion results - Plastic cured

1		2		3	
Depth	% Cl	Depth	% Cl	Depth	% Cl
[mm]	[conc.]	[mm]	[conc.]	[mm]	[conc.]
1.9	0.60	1.4	0.66	1.2	0.58
7.0	0.40	6.3	0.49	5.5	0.52
11.5	0.15	11.0	0.13	9.8	0.18
20.5	0.01	15.6	0.02	14.0	0.01
25.6	0.01	20.6	0.01	18.4	0.01
31.0	0.01	25.6	0.01	22.2	0.01

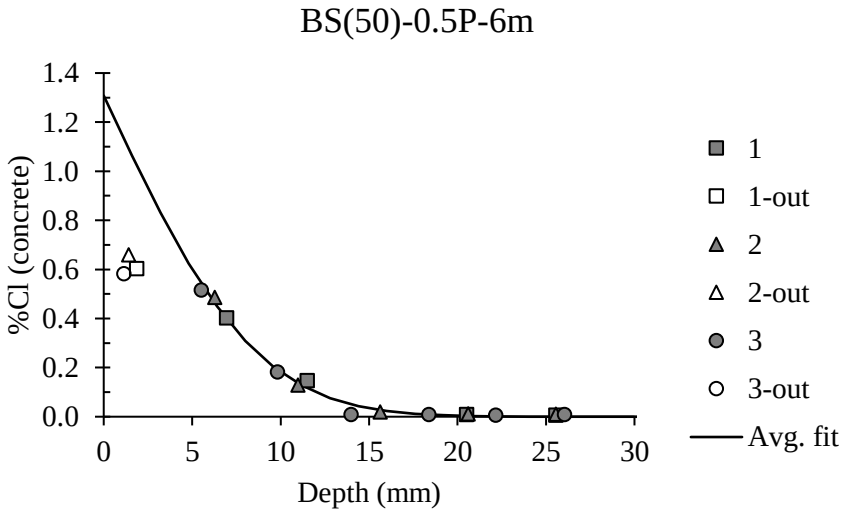

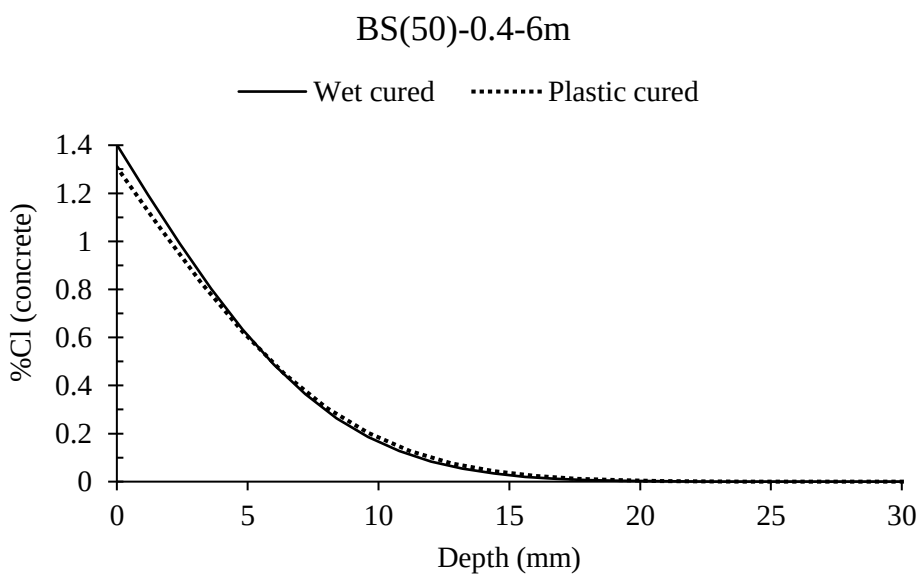
BS(50)-0.4-6m
Wet cured
Plastic cured
%Cl (concrete)
1.4
1.2
1
0.8
0.6
0.4
0.2
0
0
5
10
15
20
25
30
Depth (mm)

Fitted profiles - overall (BS(50)-0.5)

Wet cured		Plastic cured	
0.0	1.402	0.0	1.308
1.2	1.193	1.6	1.063
2.4	0.991	3.2	0.831
3.6	0.803	4.8	0.624
4.8	0.634	6.4	0.449
6.0	0.487	8.0	0.309
7.2	0.364	9.6	0.203
8.4	0.264	11.2	0.127
9.6	0.186	12.8	0.076
10.8	0.127	14.4	0.043
12.0	0.084	16.0	0.023
13.2	0.054	17.6	0.012
14.4	0.034	19.2	0.006
15.6	0.02	20.8	0.003
16.8	0.012	22.4	0.001
18.0	0.007	24.0	0.000
19.2	0.004	25.6	0.000
20.4	0.002	27.2	0.000
21.6	0.001	28.8	0.000
22.8	0	30.4	0.000
24.0	0	32.0	0.000
25.2	0	33.6	0.000
26.4	0	35.2	0.000
27.6	0	36.8	0.000
28.8	0	38.4	0.000
30.0	0	40.0	0.000
Cl depth (mm)	23		24

Initial Cl content= 0

Overall fit

Curing	D_a	C_s	r^2
W	1.3E-12	1.4	0.99
P	1.5E-12	1.3	0.99

Individual fit

W	D_a	C_s	r^2
Core 1	1.3E-12	1.4	1.00
Core 2	1.0E-12	2.0	1.00
Core 3	1.3E-12	1.3	1.00
Mean	**1.2E-12**	**1.6**	
SD	1.5E-13	0.35	
CV, %	13	22	

P	D_a	C_s	r^2
Core 1	1.9E-12	1.1	1.00
Core 2	1.3E-12	1.5	1.00
Core 3	1.3E-12	1.3	0.99
Mean	**1.5E-12**	**1.3**	
SD	3.3E-13	0.19	
CV, %	22	14	

BS(50)-0.6

Bulk diffusion results - Wet cured

1		2		3	
Depth	% Cl	Depth	% Cl	Depth	% Cl
[mm]	[conc.]	[mm]	[conc.]	[mm]	[conc.]
0.7	0.68	1.2	0.59	1.0	0.63
5.3	0.52	5.6	0.45	5.3	0.53
10.2	0.22	9.6	0.25	9.5	0.25
14.5	0.05	13.6	0.08	13.3	0.07
19.0	0.01	18.0	0.02	17.0	0.02
23.2	0.01	22.1	0.01	20.7	0.01
27.2	0.01	26.6	0.01	24.0	0.01

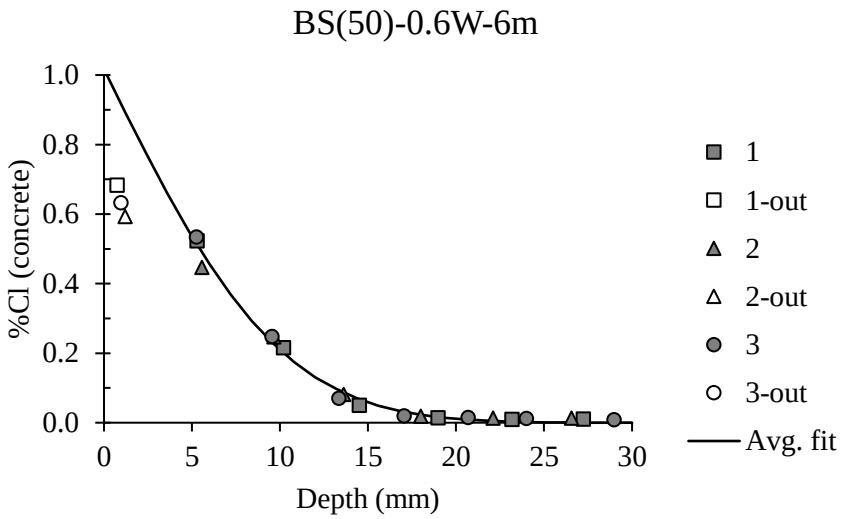

Bulk diffusion results - Plastic cured

1		2		3	
Depth	% Cl	Depth	% Cl	Depth	% Cl
[mm]	[conc.]	[mm]	[conc.]	[mm]	[conc.]
0.4	0.64	1.1	0.65	3.6	0.56
3.6	0.60	5.1	0.55	7.5	0.28
7.5	0.38	9.2	0.26	10.8	0.13
11.9	0.17	13.1	0.12	14.1	0.06
16.1	0.05	17.0	0.04	17.8	0.02
19.9	0.01	21.6	0.01	22.7	0.01

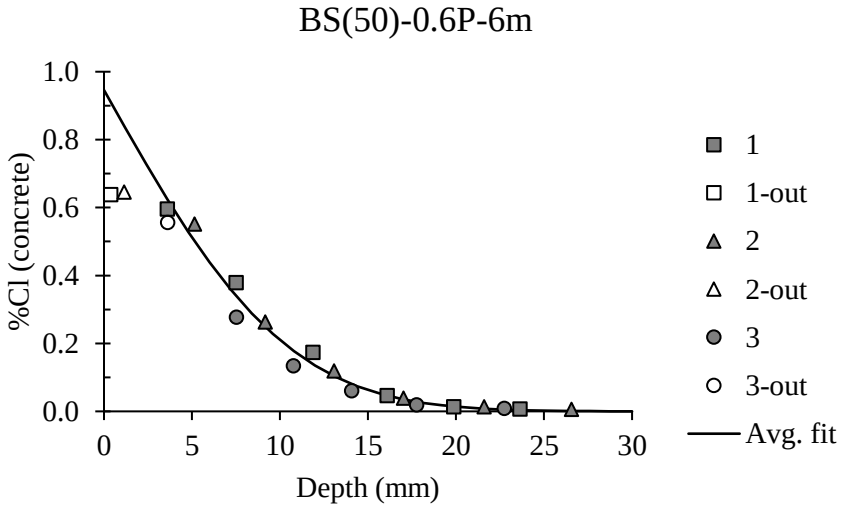

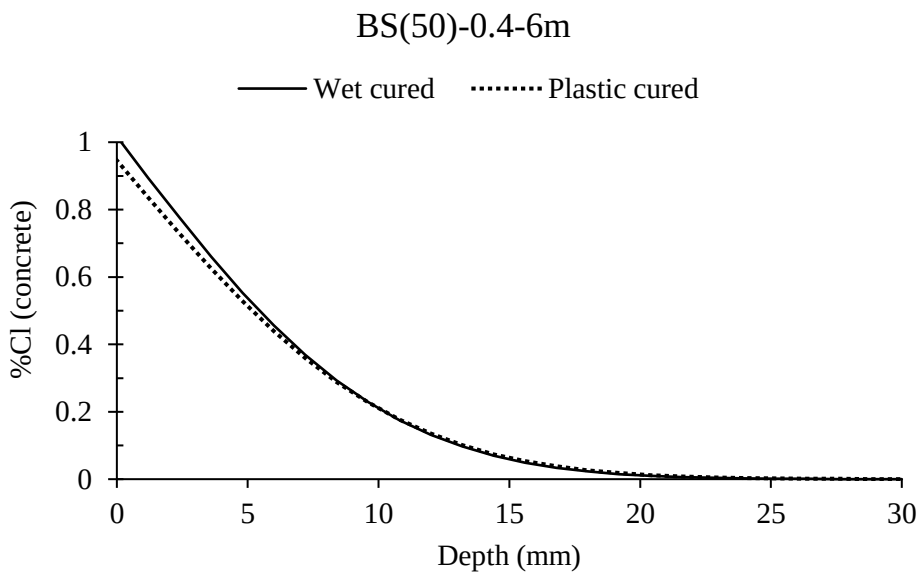
BS(50)-0.4-6m
Wet cured
Plastic cured
%Cl (concrete)
1
0.8
0.6
0.4
0.2
0
0
5
10
15
20
25
30
Depth (mm)

Fitted profiles - overall (BS(50)-0.5)

Wet cured		Plastic cured	
0.0	1.017	0.0	0.946
1.2	0.894	1.2	0.836
2.4	0.775	2.4	0.728
3.6	0.66	3.6	0.625
4.8	0.553	4.8	0.528
6.0	0.456	6.0	0.439
7.2	0.369	7.2	0.359
8.4	0.293	8.4	0.288
9.6	0.229	9.6	0.228
10.8	0.175	10.8	0.177
12.0	0.131	12.0	0.135
13.2	0.097	13.2	0.101
14.4	0.07	14.4	0.074
15.6	0.049	15.6	0.054
16.8	0.034	16.8	0.038
18.0	0.023	18.0	0.026
19.2	0.015	19.2	0.018
20.4	0.01	20.4	0.012
21.6	0.006	21.6	0.008
22.8	0.004	22.8	0.005
24.0	0.002	24.0	0.003
25.2	0.001	25.2	0.002
26.4	0.001	26.4	0.001
27.6	0	27.6	0.001
28.8	0	28.8	0.000
30.0	0	30.0	0.000
Cl depth (mm)	28		29

Initial Cl content= 0.004

Overall fit

Curing	D_a	C_s	r^2
W	2.0E-12	1.0	0.99
P	2.2E-12	0.9	0.98

Individual fit

W	D_a	C_s	r^2
Core 1	2.0E-12	1.1	1.00
Core 2	2.3E-12	0.9	0.99
Core 3	1.9E-12	1.1	1.00
Mean	**2.0E-12**	**1.0**	
SD	2.4E-13	0.11	
CV, %	12	11	

P	D_a	C_s	r^2
Core 1	2.7E-12	0.9	1.00
Core 2	2.1E-12	1.0	1.00
Core 3	1.9E-12	0.8	1.00
Mean	**2.2E-12**	**0.9**	
SD	3.8E-13	0.11	
CV, %	17	12	

BS(75)-0.4

Bulk diffusion results - Wet cured

1		2		3	
Depth	% Cl	Depth	% Cl	Depth	% Cl
[mm]	[conc.]	[mm]	[conc.]	[mm]	[conc.]
1.9	0.67	1.4	0.79	1.0	0.66
7.0	0.17	5.6	0.29	5.6	0.31
11.4	0.08	9.6	0.10	10.6	0.08
15.7	0.05	14.6	0.05	15.3	0.04
20.8	0.02	20.3	0.03	20.4	0.03
0.0	0.00	0.0	0.00	0.0	0.00
0.0	0.00	0.0	0.00	0.0	0.00

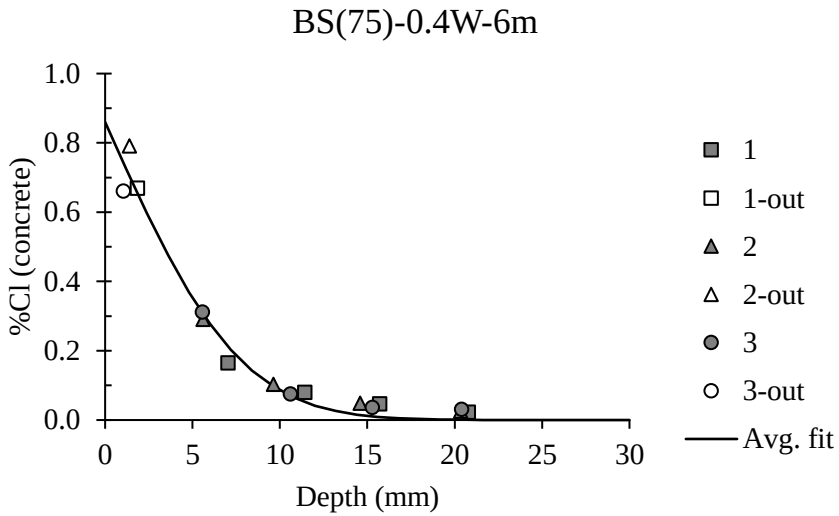

Bulk diffusion results - Plastic cured

1		2		3	
Depth	% Cl	Depth	% Cl	Depth	% Cl
[mm]	[conc.]	[mm]	[conc.]	[mm]	[conc.]
1.3	0.53	1.5	0.69	1.5	0.53
5.4	0.31	6.2	0.24	6.2	0.25
9.2	0.07	10.3	0.09	10.8	0.10
13.2	0.03	14.1	0.04	15.8	0.04
17.6	0.03	19.1	0.04	20.8	0.04
22.7	0.03	25.2	0.03	0.0	0.00

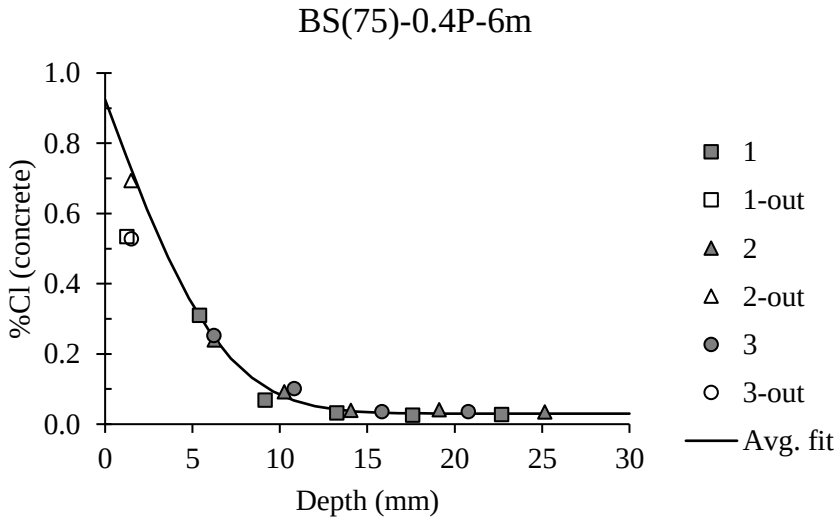

Bulk diffusion results - Wet-dry

1		2	
Depth [mm]	% Cl [conc.]	Depth [mm]	% Cl [conc.]
2.0	0.592	1.3	0.673
6.8	0.203	6.1	0.194
10.9	0.079	11.2	0.065
16.0	0.033	15.9	0.050
21.3	0.027	20.4	0.011
26.6	0.041	25.4	0.017

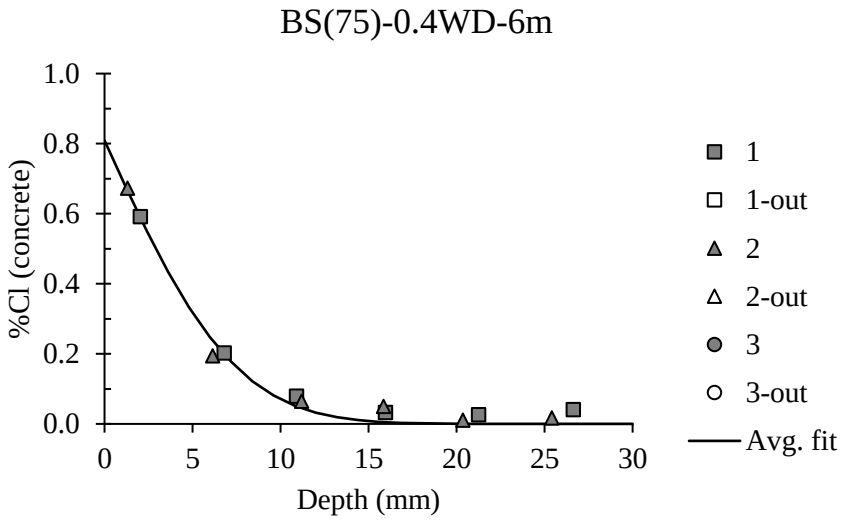

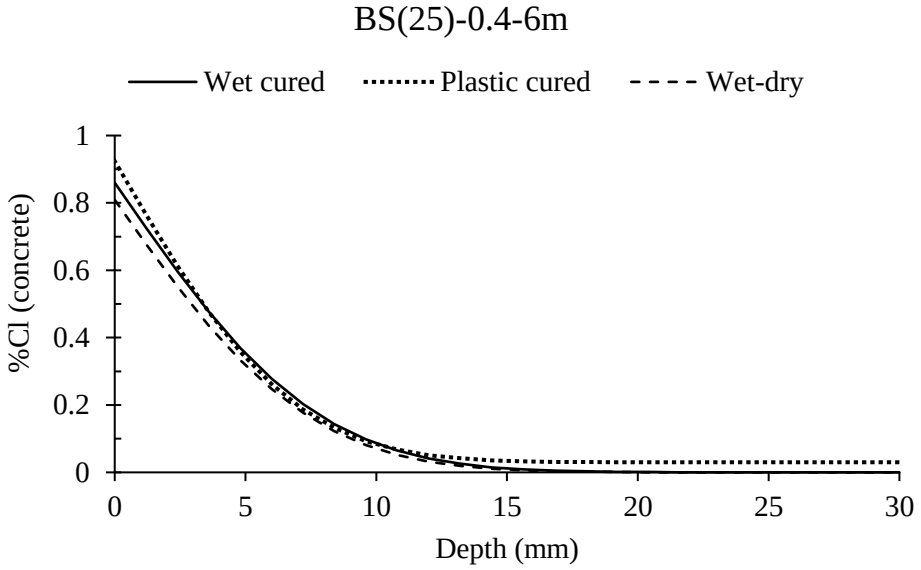

Fitted profiles - overall (BS(75)-0.4)

Wet cured		Plastic cured		Wet-dry	
0.0	0.86	0.0	0.924	0.0	0.8
1.2	0.725	1.2	0.764	1.2	0.677
2.4	0.596	2.4	0.612	2.4	0.551
3.6	0.476	3.6	0.475	3.6	0.435
4.8	0.369	4.8	0.358	4.8	0.333
6.0	0.278	6.0	0.262	6.0	0.247
7.2	0.203	7.2	0.187	7.2	0.177
8.4	0.143	8.4	0.132	8.4	0.122
9.6	0.098	9.6	0.093	9.6	0.081
10.8	0.065	10.8	0.068	10.8	0.052
12.0	0.041	12.0	0.051	12.0	0.032
13.2	0.026	13.2	0.042	13.2	0.019
14.4	0.015	14.4	0.036	14.4	0.011
15.6	0.009	15.6	0.033	15.6	0.006
16.8	0.005	16.8	0.031	16.8	0.003
18.0	0.003	18.0	0.031	18.0	0.002
19.2	0.001	19.2	0.030	19.2	0.001
20.4	0.001	20.4	0.030	20.4	0.000
21.6	0	21.6	0.030	21.6	0.000
22.8	0	22.8	0.030	22.8	0.000
24.0	0	24.0	0.030	24.0	0.000
25.2	0	25.2	0.030	25.2	0.000
26.4	0	26.4	0.030	26.4	0.000
27.6	0	27.6	0.030	27.6	0.000
28.8	0	28.8	0.030	28.8	0.000
30.0	0	30.0	0.030	30.0	0.000
Cl depth (mm)	22		19		20

Initial Cl content=

Overall fit

Curing	D_a	C_s	r^2
W	1.2E-12	0.9	0.98
P	1.2E-12	0.7	0.97
WD	1.1E-12	0.8	0.99

*Better fit was obtained with the inclusion of first points. Otherwise, lower Cs was obtained than the first points.

Individual fit

*Curve-fitting was not possible for individual data set due to few data points

I.2 Exposure duration: 365 days

PC-0.4

Bulk diffusion results - Wet cured

1		2		3	
Depth	% Cl	Depth	% Cl	Depth	% Cl
[mm]	[conc.]	[mm]	[conc.]	[mm]	[conc.]
2.0	1.01	0.8	0.97	0.0	0.00
8.1	0.65	6.1	0.76	0.0	0.00
13.8	0.44	12.6	0.46	0.0	0.00
19.1	0.27	18.4	0.28	0.0	0.00
24.9	0.14	23.7	0.15	0.0	0.00
30.7	0.06	29.2	0.05	0.0	0.00
36.6	0.01	35.0	0.01	0.0	0.00

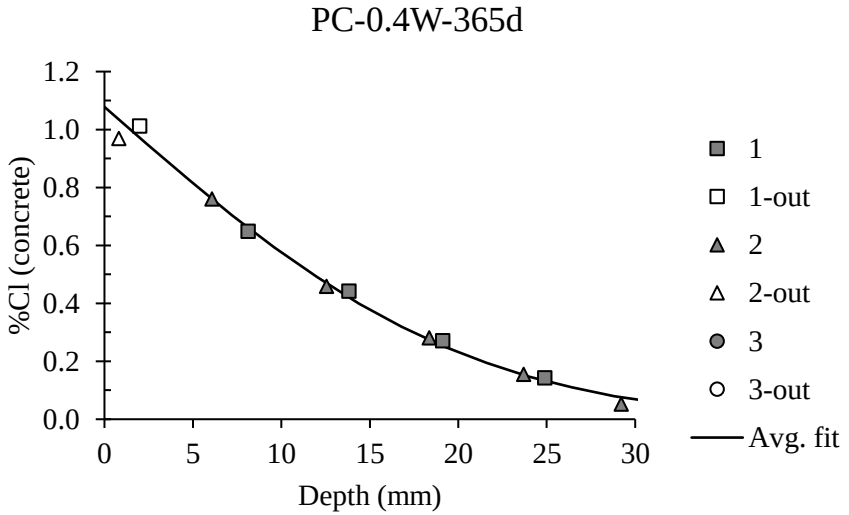

Bulk diffusion results - Plastic cured

1		2		3	
Depth	% Cl	Depth	% Cl	Depth	% Cl
[mm]	[conc.]	[mm]	[conc.]	[mm]	[conc.]
1.5	1.07	2.0	0.73	3.6	0.98
6.7	0.72	7.6	0.44	9.7	0.53
12.3	0.47	13.3	0.37	14.4	0.35
17.8	0.26	18.8	0.25	19.3	0.26
22.9	0.15	23.2	0.13	23.8	0.15
28.3	0.07	27.4	0.07	30.1	0.08

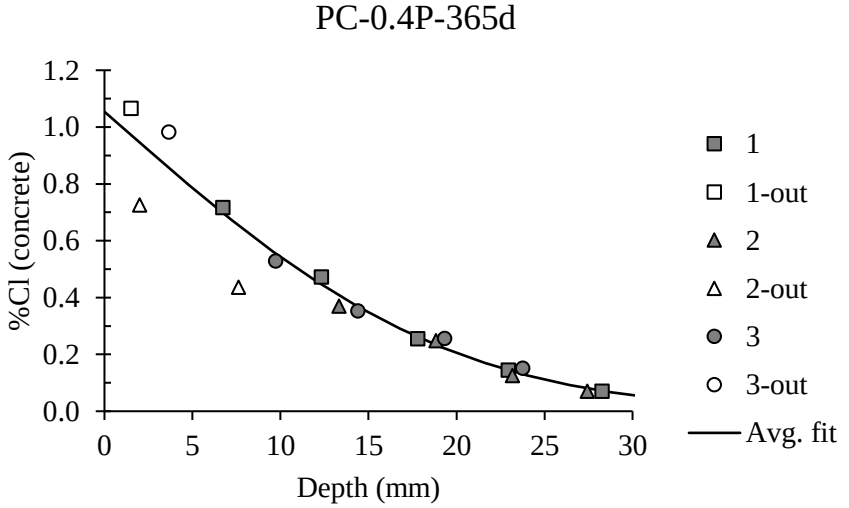

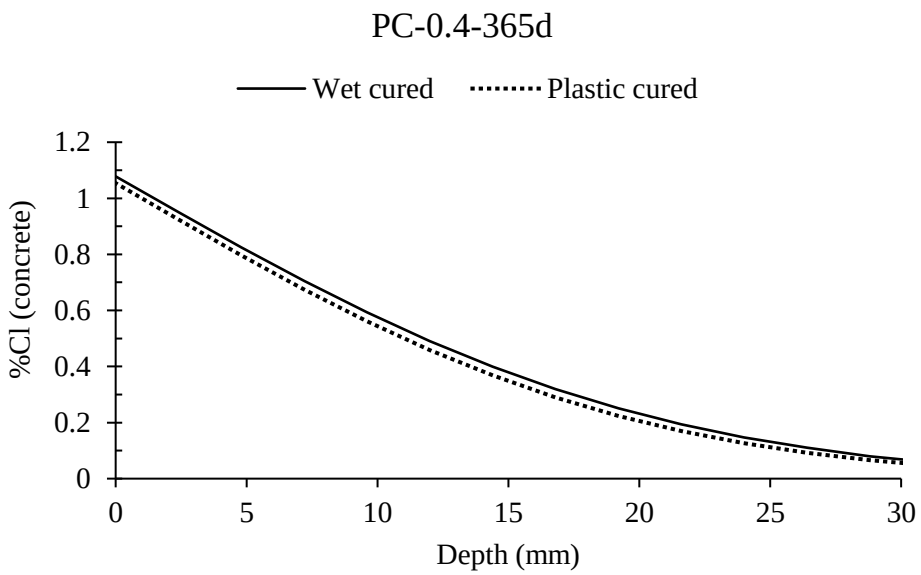
PC-0.4-365d
Wet cured
Plastic cured
%Cl (concrete)
1.2
1
0.8
0.6
0.4
0.2
0
0
5
10
15
20
25
30
Depth (mm)

Fitted profiles - overall (PC-0.4)

Wet cured		Plastic cured	
0.0	1.078	0.0	1.054
2.4	0.95	2.4	0.924
4.8	0.825	4.8	0.796
7.2	0.705	7.2	0.674
9.6	0.593	9.6	0.561
12.0	0.491	12.0	0.459
14.4	0.399	14.4	0.368
16.8	0.319	16.8	0.290
19.2	0.251	19.2	0.224
21.6	0.194	21.6	0.170
24.0	0.147	24.0	0.126
26.4	0.11	26.4	0.092
28.8	0.08	28.8	0.066
31.2	0.058	31.2	0.047
33.6	0.041	33.6	0.033
36.0	0.029	36.0	0.023
38.4	0.021	38.4	0.016
40.8	0.015	40.8	0.011
43.2	0.01	43.2	0.008
45.6	0.008	45.6	0.006
48.0	0.006	48.0	0.005
50.4	0.005	50.4	0.004
52.8	0.004	52.8	0.004
55.2	0.004	55.2	0.003
57.6	0.003	57.6	0.003
60.0	0.003	60.0	0.003
Cl depth (mm)	58		55
Initial Cl content=			0.003

Overall fit

Curing	D_a	C_s	r^2
W	8.2E-12	1.1	1.00
P	7.6E-12	1.1	0.99

Individual fit

W	D_a	C_s	r^2
Core 1	8.7E-12	1.1	1.00
Core 2	7.8E-12	1.1	1.00
Core 3	0.0E+00	0.0	0.00
Mean	**5.5E-12**	**0.7**	
SD	4.8E-12	0.62	
CV, %	87	87	

P	D_a	C_s	r^2
Core 1	7.2E-12	1.1	1.00
Core 2	7.7E-12	1.0	0.99
Core 3	9.2E-12	0.9	0.99
Mean	**8.0E-12**	**1.0**	
SD	1.0E-12	0.09	
CV, %	13	9	

FA(30)-0.4

Bulk diffusion results - Wet cured

1		2	
Depth	% Cl	Depth	% Cl
[mm]	[conc.]	[mm]	[conc.]
2.2	0.71	1.6	0.71
7.8	0.44	7.0	0.58
13.5	0.19	12.8	0.21
19.6	0.02	18.5	0.01
25.2	0.00	23.8	0.06
30.7	0.00	29.1	0.01
36.0	0.01	34.5	0.01

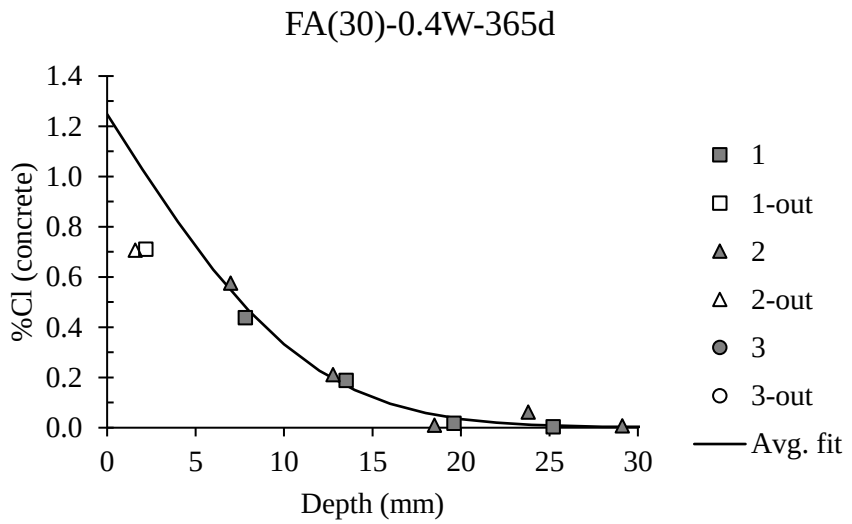

Bulk diffusion results - Plastic cured

1		2		3	
Depth	% Cl	Depth	% Cl	Depth	% Cl
[mm]	[conc.]	[mm]	[conc.]	[mm]	[conc.]
1.7	0.72	2.1	0.88	2.4	0.64
7.1	0.42	7.4	0.66	6.8	0.57
13.0	0.17	12.4	0.26	10.8	0.37
18.7	0.01	17.6	0.004	14.7	0.14
23.9	0.01	33.1	0.005	18.9	0.03
29.4	0.004	38.6	0.004	23.2	0.004

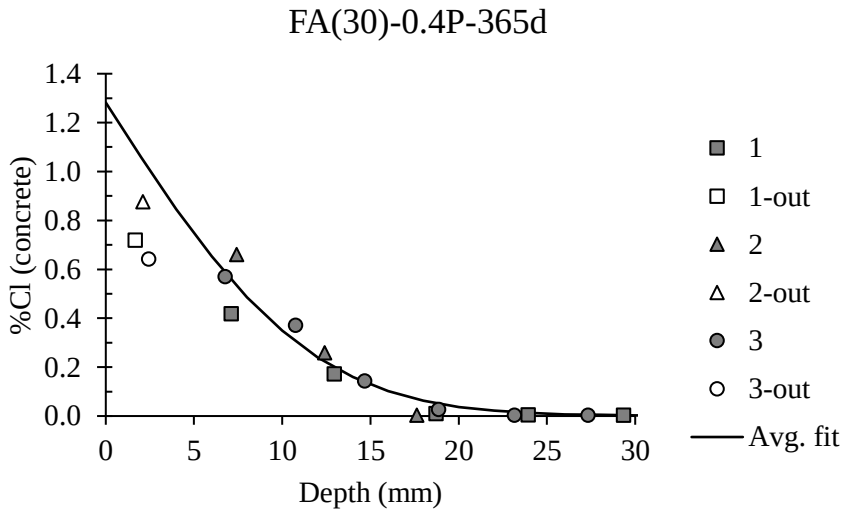

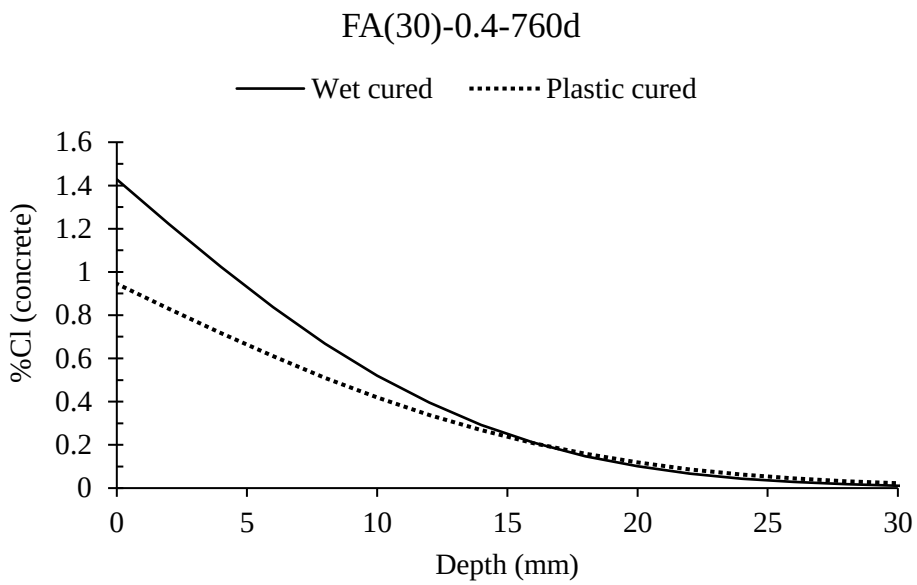
FA(30)-0.4-760d
Wet cured
Plastic cured
%Cl (concrete)
1.6
1.4
1.2
1
0.8
0.6
0.4
0.2
0
0
5
10
15
20
25
30
Depth (mm)

Fitted profiles - overall (FA(30)-0.4)

Wet cured		Plastic cured	
0.0	1.248	0.0	1.282
2.0	1.028	2.0	1.059
4.0	0.819	4.0	0.846
6.0	0.629	6.0	0.653
8.0	0.466	8.0	0.486
10.0	0.332	10.0	0.349
12.0	0.227	12.0	0.240
14.0	0.15	14.0	0.160
16.0	0.095	16.0	0.102
18.0	0.058	18.0	0.063
20.0	0.034	20.0	0.037
22.0	0.02	22.0	0.022
24.0	0.011	24.0	0.013
26.0	0.007	26.0	0.007
28.0	0.004	28.0	0.005
30.0	0.003	30.0	0.003
32.0	0.002	32.0	0.003
34.0	0.002	34.0	0.002
36.0	0.002	36.0	0.002
38.0	0.002	38.0	0.002
40.0	0.002	40.0	0.002
42.0	0.002	42.0	0.002
44.0	0.002	44.0	0.002
46.0	0.002	46.0	0.002
48.0	0.002	48.0	0.002
50.0	0.002	50.0	0.002
Cl depth (mm)	32		34
	Initial Cl content=		0.002

Overall fit

Curing	D_a	C_s	r^2
W	1.3E-12	1.2	0.98
P	1.3E-12	1.3	0.94

Individual fit

W	D_a	C_s	r^2
Core 1	1.4E-12	1.1	0.99
Core 2	1.2E-12	1.4	0.98
Core 3	--	--	--
Mean	**1.3E-12**	**1.2**	
SD	1.6E-13	0.20	
CV, %	12	17	

P	D_a	C_s	r^2
Core 1	1.3E-12	1.0	0.99
Core 2	1.0E-12	1.9	0.99
Core 3	1.5E-12	1.2	0.99
Mean	**1.3E-12**	**1.4**	
SD	2.3E-13	0.47	
CV, %	18	35	

BS(50)-0.4

Bulk diffusion results - Wet cured

1		2	
Depth	% Cl	Depth	% Cl
[mm]	[conc.]	[mm]	[conc.]
2.3	0.86	1.3	0.83
8.6	0.30	6.4	0.37
14.7	0.02	11.9	0.04
20.2	0.01	17.2	0.01
25.1	0.01	22.9	0.01
29.5	0.01	28.8	0.01
34.7	0.01	34.0	0.01

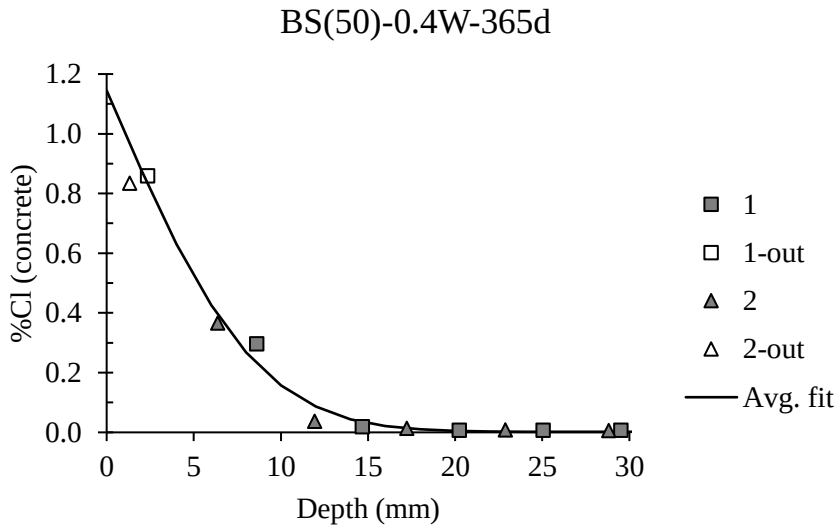

Fitted profiles - overall (BS(50)-0.4)

Wet cured	
0.0	1.145
2.0	0.877
4.0	0.631
6.0	0.426
8.0	0.268
10.0	0.157
12.0	0.086
14.0	0.044
16.0	0.021
18.0	0.01
20.0	0.005
22.0	0.003
24.0	0.002
26.0	0.002
28.0	0.002
30.0	0.002
32.0	0.002
34.0	0.002
36.0	0.002
38.0	0.002
40.0	0.002
42.0	0.002
44.0	0.002
46.0	0.002
48.0	0.002
50.0	0.002
Cl depth (mm)	24

Initial Cl content= 0.002

Overall fit

Curing	D_a	C_s	r^2
W	7.1E-13	1.1	0.96

Individual fit

W	D_a	C_s	r^2
Core 1	0.0E+00	0.0	0.00
Core 2	0.0E+00	0.0	0.00
Core 3	0.0E+00	0.0	0.00
Mean	**0.0E+00**	**0.0**	
SD	0.0E+00	0.00	
CV, %	#DIV/0!	#DIV/0!	

I.3 Exposure duration: 760 days

PC-0.4

Bulk diffusion results - Wet cured

1		2	
Depth	% Cl	Depth	% Cl
[mm]	[conc.]	[mm]	[conc.]
1.9	0.93	2.2	0.88
7.8	0.81	8.9	0.64
13.7	0.50	15.2	0.38
20.5	0.37	21.3	0.31
28.3	0.21	27.2	0.21
37.4	0.10	32.7	0.14

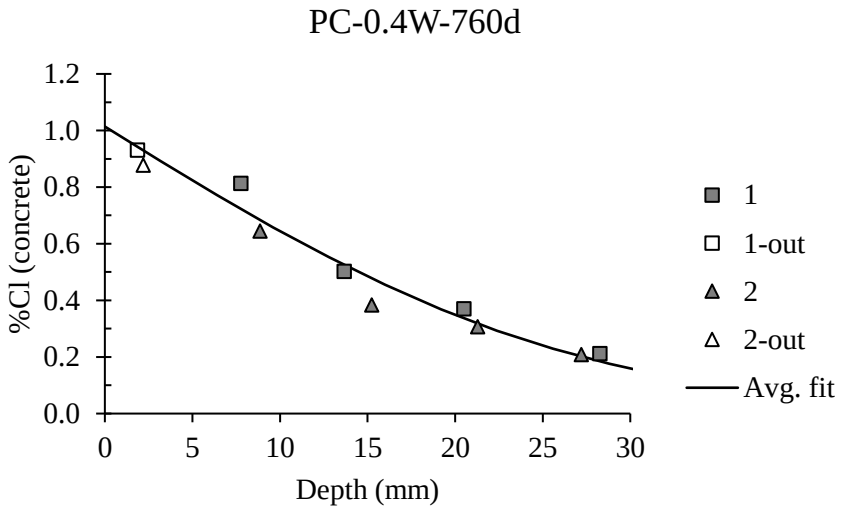

Bulk diffusion results - Plastic cured

1		2	
Depth	% Cl	Depth	% Cl
[mm]	[conc.]	[mm]	[conc.]
1.6	0.95	1.7	1.06
6.7	0.73	7.6	0.65
12.2	0.51	14.2	0.46
18.8	0.33	20.4	0.29
25.9	0.22	26.6	0.21
34.3	0.11	33.8	0.12

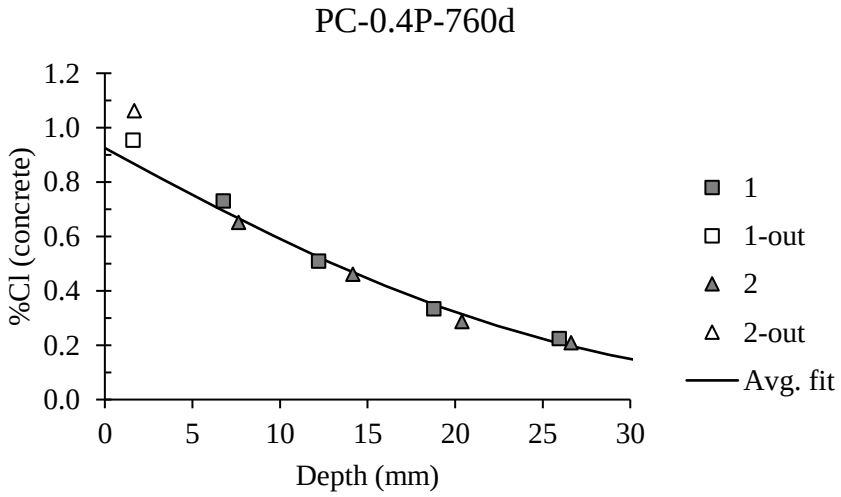

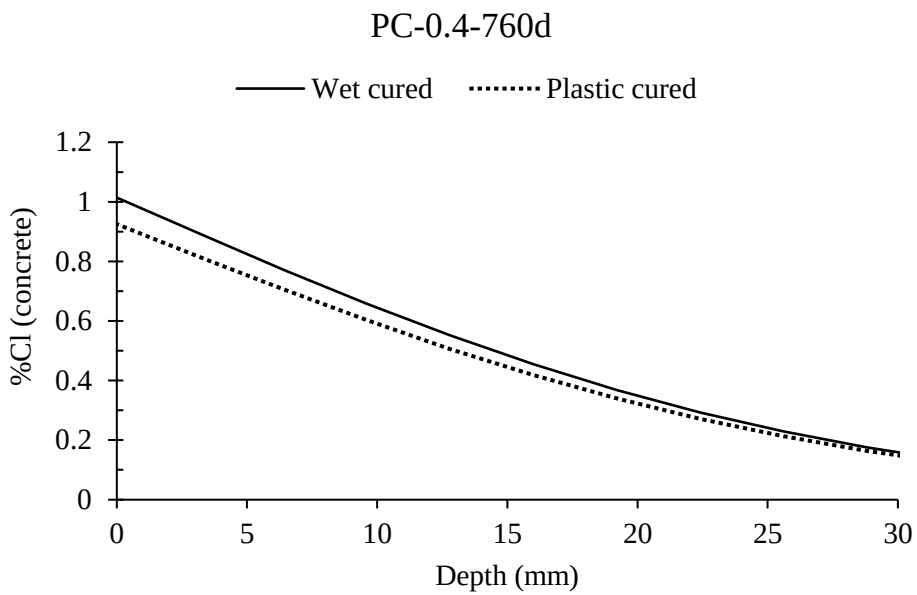
PC-0.4-760d
Wet cured
Plastic cured
%Cl (concrete)
1.2
1
0.8
0.6
0.4
0.2
0
0
5
10
15
20
25
30
Depth (mm)

Fitted profiles - overall (PC-0.4)

Wet cured		Plastic cured	
0.0	1.014	0.0	0.925
3.2	0.892	3.2	0.814
6.4	0.772	6.4	0.706
9.6	0.658	9.6	0.603
12.8	0.552	12.8	0.506
16.0	0.455	16.0	0.418
19.2	0.368	19.2	0.340
22.4	0.293	22.4	0.271
25.6	0.229	25.6	0.213
28.8	0.176	28.8	0.164
32.0	0.132	32.0	0.124
35.2	0.098	35.2	0.092
38.4	0.072	38.4	0.068
41.6	0.051	41.6	0.049
44.8	0.036	44.8	0.035
48.0	0.026	48.0	0.025
51.2	0.018	51.2	0.018
54.4	0.013	54.4	0.013
57.6	0.009	57.6	0.009
60.8	0.007	60.8	0.007
64.0	0.005	64.0	0.005
67.2	0.004	67.2	0.004
70.4	0.004	70.4	0.004
73.6	0.003	73.6	0.003
76.8	0.003	76.8	0.003
80.0	0.003	80.0	0.003
Cl depth (mm)	74		74

Initial Cl content= 0.003

Overall fit

Curing	D_a	C_s	r^2
W	3.4E-12	1.0	0.95
P	3.4E-12	0.9	0.99

Individual fit

W	D_a	C_s	r^2
Core 1	3.3E-12	1.1	0.98
Core 2	3.6E-12	0.9	0.97
Mean	**3.5E-12**	**1.0**	
SD	2.0E-13	0.14	
CV, %	6	14	

P	D_a	C_s	r^2
Core 1	3.3E-12	1.0	0.99
Core 2	3.6E-12	0.9	1.00
Mean	**3.5E-12**	**0.9**	
SD	1.9E-13	0.04	
CV, %	6	5	

FA(30)-0.4

Bulk diffusion results - Wet cured

1		2	
Depth	% Cl	Depth	% Cl
[mm]	[conc.]	[mm]	[conc.]
2.2	0.77	1.9	0.95
8.1	0.62	7.1	0.73
13.5	0.34	12.5	0.47
18.6	0.11	17.6	0.13
23.9	0.01	22.1	0.003
29.6	0.03	--	--

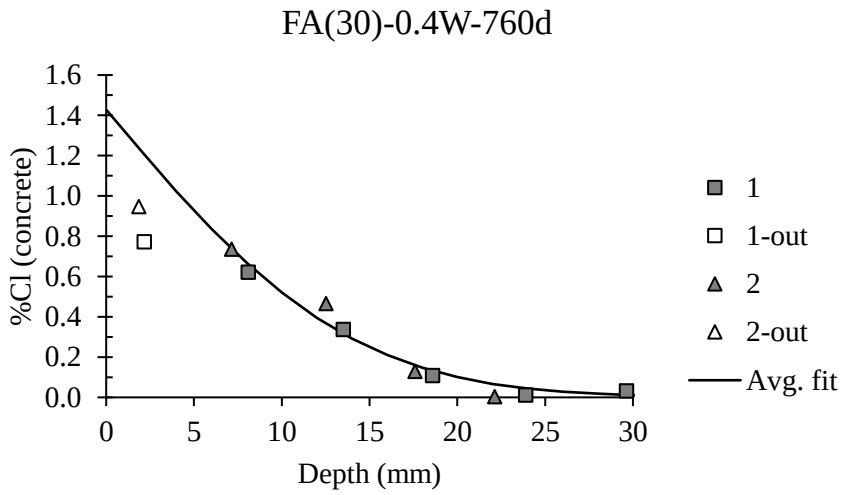

Bulk diffusion results - Plastic cured

1		2	
Depth	% Cl	Depth	% Cl
[mm]	[conc.]	[mm]	[conc.]
1.5	0.77	1.4	0.61
7.2	0.50	6.9	0.58
13.1	0.36	13.4	0.34
17.9	0.15	19.3	0.04

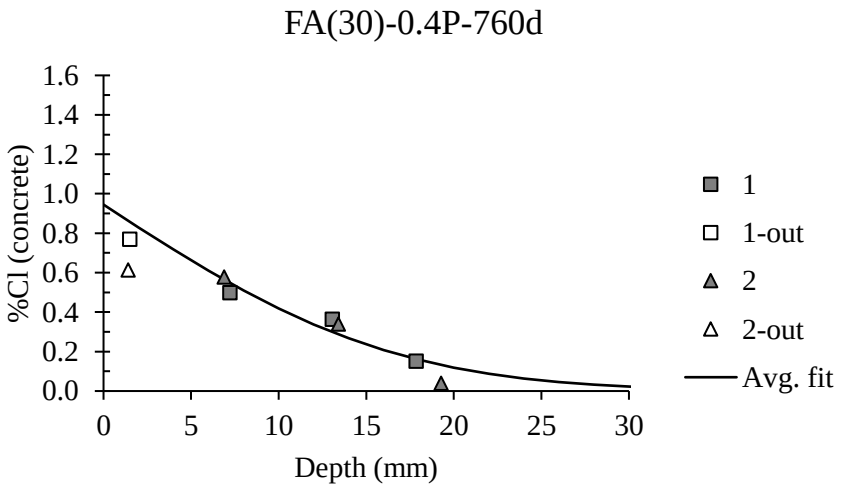

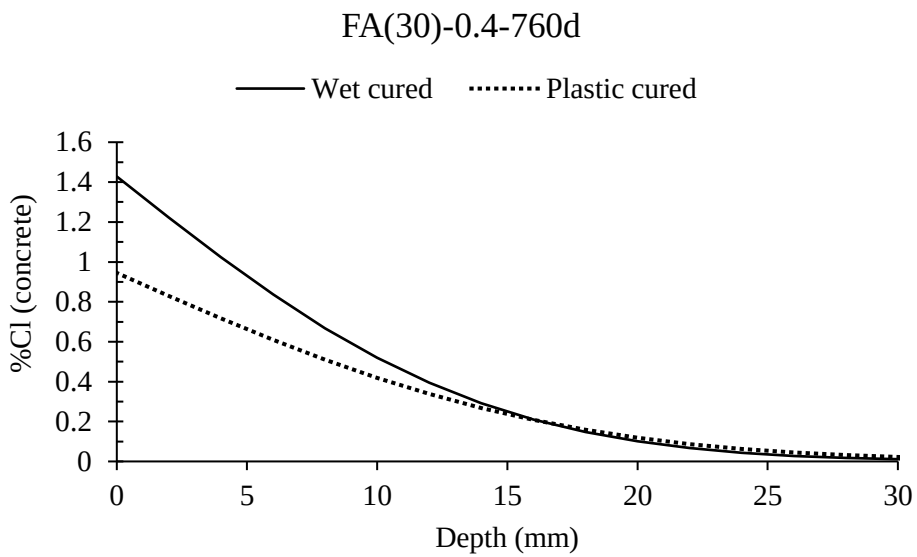
FA(30)-0.4-760d
Wet cured
Plastic cured
%Cl (concrete)
1.6
1.4
1.2
1
0.8
0.6
0.4
0.2
0
0
5
10
15
20
25
30
Depth (mm)

Fitted profiles - overall (FA(30)-0.4)

Wet cured		Plastic cured	
0.0	1.428	0.0	0.945
2.0	1.222	2.0	0.829
4.0	1.023	4.0	0.717
6.0	0.837	6.0	0.610
8.0	0.668	8.0	0.510
10.0	0.52	10.0	0.419
12.0	0.395	12.0	0.338
14.0	0.292	14.0	0.268
16.0	0.21	16.0	0.208
18.0	0.147	18.0	0.159
20.0	0.101	20.0	0.119
22.0	0.067	22.0	0.087
24.0	0.044	24.0	0.063
26.0	0.028	26.0	0.045
28.0	0.018	28.0	0.032
30.0	0.011	30.0	0.022
32.0	0.007	32.0	0.015
34.0	0.005	34.0	0.010
36.0	0.004	36.0	0.007
38.0	0.003	38.0	0.005
40.0	0.002	40.0	0.004
42.0	0.002	42.0	0.003
44.0	0.002	44.0	0.003
46.0	0.002	46.0	0.002
48.0	0.002	48.0	0.002
50.0	0.002	50.0	0.002
Cl depth (mm)	40		46
Initial Cl content=			0.002

Overall fit

Curing	D_a	C_s	r^2
W	9.2E-13	1.4	0.97
P	1.3E-12	0.9	0.91

Individual fit

W	D_a	C_s	r^2
Core 1	9.3E-13	1.4	0.99
Core 2	9.3E-13	1.5	0.96
Mean	**9.3E-13**	**1.4**	
SD	3.0E-15	0.08	
CV, %	0	5	

BS(50)-0.4

Bulk diffusion results - Wet cured

1	
Depth	% Cl
[mm]	[conc.]
1.4	0.67
6.5	0.51
11.5	0.21
16.5	0.06
22.7	0.00
28.6	0.01
81.3	0.02

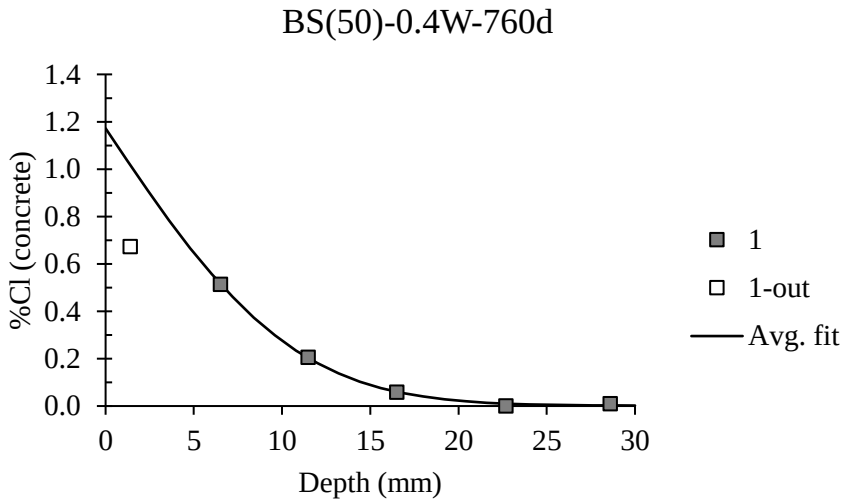

Fitted profiles - overall (BS(50)-0.4)

Wet cured	
0.0	1.172
1.2	1.039
2.4	0.909
3.6	0.784
4.8	0.666
6.0	0.558
7.2	0.46
8.4	0.373
9.6	0.298
10.8	0.234
12.0	0.181
13.2	0.138
14.4	0.103
15.6	0.076
16.8	0.055
18.0	0.04
19.2	0.028
20.4	0.02
21.6	0.014
22.8	0.01
24.0	0.007
25.2	0.005
26.4	0.004
27.6	0.003
28.8	0.003
30.0	0.002
Cl depth (mm)	30

Initial Cl content= 0.002

Curing	D_a	C_s	r^2
W (core 1)	5.4E-13	1.2	1.00

LIST OF APPENDIX REFERENCES

Alexander, M.G. & Streicher, P.E. 1998. Proposal for a rapid chloride binding test for concrete. In *International symposium on high strength concrete and reactive powder concretes*. Sherbrooke: University of Sherbrooke. 421–434.

Angst, U., Elsener, B., Larsen, C.K. & Vennesland, Ø. 2010. Potentiometric determination of the chloride ion activity in cement based materials. *Journal of Applied Electrochemistry*. 40(3):561–573. DOI: 10.1007/s10800-009-0029-6.

Arya, C. & Xu, Y. 1995. Effect of cement type on chloride binding and corrosion of steel in concrete. *Cement and Concrete Research*. 25(4):893–902. DOI: 10.1016/0008-8846(95)00080-V.

ASTM C1152. 2004. Standard Test Method for Acid-Soluble Chloride in Mortar and Concrete. *ASTM International*. DOI: 10.1520/C1152.

ASTM C1218. 2020. Standard Test Method for Water-Soluble Chloride in Mortar and Concrete. *ASTM International*. DOI: 10.1520/C1218_C1218M-20.

Atkins, P. & Paula, J. De. 2006. *Atkin's Physical Chemistry*. 8th ed. Oxford University Press.

Atkins, C.P., Carter, M.A. & Scantlebury, J.D. 2001. Sources of error in using silver/silver chloride electrodes to monitor chloride activity in concrete. *Cement and Concrete Research*. 1207–1211.

Avet, F. & Scrivener, K. 2020. Influence of pH on the chloride binding capacity of Limestone Calcined Clay Cements (LC3). *Cement and Concrete Research*. 131. DOI: 10.1016/j.cemconres.2020.106031.

Bahman-Zadeh, F., Ramezanianpour, A.A. & Zolfagharnasab, A. 2022. Effect of carbonation on chloride binding capacity of limestone calcined clay cement (LC3) and binary pastes. *Journal of Building Engineering*. 52. DOI: 10.1016/j.jobe.2022.104447.

Balonis, M., Lothenbach, B., Le Saout, G. & Glasser, F.P. 2010. Impact of chloride on the mineralogy of hydrated Portland cement systems. *Cement and Concrete Research*. 40(7):1009–1022. DOI: 10.1016/j.cemconres.2010.03.002.

Barneyback, R.S. & Diamond, S. 1981. Expression and analysis of pore fluids from hardened cement pastes and mortars. *Cement and Concrete Research*. II:279–285.

Birnin-Yauri, U.A. & Glasser, F.P. 1998. Friedel's salt, Ca2Al(OH)6(Cl,OH)·2H2O: Its solid solutions and their role in chloride binding. *Cement and Concrete Research*. 28(12):1713–1723. DOI: 10.1016/S0008-8846(98)00162-8.

BS 1881: Part 124. 1988. Methods for analysis of hardened concrete. *British Standard*.

BS EN 14629. 2007. Products and systems for the protection and repair of concrete structures - Test methods - Determination of chloride content in hardened concrete. *British Standard*.

Byfors, K., Hansson, C.M. & Tritthart, J. 1986. Pore solution expression as a method to determine the influence of mineral additives on chloride binding. *Cement and Concrete Research*. 16:760–770.

Castellote, M. & Andrade, C. 2001a. Round-Robin test on chloride analysis in concrete - Part II: Analysis of water soluble chloride content. *Materials and Structures/Materiaux et Constructions*. 34(244):589–598. DOI: 10.1617/13681.

Castellote, M. & Andrade, C. 2001b. TC 178-TMC: Round-Robin test on chloride analysis in concrete-Part I: Analysis of total chloride content. *Materials and Structures/Matériaux et Constructions*. 34:532–556.

Castellote, M. & Andrade, C. 2001c. Round-Robin test on chloride analysis in concrete - Part I: Analysis of total chloride content. *Materials and Structures/Materiaux et Constructions*. 34(243):532–556. DOI: 10.1617/13680.

Castellote, M., Andrade, C. & Alonso, C. 1999. Chloride-binding isotherms in concrete submitted to non-steady-state migration experiments. *Cement and Concrete Research*. 29:1799–1806.

Castellote, M., Alonso, C., Andrade, C., Castro, P. & Echeverria, M. 2001. Alkaline leaching method for the determination of the chloride content in the aqueous phase of hardened cementitious materials. *Cement and Concrete Research*. 31:233–238.

Chang, H. 2017. Chloride binding capacity of pastes influenced by carbonation under three conditions. *Cement and Concrete Composites*. 84:1–9. DOI: 10.1016/j.cemconcomp.2017.08.011.

Cheewaket, T., Jaturapitakkul, C. & Chalee, W. 2010. Long term performance of chloride binding capacity in fly ash concrete in a marine environment. *Construction and Building Materials*. 24(8):1352–1357. DOI: 10.1016/j.conbuildmat.2009.12.039.

Climent, M.A., Viqueira, E., De Vera, G. & López-Atalaya, M.M. 1999. Analysis of acid-soluble chloride in cement, mortar, and concrete by potentiometric titration without filtration steps. *Cement and Concrete Research*. 29:893–898.

Delagrave, A., Marchand, J., Ollivier, J.P., Julien, S. & Hazrati, K. 1997. Chloride binding capacity of various hydrated cement paste systems. *Advanced Cement Based Materials*. 6(1):28–35. DOI: 10.1016/S1065-7355(97)00007-2.

Dhir, R.K., El-Mohr, M.A.K. & Dyer, T.D. 1996. Chloride binding in GGBS concrete. *Cement and Concrete Research*. 26(12):1767–1773. DOI: 10.1016/S0008-8846(96)00180-9.

Dousti, A., Rashetnia, R., Ahmadi, B. & Shekarchi, M. 2013. Influence of exposure temperature on chloride diffusion in concretes incorporating silica fume or natural zeolite. *Construction and Building Materials*. 49:393–399. DOI: 10.1016/j.conbuildmat.2013.08.086.

Ghosh, P. & Tran, Q. 2015. Correlation Between Bulk and Surface Resistivity of Concrete. *International Journal of Concrete Structures and Materials*. 9(1):119–132. DOI: 10.1007/s40069-014-0094-z.

Glass, G.K., Wang, Y. & Buenfeld, N.R. 1996. An investigation of experimental methods used to determine free and total chloride contents. *Cement and Concrete Research*. 26(9):1443–1449.

Glass, G.K., Stevenson, G.M. & Buenfeld, N.R. 1998. Chloride-binding isotherms from the diffusion cell test. *Cement and Concrete Research*. 28(7):939–945.

Glasser, F.P., Kindness, A. & Stronach, S.A. 1999. Stability and solubility relationships in AFm phases Part I. Chloride, sulfate and hydroxide. *Cement and Concrete Research*. 29:861–866.

Gowers, K.R. & Millard, S.G. 1999. Measurement of concrete resistivity for assessment of corrosion severity of steel using wenner technique. *ACI Materials Journal*. 96(5):536–541. DOI: 10.14359/655.

Hirao, H., Yamada, K., Takahashi, H. & Zibara, H. 2005. Chloride binding of cement estimated by binding isotherms of hydrates. *Journal of Advanced Concrete Technology*. 3(1):77–84.

Jeffery, G.H., Bassett, J., Mendham, J. & Denney, R.C. 1989. *Vogel's textbook of quantitative chemical analysis.* V. 5. Longman Scientific & Technical.

Kayali, O., Khan, M.S.H. & Sharfuddin Ahmed, M. 2012. The role of hydrotalcite in chloride binding and corrosion protection in concretes with ground granulated blast furnace slag. *Cement and Concrete Composites*. 34(8):936–945. DOI: 10.1016/j.cemconcomp.2012.04.009.

Lothenbach, B., Scrivener, K. & Hooton, R.D. 2011. Supplementary cementitious materials. *Cement and Concrete Research*. 41(12):1244–1256. DOI: 10.1016/j.cemconres.2010.12.001.

Lumley, J.S., Gollop, R.S., Moir, G.K. & Taylor, H.F.W. 1996. Degrees of reaction of the slag in some blends with Portland cements. *Cement and Concrete Research*. 26(1):139–151.

Luo, R., Cai, Y., Wang, C. & Huang, X. 2003. Study of chloride binding and diffusion in GGBS concrete. *Cement and Concrete Research*. 33(1):1–7. DOI: 10.1016/S0008-8846(02)00712-3.

Machner, A., Hemstad, P. & De Weerdt, K. 2018. Towards the Understanding of the pH Dependency of the Chloride Binding of Portland Cement Pastes. *Nordic Concrete Research*. 58(1):143–162. DOI: 10.2478/ncr-2018-0009.

Mangat, P.S. & Molloy, B.T. 1995. Chloride binding in concrete containing PFA, gbs or silica fume under sea. *Magazine of Concrete Research*. 47(171):129–141.

Mapa, D.G., Zhu, H., Nosouhian, F., Shanahan, N., Riding, K.A. & Zayed, A. 2023. Chloride binding and diffusion of slag blended concrete mixtures. *Construction and Building Materials*. 388. DOI: 10.1016/j.conbuildmat.2023.131584.

Martín-Pérez, B., Zibara, H., Hooton, R.D. & Thomas, M.D.A. 2000. A study of the effect of chloride binding on service life predictions. *Cement and Concrete Research*. 30(8):1215–1223. DOI: 10.1016/S0008-8846(00)00339-2.

Morris, W., Moreno, E.I. & Sagüés, A.A. 1996. Practical evaluation of resistivity of concrete in test cylinders using a Wenner array probe. *Cement and Concrete Research*. 26(12):1779–1787. DOI: 10.1016/S0008-8846(96)00175-5.

Nguyen, T.S., Lorente, S. & Carcasses, M. 2009. Effect of the environment temperature on the chloride diffusion through CEM-I and CEM-V mortars: An experimental study. *Construction and Building Materials*. 23(2):795–803. DOI: 10.1016/j.conbuildmat.2008.03.004.

Nilsson, L.O., Massat, M. & Tang, L. 1994. The effect of non-linear chloride binding on the prediction of chloride penetration into concrete structures. In *ACI SP-145*. V.M. Malhotra, Ed. 469–486.

Nilsson, L.-O., Sandberg, P. & Sørensen, H.E. 1996. *HETEK: Chloride penetration into concrete - State-of-the-Art*. DOI: 10.13140/RG.2.1.2771.7526.

NT BUILD 208. 1996. Chloride content by Volhard titration. *Nordtest method*. 11.

Ogirigbo, O.R. & Black, L. 2017. Chloride binding and diffusion in slag blends: Influence of slag composition and temperature. *Construction and Building Materials*. 149:816–825. DOI: 10.1016/j.conbuildmat.2017.05.184.

Otsuki, N., Nagataki, S. & Nakashita, K. 1993. Evaluation of the AgNO3 solution spray method for measurement of chloride penetration into hardened cementitious matrix materials. *Construction and Building Materials*. 7(4):195–201.

Panesar, D.K., Eng, P. & Chidiac, S.E. 2011. Effect of Cold Temperature on the Chloride-Binding Capacity of Cement. *Journal of Cold Regions Engineering*. 25(4):133–144. DOI: 10.1061/(ASCE)CR.

Pargar, F., Koleva, D.A. & Van Breugel, K. 2017. Determination of chloride content in cementitious materials: From fundamental aspects to application of Ag/AgCl chloride sensors. *Sensors, MDPI*. 17. DOI: 10.3390/s17112482.

RILEM TC 178-TMC. 2002a. Analysis of water soluble chlorides in concrete - recommendation. *Materials and Structures*. 35(Nov.):586–588.

RILEM TC 178-TMC. 2002b. Analysis of total chloride content in concrete: Recommendation. *Materials and Structures*. 35:583–585.

Saillio, M., Baroghel-Bouny, V. & Barberon, F. 2014. Chloride binding in sound and carbonated cementitious materials with various types of binder. *Construction and Building Materials*. 68:82–91. DOI: 10.1016/j.conbuildmat.2014.05.049.

Sciencecready.com.au. 2023. *What is precipitation titration?*

Sengul, O. & Gjørv, O.E. 2009. Electrical Resistivity Measurements for Quality Control During Concrete Construction. *ACI Materials Journal*. (105):541–547. DOI: 10.14359/20195.

Shi, Z., Geiker, M.R., De Weerdt, K., Østnor, T.A., Lothenbach, B., Winnefeld, F. & Skibsted, J. 2017. Role of calcium on chloride binding in hydrated Portland cement–metakaolin–limestone blends. *Cement and Concrete Research*. 95:205–216. DOI: 10.1016/j.cemconres.2017.02.003.

Sui, S., Wilson, W., Georget, F., Maraghechi, H., Kazemi-Kamyab, H., Sun, W. & Scrivener, K. 2019. Quantification methods for chloride binding in Portland cement and limestone systems. *Cement and Concrete Research*. 125. DOI: 10.1016/j.cemconres.2019.105864.

Suryavanshi, A., Scantlebury, J. & Lyon, S. 1996. Mechanism of Friedel's salt formation in cements rich in tri-calcium aluminate. *Cement and Concrete Research*. 26(5):717–727.

Tang, L. & Nilsson, L.-O. 1993. Chloride binding capacity and binding isotherms of OPC pastes and mortars. *Cement and Concrete Research*. 23:24–253.

Tang, L., Nilsson, L. & Basheer, P.A.M. 2012. *Resistance of Concrete to Chloride Ingress - Testing and Modelling*. CRC Press.

Thomas, M.D.A., Hooton, R.D., Scott, A. & Zibara, H. 2012. The effect of supplementary cementitious materials on chloride binding in hardened cement paste. *Cement and Concrete Research*. 42(1):1–7. DOI: 10.1016/j.cemconres.2011.01.001.

Tritthart, J. 1989a. Chloride binding in cement II. The influence of the hydroxide concentration in the pore solution of hardened cement paste on chloride binding. *Cement and Concrete Research*. 19:683–691.

Tritthart, J. 1989b. Chloride binding in cement I. Investigations to determine the composition of pore water in hardened cement. *Cement and Concrete Research*. 19:586–594.

Voinitchi, D., Julien, S. & Lorente, S. 2008. The relation between electrokinetics and chloride transport through cement-based materials. *Cement and Concrete Composites*. 30(3):157–166. DOI: 10.1016/j.cemconcomp.2007.11.002.

De Weerdt, K., Orsáková, D. & Geiker, M.R. 2014. The impact of sulphate and magnesium on chloride binding in Portland cement paste. *Cement and Concrete Research*. 65:30–40. DOI: 10.1016/j.cemconres.2014.07.007.

De Weerdt, K., Colombo, A., Coppola, L., Justnes, H. & Geiker, M.R. 2015. Impact of the associated cation on chloride binding of Portland cement paste. *Cement and Concrete Research*. 68:196–202. DOI: 10.1016/j.cemconres.2014.01.027.

Xu, Y. 1997. The influence of sulphates on chloride binding and pore solution chemistry. *Cement and Concrete Research*. 27(12):1841–1850.

Yuan, Q., Shi, C., De Schutter, G., Audenaert, K. & Deng, D. 2009. Chloride binding of cement-based materials subjected to external chloride environment - A review. *Construction and Building Materials*. 23(1):1–13. DOI: 10.1016/j.conbuildmat.2008.02.004.

Yuan, Q., Deng, D., Shi, C. & De Schutter, G. 2013. Chloride binding isotherm from migration and diffusion tests. *Journal Wuhan University of Technology, Materials Science Edition*. 28(3):548–556. DOI: 10.1007/s11595-013-0729-y.

Zhu, Q., Jiang, L., Chen, Y., Xu, J. & Mo, L. 2012. Effect of chloride salt type on chloride binding behavior of concrete. *Construction and Building Materials*. 37:512–517. DOI: 10.1016/j.conbuildmat.2012.07.079.

Zibara, H. 2001. Binding of external chlorides by cement. *PhD thesis, University of Toronto*.